The Textile Institute and Woodhead Publishing

The Textile Institute is a unique organisation in textiles, clothing and footwear. Incorporated in England by a Royal Charter granted in 1925, the Institute has individual and corporate members in over 90 countries. The aim of the Institute is to facilitate learning, recognise achievement, reward excellence and disseminate information within the global textiles, clothing and footwear industries.

Historically, The Textile Institute has published books of interest to its members and the textile industry. To maintain this policy, the Institute has entered into partnership with Woodhead Publishing Limited to ensure that Institute members and the textile industry continue to have access to high calibre titles on textile science and technology.

Most Woodhead titles on textiles are now published in collaboration with The Textile Institute. Through this arrangement, the Institute provides an Editorial Board which advises Woodhead on appropriate titles for future publication and suggests possible editors and authors for these books. Each book published under this arrangement carries the Institute's logo.

Woodhead books published in collaboration with The Textile Institute are offered to Textile Institute members at a substantial discount. These books, together with those published by The Textile Institute that are still in print, are offered on the Elsevier website at: http://store.elsevier.com/. Textile Institute books still in print are also available directly from the Institute's web site at: www.textileinstitutebooks.com.

A list of Woodhead books on textiles science and technology, most of which have been published in collaboration with the Textile Institute, can be found towards the end of the contents pages.

Related titles

Performance Testing of Textiles: Methods, Technology and Applications
(ISBN 978-0-08-100570-5)

Garment Manufacturing Technology
(ISBN 978-1-78242-232-7)

High Performance Textiles and Their Applications
(ISBN 978-1-84569-180-6)

Woodhead Publishing Series in Textiles:
Number 187

Structure and Properties of High-Performance Fibers

Edited by

Gajanan Bhat

The Textile Institute

ELSEVIER

AMSTERDAM • BOSTON • CAMBRIDGE • HEIDELBERG
LONDON • NEW YORK • OXFORD • PARIS • SAN DIEGO
SAN FRANCISCO • SINGAPORE • SYDNEY • TOKYO
Woodhead Publishing is an imprint of Elsevier

Published by Woodhead Publishing in association with The Textile Institute
Woodhead Publishing is an imprint of Elsevier
The Officers' Mess Business Centre, Royston Road, Duxford, CB22 4QH, UK
50 Hampshire Street, 5th Floor, Cambridge, MA 02139, USA
The Boulevard, Langford Lane, Kidlington, OX5 1GB, UK

Notices

Knowledge and best practice in this field are constantly changing. As new research and experience broaden our understanding, changes in research methods, professional practices, or medical treatment may become necessary.

Practitioners and researchers must always rely on their own experience and knowledge in evaluating and using any information, methods, compounds, or experiments described herein. In using such information or methods they should be mindful of their own safety and the safety of others, including parties for whom they have a professional responsibility.

To the fullest extent of the law, neither the Publisher nor the authors, contributors, or editors, assume any liability for any injury and/or damage to persons or property as a matter of products liability, negligence or otherwise, or from any use or operation of any methods, products, instructions, or ideas contained in the material herein.

British Library Cataloguing-in-Publication Data
A catalogue record for this book is available from the British Library

Library of Congress Cataloging-in-Publication Data
A catalog record for this book is available from the Library of Congress

ISBN: 978-0-08-100550-7 (print)
ISBN: 978-0-08-100551-4 (online)

Publisher: Matthew Deans
Acquisition Editor: David Jackson
Editorial Project Manager: Edward Payne
Production Project Manager: Poulouse Joseph
Designer: Maria Inês Cruz

Typeset by TNQ Books and Journals

List of contributors

K. Akato The University of Tennessee, Knoxville, TN, United States

G. Bhat The University of Georgia, Athens, Georgia, United States

M.R. Buchmeiser Institute of Textile Chemistry and Chemical Fibers (ITCF Denkendorf), Denkendorf, Germany; Institute of Polymer Chemistry, University of Stuttgart, Stuttgart, Germany

J. Chang Beijing University of Chemical Technology, Beijing, China

J.M. Deitzel University of Delaware, DE, United States

B.L. Deopura IIT Delhi, New Delhi, India

J. Fang Deakin University, Victoria, Australia

E. Frank Institute of Textile Chemistry and Chemical Fibers (ITCF Denkendorf), Denkendorf, Germany

J.W. Gillespie, Jr. University of Delaware, DE, United States

N. Hiremath The University of Tennessee, Knoxville, TN, United States

M.G. Huson CSIRO, Geelong, Victoria, Australia

D. Ingildeev Institute of Textile Chemistry and Chemical Fibers (ITCF Denkendorf), Denkendorf, Germany

R. Kotek North Carolina State University, Raleigh, NC, United States

G. Li Donghua University, Songjiang District, Shanghai, China

T. Lin Deakin University, Victoria, Australia

P. McDaniel University of Delaware, DE, United States

B. Mijovic University of Zagreb, Zagreb, Croatia

K.R. Millington CSIRO Manufacturing, Geelong Technology Precinct, Waurn Ponds, Victoria, Australia

S. Mukhopadhyay IIT Delhi, New Delhi, India

K. Murugesh Babu Bapuji Institute of Engineering and Technology, Davangere, Karnataka, India

M. Najafi North Carolina State University, Raleigh, NC, United States

L. Nasri Trützschler Switzerland AG, Winterthur, Switzerland

H. Niu Beijing University of Chemical Technology, Beijing, China

J.A. Rippon CSIRO Manufacturing, Geelong Technology Precinct, Waurn Ponds, Victoria, Australia

F. Sloan Kuraray America, Inc. Fort Mill, South Carolina, United States

D. Wu Beijing University of Chemical Technology, Beijing, China

E. Zdraveva Deakin University, Victoria, Australia; University of Zagreb, Zagreb, Croatia

Woodhead Publishing Series in Textiles

1 **Watson's textile design and colour Seventh edition**
Edited by Z. Grosicki
2 **Watson's advanced textile design**
Edited by Z. Grosicki
3 **Weaving Second edition**
P. R. Lord and M. H. Mohamed
4 **Handbook of textile fibres Volume 1: Natural fibres**
J. Gordon Cook
5 **Handbook of textile fibres Volume 2: Man-made fibres**
J. Gordon Cook
6 **Recycling textile and plastic waste**
Edited by A. R. Horrocks
7 **New fibers Second edition**
T. Hongu and G. O. Phillips
8 **Atlas of fibre fracture and damage to textiles Second edition**
J. W. S. Hearle, B. Lomas and W. D. Cooke
9 **Ecotextile '98**
Edited by A. R. Horrocks
10 **Physical testing of textiles**
B. P. Saville
11 **Geometric symmetry in patterns and tilings**
C. E. Horne
12 **Handbook of technical textiles**
Edited by A. R. Horrocks and S. C. Anand
13 **Textiles in automotive engineering**
W. Fung and J. M. Hardcastle
14 **Handbook of textile design**
J. Wilson
15 **High-performance fibres**
Edited by J. W. S. Hearle
16 **Knitting technology Third edition**
D. J. Spencer
17 **Medical textiles**
Edited by S. C. Anand
18 **Regenerated cellulose fibres**
Edited by C. Woodings
19 **Silk, mohair, cashmere and other luxury fibres**
Edited by R. R. Franck

20 **Smart fibres, fabrics and clothing**
Edited by X. M. Tao
21 **Yarn texturing technology**
J. W. S. Hearle, L. Hollick and D. K. Wilson
22 **Encyclopedia of textile finishing**
H.-K. Rouette
23 **Coated and laminated textiles**
W. Fung
24 **Fancy yarns**
R. H. Gong and R. M. Wright
25 **Wool: Science and technology**
Edited by W. S. Simpson and G. Crawshaw
26 **Dictionary of textile finishing**
H.-K. Rouette
27 **Environmental impact of textiles**
K. Slater
28 **Handbook of yarn production**
P. R. Lord
29 **Textile processing with enzymes**
Edited by A. Cavaco-Paulo and G. Gübitz
30 **The China and Hong Kong denim industry**
Y. Li, L. Yao and K. W. Yeung
31 **The World Trade Organization and international denim trading**
Y. Li, Y. Shen, L. Yao and E. Newton
32 **Chemical finishing of textiles**
W. D. Schindler and P. J. Hauser
33 **Clothing appearance and fit**
J. Fan, W. Yu and L. Hunter
34 **Handbook of fibre rope technology**
H. A. McKenna, J. W. S. Hearle and N. O'Hear
35 **Structure and mechanics of woven fabrics**
J. L. Hu
36 **Synthetic fibres: Nylon, polyester, acrylic, polyolefin**
Edited by J. E. McIntyre
37 **Woollen and worsted woven fabric design**
E. G. Gilligan
38 **Analytical electrochemistry in textiles**
P. Westbroek, G. Priniotakis and P. Kiekens
39 **Bast and other plant fibres**
R. R. Franck
40 **Chemical testing of textiles**
Edited by Q. Fan
41 **Design and manufacture of textile composites**
Edited by A. C. Long
42 **Effect of mechanical and physical properties on fabric hand**
Edited by H. M. Behery
43 **New millennium fibers**
T. Hongu, M. Takigami and G. O. Phillips

44 **Textiles for protection**
Edited by R. A. Scott
45 **Textiles in sport**
Edited by R. Shishoo
46 **Wearable electronics and photonics**
Edited by X. M. Tao
47 **Biodegradable and sustainable fibres**
Edited by R. S. Blackburn
48 **Medical textiles and biomaterials for healthcare**
Edited by S. C. Anand, M. Miraftab, S. Rajendran and J. F. Kennedy
49 **Total colour management in textiles**
Edited by J. Xin
50 **Recycling in textiles**
Edited by Y. Wang
51 **Clothing biosensory engineering**
Y. Li and A. S. W. Wong
52 **Biomechanical engineering of textiles and clothing**
Edited by Y. Li and D. X.-Q. Dai
53 **Digital printing of textiles**
Edited by H. Ujiie
54 **Intelligent textiles and clothing**
Edited by H. R. Mattila
55 **Innovation and technology of women's intimate apparel**
W. Yu, J. Fan, S. C. Harlock and S. P. Ng
56 **Thermal and moisture transport in fibrous materials**
Edited by N. Pan and P. Gibson
57 **Geosynthetics in civil engineering**
Edited by R. W. Sarsby
58 **Handbook of nonwovens**
Edited by S. Russell
59 **Cotton: Science and technology**
Edited by S. Gordon and Y.-L. Hsieh
60 **Ecotextiles**
Edited by M. Miraftab and A. R. Horrocks
61 **Composite forming technologies**
Edited by A. C. Long
62 **Plasma technology for textiles**
Edited by R. Shishoo
63 **Smart textiles for medicine and healthcare**
Edited by L. Van Langenhove
64 **Sizing in clothing**
Edited by S. Ashdown
65 **Shape memory polymers and textiles**
J. L. Hu
66 **Environmental aspects of textile dyeing**
Edited by R. Christie
67 **Nanofibers and nanotechnology in textiles**
Edited by P. Brown and K. Stevens

68 **Physical properties of textile fibres Fourth edition**
W. E. Morton and J. W. S. Hearle
69 **Advances in apparel production**
Edited by C. Fairhurst
70 **Advances in fire retardant materials**
Edited by A. R. Horrocks and D. Price
71 **Polyesters and polyamides**
Edited by B. L. Deopura, R. Alagirusamy, M. Joshi and B. S. Gupta
72 **Advances in wool technology**
Edited by N. A. G. Johnson and I. Russell
73 **Military textiles**
Edited by E. Wilusz
74 **3D fibrous assemblies: Properties, applications and modelling of three-dimensional textile structures**
J. L. Hu
75 **Medical textiles and biomaterials for healthcare**
Edited by S. C. Anand, J. F. Kennedy, M. Miraftab and S. Rajendran
76 **Fabric testing**
Edited by J. L. Hu
77 **Biologically inspired textiles**
Edited by A. Abbott and M. Ellison
78 **Friction in textile materials**
Edited by B. S. Gupta
79 **Textile advances in the automotive industry**
Edited by R. Shishoo
80 **Structure and mechanics of textile fibre assemblies**
Edited by P. Schwartz
81 **Engineering textiles: Integrating the design and manufacture of textile products**
Edited by Y. E. El-Mogahzy
82 **Polyolefin fibres: Industrial and medical applications**
Edited by S. C. O. Ugbolue
83 **Smart clothes and wearable technology**
Edited by J. McCann and D. Bryson
84 **Identification of textile fibres**
Edited by M. Houck
85 **Advanced textiles for wound care**
Edited by S. Rajendran
86 **Fatigue failure of textile fibres**
Edited by M. Miraftab
87 **Advances in carpet technology**
Edited by K. Goswami
88 **Handbook of textile fibre structure Volume 1 and Volume 2**
Edited by S. J. Eichhorn, J. W. S. Hearle, M. Jaffe and T. Kikutani
89 **Advances in knitting technology**
Edited by K.-F. Au
90 **Smart textile coatings and laminates**
Edited by W. C. Smith
91 **Handbook of tensile properties of textile and technical fibres**
Edited by A. R. Bunsell

92 **Interior textiles: Design and developments**
Edited by T. Rowe
93 **Textiles for cold weather apparel**
Edited by J. T. Williams
94 **Modelling and predicting textile behaviour**
Edited by X. Chen
95 **Textiles, polymers and composites for buildings**
Edited by G. Pohl
96 **Engineering apparel fabrics and garments**
J. Fan and L. Hunter
97 **Surface modification of textiles**
Edited by Q. Wei
98 **Sustainable textiles**
Edited by R. S. Blackburn
99 **Advances in yarn spinning technology**
Edited by C. A. Lawrence
100 **Handbook of medical textiles**
Edited by V. T. Bartels
101 **Technical textile yarns**
Edited by R. Alagirusamy and A. Das
102 **Applications of nonwovens in technical textiles**
Edited by R. A. Chapman
103 **Colour measurement: Principles, advances and industrial applications**
Edited by M. L. Gulrajani
104 **Fibrous and composite materials for civil engineering applications**
Edited by R. Fangueiro
105 **New product development in textiles: Innovation and production**
Edited by L. Horne
106 **Improving comfort in clothing**
Edited by G. Song
107 **Advances in textile biotechnology**
Edited by V. A. Nierstrasz and A. Cavaco-Paulo
108 **Textiles for hygiene and infection control**
Edited by B. McCarthy
109 **Nanofunctional textiles**
Edited by Y. Li
110 **Joining textiles: Principles and applications**
Edited by I. Jones and G. Stylios
111 **Soft computing in textile engineering**
Edited by A. Majumdar
112 **Textile design**
Edited by A. Briggs-Goode and K. Townsend
113 **Biotextiles as medical implants**
Edited by M. W. King, B. S. Gupta and R. Guidoin
114 **Textile thermal bioengineering**
Edited by Y. Li
115 **Woven textile structure**
B. K. Behera and P. K. Hari

116 **Handbook of textile and industrial dyeing. Volume 1: Principles, processes and types of dyes**
Edited by M. Clark
117 **Handbook of textile and industrial dyeing. Volume 2: Applications of dyes**
Edited by M. Clark
118 **Handbook of natural fibres. Volume 1: Types, properties and factors affecting breeding and cultivation**
Edited by R. Kozłowski
119 **Handbook of natural fibres. Volume 2: Processing and applications**
Edited by R. Kozłowski
120 **Functional textiles for improved performance, protection and health**
Edited by N. Pan and G. Sun
121 **Computer technology for textiles and apparel**
Edited by J. L. Hu
122 **Advances in military textiles and personal equipment**
Edited by E. Sparks
123 **Specialist yarn and fabric structures**
Edited by R. H. Gong
124 **Handbook of sustainable textile production**
M. I. Tobler-Rohr
125 **Woven textiles: Principles, developments and applications**
Edited by K. Gandhi
126 **Textiles and fashion: Materials design and technology**
Edited by R. Sinclair
127 **Industrial cutting of textile materials**
I. Viļumsone-Nemes
128 **Colour design: Theories and applications**
Edited by J. Best
129 **False twist textured yarns**
C. Atkinson
130 **Modelling, simulation and control of the dyeing process**
R. Shamey and X. Zhao
131 **Process control in textile manufacturing**
Edited by A. Majumdar, A. Das, R. Alagirusamy and V. K. Kothari
132 **Understanding and improving the durability of textiles**
Edited by P. A. Annis
133 **Smart textiles for protection**
Edited by R. A. Chapman
134 **Functional nanofibers and applications**
Edited by Q. Wei
135 **The global textile and clothing industry: Technological advances and future challenges**
Edited by R. Shishoo
136 **Simulation in textile technology: Theory and applications**
Edited by D. Veit
137 **Pattern cutting for clothing using CAD: How to use Lectra Modaris pattern cutting software**
M. Stott

138 **Advances in the dyeing and finishing of technical textiles**
M. L. Gulrajani
139 **Multidisciplinary know-how for smart textiles developers**
Edited by T. Kirstein
140 **Handbook of fire resistant textiles**
Edited by F. Selcen Kilinc
141 **Handbook of footwear design and manufacture**
Edited by A. Luximon
142 **Textile-led design for the active ageing population**
Edited by J. McCann and D. Bryson
143 **Optimizing decision making in the apparel supply chain using artificial intelligence (AI): From production to retail**
Edited by W. K. Wong, Z. X. Guo and S. Y. S. Leung
144 **Mechanisms of flat weaving technology**
V. V. Choogin, P. Bandara and E. V. Chepelyuk
145 **Innovative jacquard textile design using digital technologies**
F. Ng and J. Zhou
146 **Advances in shape memory polymers**
J. L. Hu
147 **Design of clothing manufacturing processes: A systematic approach to planning, scheduling and control**
J. Gersak
148 **Anthropometry, apparel sizing and design**
D. Gupta and N. Zakaria
149 **Silk: Processing, properties and applications**
Edited by K. Murugesh Babu
150 **Advances in filament yarn spinning of textiles and polymers**
Edited by D. Zhang
151 **Designing apparel for consumers: The impact of body shape and size**
Edited by M.-E. Faust and S. Carrier
152 **Fashion supply chain management using radio frequency identification (RFID) technologies**
Edited by W. K. Wong and Z. X. Guo
153 **High performance textiles and their applications**
Edited by C. A. Lawrence
154 **Protective clothing: Managing thermal stress**
Edited by F. Wang and C. Gao
155 **Composite nonwoven materials**
Edited by D. Das and B. Pourdeyhimi
156 **Functional finishes for textiles: Improving comfort, performance and protection**
Edited by R. Paul
157 **Assessing the environmental impact of textiles and the clothing supply chain**
S. S. Muthu
158 **Braiding technology for textiles**
Y. Kyosev
159 **Principles of colour appearance and measurement. Volume 1: Object appearance, colour perception and instrumental measurement**
A. K. R. Choudhury

160 **Principles of colour appearance and measurement Volume 2: Visual measurement of colour, colour comparison and management**
A. K. R. Choudhury
161 **Ink jet textile printing**
C. Cie
162 **Textiles for sportswear**
Edited by R. Shishoo
163 **Advances in silk science and technology**
Edited by A. Basu
164 **Denim: Manufacture, finishing and applications**
Edited by R. Paul
165 **Fabric structures in architecture**
Edited by J. Ignasi de Llorens
166 **Electronic textiles: Smart fabrics and wearable technology**
Edited by T. Dias
167 **Advances in 3D textiles**
Edited by X. Chen
168 **Garment manufacturing technology**
Edited by R. Nayak and R. Padhye
169 **Handbook of technical textiles Second edition Volume 1: Technical textile processes**
Edited by A. R. Horrocks and S. C. Anand
170 **Handbook of technical textiles Second edition Volume 2: Technical applications**
Edited by A. R. Horrocks and S. C. Anand
171 **Sustainable apparel**
Edited by R. S. Blackburn
172 **Handbook of life cycle assessment (LCA) of textiles and clothing**
Edited by S. S. Muthu
173 **Advances in smart medical textiles: Treatments and health monitoring**
Edited by L. van Langenhove
174 **Medical textile materials**
Y. Qin
175 **Geotextiles**
Edited by R. M. Koerner
176 **Active coatings for smart textiles**
Edited by J. L. Hu
177 **Advances in braiding technology: Specialized techniques and applications**
Edited by Y. Kyosev
178 **Smart textiles and their applications**
Edited by V. Koncar
179 **Information systems for the fashion and apparel industry**
Edited by T. M. J. Choi
180 **Antimicrobial textiles**
G. Y. Sun
181 **Advances in technical nonwovens**
G. Kellie
182 **Advances in women's intimate apparel technology**
W. Yu
183 **Clothing for children and teenagers: Anthropometry, sizing and fit**
N. Zakaria

184 **Woven terry fabrics: Manufacturing & quality management**
J. P. Singh and S. K.Verma
185 **Performance testing of textiles: Methods, technology and applications**
Edited by L. Wang
186 **Electrospun nanofibers**
Edited by M. Afshari
187 **Structure and properties of high-performance fibers**
Edited by G. Bhat
188 **Thermal protective clothing for firefighters**
Edited by G. Song
189 **Activated carbon fiber and textiles**
Edited by J. Chen

Introduction to high-performance fibers

1

G. Bhat
The University of Georgia, Athens, Georgia, United States

There is continuing interest in technical textiles around the world, and this is one of the fastest growing sectors of the manufacturing industry. Many of these products use specialty fibers and the search for new and improved fibers is continuing. As a result, we need to look at the developments in high-performance fibers from time to time. It is only once in a while that new revolutionary fibers are introduced and most of the time there are incremental changes in properties and performance of specialty fibers. The field of high-performance fibers is continuously evolving, thanks to the efforts of many scientists and engineers in universities, research centers, and industries. These continuous developments allow the fabrication of products with specific property and performance requirements. In majority of the cases it is the performance requirements that drive the innovation and development, although at times discoveries in arenas other than fibers and textiles are adapted to development of high-performance fibers. While traditionally most of the developments were done by fiber-related researchers, recently more and more inventions are coming from nontraditional investigators. Such discoveries have certainly benefited the fiber industry. This book is an effort to capture the developments in the past several years on high-performance fibers.

Although most of the fibers could be used in high-performance applications in some context, there are several fibers that are exclusively developed with unique structure and properties, making them unsuitable for apparels or other typical consumer applications. At the same time, some of the common textile grade fibers have been modified to achieve additional functionality over what is expected in everyday apparel fabrics. One has to remember that the expectations of the apparels have been changing and by the combination of different materials and processing techniques, several high-performance and intelligent fabrics have been introduced lately. In fact, this trend of developing functional and intelligent textiles is rapidly growing with interest from a wide range of industries.

The perception of high performance with respect to fibers has also been changing, and it is not possible to clearly distinguish what fibers are suitable for this category. In the early developments, fibers that met the requirements in industrial applications other than apparel or home textiles, which had either higher strength/modulus or thermal stability or chemical or flame resistance, were considered high-performance fibers. Recently, there are also several smart or intelligent fibers that have been gaining a lot of attention. These smart fibers, although many have mechanical properties comparable to that of typical textile fibers, could have the ability to respond to environmental

Structure and Properties of High-Performance Fibers. http://dx.doi.org/10.1016/B978-0-08-100550-7.00001-2

conditions such as thermal, electrical, magnetic, or mechanical, or to other sources. In fact, there is increasing effort to incorporate them into textiles and recently a huge consortium has been funded from the US Department of Defense in partnership with several industries, states, and universities to bring revolutionary, smart, functional fibers from research laboratories to the manufacturing level and further incorporate them into fabrics. Of course, this exercise will possibly lead to a revolution in the high-performance fibers area as well. Whereas smart technology is likely to be important in future fabrics, such fibers are not included here as they are beyond the scope of this book.

The book has 14 chapters covering a wide range of fibers from inorganic to synthetic aliphatic, aromatic, cyclic polymeric, and natural fibers. The chapters two to four cover various carbon- and carbon nanotube (CNT)-based fibers. The second chapter reviews the important polyacrylonite (PAN)-based carbon fibers that are the most important and fastest growing categories in high-performance fibers. In addition to the overall review of the process of converting PAN precursor into carbon fibers, structure and property development during carbon fiber formation is thoroughly discussed. With increasing demand for low-cost carbon fibers, reducing the cost of precursors as well as the conversion cost is important so that an increase in the application of carbon fibers in automotives becomes a reality. The third chapter, which is on pitch-based carbon fibers, has a thorough discussion of different pitches, extrusion of pitch into fibers, and conversion of pitch into carbon fibers. There is an in-depth coverage of development of structure and relationship of structure to properties in these carbon fibers. Ever since the discovery of CNTs there has been increasing interest in them because of their extremely high strength, modulus, and electrical properties. Synthesis, structure, and properties of CNTs as well as CNT-reinforced fibers are reviewed in the fourth chapter. This chapter also covers the latest development in CNT-reinforced polymeric as well as carbon fibers and CNT yarns. Although CNTs have superior properties, the challenges to realize the properties in yarns and composite fibers have not been overcome. There is continuing effort to improve the structure and properties of CNT-incorporated fibers and yarns.

There are eight different chapters covering various synthetic organic fibers, which include chapters on fibers from polyester, rigid-rod polymers, polyethylene and propylene, nylon, polyaramids, electrospun nanofibers, and polyimides. Chapter five on aromatic polyester fibers includes the historical development, chemical structure, processing, and fiber structure and properties. These melt-spun fibers were developed as an alternate to polyaramids, which are expensive. In addition to high strength and modulus, these liquid crystalline polyester fibers show excellent flex resistance, which is desirable in many applications. Chapter six on rigid rod polymer fibers encompasses their aromatic and cyclic structures and includes poly *p*-phenylene benzobisoxazole and poly *p*-phenylene polybenzobisthiazole. Detailed discussion of polymerization, processing, structure, and properties is provided. Also approaches to improve the UV stability and other properties are addressed.

Gel-spun polyethylene fibers have the highest specific strength of any continuous fibers and the historic development of these fibers is discussed in detail in the seventh chapter. The major focus of this chapter is on the structure of these highly ordered and

oriented ultrahigh molecular weight polyethylene fibers that is responsible for their unique properties. It is shown that there may be room for further improvement in the properties of these fibers by process optimization. Chapter eight on polypropylene fibers discusses how the combination of higher molecular weight polymer with process conditions such as high-temperature drawing can lead to high-tenacity fibers. Although high-strength, high-modulus polypropylene fibers do not have high thermal stability or properties comparable to that of other high-performance fibers such as Kevlar or high-strength, high-modulus polyethylene fibers, these have properties that meet the requirements for many demanding applications, and the cost of these fibers will be a lot lower than that of other high-performance organic fibers.

Chapter nine on nylon fibers covers recent developments in spinning and postspinning treatments to produce high-performance fibers. These techniques influence the microstructure resulting in improved tensile, thermal, and chemical properties. Approaches that help to produce high-performance nylon fibers, by appropriately modifying the structure of these fibers by spinning process modification as well as postspinning operations, is elucidated. Chapter 10 on polyaramids addresses both Kevlar and Nomex-type fibers including their polymerization, fiber spinning, structure development during synthesis, and processing leading to superior properties. Recent advances in understanding their structure as well as surface modification to improve properties of composites are also of interest.

Electrospinning of nanofibers has been extensively studied and the recent developments are summarized in Chapter 11. In addition to the traditional needle electrospinning, other approaches such as needleless spinning are elaborated. Achieving various structures including controlled architecture of three-dimensional webs is discussed very well. Recent developments include forming nanofiber yarns and the ability to produce a wide range of patterns. The use of electrospun nanofibers in emerging applications such as batteries, super capacitors, solar cells, and piezoelectric devices is elaborated. Electrospinning can be used to produce nanofibers from a wide range of polymers that have a suitable solvent. High-performance polyimide fibers are discussed in Chapter 12, which covers different approaches to produce polyimide fibers and various types of polyimides. Special emphasis is given to polymer synthesis, fiber formation, imidization, and the microstructure of the fibers.

Chapters 13 and 14 are dedicated to two natural protein fibers, silk and wool. Both have been in use for a long time. Whereas silk fibers produced from silkworms have been used for thousands of years because of their unique luster, tactile properties, durability, and dyeability, lately there has been interest in high-strength, high-modulus silk fibers. Silk fibers obtained from various types of spiders have been evaluated and some of them have shown extremely high strength, modulus, elasticity, and toughness. The chemical composition and structural features that lead to improved mechanical properties as well as various types of silk worms and spiders available around the world are thoroughly discussed. Also all aspects of the sericulture industry are covered in detail. Wool, another natural fiber that has been used for many years, has unique properties and this fiber has been studied extensively to understand its structure so that synthetic fibers of comparable properties can be produced. Wool fibers have good thermal and acoustical insulation properties and have also been demonstrated to be efficient in filter

media and some medical applications. Ballistic fibers such as Kevlar have shown improved performance when blended with wool fibers. Lately, wool fibers have been used in some composite applications as well. In addition, both silk and wool are sustainable fibers.

This book has been made possible because of the contributions from a team of internationally recognized experts in their respective fields. These authors have put in a great deal of time and effort to make this possible. I am thankful to all the contributing authors for making this happen. I also extend my thanks to Ms. Sarah Lynch, Ms. Christina Cameron, Ms. Charlotte Cockle, and Mr. Edward Payne from Elsevier for their support and patiently working with us throughout the process. This book has a wealth of useful information, and it is my sincere hope that readers from academia, industry, and research institutes working in the areas related to fibers as well as others interested in high-performance fibers will immensely benefit from reading this book.

High-performance PAN-based carbon fibers and their performance requirements

2

E. Frank [1], D. Ingildeev [1], M.R. Buchmeiser [1,2]
[1]Institute of Textile Chemistry and Chemical Fibers (ITCF Denkendorf), Denkendorf, Germany; [2]Institute of Polymer Chemistry, University of Stuttgart, Stuttgart, Germany

Carbon fibers (CFs) have high tensile strengths up to 7 GPa with very good creep resistance, low densities (1.75−1.95 g/cm^3), and high moduli (200−600 GPa).[1] They lack resistance to oxidizing agents as hot air and flames, but they are resistant to all other chemical species. The good mechanical properties make CFs attractive for use in composites in the form of woven textiles as well as continuous or chopped fibers. Such composite parts can be produced through filament winding, tape winding, pultrusion, compression molding, vacuum bagging, liquid molding, and injection molding. The CF industry has been growing continuously with a focus on aerospace, military, and construction as well as medical and sporting goods.[1−4] For the automotive industry, CF-reinforced polymeric composites allow for a significant reduction in weight, which is a prerequisite for battery-driven cars.[2]

Over 98% of CFs are made from polyacrylonitrile (PAN) as precursor. Other CF precursor types are described elsewhere.[3,4] Global CF consumption and the major CF manufacturers of PAN-based CFs are summarized in Table 2.1 with their estimated capacities sorted by actual suppliers.[5] Besides the continuous growth of CF production in the last few years, the large-volume application of CF in the automotive industry has been impeded by high fiber costs and the lack of high-speed composite fabrication techniques. However, current investigations and future developments might well change the market to establish CFs as a mass product like other synthetic fibers or metals.

CFs were classified to the number of filaments, where "1K" means 1000 single filaments. In technical terms, CFs with 1−24K are called "low tow" and 24−320K and more filaments are called "large tow." A second classification describes the mechanical properties. According to a combination of tenacity and modulus of the CFs, a classification as seen in Table 2.2 is used.

Starting from a given material, a multifilament fiber is spun with typical 1000 (1K) to 320,000 (320K) filaments. This ready-spun fiber is defined as a "precursor" fiber for a CF. The precursor fiber is oxidized in air at temperatures between 200 and 300°C, strongly depending on the basic chemistry of the precursor. At temperatures up to 1600°C the oxidized precursor will be carbonized by removing hydrogen, oxygen, nitrogen, and other noncarbon elements. A process in which higher temperatures up to

Structure and Properties of High-Performance Fibers. http://dx.doi.org/10.1016/B978-0-08-100550-7.00002-4

Table 2.1 Estimated name plate CF capacity in 2015 in tons[5]

Supplier	Low tow (1–24K)	Large tow (24–320K)
Toray Industries (including Zoltek capacities), Japan	26,800	20,300
Toho Tenax (Teijin), Japan	11,500	–
Mitsubishi Rayon, Japan	10,800	2700
Mainland China	16,490	–
Hexcel, USA	9800	–
Formosa Plastics, Taiwan	8750	–
Cytec Engineered Materials, USA	2500	–
SGL Carbon Group, Germany	–	15,000
Holding Company Composite, Russia	3000	–
Kemrock, India	2500	–
Hyosung, Republic of Korea	6500	–
Taekwang Industrial, Republic of Korea	1500	–
RT-Chemcomposite (Rostec), Russia	200	–

Table 2.2 Classification of CFs[6]

Type of PAN-based CF	Tensile strength (MPa)	Tensile elastic modulus (GPa)
Low elastic modulus type	>3500	<200
Standard elastic modulus type	>2500	200–280
Intermediate elastic modulus type	>3500	280–350
High elastic modulus type	>2500	350–600
Ultrahigh elastic modulus type	>2500	>600

3000°C are used is called graphitization. Such graphitization yields CFs with moduli higher than those of carbonized fibers. The properties of the resulting carbon/graphite fibers are limited by many factors such as crystallinity, molecular orientation, and the amount of defects. The relatively inert surfaces of the carbon/graphite fibers are usually posttreated, that is, functionalized by electrochemical methods to improve their adhesion to composite matrices.

2.1 Synthesis of high-performance PAN-based CFs

2.1.1 Polymerization

PAN was first recognized as a suitable precursor material for CFs by Shindo in 1961.[7] It is currently the most important starting materials for the preparation of CFs. The polymerization of acrylonitrile (AN) is of crucial importance particularly since further steps in CF production, such as precursor fiber spinning, stabilization, and carbonization as well as the resulting CF properties, strongly depend on the characteristics of the polymer used.[8] AN can be polymerized in bulk, in suspension, in solution, and in emulsion applying free radical, ionic, or atom transfer radical polymerization.[8–38] Solution polymerization and suspension polymerization are currently the most widely used procedures for the preparation of PAN-based copolymers for CF production. In terms of continuous process control, solution polymerization of AN and related monomers is probably more satisfactory.[8,13,23–34,36,37,39] Solution polymerization can be carried out with solvents such as dimethylacetamide (DMAc), dimethylformamide (DMF), dimethylsulfoxide (DMSO), or aqueous sodium thiocyanate solutions and thus allows immediate manufacturing of spinning dopes.[8,9,40] Since the produced copolymers have high molecular weight, the polymerization reaction is usually carried out in rather low concentrated solutions. Two important drawbacks limit the application of this polymerization procedure. The conversion of the monomer to polymer reaches 50–70%, so the resulting solutions may be processed only after complete recovery of the unreacted AN from the spinning dope; however, usually it still contains 0.2–0.3 wt% of this toxic and carcinogenic monomer.[9] Another important drawback is that conventional solvent systems used for the polymerization process usually have high transfer constants. Thus the process of suspension polymerization of AN has the advantage that almost no by-products are produced and that it can be carried out at controlled conditions, so that both branching and crosslinking are avoided.[9–22] Further advantages of the reaction include the simple removal of the polymer by filtration and drying, adjustment of the molecular weights over a very wide range, and control of particle size. Particularly on a large scale, this discontinuous process permits good control over the exothermic nature of the polymerization, allowing up to 90% polymer yield.

Persulfate salts, especially potassium persulfate, ammonium persulfate, sodium metabisulfite, and iron (III) salts form the most important group of initiators are used for polymerization. Today, special attention focuses on reducing the defects of the CFs generated by the residues of the initiator system. Efforts involve but are not limited to the application of modified initiator systems disclosing/replacing conventional alkali metals and reducing traces of transition metals such as iron so that impurities at all steps of the CF production chain can be avoided (Scheme 2.1).[41]

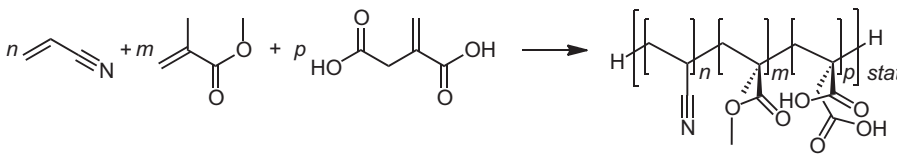

Scheme 2.1 Synthesis of a typical terpolymer consisting of acrylonitrile, methyl methacrylate, and itaconic acid.

Typically, PAN-based copolymers used for the preparation of CF have molecular weights in the range of 70,000−260,000 g/mol and a polydispersity index (PDI) of 1.5−3.5,[8,42] but with modern polymerization methods such as RAFT (reversible addition-fragmentation chain transfer) a much smaller value for the PDI of 1.34 could be achieved.[43]

The mechanical properties of CFs obtained using textile PAN with a specific comonomer content of more than 5 mol% are very limited by nonoptimized chemistry, cyclization behavior, and purity. Usually, PAN-based precursors contain a minimum of 95 mol% of AN and a maximum of 5 mol% comonomers.[41,44] These comonomers have a large impact on polymer processing as well as on the kinetics and physics of stabilization and carbonization (see later); consequently, polymer composition moved into the center of interest.[8,44,45] It is common practice for companies to produce PAN-based precursor materials by using polymerization mixtures of AN with more than one comonomer, for example, with methyl acrylate and itaconic acid. For these purposes, all monomers must have similar reactivity, that is, copolymerization parameters. Only in that case the composition of the terpolymer in terms of molar ratios at a given time will be the same as the composition of the reaction mixture with a homogeneous distribution of comonomers along the molecular chain.[8] Though the open literature provides a good base for the selection of the monomers and for precursor polymer composition,[45−81] the identification of the optimum composition of the precursor polymer (and of the processing parameters, see later) for the achievement of certain properties is still a challenging task.[82−86] In other words, to obtain high-performance fibers in terms of tensile strength and modulus, *all* process parameters including copolymer composition, molecular weights, molecular weight distribution as well as spinning, drawing, stabilization, and carbonization parameters must be taken into account. Unfortunately, a stringent and widely applicable model that allows for correlating fiber properties with process and polymer parameters is still missing. In fact, despite the tremendous progress in that field, even the correlation between CF structure and CF properties is not fully developed. In addition, an idea how polymer structure, orientation, and crystallinity transformed into the final carbonaceous structure needs to be developed.

2.1.2 Preparation of CF precursors

PAN-based polymers undergo thermally induced cyclization reactions below their melting point and can therefore not be processed in melt with conventional spinning techniques. This makes the melt spinning of pure PAN impossible unless large amounts of solvent additives and plasticizers are added. In such a melt-assisted spinning process, additives are used to reduce the interaction between PAN molecules by decoupling nitrile−nitrile association. This way the melting point of plasticized PAN is reduced to an appropriate range for melt spinning.[87−89] However, until today, no melt-spinning process has reached the CF qualities of wet-spun PAN-based precursor fibers. This is why wet spinning is still the preferred method for CF precursor manufacturing.

The choice of solvents for PAN-based copolymers is of utmost importance in the production of precursor fibers using wet-spinning processes. As already mentioned,

the highly polar nitrile groups of AN experience a strong dipole−dipole interaction, making the polymer soluble only in highly polar solvents such as DMAc, DMF, DMSO, zinc chloride, and sodium thiocyanate,[8,40] but also in ionic liquids.[90] Schildknecht listed a variety of solvent systems in which PAN is soluble.[34]

Conventional wet spinning entails extrusion of the copolymer solution into a coagulation bath where jets of the spinning dope leaving the spinneret come into contact with substances miscible with the solvent but which do not dissolve the polymer. In wet spinning, the solution concentration of 15−25 wt% $\left(10 \leq \left|\eta_0^*\right| \leq 200\text{Pa}\cdot\text{s}\right)$ strongly depends on the polymer properties such as comonomer content, molecular weight, and PDI and is adjusted to obtain a viscoelastic behavior of the polymer solution that is optimal for spinning at pressure values of 5−20 bar. Polymer solutions are spun through a spinneret with a multiplicity of holes, a total of 100−500,000 each having a diameter in the range of 40−100 μm. The line speeds at the coagulation step of the wet spinning are rarely barely than 20 m/min.[8]

There are many possible technical designs for wet-spinning processes. The precipitation bath can be situated horizontally or vertically, and different baths for washing and drawing can be applied, followed by further manufacturing operations such as application of lubricants, drying, or heat setting. The most important issue is to obtain fibers having optimum morphological structure, which is very sensitive to the composition and conditions within the coagulation bath. Thus the coagulation bath is not stationary but circulates with a finite velocity. The flow pattern in the bath is rather complex; the streamlines are usually not parallel to the axis of the spinning line, which creates unequal flow and solidification conditions for the individual filaments. Modern systems used for wet spinning often involve directed flow of the spinning bath. The aim of this modification is to make the flow pattern in the bath symmetrical and equalize the conditions experienced by the individual filaments, to promote homogeneous penetration of the nonsolvent into the bundle of filaments.

The other fundamental method of wet spinning—dry jet or air gap spinning—is a variation of wet spinning and can be applied to highly viscous spinning dopes with polymer contents up to 30 wt% and zero-shear viscosities in the range between 300 and 20,000 Pa·s (Fig. 2.1).[91] This procedure entails the extrusion of spinning dopes into an air gap of 10−200 mm where the filaments undergo jet stretch, which produces a high degree of molecular orientation, before entering a liquid coagulation bath. Further processing stages correspond to those of conventional wet spinning. This process allows the spinning dope and coagulation bath to be at different temperatures and therefore high diffusion rates can be avoided during the phase inversion process in the coagulation bath. The process is limited by the number of holes in the spinneret and usually cannot be used for tows larger than 12K.

Solidification and coagulation of a polymer solution in fiber formation is specific for the chosen spinning procedure. In jet spinning it is because of dry stretching of the filaments in an air gap, accompanied by heat dissipation transfer, followed by solvent extraction in a precipitation bath; in wet spinning the solvent is directly extracted from the polymer solution into the coagulation bath, and diffusion-controlled phase transitions play a determining role.

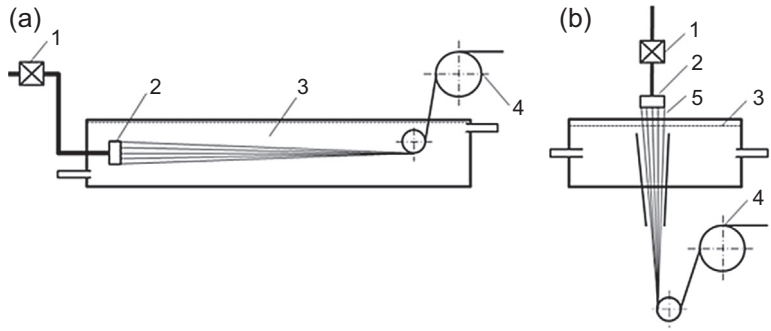

Figure 2.1 Schemes of (a) wet and (b) dry jet spinning techniques. 1, metering pump; 2, spinneret; 3, coagulation bath; 4, take-up godet; 5, air gap.

The present state of the theory of wet spinning does not enable the formulation of fundamental equations describing the process in quantitative terms. There is still some uncertainty about the deformation of a nonuniform system provided by the partially solidified spinning line, and the mechanism of mass transfer is affected by the temperature and concentration fields in the spinning dope as well as in the coagulation bath. Phase equilibria and the kinetics of phase separation are ambiguous while undoubtedly playing a decisive role in the formation of fiber structure and physical properties. The chemical structure of polymer, solvent, and nonsolvent affects both phase diagram and transport rates. Additionally, dynamics of the coagulation process are influenced by external tension, surface tension, mass exchange, and rheological effects, respectively. The only phase equilibrium data available are the so-called "coagulation values," that is, volumes of nonsolvent required for turbidimetric titration of a standard, dilute polymer solution.[62] Being specific for different comonomer systems the information about phase equilibria at higher polymer contents involved in fiber spinning is still lacking.

Very important, controllable factors in wet spinning are the temperature and the concentration gradients in the spinning bath and dope, controlling to a great extent the kinetics of mass transfer. Generally, an increase in solvent content and decrease in temperature in the bath reduce the driving force for diffusion and consequently the fluxes of solvent out of the filaments and nonsolvent directed inwards. Furthermore, the cross-sectional shape of the filaments relates to the diffusion rate of the liquids of the coagulation bath into the filaments and the transfer of the polymer solvent to the coagulation bath (Fig. 2.2).[8,40,92,93]

High coagulation rates in the spinning bath are usually accompanied by formation of a rigid "skin" on the surface of the filaments. The skin is separated by a distinct boundary from the fluid "core" and the resulting radial gradients of viscosity, modulus, etc., are extremely high. Further, diffusion-controlled solidification of the filaments rather involves the growth of the skin layer at the expense of the core, than a continuous change in the physical characteristics at all points of the cross-section. High coagulation rates usually promote the formation of an undesirable rigid skin of the precursor fiber leading to the collapse of the cross-section and therefore to noncircular, kidney-shaped fibers.[8,40,42,94] Deviation from circularity associated with solidification

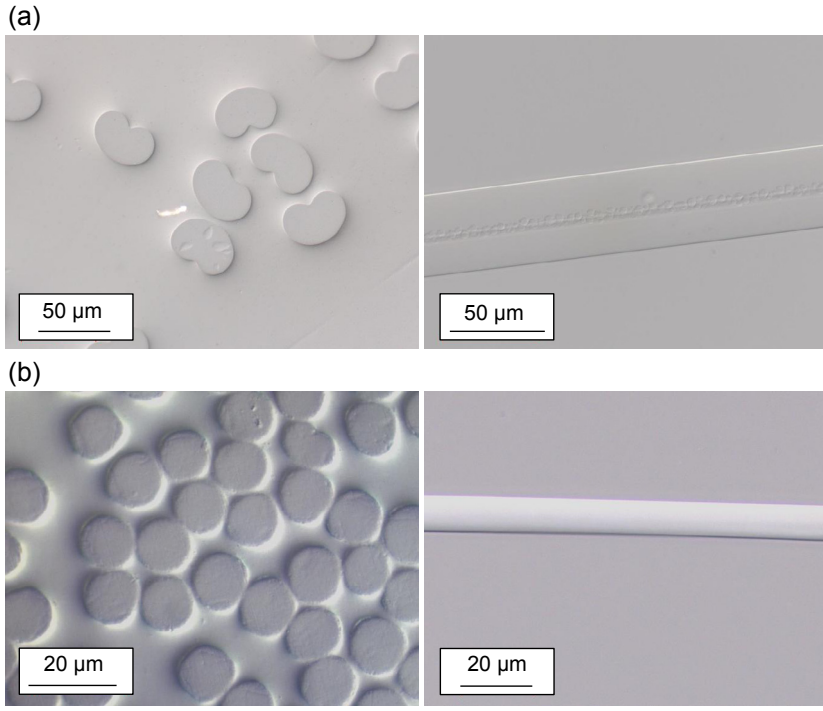

Figure 2.2 Effect of spinning conditions on the morphology of wet-spun undrawn acrylic fibers. (a) Effect of high coagulation rate on the cross-section and fiber structure. (b) Effect of low coagulation rate on the cross-section and fiber structure.

conditions affects luster, sorptional, mechanical, and physical properties as well as the subsequent oxidation and carbonization steps. The formation of dense precursor fibers with preferred circular cross-sections is obtained by low diffusion rates applying wet spinning to highly concentrated spinning dopes at elevated temperatures, with high solvent contents in the spinning bath[95–98] and low spinning bath temperatures.[95,97,99] As noted, noncircular cross-sections, usually corresponding to higher flux ratios of solvent outwards of the thread, are affected by rigidity of the solid layer as well as by osmotic pressures. Additionally, rapidly acting coagulation baths promote the formation of voids and capillaries with dimensions up to several microns leading to poor mechanical properties of the resultant CFs.

Further important structural characteristics of the resultant precursor fibers concern the formation of the supramolecular structure, that is, degree of crystallinity, crystallite orientation, crystallite size, etc., after the coagulation bath. These characteristics, being very sensitive to spinning conditions, strongly affect the behavior in drawing and in further processing operations and mechanical properties of both the precursor and the final CFs.

Once the fiber has been spun, the subsequent processing steps are basically similar, irrespective of the initial spinning technique, although handling procedures depend very much on polymer composition. Further processing steps of wet spinning include washing, drawing, finish application drying, relaxation process, and, finally,

collection. To remove excess solvent in the fibers and to increase the molecular orientation of the molecular chains, the coagulated fiber bundle is washed with hot water and/or water steam in conjunction with fiber drawing. Fibers can be drawn at elevated temperature, typically at 120−180°C, for example, by using ethylene or glycerol as a drawing medium.[42,52,100−105] A further increase in tensile properties is observed as the orientation increases through the high-temperature drawing process. Before drying, a finish is usually applied as an aqueous emulsion to act as a lubricant and antistatic. Typical finishes include sorbitan esters of long chain fatty acids, polyoxyethylene derivatives and modified polysiloxanes.[106,107] Drying and relaxation processes are necessary to remove water and to reduce the tension in the supramolecular structure of the precursor fiber after drawing. The resultant wet-spun precursor fiber tows have a relatively fine count of approximately 1.2 dtex. Large tows, above 40K, are plaited into cardboard packages using a controlled longitudinal placement, which permits the easy unloading of the tow for further processing. Lower filament counts, such as 3 and 12K, can be wound directly on a spool using precision winders.

2.1.3 Heat treatment of CF precursors

Generally, heat treatment of PAN-based fibers entails three steps, that is, oxidation, carbonization, and graphitization. The precursor fiber is first oxidized within a temperature range between 200 and 300°C, which results in the formation of an N-containing ladder-type polymer. This allows further processing at higher temperatures. After oxidation, the fibers are carbonized at temperatures up to 1200−1600°C in an inert atmosphere to obtain a turbostratic carbon structure. Then, to improve the ordering and orientation of the basal planes in the direction of the fiber axis, the fiber can be graphitized by up to 3000°C depending upon the required tensile modulus of the resultant CF. This entire procedure shall be outlined in more detail (Scheme 2.2).

2.1.3.1 Oxidization of PAN-based precursors

The basic principle used in the conversion of PAN-based precursor fibers into CFs is the treatment of the fibers in an oxidizing atmosphere at temperatures in the range between 200 and 300°C. Generally, the thermal treatment, that is, oxidation reaction of the homopolymer PAN, is a very difficult reaction to control. Because of a high conversion temperature in the oxidation step, coupled with highly exothermic reaction kinetics, the rapid evolution of heat can cause defects inside the fiber and on the surface of the filaments, particularly in larger fiber tows. However, the exothermic reaction can be influenced by suitable comonomer composition, whose presence has a significant effect on the oxidation process.[45] The functional groups present in the copolymer can cause side reactions, which depend on the nature of comonomers, the comonomer content, the comonomer distribution, the supramolecular structure of the precursor fiber, the by-products, and on any traces of chemical compounds, which may have been introduced during both polymerization and spinning, as well as on the heat treatment (Fig. 2.3).

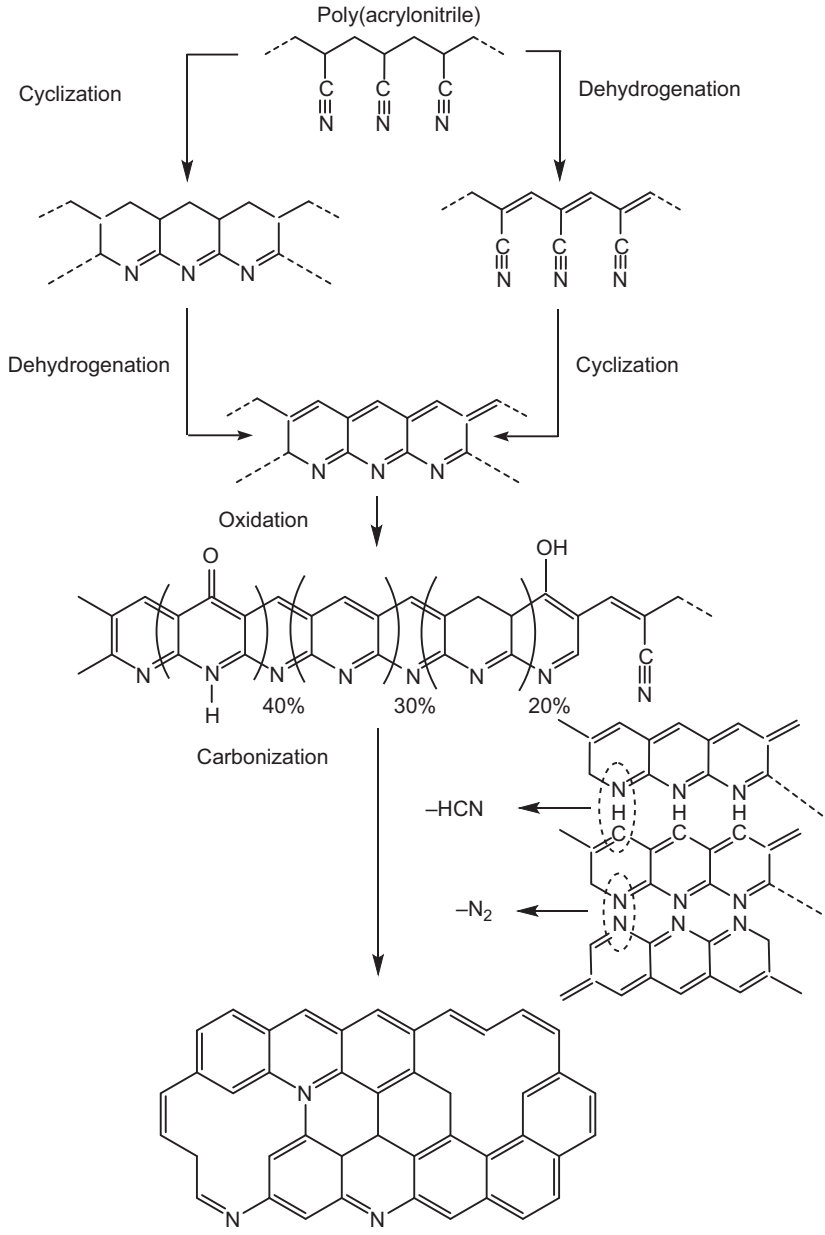

Scheme 2.2 Model reaction paths from PAN to a carbon phase.[41,108]

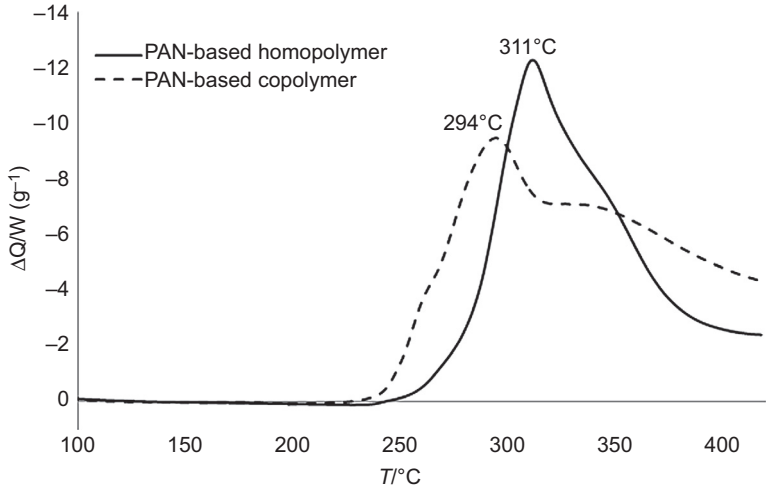

Figure 2.3 Differential scanning calorimetry of PAN-based homo- and terpolymer (acrylonitrile, methyl methacrylate, and itaconic acid) in air applying heating rate of 10K/min.

The oxidation process is accomplished by passing the fibers through an oven, which has a series of different air-heated zones gradually increasing in temperature. A significant increase in line speed can be realized by providing additional heating zones. Strict control of the exothermic reaction in the oven is achieved by maintaining a uniform temperature distribution within the oven and the single filaments thereby avoiding any overheating. The optimum air flow heats the fiber, provides oxygen for the reaction, and removes exhaust components and excess reaction heat from the fibers. Furthermore, the procedure is carried out under tension or even by applying drawing to prevent shrinkage of the filaments.[8,44] In the oxidation stage, the PAN-based fiber increases in density from 1.18 to 1.36−1.38 g/cm^3, the oxidized fibers then contain 62−70 wt% carbon, 20−24 wt% nitrogen, 5−10 wt% oxygen, and 2−4 wt% hydrogen.[13]

During the oxidation process, the polymer chains are converted into a heteroaromatic structure, similar in some aspects to the later carbon phase. Different models have been proposed for the cyclization of PAN molecules and the mechanism of formation of the ladder structure is a very complex cascade of chemical reactions, which has been investigated intensively in the last decades.[100,109−125] However, the different reactions depend heavily on the nature of the copolymers. These copolymers participate in the initial cyclization reaction and considerably influence the rate of the cyclization process. Thus the onset temperature in the presence of carboxylic acids is significantly lowered in comparison to PAN-based homopolymers.

The difference in oxidation behavior of PAN-based homo- and copolymers, as shown by differential scanning calorimetry measurements, is that the cyclization reaction of the copolymer is initiated by stabilization accelerators formed via the degradation in the copolymer compound, while the cyclization of the homopolymer is initiated

by radicals. Both reactions occur at elevated temperatures and result in a thermally stable cyclized structure. The chemical composition of the resultant ladder polymer, however, strongly depends upon the atmosphere in which the heat treatment is carried out. The rate of cyclization in oxidizing atmosphere is faster and the final CF is produced in higher yields with improved mechanical properties. As mentioned earlier, comonomers such as methyl acrylate facilitate the subsequent drawing of the fiber during the oxidation treatment. Heat treatment of PAN-based precursors under tension in an oxidizing atmosphere at temperatures over 200°C causes initiation of several thermally activated processes, involving considerable reorganization of the polymer chains and crosslinking of the molecular chains by oxygen bonds.[126,127] These interactions preserve the oriented supramolecular structure even after tension release for the following processing steps. The optimum uptake of oxygen during oxidation treatment is in the range of 8−10%.[128,129]

Alternative stabilization methods like plasma treatment,[130] electron beam-assisted cyclization,[131] or microwave-assisted processing[132] are under investigation to reduce both stabilization times and energy consumption.

2.1.3.2 Carbonization and graphitization of PAN-based precursors

In the next step of the process, the stabilized precursor fiber tows, which are capable of withstanding high temperatures, are subjected to thermal pyrolysis in an inert atmosphere and are thereby converted into CFs. The volatile compounds are removed to give CFs with a carbon yield of about 50 wt% with respect to the original precursor. At this stage, these CFs contain >98 wt% carbon, 1−2 wt% nitrogen, and 0.5 wt% hydrogen.[13]

During the early stages of the carbonization process, the rate of heating is generally low so that the evolution of the gaseous decomposition compounds does not damage the fiber. In the temperature range between 400 and 500°C, the hydroxyl groups present in the oxidized PAN fibers undergo crosslinking condensation reactions resulting in reorganization and coalescence of the cyclized sections. Goodhew et al. have found the cyclized structures undergo dehydrogenation reaction and produce a graphite-like structure bound by nitrogen atoms.[114] Intermolecular dehydrogenation occurs between 400°C and 600°C, followed by denitrogenation and formation of plain graphite layers at higher temperatures. The effect of nitrogen on the structure and properties of PAN-based fibers has been elucidated by Tsai.[133] Extended heating rates during carbonization introduce defects in the CFs, while low carbonization rates result in the loss of large amounts of nitrogen at early stages of the carbonization process, which is in fact preferred to achieve high tensile strength CFs. Most of the volatile products are evolved in the temperature range between 200 and 1000°C.[134] The evolved gases include HCN, H_2O, O_2, H_2, CO, NH_3, CH_4, high molecular weight compounds, miscellaneous tars, and finish.[8,119,120,122,135,136] As already mentioned, the ribbon polymer structure forms crosslinks in the low temperature range, and subsequently additional condensation reactions follow up to 1600°C, forming a turbostratic carbon phase.[41,109,137−139] This phase is well oriented in fiber direction, but has still many

tetrahedral carbon-type crosslinks between the graphite-type carbon layers. This particular structure is responsible for the typical high tensile strength of CFs. While the chemistry of oxidative stabilization, which results in the formation of acridone, naphthyridine, hydronaphthyridine, and other substructures as intermediates[140] has been elucidated to some extent by X-ray photoelectron spectroscopy and Fourier transform infrared spectroscopy studies[141–143] with the aid of model compounds,[144] the information about the crosslinking of the intermediate ribbon structures and the concomitant 3D structure formation during the removal of nitrogen is basically obscure.

CFs from PAN have a typical rough breaking behavior of the filaments (Fig. 2.4) and a surface with visible fibrillated structures (Fig. 2.5), depending on the coagulation conditions in the fiber preparation process.

The final step in the heat treatment of CFs at temperatures of up to 3000°C is called graphitization. At these temperatures, the ordering and orientation of the small turbostratic crystallites in the direction of the fiber axis takes place. This results in higher Young's modulus, but simultaneously leads to lower tensile strength of the final CF. The high modulus furnace employs a graphite muffle operating in a carefully controlled inert atmosphere. The conditions must be quiescent, since even a low-volume gas flow over the hot graphite element is sufficient to continually remove a molecular layer of graphite and cause severe erosion leading to premature failure.[8]

Finally, small CF tows are collected using online winders and larger tows can be collected in tubes or plated into cardboard boxes. The resulting CFs have a relatively fine count of approximately 0.8 dtex, a density of 1.8 g/cm^3. The required mechanical properties are available in low modulus, standard modulus, intermediate modulus, high modulus, and ultrahigh modulus.

To improve the properties of PAN-based CFs, carbon nanotubes (CNTs) have been added. CNTs may act as nucleation agents to improve crystallinity of the PAN precursor, which may result in a better carbon structure. A second benefit of using CNTs

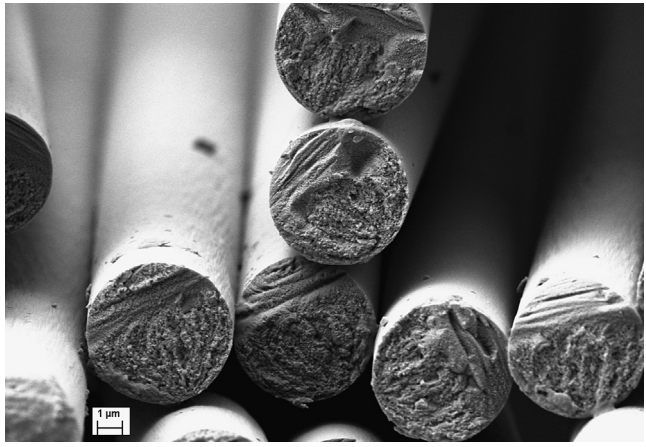

Figure 2.4 SEM of freeze break of commercial PAN-based carbon fibers.

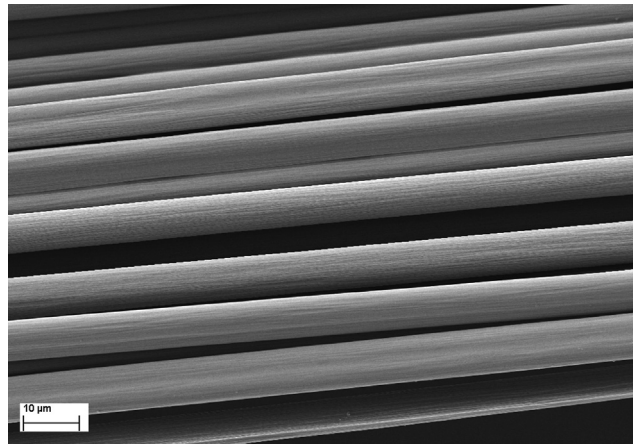

Figure 2.5 SEM of surfaces of commercial PAN-based carbon fibers.

could be the usage of their superior tensile strength and modulus, which may transfer to some percentage in CF properties.

The preparation of such composite fibers is realized by adding the CNTs in a modified form to compatibilize the surface of the CNTs to the polymer solution of PAN. With a homogeneous mixture of the CNTs in the polymer solution the preparation of the CF is accomplished via a gel-spinning process.[145] In the orientation process of the PAN polymer the CNTs become fully oriented too.

Despite the superior properties of laboratory CFs prepared by this method, there are some problems for big-scale production of such composite PAN-based CFs. The high price of the CNTs as additive compound is quite prohibitive and it is notoriously difficult to avoid any single agglomerate of CNTs, which may act as defect thereby decreasing CF strength.

2.1.3.3 Surface treatment of PAN-based precursors

To improve adhesion of CFs to matrix polymers, the final step of CF production involves the oxidative surface treatment and sizing applying solvent-based emulsions, preferably using the same chemical composition as the ultimate matrix resin. The oxidative surface treatment involves application of electrochemical or electrolytic bathes. During this procedure, the surface of the CFs is etched and roughened, thereby increasing the surface area available for interfacial fiber/matrix interaction and generating reactive chemical groups on the fiber surface. The oxidation of the surface may also be done, for example, by plasma treatment and chemical methods.[146,147] Application of thermoplastic resins, thermosetting plastics and water-based coatings with 0.5−5wt% of the sizing improves the processability of the CF to fabrics and prepregs increasing interfacial shear strength between the fiber and matrix resin.

An alternative way of functionalization for such polymeric matrices is the deposition of CNTs on the surface of the CF.[148] The CNTs act as a mechanical anchor in

polymer matrices. Using chemical vapor deposition (CVD) methods for in situ growth of the CNTs on the CF surface, the CNTs are strongly bound to the interface. But damage of the CF surface by CVD or similar processes has to be avoided because this limits the mechanical performance of the CFs.

2.2 Structure and properties of high-performance PAN-based CFs

2.2.1 Structure models of PAN-based CFs

In contrast to other allotropic forms of carbon, for example, graphite and diamond, the structure of CFs is rather complex.[149] A main structural motif of a CF is that of crystallites of more or less bent layers of preferably sp^2-hybridized carbon atoms, called turbostratic carbon. The carbon layers are disordered in stacking compared to a high crystalline graphite.

The crystallites are defined by their length L_a, thickness L_c, the interlayer distance d_{002} between the carbon layers, and the mean orientation of the crystallites, with 0 in a fully nonoriented carbon and 1 (100%) in a (theoretically) perfect oriented fiber.

A polymeric precursor has to fulfill many requirements to be applicable to CF production. This includes spinnability (see earlier) and orientation. To achieve acceptable mechanical values in terms of tensile strength and Young's modulus (stiffness), the polymer chains of the precursor must have an orientation of at least 70−80%. For high modulus CFs the orientation is typical >80%. The resulting modulus solely depends on this orientation, not on the underlying precursor system.

Unlike the two-dimensional form of carbon, graphene, which is also a substructure of CFs, the structure and morphology of a CF is complex. The crystallites dimensions L_a, L_c, and d_{002} depend on the method of measurement and are not well defined in a highly oriented carbon phase. The crystallite sizes can be measured by wide-angle X-ray scattering, Raman spectroscopy, or via transmission electron microscopy.

Another model defines the crystallites with the length L_a and the depth L_c as intersections of endless fibrils of stacked carbon layers, with voids in between the fibrils.[150] A similar model representation was discussed by Johnson in a more detailed description of penetrating carbon structures.[151]

The authors' own simulation of turbostratic carbon layers is shown in Fig. 2.6. The turbostratic layers were created from perfect graphene layers by introducing some hole defects. By stacking four layers in each of three domains and allowing them to relax at 300K for 1 ns in a ReaxFF molecular dynamics simulation. The layers start to bend in parallel in each domain and tend to misalign in stacking. The simulated layers show an increased interlayer spacing in comparison to a perfect graphitic domain.

High-modulus CFs, heat treated above 2000°C, develop a higher-ordered structure called 3D carbon. This structure development becomes clearly visible via Raman spectroscopy, where it shows up as a new peak at 2700 cm^{-1}.[152–154]

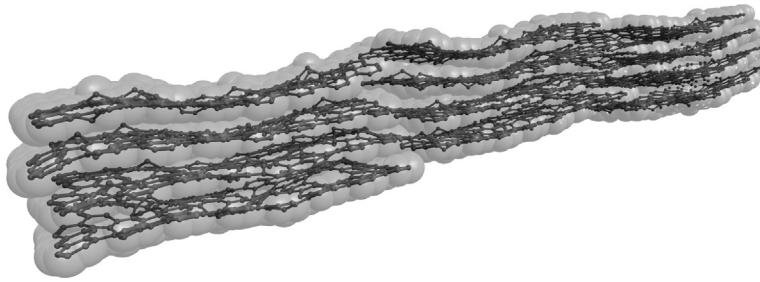

Figure 2.6 Model structure of three carbon domains with 3.3 × 2.4 × 1.5 nm volume from molecular mechanics simulation within ReaxFF at 300K after 1 ns relaxation time.

On the length scale of the entire CF, some additional features have to be discussed. Larger voids from the spinning processes and loss of material during carbonization have to be taken in consideration. Additionally, a CF typically has a core−shell structure with more graphitized carbon at the surface and more interlinked carbon structures in the core. Barnett et al. presented a model with a comprehensive representation of all macroscale features important for CF properties.

2.2.2 Properties of PAN-based CFs

PAN-based CFs are typically used as high-strength fibers with fiber strength starting in range of 3.5 up to 7 GPa and Young's modulus between 200 and 500 GPa.[3] High strength results from defect-free preparation conditions, but higher modulus fibers are a result of high-temperature treatment.[155] Apart from their outstanding mechanics, CFs have some additional unique properties. Unlike in metals, which show a decrease in conductivity with increasing temperature,[156] CFs exhibit increasing electrical conductivity with increasing temperature but also with better orientation, that is, higher modulus. Also, CFs have a low and negative thermal expansion coefficient, which is used to prepare composite parts with zero thermal expansion.[157]

Because of their electrical conductivity, which is still some orders below that of metals, PAN-based CFs are heatable by electrical power and dense layer CFs can be used to shield electromagnetic waves. Vice versa, because of their low density CFs have a low shielding effect for X-rays and have been used in medical applications. CFs are creep resistant and under inert gas they can be used up to temperatures of 2500°C. However, they become oxidized in air or similar aggressive conditions at temperatures above 450°C.

2.3 Applications of high-performance PAN-based CFs

Most PAN-based CFs have been used in the form of endless fibers for strengthening in composites, most of them in CF-reinforced plastics (CFRPs). The main industrial usage occurs in the following fields: aerospace, for example, in passenger aircrafts such as the Boing 787 "Dreamliner" and the Airbus A380 and A350 with increasing parts in

CFRPs[158]; military vessels; energy and gas storage; housings for computers and machines; and energy harvesting (wind energy).[159] The automotive industry invests a great deal into research into lightweight structures, and as a result some of the first products in electromobility are the electro-driven cars i3 and i8 from BMW in Germany.[2] Additional to their use in CFRPs there are lot of application fields, as seen in Table 2.3, depending on the textile type of the CF.

2.4 Conclusion: strengths and weaknesses of current fiber types

The available PAN-based CFs satisfy the demands of most applications, but the high price of PAN-based CFs in combination with processing costs limits large-scale applications like car building in high volume production. PAN-based CFs are the "standard" CFs in the market satisfying all types of strength in combination with intermediate modulus. Ultrahigh modulus fibers are a niche for pitch-based CFs and cannot be satisfied with PAN-based CFs.

Besides the continuous growth of CF production in the last few years, any large-volume application of CF, for example, in the automotive industry, has been impeded by high fiber costs and the lack of high-speed composite fabrication techniques. However, current investigations and future developments might well change the market to establish CFs as a mass product like other synthetic fibers or even metals.

With an increasing use of CFs for wind power and in the automotive sector, the demand for CFs in the coming 5 years is expected at least to double. To establish CFs in the mass market, prices of CFs have to be significantly reduced.

2.5 Future trends

In the medium term, alternative raw materials for CFs may be identified and implemented as a third precursor class besides PAN- and pitch-based CFs. Not only the automotive industry but also the construction industry, power industry, and mechanical engineering will require such novel, low-cost fibers when switching to new materials in price-sensitive products. Renewable raw materials such as biopolymers or polymers from biogenic sources are especially interesting sources for CFs. Therefore worldwide research projects for the investigation of biogenic CFs have been initiated. These fibers are not yet in competition with PAN-derived CFs, but provide new markets for CFs by high availability and low-cost production. The development of such alternative precursors to mature to obtain useful CFs in terms of tensile strength and modulus (stiffness) requires an immense knowledge of the underlying chemistry. Today's modern methods in analytics and computer modeling are a prerequisite to carry such fiber developments to success.

Table 2.3 Types of CFs and their major usage[6]

Types	Specifications	Major usage
Filament	A yarn consisting of numerous fibers: twisted, untwisted, twisted and untwisted	Resin reinforcement material for CF-reinforced plastics (CFRP), CF-reinforced thermoplastics (CFRTP), or carbon−carbon composites (C−C), for use in aircraft/aerospace equipment, sporting goods, and industrial equipment parts
Tow	An untwisted bundle of yarn consisting of extremely numerous fibers	Resin reinforcement material for CFRP, CFRTP, or C−C composites, for use in aircraft/aerospace equipment, sporting goods, and industrial equipment parts
Staple yarn	A yarn made via spinning of staples	Heat insulators, antifriction material, C−C composite parts
Woven fabric	A woven sheet made of filament or staple yarn	Resin reinforcement material for CFRP, CFRTP, or C−C composites, for use in aircraft/aerospace equipment, sporting goods, and industrial equipment parts
Braid	A braided yarn made of filament or tow	Resin reinforcement material particularly suitable for reinforcement of tubular products
Chopped fiber	A chopped fiber made of sized or nonsized fiber	Compounded into plastics/resins or Portland cement to improve mechanical performance, abrasion characteristics, electric conductivity, and heat resistance
Milled	Powder made by milling fiber in a ball mill, etc.	Compounded into plastics/resins or rubber to improve mechanical performance, abrasion characteristics, electric conductivity, and heat resistance
Felt/Mat	A felt or mat made by layering up of staple by carding, etc. then needle punched or strengthened by organic binders	Heat insulators, base material for molded heat insulators, protective layer for heat resistance, and base material for corrosion-resisting filters
Paper	A paper made from staple by dry or wet papermaking	Antielectrostatic sheets, electrodes, speaker cones, and heating plates

Continued

Table 2.3 Continued

Types	Specifications	Major usage
Prepreg	An intermediate material in a form of half-hardened sheets made of CFs impregnated with thermosetting resin, whose qualities are stability and sustainability to be easily applied to automatic sheet layering	Aircraft/aerospace equipment, sporting goods, and industrial equipment parts requiring low weight and high performance
Compounds	A material for injection molding, etc., made of a mixture of thermoplastics or thermosetting resins added by various additives and chopped fiber followed by compounding	Housing, etc., of office automation equipment taking advantage of electric conductivity, rigidity, and low weight

References

1. *Torayca Product Website* 2015. Available from: http://www.toraycfa.com/product.html.
2. Keichel M. Ganz neue Möglichkeiten. In: Keichel M, Schwedes O, editors. *Das Elektroauto*. Springer Fachmedien Wiesbaden; 2013. p. 73−103.
3. Frank E, et al. Carbon fibers: precursor systems, processing, structure, and properties. *Angew Chem Int Ed* 2014;**53**(21):5262−98.
4. Frank E, Buchmeiser MR. Carbon fibers. In: Kobayashi S, Müllen K, editors. *Fiber, films, resins and plastics*. Berlin Heidelberg: Springer; 2015. p. 306−10.
5. *In the starting blocks*. JEC Composites; 2015.
6. Association, T.J.C.F.M. 2015. Available from: http://www.carbonfiber.gr.jp/english/material/type.html.
7. Shindo A, Report of the Government Industrial Research Institute, Osaka, Japan 1961.
8. Morgan P. *Carbon fibers and their composites*. Boca Raton: CRC Press; 2005.
9. Sandler SR. *Polymer synthesis*, vol. 1. New York and London: Academic Press; 1974.
10. Ashina Y, Oshima I, Sekine K. *Temperature control in suspension Polymerisation*. USA: Nitto Chemical Industry Co., Mitsubishi Rayon Co.; 1972.
11. Bacon RGR. *Trans Faraday Soc* 1946;**42**:140−55.
12. Bero M, Rosner T. Polymerisationskinetik von Acrylnitril in wässriger Lösung. *Makromol Chem* 1970;**136**(1):1−10.
13. von Falkai B, Bonart R. *Synthesefasern − Grundlagen, Technologie, Verarbeitung und Anwendung*. Weinheim: Verlag Chemie; 1981.
14. Fritzsche P, Ulbricht J. *Faserforsch U Textiltechn* 1963;**14**:320.
15. Fritzsche P, Ulbricht J. *Faserforsch U Textiltechn* 1964;**15**:93.
16. Gabrielyan GA, Rogovin ZA. *J Text Inst* 1964;**55**:26.
17. Grim JM. *Chem Abstr* 1952;**46**.

18. Lewin M. *Handbook of fiber chemistry*. CRC Press; 2007.
19. Peebles LH. A kinetic model of persulfate−bisulfite-initiated acrylonitrile polymerization. *J Appl Polym Sci* 1973;**17**(1):113.
20. Price JA, Thomas WM, Padbury JJ. *Chem Abstr* 1953;**47**:670.
21. Shashoua VE. In: Sorenson WR, Campbell TW, editors. *Preparative methods of polymeric chemistry*. New York: Wiley (Interscience); 1968. p. 235.
22. Wilkinson WK. *Macromol Symp* 1966;**2**:78.
23. Parker RB, Mokler BV. Kalvar Corporation 1964.
24. Chaney DW. *Acrylonitrile copolymers and method of producing them*. USA: American Viscose Corporation; 1951.
25. Schmidt WG, Courtaulds L, editors. Courtaulds, Ltd.: Great Britain; 1958.
26. Czajlik J, et al. *Eur Polym J* 1978;**14**:1059−66.
27. Feldman D. *Mater Plast* 1966;**3**:25.
28. Kiuchi H. *Chem Abstr* 1964;**61**:7107.
29. Blades H. Polyamide fibers and films. *Chem Abstr* 1962:14483. Union Rheinische Braunkohlen Kraftstoff.
30. Kropa EL. *Process for producing polymeric materials*. USA: Old Greenwich Con.; 1944.
31. Miyama H, Harumiya N, Takeda A. *J Polym Sci Part A* 1972;**10**(3):943.
32. Murgulescu IG, Oncescu T, Vlagiu II. *Chem Abstr* 1972;**77**:75804.
33. Peebles LH. Polyacrylonitrile prepared in ethylene carbonate solution. III. Molecular parameters. *J Polym Sci Part A* 1965:341.
34. Schildknecht CE. *Vinyl and related polymers: their preparations, properties, and applications in rubbers, plastics, fibers, and in medical and industrial arts*. New York: Wiley & Sons; 1952.
35. Szafko J, Turska E. Free radical polymerization of some monomers in dimethyl formamide. *Makromol Chem* 1972;**156**:297−310 (Copyright (C) 2013 American Chemical Society (ACS). All Rights Reserved.).
36. Thomas WM. Mechanism of acrylonitrile polymerization. *Fortschr Hochpolym Forsch* 1961;**2**:401.
37. Wilkinson WK. *Process for polymerizing methacrylonitrile*. Wilmington: USA: E.I. du Pont, Del; 1963.
38. Szafko J, Turska E. Copolymerization of acrylonitrile and methyl esters of α-substituted acrylic acids. *Makromol Chem* 1972;**156**:311−20 (Copyright (C) 2013 American Chemical Society (ACS). All Rights Reserved.).
39. Szafko J, Turska E. *Makromol Chem* 1972:156. 297, 311.
40. Ziabicki A. *Fundamentals of fibre formation: the science of fibre spinning and drawing*. John Wiley & Sons; 1976.
41. Frank E, Hermanutz F, Buchmeiser MR. Carbon fibers: precursors, manufacturing and properties. *Macromol Mater Eng* 2012;**297**(6):493−501.
42. Chung DDL. *Carbon fiber composites*. Newton: Butterworth-Heinemann; 1994.
43. Spörl JM, et al. Carbon fibers prepared from tailored reversible-addition-fragmentation transfer copolymerization-derived poly(acrylonitrile)-co-poly(methylmethacrylate). *J Polym Sci Part A Polym Chem* 2014;**52**(9):1322−33.
44. Donnet JB, Bansal RC. In: Dekker M, editor. *Carbon fibers*. 2nd ed., vol. 10. New York: Marcel Dekker; 1990. p. 1−145.
45. Tsai J-S, Lin C-H. *J Appl Polym Sci* 1991;**43**:679.
46. Kibayashi M, et al. *Carbon fibers, acrylic fibers and process for producing the acrylic fibers*. USA: Toray Industries, Inc.; 2002.
47. Anders RJ, Sweeny W, 1958. E.I. du Pont: USA.

48. Otani T, Setsuie T, Yoshida K. *Method for producing acrylic fiber precursors*. USA: Mitsubishi Rayon Co., Ltd.; 1987.
49. Nishihara Y, Furuya Y, Toramaru M. In: M.R. Co., editor. *Production of high-strength carbon Fiber*. Japan: Mitsubishi Rayon Co.; 1987.
50. Kai Y, Kuboyama M. In: M.R. Co., editor. *Production of carbon fiber*. Japan: Asahi Chemical; 1990.
51. Hajikano A, Yamamoto T, Kubota T. In: M.R. Co., editor. *Precursor for carbon fiber*. Japan: Mitsubishi Rayon Co.; 1992.
52. Hajikano A, et al. In: M.R. Co., editor. *Acrylonitrile precursor fiber*. Japan: Mitsubishi Rayon Co.; 1993.
53. Stuetz DE, Gump KH. In: C. Corporation, editor. *Thermal stabilization of fibrous material made from acrylic polymers*. Great Britain: Celanese Corporation; 1969.
54. Fitzer E, Müller DJ. *Makromol Chem* 1971;**144**:117.
55. Grassie N, McGuchan R. Pyrolysis of polyacrylonitrile and related polymers. *Eur Polym J* 1972;**8**:257.
56. Henrici-Olivé G, Olivé S. *Adv Polym Sci* 1983;**51**:36.
57. Yoshinori T, Hiroshi O. Carbon fiber. In: M.T.C. Inc., editor. *Japan Kokai Tokkyo Koho*. Japan: Mitsubishi Toasty Chemical Inc.; 1987.
58. Morita K, et al. In: T.I. Inc., editor. *Heat-treated products of acrylonitrile copolymers and processes for the preparation thereof*. Great Britain: Toray Industries Inc.; 1969.
59. Hiramatsu T, Higuchi T, Mitsui S. In: T.I. Inc., editor. *High-tenacity carbon fiber manufacture*. Japan: Toray Industries Inc.; 1983.
60. Takeda S, Tsunoda A. Production of precursor yarn for carbon fiber. In: T.I. Inc., editor. *Japan Kokai Tokkyo Koho*. Japan: Toray Industries Inc.; 1983.
61. Haruo O, Masahi O, Hiroyoshi T. Production of acrylic flameproof fiber. In: T.I. Inc., editor. *Japan Kokai Tokkyo Koho*. Japan: Toray Industries Inc.; 1984.
62. Yamane S, Higuchi T, Yamasaki K. *Process for produncing high strength, high modulus carbon fibers*. Toray Industries Inc.; 1987.
63. Matsuhisa Y, Ono K, Hiramatsu T. *Highly dense acryl based carbon fiber*. Toray Industries Inc.; 1990.
64. Yamazaki J, Shirakata M, Adachi Y. In: T.I. Inc., editor. *Production of acrylic precursor yarn for carbon fiber*. Japan: Toray Industries Inc.; 1991.
65. Kobayashi M, Takada N. *Carbon fiber and its production*. Toray Industries Inc.; 1993.
66. Hiramatsu T, Higuchi T, Mitsui S. In: T.I. Inc., editor. *Carbon fiber bundle of high strenth and elongation*. Japan: Toray Industries Inc.; 1983.
67. Iharaki T, Yoshino S. Production of carbon fiber having high strength. In: A.C. Industry, editor. *Japan Kokai Tokkyo Koho*. Japan: Asahi Chemical Industry; 1986.
68. Ogawa T, Wakita E, Kobayashi T, A.K.K. KK, editors. *Asahi Kasei Kogyo KK*; 1974 [Great Britain].
69. Park LY, et al. 233. The effect of chain length on the conductivity of polyacetylene. Potential dependence of the conductivity of a series of polyenes prepared by a living polymerization method. *Chem Mater* 1992;**4**:1388.
70. Imai K, Senchi H. Production of flameproofing yarn for carbon fiber and flame proofing furnace. In: *Japan Kokai Tokkyo Koho*. Japan: Nikkiso Co., Ltd.; 1982.
71. Moutaud G, Loiseau J-P, Desmicht D. *New method of producing carbon fibres with a high modulus of elasticity*. Le Carbone Lorraine; 1969.
72. Kishimoto S, Okazaki S. *Process for producing carbon fibers*. US: Japan Exlan Co., Ltd.; 1977.
73. Tominari K, Ishimoto T. *Polymerization process*. Mitsui Petrochemicals Ind. Ltd.; 1984.

74. Takeji O, Takashi F, Tadao K. Production of carbon yarn. In: *Japan Kokai Tokkyo Koho*. Japan: Mitsubishi Rayon Co., Ltd.; 1984.
75. Imai Y, et al. Production of carbon fiber. In: M.R.C. Ltd., editor. *Japan Kokai Tokkyo Koho*. Japan: Mitsubishi Rayon Co., Ltd.; 1985.
76. Sasaki S, et al. *Production of carbon fiber*. Mitsubishi Rayon Co., Ltd; 1987.
77. Imai Y, et al. *Process for producing carbon fibers of high tenacity and modulus of elasticity*. USA: Mitsubishi Rayon Co., Ltd.; 1991.
78. Mackenzie HD, Reeder F. In: C. Ltd., editor. *Improvements in and relating to polyacrylonitrile solutions*. Great Britain: Courtaulds Ltd.; 1963.
79. Moreton R, McLonghlin, H. P., R.A. Establishment, editor.
80. Platonova NV, et al. *Vysokomol Soedin* 1988;**30**(5):1056. Ser A.
81. Kiselev GA, et al. *Composition for spinning carbon fiber precursors*. Leningrad Institute of Textile and Light Industry, USSR; All-Union Scientific-Research Institute of Synthetic Fibers; 1984.
82. Hirotaka S, Hiroaki K. *Manufacturing process of isotactic copolymer for carbon fiber precursor*. Japan: Teijin Ltd.; 2006.
83. Kuwahara H, Suzuki H, Matsumura S. *Polymer for carbon fiber precursor*. USA: Teijin Ltd.; 2008.
84. Warren CD, et al. Multi-task research program to develop commodity grade, lower cost carbon fiber. In: *Proceedings of the SAMPE Fall technical conference*; 2008 [Memphis, TN, USA].
85. Dasarathy H, et al. Low cost carbon fiber from chemically modified acrylics. In: *Proceedings of the International SAMPE technical conference*; 2002 [Baltimore, MD, USA].
86. Bajaj P, Paliwal DK, Gupta AK. *J Appl Polym Sci* 1998;**67**:1647−59.
87. Daumit GP, et al. *Formation of melt-spun acrylic fibers wich are well suited for thermal conversion to high strength carbon fibers*. Basf Aktiengesellschaft; 1990.
88. Daumit GP, et al. *Formation of melt-spun acrylic fibers which are particularly suited for thermal conversion to high strength carbon fibers*. USA: Basf Aktiengesellschaft; 1990.
89. Daumit GP, et al. *Formation of melt-spun acrylic fibers possessing a highly uniform internal structure which are particularly suited for thermal conversion to quality carbon fibers*. USA: Basf Aktiengesellschaft; 1990.
90. Ingildeev D, et al. Novel cellulose/polymer blend fibers obtained using ionic liquids. *Macromol Mater Eng* 2012;**297**:585−94 (New Trends in High-Performance Fibers and Fiber Technology).
91. Blades H. *Dry jet wet spinning process*. United States: Du Pont; 1972.
92. Gröbe V, Meyer K. *Faserforsch Textiltechnik* 1969;**467**(20).
93. Craig JP, Knudsen JP, Holland VF. Characterization of acrylic fiber structure. *Text Res J* 1962;**32**(6):435−48.
94. Hartig S, Peter E, Dohrn W. *Lenzing Ber* 1973;**35**:17.
95. Knudsen JP. *Text Res J* 1963;**33**:13.
96. Duwe G, Mann G, Gröbe A. *Faserforsch Textiltechnik* 1966;**17**:142.
97. Takeda H, Nukushima Y. *Kogyo Kagaku Zasshi* 1964;**67**:626.
98. Gröbe A, Mann G. *Faserforsch Textiltechnik* 1966;**17**:315.
99. Takahashi M, Watanabe M. *Sen-I Gakkaishi* 1960;**16**:7.
100. Uchida S. In: J.E.C. Ltd., editor. *Production of acrylic fibre having high physical property*. Japan: Japan Exclan Co., Ltd.; 1987.
101. Nishihara Y, Furuya Y, Toramaru M. *Production of high-strength carbon fiber*. Japan: Mitsubishi Rayon Co., Ltd.; 1988.

102. Zenke D, et al. *VERFAHREN ZUR HERSTELLUNG VON POLYARYNITRILFAEDEN MIT HOHER FESTIGKEIT UND HOHEM ELASTIZITAETSMODUL*. Akademie der Wissenschaften der DDR; 1990.
103. Kashani-Shirazi R. *Hochfeste Polyacrylnitrilfasern hohen Moduls, Verfahren zu deren Herstellung und deren Verwendung*. Europe: Hoechst Aktiengesellschaft; 1987.
104. Cerf M, Colombie D, N′Zudie TD. *Method for making acrylonitrile fibers*. US: Hunton & Williams LLP; 1988.
105. Nishihara Y, Nishimura K. *Production of high-tenacity acrylic fiber having excellent abrasion resistance*. Japan: Mitsubishi Rayon Co., Ltd.; 1993.
106. Funakoshi Y, Maeda Y. *Surface method of resin molded article*. Japan: Matsushita Electric Ind. Co., Ltd.; 1985.
107. Shiromoto Y, Okuda A, Mitsui S. In: T.I. Inc, editor. *Production of precursor yarn for carbon fiber − NEU SUCHEN*. Japan: Toray Ind. Inc.; 1983.
108. Watt W, Johnson W. Mechanism of oxidisation of polyacrylonitrile fibre. *Nature* 1975; **257**:210−2.
109. Huang X. Fabrication and properties of carbon fibers. *Materials* 2009;**2**:2369−403.
110. Houtz RC. *J Text Res* 1950;**20**:786−801.
111. Schurz J. *J Polym Sci* 1958;**28**:438−9.
112. Standage A, Matkowski R. *Eur Polym J* 1971;**7**:775−83.
113. Friedlander HN, et al. *Macromolecules* 1968;**1**:79−86.
114. Goodhew PJ, Clarke AJ, Bailey JE. A review of the fabrication and properties of carbon fibres. *Mater Sci Eng* 1975;**17**(1):3−30.
115. Clarke AJ, Bailey JE. *Nature* 1973;**243**:146−50.
116. Bailey JE, Clarke AJ. *Chem Ber* 1970;**6**:484−9.
117. Lora J. Industrial commercial lignins: sources, properties and applications. In: *Monomers, polymers and composites from renewable resources*. Amsterdam: Elsevier Ltd.; 2008. p. 225−41.
118. Baker DA, Rials TG. Recent advances in low-cost carbon fiber manufacture from lignin. *J Appl Polym Sci* 2013;**130**:713−28.
119. Nordström Y, Joffe R, Sjöholm E. Mechanical characterization and application of Weibull statistics to the strength of softwood lignin-based carbon fibers. *J Appl Polym Sci* 2013; **130**:3689−97.
120. Baker FS, Gallego NC, Baker DA. *DOE FY 2009 progress report for light weighting materials, part 7.A*. 2009.
121. Sundquist J. Organosolv pulping. In: Gullichsen J, Fogelholm C-J, editors. *Papermaking science and technology, book 6B, chemical pulping*. Finnish Paper Engineers' Association and TAPPI; 1999. p. 411−27.
122. Pan X, et al. Biorefining of softwoods using ethanol organosolv pulping: preliminary evaluation of process streams for manufacture of fuel-grade ethanol and co-products. *Biotechnol Bioeng* 2005;**90**(4):473−81.
123. Wang Y, et al. Structural identification of polyacrylonitrile during thermal treatment by selective 13C labeling and solid-state 13C NMR spectroscopy. *Macromolecules* 2014; **47**(12):3901−8.
124. Coleman MM, Sivy GT. *Carbon* 1981;**19**:133.
125. Sivy GT, Coleman MM. *Carbon* 1981;**19**:127.
126. Raskovic V, Marinkovic S. *Carbon* 1975;**13**:535−8.
127. Donnet JB, Ehrburger P. *Carbon* 1977;**15**:143.
128. Grassie N, Hay JN. *J Polym Sci Part A Polym Chem* 1962;**56**:189.
129. Fitzer E, Heine M, Jacobsen G. In: *International symposium on carbon*; 1982 [Toyohashi, Japan].

130. White SM, Spruiell JE, Paulauskas FL. Fundamental studies of stabilization of polyacrylonitrile precursor, part 1: effects of thermal and environmental treatments. In: *Proceedings of the International SAMPE technical conference*; 2006 [Long Beach, CA, USA].
131. Dietrich J, Hirt P, Herlinger H. *Eur Polym J* 1996;**32**.
132. Paulauskas FL, White TL, Spruiell JE. Structure and properties of carbon fibers produced using microwave-assisted plasma technology. In: *Proceedings of the International SAMPE technical conference*; 2006.
133. Tsai JS. *Text Res J* 1994;**64**(12):772−4.
134. Raskovic V, Marinkovic S. *Carbon* 1978;**16**:351−7.
135. Bromley J. Gas evolution processes during the formation of carbon fibers. In: *International conference on carbon fibers, their composites and applications*; 1971 [London].
136. Johansson A, Aaltonen O, Ylinen P. Organosolv pulping − methods and pulp properties. *Biomass* 1987;**13**(1):45−65.
137. Wangxi Z, Jie L, Gang W. Evolution of structure and properties of PAN precursors during their conversion to carbon fibers. *Carbon* 2003;**41**:2805−12.
138. O'Neil D. Precursor for carbon and graphite fibers. *Int J Polym Mater* 1979;**7**:203−18.
139. Johnson DJ, Tomizuka I, Watanabe O. Fine structure of lignin-based carbon fibers. *Carbon* 1975;**13**:321−5 (Copyright (C) 2013 American Chemical Society (ACS). All Rights Reserved.).
140. Morita K, et al. Characterization of commercially available PAN (polyacrylonitrile)-based carbon fibers. *Pure Appl Chem* 1986;**58**:455−68.
141. Shimada I, et al. FT-IR study of the stabilization reaction of polyacrylonitrile in the production of carbon fibers. *J Polym Sci A Polym Chem* 1986;**24**:1989−95.
142. Sivy GT, Gordon B, Coleman MM. Studies of the degradation of copolymers of acrylonitrile and acrylamide in air at 200°C. Speculations on the role of the preoxidation step in carbon fiber formation. *Carbon* 1983;**21**(6):573−8.
143. Varma SP, Lal BB, Srivastava NK. IR studies on preoxidized PAN fibers. *Carbon* 1976; **14**:207−9.
144. Takahagi T, et al. XPS studies on the chemical structure of the stabilized polyacrylonitrile fiber in the carbon fiber production process. *J Polym Sci A Polym Chem* 1986;**24**:3101−7.
145. Newcomb BA, et al. Processing, structure, and properties of gel spun PAN and PAN/CNT fibers and gel spun PAN based carbon fibers. *Polym Eng Sci* 2015:2603−14.
146. Donnet JB, et al. Plasma treatment effect on the surface energy of carbon and carbon fibers. *Carbon* 1986;**24**(6):757−70.
147. Desimoni E, et al. Controlled chemical oxidation of carbon fibres: an XPS−XAES−SEM study. *Surf Interface Analysis* 1993;**20**(11):909−18.
148. De Greef N, et al. Direct growth of carbon nanotubes on carbon fibers: effect of the CVD parameters on the degradation of mechanical properties of carbon fibers. *Diam Relat Mater* 2015;**51**:39−48.
149. Dresselhaus MS, et al. Graphite fibers and filaments. In: Cardona M, et al., editors. *Materials Science*, vol. 5. Berlin, Heidelberg, New York, London, Paris, Tokyo: Springer-Verlag; 1988.
150. Fourdeaux A, Perret R, Ruland W. General structural features of carbon fibres. In: *Proceedings of the International conference on carbon Fibres, their composites and applications: plastics and polymer Conf. Supplement*. London: Maney Publishing; 1971.
151. Johnson DJ. Structure property relationships in carbon fibres. *J Phys D Appl Phys* 1987; **20**(3):285−91.
152. Tuinstra F, Koenig JL. Raman Spectrum of Graphite. *J Chem Phys* 1970;**53**:1126.

153. Nemanich RJ, Solin SA. Observation of an anomolously sharp feature in the 2nd order Raman spectrum of graphite. *Solid State Commun* 1977;**23**:417−20 (Copyright (C) 2013 American Chemical Society (ACS). All Rights Reserved.).
154. Tsu R, Gonzalez HJ, Hernandez CI. Observation of splitting of the E2g mode and two-phonon spectrum in graphites. *Solid State Commun* 1978;**27**:507−10 (Copyright (C) 2013 American Chemical Society (ACS). All Rights Reserved.).
155. Bunsell AR. *Fibre reinforcements for composite materials*. Elsevier; 1988.
156. Nysten B, et al. Microstructure and negative magnetoresistance in pitch-derived carbon fibres. *J Phys D Appl Phys* 1991;**24**(5):714.
157. Zweben C. Advances in composite materials for thermal management in electronic packaging. *JOM* 1998;**50**(6):47−51.
158. Hartley K. *The political economy of aerospace industries: a key driver of growth and international competitiveness?*. Edward Elgar Publishing Limited; 2014.
159. Most relevant market segments for new low cost CFs and 2020 forecast per macro-area. In: *Composites World's annual carbon fibre 2011 conference, Washington, D.C., Dec. 5−7th 2011*; 2011.

High-performance pitch-based carbon fibers

3

M.G. Huson
CSIRO, Geelong, Victoria, Australia

3.1 Introduction

More than a 100 years ago fiber was carbonized by Thomas Edison in his production of incandescent filaments for the world's first commercially viable light bulb. He used cardboard and later bamboo filaments as his starting material to produce carbonized thread. Today carbon fiber is manufactured from a precursor fiber, which is generally spun from polyacrylonitrile (PAN), pitch or rayon. Approximately 95% of all carbon fiber produced is derived from PAN, the remaining 5% being made mostly from pitch with a very small amount made from rayon. Many other polymers have also been investigated for their potential as carbon fiber precursors, mainly with a view to reducing the processing cost or improving the mechanical properties of the resultant carbon fibers. To date none of these have become commercial.

Pitch-based carbon fiber is categorized as either general performance carbon fiber (GPCF) or high-performance carbon fiber (HPCF). GPCF is made from isotropic pitch (Maeda et al., 1993; Mora et al., 2002; Wazir and Kakakhel, 2009; Zeng et al., 1993a,b) and has a tensile strength up to 1000 MPa and a tensile modulus of 30−60 GPa. It is used mainly in less mechanically demanding applications such as reinforced concrete, thermal insulation, electrodes, or activated carbons (Bahl et al., 1998, Mora et al., 2002). The focus of this chapter is on HPCF, which is made from anisotropic or mesophase pitch.

Fifty years ago Brooks and Taylor (1965) reported a liquid crystal-like mesophase in pitch, which upon heating to high temperature formed graphitic carbon. Later White et al. (1967) showed that the mesophase could be oriented by flow and shear and that the structure persisted during the graphitization heat treatment. Singer (1978) built on this knowledge, showing that at the correct temperature and viscosity fibers could be drawn; the fibers being highly oriented with the graphite layer planes lying along the fiber axis. Heating these fibers resulted in graphitization and the formation of the first high-strength carbon fibers based on pitch. Singer's work, along with that of McHenry and Lewis, formed the basis of Union Carbide's industrial process for making mesophase pitch-based carbon fiber (Lewis et al., 1976, 1977; McHenry, 1977; Singer, 1977).

Pitch-based carbon fiber is generally more graphitic than PAN-based carbon fiber and consequently has a higher modulus (Fig. 3.1); the stiffer grades approaching the 1060 GPa value listed for graphite (Blakslee et al., 1970). The higher graphitic content also results in improved electrical and thermal conductivity for pitch-based carbon

Structure and Properties of High-Performance Fibers. http://dx.doi.org/10.1016/B978-0-08-100550-7.00003-6

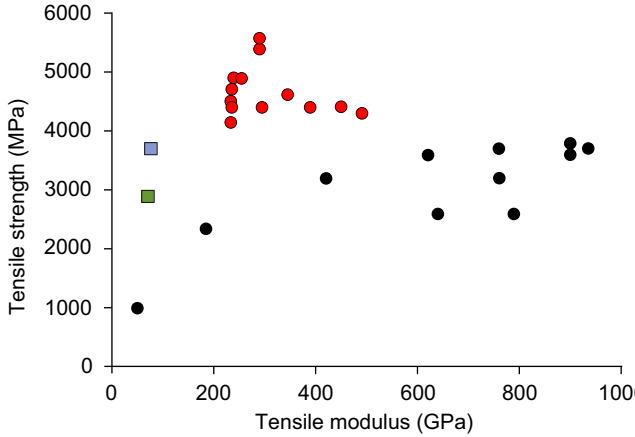

Figure 3.1 Tensile strength and modulus of Mitsubishi PAN-based (●) and pitch-based (●) carbon fibers as well as E glass (■) and Kevlar 29 (■), two other typical reinforcing fibers. Adapted with permission from Mitsubishi Rayon Co. Ltd. Data from product brochures.

fiber compared to PAN-based carbon fiber. The improved properties come at a cost, however, and so products such as Dialead K13D2U, with a tensile modulus of 935 GPa and thermal conductivity of 800 W/m K, have been limited to high value applications such as heat release materials for electronics devices loaded into satellites. Likewise, Thornel P-120 fiber with a modulus of 830 GPa and a linear coefficient of thermal expansion (CTE) of $-1.6 \times 10^{-6}\ \mathrm{K}^{-1}$ has been used in satellite structures but comes at a cost of more than $4000/kg (Brosius, 2014).

There are currently three main producers of high-performance pitch-based carbon fiber (Grégr, 2010):

1. Mitsubishi Plastics Inc., which markets products under the brand name "Dialead" and has a market share of about 70%
2. Cytec, which markets products under the brand name "Thornel" and has a 20% market share
3. Nippon Graphite Fiber Corporation, Ltd. (NGF) with products marketed under the brand name "Granoc" and a 10% market share.

3.2 Pitch precursors

3.2.1 General

Pitch is a black tar-like substance comprising hundreds of three to eight ringed aromatic compounds, the exact composition varying depending on the source of the raw material and the method of processing. It is also sometimes referred to as asphalt or bitumen. It occurs naturally in several parts of the world but most pitch is produced as the by-product of refining petroleum, or the destructive distillation of coal. Petroleum pitch typically has more alkyl-substituted polycyclic aromatic hydrocarbons

Figure 3.2 University of Queensland pitch drop experiment showing the viscoelastic nature of pitch.
Reproduced from https://en.wikipedia.org/wiki/Pitch_drop_experiment.

than coal tar pitch, that is, it has lower aromaticity and a higher degree of substitution of the aromatic ring (Choi and Yang, 2001). A so-called synthetic mesophase pitch can also be prepared from ring compounds such as naphthalene (Mochida et al., 1990a, 2004).

Pitch is a viscoelastic polymer with a molecular mass ranging between 180 and 600 g/mol (Ozel and Bartle, 2002). Although a brittle solid at room temperature, it can flow slowly as demonstrated in the University of Queensland pitch drop experiment where nine drops have fallen since the experiment was set up in 1930 (Fig. 3.2).

Raw pitch is a complex blend of polyaromatic molecules and heterocyclic compounds. As a general rule it is isotropic and is composed of four fractions (Barraza-Burgos and Ospina-Espinosa, 2012): (1) saturated aliphatic components of low molecular weight; (2) naphthalene aromatic compounds, which have low molecular weight with saturated rings; (3) polar aromatic compounds of medium molecular weight with some heterocyclic molecules; and (4) asphaltenes of high molecular weight and a degree of aromaticity. In addition, pitch contains a number of solid impurities. It has a softening point between 60 and 150°C, which is often too low for melt spinning and thus pitch needs to be treated to increase the viscosity and softening point. Most of the pitch produced is converted into bitumen for use in road surfacing; however, its use as a precursor for carbon fiber is also important.

3.2.2 Isotropic pitch

For the preparation of isotropic pitch suitable for spinning into fibers, the material needs to be processed carefully to avoid the formation of mesophase, which occurs

readily during heat treatment at 350−450°C (Morgan, 2005e). During heating at temperatures <350°C, volatiles are released and dehydrogenation, crosslinking, and condensation reactions occur leading to an increase in molecular mass. The combined effect is an increase in the softening temperature. While molten the pitch is filtered to remove the solid particles. The heat treatment can be done using a range of different solvent extraction and thermal methods of which the wiped film evaporator method (Sawran et al., 1985, 1987) and the air-blowing method (Maeda et al., 1993; Zeng et al., 1990, 1993b) are two that are commonly used. Fig. 3.3 shows the increase in softening point for a coal tar pitch air blown at three different temperatures.

Isotropic pitch is used directly to make GPCF (Maeda et al., 1993; Mora et al., 2002; Wazir and Kakakhel, 2009; Zeng et al., 1993a,b) for use in insulation felts, water purification, as reinforcing fillers for concrete, and in carbon−carbon composites. It is currently produced commercially from petroleum by Kureha Corporation (brand name "Kreca") and from coal tar by Osaka Gas Chemicals Co. (brand name "Donacarbo") and is supplied as yarn, fabric, felt, chopped fiber, and paper. It can also be converted to mesophase pitch to make HPCF.

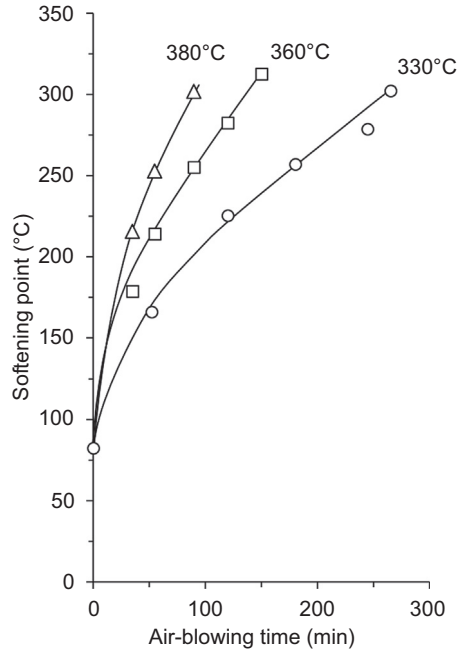

Figure 3.3 The increase in softening point for a coal tar pitch air blown at three different temperatures.
Adapted from Maeda, T., Ming Zeng, S., Tokumitsu, K., Mondori, J., Mochida, I., 1993. Preparation of isotropic pitch precursors for general purpose carbon fibers (GPCF) by air blowing—I. Preparation of spinnable isotropic pitch precursor from coal tar by air blowing. Carbon 31, 407−412 with permission of Elsevier.

3.2.3 Mesophase pitch

3.2.3.1 Mesophase formation

When isotropic pitch is heated in the range from 350 to 450°C a mesophase is produced (Fig. 3.4), the rate of formation increasing with temperature. The initial step involves condensation and dehydrogenation reactions leading to an increase in molecular mass of the aromatic pitch molecules (Greinke, 1986). These planar polyaromatic molecules then stack together to form a so-called molecular assembly unit. These units subsequently self-assemble into microdomains, which are the anisotropic spheres first discovered by Brooks and Taylor (1965). This process is shown schematically in Fig. 3.5. During spinning, these microdomains are deformed and aligned along the fiber axis and upon heating to high temperature they form the graphitic units present in carbon fiber.

A wide variety of mesophase pitches can be made by varying the starting material (petroleum, coal, or synthetic) as well as the process by which the isotropic pitch is converted into mesophase pitch. Fig. 3.6 shows the effect of time and temperature of heating on the formation of mesophase. Each process yields a product with a

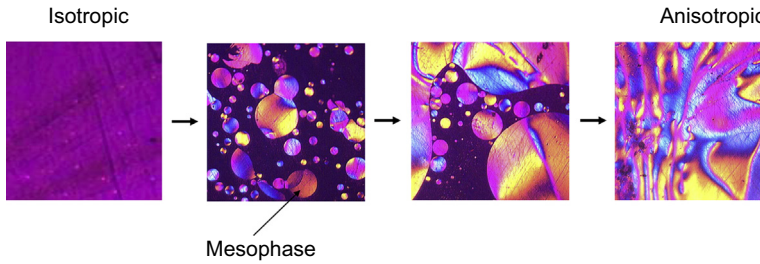

Figure 3.4 Formation of mesophase pitch from isotropic pitch on heating in the range from 350 to 450°C.
Adapted from Ania, C., 2007. Pitch based carbon materials. In: ITA Annual Conference. (Palma de Mallorca) courtesy of M. Granda (Instituto Nacional del Carbón, CSIC).

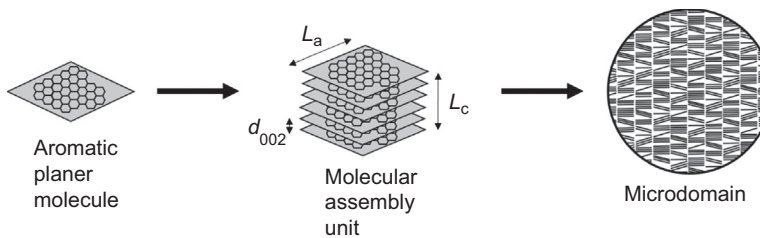

Figure 3.5 Formation of the stacked molecular assembly unit and microdomain unit from aromatic planar molecules in liquid crystal mesophase pitch. Also shown are the crystallite length (L_a), crystallite thickness (L_c), and the interplanar spacing (d_{002}).
Adapted from Yoon, S.-H., Korai, Y., Mochia, I., Yokogawa, K., Fukuyama, S., Yoshimura, M., 1996. Axial nano-scale microstructures in graphitized fibers inherited from liquid crystal mesophase pitch. Carbon 34, 83–88 with permission of Elsevier.

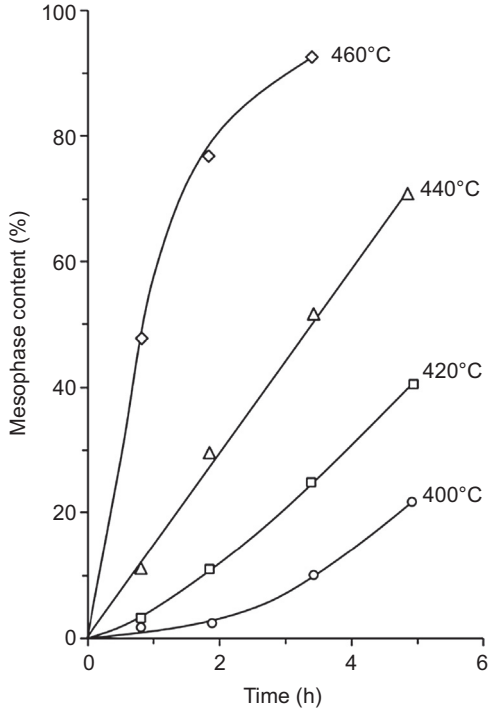

Figure 3.6 The time and temperature dependence of the formation of mesophase when an isotropic pitch is heated.
Adapted from Tillmanns, H., Pietzka, G., Pauls, H., 1978. Influence of the quinoline-insoluble matter in pitch on carbonization behaviour and structure of pitch coke. Fuel 57, 171−173 with permission of Elsevier.

different molecular weight distribution (the averages range from 800 to 1200 g/mol) and a different concentration of aliphatic side chains on the individual mesophase molecules. Consequently, their viscosity characteristics differ and their rate of stabilization differs as well. Nevertheless, all of these mesophase products reach a viscosity of approximately 200 Pa s, well below their degradation temperature, allowing them to be melt spun into fiber form. Also, although somewhat irregular, all of the individual mesophase molecules are disk-like in shape (Gillespie et al., 2005). De Castro (2006) has written a comprehensive review on the generation of mesophase in coal tar and petroleum pitches.

3.2.3.2 Coal tar and petroleum pitch

For coal tar and petroleum pitch it is common to characterize the pitch based on its solubility in a range of solvents such as *n*-pentane, carbon disulfide, carbon tetrachloride, benzene, toluene, pyridine, and quinoline. The quinoline insoluble (QI) fraction is particularly important and its influence on the formation of mesophase has been

extensively studied (Marsh and Carolyn, 1986; Moriyama et al., 2004; Stadelhofer, 1980; Tillmanns et al., 1978). QI is generally absent in petroleum pitches but present to a small degree in coal tar pitches (Lafdi et al., 1991).

For QI-free pitch, Tillmanns et al. (1978) showed that below a soaking temperature of 440°C an induction period is observed (Fig. 3.6). At soaking temperatures of 440 and 460°C there is an almost linear relation between heating time and mesophase content. From these results they postulated that the nucleation of mesophase spheres is completed within 2−3 h at temperatures of 400−420°C, and that at higher temperatures the increase of mesophase content is mainly determined by the formation and growth of many small mesophase spheres, which grow fast and/or agglomerate. Moriyama et al. (2004) compared a coal tar pitch free of QI with one containing 3% QI and showed that the presence of QI increased the total frequency of sphere generation, decreased the rate constant of coalescence, and decreased the linear growth rate. Tillmanns et al. (1978) showed that the presence of QI in the pitch acted as nucleating agents, eliminating the induction period. The addition of 20% QI, for instance, resulted in almost double the amount of mesophase being formed in 3.5 h at 420°C. In contrast Marsh and Carolyn (1986) noted that QI material, or other particulates, can retard the development of mesophase and suppress coalescence, thereby affecting the optical texture of the resultant carbonized material. Stadelhofer (1980) reported no accelerating effect upon the addition of up to 10 wt% QI, either in admixed or natural form. They claimed that their findings are consistent with the view that the rate-controlling step of mesophase formation is a dehydrogenative polymerization. Ferritto and Weiler (1968) reported that QI levels had an effect on graphite physical properties, such as coefficient of thermal expansion, flexural strength, apparent density, and electrical resistivity. However, they found that just as important as the concentration of QI was the process route, by which specific QI levels are attained.

There are many practical ways to convert isotropic pitch to mesophase pitch suitable for spinning (Morgan, 2005e), leading to a range of variants such as neomesophase, dormant mesophase, and premesophase. However, most processes involve two stages: (1) removal of low-molecular-weight species, and (2) heat treatment of high-molecular-weight fractions (asphaltenes and preasphaltenes) to temperatures between 300 and 500°C to facilitate polymerization and condensation reactions, which result in the formation of the mesophase (Barraza et al., 2014).

The removal of low-molecular-weight species is achieved in a variety of ways, including heating (Lewis et al., 1977; Mochida et al., 2006), solvent extraction (Ozel and Bartle, 2002; Park et al., 1988a,b), vacuum distillation (Mochida et al., 2006; Park and Mochida, 1989), and sparging with an inert gas (Barr, 1975; Choi and Yang, 2001; Chwastiak and Lewis, 1978). The resultant pitch has increased molecular mass and viscosity, which increases further during heat treatment between 300 and 500°C. Smaller aromatics combine into multi-ring systems, with molecular weights of ca. 1200−1400 g/mol, which eventually assemble into molecular assembly units as shown in Fig. 3.5. The final step is the formation of liquid crystal mesophase spheres, which nucleate and grow, eventually coalescing and reaching a level of 60−90% mesophase (Figs. 3.4 and 3.6).

3.2.3.3 Synthetic pitch

Synthetic pitch, prepared from the polymerization of compounds such as naphthalene and its derivatives, has attracted much attention over several decades. A key researcher in this area has been Mochida who, with his coworkers, has published prolifically in this area (Korai et al., 1991; Mochida et al., 1990a, 1992, 1993, 2000, 2004, 2006); their work leading to the commercial production of mesophase pitch by the Mitsubishi Gas Chemical Co. (MGC) in 1991 (Mochida et al., 2004). At one stage 1500 tonne/year was produced for the production of high-performance carbon fiber and anodic materials for lithium-ion batteries; however, it is no longer currently being produced commercially because of the cost of production (Yoon, 2015).

Most of the focus was on naphthalene, methylnaphthalene, or their mixtures as raw materials, with HF/BF_3 as the catalyst for the aromatic condensation or polymerization (Mochida et al., 1990a, 2000). HF/BF_3 is a strong Friedel–Crafts catalyst, which is readily recovered from the final product because of the low boiling points, 19.9 and −101.1°C, respectively, of both components. Fig. 3.7 shows the reaction scheme for the catalytic synthesis of mesophase pitch by aromatic condensation of naphthalene.

MGC assigned the trade name AR-resin to a series of their particular mesophase pitches (Mochida et al., 2004). Since the preparation of these pitches is carried out

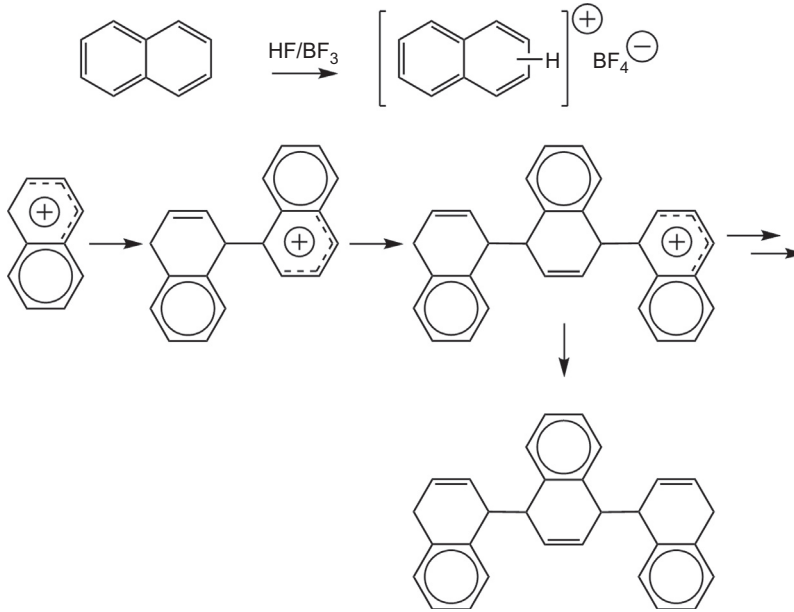

Figure 3.7 Synthesis of mesophase pitch from naphthalene using HF/BF_3 as catalyst. Reproduced from Mochida, I., Korai, Y., Ku, C.-H., Watanabe, F., Sakai, Y., 2000. Chemistry of synthesis, structure, preparation and application of aromatic-derived mesophase pitch. Carbon 38, 305–328 with permission of Elsevier.

at a relatively low reaction temperature (200−300°C) through the cationic polymerization mechanism, a homogeneous product with high naphthenic content, high solvent solubility, low softening point, and a monomodal narrow molecular weight distribution is produced. The gel effect (Tromsdorff−Norrish effect) caused by the rapid polymerization and gelation of polymers, which is often observable in radical polymerizations (Elias, 2013), can be avoided.

A wide variety of synthetic mesophase pitches can be made (Mochida et al., 2000, 2004) by varying the starting material (different ho-mooligomers), using mixed aromatic hydrocarbons (co-oligomers), mixing of different pitches (blends), or mixing isotropic and mesophase pitch together. Fig. 3.8 shows the effect of varying composition on the rheological properties of the pitch. The existence of methyl groups lowers the softening point (Korai et al., 1991; Mochida et al., 1993, 2006) and viscosity (Mochida et al., 1993, 2004) leading to improved spinnability. Stabilization reactivity is also improved, with stabilization completed within 10 min at 270°C (Huang, 2009). Methyl groups in the monomer also lead to much higher stacking (6 nm, around 18 aromatic planes) than other mesophase pitches. The degree of such stacking should also influence the properties of the resultant carbon fiber (Mochida et al., 2001).

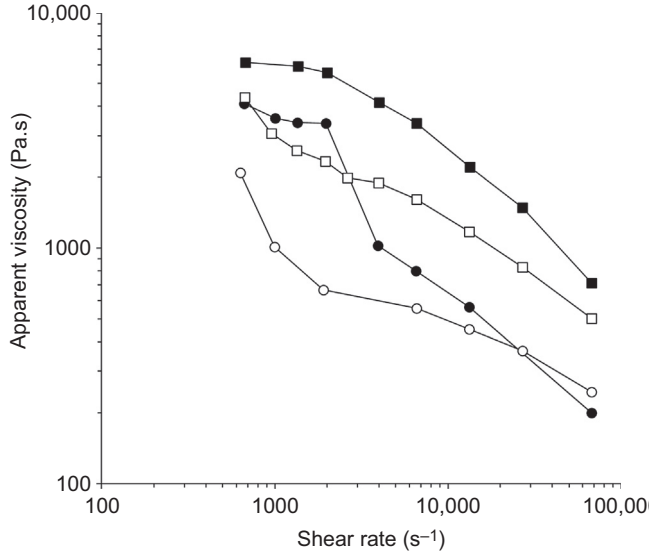

Figure 3.8 Relationship between viscosity and shear rate of mesophase pitches derived from naphthalene (■), methylnaphthalene (○), 3:7 methylnaphthalene/ naphthalene cooligomerization (□), and 3:7 methylnaphthalene/ naphthalene blending (●).
Adapted from Korai, Y., Yoon, S-H., Oka, H., Mochida, I., Nakamura, T., Kato, I., Sakai, Y., 1998. The properties of co-oligomerized mesophase pitch from methylnaphthalene and naphthalene catalyzed by HF/BF_3. Carbon 36, 369−375 with permission of Elsevier.

3.3 Manufacturing of carbon fibers

The conversion of mesophase pitch fiber to carbon fiber follows a similar process to that used to convert PAN polymer to carbon fiber. The first stage is to spin a fiber. In the case of mesophase pitch this involves hot melt spinning whereas PAN is solution spun from a solvent such as dimethylacetamide or dimethylsulfoxide. The fiber is then stabilized by heating in an oxidizing atmosphere, before being exposed to higher temperatures in an inert atmosphere to effect carbonization and graphitization. In general the tension is much lower for mesophase pitch fibers than traditionally used for PAN fibers to accommodate the low strength of the as-spun pitch fibers. The final stage involves surface treatment to protect the surface and prime it to promote adhesion with a matrix polymer.

3.3.1 Spinning of precursor fibers

3.3.1.1 General

The melt spinning of polymers is a relatively straightforward process, requiring the polymer to be heated until it melts and/or softens enough to extrude readily through a spinneret to produce fibers. The fibers are then cooled and drawn to impart molecular orientation and strength (Fig. 3.9). However, in the case of mesophase pitch the process is technically very challenging, mainly because of the extreme temperature sensitivity of the pitch and the brittle nature of the resultant fiber. Additionally, the mesophase spinning dope generally contains both anisotropic and isotropic phases, which, because of differences in their viscosities and densities, create inconsistencies in the spinning process (Huang, 2009). To successfully spin mesophase pitch the viscosity needs to be controlled in the range 10−200 Pa·s (Huang, 2009). There are a number of factors that affect the viscosity, namely, the nature of the raw material, temperature, flow rate, molecular weight, and mesophase content. All of these need to be optimized for melt spinning. In addition, there are numerous additional processing parameters such as cross air velocity, quench temperature, and winder velocity (drawing) that can have a dramatic effect on the pitch fiber properties. By applying heat, mass, and momentum balances, Edie and Dunham (1989) showed that the stress on mesophase fibers is extremely sensitive to small changes in these process conditions, easily reaching 20% of the stress required to break the fiber under typical process conditions. By contrast, during the melt extrusion of a nylon filament the tensile stress is typically $<1\%$ of the fiber strength (Edie, 1998).

The shear force aligns the anisotropic phase to form a well-oriented structure with a relatively large crystallite size (Huang, 2009). The stress profile on the fiber as a consequence of spinning and drawing influences the morphology of the mesophase fibers and in most cases this transverse microstructure is retained after carbonization. Typical transverse microstructures observed in carbonized mesophase fibers are shown in Fig. 3.10.

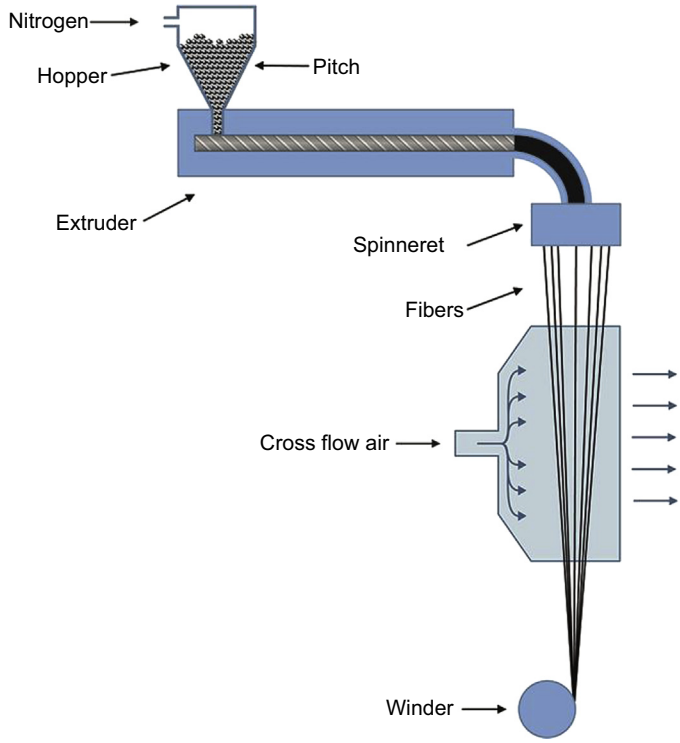

Figure 3.9 Process variables in a melt-spinning process.
Adapted from Edie, D.D., Dunham, M.G., 1989. Melt spinning pitch-based carbon fibers. Carbon 27, 647−655.

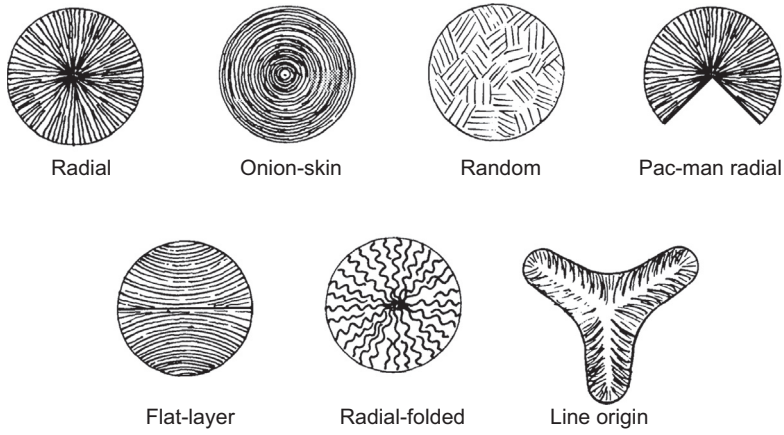

Figure 3.10 Typical transverse microstructures observed in pitch-based carbon fibers.
Adapted with kind permission from Springer Science+Business Media: Carbon Fibers, Filaments and Composites. In: Figueiredo, J.L., Bernardo, C.A., Baker, R.T.K., Hüttinger, K.J. (Eds.), Pitch and mesophase fibers, 1990, (Edie), Fig. 16.

3.3.1.2 Raw material

Natural pitches prepared from coal tar or petroleum residue have very different structures and molecular weights, originating from the lighter and heavier components, respectively, in their parent feedstock (Watanabe et al., 1999). This makes them difficult to spin and a lot of work has gone into developing methods to prepare different pitches for spinning. The processes all strive to modify the viscosity and softening point by manipulating the molecular mass distribution of the pitch and the ratio of isotropic to anisotropic material. The processes are often not distinguishable from the processes reported earlier for the conversion of isotropic pitch to mesophase pitch, involving the removal of volatile compounds followed by heat treatment to generate the anisotropic mesophase.

Hydrogenation is also sometimes used to improve the properties of mesophase pitch by introducing naphthenic groups (Mochida et al., 2004). The naphthenic groups help to maintain the low softening point necessary for stable spinning and reasonable stabilization reactivity. Hydrogenation has also been used to generate premesophase and dormant mesophase, which affords some advantages in spinning (Bahl et al., 1998).

The ratio of isotropic to anisotropic material is influenced by these treatments but can also be adjusted by blending isotropic and anisotropic pitches. Matsumura (1987) showed a strong dependence of the softening point on the isotropic content of a range of pitches (Fig. 3.11) while Yao et al. (2012) blended coal tar-derived isotropic pitch with 100% mesophase naphthalene-derived pitch and showed improved

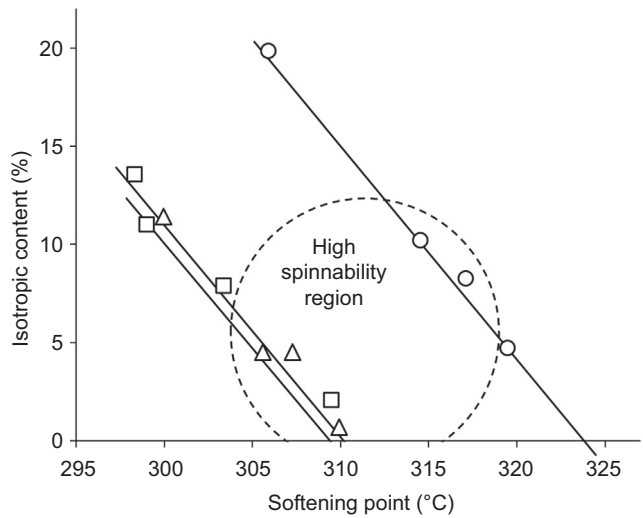

Figure 3.11 Influence of isotropic content and pitch type on softening point; QI less pitch (○), high distillate pitch (□), and high β-resin pitch (△).
Adapted from Matsumura, Y., 1987. Development of pitch-based advanced carbon materials. Journal of the Japan Petroleum Institute 30, 291−300.

spinnability for blends containing <30% isotropic pitch with no loss of carbon fiber properties. Toshima et al. (1992) showed that blending partially isotropic pitches prepared from naphthalene with a fluidized catalytic cracking-decant oil-derived mesophase pitch significantly reduced the viscosity, allowing better spinnability. The tensile strength of the resultant carbon fibers was significantly reduced by blending; however, the Young's modulus was considerably improved.

As stated earlier, for synthetic pitches the existence of methyl groups on the aromatic ring structures lowers the softening point (Korai et al., 1991; Mochida et al., 1993, 2006) and viscosity (Mochida et al., 1993, 2004) (Fig. 3.8) leading to improved spinnability (Huang, 2009; Korai et al., 1991).

3.3.1.3 Processing parameters

Spinning temperature

Viscosity is probably the single most important property that affects the spinnability of pitch and the easiest way to modify the viscosity is to alter the temperature. Fig. 3.12 shows that the viscosity–temperature data for a mesophase pitch, an isotropic pitch, and also a typical thermoplastic polymer (nylon 6) follows the Arrhenius equation, with the slope equal to the activation energy divided by the gas constant (E_a/R) (Edie and Dunham, 1989). The slope is thus a measure of the sensitivity of the viscosity to temperature changes. It is immediately obvious that mesophase pitch softens at a

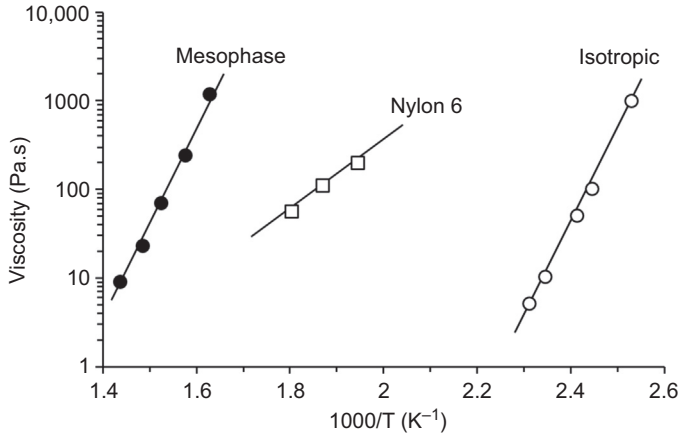

Figure 3.12 The dependence of viscosity on temperature for an isotropic petroleum pitch (Ashland 240), a mesophase pitch (produced by pyrolysis of Ashland 240), and nylon 6, a typical melt-spun thermoplastic.
Adapted with kind permission from Springer Science+Business Media: Carbon Fibers, Filaments and Composites. In: Figueiredo, J.L., Bernardo, C.A., Baker, R.T.K., Hüttinger, K.J. (Eds.), Pitch and mesophase fibers, 1990, (Edie), Fig. 8. Data from Whitehouse, S., Rand, B., 1987. Rheology of mesophase pitch from A240.In: 18th Biennial Conference on Carbon, American Carbon Society, Worcester, Mass, pp. 175–176; Edie, D.D., Dunham, M.G., 1989. Melt spinning pitch-based carbon fibers. Carbon 27, 647–655.

much higher temperature than isotropic pitch and that temperature has a much greater effect on the viscosity of pitch than typically seen for thermoplastics. It can be estimated that a 20°C decrease in temperature results in a three- to fivefold increase in viscosity for solvent-extracted mesophase pitch compared to a twofold increase for nylon 6.

This extreme temperature dependency is the primary reason why mesophase pitch is difficult to melt spin. Consequently, the temperature needs to be closely controlled. Spinning at too low a temperature leads to brittle fracture during drawing caused by the excessive viscosity. On the other hand, too high a temperature can lead to degradation and jet breakup of the pitch (Edie and Dunham, 1989). The spinning temperature affects the degree of orientation of as-spun fibers (Barnes et al., 1998; Yoon et al., 1993a, 1997), which in turn influences the structure of the melt-spun fiber (Jones et al., 1993) as well as that of the final carbon fiber (Hong et al., 2000; Jones et al., 1993; Matsumoto, 1985; Otani and Oya, 1986; Yoon et al., 1993a) including its propensity for crack formation (Yoon et al., 1993a, 1997). Otani and Oya (1986) spun fibers from two different pitches and showed that the structure varied from pac-man or cracked radial to radial to mixed or random and finally onion-skin as the temperature of spinning was increased (Fig. 3.13). While it is recognized that changing the spinning conditions can affect the final carbon fiber structure it appears that this macrostructure has little effect on the mechanical properties of the fibers (Huang and Young, 1995).

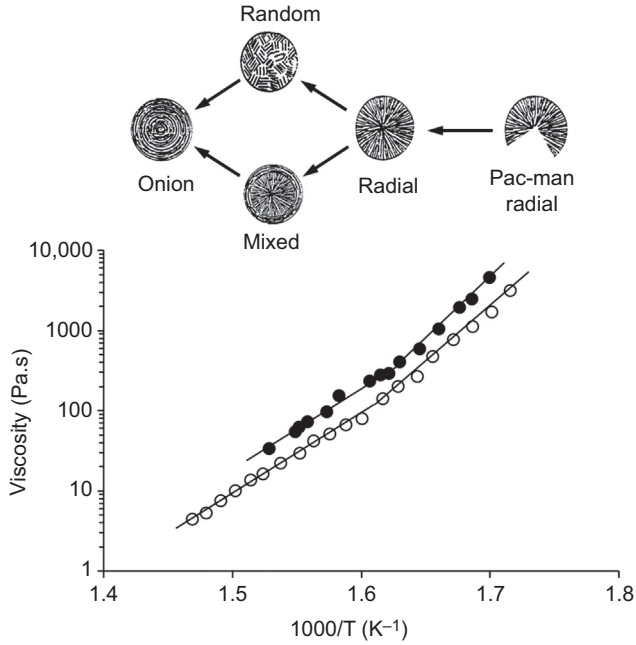

Figure 3.13 Temperature dependence of the viscosity of two different mesophase pitches and schematics of the microstructure of the fibers spun at temperatures from 300 to 400°C.
Adapted with permission from Otani, S., Oya, A., 1986. Progress of Pitch-Based Carbon Fiber in Japan. In: Petroleum-Derived Carbons. Copyright (1986) American Chemical Society.

Barnes et al. (1998) spun a naphthalene-derived mesophase pitch and reported an improved degree of orientation of the graphene basal planes with respect to the fiber axis as the spinning temperature was increased and a commensurate increase in orientation, tensile properties, and electrical conductivity for the associated final fibers. The fibers exhibited a radial-folded transverse texture at all spinning temperatures. This is consistent with the work of several researchers (Hamada et al., 1990; Matsumura, 1987; Yoon et al., 1993a, 1994b) who showed that the degree of alignment of crystallites increased with an increase in spinning temperature and hence a decrease in viscosity. The degree of alignment also increased with an increase in fiber diameter (Hamada et al., 1990; Lu et al., 2002b; Matsumura, 1987; Kurtz, 1983). The increased alignment as shear decreases is at odds with what is observed for typical thermoplastic polymers and comes about because of the polydomain liquid crystalline structure of mesophase pitch. It has been explained by Hamada et al. (1990) as a balance between the extent of microscopic disorder introduced during extrusion and the rate of recovery of the crystallites immediately after the extrusion from the capillary.

Increasing the melt-spinning temperature also results in an increase in crystallite size (L_c) (Hamada et al., 1990), a decrease in lattice or interplanar spacing (d_{002}), and an increase in tensile strength and modulus in the final carbon fiber (Jones et al., 1993; Korai et al., 1997). A more comprehensive dataset was obtained by Murakami et al. (1997) who tested seven different pitches derived from naphthalene, fluidized catalytic cracking-decant oil, and coal tar, and while all showed an increase in properties with decreased spinning viscosity some were more sensitive than others (Fig. 3.14). They claimed that aromaticity and the compactness factor of the pitch were closely related to the dependence of Young's modulus of carbon fibers on spinning viscosity; however, this is not readily apparent from the data presented. In general, spinning at higher temperature is preferred, providing a higher degree of orientation and thus better alignment as well as lower viscosity in the spinneret.

As a general principal, the orientation and perfection of crystallites that are developed in the as-spun pitch have a strong influence on the subsequent fiber properties. Yang et al. (2003) sought to exploit this idea by solid-phase annealing of mesophase pitch-derived spun fiber as a very simple and effective method to increase the properties of the final carbon fiber. They showed that annealing a methylnaphthalene-based pitch fiber at 200°C for 1 h improved the stacking height of the crystallites in the as-spun fiber from 3.5 to 5.0 nm and in its graphitized fiber from 40 to 90 nm, leading to improved thermal conductivity and tensile modulus of the graphitized fiber.

Flow rate, winder velocity and quenching conditions

The effects of flow rate are complex (Edie, 2001). Mesophase pitch behaves like a non-Newtonian fluid with viscosity decreasing as the flow rate increases (Edie, 2001; Korai et al., 1998; Mochida et al., 2004; Yoon et al., 1994b) (Fig. 3.8). Often three distinct regions are present, non-Newtonian behavior at low and high flow rates and Newtonian behavior at intermediate flow rates when the polydomain structure becomes fully deformed (Edie, 2001). Together with the winder velocity, the flow rate through the spinnerets dictates the drawdown ratio, and with the cross air temperature and

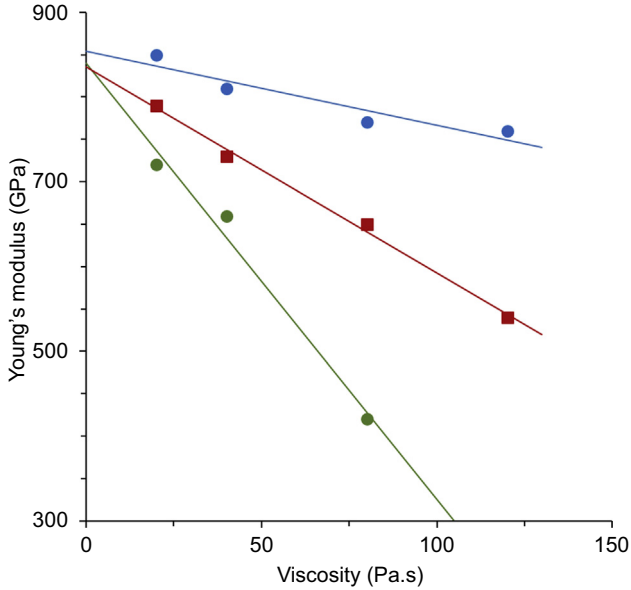

Figure 3.14 Effect of spinning dope viscosity on the tensile modulus of carbon fibers manufactured from naphthalene derived pitch (● and ●) and coal tar pitch (■). Adapted from Murakami, K., Toshima, H., Yamamoto, M., 1997. Effect of mesophase pitches on tensile modulus of pitch-based carbon fibers. Sen'i Gakkaishi 53, 73−78.

velocity it dictates the quench conditions. More rapid quenching hinders the stacking of the planar aromatic molecules during cooling, giving smaller L_c values (Yoon et al., 1993a), and also has a significant influence on the crystallite orientation (Kurtz, 1983). The drawdown ratio is defined as the ratio between the winder velocity and the flow rate, thus higher winding speeds or lower flow rates lead to greater drawdown. As discussed in the previous section, and unlike traditional thermoplastic polymers, this generally hinders crystallite alignment and leads to weaker fibers. A greater drawdown ratio also causes an increase in the velocity gradient along the fiber resulting in higher stress within the filament, thus limiting the fineness of the fibers that can be produced (Edie and Dunham, 1989). The alignment of crystallites in the melt-spun fiber is important as Barnes et al. (1998) have shown a strong correlation between as-spun and graphitized orientation.

Die shape

The structure of the fiber has also been shown to be sensitive to the shear stress generated at the spinneret and the residence time in the dye. These parameters are controlled by the diameter of the spinneret (D), the length of the die (L), and the D/L ratio and by varying them Matsumoto (1985) showed he could generate carbon fiber with radial, radial with a crack (pac-man radial), or random internal structure. The design of the die can also influence both the structure and properties of the resultant carbon fiber. Fig. 3.15 shows examples of three different designs leading to structures that have

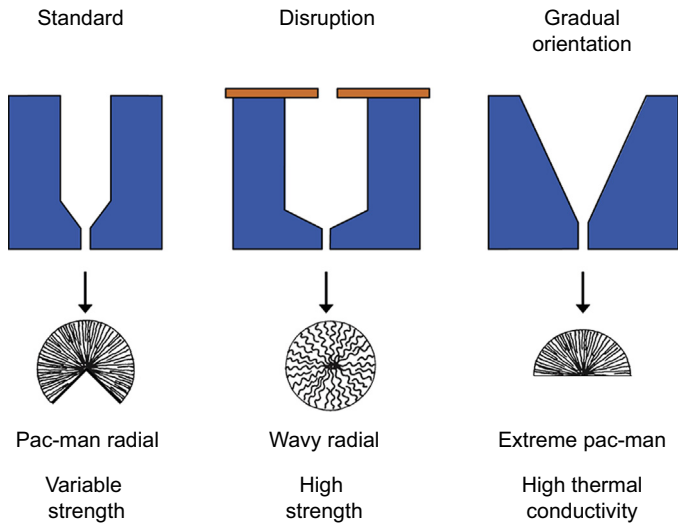

Figure 3.15 Different die designs and the effect on the resultant fiber structure and properties. Adapted from Bahl, O.P., Shen, Z., Lavin, J.G., Ross, R.A., 1998. Manufacture of carbon fibers. In: Donnet, J.-B., Wang, T.K., Rebouillat, S., Peng, J.C.M. (Eds.), Carbon Fibers. third ed. Marcel Dekker, New York with permission of Taylor and Francis Group LLC Books.

been labeled as pac-man radial, wavy radial, and extreme pac-man (Bahl et al., 1998). Similarly, Matsumoto et al. (1993) spun coal tar mesophase pitch using a spinneret with different shapes and sizes of cross-sections of the pitch reservoir. Disruption was investigated by adding a fine mesh filter to the reservoir. They found that the use of a reservoir of noncircular cross-section and a mesh filter resulted in a carbon fiber with a distorted radial-type structure in the transverse section, no crack along the fiber axis, and improved tensile strength.

3.3.2 Stabilization

Since mesophase pitch is a thermoplastic, if the fibers are heated they will eventually soften and flow leading to the sticking together of adjacent fibers or in the extreme case dripping and complete loss of fiber form. The softening point depends on the pitch precursor, the mesophase content, and the molecular mass and its distribution. Heating pitch in air to a temperature below this softening point results in dehydrogenation, cyclization, and most importantly crosslinking, thus stabilizing the fiber. Typically, mesophase pitch fibers are heated in the range 275−350°C for 5−60 min to achieve stabilization (Morgan, 2005a).

The reactions are exothermic (Chi and Shen, 1996; Stevens and Diefendorf, 1986; Yoon et al., 1994a) and result in a weight gain that is dependent on the composition of the pitch (Mochida et al., 1989; Yoon et al., 1994a; Yao et al., 2014), the environment (air or oxygen), the time and temperature of heating (Fathollahi et al., 2005a,b), the rate of heating (Yoon et al., 1993b), and the fiber diameter (Stevens and

Diefendorf, 1986; Yoon et al., 1994a). Elemental analysis confirmed that for pitch fibers stabilized at 260°C the mass increase is caused by increased oxygen content (Stevens and Diefendorf, 1986) while Shen et al. (1993, 2005) showed an increase in O/C ratio and a decrease in H/C ratio as the temperature of stabilization increased. Stevens and Diefendorf (1986) judged that a weight gain of approximately 6% is required to stabilize a fiber enough for carbonization, and showed that this could be achieved by heating a pitch fiber, spun from a solvent-extracted fraction of Ashland 240, in air for 40 min at 260°C. Heating for an additional hour only increased the oxygen content by a further 2% whereas changing the gas from air to oxygen doubled the weight gain.

The reaction is controlled by the oxidative reactivity of the aromatic pitch and the rate of diffusion of oxygen into the fiber. Depending on the time and temperature of the stabilization, as well as the physical dimensions of the fiber, the fiber can exhibit an oxygen gradient from the surface to the center of the fiber (Lu et al., 2002a; Matsumoto and Mochida, 1993; Mochida et al., 1989) (Fig. 3.16). This in turn can lead to a skin–core structure in the graphitized fiber (Lu et al., 2002a; Mochida et al., 1990b). A possible sequence of reactions leading to the formation of oxygen bridge-like crosslinks has been suggested by Shen et al. (2005) and is depicted in Fig. 3.17.

The as-spun mesophase pitch fiber is quite weak with a tensile strength of about 40–60 MPa and a modulus of less than 5 GPa (Mochida et al., 1988a,b; McHugh et al., 1992). Stabilization improves the properties; however, the fibers are still weak. Matsumoto and Mochida (1993) showed that the strength increase was dependent on the temperature of stabilization but could be as much as fivefold.

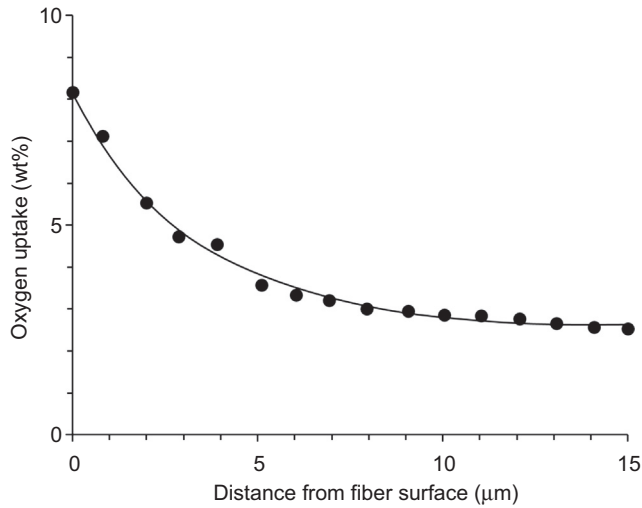

Figure 3.16 Electron probe X-ray microanalysis data showing the concentration of oxygen in a 30 μm coal tar-derived mesophase pitch fiber stabilized in air at 300°C for 15 min.
Adapted from Mochida, I., Toshima, H., Korai, Y., Hino, T., 1989. Oxygen distribution in the mesophase pitch fibre after oxidative stabilization. Journal of Materials Science 24, 389–394.

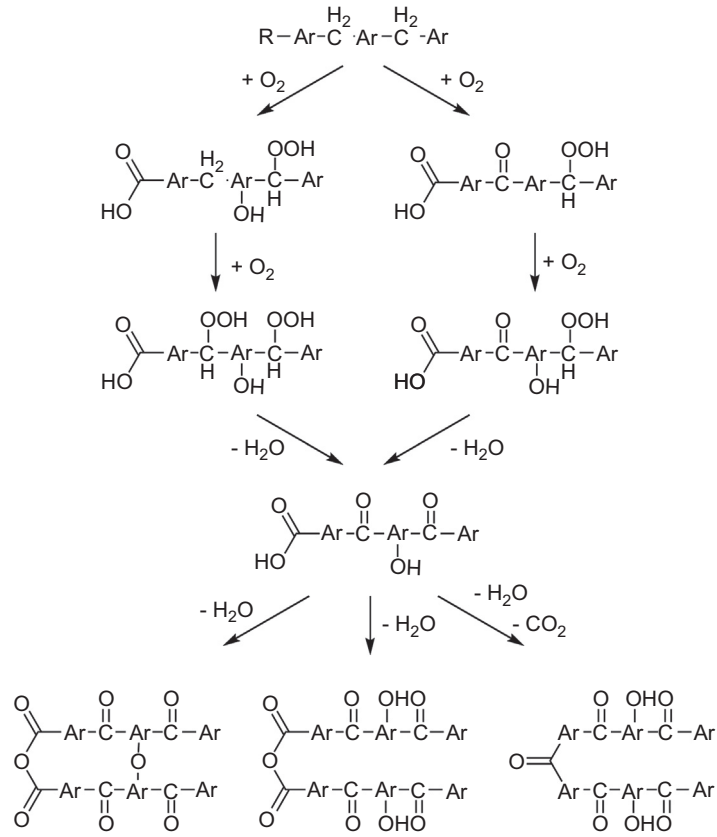

Figure 3.17 Proposed reaction sequence for the oxidation of pitch during stabilization. Reproduced from Shen, Z.-M., Chi, W.-D., Zhang, X.-J., Chang, W.-P., 2005. Carbon fibers from petroleum pitch. New Carbon Materials 20, 1−7 with permission of Elsevier.

The low strength of the as-spun fiber requires that the oxidation ovens are designed so that the weak pitch fiber never has to support its own weight until after it is carbonized. Fibers may be supported by a conveyor belt but more often are oxidized while still on the spool used for spinning. The heat-resistant spool is specially designed (Barnett, 1959) to allow ready ingress of the oxidizing gas and easy removal of heat generated during the exothermic reaction.

Matsumoto and Mochida (1993) showed that increasing the stabilizing temperature increased the strength of the stabilized fiber; however, the effect on the final graphitized fiber properties was complicated (Liu, 2010; Matsumoto and Mochida, 1992; Mochida et al., 1994; Shen et al., 1993, 2005; Yoon et al., 1994a). Matsumoto and Mochida (1992) showed that both the oxidizing temperature and the time to reach this temperature influenced the final carbon fiber properties with the graphitized fiber showing the maximum tensile properties whenever the oxidized fiber gained the maximum weight, regardless of the heating rates. In contrast, Shen et al. (2005) found

that there was an optimum oxygen content to achieve maximum tensile strength of the final graphitized carbon fiber. For a petroleum-based mesophase pitch fiber the optimum was 8% oxygen, achieved during stabilization at 300°C. Yoon et al. (1994a) showed that slower heating rates resulted in improved tensile properties of the resultant carbon fiber and attributed the improvement to less decomposition of oxygen functional groups during the stabilization, resulting in fewer defects being introduced into the fiber. Mochida et al. (1994) reported that the maximum tensile strength was dependent not only on the final stabilization temperature but also on the rate of heating to reach the stabilizing temperature and the spinning temperature (Fig. 3.18(a)). The tensile modulus was similarly dependent on these parameters (Fig. 3.18(b)). Both

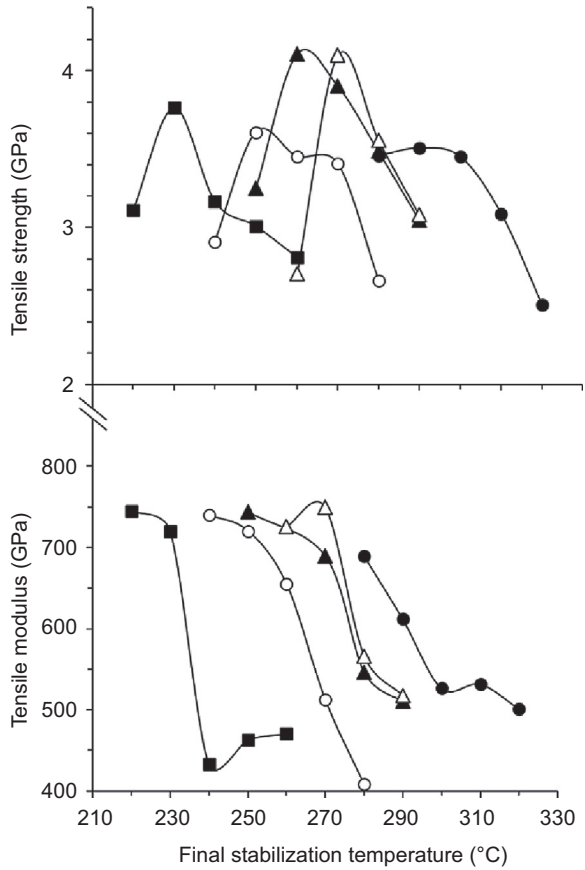

Figure 3.18 Relationship between the tensile properties and the final stabilizing temperature. Spinning temperature and heating rate at stabilization: ■, 315°C, 0.1°C/min; ○, 325°C, 0.5°C/min; ▲, 315°C, 0.5°C/min; △, 310°C, 0.5°C/min; ●, 315°C, 2.0°C/min.
Adapted from Mochida, I., Ling, L., Korai, Y., 1994. Some factors for the high performances of mesophase pitch based carbon fibre. Journal of Materials Science 29, 3050−3056 with kind permission from Springer Science+Business Media, Figs. 1 and 2.

McHugh et al. (1992) and Liu (2010) showed that the soak time was also critical. Increasing the soak time from 60 to 360 min at 360°C resulted in a 46% increase in tensile strength and 163% increase in modulus of the resultant carbon fiber (Liu, 2010). By adopting a two-step stabilization (275°C/1 h followed by 375°C/1 h) Liu could achieve similar improvements in properties (46% increase in tensile strength and 222% increase in modulus) at much shorter times. Oxidation temperature has also been shown to influence the electrical resistivity and thermal conductivity of the final fiber (Ma et al., 2006).

The presence of naphthenic groups, short alkyl side chains, and isolated aromatic C−H in the pitch is believed to increase the reactivity of pitch and allow stabilization in a relatively short time (Mochida et al., 1991a). Thus mesophase pitch prepared from coal tar pitch or petroleum pitch is generally less reactive to oxidation than synthetic pitch (Huang, 2009; Mochida et al., 1990a, 2000). Hydrogenation may be used to improve mesophase pitch by introducing naphthenic groups into the precursor pitch with the aid of a hydrogen donor solvent or catalyst but the process is costly (Mochida et al., 2000). Yoon et al. (1994a) reported that pitch fiber from both methylnaphthalene and naphthalene-derived mesophase pitches showed higher oxidation reactivity than natural pitch from coal tar or petroleum. The existence of methyl groups increased the stabilization reactivity, thus mesophase pitch based on methylnaphthalene is more reactive than pitch derived from naphthalene (Korai et al., 1991; Yoon et al., 1993b, 1994a).

Attempts have also been made to stabilize fibers by extracting chemical structures with limited oxidative reactivity from coal tar pitch using a solvent such as tetrahydrofuran or benzene (Park et al., 1988a,b). The extraction is intended to act as a stand-alone stabilization method allowing direct carbonization (Park et al., 1988b) or in combination with thermal stabilization to shorten the process (Park et al., 1988a). The combination of thermal oxidation and solvent extraction has also been used to produce fibers with a skin−core structure (Mochida et al., 1991b).

Since the stabilization reaction is controlled by the diffusion of oxygen into the fiber, which is a slow process, there is a temptation to raise the temperature to drive the reaction. However, the reaction is strongly exothermic ($\sim$2000 J/g of fiber), thus there is the danger of the reaction becoming autocatalytic, creating the equivalent of a charcoal fire and destroying the fiber (Lavin, 2001). Also at about 270°C, the Boudouard reaction becomes important. In this reaction, oxygen is chemisorbed onto the surface of the fiber and reacts with the carbon. During carbonization it is removed as CO and CO_2, potentially causing pitting and a loss of strength in the carbonized fiber.

3.3.3 Carbonization and graphitization

To develop the final mechanical properties the stabilized fiber must be further heat treated. This is done in an inert atmosphere, typically in two stages called carbonization and graphitization. The fibers are still relatively weak; however, since the basic alignment is introduced at the spinning step (Mochida et al., 1996) pitch-based carbon

fiber can undergo carbonization and graphitization with the fiber in the relaxed state, an advantage over PAN-based fiber (Lavin, 2001). Carbonization is generally carried out at temperatures below 2000°C and may itself involve several stages. A typical carbonizing heat treatment in inert nitrogen may involve 0.5−5 min at 700°C followed by 0.5 min at 900°C and then final heating in the range from 1500 to 2000°C (Morgan, 2005a). During the first stage of carbonization (sometimes referred to as precarbonization) heteroatoms such as H, N, O, and S are eliminated in the form of H_2O, CO, N_2, SO_2, CH_4, H_2, and CO_2 resulting in a substantial weight loss and a reduction in diameter of about 15% (Liu, 2010; Ogale et al., 2002). As a general rule this diameter reduction is less in pitch-based fibers than PAN-based fibers because of the higher carbon content of pitch compared to PAN. Partly because of this, but mainly because of the difficulty of spinning fine pitch-based fibers, the pitch-based fibers generally have a greater diameter. If carbonization is carried out too rapidly then the rapid evolution of these volatiles can result in the disruption of the structure and the creation of defects leading to a loss of strength in the final carbon fiber (Jones et al., 1997). Jones et al. (1997) showed two major increases in crystallite misalignment during heat treatment and ascribed them to the release of CO_2 and CO at 300°C followed by the release of CH_4 and H_2 at around 500−600°C. As these molecules diffuse through the fibers, they disrupt the crystallites, increasing the amount of basal plane misorientation with respect to the fiber axis. At temperatures above 1000°C the main gas evolved is H_2 (Edie, 1990) with pitch molecules reacting to form the final turbostratic graphite-like structure.

Graphitization involves heat treating for 10 s to 5 min at temperatures above 2000°C, often approaching 3000°C (Lavin, 2001; Mochida et al., 1991b; Morgan, 2005a). While some volatiles are still eluted from the fiber, the main changes taking place are an increase in the axial alignment, size, and perfection of crystalline lamellae (Bright and Singer, 1979; Ogale et al., 2002; Morgan, 2005d).

The exact dwell or soak times and temperatures of heat treatment, along with the choice of pitch and the spinning and stabilization conditions, can be varied to produce a range of grades of carbon fiber. Efforts have also been made to reduce the cost of production by reducing the time of heating. Greene et al. (2002) reported significant structural evolution and property development for a furnace residence time as brief as 0.7 s at 3000°C, and used a simple energy consumption analysis to show that this process may have cost benefits.

3.3.4 Surface treatment

Prior to winding the continuous filaments on bobbins, the surface of carbon fiber is usually treated to improve handling properties and adhesion to the matrix resin. Treatment is the same as that used for PAN-based fibers and generally involves some form of oxidation to increase the surface energy of the fiber, followed by the application of a coating or size.

A range of oxidizing treatments exists, but most commonly a continuous electrolytic surface treatment process is employed, which permits a good measure of control to be exercised. The fiber is made the anode by passing it over an anodic roller in a setup as

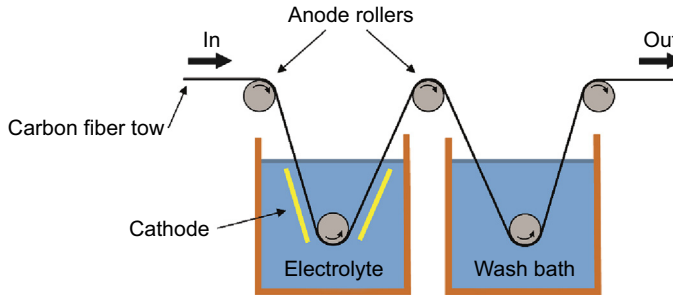

Figure 3.19 Schematic diagram depicting the continuous electrolytic surface treatment process. Adapted from Morgan, P., 2005b. Guidelines for the Design of Equipment for Carbon Fiber Plant. Carbon Fibers and Their Composites with permission of CRC Press, Boca Raton, FL.

depicted in Fig. 3.19. Many different electrolytes have been used, but typically these are water soluble compounds such as ammonium bicarbonate, sodium hypochlorite, sulfuric acid, or nitric acid (Morgan, 2005f). Ammonium bicarbonate, which decomposes at a relatively low temperature, is particularly attractive since any residual electrolyte will volatilize during drying. During the electrolytic process, oxygen is produced at the anodic carbon fiber surface, which reacts with the fiber to produce oxygen containing chemical groups and in the process roughens the surface of each filament. Together the reactive chemical groups and the increased surface area improve wetting and bonding between the fiber and matrix. The electrical current requirements for the surface treatment of high modulus fiber are relatively high and there can be an appreciable heating effect. This may necessitate cooling of the electrolyte to control the rate of treatment and in some cases to avoid thermal decomposition (Morgan, 2005c).

The varied forms of oxidative treatment that can be used with carbon fibers are well reviewed for PAN-based fibers by Morgan (2005f); however, much less information is reported in the literature for pitch-based fibers. Itoi and Yamada (1992) treated pitch-based carbon fiber with nitric acid and hydrogen peroxide and obtained improved polyethernitrile composites. Improvements in fiber/matrix adhesion has been shown for epoxy composites after treatment of the pitch-based carbon fiber with hydrogen peroxide solution (Lin and Yip, 1989), oxygen and nitrogen ion beams (Lin and Yip, 1993), and in an electrolytic process using ammonium bicarbonate, sodium bicarbonate, sodium carbonate, sodium hydroxide, and sulfuric acid as the electrolyte (Nakanishi et al., 1995; Yumitori and Nakanishi, 1996a,b). For two PAN-based and two pitch-based carbon fibers, interfacial shear strength (IFSS) was shown to be correlated with the combined oxygen plus nitrogen concentration on the fiber surface, independent of fiber type (Nakanishi et al., 1995). In contrast, sizing content had no effect on IFSS. Redick and Barnes (1986, 1991) claimed that the exposure of pitch-based carbon fibers to ozone for as little as 30 s resulted in an increase of 60−70% in the IFSS of the carbon fiber/epoxy composite manufactured from the treated fiber, signifying improved fiber/matrix adhesion. Rich et al. (2009, 2013) showed a synergistic effect when ozone was used in the presence of high intensity ultraviolet light. In studies on both PAN- and pitch-based carbon fibers

they showed significant increases in the IFSS for both fiber types. For the composite made from the pitch-based carbon fiber (Dialead K63712), the IFSS more than doubled after treatment. The ultraviolet light plus ozone treatment did not adversely affect the fiber tensile properties.

Sizing is reputed to improve interfilamentary adhesion, aid in wetting out the fiber in resin matrices, and act as a lubricant to prevent fiber damage during subsequent textile processing such as weaving (Morgan, 2005f). It is generally applied by deposition from a polymer solution, by passing the tow through a bath containing the sizing material as depicted in Fig. 3.20. Alternative methods include electrodeposition, electropolymerization, and plasma polymerization (Morgan, 2005f). Initially, solvent-based sizes were used, which gave excellent interfilament penetration, but these were discontinued on health and cost grounds. Invariably, the present sizes are water-based emulsions, preferably using the same chemical class as the ultimate polymer matrix (Morgan, 2005c). It is normally applied at a level of 1−2% and formulated to be compatible with epoxy-based composites (Mason, 2004). With the growth of nonepoxy thermosets as well as carbon fiber-reinforced thermoplastics, specialty sizing optimized for a specific matrix is now available and may become more important in the future.

3.4 Structure and properties

3.4.1 Heat treatment temperature and structure

Carbon fiber has a structurally disordered or turbostratic structure, which develops during the carbonization and graphitization stages of production (Fig. 3.21). The graphite

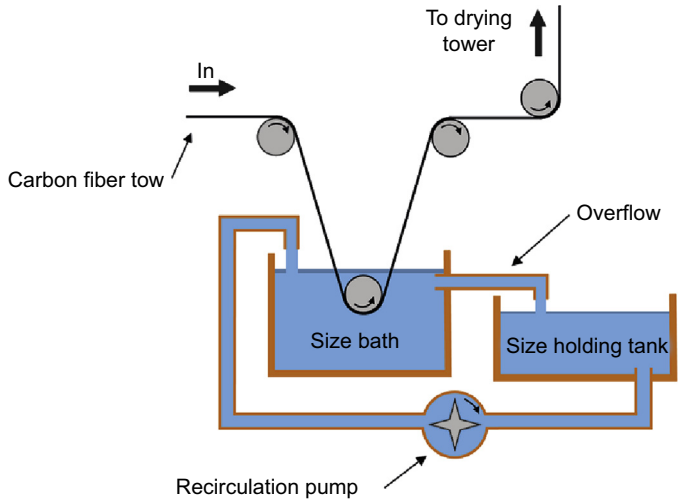

Figure 3.20 Schematic diagram depicting the application of a polymeric size to the fiber surface. Adapted from Morgan, P., 2005b. Guidelines for the Design of Equipment for Carbon Fiber Plant. Carbon Fibers and Their Composites with permission of CRC Press, Boca Raton, FL.

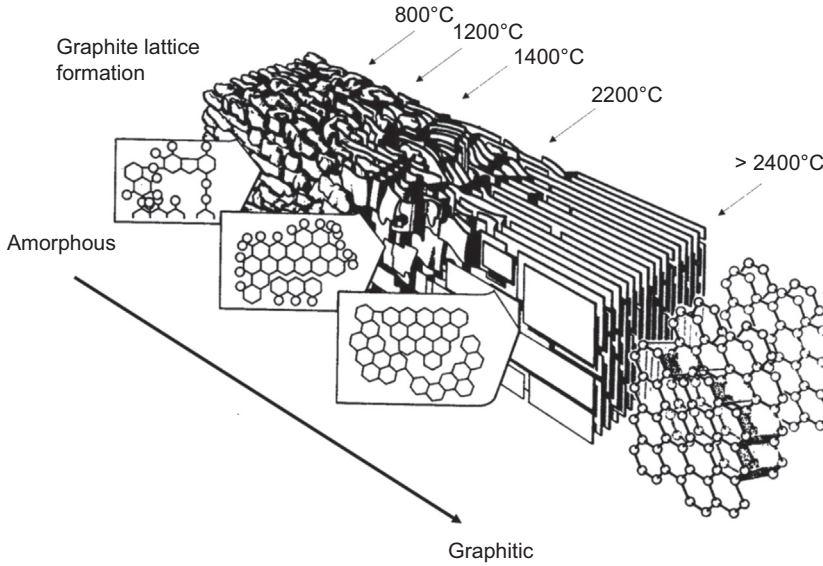

Figure 3.21 The evolution of the structure of pitch-based carbon fiber as nongraphitic mesophase is converted to graphitized carbon as it progresses through carbonization and graphitization.
Adapted from Marsh, H., Griffiths, J., 1982. A high resolution electron-microscopy study of graphitization and graphitizable carbon. In: International Symposium on Carbon: New Processing and New Applications, Toyohashi, Japan, pp. 81−83.

crystallites become larger, denser, and more aligned with the fiber axis during the process, leading to a dramatic improvement in tensile and thermal properties. As the heat treatment temperature increases, the graphite crystallites (Fig. 3.5) increase in size both perpendicular to (L_c) and parallel to (L_a) the graphite layers (Bright and Singer, 1979; Fitzer, 1989; Fitzer and Manocha, 1998; Jones et al., 1997; Matsumoto, 1985; Ogale et al., 2002; Shen et al., 2005; Takaku and Shioya, 1990) (Fig. 3.22). Concurrently, there is a decrease in the interplanar spacing (d_{002}) of the crystallites (Bright and Singer, 1979; Fitzer, 1989; Fitzer and Manocha, 1998; Jones et al., 1997; Ogale et al., 2002; Shen et al., 2005; Takaku and Shioya, 1990) (Fig. 3.22). With increased temperature the interplanar spacing approaches the theoretical value of 0.335 nm for graphite (Kowalski, 1987). In addition, Takaku and Shioya (1990) reported a substantial increase in the volume fraction of crystallites; from 50% when heated to 1200°C to about 90% when heated to 2600°C. At the same time there was a small increase in the microvoid content from 0 to 2%. The large size of these pores, as measured by small angle X-ray scattering, has been suggested as the most likely cause of the much lower tensile strength in pitch-based fibers when compared to PAN-based fibers (Ozcan et al., 2014).

The full width at half maximum (FWHM), in degrees, of the intensity of the wide angle X-ray scattering (WAXS) azimuthal scan is a commonly used measure of the graphene layer degree of misorientation (Ruland, 1968). Fig. 3.23 shows the results

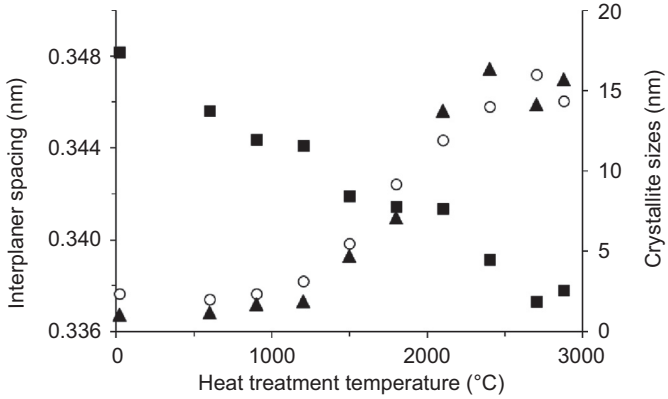

Figure 3.22 Change in interplanar spacing (■) and crystallite dimensions (L_c, ○; L_a, ▲) for a synthetic pitch fiber heat treated to various temperatures.
Adapted from Ogale, A.A., Lin, C., Anderson, D.P., Kearns, K.M., 2002. Orientation and dimensional changes in mesophase pitch-based carbon fibers. Carbon 40, 1309−1319 with permission of Elsevier.

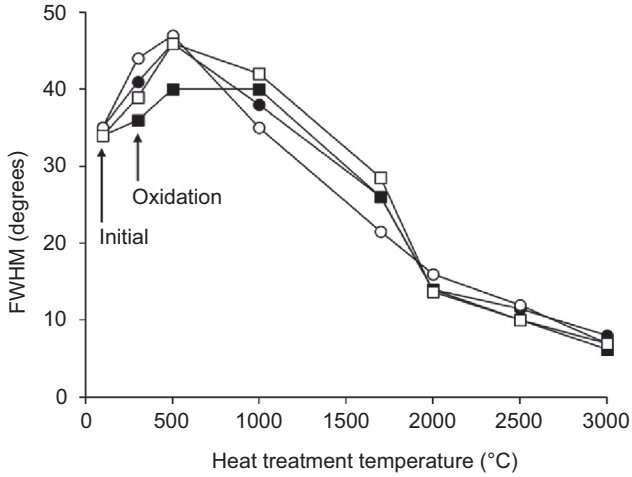

Figure 3.23 Effect of oxidation as well as carbonizing and graphitizing temperature on the degree of misorientation (FWHM) of mesophase pitch fibers with a radial (○, ●) or random (□, ■) structure and oxidized in a single (open symbols) or two-stage (closed symbols) process.
Adapted from Bright, A.A., Singer, L.S., 1979. The electronic and structural characteristics of carbon fibers from mesophase pitch. Carbon 17, 59−69 with permission of Elsevier.

for four petroleum-based pitch fibers having either a radial or predominantly random transverse structure and stabilized via either a one-stage process or a two-stage process. After stabilization and at low carbonizing temperatures there are slight differences between fibers with different structures and stabilization procedures; however, above 2000°C these differences disappear. The results suggest that there may be some deterioration in alignment at low carbonizing temperatures; however,

above 1000°C the crystallite orientation increases dramatically for all four fiber types as the heat treatment temperature increases. Jones et al. (1997) and Ogale et al. (2002) showed similar results for naphthalene-based mesophase pitch fibers. Several workers (Jones et al., 1997; Yuan et al., 2014) used Raman spectroscopy D/G ratios as a measure of the graphitization of the fiber. The G (graphitic) and D (disordered-induced) bands occur around 1580 cm^{-1} and 1350 cm^{-1}, respectively and are attributed to stretching vibrations of the sp^2 (graphitic) and sp^3 (disordered or diamond-like) geometries of carbon C−C bonds (Huson et al., 2014). D/G ratios initially increase (Jones et al., 1997) showing the disruption to the structure caused by the evolution of gases during the early stages of carbonization (Fig. 3.24). Consistent with the WAXS results this is followed by a rapid decrease in disorder at temperatures above 1000°C (Jones et al., 1997; Yuan et al., 2014) with a ribbon-shaped fiber graphitized at 3000°C having a Raman spectrum similar to that of stress-annealed pyrolytic graphite (Yuan et al., 2014).

3.4.2 Tensile properties

The increased size, volume fraction, and alignment of the crystallites, as well as the reduced interplanar spacing, result in a significant increase in the properties of the carbon fiber. Several authors have shown that tensile strength and modulus increase with heat treatment temperature, with the modulus generally increasing more sharply in the graphitization temperature range (Bright and Singer, 1979; Edie, 1990; Matsumoto, 1985; Mochida et al., 1994; Yuan et al., 2014; Shen et al., 2005; Qin et al., 2012). Fig. 3.25 shows the results for mesophase pitch derived from naphthalene.

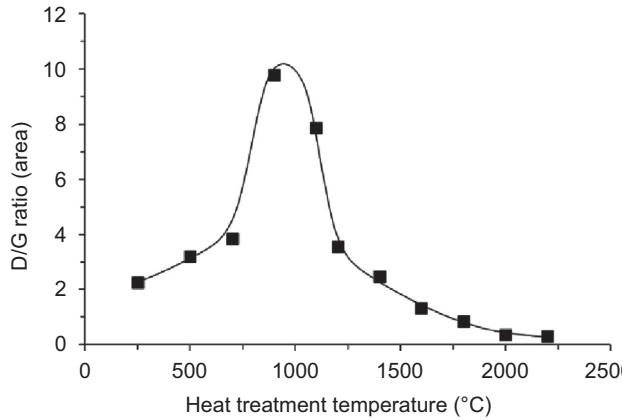

Figure 3.24 Effect of carbonizing and graphitizing temperature on the degree of graphitization, as measured by the D/G ratio, of a synthetic pitch-based fiber.
Adapted from Jones, S.P., Fain, C.C., Edie, D.D., 1997. Structural development in mesophase pitch based carbon fibers produced from naphthalene. Carbon 35, 1533−1543 with permission of Elsevier.

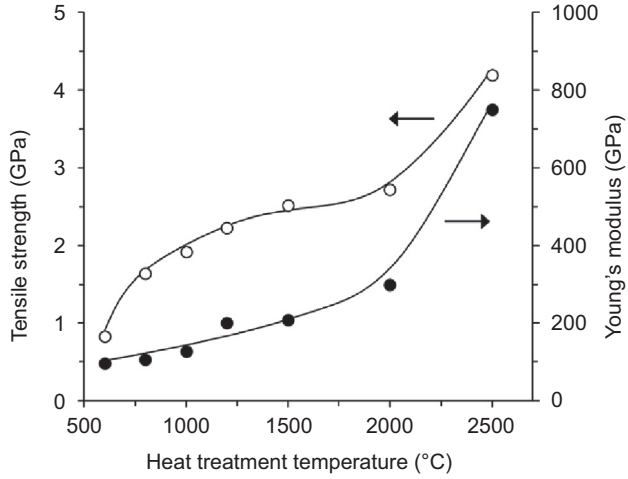

Figure 3.25 Change in tensile strength and modulus of mesophase pitch fibers as a function of carbonizing and graphitizing temperature.
Adapted with kind permission from Springer Science+Business Media: Journal of Materials Science, Some factors for the high performances of mesophase pitch based carbon fibre, vol. 29, 1994, 3050−3056, (Mochida et al.), Fig. 6.

While it is well known that as the graphitization temperature increases, modulus, tensile strength, and crystallite size (L_a and L_c) increase and interplanar spacing decreases (Ogale et al., 2002; Bright and Singer, 1979; Fitzer, 1989; Jones et al., 1997; Matsumoto, 1985; Mochida et al., 1994; Shen et al., 2005; Takaku and Shioya, 1990), there has been no detailed report showing the extent of the correlations between the different parameters. The modulus has, however, been shown to be strongly correlated with the degree of orientation of the graphite crystallites (Barnes et al., 1998; Bright and Singer, 1979; Brydges et al., 1969; Fitzer and Manocha, 1998; Johnson and Watt, 1967; Matsumura, 1987). Bright and Singer (1979) show a strong exponential relationship (Fig. 3.26) between the modulus of the fiber and the crystallite alignment as measured by WAXS. Note that the trendline extrapolates back to 1045 GPa, close to the value of 1065 GPa for perfectly oriented graphite. Fitzer (1989) and Fitzer and Manocha (1998) showed a similar exponential relationship.

All the mesophase pitch-based fibers have a sheet-like microstructure. As the modulus increases, the crystallite sheets tend to be more well defined and less curved (Huang and Young, 1995). Fig. 3.27 shows this for the ultrahigh modulus K13D2U fiber, which has a modulus of 940 GPa (Naito et al., 2008).

3.4.3 Electrical resistivity and thermal conductivity

One of the distinguishing features of mesophase pitch-based carbon fiber is the very high level of thermal conductivity attainable. Values of up to 1120 W/m K have been reported at room temperature (Adams et al., 1998; Gallego and Edie, 2001;

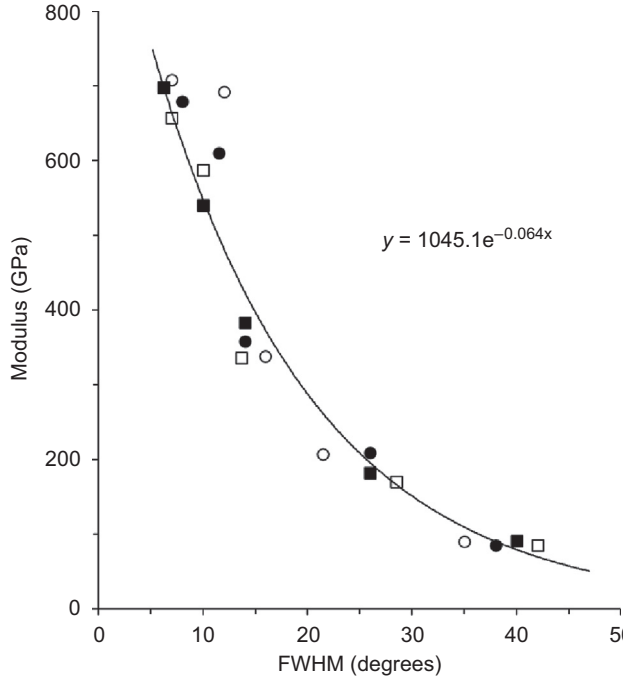

Figure 3.26 Tensile modulus of petroleum-based mesophase pitch fibers as a function of orientation of the crystallites. Note that FWHM is a measure of the misorientation. The data are for mesophase pitch fibers with a radial (○, ●) or random (□, ■) structure and oxidized in a single (open symbols) or two-stage (closed symbols) process.
Adapted from Bright, A.A., Singer, L.S., 1979. The electronic and structural characteristics of carbon fibers from mesophase pitch. Carbon 17, 59−69 with permission of Elsevier.

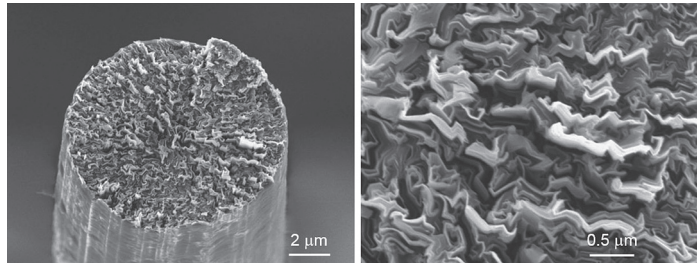

Figure 3.27 SEM image of the fracture surface of a K13D2U fiber at low (left) and high (right) magnification showing the sheet-like microstructure.
Reproduced from Naito, K., Tanaka, Y., Yang, J.-M., Kagawa, Y., 2008. Tensile properties of ultrahigh strength PAN-based, ultrahigh modulus pitch-based and high ductility pitch-based carbon fibers. Carbon 46, 189−195 with permission of Elsevier.

Ma et al., 2006), almost three times the levels found for copper (Edie et al., 1993; Lavin et al., 1993). If the data are normalized to account for the higher density of the metals then the specific thermal conductivity is more than10 times that of copper. Several researchers (Heremans et al., 1985; Kowalski, 1987; Lavin et al., 1993; Lu et al., 2002a; Zhang et al., 2000) have shown a strong relationship between electrical resistivity (ρ) and thermal conductivity (K) (Fig. 3.28) with Lavin et al. (1993) proposing the hyperbolic relationship:

$$K = 440,000/(100\rho + 258) - 295$$

where ρ is expressed in μΩm and K is expressed in W/m K. More recently Emmerich (2014) used a model of continuous defective graphene nanoribbons, arranged in stacks, to predict the relationship between several physical properties (modulus, K, ρ, CTE, and L_a) of mesophase pitch-based carbon fibers. The relationship between ρ and K was given by:

$$K = 1/(0.0001949 + 0.0007090\rho)$$

From the data plotted in Fig. 3.28 it can be seen that the Lavin equation predicts the thermal conductivity very well for a wide range of carbon fibers but underestimates the

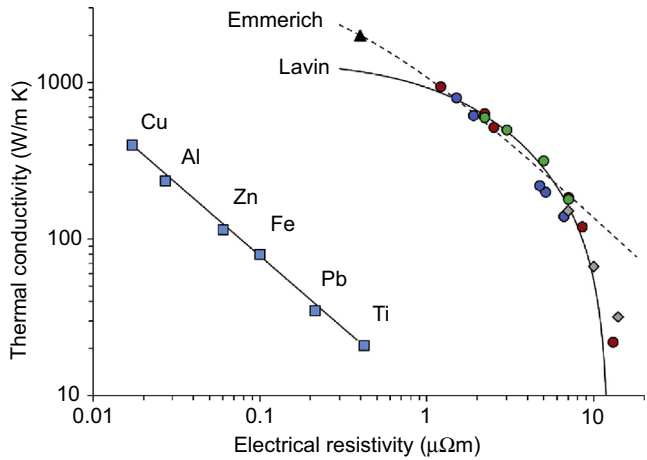

Figure 3.28 Relationship between thermal conductivity and electrical resistivity for a range of mesophase pitch-based carbon fibers (Cytec, ●; Mitsubishi, ●; NGF, ●), PAN-based carbon fibers (◆), as well as single crystal graphite (▲) and some typical metals (■).
Adapted from Kowalski, I.M., 1987, New high performance domestically produced carbon fibers. In: Carson, R., Burg, M., Kjoller, K.J. & Riel, F.J. (Eds.) 32nd International SAMPE Symposium. Anaheim, CA. Reprinted by permission from the society for the Advancement of Material and Process Engineering (SAMPE). The data used are from Emmerich, F.G., 2014. Young's modulus, thermal conductivity, electrical resistivity and coefficient of thermal expansion of mesophase pitch-based carbon fibers. Carbon 79, 274−293.

thermal conductivity of graphite by almost 50%. The Emmerich equation, on the other hand, predicts the thermal conductivity very well for graphite and the highly graphitized fibers, but overestimates the thermal conductivity of the less graphitized fibers by a considerable margin. Fig. 3.28 includes values for typical metals and shows that pitch-based carbon fibers can match, and in some cases exceed, the thermal conductivity of metals; however, the electrical conductivity is still several orders of magnitude lower. Because of the difficulty of measuring thermal conductivity it is often calculated based on one of the relationships described above (Edie et al., 1993; Yuan et al., 2014).

The enhanced perfection and orientation of the crystallites that results in high modulus fibers also has a profound effect on the electrical and thermal properties of the carbon fibers. The increased crystallite size, reduced interplanar spacing, and improved orientation result in a decrease in electrical resistivity and an increase in thermal conductivity. Heremans et al. (1985) investigated the electrical and thermal properties of pitch-based, PAN-based, and vapor-grown fibers and showed that, regardless of source, there was a strong correlation between electrical resistivity and crystallite dimensions, with resistivity decreasing as crystallite size increased and interplanar spacing decreased (Fig. 3.29). They used X-ray diffraction to measure the crystallite thickness (L_c) and interplanar spacing and coupled these results with thermal conductivity data to deduce the defect-limited phonon mean free path (L_ϕ), which is a measure of the in-plane order and approximately equal to the crystallite length (L_a). Similar correlations were found between the crystallite dimensions and the thermal conductivity. Consistent with Heremans' results, Barnes et al. (1998) showed, in a limited number of petroleum pitch-based graphitized fibers, that the electrical resistivity decreases as a result of increases in L_a and L_c and a decrease in interplanar spacing. They also showed that the reduced electrical resistivity was associated with improved orientation of the crystallites along the fiber axis. Adams et al. (1998) constructed a composite plot of thermal conductivity (K) versus interplanar

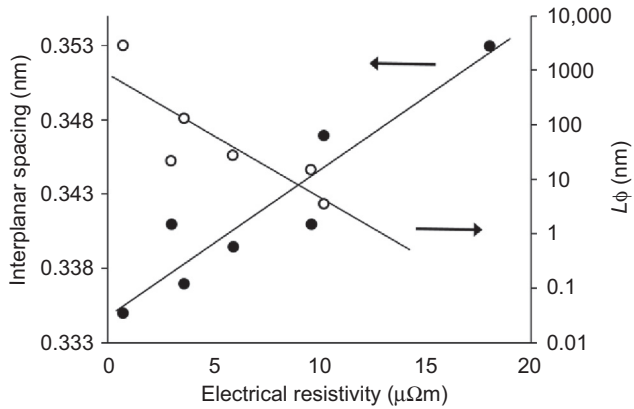

Figure 3.29 Relationship between electrical resistivity and crystallite dimensions for a range of pitch-based and PAN-based carbon fibers.
Data from Heremans, J., Rahim, I., Dresselhaus, M.S., 1985. Thermal conductivity and Raman spectra of carbon fibers. Physical Review B 32, 6742−6747.

spacing (d_{002}) for the five mesophase pitch fibers they had characterized as well as the data from Heremans et al. (1985), supplier data, and data from Nysten et al. (1991). They showed a general trend of increasing K with decreasing d_{002}; however, in the low-K regime, large decreases in interplanar spacing down to about 0.338 nm only had a small effect on K. They postulated that in this regime, the structure is essentially turbostratic, and defects greatly limit thermal transport (Fig. 3.30).

Several authors (Lavin et al., 1993; Wang et al., 2008) have shown the temperature dependence of resistivity and thermal conductivity with the conductivity being particularly sensitive to temperature. In an attempt to make fibers with superior thermal conductivity, many authors (Edie et al., 1993, 1994; Ma et al., 2006; Yuan et al., 2014) have produced ribbon-shaped mesophase pitch-based fibers, on the grounds that fibers with a rectangular cross-sectional shape show better crystallite orientation than those of traditional commercial round fibers (Ma et al., 2006). For a naphthalene-derived mesophase pitch fiber, Yuan et al. (2014) reported larger crystallite sizes and higher orientation of crystallites in comparison with corresponding round-shaped fibers.

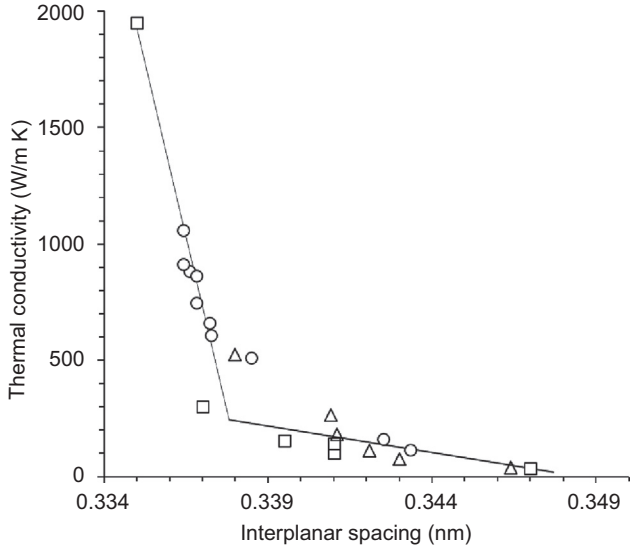

Figure 3.30 Relationship between thermal conductivity and interplanar spacing for a range of pitch-based and PAN-based carbon fibers.
Adapted from Adams, P.M., Katzman, H.A., Rellick, G.S., Stupian, G.W., 1998. Characterization of high thermal conductivity carbon fibers and a self-reinforced graphite panel. Carbon 36, 233–245 with permission of Elsevier. Data from Heremans, J., Rahim, I., Dresselhaus, M.S., 1985. Thermal conductivity and Raman spectra of carbon fibers. Physical Review B 32, 6742–6747 (□), Adams, P.M., Katzman, H.A., Rellick, G.S., Stupian, G.W., 1998. Characterization of high thermal conductivity carbon fibers and a self-reinforced graphite panel. Carbon 36, 233–245 (○), and Nysten, B., Issi, J.P., Barton, R., Boyington, D.R., Lavin, J.G., 1991. Determination of lattice defects in carbon fibers by means of thermal-conductivity measurements. Physical Review B 44, 2142–2148 (△).

3.4.4 Coefficient of thermal expansion

One of the more unusual properties of carbon fibers is that they are strongly anisotropic with respect to CTE, with a small negative CTE in the axial direction and a positive CTE in the transverse or radial direction. The anisotropy of the thermal expansion is a consequence of the graphite crystallite being anisotropic because of the contrast between the strong sp^2 hybridized C−C bonds within basal planes (a-axis) and the weak Van der Waals interactions between the basal planes (c-axis). As a result, there is a large difference between the room temperature values of the CTE of graphite single crystals measured perpendicular to the basal planes ($\alpha_c = 27.0 \times 10^{-6}\ K^{-1}$) and parallel to the basal planes ($\alpha_a = -1.5 \times 10^{-6}\ K^{-1}$) (Nelson and Riley, 1945). The small negative CTE value parallel to the basal planes is believed to result from a Poisson's contraction associated with the large expansion perpendicular to the basal planes (Hacker et al., 2000).

Both α_a and α_c have been shown to vary with temperature (Nelson and Riley, 1945; Morgan, 1972) (Fig. 3.31) and this thermal expansion of the hexagonal lattice of graphite single crystals has been explained theoretically by Riley (1945) using the quantum theory of specific heats. The coefficient of expansion perpendicular to the basal planes decreases with increasing stacking order or graphitic perfection (Kellett and Richards, 1971).

Measuring the CTE of carbon fiber is more challenging than measuring it in graphite because of the small radial dimensions and the fact that the structure is turbostratic. This rules out the use of dilatometry and also X-ray diffraction, which has been used to measure the expansion of the interplanar spacing in graphite. Nevertheless several authors have reported values for the CTE of carbon fiber in both the axial and transverse direction. The values are quite varied; however, most report results

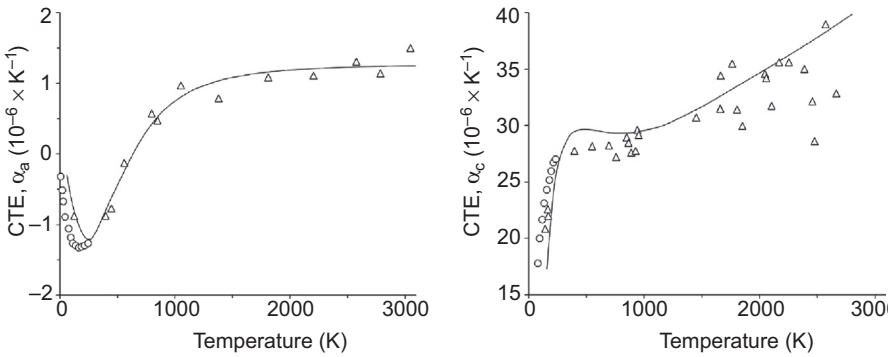

Figure 3.31 Theoretical (*line*) and experimental (*data points*) temperature dependence of the coefficient of thermal expansion (CTE) of graphite parallel to (*left*, α_a) and perpendicular to (*right*, α_c) the basal planes.
Adapted from Morgan, W.C., 1972. Thermal expansion coefficients of graphite crystals. Carbon 10, 73−79 with permission of Elsevier. Experimental data (○) from Bailey, A.C., 1970. Anisotropic Thermal expansion of pyrolytic graphite at low temperatures. Journal of Applied Physics 41, 5088 and derived data (△) from Morgan, W.C., 1972. Thermal expansion coefficients of graphite crystals. Carbon 10, 73−79.

that, for well-oriented fibers, are similar to graphite. In the axial direction the CTE has been measured by changing the temperature and keeping a bundle of fibers under constant tension (Ozbek et al., 1991; Pradere and Sauder, 2008; Sauder et al., 2002; Tanabe et al., 1991), fixing the ends of a single fiber or bundle of fibers and measuring the amount of sag (Trinquecoste et al., 1996; Wasan, 1979; Williams, 1968) and using TEM to measure the dimensional changes in single fibers (Kulkarni and Ochoa, 2006). Most workers report a small negative value below about 400°C rising to $2-3 \times 10^{-6}\ K^{-1}$ at 1000°C (Kulkarni and Ochoa, 2006; Ozbek et al., 1991; Singer, 1981; Tanabe et al., 1991; Williams, 1968; Wolff, 1987). Naturally, the sag method will not be accurate below 400°C as it relies on expansion of the fiber. Similar results were found for fibers embedded in an epoxy composite (Wagoner and Bacon, 1989). The axial CTE has been shown to decrease as Young's modulus increases for fibers with a modulus up to 680 GPa (Wolff, 1987) suggesting that CTE, like modulus, is dependent on crystal structure and orientation (Fig. 3.32). The abrupt change in the slope of the curve above about 680 GPa is believed to be caused by a decoupling of the CTE dependence on preferred orientation (Wolff, 1987). In the extreme, both modulus and axial CTE approach the values reported for graphite.

Measurement of the CTE in the radial or transverse direction is even more challenging. Several workers have measured the dimensional changes in single fibers using TEM (Kulkarni and Ochoa, 2006; Rozploch and Marciniak, 1986; Marciniak and Rozptoch, 1979) or laser diffraction (Pradere and Sauder, 2008; Praderea et al., 2007;

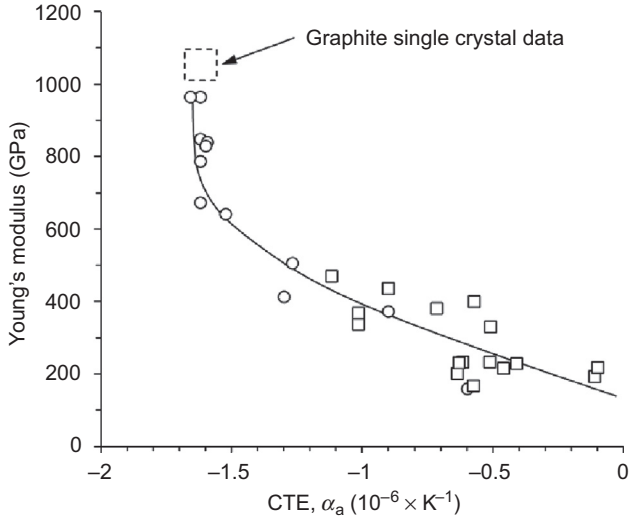

Figure 3.32 Relationship between axial fiber modulus and axial CTE of both PAN- (□) and pitch- (○) based carbon fibers.
Adapted from Wolff, E.G., 1987. Stiffness-thermal expansion relationships in high modulus carbon fibers. Journal of Composite Materials 21, 81−97 with permission of SAGE. Data from Wolff, E.G., 1987. Stiffness-thermal expansion relationships in high modulus carbon fibers. Journal of Composite Materials 21, 81−97 plus supplier datasheets.

Sheaffer, 1987) and reported values ranging from 4 to 41 $\times$ 10^{-6} K^{-1} for a variety of pitch- and PAN-based fibers. It is difficult to assess the accuracy of these measurements; however, it is worth noting that in general the cross-section of the fibers are not circular, therefore a small twist during heating is sufficient to change the observed dimensions and generate large errors. Rozploch and Marciniak (1986) claim that for their method the reproducibility is better than 95%. An interesting approach was used by Fanning (1972) who generated a binder-less bonded bundle by subjecting fibers to high temperature (2760°C) and pressure (100 MPa) over several hours. The bonded bundles were then gently hand abraded into rectangular cross-sections and tested in a dilatometer. Using this method the transverse CTE of Thornel 50, a rayon-based carbon fiber, was shown to increase from 8 $\times$ 10^{-6} K^{-1} at 100°C to 16 $\times$ 10^{-6} K^{-1} at 1000°C. A concern would be how much the original fiber structure is changed by the bonding process. Other workers (Wagoner and Bacon, 1989; Wagoner et al., 1987; Wolff, 1987) have measured the CTE of unidirectional carbon fiber composites and calculated the transverse CTE of the fibers. This provides ease of handling but requires accurate measurement of the fiber volume fraction. Wolff (1987) reported values of 16 and 17 $\times$ 10^{-6} K^{-1} for P120 and P140 high-modulus pitch-based fibers, respectively.

3.4.5 Heterogeneity

Modern instrumentation has made it possible to determine the heterogeneity in the structure and properties of single fibers. Fig. 3.33 shows the results from several different techniques. Paris et al. (2002) used a high intensity X-ray synchrotron beam to show the changes in orientation of crystallites, as a function of the position across the fiber diameter, in a fiber exhibiting a skin−core structure (Fig. 3.33(a)). Note that the FWHM of the intensity of the wide angle X-ray diffraction azimuthal scan is a measure of the graphene layer degree of misorientation. The scanning probe microscope (SPM), often referred to as an atomic force microscope, is capable of collecting images based on the sample's mechanical properties. Fig. 3.33(b) is a modulus map of T300 PAN-based carbon fiber cross-sections showing the core−sheath structure of the fibers, with the core exhibiting a lower modulus. Huson et al. (2014) used nanoindentation, micro-Raman and inverse gas chromatography (IGC) to show heterogeneity in PAN-based IM7 and M46J carbon fibers as well as a pitch-based P25 fiber. It was found that the transverse modulus varied along the length of the fibers as did the extent of graphitization, as measured by the micro-Raman D/G ratio. This is particularly evident in the pitch-based fiber (Fig. 3.33(c)). IGC showed considerable heterogeneity in the surface energy of a PAN-based Panex 35 carbon fiber, especially prior to the application of the sizing material.

3.5 Applications of high-performance pitch-based carbon fibers

In general, carbon fibers find application wherever high strength, high stiffness, and low weight are required. Table 3.1 highlights the primary attractiveness of carbon

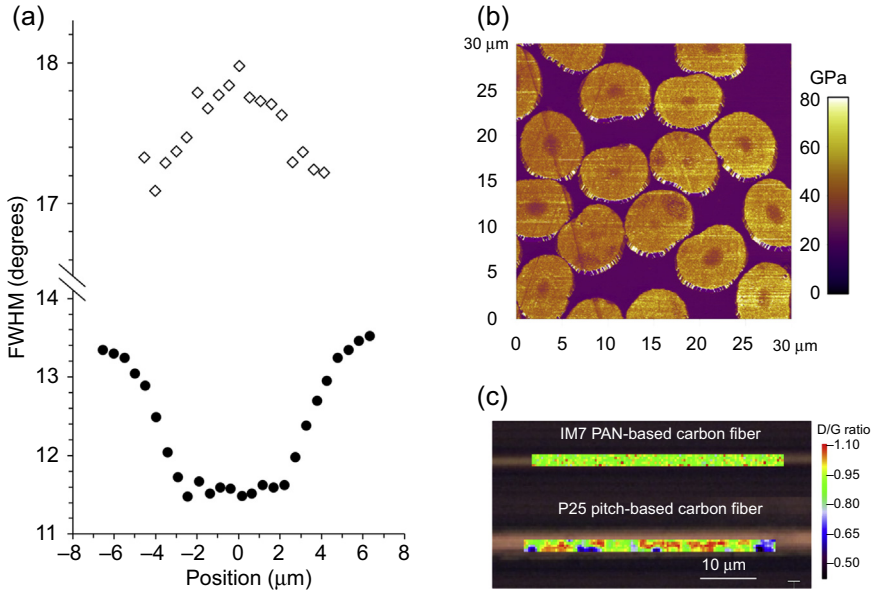

Figure 3.33 Heterogeneity of carbon fibers as shown by (a) variation in orientation (FWHM) across the diameter of HTA7-24 PAN-based (◇) and FT500 pitch-based (•) carbon fibers. *Adapted from Paris, O., Loidl, D., Peterlik, H., 2002. Texture of PAN- and pitch-based carbon fibers. Carbon 40 551−555 with permission of Elsevier.* (b) SPM modulus map of T300 PAN-based carbon fiber cross-sections embedded in an epoxy matrix (*image courtesy of M. Kocun, Asylum Research*) and (c) Raman D/G ratio maps obtained from the surface of an IM7 PAN-based carbon fiber and a P25 pitch-based carbon fiber. *Reproduced from Huson, M.G., Church, J.S., Kafi, A.A., Woodhead, A.L., Khoo, J., Kiran, M.S.R.N., Bradby, J.E., Fox, B.L., 2014. Heterogeneity of carbon fibre. Carbon 68, 240−249.*

fiber. On a weight basis, carbon fiber composite is 2−5 times stronger (specific yield stress) and stiffer (specific modulus) than aluminum. Often bending rigidity is the property of most interest, which for a beam will vary as the third power of the radius or thickness and hence performance of the beam will depend on Young's modulus divided by density cubed. When these values are compared, carbon fiber composites are even more appealing.

The three main areas of carbon fiber application are (Rebouillat et al., 1998):

1. High technology including aerospace and nuclear engineering
2. General engineering and transportation including bearings, gears, wind turbine blades, car bodies, and boats
3. Sporting goods including golf clubs, tennis racquets, and bicycles

The main driver for the use of carbon fiber composites in the aerospace and automotive industry is weight reduction with the resultant savings in fuel. Each kilogram reduction in weight of an aircraft saves US$3000 per year in fuel costs (ie, US$90,000 over the lifetime of the aircraft). These economic pressures are clearly driving a strong interest in carbon fiber from the aerospace industry. Likewise fuel savings are the

Table 3.1 Comparison of mechanical properties of a range of common structural materials

Material	Yield stress (YS) (MPa)	Modulus (E) (GPa)	Density (ρ) (g/cm^3)	Specific modulus (E/ρ) ($10^6\ m^2/s^2$)	Specific bending rigidity (E/ρ^3) ($m^8/kg^2\ s^2$)	Specific yield stress (YS/ρ^1) ($10^6\ m^2/s^2$)
Stainless steel (Bristol Supersonic)	1081	215	7.83	27.5	0.4	0.14
Titanium alloy Ti-6AI-4V	830	110	4.43	24.8	1.3	0.19
Aluminum alloy 7075-T6 (Boeing 707)	470	72	2.8	25.7	3.3	0.17
Mg alloy	200	45	1.8	25.0	7.7	0.11
Carbon fiber reinforced epoxy	1300	192	1.5	128.0	56.9	0.87
Sitka spruce (Spruce Goose)	39	9.4	0.42	22.4	126.9	0.1

economic driver in the automobile industry. A recent study of the cradle-to-grave energy usage of an Audi A3 with a 200,000-km lifetime gave the following breakdown of the energy usage:

Material production	6%
Manufacture of car	6%
Fuel during usage	84%
Parts and servicing	3%
Recycling at end of life	1%

The differentiating properties of mesophase pitch-based carbon fibers, compared to PAN-based fibers, are their high modulus and exceptional thermal properties. The most thermally conductive, commercially available mesophase pitch-based carbon fiber (K1100) has a nominal thermal conductivity value of 1000 W/m K, superior to that of metals such as silver and copper (Fig. 3.28). K13D2U fiber has a thermal conductivity of 800 W/m K along with a modulus of 935 GPa. Consequently, mesophase pitch-based carbon fibers have found applications where these properties are critical.

Effective devices for thermomanagement such as heat exchangers, heat release, and heating walls can be designed using the fiber as the filler of the composite (Mochida et al., 2000).

Carbon fibers are one of the few materials with a negative CTE, with pitch-based fibers having the highest negative values. Combining these fibers with an epoxy, which has a positive CTE, allows the production of composites with zero CTE, making them ideal for critical applications in space where the ability to withstand large thermal gradients while maintaining dimensional stability is important (Kowalski, 1987).

It is well known that materials with high stiffness and reduced weight achieve vibration damping in a shorter period of time, improving productivity. Thus composites containing ultrahigh modulus pitch-based fibers are often used as rollers, robot arms, or machine tooling where high-speed operation and accuracy are required. Fig. 3.34 shows the superior damping performance of a composite containing XN-80 pitch-based fiber with a modulus of 780 GPa, compared to a composite containing PAN-based fiber with a modulus of 230 GPa. Carbon fiber composite rollers in particular have become popular, replacing the traditional steel or aluminum rollers in the film and papermaking industries. The lighter, stiffer rollers provide a range of benefits, including fewer, less powerful motors, longer bearing life, and wider web width because of less deflection in the longer rollers (Fig. 3.35). Liquid crystal displays

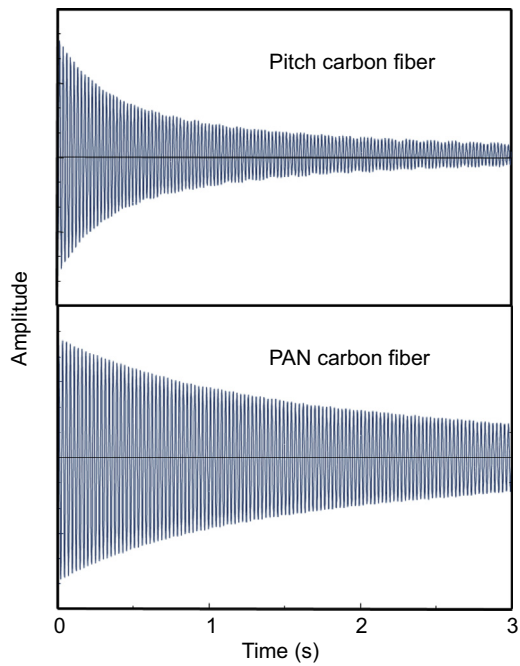

Figure 3.34 Damping performance of a composite containing XN-80 pitch-based carbon fiber (modulus 780 GPa) compared to one containing PAN-based carbon fiber (modulus 230 GPa). Image courtesy of Hideyuki Ohno, Nippon Graphite Fiber Corporation.

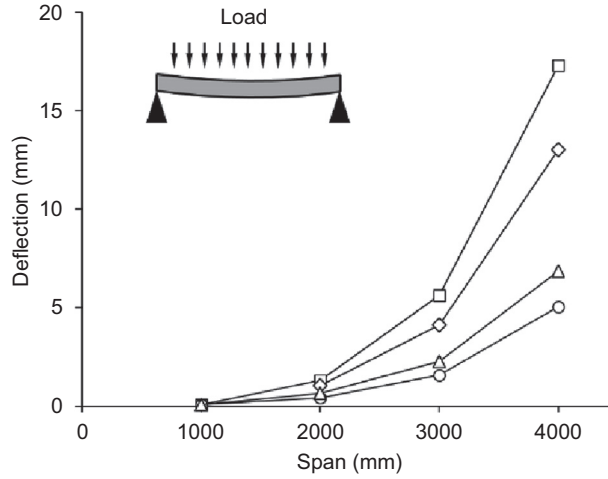

Figure 3.35 The deflection of rollers from different materials under a uniformly distributed load of 1000 N/m. Rollers manufactured from aluminum (□), 230 GPa modulus PAN-based carbon fiber composite (◇), steel (△), and 640 GPa modulus pitch-based carbon fiber composite (○). Adapted from Yoshiya, A., July 2001. Characteristics and Applications of Pitch-based Carbon Rollers. Paper, Film & Foil Convertech Pacific, pp. 38–40 with permission of the author.

(LCDs) are composed of a liquid crystal layer sandwiched between two glass plates and many functional polymer films. The greater precision achievable with these high performance rollers has resulted in them being preferred in the manufacture of these films and laminates and thus they have played a leading role in the expansion of LCDs in recent years (Yoshiya, 2001, 2011).

3.6 Conclusion

High-performance pitch-based carbon fiber fulfills a small but nevertheless important role in the broader carbon fiber landscape. While it can be made with a range of properties, it is the high modulus, high thermal conductivity, low electrical resistivity, and low negative CTE grades that distinguish pitch-based carbon fiber from PAN-based carbon fiber. Pitch-based carbon fiber is currently made from both coal tar and petroleum feedstocks and occupies about 10% market share. This is unlikely to change although the global push towards the use of renewable resources counts in its favor. An enormous effort went into producing high-performance carbon fiber from synthetic pitches based on naphthalene, culminating briefly in significant commercial production. While this product is no longer produced commercially, much knowledge was gained on the structure and properties of mesophase pitch fibers during the almost two decades of research in this area.

The current push in carbon fiber production is to make cheaper fibers for use in general engineering and the automotive industry. The precursor material should ideally be from a renewable source and/or be a waste product and preferably be able to be

converted into a fiber by melt spinning rather than by solution spinning. Pitch fulfills most of these requirements, thus if the processing costs can be reduced pitch-based carbon fiber may yet increase its market share.

References

Adams, P.M., Katzman, H.A., Rellick, G.S., Stupian, G.W., 1998. Characterization of high thermal conductivity carbon fibers and a self-reinforced graphite panel. Carbon 36, 233−245.

Ania, C., 2007. Pitch based carbon materials. In: ITA Annual Conference. Palma de Mallorca.

Bahl, O.P., Shen, Z., Lavin, J.G., Ross, R.A., 1998. Manufacture of carbon fibers. In: Donnet, J.-B., Wang, T.K., Rebouillat, S., Peng, J.C.M. (Eds.), Carbon Fibers, third ed. Marcel Dekker, New York.

Bailey, A.C., 1970. Anisotropic thermal expansion of pyrolytic graphite at low temperatures. Journal of Applied Physics 41, 5088.

Barnes, R.D., Redick, H.E., 1991. Surface Treatment of Pitch-Based Carbon Fibers. Patent Number CA1282564 C.

Barnes, A.B., Dauché, F.M., Gallego, N.C., Fain, C.C., Thies, M.C., 1998. As-spun orientation as an indication of graphitized properties of mesophase-based carbon fiber. Carbon 36, 855−860.

Barnett, I., 1959. Thermal Modification of Acrylonitrile Yarns (United States patent application, Patent Version Number 2,913,802).

Barr, J.B., 1975. High modulus carbon fibers from pitch precursor. Applied Polymer Symposia 29, 161−173.

Barraza, J., Muñoz, N., Barona, L., 2014. Asphaltenes and preasphaltenes from coal liquid extracts: feedstocks to obtain carbon mesophase. Revista Facultad de Ingeniería Universidad de Antioquia 86−98.

Barraza-Burgos, J.-M., Ospina-Espinosa, J.-M., 2012. Effect of pitch petroleum oxidation on mesophase production. CT&F − Ciencia, Tecnología Y Futuro 4.

Blakslee, O.L., Proctor, D.G., Seldin, E.J., Spence, G.B., Weng, T., 1970. Elastic constants of compression-annealed pyrolytic graphite. Journal of Applied Physics 41, 3373−3382.

Bright, A.A., Singer, L.S., 1979. The electronic and structural characteristics of carbon fibers from mesophase pitch. Carbon 17, 59−69.

Brooks, J.D., Taylor, G.H., 1965. The formation of graphitizing carbons from the liquid phase. Carbon 3, 185−193.

Brosius, D., September 2014. What Will Be the Next Major Iteration in Carbon Fiber? Composites World.

Brydges, W.T., Badami, D.V., Joiner, J.C., 1969. The structure and elastic properties of carbon fibers. Applied Polymer Symposia 9, 255−261.

Chi, W., Shen, Z., 1996. Mechanism and kinetics of air stabilisation of petroleum pitch fibers. In: Carbon '96: Extended Abstracts of European Carbon Conference, pp. 395−396. Newcastle, UK.

Choi, Y.O., Yang, K.S., 2001. Preparation of carbon fiber from heavy oil residue through bromination. Fibers and Polymers 2, 178−183.

Chwastiak, S., Lewis, I.C., 1978. Solubility of mesophase pitch. Carbon 16, 156−157.

De Castro, L.D., 2006. Anisotropy and mesophase formation towards carbon fibre production from coal tar and petroleum pitches − a review. Journal of the Brazilian Chemical Society 17, 1096−1108.

Edie, D.D., Dunham, M.G., 1989. Melt spinning pitch-based carbon fibers. Carbon 27, 647−655.

Edie, D.D., Fain, C.C., Robinson, K.E., Harper, A.M., Rogers, D.K., 1993. Ribbon-shape carbon fibers for thermal management. Carbon 31, 941−949.

Edie, D.D., Robinson, K.E., Fleurot, O., Jones, S.P., Fain, C.C., 1994. High thermal conductivity ribbon fibers from naphthalene-based mesophase. Carbon 32, 1045−1054.

Edie, D., 1990. Pitch and mesophase fibers. In: Figueiredo, J.L., Bernardo, C.A., Baker, R.T.K., Hüttinger, K.J. (Eds.), Carbon Fibers Filaments and Composites. Springer, Netherlands.

Edie, D.D., 1998. The effect of processing on the structure and properties of carbon fibers. Carbon 36, 345−362.

Edie, D.D., 2001. Carbon fiber processing and structure/property relations. In: Rand, B., Appleyard, S.P., Yardim, M.F. (Eds.), Design and Control of Structure of Advanced Carbon Materials for Enhanced Performance. Springer, Netherlands.

Elias, H.G., 2013. Macromolecules: Volume 2: Synthesis, Materials, and Technology. Springer.

Emmerich, F.G., 2014. Young's modulus, thermal conductivity, electrical resistivity and coefficient of thermal expansion of mesophase pitch-based carbon fibers. Carbon 79, 274−293.

Fanning, R.C., 1972. Transverse thermal expansion characteristics of graphite fibers. Carbon 10, 331.

Fathollahi, B., Chau, P.C., White, J.L., 2005a. Injection and stabilization of mesophase pitch in the fabrication of carbon−carbon composites: Part II. Stabilization process. Carbon 43, 135−141.

Fathollahi, B., Jones, B., Chau, P.C., White, J.L., 2005b. Injection and stabilization of mesophase pitch in the fabrication of carbon−carbon composites. Part III: mesophase stabilization at low temperatures and elevated oxidation pressures. Carbon 43, 143−151.

Ferritto, J.J., Weiler, J., 1968. The effect of pitch quinoline insolubles on graphite properties. In: ACS Fuels Fall Conference. Atlantic City.

Fitzer, E., Manocha, L.M., 1998. Carbon fibers. In: Fitzer, E., Manocha, L.M. (Eds.), Carbon Reinforcements and Carbon/Carbon Composites. Springer-Verlag, Berlin.

Fitzer, E., 1989. Pan-based carbon fibers—present state and trend of the technology from the viewpoint of possibilities and limits to influence and to control the fiber properties by the process parameters. Carbon 27, 621−645.

Gallego, N.C., Edie, D.D., 2001. Structure−property relationships for high thermal conductivity carbon fibers. Composites Part A: Applied Science and Manufacturing 32, 1031−1038.

Gillespie, J.J.W., Devault, J.B., Gabara, V., Kardos, J.L., Schadler, L.S., 2005. High-performance Structural Fibers for Advanced Polymer Matrix Composites. National Academies Press, Washington, DC.

Greene, M.L., Schwartz, R.W., Treleaven, J.W., 2002. Short residence time graphitization of mesophase pitch-based carbon fibers. Carbon 40, 1217−1226.

Grégr, J., 2010. The complete list of commercial carbon fibers. In: 7th International Conference − TEXSCI Liberec, Czech Republic.

Greinke, R.A., 1986. Kinetics of petroleum pitch polymerization by gel permeation chromatography. Carbon 24, 677−686.

Hacker, P.J., Neighbour, G.B., McEnaney, B., 2000. The coefficient of thermal expansion of nuclear graphite with increasing thermal oxidation. Journal of Physics D: Applied Physics 33, 991−998.

Hamada, T., Furuyama, M., Sajiki, Y., Tomioka, T., Endo, M., 1990. Preferred orientation of pitch precursor fibers. Journal of Materials Research 5, 1271−1280.

Heremans, J., Rahim, I., Dresselhaus, M.S., 1985. Thermal conductivity and Raman spectra of carbon fibers. Physical Review B 32, 6742–6747.

Hong, S.-H., Korai, Y., Mochida, I., 2000. Mesoscopic texture at the skin area of mesophase pitch-based carbon fiber. Carbon 38, 805–815.

Huang, Y., Young, R.J., 1995. Effect of fibre microstructure upon the modulus of PAN- and pitch-based carbon fibres. Carbon 33, 97–107.

Huang, X., 2009. Fabrication and properties of carbon fibers. Materials 2, 2369–2403.

Huson, M.G., Church, J.S., Kafi, A.A., Woodhead, A.L., Khoo, J., Kiran, M.S.R.N., Bradby, J.E., Fox, B.L., 2014. Heterogeneity of carbon fibre. Carbon 68, 240–249.

Itoi, M., Yamada, Y., 1992. Effect of surface treatment of pitch-based carbon fiber on mechanical properties of polyether nitrile composites. Polymer Composites 13, 15–29.

Johnson, W., Watt, W., 1967. Structure of high modulus carbon fibres. Nature 215, 384–386.

Jones, S.P., Rogers, D.K., Liu, G.Z., Fain, C.C., Edie, D.D., 1993. Structural development in mesophase pitch-based carbon fibers. In: Proceedings of 21st Biennial Conference on Carbon. American Carbon Society, Buffalo, NY, pp. 354–355.

Jones, S.P., Fain, C.C., Edie, D.D., 1997. Structural development in mesophase pitch based carbon fibers produced from naphthalene. Carbon 35, 1533–1543.

Kellett, E.A., Richards, B.P., 1971. The *c*-axis thermal expansion of carbons and graphites. Journal of Applied Crystallography 4, 1–8.

Korai, Y., Nakamura, M., Mochida, I., Sakai, Y., Fujiyama, S., 1991. Mesophase pitches prepared from methylnaphthalene by the aid of HF/BF_3. Carbon 29, 561–567.

Korai, Y., Ishida, S., Watanabe, F., Yoon, S.H., Wang, Y.G., Mochida, I., Kato, I., Nakamura, T., Sakai, Y., Komatsu, M., 1997. Preparation of carbon fiber from isotropic pitch containing mesophase spheres. Carbon 35, 1733–1737.

Korai, Y., Yoon, S.-H., Oka, H., Mochida, I., Nakamura, T., Kato, I., Sakai, Y., 1998. The properties of co-oligomerized mesophase pitch from methylnaphthalene and naphthalene catalyzed by HF/BF_3. Carbon 36, 369–375.

Kowalski, I.M., 1987. New high performance domestically produced carbon fibers. In: Carson, R., Burg, M., Kjoller, K.J., Riel, F.J. (Eds.), 32nd International SAMPE Symposium. Anaheim, CA.

Kulkarni, R., Ochoa, O., 2006. Transverse and longitudinal CTE measurements of carbon fibers and their impact on interfacial residual stresses in composites. Journal of Composite Materials 40, 733–754.

Kurtz, D.S., 1983. Molecular Preferred Orientation in High Modulus Carbon Fiber Produced from Mesophase Pitch. MSc. Rensselaer Polytechnic Institute.

Lafdi, K., Bonnamy, S., Oberlin, A., 1991. Mechanism of anisotropy occurrence in a pitch precursor of carbon fibres: Part I—Pitches A and B. Carbon 29, 831–847.

Lavin, J.G., Boyington, D.R., Lahijani, J., Nystem, B., Issi, J.P., 1993. The correlation of thermal conductivity with electrical resistivity in mesophase pitch-based carbon fiber. Carbon 31, 1001–1002.

Lavin, J.G., 2001. Mesophase precursors for advanced carbon fibers: Pitches, stabilization and carbonization. In: Rand, B., Appleyard, S.P., Yardim, M.F. (Eds.), Design and Control of Structure of Advanced Carbon Materials for Enhanced Performance. Springer, Netherlands.

Lewis, I.C., Mchenry, E.R., Singer, L.S., 1976. Process for Producing Carbon Fibers from Mesophase Pitch (U.S. patent application, Patent Version Number 3976729).

Lewis, I.C., Mchenry, E.R., Singer, L.S., 1977. Process for Producing Mesophase Pitch (U.S. patent application, Patent Version Number 4,017,327).

Lin, S.S., Yip, P.W., 1989. Surface adhesion of carbon fibers after chemical treatments. In: 19th Biennial Conference on Carbon. Penn State University, pp. 244–245.

Lin, S.-S., Yip, P.W., 1993. Improved mechanical strengths of epoxy composites obtained from ion beam treated carbon fibers. In: Materials Research Society Symposium, pp. 381−386.
Liu, C., 2010. Mesophase Pitch-based Carbon Fiber and its Composites: Preparation and Characterization. MSc. University of Tennessee.
Lu, S., Blanco, C., Appleyard, S., Hammond, C., Rand, B., 2002a. Texture studies of carbon and graphite tapes by XRD texture goniometry. Journal of Materials Science 37, 5283−5290.
Lu, S., Blanco, C., Rand, B., 2002b. Large diameter carbon fibres from mesophase pitch. Carbon 40, 2109−2116.
Ma, Z., Shi, J., Song, Y., Guo, Q., Zhai, G., Liu, L., 2006. Carbon with high thermal conductivity, prepared from ribbon-shaped mesosphase pitch-based fibers. Carbon 44, 1298−1301.
Maeda, T., Ming Zeng, S., Tokumitsu, K., Mondori, J., Mochida, I., 1993. Preparation of isotropic pitch precursors for general purpose carbon fibers (GPCF) by air blowing—I. Preparation of spinnable isotropic pitch precursor from coal tar by air blowing. Carbon 31, 407−412.
Marciniak, W., Rozptoch, F., 1979. Measurement of the radial thermal expansion coefficient of carbon fibres. High Temperatures−High Pressures 11, 709−710.
Marsh, H., Carolyn, S.L., 1986. The Chemistry of Mesophase Formation. Petroleum-Derived Carbons. American Chemical Society.
Marsh, H., Griffiths, J., 1982. A high resolution electron-microscopy study of graphitization and graphitizable carbon. In: International Symposium on Carbon: New Processing and New Applications, pp. 81−83. Toyohashi, Japan.
Mason, K., March 2004. Advances in Sizings and Surface Treatments for Carbon Fibers. High-Performance Composites (Online), Available: http://www.compositesworld.com/articles/advances-in-sizings-and-surface-treatments-for-carbon-fibers.
Matsumoto, T., Mochida, I., 1992. A structural study on oxidative stabilization of mesophase pitch fibers derived from coaltar. Carbon 30, 1041−1046.
Matsumoto, T., Mochida, I., 1993. Oxygen distribution in oxidatively stabilized mesophase pitch fiber. Carbon 31, 143−147.
Matsumoto, M., Iwashita, T., Arai, Y., Tomioka, T., 1993. Effect of spinning conditions on structures of pitch-based carbon fiber. Carbon 31, 715−720.
Matsumoto, T., 1985. Mesophase pitch and its carbon fibers. Pure and Applied Chemistry 57, 1553−1562.
Matsumura, Y., 1987. Development of pitch-based advanced carbon materials. Journal of the Japan Petroleum Institute 30, 291−300.
McHenry, E.R., 1977. Process for Producing Mesophase Pitch (U.S. patent application, Patent Number 4,026,788).
McHugh, J.J., Liu, G.Z., Edie, D.D., 1992. An evaluation of naphthalene-based mesophase as a carbon fiber precursor. TANSO 1992, 417−425.
Mochida, I., Toshima, H., Korai, Y., Matsumoto, T., 1988a. Blending mesophase pitch to improve its properties as a precursor for carbon fibre: Part 1. Blending of PVC pitch into coal tar and petroleum-derived mesophase pitches. Journal of Materials Science 23, 670−677.
Mochida, I., Toshima, H., Korai, Y., Naito, T., 1988b. Modification of mesophase pitch by blending; Part 2. Modification of mesophase pitch fibre precursor with thermoresisting polyphenyleneoxide (PPO). Journal of Materials Science 23, 678−686.
Mochida, I., Toshima, H., Korai, Y., Hino, T., 1989. Oxygen distribution in the mesophase pitch fibre after oxidative stabilization. Journal of Materials Science 24, 389−394.

Mochida, I., Shimizu, K., Korai, Y., Otsuka, H., Sakai, Y., Fujiyama, S., 1990a. Preparation of mesophase pitch from aromatic hydrocarbons by the aid of HF/BF_3. Carbon 28, 311−319.

Mochida, I., Zeng, S.-M., Korai, Y., Toshima, H., 1990b. The introduction of a skin-core structure in mesophase pitch fibers by oxidative stabilization. Carbon 28, 193−198.

Mochida, I., Korai, Y., Azuma, A., Kakuta, M., Kitajima, E., 1991a. Structure and stabilization reactivity of mesophase pitch derived from f c c-decant oils. Journal of Materials Science 26, 4836−4844.

Mochida, I., Zeng, S.-M., Korai, Y., Hino, T., Toshima, H., 1991b. The introduction of a skin-core structure in mesophase pitch fibers through a successive stabilization by oxidation and solvent extraction. Carbon 29, 23−29.

Mochida, I., Shimizu, K., Korai, Y., Sakai, Y., Fujiyama, S., Toshima, H., Hono, T., 1992. Mesophase pitch catalytically prepared from anthracene with HF/BF_3. Carbon 30, 55−61.

Mochida, I., Yoon, S.-H., Korai, Y., 1993. Preparation and structure of mesophase pitch-based thin carbon tape. Journal of Materials Science 28, 2135−2140.

Mochida, I., Ling, L., Korai, Y., 1994. Some factors for the high performances of mesophase pitch based carbon fibre. Journal of Materials Science 29, 3050−3056.

Mochida, I., Yoon, S.H., Takano, N., Fortin, F., Korai, Y., Yokogawa, K., 1996. Microstructure of mesophase pitch-based carbon fiber and its control. Carbon 34, 941−956.

Mochida, I., Korai, Y., Ku, C.-H., Watanabe, F., Sakai, Y., 2000. Chemistry of synthesis, structure, preparation and application of aromatic-derived mesophase pitch. Carbon 38, 305−328.

Mochida, I., Korai, Y., Wang, Y.-G., Hong, S.-H., 2001. Preparation and properties of mesophase pitches. In: Delhaes, P. (Ed.), Graphite and Precursors. Gordon & Breach, Australia.

Mochida, I., Yoon, S.-H., Korai, Y., 2004. Synthesis and application of mesophase pitch. In: American Carbon Society, Proceedings of the Carbon Conference. Providence, Rhode Island.

Mochida, I., Yoon, S.-H., Qiao, W., 2006. Catalysts in syntheses of carbon and carbon precursors. Journal of the Brazilian Chemical Society 17, 1059−1073.

Mora, E., Blanco, C., Prada, V., Santamarŕa, R., Granda, M., Menéndez, R., 2002. A study of pitch-based precursors for general purpose carbon fibres. Carbon 40, 2719−2725.

Morgan, W.C., 1972. Thermal expansion coefficients of graphite crystals. Carbon 10, 73−79.

Morgan, P., 2005a. Carbon Fiber Production Using a Pitch Based Precursor. Carbon Fibers and Their Composites. CRC Press, Boca Raton, Fl.

Morgan, P., 2005b. Guidelines for the Design of Equipment for Carbon Fiber Plant. Carbon Fibers and Their Composites. CRC Press, Boca Raton, Fl.

Morgan, P., 2005c. Carbon Fibers and Their Composites. CRC Press, Boca Raton, Fl, p. 203.

Morgan, P., 2005d. Carbon Fibers and Their Composites. CRC Press, Boca Raton, Fl, p. 798.

Morgan, P., 2005e. Precursors for Carbon Fiber Manufacture. Carbon Fibers and Their Composites. CRC Press, Boca Raton, FL.

Morgan, P., 2005f. Surface Treatment and Sizing of Carbon Fibers. Carbon Fibers and Their Composites. CRC Press, Boca Raton, Fl.

Moriyama, R., Hayashi, J.I., Chiba, T., 2004. Effects of quinoline-insoluble particles on the elemental processes of mesophase sphere formation. Carbon 42, 2443−2449.

Murakami, K., Toshima, H., Yamamoto, M., 1997. Effect of mesophase pitches on tensile modulus of pitch-based carbon fibers. Sen'i Gakkaishi 53, 73−78.

Naito, K., Tanaka, Y., Yang, J.-M., Kagawa, Y., 2008. Tensile properties of ultrahigh strength PAN-based, ultrahigh modulus pitch-based and high ductility pitch-based carbon fibers. Carbon 46, 189−195.

Nakanishi, Y., Itoh, H., Ejiri, H., 1995. Influence of surface treatment and sizing agent on carbon fiber and the interface properties of CFRP. In: Tenth International Conference on Composite Materials. ICCM-10, Whistler B.C. Canada.

Nelson, J.B., Riley, D.P., 1945. The thermal expansion of graphite from 15°C to 800°C: Part I. Experimental. Proceedings of the Physical Society 57, 477−486.

Nysten, B., Issi, J.P., Barton, R., Boyington, D.R., Lavin, J.G., 1991. Determination of lattice defects in carbon fibers by means of thermal-conductivity measurements. Physical Review B 44, 2142−2148.

Ogale, A.A., Lin, C., Anderson, D.P., Kearns, K.M., 2002. Orientation and dimensional changes in mesophase pitch-based carbon fibers. Carbon 40, 1309−1319.

Otani, S., Oya, A., 1986. Progress of Pitch-based Carbon Fiber in Japan. Petroleum-Derived Carbons. American Chemical Society.

Ozbek, S., Jenkins, G.M., Isaac, D.H., 1991. Thermal expansion and creep of carbon fibres. In: 20th Biennial Conference on Carbon. American Carbon Society, Palo Alto, pp. 270−271.

Ozcan, S., Vautard, F., Naskar, A.K., 2014. Designing the structure of carbon fibers for optimal mechanical properties. In: Naskar, A.K., Hoffman, W.P. (Eds.), Polymer Precursor-derived Carbon. American Chemical Society, Washington, DC.

Ozel, M.Z., Bartle, K.D., 2002. Production of mesophase pitch from coal tar and petroleum pitches using supercritical fluid extraction. Turkish Journal of Chemistry 26, 417−424.

Paris, O., Loidl, D., Peterlik, H., 2002. Texture of PAN- and pitch-based carbon fibers. Carbon 40, 551−555.

Park, Y.D., Mochida, I., 1989. A two-stage preparation of mesophase pitch from the vacuum residue of FCC decant oil. Carbon 27, 925−929.

Park, Y., Toshima, H., Korai, Y., Mochida, I., Matsumoto, T., 1988a. Rapid stabilization of mesophase pitch-based carbon fibre by solvent extraction and successive oxidation. Journal of Materials Science Letters 7, 1318−1320.

Park, Y.D., Mochida, I., Matsumoto, T., 1988b. Extractive stabilization of mesophase pitch fiber. Carbon 26, 375−380.

Pradere, C., Sauder, C., 2008. Transverse and longitudinal coefficient of thermal expansion of carbon fibers at high temperatures (300−2500K). Carbon 46, 1874−1884.

Praderea, C., Batsalea, J.C., Goyhenecheb, J.M., Paillerb, R., Dilhairec, S., 2007. Estimation of the transverse coefficient of thermal expansion on carbon fibers at very high temperature. Inverse Problems in Science and Engineering 15, 77−89.

Qin, X., Lu, Y., Xiao, H., Wen, Y., Yu, T., 2012. A comparison of the effect of graphitization on microstructures and properties of polyacrylonitrile and mesophase pitch-based carbon fibers. Carbon 50, 4459−4469.

Rebouillat, S., Peng, J.C.M., Donnet, J.-B., Ryu, S.-K., 1998. Carbon fiber applications. In: Donnet, J.-B., Wang, T.K., Peng, J.C.M., Rebouillat, S. (Eds.), Carbon Fibers, third ed. Marcel Dekker, Inc., New York.

Redick, H.E., Barnes, R.D., 1986. Surface Treatment of Pitch-based Carbon Fibers (United States patent application, International Patent Number 4,608,402).

Rich, M.J., Drzal, L.T., Rook, B.P., Askeland, P., Drown, E.K., 2009. Novel carbon fiber surface treatment with ultraviolet light in ozone to promote composite mechanical properties. In: The 17th International Conference on Composite Materials. ICCM 17, Edinburgh, UK.

Rich, M.J., Drown, E.K., Askeland, P., Drzal, L.T., 2013. Surface treatment of carbon fibers by ultraviolet light+ozone: Its effect on fiber surface area and topography. In: The 19th International Conference on Composite Materials. ICCM 19, Montreal, Canada, pp. 1196−1204.

Riley, D.P., 1945. The thermal expansion of graphite: Part II. Theoretical. Proceedings of the Physical Society 57, 486–495.

Rozploch, F., Marciniak, W., 1986. Radial thermal expansion of carbon fibres. High Temperatures-High Pressures 18, 585–587.

Ruland, W., 1968. X-ray diffraction studies on carbon and graphite. In: Walker, P.L. (Ed.), Chemistry and Physics of Carbon: A Series of Advances. Marcel Dekker, New York.

Sauder, C., Lamon, J., Pailler, R., 2002. Thermomechanical properties of carbon fibres at high temperatures (up to 2000°C). Composites Science and Technology 62, 499–504.

Sawran, W.R., Turrill, F.H., Newman, J.W., Hall, N.W., 1985. Process for the Manufacture of Carbon Fibers (United States patent application, Patent Version Number 4,497,789).

Sawran, W.R., Turrill, F.H., Newman, J.W., Hall, N.W., Ward, C., 1987. Process for the Manufacture of Carbon Fibers and Feedstock Therefor (United States patent application, Patent Version Number 4,671,864).

Sheaffer, P.M., 1987. Transverse thermal expansion of carbon fibers. In: Extended Abstracts of the 18th Biennial Conference on Carbon. Worcester Polytechnic Institute, Worcester, MA., pp. 20–21

Shen, Z., Guo, H., Shi, Y., Chang, W., Wang, Y., Shang, Y., 1993. Study on the heat treatment process of mesophase pitch fibres. In: 21st Biennial Conference on Carbon. American Carbon Society, Buffalo, New York, pp. 352–353.

Shen, Z.-M., Chi, W.-D., Zhang, X.-J., Chang, W.-P., 2005. Carbon fibers from petroleum pitch. New Carbon Materials 20, 1–7.

Singer, L.S., 1977. High Modulus High Strength Fibers Produced from Mesophase Pitch (U.S. patent application, Patent Number 4,005,183).

Singer, L.S., 1978. The mesophase and high modulus carbon fibers from pitch. Carbon 16, 409–415.

Singer, L.S., 1981. Carbon fibres from mesophase pitch. Fuel 60, 839–847.

Stadelhofer, J.W., 1980. Examination of the influence of natural quinoline-insoluble material on the kinetics of mesophase formation. Fuel 59, 360–361.

Stevens, W.C., Diefendorf, R.J., 1986. Thermosetting of mesophase pitches: I. Experimental. In: Carbon '86, 4th International Carbon Conference. Deutschen Keramischen Gesellschaft, Baden-Baden, pp. 37–39.

Takaku, A., Shioya, M., 1990. X-ray measurements and the structure of polyacrylonitrile- and pitch-based carbon fibres. Journal of Materials Science 25, 4873–4879.

Tanabe, Y., Yasuda, E., Yamaguchi, K., Inagaki, M., Yamada, Y., 1991. Studies on "mesophase"-pitch-based carbon fibers: Part II. Mechanical properties and thermal expansion. TANSO 66–73.

Tillmanns, H., Pietzka, G., Pauls, H., 1978. Influence of the quinoline-insoluble matter in pitch on carbonization behaviour and structure of pitch coke. Fuel 57, 171–173.

Toshima, H., Mochida, I., Korai, Y., Hino, T., 1992. Modification of petroleum-derived mesophase pitch by blending naphthalene-derived partially isotropic pitches. Carbon 30, 773–779.

Trinquecoste, M., Carlier, J.L., Derré, A., Delhaès, P., Chadeyron, P., 1996. High temperature thermal and mechanical properties of high tensile carbon single filaments. Carbon 34, 923–929.

Wagoner, G., Bacon, R., 1989. Elastic constants and thermal expansion coefficients of various carbon fibers. In: Extended Abstracts of 19th Biennial Carbon Conference. Penn State University, State College, PA, pp. 296–297.

Wagoner, G., Smith, R.E., Bacon, R., 1987. Thermal expansion and elastic constant measurement of carbon fibers. In: Extended Abstracts of 18th Biennial Carbon Conference. Worcester Polytechnic Institute, Worcester, MA, pp. 415–416.

Wang, J.-L., Gu, M., Ma, W.-G., Zhang, X., Song, Y., 2008. Temperature dependence of the thermal conductivity of individual pitch-derived carbon fibers. New Carbon Materials 23, 259–263.

Wasan, V.P., 1979. Sag method for the determination of coefficient of linear thermal expansion of carbon fibres. Carbon 17, 55–58.

Watanabe, F., Ishida, S., Korai, Y., Mochida, I., Kato, I., Sakai, Y., Kamatsu, M., 1999. Pitch-based carbon fiber of high compressive strength prepared from synthetic isotropic pitch containing mesophase spheres. Carbon 37, 961–967.

Wazir, A.H., Kakakhel, L., 2009. Preparation and characterization of pitch-based carbon fibers. New Carbon Materials 24, 83–88.

White, J.L., Guthrie, G.L., Gardner, J.O., 1967. Mesophase microstructures in carbonized coal-tar pitch. Carbon 5, 517–518.

Whitehouse, S., Rand, B., 1987. Rheology of mesophase pitch from A240. In: 18th Biennial Conference on Carbon. American Carbon Society, Worcester, Mass, pp. 175–176.

Williams, W.S., 1968. Thermal expansion of carbon fibers. American Ceramic Society Bulletin 47, 760.

Wolff, E.G., 1987. Stiffness-thermal expansion relationships in high modulus carbon fibers. Journal of Composite Materials 21, 81–97.

Yang, H., Yoon, S.-H., Korai, Y., Mochida, I., Katou, O., 2003. Improving graphitization degree of mesophase pitch-derived carbon fiber by solid-phase annealing of spun fiber. Carbon 41, 397–403.

Yao, Y., Chen, J., Liu, L., Dong, Y., Liu, A., 2012. Tailoring structures and properties of mesophase pitch-based carbon fibers based on isotropic/mesophase incompatible blends. Journal of Materials Science 47, 5509–5516.

Yao, Y., Liu, L., Chen, J., Dong, Y., Liu, A., 2014. Enhanced oxidation performance of pitch fibers formed from a heterogeneous pitch blend. Carbon 73, 325–332.

Yoon, S.-H., Korai, Y., Mochida, I., 1993a. Spinning characteristics of mesophase pitches derived from naphthalene and methylnaphthalene with HF/BF_3. Carbon 31, 849–856.

Yoon, S.H., Korai, Y., Mochida, I., 1993b. Stabilization process of mesophase pitch fibers studied by thermal analysis systems. In: Proceedings of 21st Biennial Conference on Carbon. Buffalo, NY.

Yoon, S.-H., Korai, Y., Mochida, I., 1994a. Assessment and optimization of the stabilization process of mesophase pitch fibers by thermal analyses. Carbon 32, 281–287.

Yoon, S.-H., Korai, Y., Mochida, I., Kato, I., 1994b. The flow properties of mesophase pitches derived from methylnaphthalene and naphthalene in the temperature range of their spinning. Carbon 32, 273–280.

Yoon, S.-H., Korai, Y., Mochia, I., Yokogawa, K., Fukuyama, S., Yoshimura, M., 1996. Axial nano-scale microstructures in graphitized fibers inherited from liquid crystal mesophase pitch. Carbon 34, 83–88.

Yoon, S.-H., Takano, N., Korai, Y., Mochida, I., 1997. Crack formation in mesophase pitch-based carbon fibres: Part I. Some influential factors for crack formation. Journal of Materials Science 32, 2753–2758.

Yoon, S.-H., 2015. RE: Personal Communication.

Yoshiya, A., July 2001. Characteristics and applications of pitch-based carbon rollers. *Paper, Film & Foil Convertech Pacific*, pp. 38–40.

Yoshiya, A., May/June 2011. "Carboleader" high-performance carbon fiber composite rollers for the film industry. *Convertech & e-Print*, pp. 83–88.

Yuan, G., Li, X., Dong, Z., Westwood, A., Rand, B., Cui, Z., Cong, Y., Zhang, J., Li, Y., Zhang, Z., Wang, J., 2014. The structure and properties of ribbon-shaped carbon fibers with high orientation. Carbon 68, 426–439.

Yumitori, S., Nakanishi, Y., 1996a. Effect of anodic oxidation of coal tar pitch-based carbon fibre on adhesion in epoxy matrix: Part 1. Comparison between H_2SO_4 and NaOH solutions. Composites Part A: Applied Science and Manufacturing 27, 1051−1058.

Yumitori, S., Nakanishi, Y., 1996b. Effect of anodic oxidation of coal tar pitch-based carbon fibre on adhesion in epoxy matrix: Part 2. Comparative study of three alkaline solutions. Composites Part A: Applied Science and Manufacturing 27, 1059−1066.

Zeng, S.-M., Korai, Y., Mochida, I., Hino, T., Toshima, H., 1990. The creation of a skin-core structure in petroleum derived mesophase pitch based carbon fiber. Bulletin of the Chemical Society of Japan 63, 2083−2088.

Zeng, S.M., Maeda, T., Mondori, J., Tokumitsu, K., Mochida, I., 1993a. Preparation of isotropic pitch precursors for general purpose carbon fibers (GPCF) by air blowing—III. Air blowing of isotropic naphthalene and hydrogenated coal tar pitches with addition of 1,8-dinitronaphthalene. Carbon 31, 421−426.

Zeng, S.M., Maeda, T., Tokumitsu, K., Mondori, J., Mochida, I., 1993b. Preparation of isotropic pitch precursors for general purpose carbon fibers (GPCF) by air blowing—II. Air blowing of coal tar, hydrogenated coal tar, and petroleum pitches. Carbon 31, 413−419.

Zhang, X., Fujiwara, S., Fujii, M., 2000. Measurements of thermal conductivity and electrical conductivity of a single carbon fiber. International Journal of Thermophysics 21, 965−980.

High-performance carbon nanofibers and nanotubes

4

N. Hiremath [1], G. Bhat [2]
[1]The University of Tennessee, Knoxville, TN, United States; [2]The University of Georgia, Athens, Georgia, United States

4.1 Carbon nanotubes (CNTs)

4.1.1 Introduction to CNTs

In this chapter, a brief overview on the discovery, structure, theory, and synthesis of CNTs is presented. Though it is important to understand the precise structure of a CNT, it is not easy to conceive, as there are many theories related to its explanations [1]. Only an overview on CNT structure and its various symmetrical aspects is discussed. Readers are requested to refer to the references for a deeper understanding of the physics of CNTs.

Smalley and Kroto in 1985 started their work to identify the products of vaporization of graphite, because their motive was to understand the processes that occur on stars. They used high-energy lasers to vaporize graphite in a helium atmosphere and found that the soot contained C_{60}, a carbon nanosphere or the famous "buckminsterfullerene." In similar experiments, Krätschmer and Huffman in 1990 were able to find 90% C_{60} and 10% C_{70}. In 1991, Iijima, in the NEC laboratories in Japan, discovered CNTs that were cylindrical in nature with closed ends. CNTs are cylindrically arranged carbon atoms as shown in Fig. 4.1. The CNTs gained importance as reinforcing materials in the polymer and metal matrix because of their inherent strength. The tensile strength of CNTs is ~1 TPa, which is at least 200 times higher than that of steel of similar dimensions. To understand its property better, it is important to understand the structure of CNTs. CNTs are synthesized from various techniques associated with various advantages and disadvantages. Each of the techniques is discussed and a table is provided to differentiate between the techniques. There are two types of CNTs, single-walled nanotubes (SWNTs) and multiwalled nanotubes

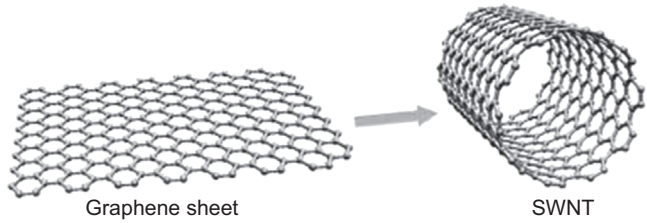

Figure 4.1 Schematic of a carbon nanotube [2].

Structure and Properties of High-Performance Fibers. http://dx.doi.org/10.1016/B978-0-08-100550-7.00004-8

(MWNTs). SWNTs contain one layer of carbon atom sheet or graphene while MWNTs are made up of multiple layers of graphene concentrically or spirally formed [1]. CNTs are also spun into yarns directly from the chemical vapor deposition (CVD) instrument.

4.1.2 Structure of CNTs

The structure of CNTs' "archetypal" armchair and zig-zag can be understood by bisecting along the threefold and fivefold axes. To understand the chirality of the structure of the nanotube, we have to open up the nanotube to form a layer of carbon atoms, a graphene sheet. It is hard to implement the rules of crystallography even though the structure of a CNT is crystalline in nature. Certain biological structures come close to that of CNTs; however, the factors governing these cylindrical biological structures are insufficient for CNT structure analysis. Many scientists have introduced different methods to explain the nature of formation of the nanotube. Theoretical structure analysis has helped understand the electronic and vibrational properties of CNTs. Experimental studies using high-resolution electron microscopy have helped further understand and affirm the structure of CNTs [1,3].

The two possible symmetric structures of nanotubes are armchair and zig-zag. In reality, the hexagons on the CNTs arrange helically along the CNT axis. The degree of helical arrangement or chirality is given by θ. To understand the structure in terms of vector, **C**, which joins two equivalent points on the graphene layer as shown in Fig. 4.2, vectors $\mathbf{a}_1$ and $\mathbf{a}_2$, a cylinder is formed when the graphene sheet is rolled

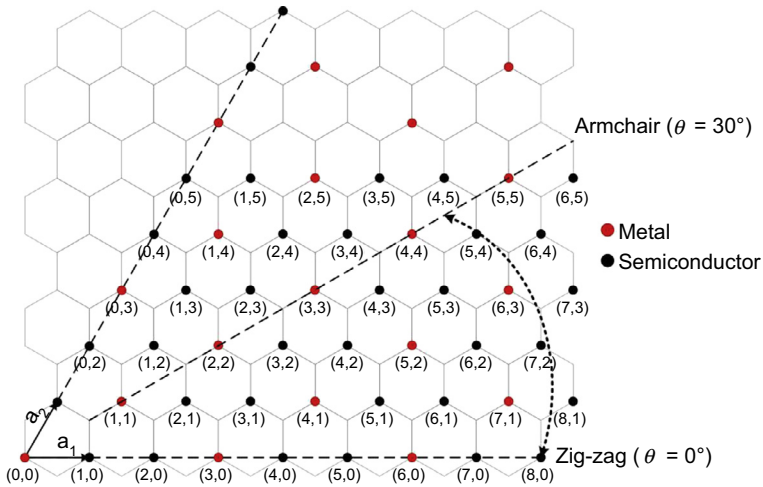

Figure 4.2 A graphene sheet explaining the formation of different types of carbon nanotubes. $\mathbf{a}_1$ and $\mathbf{a}_2$ are the vectors. Red dots are carbon atoms, which inherit metallic behavior, and the black dots inherit semiconductor behavior.
Based on Harris PJ. Carbon nanotubes and related structures. Cambridge University Press; 2001.

such that the two end points of the vector are superimposed. From Fig. 4.2, integer (n, m) represents a tubular structure. Therefore vector **C** could be expressed as:

$$\mathbf{C} = n\mathbf{a}_1 + m\mathbf{a}_2$$

where $\mathbf{a}_1$ and $\mathbf{a}_2$ are of length 0.246 nm as the C−C bond length is 0.142 nm. Furthermore, it is explicit that for $n = m$, armchair tubes (with $\theta = 30°$) could be formed and for $m = 0$, zig-zag tubes (with $\theta = 0°$) could be formed. For these tubes the diameter d could be calculated by the expression [1,3]:

$$d = \frac{0.246\sqrt{(n^2 + nm + m^2)}}{\pi}$$

and the angle of chirality could be expressed by θ:

$$\theta = \sin^{-1}\frac{\sqrt{3m}}{2\sqrt{n^2 + nm + m^2}}$$

A unit CNT has the form translation of a cylinder. In Figs. 4.3 and 4.4, unit cells of armchair and zig-zag are shown. In the armchair-type structure the width of the unit cell is same as vector a, while for zig-zag it is $\sqrt{3}$a. The length of the unit cell depends

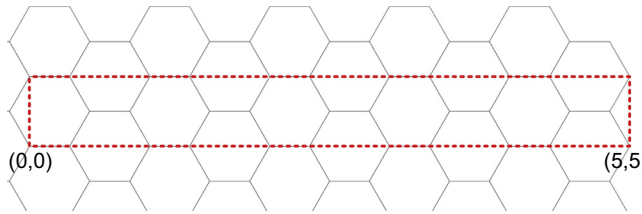

Figure 4.3 A typical unit cell of armchair type of carbon nanotubes.
Inspired by Harris PJ. Carbon nanotubes and related structures. Cambridge University Press; 2001.

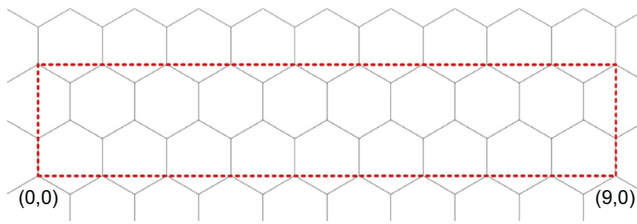

Figure 4.4 A typical unit cell of zig-zag type of carbon nanotubes.
Inspired by Harris PJ. Carbon nanotubes and related structures. Cambridge University Press; 2001.

on the diameter of the CNT. Furthermore, chiral structures lower symmetry results. The number of carbon atoms in the unit cell can be calculated by the expression:

$$N = 2\left(n^2 + nm + m^2\right)d_{\mathrm{H}} \quad \text{if} \quad n - m \neq 3xd_{\mathrm{H}}$$

and:

$$N = 2\left(n^2 + nm + m^2\right)3d_{\mathrm{H}} \quad \text{if} \quad n - m = 3xd_{\mathrm{H}}$$

where d_{H} is highest common factor of n and m and x is some integer.

4.1.3 Theory

Since CNTs have diameters smaller than 10 nm, these structures exhibit quantum mechanical behavior. Many scientists have investigated the physics of CNT structure and have claimed that CNTs possess a metallic or semiconductor-like nature. Certain structures with a precise diameter (all armchair structures and n, m multiples of 3) exhibit a metal-like character and others behave as semiconductors. As the CNTs are highly anisotropic, electron mobility along the basal planes is high while mobility perpendicular to the planes is low [1,3]. Wallace in 1947 calculated band structures for conduction only in planes, while ignoring conduction between the planes. The expression is as follows:

$$E_{2\mathrm{D}}(k_x, k_y) = \pm\gamma_0\sqrt{\left\{1 + 4\cos\left(\frac{\sqrt{(3)}}{2}k_x a\right)\cos\left(\frac{k_y a}{2}\right) + 4\cos^2\left(\frac{k_y a}{2}\right)\right\}}$$

where γ_0 is the nearest-neighbor transfer integral and $a = 0.246$ nm, the in-plane lattice constant. E is energy in 2D k-space where k_x and k_y are the wave numbers in the x and y directions, respectively.

This expression is for a 2D graphite structure with two atoms in the unit cell. This yields four valence bands (three σ bands and one π band). Fig. 4.5 shows the E (energy) versus k (wave number) data for the 2D graphite structure along K−Γ−M [4]. Fig. 4.6 shows the density of states for armchair and zig-zag CNT structures [5].

4.1.4 Synthesis of CNTs

To achieve the amazing properties of ideal CNTs, it is critical that the CNTs should be fabricated to 100% purity. In reality, this is extremely difficult. Various other carbon materials such as amorphous carbon, other carbon nanoparticles, etc., act as impurities. Some of the synthesis techniques used to fabricate high-purity CNTs are briefly discussed herein and Table 4.1 provides a summary of the synthesis techniques.

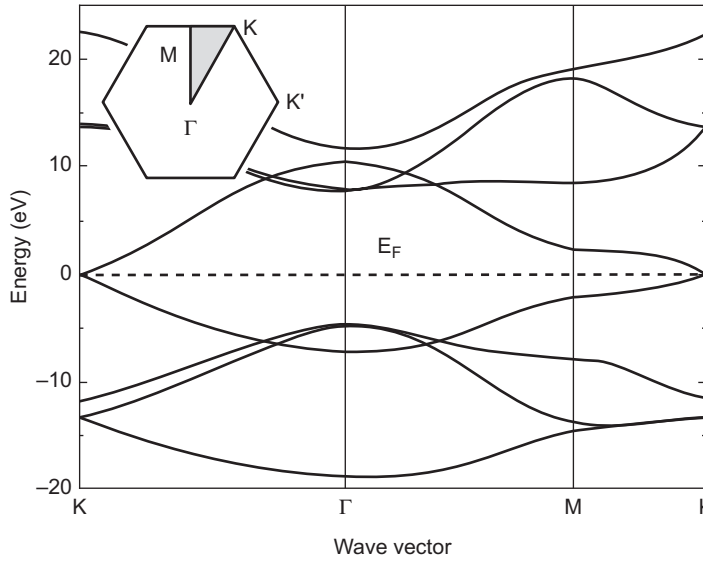

Figure 4.5 Energy versus k-vector along the K−Γ−M direction of a 2D graphite structure [4].

4.1.4.1 Arc discharge

A low-voltage (12−25 V), high-current (50−120 A) power supply on graphite electrodes (5−20 mm in diameter) placed 1 mm apart in the presence of He or Ar gas (100−1000 torr) produces CNTs with typical yields ranging from 30% to 90%, as shown in Fig. 4.7. In the arc-discharge method, variations are made in the procedure to tune the properties of the CNTs. By mixing different gases, Ar and He, the properties can be varied, for example, a higher Ar:He ratio produces smaller diameter CNTs [3]. This batch process is inexpensive and yields high-purity CNTs with varying lengths.

4.1.4.2 Laser ablation technique

A cobalt/nickel with graphite composite target is evaporated by pulsed or continuous laser by placing the electrode in a quartz tube, at 1200°C, in an inert atmosphere of He or Ar, at 500 torr, with a typical yield of about 70%. A metal-impregnated graphite target produces SWNTs and a pure graphite target produces MWNTs and fullerenes. A schematic of a laser ablation technique is shown in Fig. 4.8. The CNTs are deposited on the cold finger [3]. This is a batch process and yields high-purity CNTs with good diameter control. This is a very expensive process as the high-energy laser beam is expensive to make and requires an ultraclean inert atmosphere.

4.1.4.3 Chemical vapor deposition

Gaseous carbon feedstock, such as methane, is passed over metal nanoparticles at temperatures ranging from 550 to 1200°C, where the feedstock reacts with the

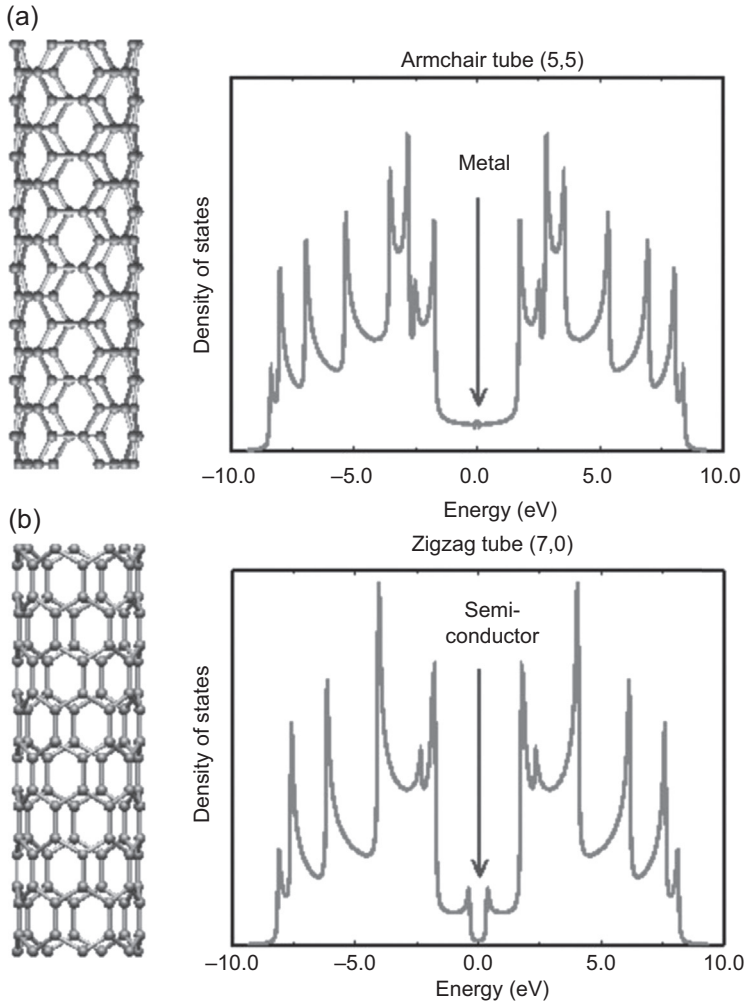

Figure 4.6 Density of states for (a) armchair and (b) zig-zag CNTs [5].

nanoparticles to produce SWNTs. This method provides higher purity of CNTs (99%) in bulk quantities. Other types of CVD include hot filament, water assisted, oxygen assisted, microwave plasma, radio frequency, thermal, plasma enhanced, etc. [3].

Some of the recent advancements in CNT synthesis involve finding new precursors, for example, coal, and new processing methods, such as the solar furnace. Coal is much less expensive than graphite and high-purity hydrocarbon gas sources. Even though CNTs can be produced from both arc-discharge and thermal plasma jet with coal as precursor, large-scale production is not currently possible [6]. However, CVD can be used to synthesize CNTs in large quantities by optimizing the experimental conditions.

Table 4.1 Advantages and disadvantages of the various synthesis techniques discussed [9]

Methods	Typical yield	Advantages	Disadvantages
Arc discharge	30−90%	Simple process, inexpensive, high yield and high purity, diameter = 1−20 nm	Shorter tubes with random length, batch process
Laser ablation	~70%	High purity, good diameter control	Cost of the equipment is high, batch process
Chemical vapor deposition	~95%	High purity, long tubes, easy processing, continuous process, diameter = 0.8−2 nm	High defects present
Solar furnace	~60%	Diameter = 1.2−1.6 nm	Very slow process and random length tubes

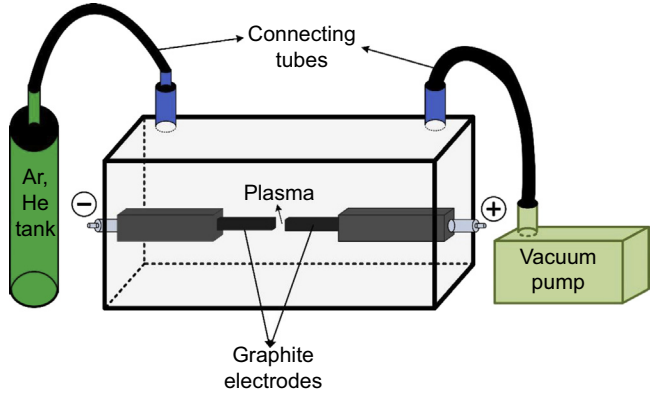

Figure 4.7 A schematic of arc-discharge tube with a small gap between electrodes.

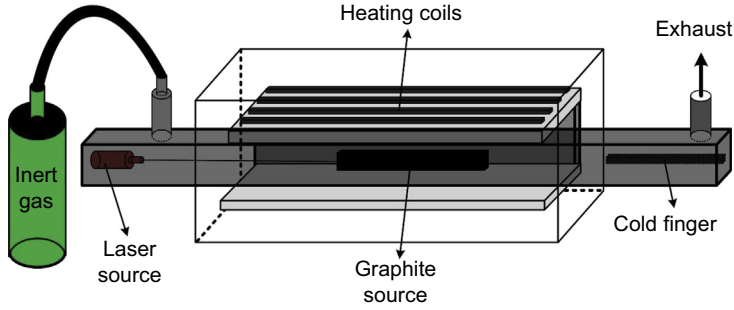

Figure 4.8 A schematic of the laser ablation technique.

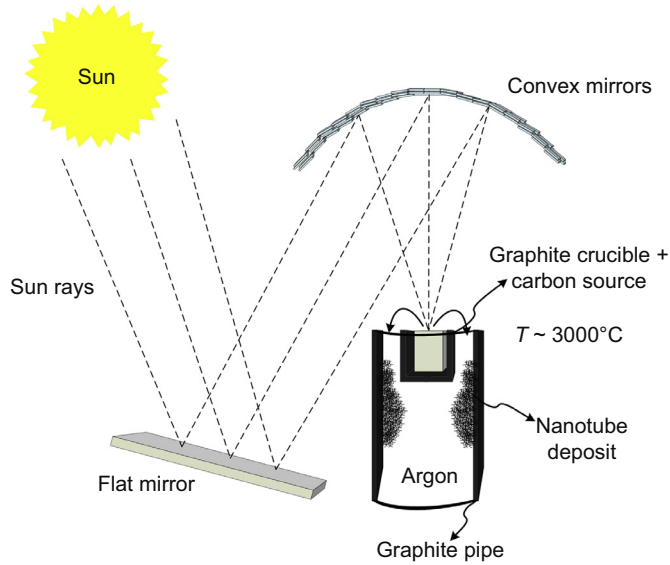

Figure 4.9 A schematic of CNTs produced by solar furnace technique.

4.1.4.4 Solar furnace

In the solar furnace method as shown in Fig. 4.9, the graphite source with metal catalyst is placed in a graphite crucible. A highly directed solar beam hits the source creating a temperature of about 3000K, triggering evaporation of carbon and resulting in soot settling on the walls of the graphite tube. This soot on the walls of the graphite pipe contains CNTs and other forms of carbon nanostructures such as fullerenes. The diameter of the CNTs produced by this method lies in the range of 1.2−1.5 nm, with high purity comparable to those of CNTs produced by the laser ablation technique [7,8]. However, the lengths of the tubes are random and it is a very slow process with a yield of up to 60%.

4.2 Carbon nanotube-based fibers

4.2.1 CNT-based composite fibers

The high-performance fiber industry has changed the face of the textile market, because of the properties the high-performance fibers inherit, such as nylon, polyester, etc. To make composite fibers, many researchers have studied new processes and materials that deliver high strength. A polymer matrix with CNTs has proven to increase the strength and modulus considerably; however, the results have fallen far short of the expected theoretical values. Table 4.2 summarizes the strength and modulus of various compositions of composite fibers derived

Table 4.2 CNT/polymer composites and their tensile strength, elastic modulus, and toughness

Composite fiber (CNT wt% + polymer)	Tensile strength (GPa)	Elastic modulus (GPa)	Toughness	References
Carbonized PAN	2.0 ± 0.4	302 ± 32	N/A	[20,21]
Carbonized PAN + 1 wt% SWNT	3.2 ± 0.4	450 ± 49	N/A	
Nylon 6	0.045	0.44	N/A	[13]
Nylon 6 + 0.1 wt% SWNT	0.086	0.54	N/A	
Nylon 6 + 0.2 wt% SWNT	0.093	0.66	N/A	
Nylon 6 + 0.5 wt% SWNT	0.083	0.84	N/A	
Nylon 6 + 1.0 wt% SWNT	0.083	1.15	N/A	
Nylon 6 + 1.5 wt% SWNT	0.075	1.2	N/A	
PAN	0.9 ± 0.18	22.1 ± 1.2	35 ± 9 MPa	[22]
PAN + 0.5 wt% SWNT	1.06 ± 0.14	25.5 ± 0.8	41 ± 8 MPa	
PAN + 1 wt% SWNT	1.07 ± 0.14	28.7 ± 2.7	39 ± 8 MPa	
PBO	2.6 ± 0.3	138 ± 20	N/A	[23]
PBO + >10 wt% SWNT	4.2 ± 0.5	167 ± 15	N/A	
Polypropylene (PP)	0.71	6.3	7.93 dN/tex	[24]
PP + 0.5 wt% SWNT	0.84	9.3	9.37 dN/tex	
PP + 1 wt% SWNT	1.03	9.8	11.5 dN/tex	
PVA + >60 wt% SWNT	0.15	9−15	N/A	[19,25]
PVA + 60 wt% SWNT	1.8	80	570 J/g	
PVA (commercial fiber)	1.6	40	N/A	[15]
PVA + >60 wt% SWNT	1.8	78	120 ± 152 J/g	

Continued

Table 4.2 Continued

Composite fiber (CNT wt% + polymer)	Tensile strength (GPa)	Elastic modulus (GPa)	Toughness	References
PVA + 60 wt% SWNT	0.3	40	600 J/g	[14]
PVA	1.2 ± 0.3	21.8 ± 3.0	55.8 ± 12.3 J/g	[11]
PVA + 10 wt% SWNT	2.5 ± 0.1	36.3 ± 1.3	101.4 ± 11.4 J/g	
PVA + 10 wt% SWNT	4.4 ± 0.5	119.1 ± 8.6	171.6 ± 30.4	
PVA	~0.4	~13	N/A	[16]
PVA + 1 wt% SWNT	~1.2	~17.5	N/A	
PVA	1 ± 0.1	45 ± 7	22 ± 4 J/g	[17]
PVA	1.6 ± 0.1	48 ± 3	40 ± 6 J/g	
PVA + 1 wt% SWNT	1.4 ± 0.1	60 ± 6	29 ± 6 J/g	
PVA + 1 wt% SWNT	2.6 ± 0.2	71 ± 6	59 ± 7 J/g	
PVA + 2–31 wt% SWNT	~2.9	~244	N/A	[18]
UHMWPE	3.51 ± 0.13	122.6 ± 1.9	76.7 ± 7.5 MPa	[12]
UHMWPE + 5 wt% MWNT	4.17 ± 0.04	136.8 ± 3.8	110.6 ± 10.5 MPa	

MWNT, Multiwalled nanotube; *N/A*, not available; *PAN*, polyacrylonitrile; *PBO*, poly(p-phenylenebenzobisoxazole); *PVA*, poly(vinyl alcohol); *SWNT*, single-walled nanotube; *UHMWPE*, ultrahigh molecular weight polyethylene.

using CNTs as fillers [10]. From the data in the table we can see that for carbonized polyacrylonitrite (PAN) with 1 wt% SWNT, the tensile strength and modulus increased by 60% and 49%, respectively. For nylon 6, from addition of 1.5 wt% of SWNT, the tensile strength and modulus have increased by ~66% and 172%, respectively. Similarly, for PAN with 1 wt% SWNT, the tensile strength and modulus have increased by ~18% and ~30%, respectively. About a fourfold increase in strength and about a sixfold increase in modulus are reported by Meng et al. in the case of poly(vinyl alcohol) (PVA) +10 wt% [11] SWNT. About an 18% increase in strength and an 11% increase in modulus are observed in the case of ultrahigh molecular weight polyethylene (UHMWPE) +5 wt% MWNT, as reported by Ruan et al. [12]. A brief overview of various composite fibers, mentioned in Table 4.2, is summarized in the following sections. Figs. 4.10(a,b) and 4.11(a,b) are pictorial representations of the difference between the tensile strength and elastic modulus of various composite fibers discussed in Table 4.2.

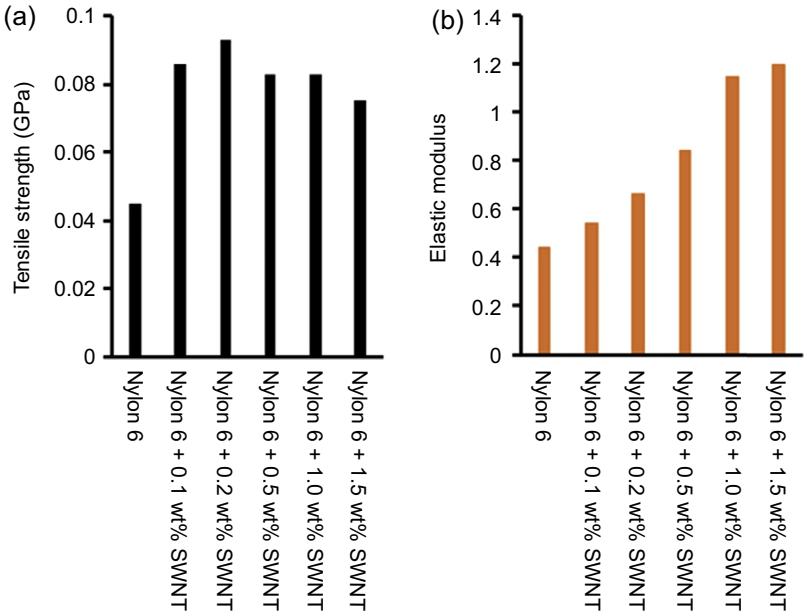

Figure 4.10 (a) and (b) Tensile strength and elastic modulus data for nylon 6-CNT-based composite fibers based on data from [13].

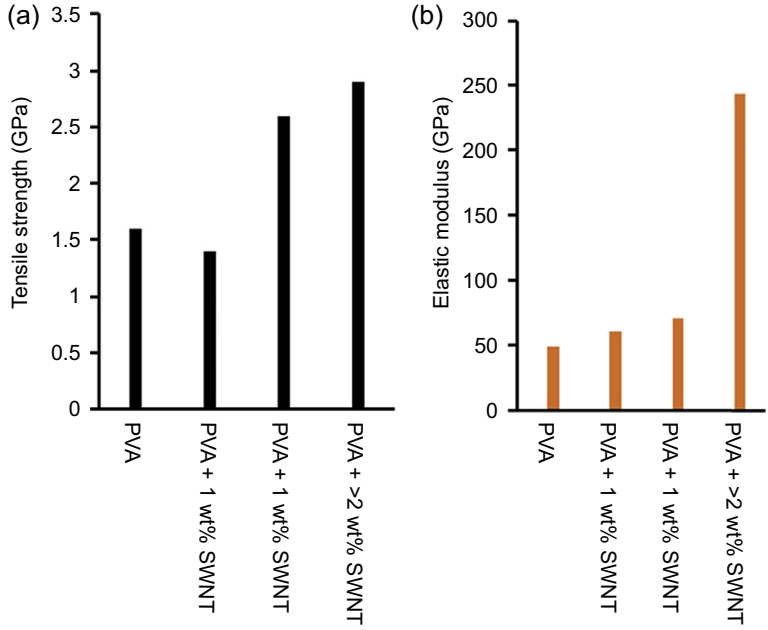

Figure 4.11 (a) and (b) Tensile strength and elastic modulus data for PVA-CNT-based composite fibers from various researchers based on data from [17,18].

4.2.1.1 Nylon-CNT composite fiber

The CNT-caprolactam sonicated suspension was heated and mechanically stirred to 250°C with 6-aminocaproic acid. Following the mixture formation, the product was poured in water and the hard polymer was precipitated. The polymer was broken into small pieces, heated to 250°C, and extruded using a spinneret by pressurized nitrogen gas. The fibers were then characterized with various mechanical tests. The incorporation of 1.5 wt% SWNTs into nylon 6 increased the tensile modulus and tensile strength about three and two times, respectively [13]. These improvements in strength and modulus data are compared in Fig. 4.10(a) and (b).

4.2.1.2 PBO-CNTs

High-pressure carbon monoxide nanotubes (SWNTs) were added to the poly (*p*-phenylenebenzobisoxazole) (PBO) polymerization solution in the ratio of 90:10: PBO:SWNT and 95:05. The fibers were spun using a dry-jet wet-spinning process using a piston-driven setup. The fibers were collected in the distilled water coagulation bath maintained at room temperature. The air gap was maintained at 10 cm from the spinneret to coagulation bath. The fibers with 10% SWNT in PBO showed an increase in tensile strength of 50% of the PBO fibers, and there was an increase in creep resistance as well.

4.2.1.3 PP-CNTs

The SWNTs were dispersed in decalin by sonication and the polypropylene (PP) pellets were added to the solvent mixture. The PP-SWNT mixture, in the form of coarse powder, was extruded with a spinneret of 1.22 mm diameter and the fiber was further drawn. Though the PP-SWNT composite fibers were not of enough strength compared to other composite fibers, with 1 wt% loading of nanotubes, the fiber tensile strength increased by 40% and the modulus increased by 55%. By incorporating CNTs dispersed in sodium dodecyl sulfate, a surfactant, by sonication, the solution was injected into a coflowing system of a polymer solution. The resulting CNT ribbon was taken out, dried, and characterized with mechanical properties. The strength of the ribbon was 10 times higher than high-quality bucky paper. Also knotting the fibers revealed that the fiber can be curved through 360 degrees in a few micrometers, which demonstrates the flexibility and high torsion resistance of those fibers.

4.2.1.4 PVA-CNTs

In Razal's, Dalton's and Meng's research, the PVA-CNTs composite fibers were extruded in different spinning mechanisms [11,14,15]. Razal's group used a coagulation-spinning method, which involved dispersion of SWNTs injected into a PVA solution flowing in a glass tube. In Dalton's group the aqueous dispersion of nanotubes was spun in a rotating coagulation bath of aqueous PVA solution. In Meng's group a shear-flow gel spinning method was used, in which the methanol was stirred to provide shearing as the PVA-SWNT solution was injected to form fibers.

The spun fibers were subsequently drawn on hot plates at 90°C and 160°C. Hence there were variations in the tensile strengths of the PVA-CNT composite fibers.

In Wang's research group the SWNTs were dispersed in dimethyl sulfoxide, and PVA solution was mixed to form the PVA-SWNT composite mixture [16]. The mixture was spun by solid-state spinning with a draw ratio of 5. The tape drawn from the composite (PVA-SWNT) was 200% stronger than the PVA tape of similar length. Hence addition of 1 wt% SWNTs increased the strength drastically. However, in Minus's group the PVA-SWNT composite fiber was extruded by gel-spinning method [17]. The tensile properties of the composite fibers were higher than that of the composite fibers from Wang's group. This could be caused by the spinning method, the solution preparation techniques involved and the fiber diameter, purity of CNTs, interfacial binding between the polymer and the CNTs, etc. In Young's group the PVA-CNT composite fiber was extruded using coagulation spinning [18]. The diameter of the fiber was in the range of 1−15 μm, the mean modulus was about 244 GPa, and strength about 2.9 GPa. This high strength was attributed to the distribution of the CNTs in the polymer matrix and binding. The higher the concentration of the CNTs in the matrix, the higher the load-bearing interaction. The increasing trend in strength and modulus observed with addition of CNTs in PVA fibers are shown in Figs. 4.11(a) and (b), respectively. Some of the authors [14,15,19] claim to have CNTs as high as 60 wt% in the PVA-based composite fibers; however, the percentage calculated from the procedure in the respective paper does not exceed 8 wt% of CNTs. From several studies it is well known that incorporating higher concentrations of CNTs especially above 5 wt% is extremely difficult and it is hard to believe that the authors produced PVA samples with a 60 wt% CNT loading.

4.2.1.5 UHMWPE-CNTs

In Ruan's group, multiwalled CNTs were used as reinforcement in the polymer matrix: 5 wt% MWCNTs were reinforced in gel-spun UHMWPE resulting in a yield strength of 4.2 GPa and strain at break of 5%. By reinforcement of CNTs in UHMWPE there was an increase of 18.8% in tensile strength and 15.4% in ductility. In addition, a 44.2% increase in energy to fracture was observed.

4.2.2 CNT-based CFs

CNT-based carbon fibers (CFs) are produced by various approaches, such as aqueous dispersion, dispersion in strong acids, drawing from CNT forests, drawing from CVD reactor in the form of aerogel, etc. They are relatively ductile when compared to PAN- or pitch-based CFs because the knot efficiency of the CNT-based CF is ∼1 while PAN- or pitch-based CFs cannot be knotted [26]. The tensile strength and modulus of CFs are higher for CNT fiber spun from CNT forests and from CVD reactors. However, stretching the CFs aligns the CNTs and improves the mechanical properties by increasing the interaction between CNTs. Longer CNTs do help to improve the performance, chemical modification, gamma-ray induced crosslinking, heat treatment, etc.,

on the CNTs' surface, which further enhances internanotube interaction, resulting in increase in strength. However, the compressive strength achieved was low [26].

When synthesizing CNTs by various processes discussed in Section 4.4, if there is a possibility to isolate the pure CNTs, the quality of the CF produced using such nanotubes would yield higher strength and modulus. However, during the preparation of CNTs there are various other structures generated, such as fullerenes and amorphous carbon agglomerates, and these structures are the weak points or defects in CNT-based CFs [1]. Furthermore, the CNTs that are produced with highest purity must also be dispersed well in the medium of interest. Generally, the CNTs are dispersed in suitable polymers and melt drawn to high draw ratios. Increasing the draw ratio helps align the CNTs in the polymer matrix and hence increases the strength of the CFs. CNTs can also be grafted into the CFs, such as PAN or pitch based, to increase the alignment of the polymer matrix or to act as the load-bearing structures in the CF matrix [27].

Carbon nanofibers (CNFs) produced by the pyrolysis of cellulose contain no skin–core morphology, resulting in high tensile modulus of 60 and 100 GPa, when carbonized at 1500 and 2200°C, respectively [28]. By producing high purity and continuous nanotubes the internanotube interaction can be increased resulting in high-strength CFs. In an attempt to make the CNTs long, in 2009, a research group from Peking University, China, led by Qunqing Li, grew ultralong single-wall CNTs using an improved CVD technique [29]. Using ethanol or methane as the feed and an Fe-Mo monodispersed catalyst, super-aligned ultralong CNT was grown for a length of 18.5 cm. Homogeneous temperature spatially during the growth process is the key for constant electrical characteristics. However, improving the mechanical properties of the CNTs along the length is also equally important for high-strength materials applications. In 2013, Zhang reported that 550-mm long CNTs were fabricated using a floating CVD process and catalyst activation/deactivation probability. Following optimized processing parameters, half-meter long CNTs fabricated exhibited a tensile stress of up to 120 GPa [30].

4.3 CNT yarns

CNT yarns are derived from spinning CNTs to form a yarn. A CNT yarn is analogous to a spun yarn from short 25–40-nm staple fibers by orienting and twisting them, in terms of structural formation. CNTs are grown in a CVD reactor and are spun directly from the reactor in the form of aerogel or the CNTs are grown on a substrate and spun in a batch process as shown in Fig. 4.12(a) and (b). The liquid feedstock is continuously fed into the CVD reactor, an aerogel is formed, and a wind-up bar (at an angle) collects CNT aerogel in the reactor and forms a yarn, which is further collected on a spindle. In the other approach, a CNT forest is grown on a substrate, the CNTs (they are sticky because of high surface area and high purity) stick to each other, and when pulled out of the substrate and twisted a yarn is formed as shown in Fig. 4.12(b).

CNT yarns bought from generalnanollc.com, Cincinnati, Ohio, were characterized using various techniques such as scanning electron microscopy (SEM), transmission

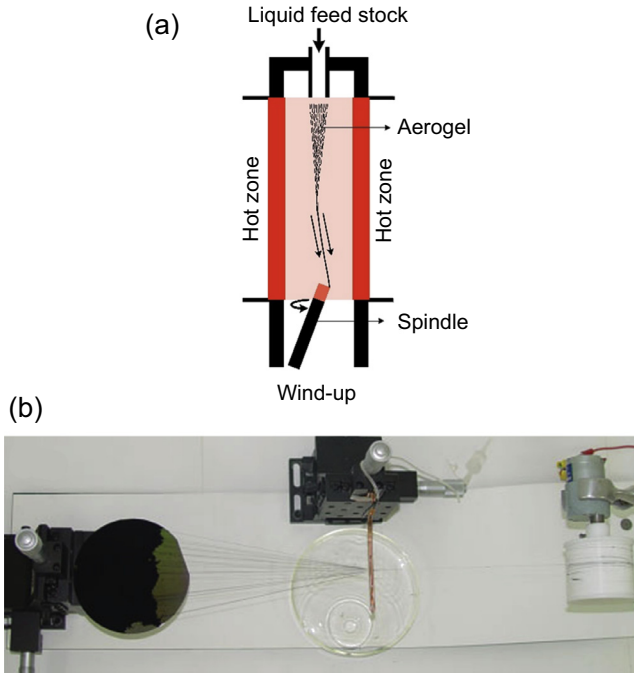

Figure 4.12 (a) CNT yarn spun from CVD reactor and wound on a spindle. Schematic based on [31]. (b) CNT forest grown on silicon substrate and spun with a twisting instrument and collected on a spindle [32].

electron microscopy (TEM), focused ion beam (FIB), and tensile testing. SEM photographs show that there is lot of vacancy present in the structure of the CNT yarns (Fig. 4.13). The orientation of the nanotubes on the surface shows that there is significant opportunity to enhance the nanotube organization to increase the strength and improve the mechanical properties.

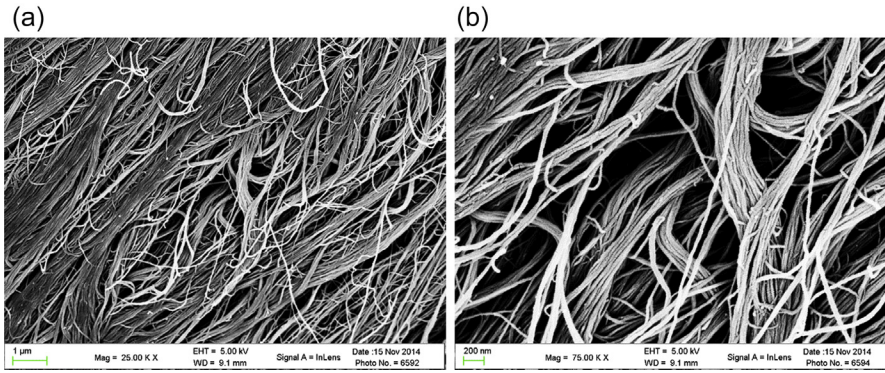

Figure 4.13 (a) SEM image of CNT yarn at lower magnification depicting porous structure, and (b) at higher magnification showing larger voids.

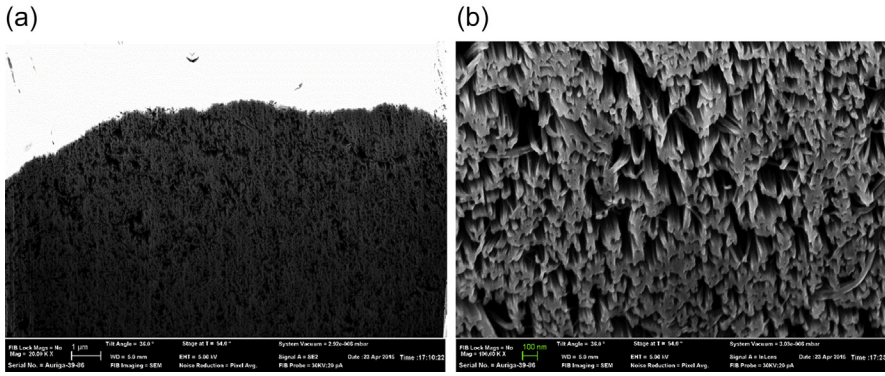

Figure 4.14 (a) Cross-section of CNT yarn at lower magnification showing highly porous structure. (b) Cross-section of CNT yarn at higher magnification showing porosity.

FIB was carried out to investigate the cross-section of the yarn. The CNT yarns show the presence of vacancy in the cross-section (Fig. 4.14). The striations in the images are caused by the ion beam milling marks. As the void in the yarn is also large, further densifying and improving the interaction/bonding between the nanotubes should enhance the strength and other mechanical properties. Furthermore, milling along the length of the yarn shows that the CNTs are arranged in various directions and the nanotubes in the yarn are not completely oriented along the yarn axis.

Tensile testing of the yarn was performed on MTS Systems Corporation single filament tensile tester at Oakridge National Laboratories (ORNL). Three types of yarns were tested, CNT yarn from generalnanollc.com (CY-1), single ply (CY-2), and acetone densified (CY-3) from nanocomptech.com. Tensile strength and modulus of these samples are as shown in Fig. 4.15. The differences in observed tensile data can be attributed to the packing and diameter of the yarn. The CY-1 average diameter is 46 ± 4 μm while CY-2 and CY-3 are about 62 ± 6 μm.

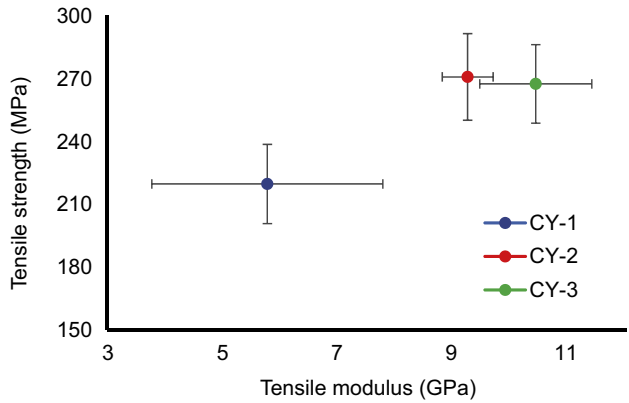

Figure 4.15 Tensile testing data of carbon yarns tested at the ORNL facility. CY-1 is CNT yarn from generalnanollc.com, CY-2 is single ply, and CY-3 is acetone densified.

The CNT yarns can further be improved by infiltrating polymer or by crosslinking using irradiation techniques. In one of the studies, chemical functionalization and electron beam irradiation was carried out on the CNT sheets [33]. The tensile strength increased by 88% when the CNT sheets were chemically crosslinked and further irradiated with electron beam. Crosslinking improves the bonding between the nanotubes while irradiation physically welds one nanotube to the other or bunch of nanotubes to other nanotubes. This increases the load-bearing capacity and the material does not experience catastrophic failure. Such a drastic increase in mechanical properties is desired in futuristic aerospace applications, advanced composites, etc.

4.4 Carbon nanofibers

4.4.1 Introduction to carbon nanofibers

CNFs are sp^2-based linear structures with a diameter of $\approx$100 nm and a length of $\approx$200 μm. These nanodiameter fibers are scientifically prominent because of their unique physical, mechanical, and chemical properties. For the high specific area, flexibility, and high mechanical strength, CNFs could be used in tough composites for vehicle and aerospace applications, biosensors, electrodes and supercapacitors, tissue engineering scaffolds, etc. The difference between CNFs and CFs is the diameter. Conventional CFs have diameters of several micrometers while CNFs have several nanometer-sized diameters. In addition, CNFs are different from CNTs in their geometry, from concentric CNTs containing an entire hollow core, CNFs have regularly stacked, truncated conical or planar layers along the fiber length as shown in Fig. 4.16. Furthermore, because of the cup-stacked structure, CNFs carry semiconducting behavior and because both inner and outer surfaces are chemically active they are well suited for catalysts, reinforcing fillers in composites,

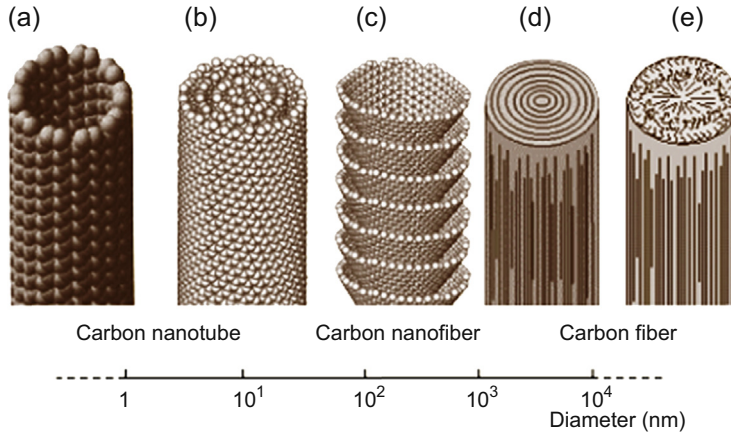

Figure 4.16 Schematic of size and morphology distribution of various nanotubular structures [34].

photochemical cells, etc. [34]. In conjunction, CNFs can be made from electrospinning of organic polymers with thermal treatment in an inert atmosphere. Electrospun nanofibers have high surface area, nanometer range diameter, and web-like morphology suited for high-performance nanocomposites for tissue engineering applications and energy storage devices.

4.4.1.1 History of CNFs

As the conventional CFs were expensive for composite applications in the early 1970s and 1980s, an effort to make vapor-grown CNFs or CNFs from a hydrocarbon source was initiated in Japan, the Soviet Union, the United States, and France. The CNFs synthesized from the CVD technique would emulate the properties of conventional CFs of the respective size and at a cheaper price than CFs. CNFs are grown to lengths of up to 200 μm using iron catalyst in methane or benzene as feed and hydrogen as diluting gas. In the early 1980s, fibrils.com (Hyperion) attempted to develop nanofibers on dispersed catalyst nanoparticles in the CVD with hydrocarbon gases at high temperatures. The resulting fibers were relatively longer and entangled with cylinder-like morphology. In 1991, Applied Sciences, Inc., in association with General Motors research, started making and marketing Pyrograf I and III (CNFs processed at 1500°C and 2900°C respectively). These fibers have a structure similar to a spirally wound ribbon, and are manufactured with varying thicknesses of surface vapor deposition of carbon. The cost of 1 kg of CNF is US$200 [35]. Because they are less expensive than nanotubes, many research groups have incorporated CNFs in composites and composite filaments. CNFs are also highly entangled, and orienting them in a particular direction is a challenge. CNFs, because of their electrical and thermal conductivity, are used in electrostatic discharge applications, radio-frequency interference, etc. Nevertheless, efforts are continuing to make them aligned in a filament-spinning direction to exploit their mechanical properties. CNFs are also used in making papers for supercapacitors and fuel cell membranes for electromagnetic interference shielding applications with improved 2D mechanical properties. They can also be isotropically reinforced in resins for making injection-molded thermoplastic parts. Because CNFs inherit exceptional mechanical properties, high electrical and thermal conductivities, they can be deployed in a wide range of matrices including but not limited to thermoplastics, thermosets, elastomers, ceramics, and metals. Moreover, because of the unique surface of CNFs, functionalization and other surface modification compatibilizing with the host polymer is easier than with the CNTs [34,35].

4.4.2 Structure of carbon nanofibers

Carbon or graphite fibers are important graphitic materials that are closely associated with CNFs in terms of structure and properties. They have received a lot of attention as they are used in aerospace and automotive, construction, sports, electronic device, biosensor, and tissue engineering applications. The specific strength (strength/weight) and specific modulus (stiffness/weight) of CF-reinforced composites explain their importance as engineering materials, because of the high performance of their CF

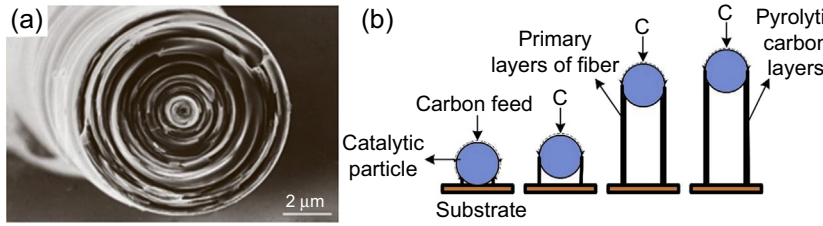

Figure 4.17 (a) Annular ring type of morphology of CNFs and (b) schematic of catalytic growth process of CNFs [34].

constituents [34]. The temperature and pressure required to make a CF from the liquid phase is at the triple point ($T = 4100$K, $p = 123$ kbar). Industrial execution is impossible as there are no materials available on Earth that could be stable at that high pressure and temperature. CFs are therefore prepared from organic precursors such as pitch and PAN. This is achieved in three steps, including stabilization of a precursor fiber in air ($T \approx 300°$C), carbonization at $\approx 1100°$C, and subsequent graphitization (at $>2500°$C). Fibers that are treated up to the carbonization step are called CFs (high strength) while those treated until the graphitization step are called graphite fibers (high modulus) [34].

CNFs have a very special structure like annular rings on a tree (Fig. 4.17) and are synthesized from hydrocarbon gas, using a catalytic growth process outlined in Fig. 4.17(b) [34,36,37]. Nanoparticles of transition metal such as Fe, Ni, Co, and Cu are dispersed on a ceramic substrate and a hydrocarbon gas diluted with hydrogen is introduced into the chamber at 1100°C. Hydrocarbon decomposes on the catalyst Fe nanoparticles to uptake carbon atoms and hollow well-organized graphitic hexagonal sp^2-based CNFs are formed. The rapid growth rate of several tens of μm/min enables production of commercially viable quantities of CNFs [34,38]. The shape of the primary hollow tubule is formed by the shape of the catalytic nanoparticle; the tubule is thickened by a successive deposition of pyrolytic carbon layers on the primary tubular core in the (CVD) process. The graphitization process (3000°C) introduces a fully developed graphite structure in the peripheral region of a CNF, exhibiting a polygonal shape.

4.4.3 Synthesis of CNFs

4.4.3.1 Chemical vapor deposition technique

A catalytic thermal CVD synthesis method is generally accepted for large-scale production of CNFs [34,39,40]. By controlling the synthesis conditions, the diameter, crystallinity, and orientation of the cone angle can be manipulated. CNFs are characterized in terms of their microstructure, oxidation behavior, and also graphitizability and are compared with those of conventional tubular types of CNFs. Their structural characteristics and low production cost make it possible to use them in fabrication of absorbent materials, field emitters, gas storage components, composite materials, etc.

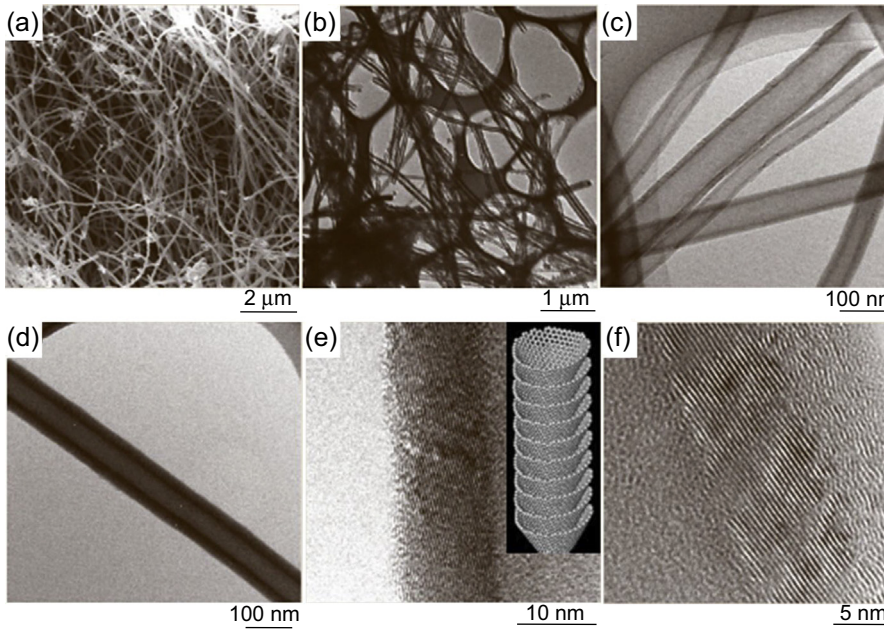

Figure 4.18 (a) SEM image of CNFs showing a long and straight morphology. (b) TEM image of CNFs with a hollow core at low resolution. (c) TEM image of uncoated CNFs with a large hollow core. (d) TEM image of coated CNFs with a large hollow core. (e) TEM image of uncoated CNFs (*inset*: schematic model of a CNF). (f) TEM image of a coated CNF [34].

Electron microscopy imaging (Fig. 4.18(a–c)) shows relatively long (~200 µm) and straight CNFs with a hollow core along the fiber length, with diameters ranging from 50 to 150 nm. One of the prominent feature of the CNFs is a large hollow core. In addition, there are a number of differences in the ratio of outer to inner diameter, that is, the wall thickness of the CNFs, as shown in the TEM images of Fig. 4.18(d). High-resolution TEM studies on the CNFs reveal a truncated cone microstructure (Fig. 4.18(e)); other types of nanofiber contain a coating of amorphous carbon (Fig. 4.18(f)). The angle of the cone in the CNFs with respect to fiber axis is in the range of 45–80 degrees. The stacked conical graphene sheets of (110) planes with ABAB stacking are primarily the effect of catalytic nanoparticles, while the outer thickening of the walls, the amorphous carbon, are formed during the growth process (Fig. 4.18(e)) [34].

4.4.3.2 Electrospinning technique

PAN polymer dissolved in dimethylformamide (DMF) is extruded from a spinneret and collected on a charged plate in the form of a web. As PAN is a well-known CF precursor, electrospinning nanofibers on a substrate and stabilizing followed by carbonizing delivers CNFs. During stabilization reaction (in air) the color of the PAN nanofibers changes from white to dark brown, and further carbonization

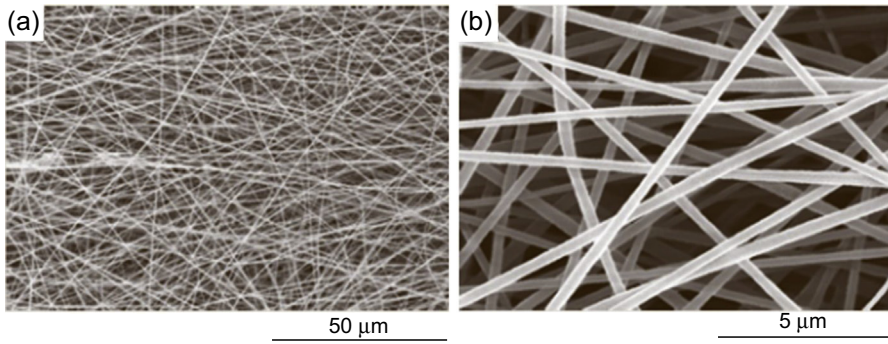

Figure 4.19 (a) and (b) SEM images of electrospun nanofibers [34].

(in N_2 or Ar) leads to black-colored nanofiber webs. Oxidative stabilization is required to inherit the thermoset properties in PAN and maintain the structural integrity [41,42]. Chemical kinetics is affected by the surface area available in the precursor fibers, and the oxidation mechanism could be understood by performing differential scanning calorimetry [34,41,42]. Typical SEM images of electrospun PAN nanofibers are shown in Fig. 4.19(a) and (b). As it is observed, the nanofibers are long and straight and as the treatment temperature is increased the surface morphology also changes. In this particular example the nanofibers treated at various temperatures do not show much morphological evolution; however, when the nanofiber web is treated to 2800°C the surface of the nanofibers shows a smooth to wrinkled surface while the cross-section shows facetted morphology. This is mainly because of a large change in density and densification of carbon atoms (specific gravity changes from 0.690 to 1.999) [34]. Using this electrospinning process, high purity and uniform nanofiber morphology could be achieved with high throughput.

4.5 CNF based composite filaments

In this section PAN- and CNF-based composite filaments will be discussed. A low-molecular-weight textile grade PAN was dissolved in DMF. The concentration of the PAN was 12 wt% in DMF. The high heat-treated (2900°C) CNFs obtained from Applied Science Inc. in the amount of 3.2 wt% of 12 wt% PAN was added to the PAN solution and stirred for 48 h for uniform dispersion. Following dispersion of CNFs in PAN, the solution was filtered to remove any agglomerates. It was noticed that longer stirring time helps to break down the agglomerates and disperse them. The filtered PAN-CNFs solution was subjected to degassing, for 2 h, in a lab-scale degassing glassware. The filtered and degassed PAN-CNF solution was used in a home-built single-filament wet-spinning schematic as shown in Fig. 4.20.

Three-milliliter syringes, from BD, with pistons were used as injector and 30 gauge, 160 µm inner diameter needles, from CML supply, were used as spinnerets. The coagulation bath was kept below 0°C so as to reduce the rate of diffusion. Higher bath

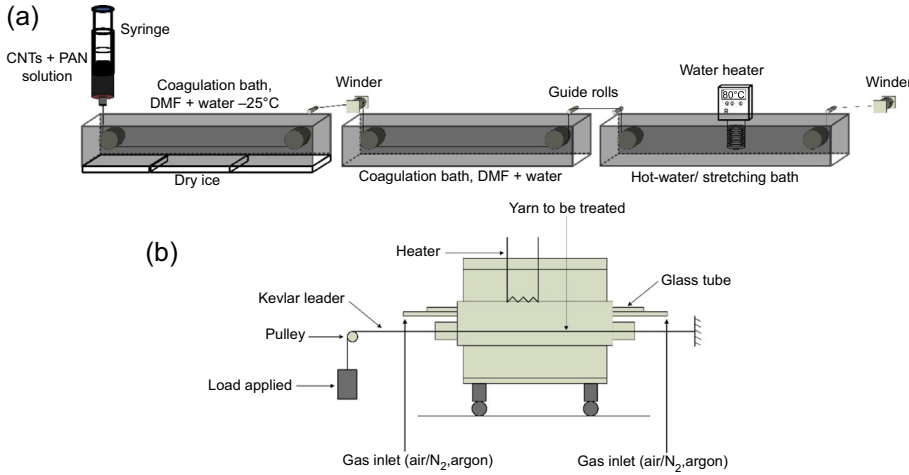

Figure 4.20 (a) Schematic of lab-scale wet-spinning setup used for synthesizing CNF-based precursor fibers. (b) Schematic of tube furnace used for oxidation and carbonization of the precursor fibers.

temperature can result in circular fibers; however, the void content is also very high. Colder coagulation bath delivers oval- to bean-shaped fibers but the fiber formation is uniform in nature. The first bath concentration was kept solvent rich (about 65% DMF to water) and the draw ratio was kept at 1 to 1.22; a higher draw ratio in the first coagulation bath results in weak filament properties. Following coagulation in the first bath, the filament was subjected to a second coagulation bath with a higher concentration of non-solvent (about 70% water to 30% DMF) and stretched in a hot water bath (90°C). The total draw ratio was maintained at 6 to 7.7. Higher draw ratios, when tried, resulted in filament breakages. The final diameter of the filament was about ~22 μm. SEM and FIB imaging shows (Fig. 4.21) uniform distribution of CNFs in the PAN matrix in cross-section. The precursor filaments' tensile strength and modulus were found to be 157.2 ± 40.67 MPa and 4.82 ± 1.38 GPa, respectively. Pristine PAN fibers, wet spun at similar conditions as PAN + CNF fibers, had tensile strength of 54.60 ± 23.58 MPa.

Following wet spinning, the PAN + CNF composite filaments were subjected to stabilization (300°C) and carbonization (1100°C). A lab-scale tube furnace as shown in Fig. 4.20(b) was used. The filaments were subjected to tension (~0.7 MPa/1000 filaments) during oxidation and (~5 MPa/1000 filaments) during carbonization. SEM and FIB images are as shown in Fig. 4.21(c) and (d). FIB revealed that the nanofibers bond well with the polymer matrix and carbonized samples show uniformly distributed CNFs. Tensile testing of the carbonized samples showed tensile strength and modulus of 427 ± 148 MPa and 70 ± 8.2 GPa, respectively. The strength and modulus improved by 2.7 times and 14.5 times, respectively, compared to the precursor fibers (Fig. 4.22). Extruding the filament using a finer spinneret results in smaller diameter precursor fibers and hence lower defects than the larger diameter and hence affects the final tensile strength of the carbonized sample.

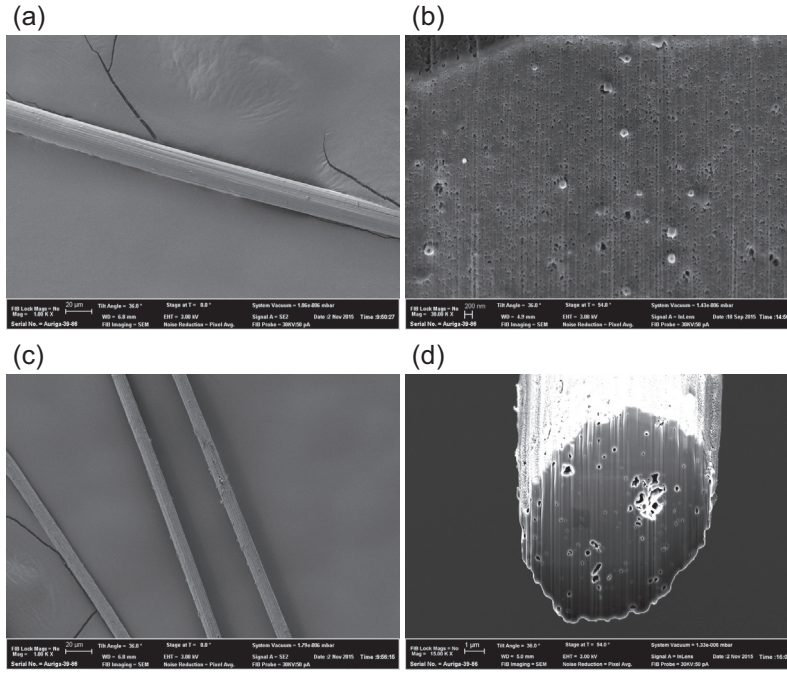

Figure 4.21 (a) and (b) are SEM and FIB images of precursor fibers. CNFs can be observed in the cross-section image of precursor fiber. (c) and (d) are SEM and FIB images of carbonized fibers. CNFs can be observed in the cross-section of the carbonized fiber.

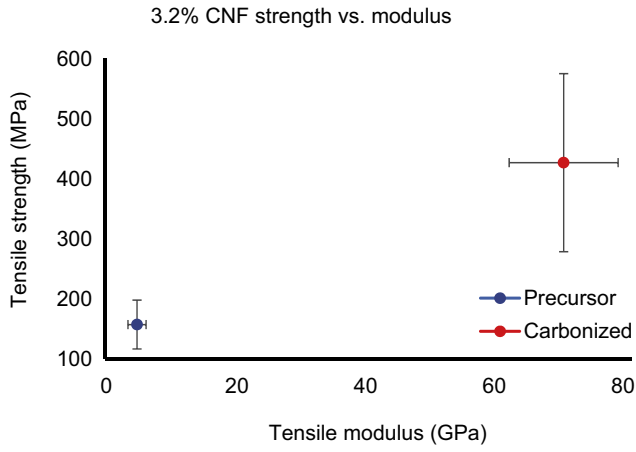

Figure 4.22 Strength versus modulus data of 3.2% CNF in 12% PAN fibers. The strength increased by 2.7 times while the modulus increased by 14.5 times.

Table 4.3 Summary of physical properties of CNFs and CNTs

Property	CNFs	CNTs
Diameter (nm)	50–200	5–50
Length (μm)	50–100	1–100
Aspect ratio	250–2000	100–10,000
Density (g/cm^3)	≈2	≈1.75
Thermal conductivity (W/mK)	1950	3000–6000
Resistivity (Ω cm)	1×10^{-4}	1×10^{-4} to 2×10^{-3}
Strength GPa	2.92	10–60
Modulus GPa	240	1000

4.6 Comparison of CNT and CNF properties

CNTs and CNFs are both used as reinforcement nanomaterials to increase the mechanical and physical properties of the composite filaments. However, to enhance the properties of the composite filaments, the properties of CNTs and CNFs should also be understood. As the synthesis procedure for nanotubes and nanofibers are similar (CVD), the physical properties are different. As seen in Table 4.3, important physical properties are compared. The aspect ratio of the nanofibers is smaller than nanotubes; however, the density is higher. The diameter of CNFs is larger than that of CNTs. The strength and modulus of CNFs are smaller than that of CNTs. However, as the nanofibers are larger than the nanotubes, dispersion and suspension are better. Thermal conductivity of CNTs is again higher than that of CNFs but the electrical resistivity of CNFs is lower than CNTs, which makes them better inexpensive candidates for electrical discharge applications of composite materials.

4.7 Surface modification and dispersion techniques of CNTs and CNFs for composite applications

Surface modification is carried out to achieve uniform distribution of CNTs or CNFs as these nanofillers have very high surface area, but do not blend well with polymer matrix. In Fig. 4.23, an example of electrochemical covalent surface modification of CNTs is shown. Here aryldiazonium salts are used, with a single electronic reduction yielding dinitrogen and a free radical species. The electrogenerated radical ion covalently bonds to the surface of CNTs. Polymerization of the radical species on the CNT surface occurs for R═NO and R═Br, CH_2Cl, SO_3H, COOH. The thickness of the deposited coating is controlled by the magnitude and direction of the potential applied [43].

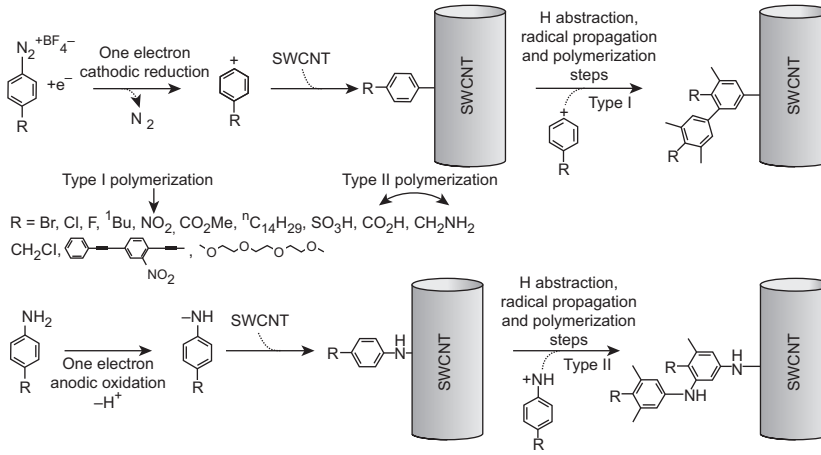

Figure 4.23 Example of radical additions using electrochemical reactions for CNT surface modification [43].

In Fig. 4.24, various types of surface modification of CNTs or CNFs are summarized. Acid cutting with HNO_3 or a mixture of concentrated H_2SO_4 and HNO_3 cuts the length of the nanotubes and the defect sites are converted to COOH. In halogenation, the strong element, fluorine, can be attached to the side walls of the CNTs at higher temperatures up to 600°C. However, by halogenation, the CNTs lose their metallic or semiconducting nature to become an insulator (sp^3 hybridization). In the case of nucleophilic additions, a solvent-free amination of CNTs leads to addition of octadecylamine to a graphitic network of CNTs. Carbenes are also added in nucleophilic type of additions. In electrophilic addition, chloroform in the presence of Lewis acid followed by hydrolysis results in hydroxyl groups attached to the surface of the CNTs. Electrophilic addition of CNTs make them dispersible in standard organic solvents. Carbenes and nitrines both react with CNTs to attach cycloaddition materials. Various types of functional groups have been attached to the CNT surface incorporating different azides. In polymer grafting methods, the grafting site on the CNTs should be graphitic in nature (π-bonds are responsible for covalent bonding) [44]. Polymers such as poly(methyl methacrylate) (PMMA) reacts with CNTs in the presence of monochlorobenzene in the ultrasonication process. The PMMA attaches to the CNT surface forming polymer-grafted CNTs. Other types of reactions such as hydrogenation and oxidative or reductive couplings are also used as surface modification techniques. For more information regarding the actual surface modification techniques, readers should refer to the references [45].

In the case of CNFs, mostly the surface is oxidized by soaking the CNFs in $H_2SO_4 + HNO_3$ at various temperatures followed by acylation. Following this process, the functional groups will be grafted to the CNF surface by the reaction between the oxidized CNF and the functional groups. However, as CNTs and CNFs are nanomaterials with similar physical and chemical properties, most of the surface modification techniques discussed in Fig. 4.24 hold good for CNFs as well.

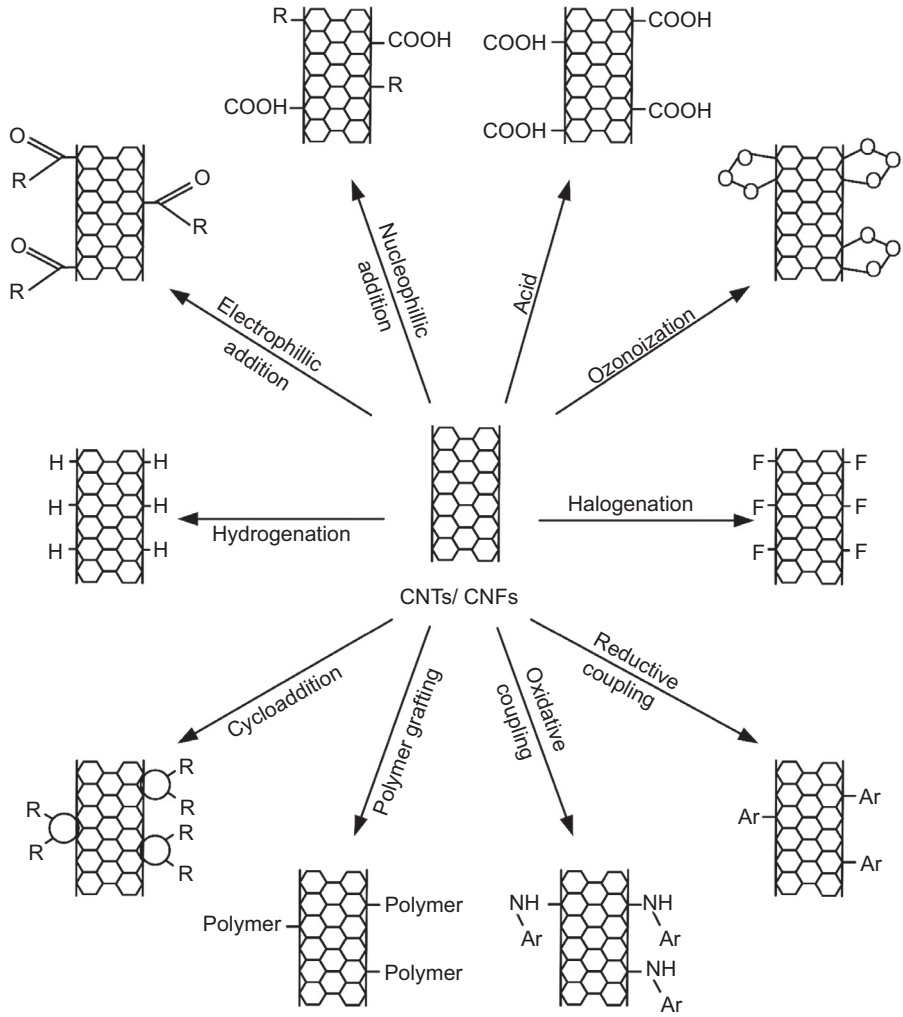

Figure 4.24 Summary of frequently followed surface modification of CNTs or CNFs [45].

4.8 Applications

In this section, a brief overview of various applications of CFs and CNTs or CNFs with a matrix or by themselves or other capabilities is presented. CF-based composites are used in fairings, flight control surfaces, landing gear doors, floor beams and floorboards, and primary wing and fuselage structures on new-generation aircraft (Boeing 787 and Airbus A 350 XWB). The Boeing 787 Dreamliner is made of almost 50% of CF-based composite material while the Airbus A350 XWB contains almost 53% of CF-based composite materials. Because of the increase in composite use, fuel

efficiency is up by 25% as claimed by Airbus [46]. The sporting goods industry accounts for 18−20% of the CF market. CF composites are used in golf shafts, hockey sticks, rackets, fishing rods, ski poles, snowboards, sailboard masts, marine hulls, backpack frames, tent poles, bicycle frames, etc. The CFs used in the various sports equipment not only provide light weight but also improve sporting performance [47]. The most recent example of CFs used in the automotive industry is the BMW i3 electric vehicle. Because of the use of CFs in the BMW i3, nearly 550 lb in weight reduction was achieved as compared to the regular all aluminum body. BMW claims that because of this reduction in weight the car will have an additional range of 80−100 miles per full charge. Other commercially available CF-based cars are Aston Martin, Ferrari, Lamborghini race cars, etc. CFs are also used in boats, which make them much lighter, highly durable, and performance oriented. Other major commercial uses of CFs are in windmill blades. The CF rib runs through the length of the blade and at the root of the blade. Over the rib, fiber glass forms the blades. It is extremely important for the blade to be light weight so that maximum amount of electricity is produced.

The electrical conductivity of CNTs was an initially exploited property. MWNTs impregnated with polymers help in the automotive industry to dissipate electrostatic charge buildup in mirror housings, fuel lines, and filters [48,49]. Also CNTs mixed with polymers are used for electromagnetic interference shielding in the microelectronics industry. Engineered CNTs mixed with polymers increase CNT interactions and improve energy damping especially in the sports industry, such as in tennis racquets, baseball bats, bicycle frames, golf clubs, hockey sticks, fishing rods, etc. [50,51]. CNTs made into CF yarn have very high tensile strength and are used where both good electrical and mechanical properties of a material are required [52,53]. Other than carbon composites with polymers, CNTs added to metals are known to increase tensile strength and modulus [54,55]. Such high-performance CNT-metal composite materials are normally used in aircraft and the automotive industry where weight and strength are prime competing factors [56]. CNTs are nowadays used in conductive polymer technology. As CNTs inherit high electrical conductivity, CNT-based conductive polymer coating prevents corrosion in metals [57]. Indium tin oxide is very expensive because of the scarcity of indium, a rare earth metal; hence CNT-based conductive films are used for capacitive or resistive screens [58]. SWNTs were first used in field-effect transistor (FET) architectures. In 1998 the first CNT-based FET was designed using SWNTs [59]. SWNT FETs with 10 nm channel lengths, a current density of nearly 2.4 mA/μm at 0.5 V are observed, greater than that of the silicon devices of similar size [60−62]. Another example of CNT-based application in microelectronics is the thin film transistor (TFT), organic light-emitting diode (OLED) displays [63−65]. The greatest advantage of OLEDs is that the TFTs are flexible and hence future screens could be made to bend with functionality restored without disturbing the structure [66,67]. Lithium-ion batteries in laptops and mobile phones contain the use of MWNTs [66,68]. CNTs are also used in fuel cells as catalyst support reducing the use of platinum by 60% [69]. In solar cells the use of CNTs not only reduces the undesired carrier recombination but also resists photooxidation [70,71]. Continued research in CNTs as components of biosensors and medical devices is because of the chemical and biological compatibility of

CNTs with DNA and proteins [72,73]. SWNT-based biosensors show large changes in electrical resistance and optical properties in response because of the surface binding of target molecules on CNTs [74−76].

4.9 Future trends

CNTs or nanofibers are the major building blocks of future high-strength and high-performance composites. High-performance composites are important as they possess a high strength to weight ratio, increasing energy efficiency and payload size/range in the field of application. However, these composites, because they are in their early stage of usage, are extremely expensive. Making these composites inexpensive is the focus of many researchers, companies, and end users in this field. The addition of CNTs or CNFs to enhance properties of CFs is also being researched by scientists and industry experts for CF-based applications. Increasing the use of CFs reinforced with CNTs or CNFs in various applications reduces the cost of the composites.

References

[1] Harris PJ. Carbon nanotubes and related structures. Cambridge University Press; 2001.
[2] Prasek J, et al. Methods for carbon nanotubes synthesis—review. Journal of Materials Chemistry 2011;21(40):15872−84.
[3] O'connell MJ. Carbon nanotubes: properties and applications. CRC Press; 2006.
[4] Ando T. Theory of transport in carbon nanotubes. Semiconductor Science and Technology 2000;15(6):R13.
[5] Terrones M. Science and technology of the twenty-first century: synthesis, properties, and applications of carbon nanotubes. Annual Review of Materials Research 2003;33(1): 419−501.
[6] Moothi K, et al. Coal as a carbon source for carbon nanotube synthesis. Carbon 2012; 50(8):2679−90.
[7] Flamant G, et al. Solar processing of materials: opportunities and new frontiers. Solar Energy 1999;66(2):117−32.
[8] Laplaze D, et al. Carbon nanotubes: the solar approach. Carbon 1998;36(5):685−8.
[9] Szabó A, et al. Synthesis methods of carbon nanotubes and related materials. Materials 2010;3(5):3092−140.
[10] Song K, et al. Structural polymer-based carbon nanotube composite fibers: understanding the processing−structure−performance relationship. Materials 2013;6(6):2543−77.
[11] Meng J, et al. Forming crystalline polymer-nano interphase structures for high-modulus and high-tensile/strength composite fibers. Macromolecular Materials and Engineering 2013;299(2):144−53.
[12] Ruan S, Gao P, Yu T. Ultra-strong gel-spun UHMWPE fibers reinforced using multiwalled carbon nanotubes. Polymer 2006;47(5):1604−11.
[13] Gao J, et al. Continuous spinning of a single-walled carbon nanotube-nylon composite fiber. Journal of the American Chemical Society 2005;127(11):3847−54.
[14] Dalton AB, et al. Continuous carbon nanotube composite fibers: properties, potential applications, and problems. Journal of Materials Chemistry 2004;14(1):1−3.

[15] Razal JM, et al. Arbitrarily shaped fiber assemblies from spun carbon nanotube gel fibers. Advanced Functional Materials 2007;17(15):2918−24.
[16] Wang Z, Ciselli P, Peijs T. The extraordinary reinforcing efficiency of single-walled carbon nanotubes in oriented poly (vinyl alcohol) tapes. Nanotechnology 2007;18(45): 455709.
[17] Minus ML, Chae HG, Kumar S. Interfacial crystallization in gel-spun poly (vinyl alcohol)/ single-wall carbon nanotube composite fibers. Macromolecular Chemistry and Physics 2009;210(21):1799−808.
[18] Young K, et al. Strong dependence of mechanical properties on fiber diameter for polymer-nanotube composite fibers: differentiating defect from orientation effects. ACS Nano 2010; 4(11):6989−97.
[19] Vigolo B, et al. Macroscopic fibers and ribbons of oriented carbon nanotubes. Science 2000;290(5495):1331−4.
[20] Chae HG, et al. Carbon nanotube reinforced small diameter polyacrylonitrile based carbon fiber. Composites Science and Technology 2009;69(3):406−13.
[21] Chae HG, et al. Stabilization and carbonization of gel spun polyacrylonitrile/single wall carbon nanotube composite fibers. Polymer 2007;48(13):3781−9.
[22] Chae HG, Minus ML, Kumar S. Oriented and exfoliated single wall carbon nanotubes in polyacrylonitrile. Polymer 2006;47(10):3494−504.
[23] Kumar S, et al. Synthesis, structure, and properties of PBO/SWNT composites. Macromolecules 2002;35(24):9039−43.
[24] Kearns JC, Shambaugh RL. Polypropylene fibers reinforced with carbon nanotubes. Journal of Applied Polymer Science 2002;86(8):2079−84.
[25] Dalton AB, et al. Super-tough carbon-nanotube fibres. Nature 2003;423(6941):703.
[26] Liu Y, Kumar S. Recent progress in fabrication, structure, and properties of carbon fibers. Polymer Reviews 2012;52(3−4):234−58.
[27] Song Q, et al. Grafting straight carbon nanotubes radially onto carbon fibers and their effect on the mechanical properties of carbon/carbon composites. Carbon 2012;50(10):3949−52.
[28] Deng L, et al. Carbon nanofibres produced from electrospun cellulose nanofibres. Carbon 2013;58:66−75.
[29] Wang X, et al. Fabrication of ultralong and electrically uniform single-walled carbon nanotubes on clean substrates. Nano Letters 2009;9(9):3137−41.
[30] Zhang R, et al. Growth of half-meter long carbon nanotubes based on Schulz−Flory distribution. ACS Nano 2013;7(7):6156−61.
[31] Li Y-L, Kinloch IA, Windle AH. Direct spinning of carbon nanotube fibers from chemical vapor deposition synthesis. Science 2004;304(5668):276−8.
[32] Zhang X, et al. Spinning and processing continuous yarns from 4-inch wafer scale super-aligned carbon nanotube arrays. Advanced Materials 2006;18(12):1505.
[33] Miller SG, et al. Increased tensile strength of carbon nanotube yarns and sheets through chemical modification and electron beam irradiation. ACS Applied Materials and Interfaces 2014;6(9):6120−6.
[34] Vajtai R. Springer handbook of nanomaterials. Springer Science & Business Media; 2013.
[35] Tibbetts GG, et al. A review of the fabrication and properties of vapor-grown carbon nanofiber/polymer composites. Composites Science and Technology 2007;67(7): 1709−18.
[36] Baker R. Catalytic growth of carbon filaments. Carbon 1989;27(3):315−23.
[37] Oberlin A, Endo M, Koyama T. Filamentous growth of carbon through benzene decomposition. Journal of Crystal Growth 1976;32(3):335−49.

[38] Bacon R, Bowman J. Production and properties of graphite whiskers. Bulletin of the American Physical Society 1957;2:131.
[39] Dai H, et al. Single-wall nanotubes produced by metal-catalyzed disproportionation of carbon monoxide. Chemical Physics Letters 1996;260(3):471–5.
[40] Rao C, Sen R. Large aligned-nanotube bundles from ferrocene pyrolysis. Chemical Communications 1998;15:1525–6.
[41] Jiang H, et al. Structural characteristics of polyacrylonitrile (PAN) fibers during oxidative stabilization. Composites Science and Technology 1987;29(1):33–44.
[42] Ogawa H, Saito K. Oxidation behavior of polyacrylonitrile fibers evaluated by new stabilization index. Carbon 1995;33(6):783–8.
[43] Wildgoose GG, et al. Chemically modified carbon nanotubes for use in electroanalysis. Microchimica Acta 2006;152(3–4):187–214.
[44] Tsubokawa N. Preparation and properties of polymer-grafted carbon nanotubes and nanofibers. Polymer Journal 2005;37(9):637–55.
[45] Wu H-C, et al. Chemistry of carbon nanotubes in biomedical applications. Journal of Materials Chemistry 2010;20(6):1036–52.
[46] Boeing. http://www.boeing.com/commercial/aeromagazine/articles/qtr_4_06/article_04_2.html, 2015. Available from: http://www.boeing.com/commercial/aeromagazine/articles/qtr_4_06/article_04_2.html.
[47] Toray. http://www.toray.us/, 2015. Available from: http://www.toray.us/.
[48] Bauhofer W, Kovacs JZ. A review and analysis of electrical percolation in carbon nanotube polymer composites. Composites Science and Technology 2009;69(10):1486–98.
[49] Chou T-W, et al. An assessment of the science and technology of carbon nanotube-based fibers and composites. Composites Science and Technology 2010;70(1):1–19.
[50] Gojny F, et al. Carbon nanotube-reinforced epoxy-composites: enhanced stiffness and fracture toughness at low nanotube content. Composites Science and Technology 2004;64(15):2363–71.
[51] Suhr J, et al. Viscoelasticity in carbon nanotube composites. Nature Materials 2005;4(2):134–7.
[52] Bakshi SR, Agarwal A. An analysis of the factors affecting strengthening in carbon nanotube reinforced aluminum composites. Carbon 2011;49(2):533–44.
[53] Kashiwagi T, et al. Nanoparticle networks reduce the flammability of polymer nanocomposites. Nature Materials 2005;4(12):928–33.
[54] Coleman JN, et al. Small but strong: a review of the mechanical properties of carbon nanotube–polymer composites. Carbon 2006;44(9):1624–52.
[55] Zhang M, Atkinson KR, Baughman RH. Multifunctional carbon nanotube yarns by downsizing an ancient technology. Science 2004;306(5700):1358–61.
[56] De Volder MF, et al. Carbon nanotubes: present and future commercial applications. Science 2013;339(6119):535–9.
[57] Beigbeder A, et al. Preparation and characterisation of silicone-based coatings filled with carbon nanotubes and natural sepiolite and their application as marine fouling-release coatings. Biofouling 2008;24(4):291–302.
[58] Wu Z, et al. Transparent, conductive carbon nanotube films. Science 2004;305(5688):1273–6.
[59] Ionescu AM, Riel H. Tunnel field-effect transistors as energy-efficient electronic switches. Nature 2011;479(7373):329–37.
[60] Appenzeller J, et al. Band-to-band tunneling in carbon nanotube field-effect transistors. Physical Review Letters 2004;93(19):196805.

[61] Franklin AD, et al. Sub-10 nm carbon nanotube transistor. Nano letters 2012;12(2): 758−62.
[62] Jensen K, et al. Nanotube radio. Nano letters 2007;7(11):3508−11.
[63] Chen Z, et al. Protein microarrays with carbon nanotubes as multicolor Raman labels. Nature Biotechnology 2008;26(11):1285−92.
[64] Jung M, et al. All-printed and roll-to-roll-printable 13.56-MHz-operated 1-bit RF tag on plastic foils. Electron Devices, IEEE Transactions on 2010;57(3):571−80.
[65] Sun D-M, et al. Flexible high-performance carbon nanotube integrated circuits. Nature Nanotechnology 2011;6(3):156−61.
[66] Dai L, et al. Carbon nanomaterials for advanced energy conversion and storage. Small 2012;8(8):1130−66.
[67] Rueckes T, et al. Carbon nanotube-based nonvolatile random access memory for molecular computing. Science 2000;289(5476):94−7.
[68] Köhler AR, et al. Studying the potential release of carbon nanotubes throughout the application life cycle. Journal of Cleaner Production 2008;16(8):927−37.
[69] Evanoff K, et al. Ultra strong silicon-coated carbon nanotube nonwoven fabric as a multifunctional lithium-ion battery anode. ACS Nano 2012;6(11):9837−45.
[70] Gao G, Vecitis CD. Electrochemical carbon nanotube filter oxidative performance as a function of surface chemistry. Environmental Science and Technology 2011;45(22): 9726−34.
[71] Le Goff A, et al. From hydrogenases to noble metal−free catalytic nanomaterials for H2 production and uptake. Science 2009;326(5958):1384−7.
[72] De La Zerda A, et al. Carbon nanotubes as photoacoustic molecular imaging agents in living mice. Nature Nanotechnology 2008;3(9):557−62.
[73] Heller DA, et al. Single-walled carbon nanotube spectroscopy in live cells: towards long-term labels and optical sensors. Advanced Materials 2005;17(23):2793−9.
[74] Heller DA, et al. Multimodal optical sensing and analyte specificity using single-walled carbon nanotubes. Nature Nanotechnology 2008;4(2):114−20.
[75] Kam NWS, et al. Carbon nanotubes as multifunctional biological transporters and near-infrared agents for selective cancer cell destruction. Proceedings of the National Academy of Sciences of the United States of America 2005;102(33):11600−5.
[76] Kurkina T, et al. Label-free detection of few copies of DNA with carbon nanotube impedance biosensors. Angewandte Chemie International Edition 2011;50(16):3710−4.

Liquid crystal aromatic polyesterarylate (LCP) fibers: structure, properties, and applications

5

F. Sloan
Kuraray America, Inc. Fort Mill, South Carolina, United States

5.1 Introduction

There are many types and grades of industrial polyester fibers, including polyethylene terephthalate (PET), which is the most common industrial fiber used today. High-modulus low-shrinkage PET fibers are used in passenger car tires, mooring ropes, and other large-scale industrial end uses, with strength of 8−9 g per denier and elongations of 10−20% [1]. There are also specialty polyester fibers, such as polyethylene naphthalate, polybutylene terephthalate, etc. These polyester-based fibers have tensile strengths in a range of 4−10 g per denier, with elongations tailorable within a range of 6−45%. Liquid crystal polyester (LCP) fibers, by contrast, can achieve tenacities in excess of 28 g per denier (3.4 GPa) with elongations of only 3−4%. This class of fibers has found increasing use in demanding end uses requiring dimensional stability and durability across a wide range of environments.

The first liquid crystal super fibers were of the *ar*omatic poly*amid*e (aramid) family, for example, Kevlar, developed by DuPont in the 1960s. The success of aramid fiber led to a great deal of research into liquid crystal polymers, not only based on polyamide chemistry but also polyester. Much work was done by Calundann et al. [2,3] of Celanese, evaluating a wide range of monomers for polymer and copolymer production. Although many of those candidate polymers are in wide use today for engineering applications, only one was moved forward for fiber production, and this became the fiber product commonly known by the generic names LCP or polyarylate, or by the trade name Vectran.

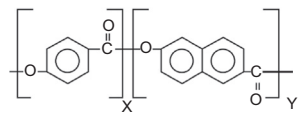

5.2 LCP polymer development history

As is true for most industrial fibers, the original target market for LCP fiber was for high-volume passenger tires. However, although providing interesting properties for

Structure and Properties of High-Performance Fibers. http://dx.doi.org/10.1016/B978-0-08-100550-7.00005-X

tires, the fiber was not compatible with the rapid manufacturing processes required for the tire industry. In addition, the relatively high cost of LCP fiber compared with tire-grade polyester fiber put the automotive market out of reach commercially.

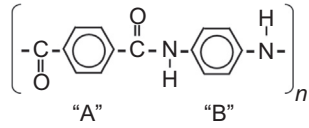

Most high-performance polymers are produced as repeating chain polymers. For example, if we represent the diacid of aramid production as A and the diamine as B, then the polymer created by reacting these two monomers has a regular, repeating, A-B-A-B-A-B… molecular structure. However, with many aromatic monomers, the repeating structures thus created have very high crystallinity and are thermodynamically very stable, with theoretical melting temperatures in excess of actual charring or decomposition temperatures. For that reason they are not easily tractable, that is, they cannot be processed using traditional melt flow systems. As a result, fiber production requires complex wet-spinning methods, such as spinning in very strong acids.

In developing their LCP technology, Celanese under Calundann et al. pursued a somewhat different strategy as compared with the aramid fiber production developed by DuPont. To be able to utilize the polymer in more common melt-driven processes such as injection molding and melt spinning, Celanese sought a polymer that had high performance but that was melt processable. Many different compounds were tried but, as in the case of aramid, the decomposition temperature was usually reached before melting. The breakthrough came from work with bifunctional monomers that self-react to form random copolymers [2].

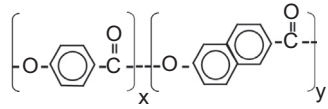

Consider aromatic monomers having both acid and alcohol functionality, for example, hydroxyl acids. Reacting a blend of such monomers creates a random copolymer, for example, A-B-A-A-B-B-A-BBB-AA, etc. Such a copolymer is shown here, combining 4-hydroxy benzoic acid (HBA) with 6-hydroxy naphthoic acid (HNA). One consequence of random copolymerization is a depression of the melt point to values lower than that of polymers created from 100% of either constituent monomer. In a certain range of A:B mole ratio, the melting temperature is depressed so that the polymer can be processed with traditional methods, as shown schematically by the thermotropic envelope of Fig. 5.1.

Liquid crystal polymers get their physical properties because of electron sharing among adjacent aromatic groups. For example, ester and amide connecting units have excess electrons and therefore contribute to sharing of electron resonance along

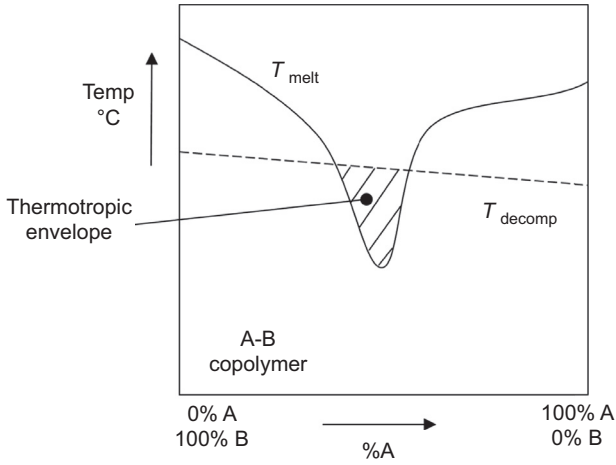

Figure 5.1 Region of melt processing for an A:B random copolymer [4].

the molecular chain. The lowest energy state occurs when adjacent phenyl rings lie in the same plane, creating a rigid, ribbon-like molecule conducive to crystal formation. When the molecules are free to move about, for example, in the liquid state, they naturally form crystals as the rigid ribbon segments align and are attracted to one another by van der Waals' forces. (This tendency to form crystals in the liquid state gave rise to the term liquid crystal.) Polymers forming crystals in the melt are called thermotropic LCPs, whereas polymers forming crystals in solution (eg, in acids) are referred to as lyotropic.

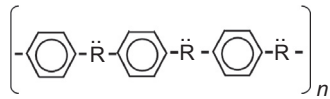

5.3 LCP polymer synthesis

The majority of industrial main-chain aromatic thermotropic LCPs are formed via polycondensation reactions, as discussed elsewhere [3]. Polymerization is conducted in an inert atmosphere to minimize oxidation, at temperatures 50−80°C higher than the monomer melting points. Catalysts such as acetate salts can be added to improve reaction rates. Vacuum is applied to the low viscosity melt to remove excess condensate, for example, acetic acid, thus driving the reaction forward to higher molecular weights. The resulting polymer can then be extruded, cooled, and chipped as in normal polyester production. A simple polymerization reaction for an HBA/HNA polymer is shown in Fig. 5.2.

Liquid crystal polymers have been the subject of many reviews and texts [5−8]. Commercially important LCP attributes include high strength, toughness, dimensional

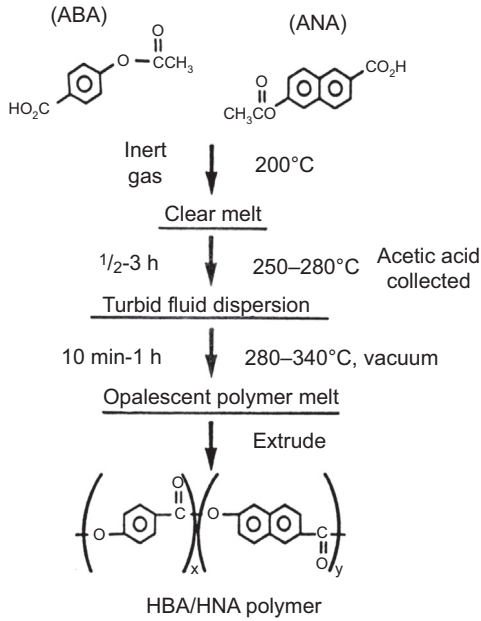

Figure 5.2 Condensation polymerization of HBA/HNA copolymer LCP [3].

stability, heat tolerance, and resistance to organic solvents. Several thermotropic LCP polymers are available commercially today, for example, Xydar, Vectra, Zenite, and Laperos [9].

5.4 LCP fiber manufacturing

Many common high-performance fibers are produced using complex spinning processes that require recovery and recycling of aggressive polymer solvents. For example, aramid fibers are spun in strong acids similar to the scheme of Fig. 5.3. The molecular weight of the polymer is developed in the acid solution, and once a target molecular weight is reached, then the solution is spun to form continuous filaments. Once formed, the filaments are drawn, washed, and the acid recycled and reused in the production process. The use of strong acids presents challenges for containment and for ensuring safe and environmentally friendly practices for solvent handling.

In contrast, many LCP polymers are amenable to common melt-spinning practices, for example, Fig. 5.4, although the fiber cannot be drawn in the traditional manner. The inability to draw the fiber means that fiber diameter is determined directly by the spun polymer diameter. This requires specially designed spinnerets and melt extruders. After spinning, a solid-state polymerization process is used to increase the molecular weight of the fiber, thereby improving the mechanical and thermal properties.

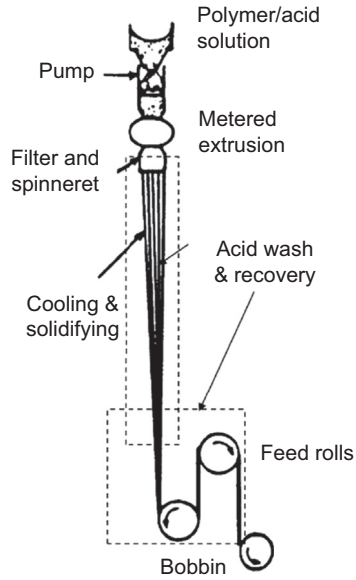

Figure 5.3 Wet (acid) fiber-spinning process used for lyotropic polymers
Modified from Chung T-S, Calundann GW, East AJ. Liquid-crystal polymers and their applications. In: Cheremisinoff NP. editor. Encyclopedia of engineering materials, vol. 2. Marcel Dekker Publisher; 1989. p. 625−75.

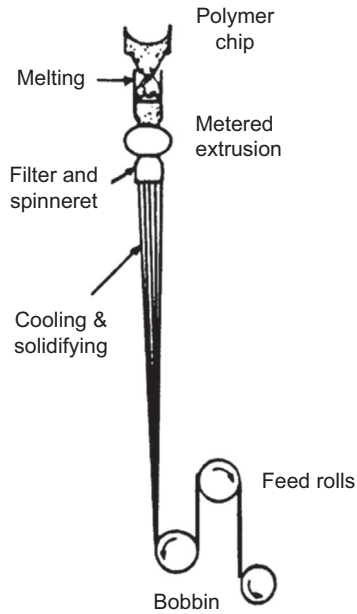

Figure 5.4 Dry melt fiber-spinning process used for thermotropic LCP polymers [3].

Celanese (Beers et al., [10−12]) worked in cooperation with Kuraray (Kuraray Co., Ltd., Tokyo, Japan) during the late 1980s to produce the first commercial output of LCP fibers in 1990 (Nakagawa et al., [13]). Kuraray has produced LCP fibers (Vectran) commercially since 1990. Today commercial production capacity is approximately 1000 MT/year. Although commercially significant, this is a very small capacity compared, for example, to worldwide aramid production, which is estimated to be in excess of 70,000 MT/year.

5.5 LCP fiber structure and properties

When liquid crystal polymers are spun into fibers, some alignment of the crystal domains occurs, as shown schematically in Fig. 5.5. Some alignment to the spinning direction also occurs in amorphous polymers such as PET, but in LCPs the aligned crystal domains lead to much greater physical properties.

The fibrillar structure of high-performance fibers has been described by many authors, for example, as shown in Fig. 5.6. Sawyer et al. [14−16] and others, for example, Masuda et al. [17], have described the actual orientation of crystal domains in LCP fibers using SEM and other analytical techniques. Domains for thermotropic LCPs were found to be not parallel with the fiber direction as in lyotropic LCPs, but rather followed a slightly meandering pathway, contributing to the greater tolerance to compression fatigue found in LCP fibers.

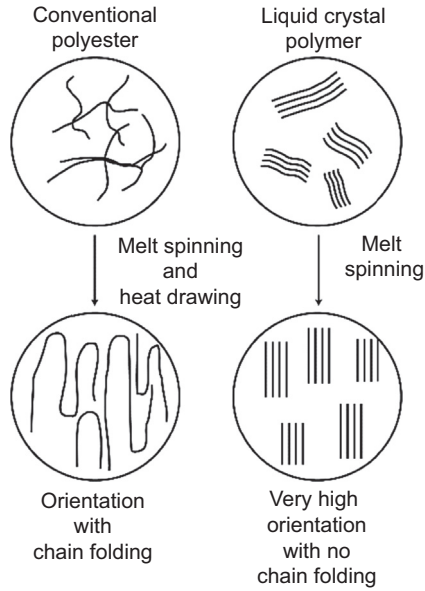

Figure 5.5 Molecular and crystal orientation in spun polymers [12].

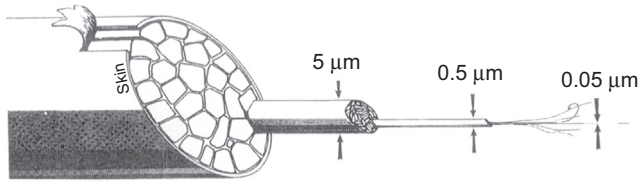

Figure 5.6 Fibrillar structure of LCP fibers [14].

5.5.1 Mechanical properties

Table 5.1 compares LCP fiber tensile properties with other engineering materials. LCP has tensile strength greater than five times that of aluminum, with similar tensile modulus, with only half the density. As with aramid and also high-modulus polyethylene (HMPE), LCP fibers are available in standard modulus and high modulus grades. (Unless noted otherwise, all LCP fiber data presented in this chapter refer to standard modulus LCP.) The compressive strength and modulus of LCP and other polymer-based fibers are much lower, which limits their use in composites to secondary structure, hybrids, or flexible applications [19].

5.5.2 Tension fatigue

LCP fibers have excellent tension−tension fatigue properties, as has been shown in studies of fiber ropes. For example, Fig. 5.7 shows LCP tension fatigue data generated

Table 5.1 Tensile properties of various engineering materials [18]

Material description	Density (g/cm^3)	Tensile strength (GPa)	Specific strength[a] (km)	Tensile modulus (GPa)	Specific modulus[b] (km)
LCP std modulus[c]	1.4	3.2	229	75	5300
LCP high modulus[d]	1.4	3.0	215	103	7400
Titanium	4.5	1.3	29	110	2500
Stainless steel	7.9	2.0	26	210	2700
Aluminum	2.8	0.6	22	70	2600
E-glass	2.6	3.4	130	72	2800
Graphite (AS4)	1.8	4.3	240	230	13,000

[a]Specific strength = strength/density (also divided by acceleration of gravity for SI units). Also known as breaking length, the length of fiber that could be held in a vertical direction without breaking.
[b]Specific modulus = modulus/density (also divided by acceleration of gravity for SI units).
[c]Std (standard) modulus LCP is Vectran HT grade.
[d]High modulus LCP is Vectran UM grade.

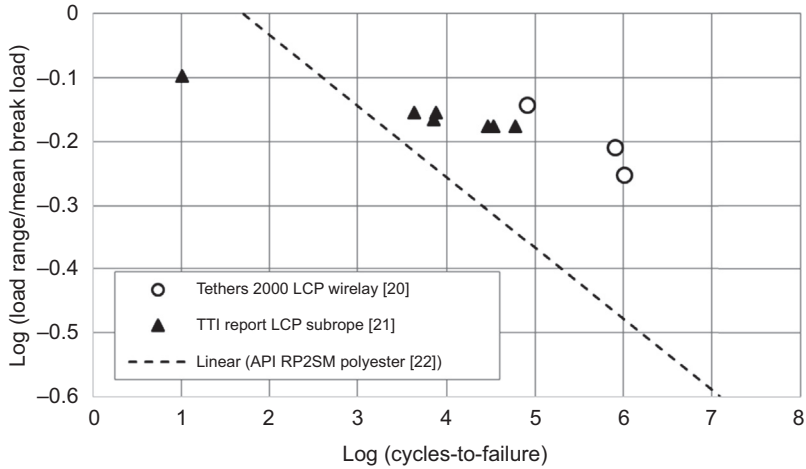

Figure 5.7 Tension−tension fatigue data for LCP fiber ropes.

during studies of offshore mooring lines [20,21]. The available data suggest that LCP subropes will have a fatigue life similar to polyester [22] when load ranges are within typical design levels.

5.5.3 Creep and stress relaxation

Data from one early study of stress relaxation in LCP fiber ropes is shown in Fig. 5.8. In this study, elongations were fixed using turnbuckles in series with load cells to set

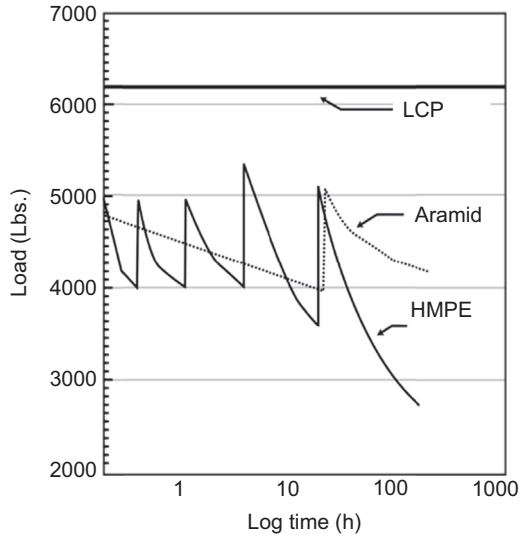

Figure 5.8 Stress relaxation experiment in fiber ropes [23].

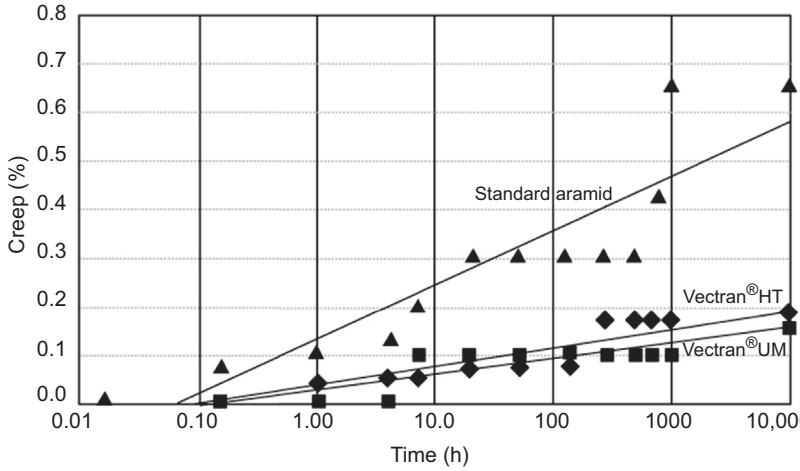

Figure 5.9 Creep elongation for LCP and aramid fibers at 30% load [18].

initial tensions in several high-performance ropes. Load decreased over time in each rope because of stress relaxation, and was reset using the turnbuckle when tension fell below a predetermined level. The frequency of retensioning was taken as a relative measure of creep performance. The indication of this study was that the LCP rope did not creep; however, this was more likely a limitation on the resolution of the load cell.

The creep rate of LCP fiber is well defined, with creep elongation proportional to log(time) as shown in Fig. 5.9. Creep elongation rate for polymer fibers depends on applied load and ambient temperature. Creep rupture time is also dependent on load and temperature. Fig. 5.10 shows a creep rupture curve for 25°C for LCP fiber, as developed using an isothermal technique (Scarborough et al. [24]), and also supporting data at 40°C [25].

5.5.4 Thermal properties

LCP fiber is spun as a thermoplastic but the polymer structure and molecular weight are further developed during solid-state polymerization. This process gives the fiber interesting thermal properties between a thermoplastic and a thermoset. LCP fiber has very good dimensional stability, with very low shrinkage at elevated temperatures as shown in Table 5.2. The limiting oxygen index of LCP fiber is similar to that of aramids.

Similar to other polymeric fibers, LCP fiber loses strength as temperature increases, as shown in Fig. 5.11. This reduction of physical properties at elevated temperatures is attributed to activation of the amorphous regions remaining between crystalline domains. Residual strength remains high after short-term exposure to moderate temperatures, as shown in Fig. 5.12 (24-h thermal soak). LCP is also stable to repeated (cyclic) thermal exposure, as shown in Fig. 5.13. Continuous long-term exposure to temperature extremes is shown in Fig. 5.14. During dry exposure, only a 10–20% loss in residual strength was seen after 300 h at 250°C, as shown in Fig. 5.14(a).

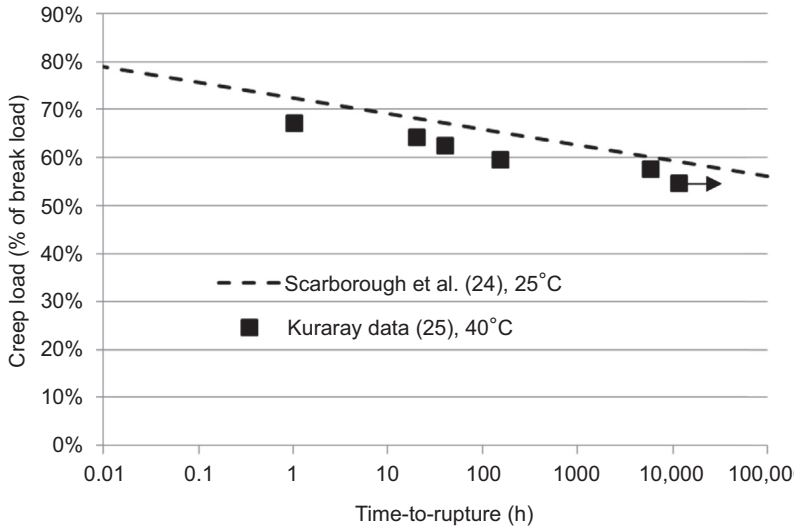

Figure 5.10 Time-to-rupture (stress or creep rupture) data.

Table 5.2 LCP and aramid thermal properties [18]

Fiber thermal property	LCP		Aramid	
	Standard modulus	**High modulus**	**Standard modulus**	**High modulus**
Limiting oxygen index	28	30	30	30
Melting point, °C	None	350	None	None
Hot air shrinkage, 180°C, 30 min, %	<0.2	<0.1	<0.2	<0.1
Boiling water shrinkage, 180°C, 30 min, %	<0.2	<0.1	<0.2	<0.1
50% strength retention[a], °C	145	150	400	230
Thermogravimetric analysis (20% weight loss), °C	>450	>450	>450	>450

[a]Estimated from Fig. 5.11.

A combination of high heat and moisture has a more significant hydrolysis effect, similar to that occurring in other polyester-based fibers (Fig. 5.14(b)).

The strength of LCP fibers increases up to 20% at cryogenic temperatures, as shown in Fig. 5.15. LCP fiber performance at low temperature extremes has been studied extensively by NASA, at temperatures as low as −100°C, for programs such as the Mars Explorer Robot landing airbags, space shuttle extravehicular safety/equipment tethers, and inflatable habitats [26,27]. LCP fiber has also been evaluated for use in applications in direct contact with liquefied natural gas at −160°C.

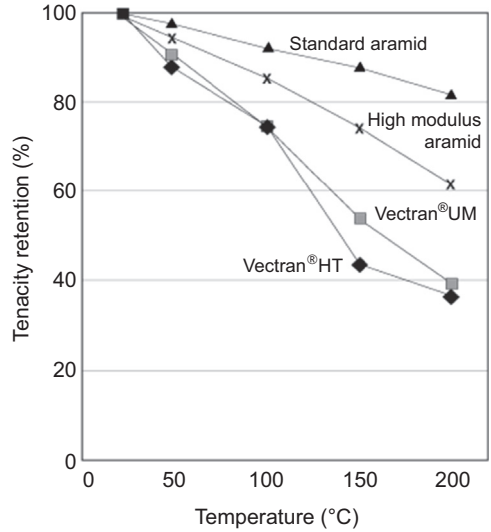

Figure 5.11 Strength reduction in LCP fibers tested at elevated temperatures [18].

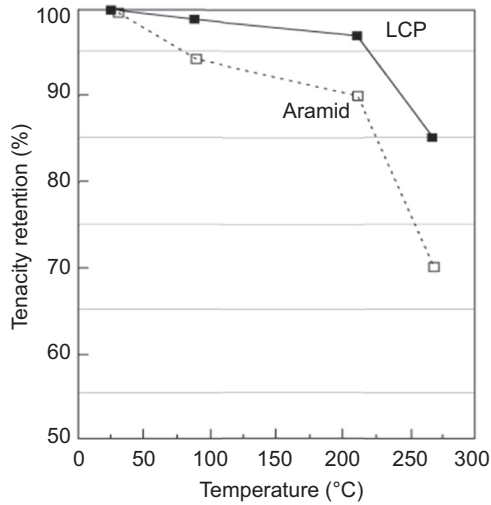

Figure 5.12 Effect of 24-h elevated temperature exposure on residual strength in LCP fibers [18].

5.5.5 Chemical properties

One benefit of LCP fibers compared to aramid is the very low equilibrium moisture content, as shown in Table 5.3. Similar to other polyesters that tend to be hydrophobic, LCP fibers exhibit near-zero equilibrium moisture absorption. This largely eliminates the need for humidity controlled storage environments or extensive predrying prior to

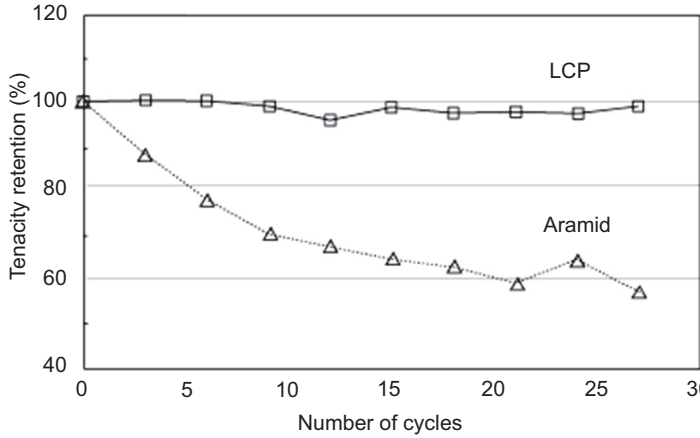

Figure 5.13 Effect of high temperature cycling on LCP fibers (each cycle 8 h at 195°C) [18].

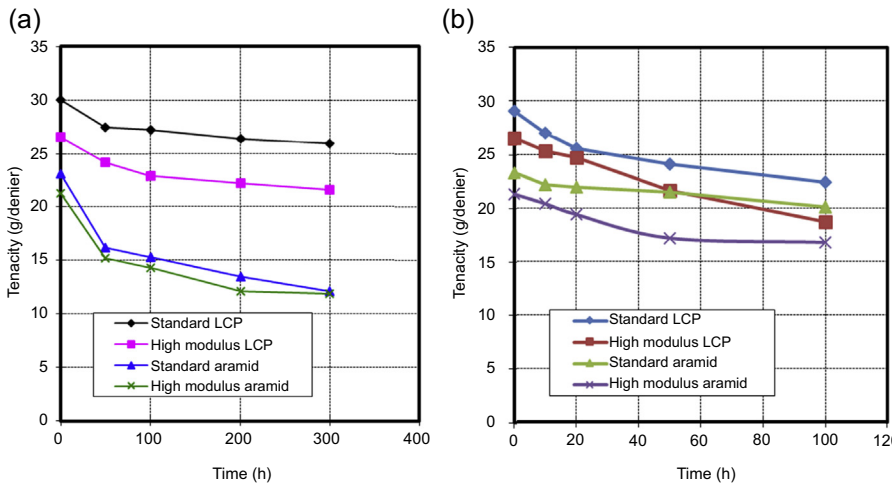

Figure 5.14 Effect of elevated temperature on LCP fibers under dry heat and wet heat (steam) conditions [18]: (a) dry air 250°C, (b) wet steam 120°C.

overcoating with polymer melts, for example,. during fabric coating or extrusion of polymer cable jackets. The presence of significant moisture during these operations can lead to blistering, bubbles, or other surface defects. The tendency to absorb moisture from the environment can also cause long-term microcracking issues in fiber-reinforced composite materials, as has been reported with aramids.

LCP fibers, because of their polyester basis, tend to be stable against common acids, but are attacked in high pH solutions such as caustics, concentrated bases, or ammonia solutions. LCP is also stable against bleach solutions commonly used in industrial

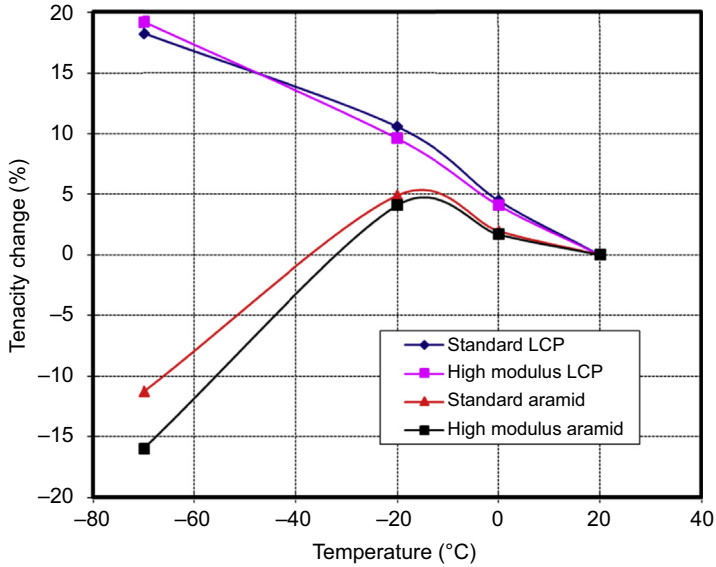

Figure 5.15 Effect of cryogenic conditions on strength of LCP fibers [18].

Table 5.3 Equilibrium moisture regain of LCP fibers (%) [18]

Temperature (°C)	Relative humidity (%)	LCP		Aramid	
		Regular	High modulus	Regular	High modulus
20	65	<0.1	<0.1	4.2	4.1
20	80	<0.1	<0.1	4.8	4.8
20	90	<0.1	<0.1	5.4	5.5

laundering, as shown in Fig. 5.16. An abbreviated chart of chemical resistance against a variety of solutions is shown in Table 5.4.

5.5.6 *Effect of UV and radiation*

As with many aromatic polymers, LCP fibers are subject to degradation by the high-energy UV rays in natural sunlight. Testing in simulated sun environments shows rapid degradation of individual fibers. However, the effect appears to be self-blocking, and so the effects are dependent on product form and variables such as diameter/size, finishes/coatings, twist levels, pick counts, etc. Fig. 5.17 shows that many high-performance fibers can be damaged by sunlight exposure, and should be protected with simple measures such as overbraided jackets and/or UV-blocking coatings. In the worst case (eg, low-twist, single fibers, no coatings), LCP and other

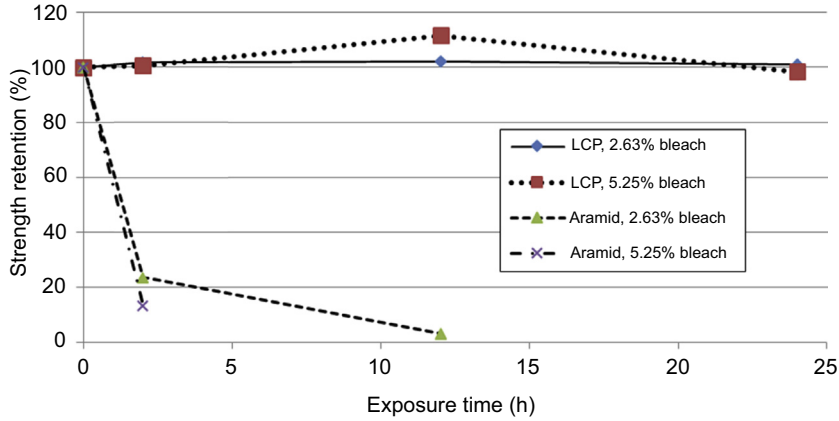

Figure 5.16 Effect of hypochlorite (bleach) solution on LCP fibers [18].

Table 5.4 Chemical resistance of LCP fiber to common reagents [18]

					Retained strength (%)	
Reagent	**Formula**	**Concentration (%)**	**Temperature (°C)**	**Time (h)**	**LCP**	**Aramid**
Sulfuric acid	H_2SO_4	10	100	10	96	40
Nitric acid	NHO_3	10	70	10	95	23
Caustic soda	NaOH	10	70	20	66	21
Acetone	CH_3COCH_3	100	20	10,000	99	99
Methanol	CH_3OH	100	20	100	96	94
Ammonia	NH_4OH	10	70	24	35	95
Mineral oil		100	20	10,000	100	100

See complete table in Vectran® grasp the world of tomorrow, technical data brochure. Houston: Kuraray America, Inc.; 2010.

high-performance fibers may not retain acceptable performance after long-term UV exposure (eg, Fig. 5.18).

LCP fibers are transparent to microwave energy and are virtually unaffected by high levels of radiation. Table 5.5 shows results of X-ray exposure on LCP fibers (gamma radiation, cobalt-60). Total exposure time was 30 min or 4800 rad. LCP polymer data [28] show minimal effect on properties after exposure to 500 Mrad.

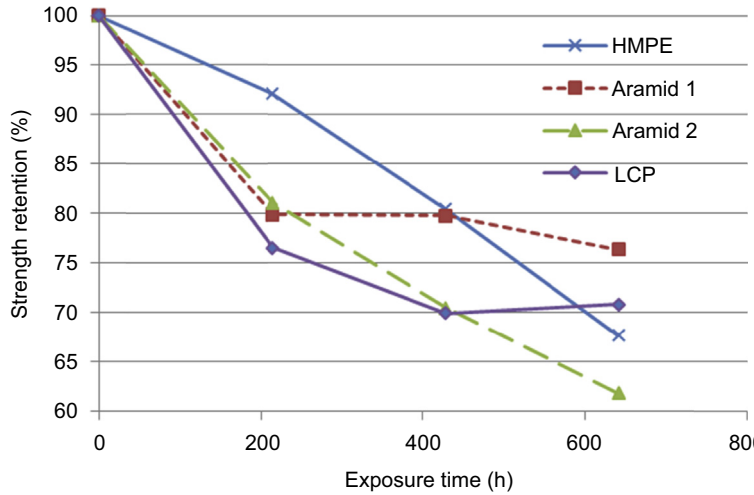

Figure 5.17 Effect of simulated sunlight (xenon-arc) on $^{1}/_{4}$ ″ (6 mm) diameter 12-strand ropes [18].

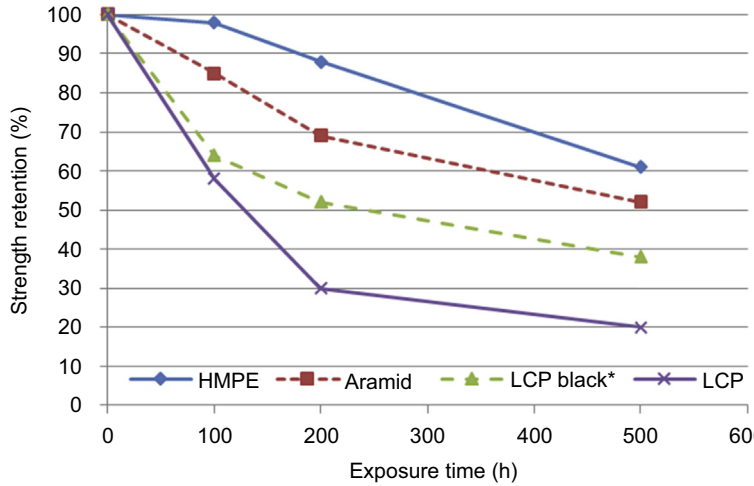

Figure 5.18 Effect of simulated sunlight (carbon-arc) on single-end 1500 denier fibers [18] (*LCP Black is pigment-dyed).

5.5.7 Abrasion resistance

LCP has excellent resistance to yarn-on-yarn abrasion, which is an important property for fatigue resistance in ropes, cables, and slings. Internal fiber interaction occurs whenever flexible strength members are moved or loaded, and poor yarn-to-yarn abrasion performance translates to limited life in the field, or low residual strength after service. Similar to polyester fiber, the abrasion resistance of LCP improves in the wet condition, as shown in Table 5.6.

Table 5.5 Effect of gamma radiation on LCP fiber tenacity [18]

Sample	Denier (dTex)	Twist (t/m)	Before X-ray		After X-ray		Strength retention (%)
			Tenacity (cN/dtex)	Elongation (%)	Tenacity (cN/dtex)	Elongation (%)	
Standard LCP	1670	80	25.5	3.8	25.1	4.3	98
High modulus LCP	1580	80	21.1	2.6	23.2	3.1	110
Standard aramid	1670	80	20.0	4.5	21.5	4.3	108

Energy equivalent to 1800 times levels used in medical soft X-ray photography.
Soft X-ray, 9600 rad/h at 1 m, 30 min exposure time.

Table 5.6 Yarn-on-yarn abrasion results [18]

Yarn designation	Average cycles-to-failure	
	Dry	Wet
LCP	16,672	21,924
Aramid 1	1178	705
Aramid 2	1773	759
Aramid 3	974	486
PBO	2153	–
HMPE (1600d)	8518	23,619

Test Method CI-1503, 1500 denier, single-end no-twist, 1.5 wraps, 500 g load, 66 cpm.
HMPE, high-modulus polyethylene; *PBO*, poly(*p*-phenylenebenzobisoxazole).

5.5.8 Flex fatigue

Flex or bending fatigue is a critical concern in many applications where yarns or fabrics are subject to repeated folding or creasing. Examples include ropes, sailcloth, inflatable and/or temporary structures, etc. Improving the service life of products by increasing the flex fatigue resistance is an important driver for the use of LCP fibers in a variety of applications.

The actual mechanism of flex fatigue has been a subject of considerable study because of the significant variability in flex failure resistance of fibers made from linear chain polymers. For example, typical polyesters, LCP (wholly aromatic polyesters), and aramids (wholly aromatic polyamides) all exhibit a similar microfibrillar structure. In addition, the ultimate compressive strength of high modulus organic fibers is generally about 1/10th of the ultimate tensile strength, and for all of these examples, the first visual manifestation of flex damage is the appearance of kink bands in the fiber. Kink bands, often explained as dislocations (buckling or breaking) in the molecular chains, could involve the entire microfibril, or propagate through the microfibril with repeated flexing or compressive strain at the same location.

In spite of these structural commonalities, these fibers differ considerably in their resistance to flex fatigue. Typical polyester cannot provide the tensile and thermal properties of high-performance fibers, but it does offer higher flex fatigue resistance when cycled at a similar percentage of its ultimate break load. LCP routinely outperforms aramids when tested for fatigue resistance and tenacity retention in yarn, rope/cable, and fabric forms.

Comparative flex fatigue data for yarns appears in Table 5.7. While aramid results varied considerably with type, LCP clearly outperforms the aramid class, including poly(*p*-phenylenebenzobisoxazole) (PBO). Flexural test data should always be considered only as a tool to rank various materials. Controlled component testing cannot always reflect actual results in the product's end use environment and

Table 5.7 Flex fatigue results (single yarns) [18]

Yarn designation	Cycles-to-failure
LCP	115,113
Aramid 1	5114
Aramid 2	40,666
Aramid 3	1383
PBO	23,821

Tested per ASTM D2176-97a (Tinius–Olsen), modified for yarn, 1500 denier, 2 kg weight.
PBO, poly(*p*-phenylenebenzobisoxazole).

construction. However, relative material rankings are consistent from test to test, as seen in Table 5.8 using small cords.

An aerospace company compared flex fatigue resistance of LCP to aramids in coated fabric form. In this study, base fabrics of aramid and LCP were coated in an identical fashion with the company's proprietary formulation. Specimens 1″ (weft direction) × 60″ were cut and tested to simulate hard creasing and folding in a cyclic fashion. Each cycle consisted of folding the sample in half, dragging a 10 lb steel roller over the fold, refolding the specimen at the same point but in the opposite direction, and again dragging the roller over the fold. Strength losses were compared using a test compliant with FED-STD-191, Test Method 5102. As Table 5.9 illustrates, LCP tenacity losses were minimal after 100 cycles, with the tensile failure point occurring away from the fatigued fold line. Aramid strength losses were significant, with tensile failures occurring at the fold line.

Fig. 5.19 shows residual strength of fibers as a function of flex cycles per ASTM D2176. The load-bearing capacity of the LCP fibers was twice that of aramid after as few as 500 cycles, and the gap widened as cycling continued. Microscopic

Table 5.8 Flex fatigue results (small cords) [18]

Yarn designation	Cycles-to-failure
LCP	41,909
Aramid 1	2115
Aramid 2	14,963
Aramid 3	8143
PBO	25,158

Cord construction: parallel core/extruded jacket.
Test conditions: 0.085″ diameter cords, 1.78″ diameter pulley, 100 lb test load, 58 cpm, 5 tests/sample.
PBO, poly(*p*-phenylenebenzobisoxazole).

Table 5.9 Flex fatigue resistance of LCP-coated fabric [18]

Base material	Tenacity loss after 100 cycles (%)	Failure location
LCP	0.8	Away from fatigued crease
Aramid	22.9	At crease

Fabric strength tested per FED-STD-191, Test Method 5102, 1″ width strips.

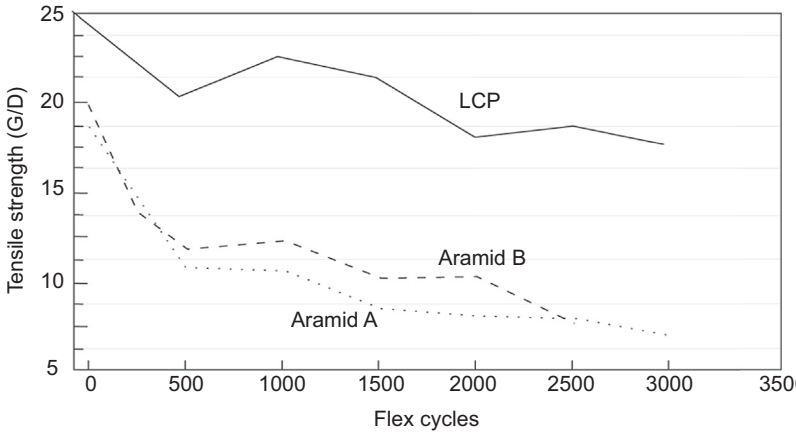

Figure 5.19 Flex fold cycling of LCP and aramid fibers [18].

examination showed that in LCP kink band formation increased with cycle count as expected; however, the bands did not rapidly progress into cracks and split microfibrils as noted with aramids. Possibly kink band formation in aramids was initiated at much lower cycle counts, but catastrophic failure later masked or interfered with microscopic examination.

To better understand the basic mechanisms of flex fatigue, residual strength of LCP and aramid fibers after cyclic compression fatigue was studied using individual filaments, by Saito et al. [29–31]. Fig. 5.20 shows residual strength of individual LCP filaments after cycling to levels around the critical compression strain where kink bands begin to form (roughly 0.6% compressive strain for LCP and 0.9% for aramid) [29,30]. Compressive cycling at 50% of this critical strain caused only minor fiber damage or reduction in residual tensile strength. However, at strains 100% of the critical level or higher, damage began to increase after as few as 10 cycles for aramid [31], compared to more than 10,000 cycles for LCP.

Flex fatigue failure mechanisms are not simple, and elucidating differences between the resistances of various fibers is not straightforward. However, one relevant consideration might be the relative extent of crystalline order in these fibers. For example, standard polyester fibers are ordered along the axis with considerable amorphous

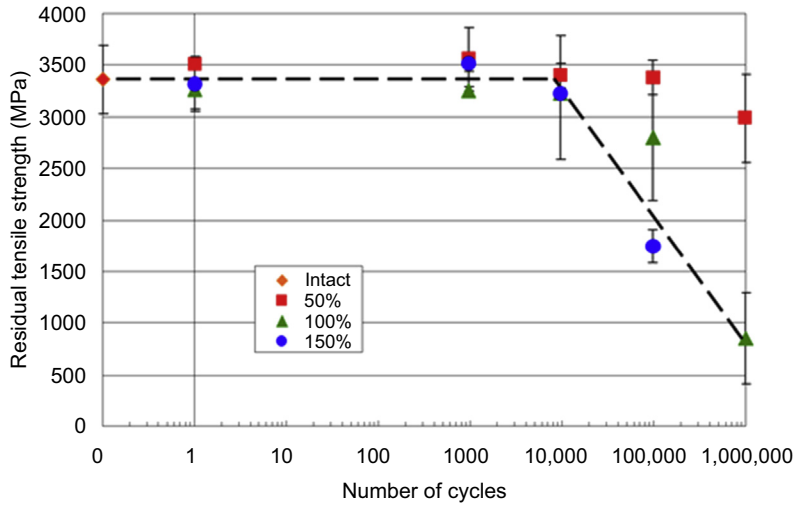

Figure 5.20 Single-filament compression fatigue resistance of LCP fibers [29].

content. LCP is oriented along the axis with very few amorphous regions and no observed three-dimensional crystallinity. Aramids have a much greater degree of intermolecular bonding because of hydrogen bonding between adjacent molecules, that is, a more three-dimensional molecular structure. While each of these fibers has exhibited kink band formation in response to compressive strains, lower degrees of dimensional order may more effectively block damage propagation across microfibrils and/or fibers.

5.5.9 Cut resistance

There are a variety of cut resistance test methods, and uniformity/consistency of test sample and cutting edge is critical in all such tests. Cut testing methods developed by Kuraray [18], utilizing fixed blades and knitted spun yarn samples (Fig. 5.21), gave the results shown in Table 5.10.

Fig. 5.22 shows the result of slash testing [25] conducted per the Home Office SDB Slash Resistance Standard for UK Police [32]. LCP fibers are often used either alone or blended with other fibers in engineered yarns, knits, and fabrics, for applications requiring resistance to blade threats such as slashing attack.

5.6 LCP fiber applications

LCP fiber is one of several high-performance fibers available commercially today, for example, HMPE, para-aramid, copolymer aramid, PBO, etc. All of these fibers are used in applications demanding high strength and low elongation. Therefore in short-term end uses there is often not sufficient difference in tensile performance to

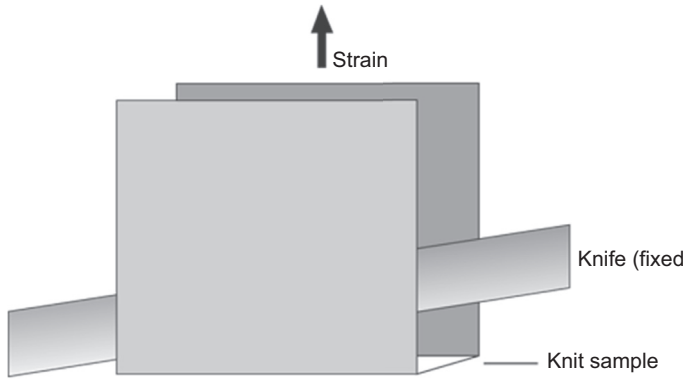

Figure 5.21 Cut resistance test method used by Kuraray for the material rankings of Table 5.10 [18].

Table 5.10 Cut Resistance of spun yarn samples [18]

Material	Relative cutting load
LCP	100
Aramid	73
Polyester	4

Samples: 20s/2s cotton count, knit hose construction.
Tested per Kuraray cut method of Fig. 5.21.

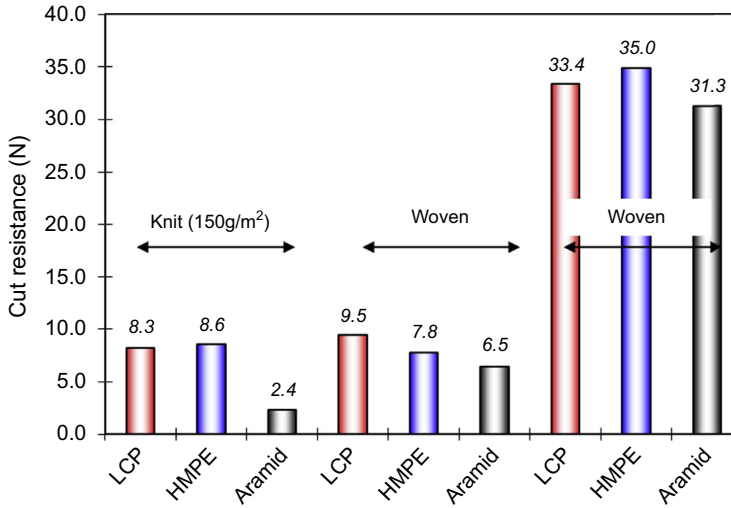

Figure 5.22 Results of slash testing using UK Home Office SDB method [25,32].

justify the higher cost of LCP, for example, compared to HMPE or aramid alternatives. However, in applications that value long-term stability of physical properties and dimensions, LCP has proven to meet end use requirements over a wide range of temperatures and environments. Some of these application areas are described next. Of course, many applications are proprietary to specific converters or customers and so are not described.

5.6.1 Rope and cordage

LCP fibers are used in many specialty rope and cordage applications where low creep elongation over an extended period of time is required by the end use. Examples include mooring tethers, tension cables, actuator cables, for example, as used in robotics, and other specialty rope/cordage applications. LCP fibers and ropes are also finding use in bending fatigue applications, such as continuous bend-over-sheave (CBOS), often in blends with HMPE. Because of the very good resistance to internal abrasion, creep, and flex fatigue, in many operating conditions LCP or LCP/HMPE blends offer superior performance to HMPE and aramids [33,34]. Properties of LCP fibers in rope applications have been presented elsewhere [35].

5.6.2 Cables/umbilicals

One of the first applications for LCP fibers was in sensor cables, for hydrophone streamer cables used by submarines to enhance their ability to locate objects under water. Dimensional stability is important wherever regularly spaced sensors are used with software that relies on specified spacing to accurately interpret incoming sensor data. Dimensional stability is also important in electromechanical cables where LCP is used as a strength member or as part of a served or braided protective jacket. Cable designers depend on LCP to keep load away from low-strength, low-elongation materials such as fiber-optic cables. LCP also increases bursting strength in high-pressure hydraulic/pneumatic hoses used in specialty umbilicals. Depending on the design requirements, use of LCP fibers can reduce overall product diameter because of its somewhat higher performance, or can be used to maintain performance at a reduced overall weight.

Cable manufacturers also benefit from the very low equilibrium moisture content of LCP fibers. This means lower off-gassing of moisture and therefore less blistering/bubbling when the cable components are overcoated at high speed with a hot extruded polymer, for example, when producing cable jackets made from nylon or polyurethane. The reduced moisture uptake of LCP may eliminate the need for conditioned storage or drying, for example, no longer requiring the use of environmentally controlled warehouse areas.

5.6.3 Protective fabrics

As noted previously, LCP fibers combine excellent cut/slash resistance properties with resistance to damage or shrinkage during industrial laundering processes. This has led

to growing markets for LCP in industrial applications where personal protective equipment is expected to last for many usage cycles, for example, in gloves and other protective garments. High initial cost compared to more common meta- and para-aramid gloves must be weighed against the increased service life, and in many high-usage applications the overall reduction in life-cycle cost easily justifies the slightly higher initial cost.

5.6.4 Narrow fabrics, straps, lifting slings

Many companies in several countries around the world utilize LCP fibers in lifting equipment such as straps, narrow woven belts, or slings. The durability of the fiber to internal yarn-to-yarn abrasion and high-strength retention in hot weather (or when lifting outdoor sun-heated equipment) ensures safe lifting operations as well as long service life. Similar applications include heavy equipment tie-down straps and safety restraint systems.

5.6.5 Flexible composites

As discussed in a previous section, a significant advantage of LCP fibers compared to para-aramids is the ability to undergo repeated low-radius bending without significant damage to the fibers. This property has led to many applications in coated fabrics or "flexible composites," where the end use requires multiple bending cycles. For example, there are many examples of inflatable structures in military and industrial applications where the coated fabric is folded for low-volume storage when not in use, but is repeatedly deployed, inflated, deflated, and packed again. The superior flex fatigue resistance of LCP leads to much longer service life and overall product durability for inflatables such as airships, temporary barriers, emergency structures, etc. The use of LCP fibers and fabrics for inflatable applications was the subject of a recent review [19].

5.6.6 Rigid composites

There are many applications of LCP fibers in rigid composites, even though the compressive properties of LCP are much lower than that of carbon or glass. Because of the low compressive strength and modulus, similar to other organic fibers, LCP fibers are not used as reinforcement for primary structure. However, LCP fibers are used in hybrids with glass or carbon, to protect against impacts (eg, improving compression-after-impact properties), enhancing vibration damping behavior, and in some cases creating directionally designed user-friendly failure modes to reduce the possible secondary effects of catastrophic failures. LCP fibers are also used as preform stitching threads, to enhance delamination resistance, and/or hold layup patterns during initial curing stages [36–38]. LCP fibers have a very low equilibrium moisture content, and so do not contribute to long-term moisture-related problems in aerospace composite parts, for example, matrix plasticization, corrosion of adjacent metals, or microcracking.

5.6.7 Other markets

Many niche markets exist for LCP fibers, primarily in applications requiring stability of dimensions and properties over a range of loading and environmental histories. Typical end users include suppliers to military, aerospace, and industrial market segments. In many cases LCP fibers are introduced to extend service life or expand operational windows for otherwise successful applications of competing technical fibers such as aramids or HMPE. LCP fibers provide the optimum combination of thermal/dimensional stability and abrasion/flex fatigue resistance.

5.7 Future trends

Although LCP fibers have excellent overall properties, fiber producers continue to target improvements. For example, the high yarn-to-yarn abrasion resistance of LCP fibers observed in ropes, slings, and cables has generated interest in improvements. Options include (1) enhanced fiber finishes/lubricants, (2) improving heat tolerance of fibers/finishes, and (3) modifying contact area by changing filament size.

Large-scale CBOS testing of LCP ropes revealed that standard silicone oil lubricants had a tendency to become highly fluid at the high temperatures generated by friction in a bend-over-sheave test. The high temperatures reduced the viscosity of the oil and led to the finish squeezing out of the structure, with significant negative results on fatigue performance. Kuraray recently introduced a higher molecular weight silicone oil that is more stable to elevated temperature cycling. Test results in yarn-to-yarn abrasion are shown in Fig. 5.23 [39].

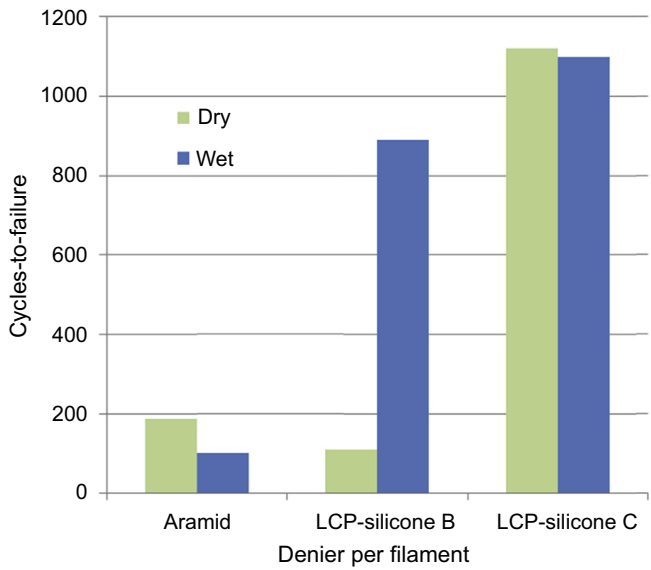

Figure 5.23 Improvement of yarn-on-yarn abrasion resistance using an improved finish [39].

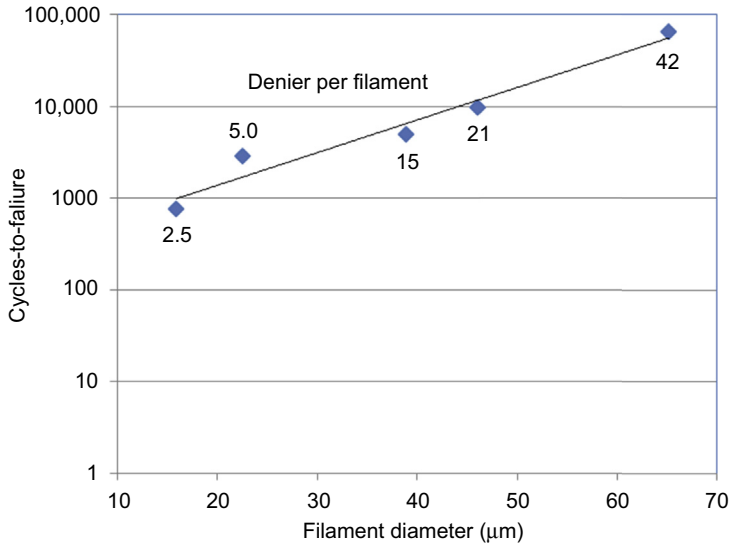

Figure 5.24 Effect of LCP filament diameter on yarn-on-yarn abrasion performance [39].

Another interesting area of research is that of increasing filament diameter. One advantage of the melt-spinning process is that many options are available for filament size and shape. Abrasion testing of several filament sizes (round cross-section) shows a very strong relationship between filament size and yarn-to-yarn abrasion resistance (Fig. 5.24 [39]). These data suggest that ropes made from larger filaments could achieve proportionally longer service lives. Large-diameter ropes generate potentially damaging internal heating during continuous cyclic bending. This heat is driven by sliding friction between millions of individual small filaments in continuous contact. Larger filaments could also reduce the maximum operating temperatures in large-diameter ropes by reducing the fiber-to-fiber contact area [40].

5.8 Summary

Wholly aromatic LCP polyester fibers are a high strength, low-elongation alternative to aramid and HMPE fibers. LCP fibers are the highest strength polyester-based fiber available, and share the dimensional and chemical stability of PET. Many designers and end users in aerospace, military, and industrial markets take advantage of LCP's unique combination of low creep, thermal stability, and high durability, in environments ranging from deep arctic seas to the surface of Mars. Work continues into fiber and finish modifications that will further improve LCP fiber properties across a wide range of end uses.

LCP fibers continue to be produced today primarily by Kuraray, and they have been the dominant supplier of LCP fibers since 1990. Other producers are likely to enter the

market in the coming years. Future expansion of fiber production is inevitable as the application base expands from low-volume niche end uses to mainstream high-volume markets.

Acknowledgments

Special thanks to all the technical staff and laboratories of Kuraray that contributed to the experimental data referenced in this document. Testing facilities for fibers, yarns, nonwovens, and textiles can be found in Kuraray sites in Okayama, Japan, Saijo, Japan, Fort Mill, South Carolina, and Houston, Texas.

References

[1] McIntyre JE, editor. Synthetic fibres: Nylon, polyester, acrylic, polyolefin. Elsevier; 2005.
[2] Calundann G, Jaffe M, Jones RS, Yoon H. High performance organic fibers for composite reinforcement. In: Bunsell AR, editor. Fibre reinforcements for composite materials. Elsevier; 1988.
[3] Chung T-S, Calundann GW, East AJ. Liquid-crystal polymers and their applications. In: Cheremisinoff NP, editor. Encyclopedia of engineering materials, vol. 2. Marcel Dekker Publisher; 1989. p. 625−75.
[4] Sloan F. Chemistry and properties of LCP fibers. In: Presented to the AIAA Aerodynamic Decelerator Systems Materials Seminar, American Institute of Aeronautics and Astronautics; May 19, 2003.
[5] Donald AM, et al. Liquid crystalline polymers. 2005.
[6] Chung TS. Thermotropic liquid crystal polymers. 2001.
[7] McChesney CE. Liquid crystal polymers. In: Engineered materials handbook, vol. II − Engineering plastics. ASM International; 1988.
[8] Dobb MG, McIntyre JE. Properties and applications of liquid-crystalline main-chain polymers. Advances in Polymer Science 1984;60/61:61−98. Springer-Verlag.
[9] Schottek J. Liquid crystal polymers (LCPs). Kunststoffe International, No. 10. Munich: CH Verlag; October 2007.
[10] Beers DE. Melt-spun wholly aromatic polyester. In: Hearle JWS, editor. High-performance fibres. Cambridge, England: Woodhead Pub. Ltd (in assoc. with The Textile Institute); 2001. p. 93−101.
[11] Beers DE. Liquid crystal Vectran fiber. In: Paper presented at Hi-Tech Textiles held at Greenville, SC, USA. Aurora (CO, USA): Maclean Hunter Presentations; July 20−22, 1993. p. 221−37. 312 pp.
[12] Beers DE, Ramirez JE. Vectran high-performance fiber. Journal of the Textile Institute 1990;81(4):561−74.
[13] Nakagawa J. Spinning of thermotropic liquid-crystal polymers. In: Advanced fiber spinning technology. Cambridge, England: Woodhead Publishing Ltd.; 1991.
[14] Sawyer LC, Chen RT, Jamieson MG, Musselman IH, Russell PE. The fibrillar hierarchy in liquid crystalline polymers. Journal of Materials Science 1993;28:225−38.
[15] Sawyer LC, Chen RT, Jamieson MG, Musselman IH, Russell PE. Microfibrillar structures in liquid-crystalline polymers. Journal of Materials Science Letters 1992;11:69−72.

[16] Sawyer LC, Jaffe M. The structure of thermotropic copolyesters. Journal of Materials Science 1986;21:1897−913.
[17] Masuda K, Takeda T, Nishizawa T. Studies on orientation of thermotropic aromatic copolyester by fused state NMR. In: Aoki H, et al., editors. Advanced materials '93, II/A: Biomaterials, organic and intelligent materials. Trans Mat Res Soc Jpn, vol. 15A; 1994.
[18] technical data brochure Vectran® grasp the world of tomorrow. Houston: Kuraray America, Inc.; 2010.
[19] Sloan F. Liquid crystal polyester fiber in flexible composite applications. In: Proc. Sampe 2012 Baltimore; May 21−24, 2012. Soc. Adv. Matls & Process Engr., SKU 57-2019.
[20] Fibre tethers 2000: High-technology fibres for Deepwater tethers and moorings. Joint Industry Project, Noble Denton Europe, National Engineering Lab, Tension Technology International; 1995.
[21] contract report TTI-IMLR-2009-645 Strength and fatigue characterization of Vectran fibre ropes − final report. Tension Technology International Ltd.; 2011.
[22] API RP2SM Recommended practice for design, manufacture, installation, and maintenance of synthetic fiber ropes for offshore mooring. American Petroleum Institute; 2001.
[23] Allan P. Final test report Vectran fibers, contract report. Lima (PA): Whitehill Manufacturing Co.; 1989.
[24] Scarborough SE, Fredrickson T, Cadogan DP, Baird G. Creep testing of high performance materials for inflatable structures. In: Proceedings SAMPE International Symposium, Long Beach, USA; May 18−22, 2008.
[25] Vectran™ technical brochure. Tokyo: Kuraray Co., Ltd.; 2015.
[26] Hinkle J, Timmers R, Dixit A, Lin JKH, Watson J. structural design, analysis, and testing of an expandable Lunar habitat. In: 50th AIAA Structures, Structural Dynamics and Materials Conference, Palm Springs, USA. AIAA; May 4−7, 2009. p. 2009−166.
[27] Fette RB, Sovinski MF. Vectran fiber time dependent behavior and additional static loading properties. NASA/TM-2004-212773. December 2004.
[28] technical brochure Vectra® liquid crystal polymer (LCP). Celanese/Ticona; 2000.
[29] Saito H, Inaba S, Nakahasi M, Katayama T, Kimpara I. Residual strength of organic monofilaments after compressive loading. In: Proceedings 18th International Conference on Composite Materials, ICCM-18, Jeju, Korea; August 21−26, 2011.
[30] Inaba N, Nakahashi M, Saito H, Kimpara I, Oomae Y, Katayama T. Study of residual tensile strength after compressive load for organic fiber. In: Proceedings 1st Japan Conference on Composite Materials, JCCM-1, Kyoto, Japan; March 9−11, 2010 [in Japanese].
[31] Saito H, Inaba S, Nakahasi M, Kimpara I. A study of residual tensile strength of organic fibers after compression loading. Technical Report to Kuraray Co., Ltd. April 28, 2010.
[32] Malbon C, Croft J. Slash Resistance Standard for UK Police (2006). 2005. Home Office Scientific Development Branch, HOSDB Pub No 48/05.
[33] Sloan F, Bull S, Longerich R. Design modifications to increase fatigue life of fiber ropes. In: Proc. Oceans 2005, vol. 1. Marine Technology Society; 2005. p. 829−35.
[34] Novak G, Winter S. Use of high-modulus fibre ropes in rope drives. In: OIPEEC Conference/5th International Ropedays − Stuttgart; March 2015. p. 165−90.
[35] Sloan F. Pitfalls of comparative rope materials testing using accelerated methods. In: Presented at 9th Intl Rope Technology Workshop, Texas A&M Univ., Marine Technology Society; March 22−24, 2011.
[36] Tan KT, Watanabe N, Iwahori Y. Stitch fiber comparison for improvement of interlaminar fracture toughness in stitched composites. Journal of Reinforced Plastics and Composites 2011;30:99−109.

[37] Jegley DC. Experimental behavior of fatigued single stiffener PRSEUS specimens. NASA/TM-2009-215955. 2009.
[38] Wood MDK, Tong L, Luo Q, Katzos A, Rispler AR. Failure of stitched composite laminates under tensile loading—experiment and simulation. Journal of Reinforced Plastics and Composites 2009;28:715—42.
[39] Uehata A, Sloan F. Developments in liquid crystal polymer (Ar-ester) fibers. In: Presented at the Techtextil North America Symposium, Las Vegas, April 21—23; 2009.
[40] Sloan F. Damage mechanisms in synthetic fibre ropes. In: Proc. OIPEEC Conf/3rd International Stuttgart Ropedays. I.M.L. Ridge; March 18—19, 2009. p. 259—71.

High-performance rigid-rod polymer fibers

6

G. Li
Donghua University, Songjiang District, Shanghai, China

6.1 Introduction

The motivation to synthesize high-performance polymeric materials has been mainly pushed by the developing aerospace and inspection industries. High strength, high modulus, excellent thermal stability as well as flame resistance are essential for application in aerospace and protective purpose in extreme conditions.

In theory, rigid-rod aromatic heterocyclic polymers have the potential to reach the level of the aforementioned requirements. The design and synthesis of these rigid-rod aromatic heterocyclic polymers was launched by the US Air Force in the 1950s [1−7]. Some companies, including at SRI International, Dow Chemical Co., Celanese (Hoechst Celenese Co.), DuPont, among others, made a great contribution to developing rigid-rod polymers in the 1970s to 1980s. After a long time of hard work and extensive study, poly(*p*-phenylene benzobisoxazole) (PBO), poly(*p*-phenylene benzobisthiazole) (PBZT), and poly(*m*-phenylene bisbenzimidazole) (PBI) were chosen as valuable rigid-rod polymers to be spun into high-performance fibers [8,9].

PBI fiber was commercialized for its thermal stability with a thermal decomposition temperature (T_d) of 550°C by Celanese in 1983 [10]. In 1991, the Toyobo Co. joined Dow Chemical Co. to develop PBO fiber. For some reason, Dow decided to stop this PBO fiber program, and Toyobo was granted a license for production of PBO fiber. In 1998, PBO fiber was ultimately commercialized by Toyobo Co. with the trade name Zylon [11]. Zylon shows superior properties, its tensile strength and modulus reach 5.8 GPa and 180 GPa, respectively, its decomposition temperature is 650°C, and its limiting oxygen index value is 68 [12,13]. However, a shortcoming of Zylon is its comparatively low axial compressive strength with a value of 0.6 GPa, which limits its uses in composites. Later, Akzo Co. claimed to have manufactured polypyridobisimidazole (PIPD, also called M5) fibers, with improved compressive strength [14−16]. Although these rigid-rod aromatic heterocyclic fibers are thermally stable, their mechanical properties are dependent on their chain conformation, intermolecular actions, as well as processing technologies.

6.2 Synthesis of rigid-rod polymers

It is difficult to produce a stiff chain polymer by connecting rigid monomer units in a linear style because of the lack of solubility in many conventional solvents and a very

Structure and Properties of High-Performance Fibers. http://dx.doi.org/10.1016/B978-0-08-100550-7.00006-1

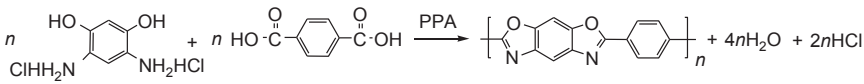

Figure 6.1 Synthesis of poly(*p*-phenylene benzobisoxazole). *PPA*, poly(phosphoric acid).

high melting temperature. The synthesis of such a polymer might appear to be a simple condensation polymerization. However, it is very difficult to carry out, as the time from scientific discovery to commercialization shows [17–20]. PBO was prepared by the reaction of 4,6-diamino resorcinol dihydrochloride (DAR) and terephthalic acid (TA) in poly(phosphoric acid) (PPA), as shown in Fig. 6.1 [13,17,18].

The polymerization mechanism of PBO has been described elsewhere [21–24]. There are some technical problems that need to be mentioned. First, dehydrochlorination of DAR will take place before polymerization. It is very common for large quantities of foam to appear with the procedure of dehydrochlorination in the reactor. This foam formation must be limited because solid monomer particles (eg, TA particles) could adhere to the inner wall of the reactor and mixing frame along with foaming, which would destroy the chemical stoichiometric quantity of the two monomers. To control the level of foaming, a low temperature or periodic cooling was applied to the reactive mixture by Wolfe et al. [13,17,18]. In their method, dehydrochlorination took a very long time. Jiang et al. [25–27] presented a novel technique for dehydrochlorination, that is, dehydrochlorination takes place at high pressure ($3-5 \times 10^5$ Pa), as shown in Fig. 6.2. Foaming could be effectively limited in this way, and dehydrochlorination could be processed at higher temperatures within a shorter time, which favors polymerization efficiency. For example, in laboratory experiments, 140–160 h is needed for dehydrochlorination in the temperature procedure at 30–60–70–90°C; while 30–40 h is enough for dehydrochlorination at 120°C with a pressure of 4×10^5 Pa [26,27]. On the other hand, the chemical stoichiometric quantity of the two monomers could remain unchanged.

Second, unlike the usual step-growth polymerizations, PBO oligomers are not randomly end capped with the two monomers, and only DAR is found at PBO oligomer

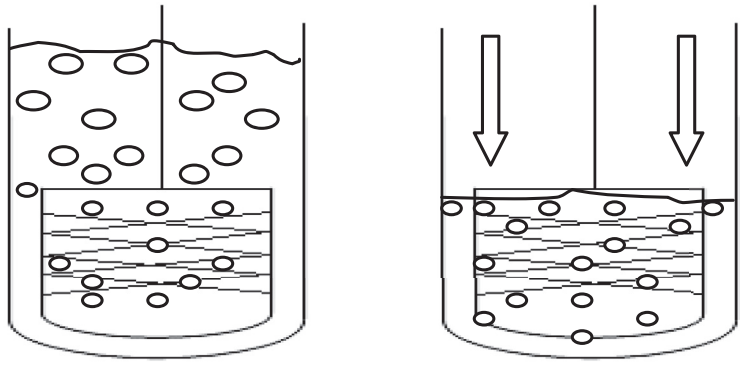

Figure 6.2 Dehydrochlorination in the atmosphere (left) and at a high pressure (right).

chain ends [21−23]. This is a result of poor solubility of TA in PPA. Therefore the particle size of TA should be less than 10 μm and is best below 5 μm to assure its dissolution. Otherwise the particles of TA might be capped by sticky oligomers before its complete dissolution, which hinders the growth of molecular weight and the formation of the nematic liquid crystalline phase. Wolfe suggested that formation of the nematic liquid crystallize phase could increase the rate of polymerization as well as the molar mass of final products [13,29,30]. The reason is that the ordering of molecules in the nematic domains increases the probability of making the reactive ends of oligomers align together thereby facilitating the reactivity [13,29].

In addition, to maintain a certain concentration of polymer (5−20 wt%) is required to form a liquid crystal phase in PPA solution [29,30]. To attain a high molecular weight of PBO, the concentration of the solvent PPA is the key factor. PPA acts as solvent, catalyst, and dehydrating agent simultaneously [21−23]. A certain P_2O_5 content (>82%, best 84%) at the end of polymerization was regarded essential to the attainment of high molecular weight. Details of the P_2O_5 adjustment method are described elsewhere [23,24].

In addition to P_2O_5 content adjustment, temperature control is technically important in the polymerization of PBO. After dehydrochlorination the reactant mixtures were allowed to stay between 130 and 150°C for a few hours for further removal of the last traces of hydrogen chloride. Then the temperature was raised to 160−170°C for several hours. Finally, the mixture should be transformed to a twin-screw extruder heated at 180−190°C for further polymerization and liquid crystal spinning at the same time [31,32].

In the case of PBZT, polymerization is quite similar to that of PBO, except 2,5-diamino-1,4 benzenedithiol dihydrochloride (DABDT) is used instead of DAR. DABDT could be synthesized by converting *p*-phenylene diamine into bis-thiourea with ammonium thiocyanate at the first. This compound is cyclized with bromine and then hydrolyzed to the oxidation susceptible monomeric potassium salt. The salt is isolated with HCl under reducing conditions to obtain DABDT. The condensation reaction of DABDT and TA is conducted in PPA by a two-stage process [4,30]. The first stage is to completely remove hydrogen chloride from DABDT under reduced nitrogen pressure at 60−80°C before adding TA. The key factors are the purity of DABDT and the particle size of TA, because DABDT is easily oxidized and TA is poorly dissolved in PPA. Solubility at 140°C is 0.0006 g per 1 g PPA [13], so that the particle size should be under 10 μm to assure dissolution. To obtain high molecular weight polymers, during the second stage P_2O_5 is added to adjust the P_2O_5 content to about 82−84%. The mixture of monomers, PPA, and P_2O_5 is stirred at 90°C to completely dissolve the solids and then slowly heated to 190−200°C and reacted for 8−10 h.

In the same way, PIPD could be prepared from 2,3,5,6-tetraaminopyridine (TAP) and 2,5-dihydroxydroxy terephthalic acid (DHTA), as given in Fig. 6.3.

TAP and DHTA were used as monomers in the polymerization. TAP hydrochloride can be synthesized by the reduction of 2,6-diamino-3,5-dinitropyridine, which is prepared by the nitration of 2,6-diaminopyridine in concentrated sulfuric acid and in phosphoric acid under a nitrogen and hydrogen atmosphere. After changing the nitration medium to oleum, high-purity products at 90−95% from the nitration and 85% yield

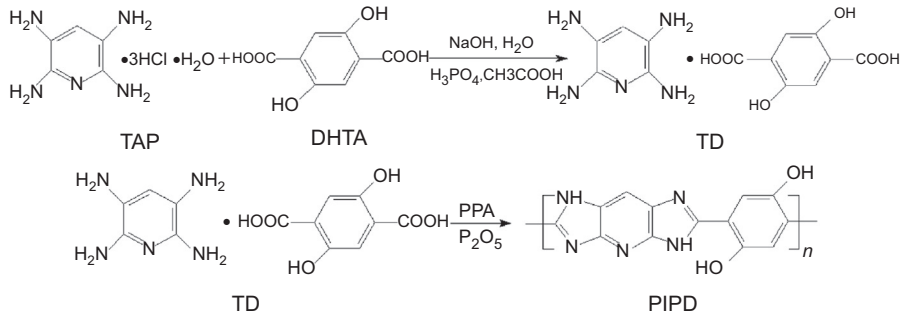

Figure 6.3 Synthesis of PIPD. *DHTA*, 2,5-dihydroxydroxyterephthalic acid; *PIPD*, polypyridobisimidazole; *TAP*, 2,3,5,6-tertra amino pyrideine.

of polymer grade purity crystal (TAP.3HCl.1H_2O) from the reduction with hydrogen can be prepared [14]. DHTA can be produced by acid-mediated aromatization (in acetic acid refluxing with 30% aqueous H_2O_2 with a sodium iodide catalyst) of diethyl succinoylsuccinate followed by hydrolysis [33]. For the polymerization of PIPD, two synthetic routes have been developed. One is the conventional method like that of PBO or PBZT using TAP hydrochloride and DHTA. The other route is the polymerization of TAP:DHTA 1:1 complex or in short expression TD complex derived from TAP phosphate, resulting in a fast polymerization cycle (typically 4−8 h) rather than >24 h and high molecular weight polymer [14]. The polymerization of homopolymer consists of taking TD complex, PPA, and P_2O_5 with a trace of tin powder into the reactor, displacing air by nitrogen, homogenizing the thick slurry, and raising the reaction temperature to 130−140°C. Mixing for at least 1.5 h at that temperature before taking the mixture to 180°C and stirring for another 1−2 h produce high molecular weight PIPD polymers.

6.3 Spinning of poly(*p*-phenylene benzobisoxazole) fibers

The polymer dopes composed of PBO macromolecules and PPA are characteristics of very high viscosity. It is almost impossible for the dopes to flow at high temperature. Therefore the prepolymer dopes were transformed from the reactor to a twin-screw extruder, which is essential for high-performance PBO fiber production. The polymerization continuously takes place during the process of dope transformation and could be accelerated in the twin-screw extruder because of the high efficiency of shearing presented by the twin-screw extruder. An illustration of reactive-extrusion liquid crystalline spinning is given in Fig. 6.4 [25,26].

Polymerized nematic liquid crystalline PBO/PPA dope is directly spun without polymer precipitation and redissolution. It is almost impossible to redissolve PBO to prepare its solution with high concentration, because it is very difficult for PBO to dissolve in many solvents, even strong acid. The processing method is dry-jet

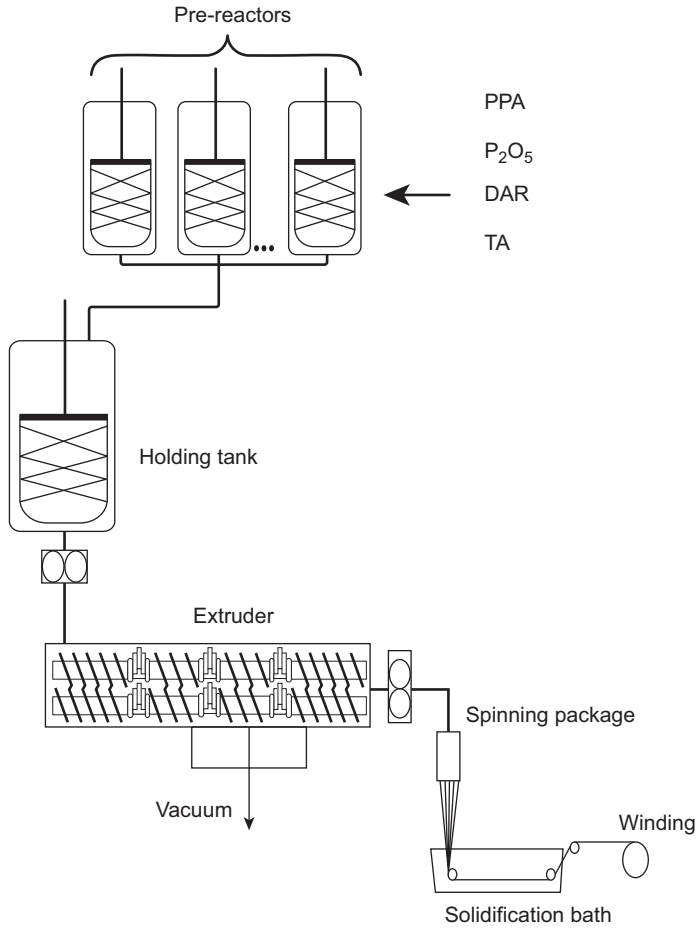

Figure 6.4 Scheme of reactive-extrusion liquid crystalline dry-jet wet spinning [25,26]. *DAR*, 4,6-diamino resorcinol dihydrochloride; *PPA*, poly(phosphoric acid).

wet spinning as show in Fig. 6.4. There are several steps included in this technique: (1) the extrusion of liquid crystal solution under heat and pressure, (2) the stream of the spinning solution goes through an air gap before entering a coagulation bath, (3) the spun stream turns into solid polymer fibers caused by the removal of PPA in the coagulation bath, (4) the coagulated fiber is washed, dried, and heat treated under tension in postprocessing. Thus each factor involved in these steps might influence the structure and properties of obtained PBO fibers. The concentration of polymer is the same as in the reactor in the 10−15 wt% range and the typical dope temperature can be optimal in the range 160−190°C. Water or 10 wt% of PPA in water at room temperature is the common coagulant. Coagulation rate can be controlled by altering the bath temperature as well as coagulation media. Coagulation conditions significantly affect the ultimate fiber structure. When the temperature of the coagulation bath changed in the

range of 25−55°C (25, 35, 45, 55°C, respectively), the degree of crystallization became smaller, from 89% to 85%, 81%, and 80%, respectively. The surface morphology of PBO fibers is also different with respect to the temperature of the coagulation bath (Fig. 6.5) [31]. The main factors that influence the surface morphology of as-spun fibers in coagulation processing are the flux ratio of solvent (PPA) and nonsolvent (water) and the rigidity of the solidified surface layer. When the coagulation bath temperature is low, the diffusion coefficient is small, thus the solidification of spun streams is lower.

Because of the difference between coagulation extent in the interior and exterior of nascent fiber, the thickness and rigidity of the fiber surface increase gradually. The tempered diffusion results in the formation of nascent fiber with circular cross-section, and possessing a smooth and regular surface morphology. The circular cross-section can alleviate stress concentration and make the drawn fibers bear stress more symmetrically during subsequent processes, which facilitates the high strength of PBO fibers.

However, at a higher bath temperature, the skin layer was solid because of intense counterdiffusion of solvent and nonsolvent. The solidification rate of the polymer was so great that the thickness and rigidity of solid skin were both greater, which holds up

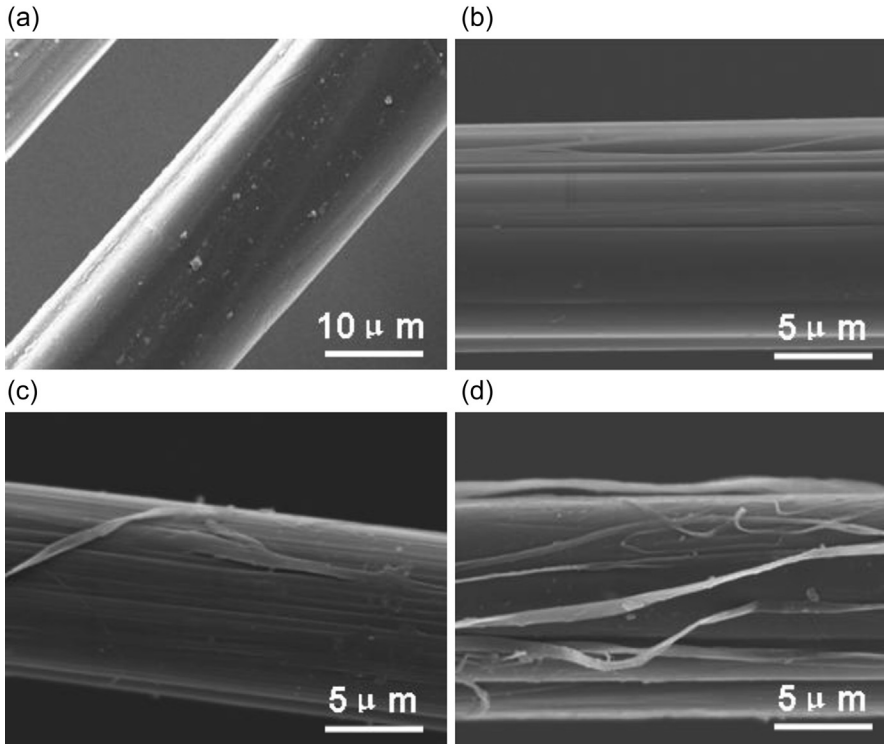

Figure 6.5 The surface morphology of poly(*p*-phenylene benzobisoxazole) fiber at different coagulation temperatures: (a) 25°C, (b) 35°C, (c) 45°C, (d) 55°C [31].

the diffusion of core solvent effectively, the stress and difference of inner and out layer of nascent fiber increasing. Finally, the surface skin of the nascent fiber collapsed and formed a lot of broken filaments on its surface [31].

It was reported that the slow coagulation assists the formation of cocrystals of the polymer and solvent [34] and leads to a lamellar structure, while high coagulation rate tends to form a nanofibrillar structure [34]. This may be the reason why lots of broken fibrillars appear on the surface of PBO fibers at a high bath temperature [31]. It is reasonable that the mechanical properties (tensile strength and tensile modulus) of DHPBO fiber become high with reduction of bath temperature (Table 6.1).

Beside bath temperature, the take-up speed is also an important factor to determine the structure and property of PBO fiber [32]. Table 6.2 shows the effect of take-up speed on performance of as-spun PBO fiber.

It is easy to understand the results listed in Table 6.2. When the extrusion rate is set, the macromolecular orientation could increase with increasing take-up speed, because more extensional flow of the liquid crystalline solution occurred during the air gap. In fact, the air gap plays an important role in providing high performance of fibers, where a very thin sheath can be formed on the surface of the spinning solution (and newly

Table 6.1 Mechanical properties of Di-hydroxyl PBO fibers at various coagulation temperatures [31]

Temperature (°C)	Tensile strength (GPa)	Tensile modulus (GPa)	Elongation (%)
25	5.33	165	2.93
35	4.85	106	4.30
55	3.53	106	3.33

Table 6.2 The effect of take-up speed on properties of poly(*p*-phenylene benzobisoxazole) (PBO)[a] fiber [32]

Take-up speed (m/min)	dtex/ filament	Tensile strength (GPa)	Tensile modulus (GPa)	Elongation at break (%)
10	5.31	3.0	101	3.0
20	4.97	3.1	104	3.0
75	3.91	4.6	122	3.8
85	3.71	4.8	125	3.8
105	3.66	5.0	129	3.8
110	3.29	5.2	131	3.8

[a]The intrinsic viscosity of PBO polymer is about 30 dL/g.

formed fiber form). Then in the followed coagulation bath, this sheath functions to affect precipitant diffusion into the fiber, which results in fewer microvoids and fine structure in the fibers [35−37].

PIPD fibers have also been spun by the dry-jet wet-spinning technique [14,38,39]. The spinning process is similar to that for PBO fibers. That is, the as-polymerized PIPD/PPA dope solution can be directly used to spin the fibers. The molecular weight of PIPD polymer is controlled in the range of 60−150K. The spinning dope is maintained above 160−180°C with a concentration of 15−20 wt%. The tensile strength and modulus of PIPD fibers are reported to be 5.36 and 350 GPa, respectively. The tensile modulus of as-spun PIPD fibers is much higher than that of PBO fibers (180 GPa).

After receiving as-spun fibers, subsequent heat treatment of these rigid-rod fibers can be run at around 500−700°C in a vacuum or a nitrogen atmosphere. Tension is necessary during the heat treatment to improve the fiber properties. Under tension applied along the fiber axles, chain orientation along the fiber axis, crystal perfection, as well as lateral order can be enhanced, resulting in an increase in tensile properties, especially modulus [40]. For PBO fibers, the temperature ranges from 550 to 600°C with a residual time of about 10 s and 400−500 MPa tension in nitrogen [41].

It has been noticed that the heat treatment parameters do not directly influence the tensile properties, that is, with the increase of temperature up to 700°C, the tensile modulus remains nearly constant [42,43]. To obtain PBO fiber with high modulus, a nonaqueous coagulation followed by heat treatment is needed. Kitagawa in Toyobo Co. Ltd. reported that the Young's modulus of the PBO fiber could be increased by 30%, that is, from 258 GPa for PBO high modulus (HM) to 352 GPa for PBO HM+, when the as-spun PBO fiber comes from nonaqueous compared to aqueous coagulation, although the tensile strength is at a lower value, 4.72 GPa for PBO HM+ and 5.59 GPa for PBO HM [43]. The property comparisons are listed in Table 6.3.

It has been considered that the slow coagulation carried on in the nonaqueous coagulation process could produce different fiber structure after heat treatment. Small-angle X-ray scattering analysis indicates that HM+ has a more homogeneous structure or is free of periodical electron density fluctuation along the fiber axis than the HM fiber [34]. The electron density fluctuation in the HM fiber comes from the presence of contrast between ordered and disordered regions; the ordered region

Table 6.3 Mechanical properties of PBO fibers

	Tensile strength (GPa)	Modulus (GPa)
PBO AS	5.55	187
PBO HM	5.59	258
PBO HM+	4.72	352

AS, means as spun; *HM+*, means high modulus-type PBO fiber by heat treatment of as-spun PBO fiber from nonaqueous coagulation; *PBO*, poly(*p*-phenylene benzobisoxazole).

forms a three-dimensional lattice and the disordered region may include defects such as molecular chain ends, conformational irregularity, and so on [35,36].

6.4 Structure and properties of rigid-rod fibers

The basic structure of PBO and PBZT fiber developed during the coagulation of liquid crystalline PBO/PPA and PBZT/PPA solution is an interconnected network of oriented microfibrils [44]. Cohen and Thomas have studied the structure formation of PBZT and PBO fibers [44–46]. According to their explanation, the first filaments are extruded from a spinneret to a swollen microfibrillar network when the nematic rigid-rod solution touches a coagulant. Passing through the coagulation process, solvent was lost from the network and dense fibrillar structure was formed. The preliminary microfibrils consisting of several rigid-rod molecular chains have typical diameters of 7–10 nm. Then several preliminary microfibrils accumulated together to form large fibrils ranging in micrometer size, as shown in Fig. 6.6 [43].

From the cross-section view of PBO fiber, there are two parts present. One is the void-free region located on the outer surface of the fibers with a layer thickness less than 0.2 μm; the other is the microvoid-containing region except for the outer layer (Fig. 6.7). This kind of structure of PBO fiber was confirmed by TEM observation given in Fig. 6.6(a) and (b) [43].

The crystal structure of these rigid-rod fibers has been investigated in detail by several research groups [47–59]. PBO, PBZT, and PIPD all have the monoclinic crystal system (Table 6.4). Their monoclinic unit cells are given in Fig. 6.8 [59].

The crystallite size for these rigid-rod fibers determined by different authors shows some difference. For example, Adams et al. [49–51] reported that as-spun PBO fibers show 5.2-nm long and 5.4-nm wide crystals and after heat treatment these crystals grew to 5.7 nm long and 10.6 nm wide. While Thomas et al. [52] found that as-spun PBO fibers have average 7.8-nm wide and 10.2-nm long crystals, they found that these crystals grew to a width of 10.0 nm and a length of 10.2 nm with 600°C

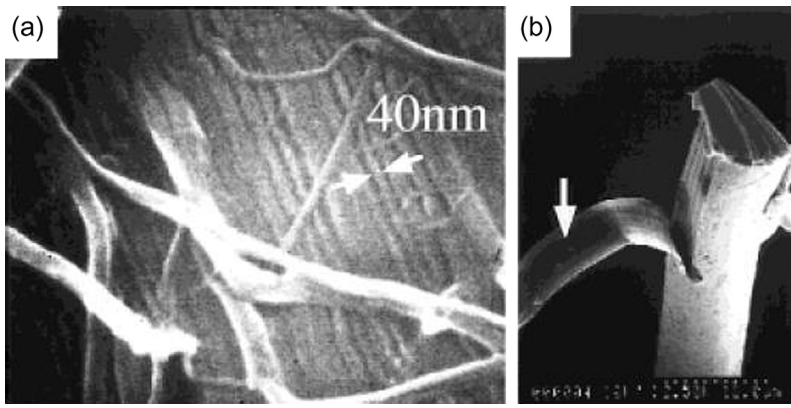

Figure 6.6 Morphology of poly(*p*-phenylene benzobisoxazole) fibers [43].

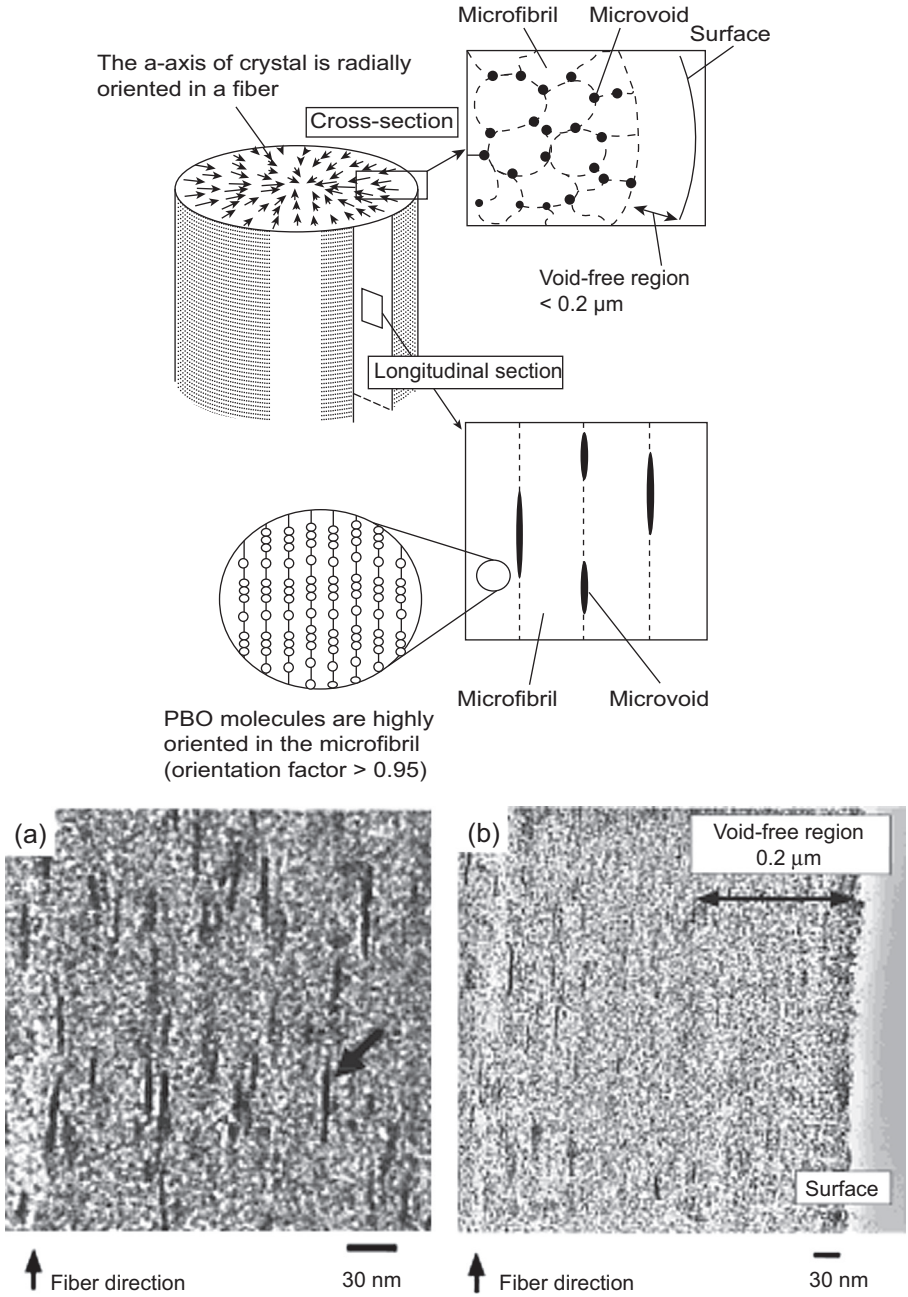

Figure 6.7 Structure model of poly(*p*-phenylene benzobisoxazole) fiber [43] and TEM images of (a) microvoid-containing region and (b) void-free region [43].

Table 6.4 Unit cell parameters of PBO, PBZT, and PIPD

Polymer	Unit cell parameters					References
	Crystal type	*a*/nm	*b*/nm	*c*/nm	γ/degree	
PBZT	Monoclinic	1.179	0.354	1.251	94.0	Fratini et al. [48,51]
	Monoclinic	1.160	0.359	1.251	92.0	Takahashi et al. [53]
PBO	Monoclinic	1.120	0.354	1.205	101.3	Fratini et al. [48,51]
	Monoclinic	0.565	0.357	0.603	101.4	Takahashi et al. [53]
PIPD	Monoclinic	1.249	0.348	1.201	90.0	Klop et al. [39]
	Monoclinic	0.668	0.348	1.202	107.0	Hageman et al. [59]
	Triclinic	0.648	0.348	1.201	105.0	Hageman et al. [59]

PBO, poly(*p*-phenylene benzobisoxazole); *PBZT*, poly(*p*-phenylene benzobisthiazole); *PIPD*, polypyridobisimidazole.

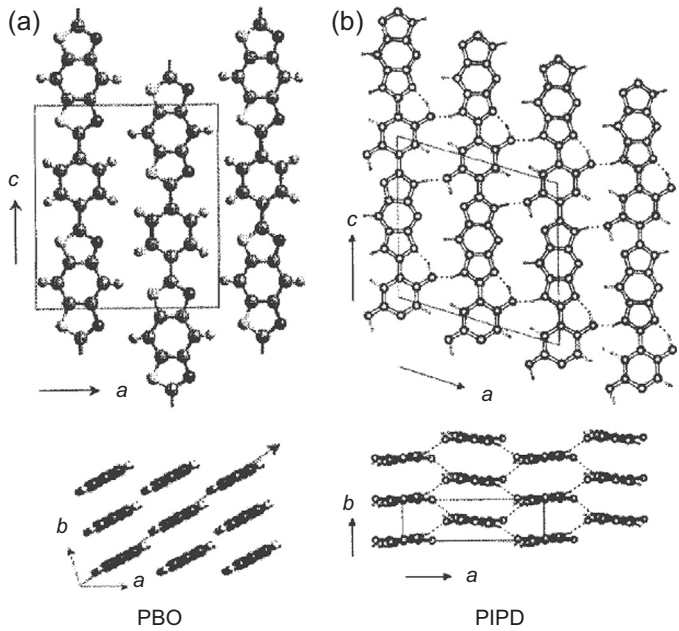

Figure 6.8 The unit cells of poly(*p*-phenylene benzobisoxazole) (PBO) and polypyridobisimidazole (PIPD) crystals [59].

heat treatment, and further to a width of 19.4 nm and a length of 14.2 nm with 650°C heat treatment. Limited growth of the crystallite along the *c*-axis after heat treatment indicates that a high degree of axial order in PBO fibers has already existed in the as-spun state. The ratios of crystallite size before and after heat treatment are 6.7 and 3.1 in the direction of axes *a* and *b* for PBZT fibers [57]. The average axial distance

Table 6.5 Average crystal size and molecular misorientation along the fiber

	PBO HM	PBO HM+	PIPD
Transverse crystalline size/nm	6.7	6.8	5.1
Axial crystalline size/nm	4.4	4.7	4.3
Misorientation angle/degree	1.25	0.95	2.34

AS, as spun; *HM*, high modulus; *PBO*, poly(*p*-phenylene benzobisoxazole); *PIPD*, polypyridobisimidazole.

between crystals is approximately 2.5 nm for as-spun PBO fiber and 3.13 nm for heat-treated PBO fiber [54,55].

Kitagawa and coauthors [56,58] compared the crystallite size for PBO HM, PBO HM+, and PIPD fibers from dark-field images. They also calculated the misorientation angle defined as the average of the angle between the lattice fringes in adjacent crystals along the fiber axis. As listed in Table 6.5, the PBO HM+ fiber has a longer persistence length along the fiber axis and less misorientation angle than HM fiber, which may be the reason why PBO HM+ shows higher modulus (320 GPa) than PBO HM fiber (260 GPa). PIPD fiber also gives a high modulus of 328 GPa although its axial crystal size is almost the same as PBO HM fiber and its misorientation angle is larger than that of PBO HM fiber. This reason may be attributed to the chemical composition of PIPD where −OH groups are present. The −OH groups could build interaction of PIPD molecules, which might play a role in stress transfer during fiber deformation leading to a high-fiber modulus [59].

The physical and mechanical properties of different rigid-rod fibers are listed in Table 6.6 [41−43]. It is clear that PBO fiber shows much higher tensile strength and tensile modulus than that of *p*-aramid fiber (Kevlar), having a decomposition temperature about 100°C. It is noticeable that the mechanical properties of PBO fiber depend on polymer molecular weight, as well as on processing conditions and post-treatment. Generally, the intrinsic viscosity of PBO reaches the level of about 30 dL/g, which is required to prepare the high-performance PBO fiber. The defects include impurities, voids, surface damage, and misaligned crystals, which may deteriorate the mechanical performance of rigid-rod fibers [40].

The stability of tensile strength and modulus upon exposure to temperature and applied conditions such as light and humidity is a key factor that influences applications of rigid-rod fibers [60,61]. PBO as-spun (AS), PBO HM, and *p*-aramid fibers were investigated under various environmental conditions to measure their tensile strength and modulus retention rate. The influence of temperature on tensile strength and modulus is given in Fig. 6.9. Both tensile strength and modulus of PBO AS, PBO HM, and *p*-aramid fibers show a reduction with increasing applied temperature. At 400°C, PBO HM fiber retains 75% and 50% of its original modulus and strength, respectively. *p*-Aramid keeps lower retention than PBO HM, 65% and 30% of the modulus and strength, respectively. In addition, high temperature together with

Table 6.6 Physical and mechanical properties of various fibers

	Density (g/cm^3)	Tensile strength (GPa)	Tensile modulus (GPa)	Elongation at break (%)	Decomposition temperature (°C)	Limiting oxygen index
PBO AS	1.54	5.8	180	3.5	650	68
PBO HM	1.56	5.8	270	2.5	650	68
Kevlar 49	1.44	3.6−4.1	130	2.8	550	28
PIPD (M5)	1.7	3.5−4.5	330	2.5	500	>50
Steel	7.8	2.8	200	1.4	–	–
Polyester	1.38	1.0	15	20	260[a]	17

AS, as spun; *HM*, high modulus; *PBO*, poly(*p*-phenylene benzobisoxazole); *PIPD*, polypyridobisimidazole.
[a]The intrinsic viscosity of polymer is a crucial factor to determine the mechanical properties of the fiber, which means the level of molecular weight.

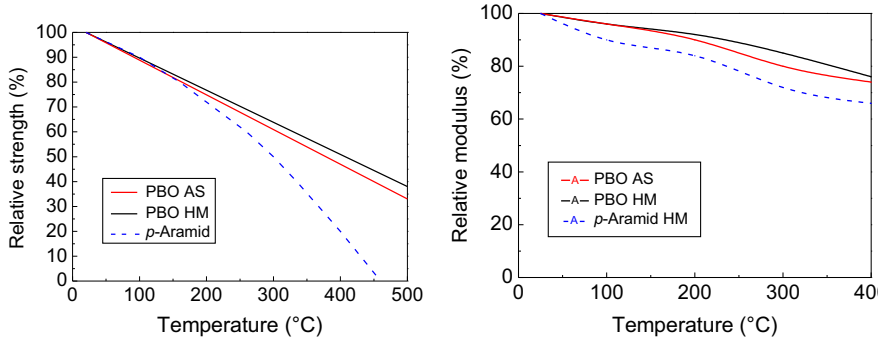

Figure 6.9 The influence of temperature on tensile strength and modulus of different fibers. *AS*, as spun; *HM*, high modulus; *PBO*, poly(*p*-phenylene benzobisoxazole).

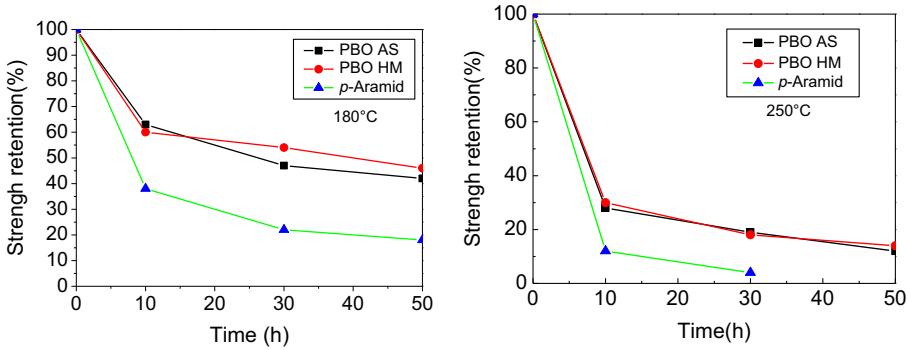

Figure 6.10 The influence of time on tensile strength of different fibers at set temperature. *AS*, as spun; *HM*, high modulus; *PBO*, poly(*p*-phenylene benzobisoxazole).

humidity has a drastic effect on strength (Fig. 6.10). At 250°C, with saturated steam, the strength retention of PBO HM is below 20% after 50 h in contrast to 45% retention at 180°C. *p*-Aramid fiber almost lost its tensile strength at 250°C for 30 h. UV exposure is also harmful to these rigid-rod fibers. After 500 h of exposure, PBO HM fiber keeps 30% of its tensile strength (Fig. 6.11). Further, exposure to visible light also affects PBI strength. It was reported that 1 month of exposure to two 35-W fluorescent lamps placed 150 cm away from the sample could reduce PBO fiber tensile strength to nearly 70% of its original value.

Unlike carbon fiber and inorganic fibers, rigid-rod fibers do not show required compressive strength for composite applications. The compressive strength of PBO fiber is in the 200−400 MPa range and for Kevlar it is about 400 MPa. Among these rigid-rod organic fibers, the PIPD fiber exhibits the highest compressive strength of about 1 GPa. By comparison, the compressive strength of carbon fiber is in the range of 1−3 GPa, and those of Al_2O_3 and SiC fibers can reach 7 GPa. Therefore there have been some efforts made to improve the stability of mechanical properties and compressive strength through physical and chemical techniques [14,16,39,57,62−75].

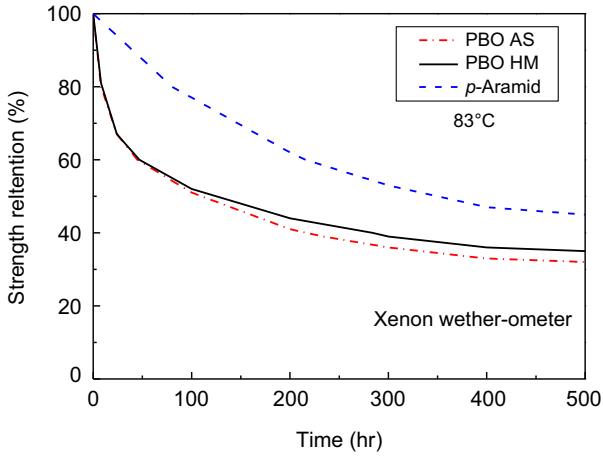

Figure 6.11 The relationship between strength and UV exposure time.

6.5 Modification of rigid-rod fibers

Besides the poor UV stability and low compressive strength of rigid-rod fibers, the surface of PBO fibers is smooth and inactive, which may lead to inferior interfacial shear strength (IFSS) when used as an enhancement for composites. Therefore the modification of these rigid-rod fibers includes chemical incorporation of functional groups and physical introduction of specific fillers to focus on designated performance improvement.

6.5.1 Chemical modification

Usually, a small fraction of multifunctional monomers was incorporated during synthesis of these rigid-rod polymers. Monomers with methyl pendant groups and dihydroxy groups are commonly added to reactive mixtures. Chemical structures of some chemically modified PBZTs and PBOs are given in Fig. 6.12.

Most of these chemically modified polymers are expected to either undergo cross-linking when heated/irradiated or form interactions between chains by hydrogen bonding. As-spun MePBZT fibers are soluble in methane sulfonic acid, while fibers heat treated between 475 and 550°C become insoluble in methane sulfonic acid. Cross-linking has occurred during heat treatment by ^{13}C solid-state NMR (Fig. 6.13) [64,65]. The compressive strength of MePBZT tension heat treated at 525°C was found to be 440 MPa, compared to 220 MPa for comparably heat-treated PBZT fibers [64]. A tetramethyl-biphenyl PBZT with the potential of forming a three-dimensional covalently bonded network has been reported. The tetramethyl-biphenyl groups may be in a minimum energy confirmation when the biphenyls are approximately 90 degrees with respect to one another based on the steric hindrance between methyl pairs on adjacent

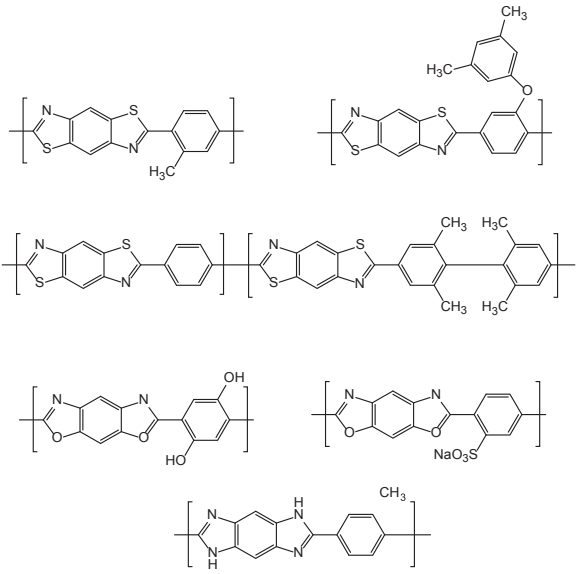

Figure 6.12 Chemical structure of modified poly(*p*-phenylene benzobisthiazole) and poly(*p*-phenylene benzobisoxazole) [68].

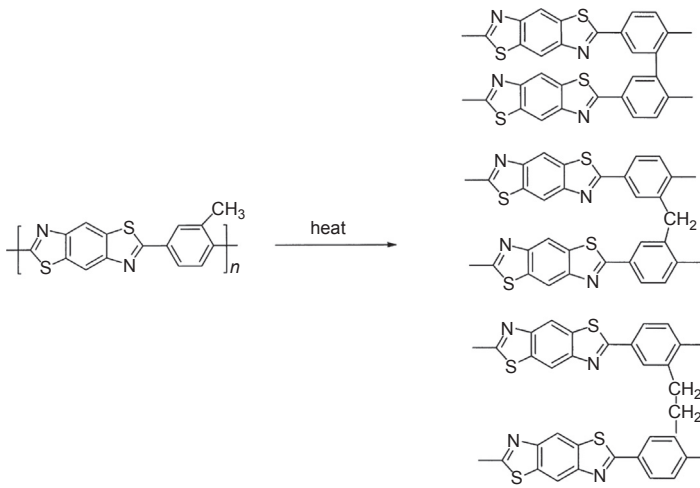

Figure 6.13 Possible products from heat-treated poly(*p*-phenylene benzobisthiazole) with the methyl pendant group.

rings. Thus cross-linking between biphenyl groups might occur in two dimensions. The compressive strength of the thermally treated 25/75 co-PBZT fibers containing 25% tetramethyl-biphenyl PBZT is about three times the compressive strength of PBZT fibers [73].

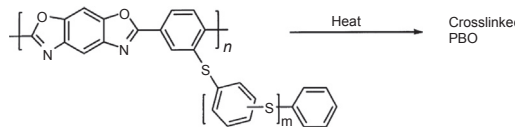

Figure 6.14 PBO with the polyphenylene pendant group [28]. *PBO*, poly(*p*-phenylene benzobisoxazole).

PBO with polyphenylene sulfide (PPS) pendant groups were made by So and coworkers at Dow (Fig. 6.14) [66]. It is well established that PPS undergoes chain extension and cross-linking upon heat treatment in air from 260 to 370°C depending on application. PBO-PPS fiber heat treated at 600°C for 30 s under nitrogen did not dissolve or break up in MSA, which was indicative of cross-linking. The compressive strength of cross-linking fiber was about 20% better than that of unmodified PBO fiber. However, the tensile strength of PBO-PPS fiber was only about 60% of that of unmodified PBO fiber because of defects caused by PPS particles in the fiber.

It is worth noticing that PIPD with similar structure as PBZT and PBO shows much higher compressive strength of 1 GPa than PBZT and PBO. The intermolecular hydrogen bonds between hydrogen of −OH and nitrogen in heterocycle rings are considered to be responsible for the improved compressive strength [16,39,74]. Inspired by the chemical structure of PIPD, Li and coauthors [75−83] proposed that introduction of hydroxyl groups or ionic groups into the macromolecular chains of PBO polymer may be an effective method to improve the compression resistance property of PBO fiber. They synthesized DHPBO polymer from the monomer of DAR, TA, as well as DHTA, as shown in Fig. 6.15. The compressive strength of as-spun DHPBO fiber reached 750 MPa when the molar ratio of DHTA was 10%, compared to 430 MPa of PBO fibers [75−80]. Fig. 6.16 shows two typical SEM images of the kink bands on PBO and DHPBO-10% fiber surface induced by axial compression. Under the same compression load, the kink band on the PBO fiber surface is very clear, while the surface of DHPBO-10% fiber still remains smooth and uniform [79].

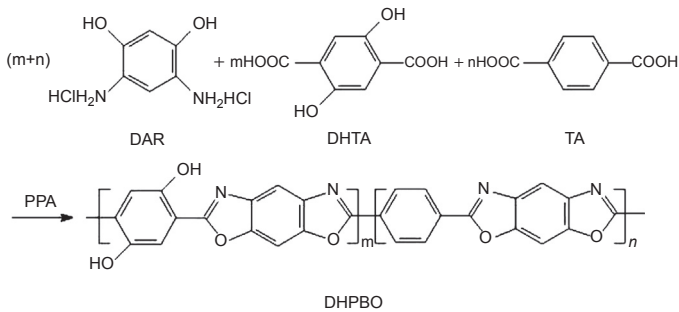

Figure 6.15 Synthesis of DHPBO from DAR, DHTA, and TA. *DAR*, 4,6-diamino resorcinol dihydrochloride; *DHTA*, 2,5-dihydroxydroxyterephthalic acid; *PPA*, poly(phosphoric acid); *TA*, terephthalic acid.

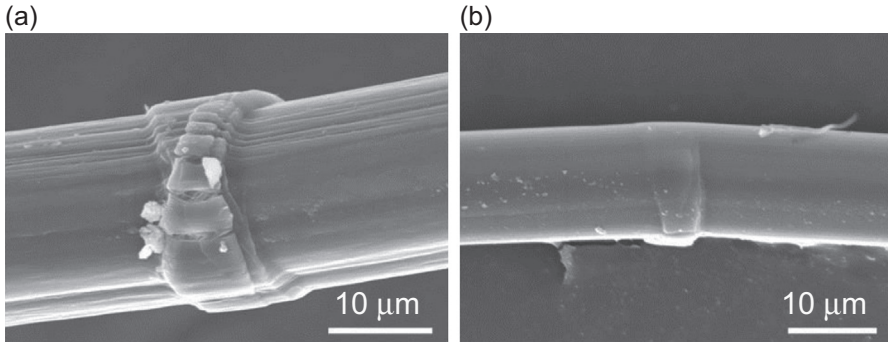

Figure 6.16 Kink band induced by axial compression bending on (a) poly(*p*-phenylene benzobisoxazole) fiber and (b) DHPBO-10% fiber under the same axial compression load [79].

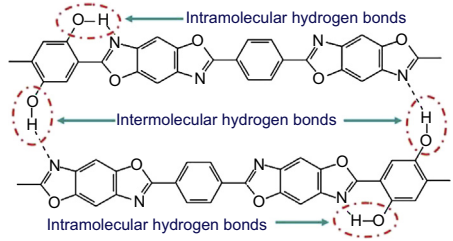

Figure 6.17 Proposed hydrogen bonds in DHPBO [79].

Based on the analysis of the FTIR spectrums of DHPBO fibers at various temperatures, the formation of intermolecular hydrogen bonds via hydroxyl groups on adjacent chains are conceivable. Fig. 6.17 illustrates the proposed relative positioning of the neighboring chains and the consequent hydrogen bond formation in DHPBO fibers. DHPBO has hydroxyl groups along its macromolecule chains, which lead to the formation of both intermolecular and intermolecular hydrogen bonds. This may be the reason why DHPBO fibers exhibit higher compressive strength than PBO fibers.

Besides the enhanced compressive strength from the hydroxyl groups' attached molecular chains, the interface interaction between fiber and matrix could also be improved because of the hydroxyl groups. DHPBO fibers with 5% and 10% of DHTA show the IFSS of 16.8 and 18.9 MPa, respectively, compared to 9.8 MPa of PBO fibers [76]. The IFSS of DHPBO fiber/epoxy resin is apparently higher than that of PBO fiber/epoxy resin. As shown in Fig. 6.18, after the pull-out test there was much more epoxy resin remaining on the surface of DHPBO fibers than on the surface of PBO fibers [80,81]. This further proves the larger interfacial adhesion of DHPBO/epoxy than that of PBO/resin. Meanwhile, DHPBO fibers provide extra benefit for UV stability [81−83]. At the same time as UV exposure, DHPBO (10%) fibers keep more retention of strength (Fig. 6.19). In fact, the present hydroxyl groups did not worsen the mechanical properties significantly (Table 6.7). In conclusion, the chemical incorporation of DHTA is an effective way to modify the performance of PBO fibers.

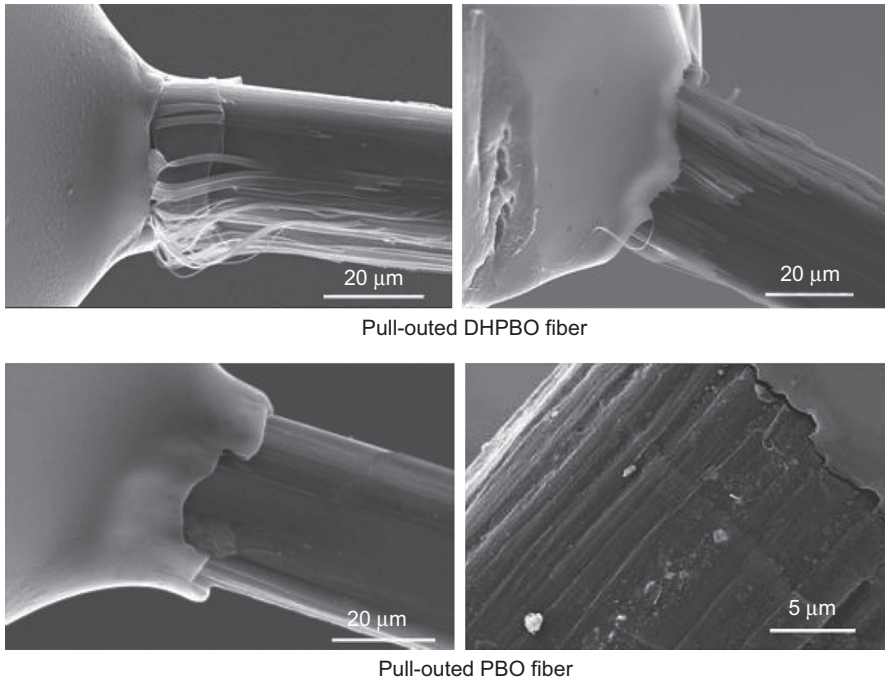

Figure 6.18 SEM micrographs of pull-outed fibers [76].

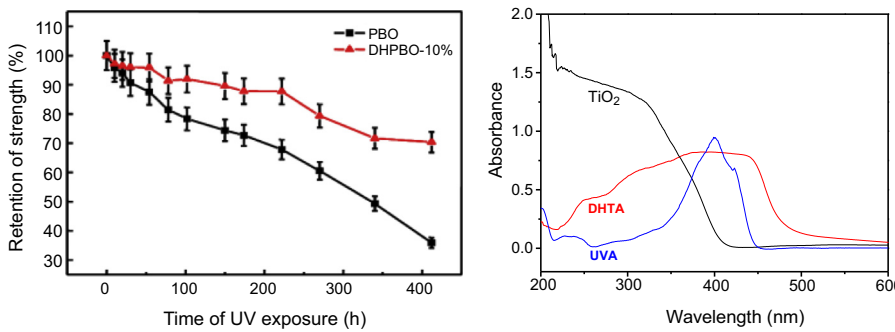

Figure 6.19 The retention of strength upon UV exposure and UV absorption of chemicals [81].

6.5.2 Physical modification

Some additives employed physically during polymerization and surface modulation by posttreatment of PBO fibers are key physical modifications. Kumar et al. [84,85] once reported that the addition of 10 wt% single-wall carbon tube to PBO could enhance the tensile strength by 60%, although there was doubt about this result because the result is difficult to realize by others. When light stabilizers were added to the reactive system together with monomers, they could remain in PBO fibers and

Table 6.7 Tensile properties of PBO and DHPBO fibers

Samples	Tensile strength (GPa)	Tensile modulus (GPa)	Elongation at break (%)
PBO	5.52	172.	3.60
DHPBO-5%	5.24	171	3.30
DHPBO-10%	5.05	143	3.27
DHPBO-20%	4.45	106	3.35

PBO, poly(*p*-phenylene benzobisoxazole).

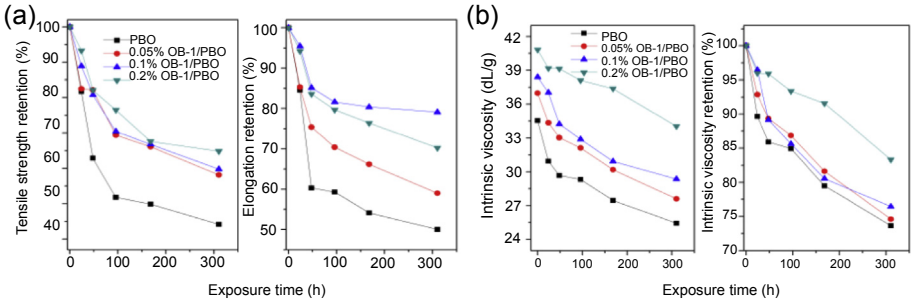

Figure 6.20 The tensile strength and elongation retention versus exposure time (a), and intrinsic viscosity versus exposure time (b).

improve light resistance to a certain extent [81,82,86,87]. Eastobrite OB-1 was once used as a light stabilizer by Jin and coauthors [86], as shown in Fig. 6.20, both the tensile strength and elongation of all fibers decrease after UV exposure with significant losses occurring after the first 100 h. For PBO fiber, at the first 100 h the tensile strength and elongation retention are only 50% and 60%, afterward the values decrease slowly to 44% and 50%, respectively, after 310 h of exposure. Meanwhile, it is obvious that only 0.05−0.2 wt% addition of OB-1 can improve the strength and elongation retention significantly. The strength and elongation retention of 0.05%OB-1/PBO is 70% at 100 h of exposure, while 310 h later it is still close to 60%. For 0.2%OB-1/PBO fiber the strength and elongation retention after 310 h of exposure is 65% and 70%, which is a 47% and 40% improvement, respectively, compared to PBO fiber. Fig. 6.21 explains that PBO absorbs both UVA-UVC and visible light with an intense absorption peak at 248 and 282 nm and the most intense absorption at 404 and 428 nm; also OB-1, 2,2′-(1,2-ethenediyldi-4,1-phenylene) bisbenzoxazole, absorbs the 200−440 nm light with peaks at 228, 238, 399, and 423 nm, and shows stronger absorptions than PBO from wavelengths of 307−430 nm. Thus OB-1 can absorb high-energy UV light of 300−400 nm wavelength, then transfer it to lower-energy visible light (400−500 nm) to avoid the UV irradiation degradation of polymers. It contains the same oxazole ring structure

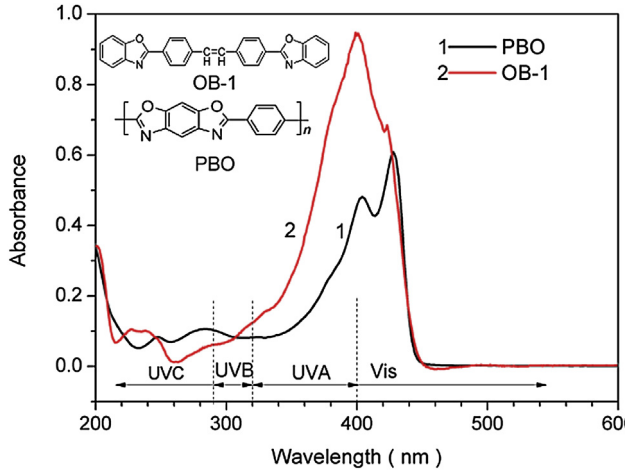

Figure 6.21 UV-Vis absorption spectrum of 2,5-dihydroxydroxyterephthalic acid , nanorutile-TiO_2, and UVA [86].

as PBO and has stronger absorption at the sensitive wavelength of PBO, which makes it a potential stabilizer for PBO fiber. From Fig. 6.20(b), the intrinsic viscosity of PBO, 0.05%OB-1/PBO, and 0.1%OB-1/PBO fibers decreases with the same trend; while for 0.2%OB-1/PBO fiber the intrinsic viscosity decreases slowly and is kept at higher retention. Clearly, the intrinsic viscosity retention of OB-1/PBO fibers is higher than that of PBO fiber under the same UV exposure conditions. After 310 h of UV exposure the intrinsic viscosity retention of both PBO and OB-1/PBO fibers is kept over 73%. These results show that chain scissions occur but not so severely, and OB-1 can protect PBO from chain scissions to some extent.

Other light stabilizers, such as 2,2′-[ethylenedi(*p*-phenylene)]bisbenzoxazole (UVA), as well as rutile nanotitanium dioxide (n-TiO_2), are also useful to protect PBO fibers from being destroyed by UV light. The UV-Vis absorption spectrum of DHTA, n-TiO_2, and UVA are compared in Fig. 6.19(b). Rutile n-TiO_2 displays the highest absorption during 200−350 nm. As expected in Fig. 6.22, PBO/n-TiO_2 could keep higher retention of tensile strength after the same time of UV exposure than PBO/UVA; DHPBO/n-TiO_2 shows the highest retention of tensile strength because of double stabilization of n-TiO_2 and DHTA [82].

6.6 Applications of rigid-rod fibers

High strength, stiffness, high-temperature stability, and fire resistance are the characteristics of these rigid-rod fibers. Thus they could be applied in appropriate areas. For example, PBI and PBO fibers are ideal in the preparation of fire clothing and special military uniforms for protective purposes. PBO fiber is strong enough to resist cutting and is used as a material to produce safe gloves. Heat-resistant roller, felt, and fabric made from PBO fibers could be used as mats in aluminum alloy and glass production

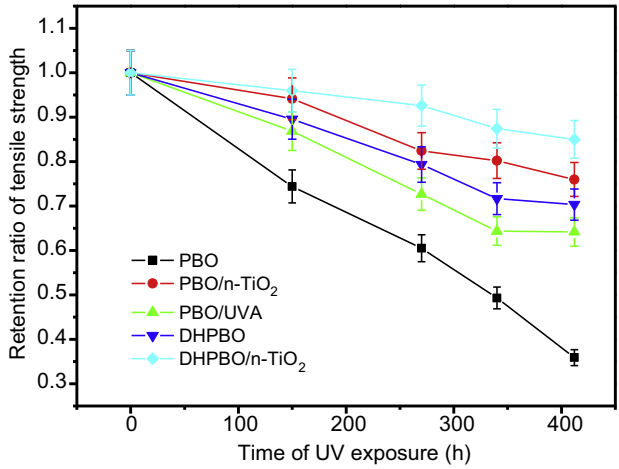

Figure 6.22 Tensile strength retention of fibers after UV exposure durations [82].

industries. The new kind of ballutes with features of balloon and parachute also consider PBO fiber as a material of high strength, stiffness, and temperature resistance, combined with low density. TenCate in the Netherlands manufactured a PBO/*p*-aramid blended fabric named Millenia with lightweight, super-strong, and heat stress reducing properties used for fire clothing. Millenia possesses outstanding cut and puncture resistance, inherent heat and flame resistance, and stays flexible and strong after exposure to flashover [88]. Second Chance Body Armor and Armor Holdings (USA) used PBO fibers in US police officers' body armor protection [89]. Navtec (USA) used PBO fibers to produce high-strength tensile materials such as cable, wire, and rigging [90]. In the aerospace area, PBO fibers were used by NASA in long-duration, high-altitude data collection. Braided PBO strands maintain the structure of polyethylene super pressure balloons [91]. A prototype of the Mars exploration balloon tested in 2002 utilized PBO tendons [92]. In motorsport, since 2001, PBO tethers were used in Formula One to fix the wheel to the chassis, thus preventing an airborne wheel from ejecting into a crowded area in the event of an accident. Starting in the 2007 season, the driver's cockpit must now be clad in special antipenetration panels made of PBO [93]. In 2011, a PBO strip was introduced to reinforce the top of the racing helmet visor and provide an overlap between the visor and helmet for additional protection after Felipe Massa's 2009 injury. In 2008 the Indy Racing League began using PBO fibers as intrusion barriers as a guarantee of safety [94].

Because of its high strength, PBO fiber is an important reinforcement to prepare composites. In the last two decades, fiber-reinforced polymer (FRP) composites have been the most common type of composite used for structural applications. Because of the combination of high strength and lightweight, PBO-FRP was developed by Furukawa Electric (Japan) in 2005 to manufacture small-diameter high-strength optical drop and indoor cables [95]. Achievable magnetic fields are determined by the strain limitation of the conductor, and the strength and stiffness of the reinforcement. PBO fiber is

used as reinforcement for producing a high magnetic field at the National High Magnetic Field Laboratory in Tallahassee, Florida, where the purpose is to develop a 100-T pulse magnet [96]. PBO-FRP sheets have been applied in the Sanyo Shinkansen as reinforcing and strengthening materials in Japan. The strengthening and rehabilitation of concrete structures and buildings may become one of new trends of PBO fiber application [97]. Conventional retrofitting techniques, such as external reinforcement with steel plates, surface concrete coating, and welded steel meshes, have proven to be complex, time expensive, and add considerable mass to the structure, which may increase the inertia forces induced by an earthquake or natural damage. Therefore the use of FRP strips as reinforcements instead of conventional methods seems a suitable solution for seismic upgrading. Currently, promising newly developed types of matrix that potentially represent a valid, sustainable, and durable alternative to epoxy are the so-called inorganic matrices such as cement-based mortars. Composite materials that employ cement-based mortars are usually referred to as fiber-reinforced cementitious matrix (FRCM) composites. FRCM composites show a promising alternative to new construction because they allow for an extension of the original service life and therefore prevent demolition of existing structures [97–99].

6.7 Concluding remarks

More than 10 years have passed since the commercial appearance of PBO, PIPD, etc., fibers; however, the application scope of these fibers and their commercial quantity is still limited. Of course, their high cost is one obstacle; another major obstacle is insufficient research focusing on a specific application to support their practical use. Designing, processing, and evaluating the products is a systematic task including different professional jobs; even new machines and equipment are needed to handle these strong materials. In the future, the development of demand-driven specific products consisting of these rigid-rod fibers may be an effective route to expand their application and production and at the same time reduce their cost.

References

[1] Arnold FE, Van Deusen RL. Macromolecules 1969;2:497.
[2] Arnold FE, Van Deusen RL. Journal of Applied Polymer Science 1971;15:2035.
[3] Wolf JF, Arnold FE. Macromolecules 1981;14:909.
[4] Wolf JF, Loo BH, Arnold FE. Macromolecules 1981;14:915.
[5] Wellman MW, Adams WW, Wolff RA, Dudies DS, Wiff DR, Fratini AV. Macromolecules 1981;14:935.
[6] Chu SG, Venkatraman S, Berry GC, Einaga Y. Macromolecules 1981;14:939.
[7] The materials science and engineering of rigid-rod polymers. In: Adams WW, Eby RK, Mclemore DE, editors. Nater. Res. Soc. Symp. Proc., vol. 134; 1989. Pittsburgh (PA).
[8] Yang HH. Aromatic high strength fibers. New York: John Wiley; 1989.
[9] Hearle JWS. High-performance fibers. (Cambridge, UK): Woodhead Publishing Ltd.; 2001.

[10] Bourbigot S, Flambard X. Fire and Materials 2002;26:155.
[11] Kuroki T, Tanaka Y, Hokudoh T, Yabuki TK. Journal of Applied Polymer Science 1997; 65:1031.
[12] Kitagawa T, Yabuki K, Young RJ. Polymer 2001;42:2102.
[13] Wolf JF. In: Mark HF, editor. Encyclopedia of polymer science and engineering, vol. 11. New York: John Wiley; 1988. p. 601.
[14] Sikkema DJ. Polymer 1998;39:5981.
[15] Lammers M, Klop EA, Northolt MG. Polymer 1998;39:5999.
[16] Sirichaisit J, Young RJ. Polymer 1999;40:3421.
[17] Wolf JF. US Pat 4335700 1980.
[18] Wolf JF, Sybert PD, Sybert JR. US Pat 4533692, 4533693, 4533724 1987.
[19] Lysenko Z. US Pat 4766244 1988.
[20] Morgan TA, Nader BS, Vosejpka P, Wu W, Kenda AS. WO95/23130 1995.
[21] So YH. Journal of Polymer Science, Part A: Polymer Chemistry 1994;32:1899.
[22] So YH, Heeschen JP, Bell B, Bonk P, Briggs M, DeCaire R. Macromoles 1998;31: 5229.
[23] So YH, Heeschen JP. Journal of Organic Chemistry 1997;62:3552.
[24] So YH, Suter UW, Romick J. Polymer Preprint 1999;40:628.
[25] Jiang JM, Zhu HJ, Li G, Jin JH, Yang SL. Journal of Applied Polymer Science 2008;109: 3133.
[26] Jiang JM, Jin JH, Yang SL, Li G. Chinese Journal of Materials Research 2006;20:435.
[27] Li G, Jiang JM, Jin JH, Yang SL. Chinese Patent ZL 02160543.2.
[28] So YH. Progress in Polymer Science 2000;25:137.
[29] Choe EW, Kim SN. Macromolecules 1981;14:920.
[30] Wolfe JF. Rigid-rod polymer synthesis: development of mesophase polymerization in strong acid solution. In: Adams WW, Edy RK, Mclemore DE, editors. The materials science and engineering of rigid-rod polymers, vol. 134; 1989. p. 134−83. Boston.
[31] Zhang T, Jin JH, Hu DY, Yang SL, Li G, Jiang JM. Science in China, Series E: Technological Sciences 2009;52:906.
[32] Zhu HJ. Doctoral thesis of Donghua University 2008.12.
[33] Sikkema DJ. Nitration of pyridine-2, 6-diamines. US Patent 5,945,537. 1999.
[34] Rakas MA, Farris RJ. Journal of Applied Polymer Science 1990;40:823.
[35] Allen SR, Filippov AG, Farris RJ, Thomas EL. Macromolecules 1981;14:1138.
[36] Allen SR, Filippov AG, Farris RJ, Thomas EL, Chenevey EC. Journal of Applied Polymer Science 1981;26:291.
[37] Allen SR, Farris RJ, Thomas EL. Journal of Materials Science 1985;20:2727.
[38] Lammers M, Klop EA, Northolt MG, Sikkema DJ. Polymer 1998;39:5999.
[39] Klop EA, Lammers M. Polymer 1998;39:5987.
[40] Allen SR, Farris RJ. In: Adams WW, Eby RK, Mclemore DE, editors. The materials science and engineering of rigid-rod polymers, vol. 134; 1989. p. 297. Boston.
[41] Pottick LA, Farris RJ, Thomas EL. Polymer Engineering & Science 1985;25:284.
[42] Kitagawa T, Ishitobi M, Yabuki K. Journal of Polymer Science, Part B: Polymer Physics 2000;38:1605.
[43] Kitagawa T, Murase H, Yabuki K. Journal of Polymer Science, Part B: Polymer Physics 1998;36:39.
[44] Cohen Y, Thomas EL. Polymer Engineering & Science 1985;25:1093.
[45] Cohen Y, Thomas EL. Macromolecules 1988;21:433.
[46] Cohen Y, Thomas EL. Macromolecules 1988;21:436.
[47] Minter JR, Shimamura K, Thomas EL. Journal of Materials Science 1981;16:3303.

[48] Fratini AV, Cross EM, O'Brion JF, Adams WW. Journal of Macromolecular Science, Part B: Physics 1985−1986;24:159.
[49] Krause SJ, Haddock TB, Vezie DL, Lenhert PG, Hwang WF, Price GE, et al. Polymer 1988;29:1354.
[50] Kumar S, Warner S, Grubb DT, Adams WW. Polymer 1994;35:5408.
[51] Fratini AV, Lenhert PG, Resch TJ, Adams WW. Materials Research Society Symposia Proceedings 1989;134:431.
[52] Martin DC, Thomas EL. Macromolecules 1991;24:2450.
[53] Takahashi Y. Macromolecules 1999;32:4010.
[54] Tashiro K, Yoshino J. Macromolecules 1998;31:5430.
[55] Tashiro K, Hama H, Yoshino J, Abe Y, Kitagawa T, Yabuki K. Journal of Polymer Science, Part B: Polymer Physics 2001;39:1296.
[56] Takahashi Y, Sul H. Journal of Polymer Science, Part B: Polymer Physics 2000;38:376.
[57] Hu XD, Jenkins SE, Min BG, Polk MB, Kumar S. Macromolecular Materials and Engineering 2003;288:823.
[58] Kitagawa T, Yabuki K, Wright AC, Young RJ. Journal of Materials Science 2014;49:6467.
[59] Hageman JCL, Van der Horst JW, De Groot RA. Polymer 1999;40:1313.
[60] Chae HG, Kumar S. Journal of Applied Polymer Science 2006;100:791.
[61] Toyobo Inc. http://www.toyobo.co.jp/e/seihin/kc/pbo/manu/fra_manu_en_.htm.
[62] Kozey VV, Jiang H, Mehta VR, Kumar S. Journal of Materials Research 1995;10:1044.
[63] Kozey VV, Kumar S. Journal of Materials Research 1994;9:2717.
[64] Mehta VR, Kumar S, Polk MB, Vanderhart DL, Arnold FE, Dang TD. Journal of Polymer Science, Part B: Polymer Physics 1996;34:1881.
[65] Dang TD, Wang CS, Click WE, Chuah HH, Tsai TT, Husband DM, et al. Polymer 1997; 38:621.
[66] So YH, Bell B, Heeschen JP, Nyquist RA, Murlick CL. Journal of Polymer Science, Part A: Polymer Chemistry 1995;33:159.
[67] Jenkins S, Jacob KL, Kumar S. Journal of Polymer Science, Part B: Polymer Physics 1998; 36:3057.
[68] Bai Y. M.S. thesis, Georgia Institute of Technology 1998.
[69] Yang F. M.S. thesis, Georgia Institute of Technology 1998.
[70] Dean DR, Husband DM, Dotrong M, Wang CS, Dotrong MH, Click WE, et al. Journal of Polymer Science, Part A: Polymer Chemistry 1997;35:3457.
[71] Yang F, Bai Y, Min BG, Kumar S, Polk MB. Polymer 2003;44:3837.
[72] Jenkins S, Jacob KI, Kumar S. In: Rozenbaum BA, Sigalov GM, editors. Heterophase network polymer, synthesis, characterization and properties. Talor and Francs; 2002.
[73] Hu X, Kumar S, Polk MB. Macromolecules 2000;33:3342.
[74] Takahashi Y. Macromolecules 2002;35:3942.
[75] Zhang T, Yang SL, Hu DY, Jin JH, Li G, Jiang JM. Polymer Bulletin 2009;62:247.
[76] Zhang T, Hu DY, Jin JH, Yang SL, Li G, Jiang JM. European Polymer Journal 2009;45: 302.
[77] Zhang T, Jin JH, Yang SL, Li G, Jiang JM. Carbohydrate Polymers 2009;78:364.
[78] Hu DY, Zhang T, Jin JH, Yang SL, Li G. Acta Materiae Compositae Sinica 2009;26:78.
[79] Zhang T, Jin JH, Yang SL, Li G, Jiang JM. ACS Applied Materials & Interfaces 2000;1: 2123.
[80] Zhang T, Jin JH, Yang SL, Li G, Jiang JM. Journal of Macromolecular Science, Part B. Physics 2009;48:1114.
[81] Zhang T, Jin JH, Yang SL, Li G, Jiang JM. Polymers for Advanced Technologies 2009;20.
[82] Zhang T, Jin JH, Yang SL, Li G, Jiang JM. Acta Chimica Sinica 2010;68:199.

[83] Luo KQ, Jin JH, Yang SL, Li G, Jiang JM. Materials Science and Engineering B 2006;132:59.
[84] Kumar S, Dang TD, Arnold FE, et al. Macromolecules 2002;35:9034.
[85] Walsh PJ, Hu XB. Journal of Applied Polymer Science 2006;102:3891.
[86] Jin JH, Li G, Yang SL, Jiang JM. Iranian Polymer Journal 2012;21:739.
[87] Jin JH, Yang SL, Li G, Jiang JM. 高分子通报 2013 [年].
[88] http://tencatefrfabrics.com/fire-service/firefighter-outer-shells/millenia-xt/.
[89] https://en.wikipedia.org/wiki/Armor_Holdings.
[90] http://www.navtecriggingsolutions.com/pbo-rigging.html.
[91] https://en.m.wikipedia.org/wiki/Zylon.
[92] Seely L, Zimmerman M, McLaughlin J. Advances in Space Research 2004;33:1736.
[93] Formula One press release. FIA Rules & Regulations Sporting Regulations 2007. Super Visor − Formula One helmets become even safer. March 30, 2011. Formula1.com.
[94] Indy-car Upgrades Planned for 2008. September 07, 2007. AutoWeek.com.
[95] Yasutomi T, Tsukamoto M, Nakajima F, Rintsu Y. Technical Report of IEICE OCS 2005;105:61.
[96] Schneider-Muntau HJ, Han K, Bednar NA, Swenson CA, Walsh R. IEEE Transactions on Applied Superconductivity 2004;14:1153.
[97] Antino TD, Carloni C, Sneed LH, Pellegrino C. Engineering Fracture Mechanics 2014;117:94.
[98] Carozzi FG, Milani G, Poggi C. Composite Structures 2014;107:711.
[99] D'Ambrisi A, Feo L, Focacci F. Composites Part B: Engineering 2012;43:2938.

High performance polyethylene fibers

7

J.M. Deitzel, P. McDaniel, J.W. Gillespie, Jr.
University of Delaware, DE, United States

7.1 Introduction

Research into the spinning of fibers from polyethylene (PE) is well into its seventh decade [1–6]. Initial fibers spun from the melt exhibited tensile modulus of 10–20 GPa, and tensile strengths of less than 1 GPa [5]. Today ultrahigh-molecular-weight polyethylene (UHMWPE) fibers are commercially available that boast average tensile strengths of ~3.7 GPa and tensile modulus of ~130 GPa [7,8] (Table 7.1). A detailed history of the development of PE fibers is worthy of a book in its own right and well beyond the scope of this chapter. In putting this chapter together, the goal of the authors has been to provide a historical roadmap highlighting the key insights that have enabled the 10-fold improvement in tensile properties, and introducing some more recent work focused on understanding how processing conditions influence the formation of the complex phase composition and morphology of these fibers and ultimately their mechanical performance. Numerous, excellent review articles and reference texts on various aspects of this topic have been written over the years, and their citations can be found in the reference section for those readers who wish to go deeper into a particular subject.

Table 7.1 Historical comparison of polyethylene fiber properties by the spinning method

Spinning process	Historical strength ranges (GPa)	Historical modulus ranges (GPa)
Melt spinning and drawing	≤1.0	~10–90
Drawing of single crystal mats	~0.5–1.0	~20–220
Surface growth fibers	~1.0–4.0	~30–140
Gel-spun fibers	~1.0–4.0	~20–130

Barham PJ, Keller A. Journal of Materials Science 1985;20:2281–2302.

Structure and Properties of High-Performance Fibers. http://dx.doi.org/10.1016/B978-0-08-100550-7.00007-3

7.1.1 Types of polyethylene

PE falls in a classification of organic materials known as polyolefins, which is the largest family of polymer materials in terms of volume in the world [9]. PE is obtained via polymerization of the ethylene monomer through either a free radical polymerization [10,11] using a peroxide initiator or through ionic polymerization through use of an organometallic catalyst like those first identified by Ziegler and Natta [11,12] or the more recent class of metallocene catalysts [11,13]. PE polymerized via free radical initiation results in a branched architecture and is generally referred to as low density polyethylene (LDPE). The presence of branching inhibits crystallization leading to a material with a density in the range of 0.9−0.94 g/cc. PE polymerized via ionic polymerization results in the formation of linear chains of carbon molecules with little or no branching [12]. The lack of branches or other defects results in a material with a high level of crystallinity and a density that ranges from 0.94 to 0.97 g/cc [14]. Commercially, linear PE is generally referred to as high density polyethylene (HDPE). It is the linear form of the PE molecule that is of interest in the production of high-performance fibers and will be the main topic of this chapter.

The simple nature of the PE molecule, an array of carbon atoms forming a linear chain, belies the wide range of properties that can be achieved through precise control of its molecular architecture and careful processing of the bulk material. Low molecular weight PEs, often referred to as paraffins [1], are waxy substances that find their use in a wide variety of applications including automotive wax, insulation, candles, and sealants for food products, among others. These materials have little in the way of mechanical strength and have a very low melting temperature [15]. PEs within this range of molecular weights are highly crystalline and exhibit little in the way of molecular entanglement needed for the formation of continuous fibers.

As molecular weight increases, significant increases in both tensile strength and thermal stability are observed [16,17]. In large part this is because of an increase in molecular entanglement and the sharing of molecules between crystallites [11]. PEs with molecular weight in the range of 10^4−10^5 Da are what one typically finds in a wide variety of commercial applications from beverage containers to composite decking materials [9]. PE in this molecular weight range is readily processable in the melt and sold in a wide variety of forms including coatings, films, injection-molded parts, and of course fibers. Fibers produced from PE in this range of molecular weights are typically spun from the melt state and then cold drawn to achieve greater tensile properties [16−21]. These materials are found in applications such as high-strength rope and outdoor tarpaulin covers. Nonwoven and spun-bonded PE fabrics produced via melt-blowing processes are found in the filtration and medical garment industries.

When the molecular weight approaches and/or exceeds 1 million Da, PE is referred to as having ultrahigh molecular weight (UHMWPE). It is this grade of material that is used to produce the high-performance fibers used in ballistic applications and applications requiring light weight and very high strength. In the bulk form this material characteristically exhibits excellent fracture strength, good wear resistance, a low coefficient of friction, and good chemical resistance [17]. Processing of UHMWPE is very difficult, because of very high melt viscosity and low “natural draw ratio” afforded by the increased level of molecular entanglement [17,21]. Commercial fibers of UHMWPE are spun from a solvated gel, which enables draw ratios in excess

Table 7.2 Tensile properties of synthetic fibers

Materials	Tensile strength (GPa)	Tensile modulus (GPa)	Density (g/cc)
Steel[a]	~2	~200	~7.75
Mesophase pitch[b] carbon fiber	3.6–3.9	520–880	2.1–2.2
PAN carbon fiber[c]	4.9–6.4	230–294	1.7–1.8
S-Glass[a]	~80	~4.5	~2.5
UHMWPE fibers[d]	2.5–3.7	70–133	0.97
Aramid[a,e]	3–3.4	70–185	1.44

The data presented in this table was assembled from the following sources:
[a]Dupont Kevlar Technical Guide.
[b]Nippon Graphite datasheet.
[c]Toray datasheet.
[d]Honeywell Spectra datasheets.
[e]Kumar, Indian Journal of Fiber and Textile Research 1991;10:52.

of 50× [22,23], yielding highly crystalline fibers with a very high degree of molecular orientation along the fiber axis. Table 7.2 provides a comparison of tensile properties for a variety of high-performance synthetic fibers.

7.2 Processing of high-performance polyethylene fibers

The goal of processing any polymer into fiber form is to optimize the subfilament structure or morphology to provide the required mechanical performance for a given application. In the case of most applications requiring high-performance fibers this often means achieving a desired balance between tensile strength, modulus, and strain to failure. Hearle and Greer [24] identify six attributes of fibers that are key to determining their final mechanical properties. They are degree of order, degree of localization of ordered domains, length to width ratio of localized units, size of localized units, degree of orientation, and molecular extent.

- *Degree of order*—In the case of PE, this refers to the overall crystallinity and crystalline perfection found in the fiber.
- *Degree of localization of order, length to width ratio of ordered domains, and size of ordered domains*—These all refer to the morphology (or shape) and spatial distribution of crystalline and amorphous domains as well as domains of intermediate phases (ie, metastable phases, constrained amorphous domains, etc.) [25–30].
- *Degree of orientation*—This refers to the degree to which the orientation molecules in the different phase domains deviate from the direction of drawing.
- *Molecular extent*—This refers to the degree to which the PE molecule has been extended along the axis of the fiber.

Each of these factors plays a role in determining the load paths and distribution of critical flaws along the length and throughout the cross-section of the fiber, which in turn determines the final properties of the filament [30].

Broadly speaking, for flexible, linear polymers the spinning process achieves the aforementioned goals by inducing a state of extensional flow that stretches the polymer chains out, inducing them to form bundles of long, fibrous crystals. Some key material and processing parameters that influence the six attributes enumerated by Hearle and Greer include: polymer weight average molecular weight [Mw], spinning temperature, and shear rate, among others [17,31–34]. In PE, the extensional flow needed to straighten out the flexible chains can be achieved via cold drawing of melt-spun filaments below PE's equilibrium melting temperature, drawing in the melt state at very high strain rates, spinning from a semidilute solution, or extrusion of solvent swollen UHMWPE followed by subsequent drawing at elevated temperatures. A brief description of each process is described in the following sections.

7.2.1 Melt spinning and drawing

7.2.1.1 Cold drawing

PE molecules are unique in that they exhibit a significant degree of molecular mobility in both crystalline and amorphous domains at temperatures well below the equilibrium melting temperature of a PE crystal (~140°C) [29,31]. It is because of this that it is possible to induce molecular orientation and annealing through drawing filaments and films at temperatures only 60°C or so above room temperature. Serious investigation into the production of high-modulus fibers by spinning PE from the melt state and subsequent drawing below the melting temperature started in the early 1970s with the works of Ward and his coworkers [16,18–20]. In 1970 Andrews and Ward carried out a series of experiments involving the "cold drawing" of fibers produced from a series of linear PEs with very well-defined molecular weight distributions. In this work, PE filaments were spun and then subsequently drawn at ambient and elevated temperatures, before undergoing tensile testing. It was observed that the achievable draw ratio for a given sample was dependent on the weight-average molecular weight. The authors also noted that increasing the draw ratio from 7 to 13 increased the measured tensile modulus from 4 to 20 GPa [16,21].

What followed through the decade of the 1970s was a string of publications from Barnham and Keller [35,36], Capaccio and Ward, Wilding and Ward, and others [18–20,32–34] that explored the effects of temperature, molecular weight, strain rate, and draw ratio on the tensile strength and modulus of different grades of linear PEs (HDPE and UHMWPE). Key observations [16,18–20,31] from this period were that linear polymers in general possess a "natural draw ratio" (ratio of initial to final cross-section) that represents the maximum extensibility for a material of a given molecular weight distribution, and that to achieve this state, drawing must occur at elevated temperature. For a given molecular weight distribution the drawing temperature should be chosen so that molecular mobility is sufficient to allow chains to move past each other, but not so great as to allow molecular relaxation at a given drawing rate (ie, maintaining a state of extensional flow) [21].

7.2.1.2 Melt drawing

While it has been demonstrated that the modulus of drawn PE fibers clearly increases with increasing draw ratio, the production of fibers through melt spinning and cold drawing was of limited use as the molecular weight of the material approaches 10^6 Da [37]. It is well understood that the melt viscosity for a linear polymer increases with increasing weight-average molecular weight [38] making the UHMWPE grades of material impossible to form fibers from the melt state. Additionally, the natural draw ratio decreases significantly with increasing molecular weight [16,18–20]. In the case of UHMWPE (>1 million Da), the natural draw ratio is limited to ~5 times or so, minimizing the amount of chain extension achievable through a cold-drawing process [21].

In the late 1980s, Bashir, Odell, and Keller [37,39,40] investigated the possibility of drawing PE fibers and films directly in the melt state. Films were made from PE samples with molecular weights ranging from 500,000 to 1 million Da, and drawn at strain rates high enough to induce extensional flow in the melt state, prior to quenching to freeze in the flow-induced microstructure. Using this approach they were able to achieve films with tensile modulus ~60–80 GPa and tensile strengths ~1.5 GPa. Additionally, examination of the crystalline morphology showed the presence of fibril crystals and shish-kebab morphologies commonly seen in highly drawn fibers. However, they found that for molecular weight higher than 10^6 Da, drawing of compression-molded films proved to be problematic because of the high melt elasticity. Additionally, the UHMWPE films retained a memory of the powder particles from which they were formed. The high level of molecular entanglement inhibited complete interdiffusion of UHMWPE molecules between the powder grains, resulting in a coarse grain structure within the film. Subsequently, Bashir and Keller explored the possibility of melt-drawing fibers from blends of HDPE containing small amounts (3% by weight) of UHMWPE with some success [40]. The process generated filaments with improved tensile modulus relative to the unblended HDPE fibers, but still short of what was achievable via solution and gel-spinning processes [17].

7.2.2 Spinning from polymer solution

7.2.2.1 Solution grown crystal drawing

It is well known that PE single crystals can be grown from a dilute solution (usually xylene at elevated temperature) and collected for further study [41–44]. Typically, PE is dissolved in a solvent, like xylene or decalin at elevated temperature and then cooled rapidly to a temperature just below the equilibrium melting temperature (T_{m0}) in solution. Upon cooling, PE lamella crystals form and precipitate out from solutions. These crystals are generally thin, flat, and diamond shaped and are composed of folded polymer chains oriented in the thickness direction [41–43]. The thickness of the PE single crystal is determined by the crystallization temperature (T_c) with thicker crystals occurring at higher T_c [43].

In the early 1960s Statton and coworkers demonstrated that it is possible to take a compressed mat of PE single crystals and draw them into filaments at elevated

temperature [44]. The authors reported a tensile modulus of 10 GPa and a tensile strength of 0.67 GPa. Subsequent efforts by Barnham and Keller, and Kanamoto [45], among others, have been carried out for a variety of molecular weights and drawing temperatures, with draw ratios in excess of 100 times and tensile modulus reported as high as 160 GPa for filaments produced from UHMW PE crystals. While this approach to filament production is not amenable to scale-up, it does demonstrate how PE crystallization from solution can produce a material with a greatly enhanced "natural draw ratio."

7.2.2.2 Surface spinning

In the late 1960s Pennings and coworkers first observed that crystallization of PE could be induced in polymer solutions at temperatures higher than those for which chain-folded PE lamellar single crystals would form, if one agitated the solution with continuous stirring at a rate great enough to create a condition of extensional flow. Pennings reasoned that stirring of the solution caused the higher-molecular-weight molecules to elongate because of the flow field in the vicinity of the stir blade, lowering the barrier for crystal nucleation. Crystals that formed in this state were long and fibrous with filament diameters ranging from $\sim$100 Å to about 1 μm in diameter [46].

Later investigations revealed that these long fibrous crystals provided a favorable surface for nucleation chain-folded crystals under the appropriate conditions [47]. The growth of these epitaxial crystals occurred at regular intervals along the length of the fibrous crystal core, earning this particular crystal morphology the name "shish-kebab" [17,48]. Originally, it was assumed that the "shish" or core filaments were composed of high-molecular-weight, extended chain crystals while the platelike "kebabs" were thought to be composed of lower-molecular-weight molecules that were free, and not incorporated into the core "shish." However, it was demonstrated that although the washing of the shish-kebab crystals in hot solvent could reduce the size of the kebabs [49], a small amount of epitaxial growth persisted.

Subsequent work by Hill, Barnham, and Keller demonstrated [35] that the state of epitaxial growth on a solution grown fibrous crystal could be altered by annealing at different temperatures below the original crystallization temperature. Smooth filaments grown from solution were observed to form what the authors refer to as "microkebabs" and that this process was reversible. The authors reasoned that the surface of solution grown fibrous crystals was in fact "hairy," composed of lengths of chain ends that had not been fully incorporated into the main body of the crystal. Under the right conditions these free chain lengths could form either chain-folded platelets or a structureless sheath [17,35].

The first successful attempt at continuous production of a solution grown fiber was reported by Zwijnenburg and Pennings [50,51]. A seed filament was dipped into a flowing solution of PE held at an elevated temperature. When the seed filament was slowly withdrawn in a direction opposite to the direction of the solution flow, a region of extensional flow in the vicinity of the seed fiber surface is created, promoting the nucleation and growth of fibrous PE crystals. These crystals adhere to the end of the seed fiber and create a continuous filament of solution grown fibrous crystals as

the seed is slowly pulled out of the solution [17]. This method is referred to as a free growth method.

A second approach by the same authors involved creating an extensional flow condition for a PE solution in the gap between two concentric cylinders, where the inner cylinder was rotating and the outer cylinder was held stationary (Fig. 7.1). Again, a seed filament was introduced into the solution and pulled out in the direction opposite the rotation of the inner cylinder. The seed filament end contacted the surface of the rotating cylinder and pulled off some of the fibrous PE crystals that had grown in the flow field (Fig. 7.1). By this method a continuous filament of fibrous PE crystals can be wound up, as long as fresh solution is introduced into the system. Using this approach, Barham and Keller [36] were able to create UHMWPE filaments with tensile modulus of 150 GPa and tensile strength of 4.5 GPa. This new approach to fiber production is referred to surface spinning and in spite of its success, its production rate is very, very slow, making it unsuitable for commercialization. However, the observations by Pennings and Keller that the filament produced in the surface-spinning process is actually being drawn from a gel that forms on the surface of the rotating drum provided key insights which led to the process by which high-performance PE fibers are produced commercially today, known as gel spinning.

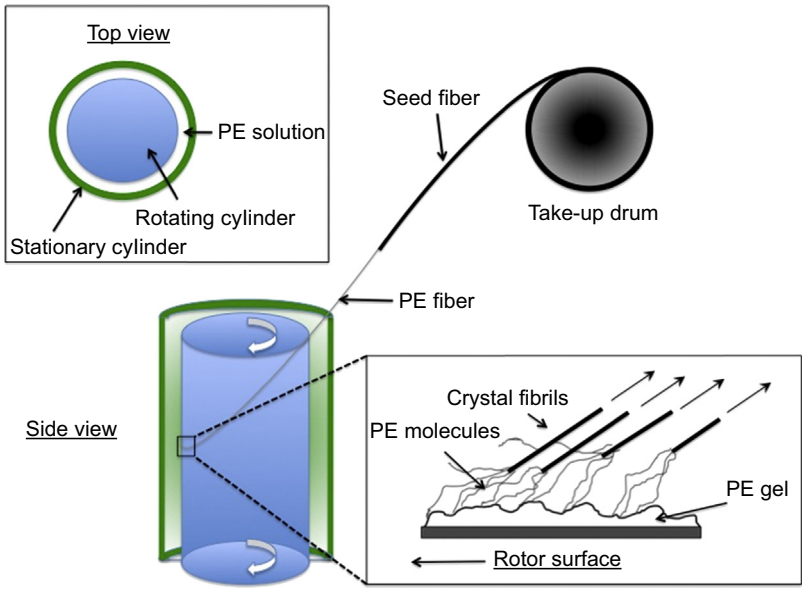

Figure 7.1 Schematic of the surface-spinning technique. Polymer solution is sheared in a gap between concentric cylinders. Elongational flow occurs at the surface of the rotating cylinder, inducing the formation of a gel of PE molecules with a low level of entanglement [36]. A seed fiber comes in contact with the rotating surface and draws out a bundle of crystalline fibrils from the gel.

7.2.3 Gel spinning of UHMWPE fibers

Understanding the nature of PE gels is key to understanding the production of fibers through the gel-spinning technique. In modern production the gels themselves are formed through swelling of the UHMWPE in solvent at elevated temperature [22,23,17]. The formation of a gel is promoted by increasing molecular weight and concentration in solution. The gel state is an ideal precursor because it significantly reduces the amount of topological constraint, that is, entanglement, experienced by polymer molecules, relative to the melt state. Research has shown that different percentages of polymer in solution lead to varying levels of entanglement, but Prevorsek and Kavesh found that 5−8 wt% polymer in solution yields optimal drawability [23]. Along this line of thinking, the solvent acts as a plasticizer on the system, thereby increasing free volume between chains that allow them to move past each other. It should also be noted that in this case, the gel is composed of physical crosslinks, instead of chemical crosslinks, in the form of crystallite junctions. Barham and Keller identify three types of junctions in the gel network based on their thermal behavior: micelles, fibrous crystals, and folded chain crystals [17]. The most common network junctions in high-molecular-weight polyethylene Gels are the fibrous crystal and folded chain crystalline types. The specific type of junction might not be as important as the fact that a networked crystalline structure exists in the first place. Nevertheless, studying the extension of these structures provided some interesting insight. Barham and Keller discuss the fact that drawing of the folded chain-type junctions might lead to unfolding of the crystal [17]. This is important because, as discussed previously, the extended lamellar crystals provide the highest values of stiffness and strength currently achieved.

Today, the gel-spinning process is the predominant way that high-performance PE fibers are produced. Trade names for UHMWPE fibers include Honeywell's Spectra family of fibers and the Dyneema fibers produced by DSM. The high strength and stiffness materials are achieved through a multistep process of extrusion and hot drawing [22,23,52−54]. First, the gel is extruded and drawn through a quenching bath. This initial step shapes the fiber and gives slight chain orientation through shear as it exits the die. After passing through the quenching bath, the fiber is subsequently heated and drawn. This process is very important in the evolution of meso/nano/crystallographic structure. For the purposes of the following discussion the prefix nano refers to length scales from ∼10 to 100 nm and meso refers to length scales between 10 and 10^3 nm. As discussed in the previous sections, research has shown that optimal drawing temperatures for PE fibers are above 110°C [31,48]. It is at this temperature that the alpha relaxation associated with PE molecules in the crystalline phase becomes thermally activated, providing favorable conditions for the unraveling of folded chain lamella crystals and promoting further growth of fibrous morphologies, where molecular chains see a high degree of extension [30,31,33,52−55]. The key to achieving the desired mechanical properties is a high draw ratio. As discussed in the previous sections, increased molecular weight leads to increases in tensile strength [38], while increasing draw ratio yields higher modulus [30]. This has traditionally been attributed to an increase in both molecular and crystal orientation [57], and improvements in

overall crystalline perfection (extended chain vs chain-folded lamella). However, it has also been shown that crystal orientation and modulus begin to plateau after a certain maximum draw ratio [53]. Some work [6] suggests that the drawing process brings about changes in mesoscale morphological structures that also contribute to improvement in tensile properties, in addition to factors of overall crystallinity and crystal orientation. The evolution of subfilament phase morphology composition and mesoscale structure during processing and its impact on filament mechanical properties is the topic of the next section.

7.3 Hierarchical structure of high-performance polyethylene fibers

7.3.1 Phase composition of PE fibers

The first report of crystallographic unit cell parameters for PE was by Bunn and Alcock in 1944 [56]. They reported an orthorhombic unit cell with the parameters, a-7.42 Å, b-4.93 Å, and c-2.534 Å obtained by wide angle X-ray diffraction (WAXD) experiments with a PE film at room temperature. Elevated temperature experiments showed that expansion of the unit cell occurred primarily along the *a*-axis, and that evidence of ordered structure disappeared around 126°C. The authors speculated that this change in the *a*-axis represented a shift toward a pseudohexagonal packing caused by twisting of the PE molecule away from its all-transplanar conformation. Much later work by a number of researchers [58] has shown that when constrained ultradrawn PE fibers are heated, they do in fact pass through a hexagonal phase prior to becoming an isotropic melt. Bunn and Alcock were also among the first to propose a mechanism for cold drawing of PE filaments that involved the cleaving of PE crystals.

In the mid-1950s several research groups observed that WAXD patterns for PE films and filaments that had undergone significant cold drawing showed additional reflections that could not be accounted for by the orthorhombic unit cell proposed by Bunn and Alcock [59,60]. These "extra" reflections have since been attributed to a metastable monoclinic unit cell that arises from deformation of the orthorhombic crystal [61−63]. This monoclinic phase has been reported widely in ultradrawn PE filaments [6,25] as is shown in Fig. 7.2. Fig. 7.2(a) is a 2D WAXD pattern obtained for a bundle of Spectra S130 fibers provided by Honeywell, while Fig. 7.2(b) is the corresponding integrated plot of intensity as a function of 2 theta of the equatorial reflections. In both the image and the 2 theta plot a small peak at ∼19 degrees is seen that corresponds to the 010 reflection of the monoclinic unit cell for PE. Its associated area contributes to about ∼4% of the total area of the diffraction pattern [6], which is consistent with what has been reported elsewhere in the literature [25].

In addition to these different crystal phases, an intermediate phase has been observed [25−28,30] via solid-state nuclear magnetic resonance (NMR) and full pattern WAXD experiments. This intermediate phase consists of axially oriented polymer chains that have a predominantly trans conformation, but lack lateral order associated with the orthorhombic crystalline phase [25]. Solid-state NMR experiments by

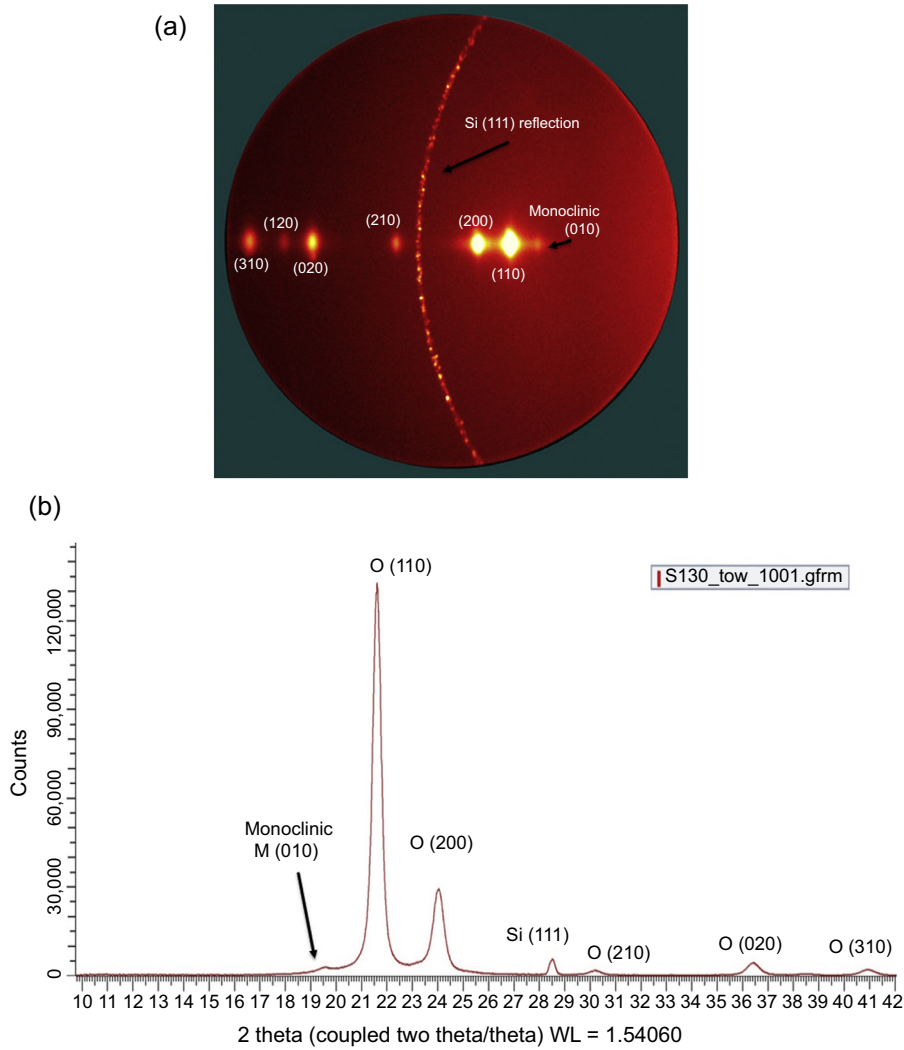

Figure 7.2 X-ray diffraction data showing mixture of orthorhombic and monoclinic crystal structures for Spectra S130 fibers.

Wunderlich et al. [25] indicate that this intermediate phase possesses 100 times greater degree of molecular mobility than that of the crystalline phase, but 1000 times less than that of molecules in a pure amorphous phase. Real-time Fourier transform-infrared spectroscopy (FTIR) [64] and Raman infrared (IR) [65] experiments were carried out on UHMWPE filaments to measure molecular conformational changes during tensile testing. The results show that it is the amorphous and intermediate components in the filament that see the greatest strain, relative to the crystalline phase, during loading of the fiber. This work is important in that it supports the idea that distribution of stress

through a PE filament is heterogeneous and that the load paths are dependent on phase composition and morphology [30].

Although these spectroscopic techniques have provided important insight into the nature of the phase composition of the UHMWPE fiber, and how these phases respond to loading, very little is understood regarding the spatial distribution of these phase domains throughout the filament, or how they link together to transmit load. The development of advanced microscopy techniques to probe these questions is a fruitful direction for future inquiry.

7.3.2 Microfibrils

Much has already been discussed in the preceding sections regarding the importance of fibrillary crystals or "shish-kebab" crystals to the final mechanical properties of a UHMWPE filament produced via melt drawing or solution spinning. Originally, these fibrous crystals were thought to be composed primarily of extended change crystals [3], but subsequent work revealed that they are composed of a series of smaller crystalline domains connected by amorphous tie molecules [25,30]. In their 1995 publication, Kavesh and Prevorsek [66] attempt to describe the structure hierarchy for gel-spun UHMWPE fibers, identifying these fibrous crystals as the fundamental building block for the gel-spun fibers, calling them microfibrils (which is the term we will use for the remainder of this discussion). These microfibrils aggregate to form bundles of macrofibrils, which in turn make up a single filament. As is seen in the images in Fig. 7.3, their description is generally consistent with microscopy data for these fibers found in the literature [6,47,69]. Fig. 7.4 shows a distribution of microfibril diameters obtained for a Spectra S130 fiber using atomic force microscopy [6]. The data follow a log normal distribution and microfiber diameters range from 10 nm to ~80 nm, with a mean diameter of ~35 nm [6]. Interestingly, when McDaniel et al. compared these results to those from filaments with different draw ratios, they reported only minimal changes in the mean microfibril diameter with increasing draw ratio, but they did

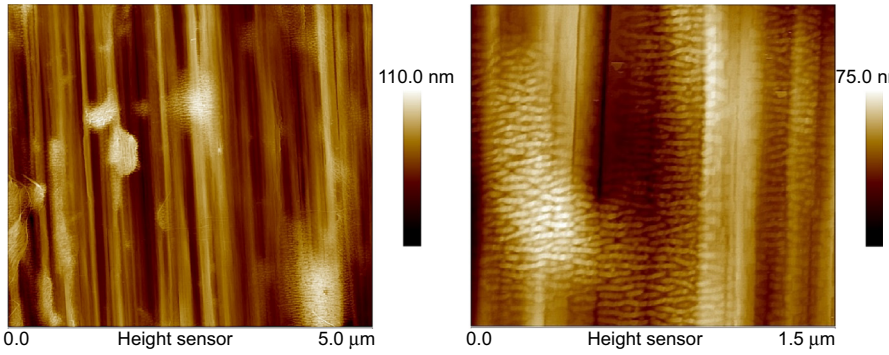

Figure 7.3 Fibril structure and epitaxial features on the surface of an S130 fiber. 5 µm scan on the surface of the fiber (left). 1.5 µm scan on a different fiber showing the large domains of epitaxial features (right).
Reproduced with permission from McDaniel PB, Deitzel JM, Gillespie Jr JW. Polymer 2015;69: 148–58.

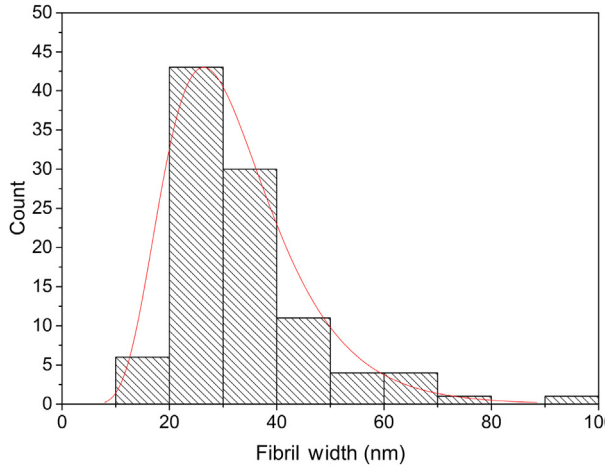

Figure 7.4 Microfibril width distribution of a high tenacity, 130 denier Spectra fiber. A log normal distribution of fibril widths was measured with the majority of fibrils falling between 20 and 40 nm in width.
Reproduced with permission from McDaniel PB, Deitzel JM, Gillespie Jr JW. Polymer 2015;69: 148−58.

observe significant narrowing of the diameter distribution as the draw ratio increased. These results are consistent with earlier work published by Pennings et al. [47], and suggests that the elevated temperature drawing of these fibers is a delicate balance between drawing larger microfibrils and melting of the smallest, least stable ones [6].

Through spectroscopic measurements described here (FTIR, WAXD, solid-state NMR, Raman IR, etc.), it has been possible to develop a picture of how crystalline domains are interconnected via taut tie molecules via an intermediate phase within the microfibril. What has not been as clear is how the microfibrils are held together in larger bundles and how load is transferred between these fibrils. Litvinov et al. [30] have suggested that drawing at elevated temperature results in the incorporation of smaller microfibrils into larger extended chain crystals. For melt-drawn fibers and films, Bashir et al. [37,40] have provided evidence that under certain conditions microfibrils appear to be connected via smaller chain-folded crystals, in arrays of interleaving shish-kebab structures. In other cases, where processing conditions and microfibril (shish) spacing is too close to promote the growth of chain-folded crystals, the microfibrils appear to be simply stuck together, possibly sharing surface chains from the "hair dressing" described by Barham and Keller [17].

For gel-spun filaments, scanning electron microscope (SEM) evaluation of fibers at different stages of drawing have shown that in the initial stages of formation, the microfibrils form a network linked by undrawn lamella crystal [47]. High-resolution atomic force microscope (AFM) experiments [6] have provided evidence that this network persists in the structure of highly drawn fibers. Examination of the disrupted microfibrils on the surface of filaments with different draw ratios shows this 2D network as illustrated in Fig. 7.5. Fig. 7.5(a) shows a high-resolution SEM image of

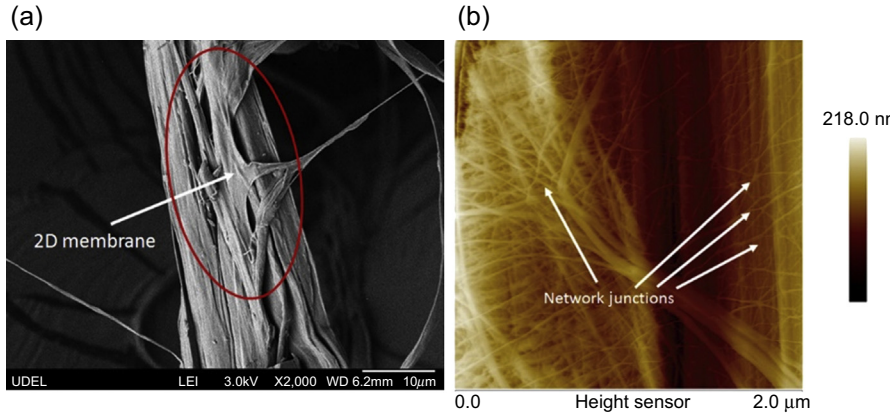

Figure 7.5 (a) Scanning electron microscope (SEM) image of interior of a split UHMWPE filament. (b) Atomic force microscope (AFM) image of the interior of a split S130 Spectra filament showing junctions between microfibrils.

a UHMWPE fiber that has been split down the middle. In addition to the expected fibrillation that one would expect to see, what looks like a thin membrane of material has been pulled from the core of the filament, suggesting a significant amount of lateral interaction between the microfibrils. In Fig. 7.5(b), high-resolution AFM examination of a similar Spectra S130 filament that has been split reveals the junctions between individual microfibrils that form a two-dimensional network. The nature of this network and the implications it has for filament properties in both tension and transverse loading is an area of ongoing investigation.

7.3.3 Epitaxial structures

The initial extruded gel fiber is composed primarily of chain-folded lamella crystals and or shish kebab crystals with large "kebab" platelets [18,50]. As these filaments undergo drawing at elevated temperature, the chain-folded lamella decrease in size and quantity as they are converted into microfibrils or "shishes." This conversion has been reported by a number of research groups [47,55] followed via microscopy and in situ small angle X-ray scattering. However, work by Maganov [67], Strawhecker [68], and McDaniels et al. [6] has reported observation of epitaxial structures on the surface of commercial ultradrawn UHMW PE fibers using AFM techniques. Fig. 7.3 shows both low and high magnification images of the surface of a Spectra S130 fiber. In the lower magnification image large clusters of epitaxial features are prevalent along the length of the fiber. Inspection at higher magnification (image on the right) shows lamella-like structures that span multiple microfibrils. Annealing experiments carried out by McDaniel [6] showed that these structures underwent further thickening at temperatures greater than 130°C, which is consistent with annealing of polymeric chain-folded lamella, rather than melting of structures composed of low-molecular-weight material. Examination [6] of samples that had been microtomed did not reveal any evidence of these large-scale structures; however, the presence of

the microshish kebabs described by Barham and Keller, and Thomas et al. [17,69] cannot be ruled out. Additionally, it is possible (even likely) that these larger epitaxial structures might be found in voids, where there is enough space to allow unconstrained nucleation and growth of these larger epitaxial features.

7.3.4 Voids

From the beginning it has been understood that the gel-spinning process produces fibers that contain a significant amount of voids, resulting from the removal of the solvent phase during the drawing process [22,50]. AFM examination of microtomed UHMWPE fibers with different draw ratios show that these voids persist even in highly drawn fibers. The results suggest that the drawing process helps consolidate microfibrils into bundles, and by default consolidating the free space into oval "voids" oriented along the direction of draw (Fig. 7.6), which were ~100 nm in diameter

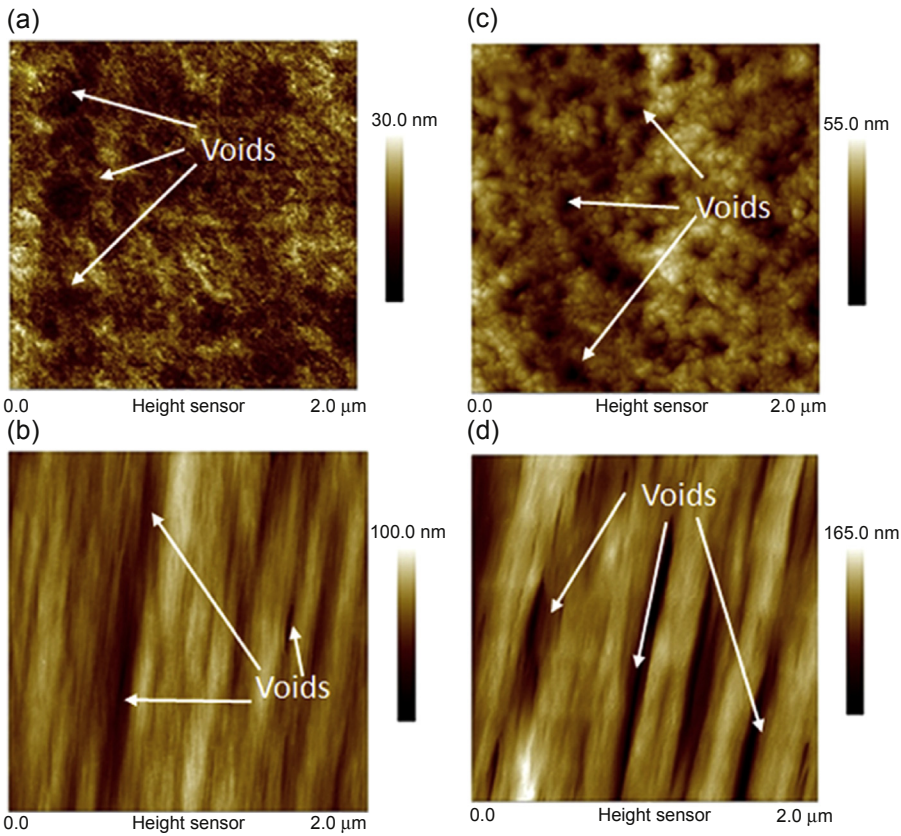

Figure 7.6 AFM images of microtomed fibers. (a) Axial image of precursor fiber. (b) Image of precursor fiber interior microtomed along the fiber axis. (c) Axial image of postdraw fiber. (d) Image of postdraw fiber microtomed along the fiber axis.
Reproduced with permission from McDaniel PB, Deitzel JM, Gillespie Jr JW. Polymer 2015;69: 148−58.

and >1 μm in length. Litvinov [30] et al. also observed the growth of nanoscale voids at ultrahigh draw ratios and speculated that these formed as a result of the fracture of PE crystals. A survey of the literature reveals little information regarding the influence of these mesoscale heterogeneities on the mechanical properties of these fibers, suggesting that this might be a fruitful area for future research.

7.4 Applications of high-performance polyethylene fibers

High-performance PE fibers are found in a variety of commercial and Department of Defense (DoD) applications, because of their light weight and extremely high strength, stiffness and durability, for example, backing material for metal and ceramic inserts for body armor and composite helmets [73]. In this application, multiple plies of unidirectional UHMWPE fabric impregnated with a thermoplastic elastomer resin (polyurethane, Kraton block copolymer) are arranged in a 0−90 configuration to form a thick section composite, which is bonded to the surface of a strike plate (ceramic or metal). The role of the UHMWPE composite is to act as a catcher's mitt, arresting the progression of the projectile and the fragments of the metal or ceramic strike face. These textiles also exhibit excellent cut resistance and are often used in protective gloves and garments used in both DoD applications and a variety of industries including the food preparation industry, automotive repair, and protective clothing in sports like fencing.

UHMWPE fibers are found in a wide variety of sporting applications requiring light weight and strength. Examples include parasails, suspension lines for parachutes and paragliders, and in rigging used in competitive sailing. UHMWPE fiber (Dyneema, Spectra) can also be found as a component in high-performance sails, often paired with a second fiber, such as carbon or Kevlar, which is more resistant to creep. UHMWPE fibers are used for bow strings in competition archery, while UHMWPE monofilament is used widely in sport fishing lines. The combination of light weight, high strength, and abrasion resistance also make UHMWPE rope popular among climbing enthusiasts.

UHMWPE fibers are used in a wide variety of rope and cordage products servicing the offshore oil and gas, industrial marine, and construction industries, as well as civilian first responders and the recreational boating industry. UHMWPE ropes are used as hawsers and cables in commercial shipping because of their high strength and low density (~0.97 g/cc), which enables them to float in sea water. Their abrasion resistance and resistance to chemical attack make these ropes attractive alternatives to metal wires and cables in corrosive environments.

7.5 Conclusion: strengths and weaknesses—the state of the art

Modern gel-spun UHMWPE fibers represent the culmination of over 50 years of research into the fundamental rheological behavior of flexible linear polymers in

both solution and the melt state. The insights gained through the development of these materials represent a significant portion of the theoretical underpinnings of modern polymer science. These materials provide an excellent combination of tensile specific strength, modulus, and toughness that is unmatched among commercially available high-performance fibers. In spite of the improvements that have occurred, the average tensile properties of commercial fibers, in particular tensile strength, still fall short of what theoretical predictions indicate is possible, suggesting that further process optimization might be feasible. For applications requiring light weight, high stiffness and strength, chemical resistance, and durability, UHMWPE fibers and textiles represent an enticing option for the designer. However, the inherently low glass transition temperature and melting temperatures of these materials make them unsuitable for load-bearing applications that must operate at temperatures significantly above ambient conditions. Additionally, the excellent chemical resistance of PE makes incorporation of these fibers into composites, where resin adhesion to the fibers is critical a significant technical challenge.

7.6 Future trends

The demand today for ever stronger, light weight textiles is great, fueling interest in the further development of materials like UHMWPE fibers and composites. The desire for further improvement in tensile properties continues to drive research into the effects of ultradrawing of gel-spun fibers [6,30,56,68] on filament structure and properties. Concerns about the environment and global warming have driven interest in developing renewable sources for precursors for the synthesis of PE and the development of gel-spinning processes using more environmentally friendly solvents [70]. Significant research over the last decade has gone into the production of high-performance PE fibers containing nanoscale filler, such as functionalized nanoalumina filler [71] and cellulosic nanofibers [72] to achieve further improvements in thermal, mechanical, and electrical properties.

Sources of further information and advice

For further information on the topics discussed in this chapter, readers are referred to the cited references of I. Ward, A. Keller, and of course A.J. Pennings. Also recommended are the following reference texts:

1. *Fiber Science* by Steve B. Warner.
2. *Handbook of Textile Fiber Structure Volume 1: Fundamentals and Manufacture Polymer Fibers*, edited by S.J. Eichhorn, J.W.S. Hearle, M. Jaffe, and T. Kikutani.
3. *The Handbook of Fiber Chemistry*, edited by Menachem Lewin.
4. *Polyolefin Composites*, edited by Thein Kyu.
5. *Macromolecular Physics* volumes 1−3 by Bernhard Wunderlich.
6. *Phase Transitions in Polymers: The Role of Metastable States* by Stephen Z.D. Cheng.

Further information regarding properties and applications of commercially available high-performance PE fibers can be found at the commercial websites: http://www.honeywell-advancedfibersandcomposites.com/http://www.dsm.com/products/dyneema/en_US/home.html.

References

[1] Bunn CW. Transactions of the Faraday Society 1939;35:482−91.
[2] Keller A. Philosophical Magazine 1957;2:1171−5.
[3] Pennings AJ. Journal of Polymer Science, Part C 1967;16:1799−812.
[4] Treloar LRG. Polymer 1960;1:95−103.
[5] Zwick MM. Applied Polymer Science Symposium 1967;6:109.
[6] McDaniel PB, Deitzel JM, Gillespie Jr JW. Polymer 2015;69:148−58.
[7] Dyneema spec sheet; http://www.dsm.com/products/dyneema/en_US/home.html.
[8] Honeywell spec sheet; http://www.honeywell-advancedfibersandcomposites.com/.
[9] Nwabunma D, Kyu T, editors. Polyolefin composites. John Wiley and Sons, Inc.; 2007.
[10] Beasley JK. Journal of the American Chemical Society 1953;75:6123−7.
[11] Odian G. Principles of polymerization. John Wiley and Sons, Inc.; 2004.
[12] Natta G. Journal of Polymer Science 1959;33:21−48.
[13] Chien JCW, Wang BP. Journal of Polymer Science, Part A: Polymer Chemistry 1988;26:3089−102.
[14] Peacock AJ. Handbook of polyethylene: structures, properties and applications. Marcel Dekker, Inc.; 2000.
[15] Wunderlich B. Thermal analysis of polymeric materials. Springer Verlag; 2005.
[16] Andrews JM, Ward IM. Journal of Materials Science 1970;5:411−7.
[17] Barham PJ, Keller A. Journal of Materials Science 1985;20:2281−302.
[18] Capaccio G, Ward IM. Nature Physical Science 1973;243:130−43.
[19] Capaccio G, Ward IM. Polymer 1974;15:233−8.
[20] Capaccio G, Ward IM. Polymer Engineering & Science 1975;15:219−24.
[21] Eichhorn SJ, Hearle JWS, Jaffe M, Kikutani T. Handbook of textile fiber structure volume 1: Fundamentals and manufactured polymer fibers. Woodhead Publishing Limited; 2009.
[22] Smith, P., & Lemstra, P.J.. (1982). Patent No. 4344908. USA.
[23] Kavesh, S., & Prevorsek, D.K.. (1982). Patent No. 4413110. USA.
[24] Hearle JWS, Greer R. Textile Progress 1970;2.
[25] Fu Y, Chen W, Pyda M, Londono D, Annis B, Boller A, et al. Journal of Macromolecular Science, Part B: Physics 1996;35:37−87.
[26] Cheng J, Fone M, Reddy VN, Schwartz KB, Fisher HP, Wunderlich B. Journal of Macromolecular Science, Part B: Physics 1994;32:2683−93.
[27] Hu W-G, Schmidt-Rohr K. Polymer 2000;41:2979−87.
[28] Tzou DL, Schmidt-Rohr K, Spiess H. Polymer 1994;35:4728−33.
[29] Chen W, Fu Y, Wunderlich B, Cheng J. Journal of Polymer Science, Part B: Polymer Physics 1994;32:2661−6.
[30] Litvinov VM, Xu J, Melian C, Demco DE, Moller M, Simmelink J. Macromolecules 2011;44:9254−66.
[31] Wilding MA, Ward IM. Journal of Polymer Science, Polymer Physics Edition 1984;22:561−75.
[32] Capaccio G, Crompton TA, Ward IM. Polymer 1976;17:644−5.

[33] Kanamoto T, Sherman ES, Porter RS. Polymer Journal 1979;11:497.
[34] Pennings AJ, Torfs J. Colloid and Polymer Science 1979;257:547.
[35] Barham P, Hill M, Keller A. Colloid and Polymer Science 1980;258:899–908.
[36] Barham PJ, Keller A. Journal of Polymer Science, Polymer Letters Edition 1979;17: 591–3.
[37] Bashir Z, Keller A. Colloid and Polymer Science 1989;267:116–24.
[38] Fatou JG, Mandelkern L. Journal of Physical Chemistry 1965;69:417–28.
[39] Odell JA, Grubb DT, Keller A. Polymer 1978;19:617.
[40] Bashir Z, Odell JA, Keller A. Journal of Materials Science 1984;19:3713–25.
[41] Geil PH. Polymer single crystals. Huntington, NY: Robert E. Krieger Publishing Company; 1973.
[42] Wunderlich B. Macromolecular physics volume II crystal nucleation, growth and annealing. Academic Press; 1976.
[43] Cheng SZ. Phase transitions in polymers: the role of metastable states. Elsevier Science; 2008.
[44] Statton WO. Journal of Applied Physics 1967;38:4149.
[45] Kanamoto T, Tsurata A, Tanaka K, Takeda M, Porter RS. Polymer Journal 1983;15:327.
[46] Pennings A. Journal of Polymer Science: Polymer Symposium 1977:55–86.
[47] Pennings A, Smook J, de Boer J, Gogolewski S, van Hutten P. Pure and Applied Chemistry 1983;55:777–98.
[48] Van Hutton P, Koning C, Pennings A. Journal of Materials Science 1985;20:1556–70.
[49] Keller A, Willmouth FM. Journal of Macromolecular Science-Physics 1972;B6:493.
[50] Zwijnenburg A, Pennings A. Colloid and Polymer Science 1976;254(10):868–81.
[51] Zwijnenburg A, Pennings A. Colloid and Polymer Science 1975;253:452.
[52] Smith, Lemestra. Journal of materials Science 1980;15:505.
[53] Hoogsteen W, van der Hooft R, Postema A, ten Brinke G. Journal of Materials Science 1988;23:3459–66.
[54] Hoogsteen W, Kormelink H, Eshuis G, ten Brinke G, Pennings A. Journal of Materials Science 1988;23:3467–74.
[55] Ohta Y, Murase H, Hashimoto T. Journal of Polymer Science, Part B: Polymer Physics 2010;48:1861–72.
[56] Bunn CW, Alcock TC. Transactions of the Faraday Society 1945;41:317–25.
[57] Northolt M, Hout R. Polymer 1985;26:310–6.
[58] Rastogi S, Odell JA. Polymer 1993;34:1523–7.
[59] Natta G. Makromolekulare Chemie 1955;16:213.
[60] Slichter WP. Journal of Polymer Science 1956;21:141.
[61] Teare PW, Holmes DR. Journal of Polymer Science 1957;24:496.
[62] Walter ER, Reding FP. Journal of Polymer Science 1956;21:557–8.
[63] Keller A. Nature 1952;169:913.
[64] Wool RP, Bretzlaff RS, Li BY, Wang CH, Boyd RH. Journal of Polymer Science, Part B: Polymer Physics 1986;24:1039–66.
[65] Prasad K, Grubb DT. Journal of Polymer Science, Part B: Polymer Physics 1989;27: 381–403.
[66] Kavesh S, Prevorsek DC. International Journal of Polymeric Materials 1995;30:15–56.
[67] Magonov SN, Sheiko SS, Deblieck R, Moller M. Macromolecules 1993;26:1380–6.
[68] Strawhecker KE, Cole DP. Morphological and local mechanical surface characterization of ballistic fibers via AFM. Journal of Applied Polymer Science 2014;131.
[69] Brady JM, Thomas EL. Polymer 1989;30:1615–22.

[70] Rajput AW, Aleem A, Arain FA. International Journal of Polymer Science, Volume (2014), Article Number: 480149. http://dx.doi.org/10.1155/2014/480149.
[71] Yeh JT, Wang CK, Yu W, Huang KS. Polymer Engineering and Science 2015;55.
[72] Yeh JT, Tsai CC, Shao JW, Xiao MZ, Chen SC. Carbohydrate Polymers 2014;101:1−10.
[73] Bhatnagar A, editor. Lightweight ballistic composites: Military and law-enforcement applications. Honeywell International; 2006.

High-modulus polypropylene fibers—through postspinning operations

8

S. Mukhopadhyay, B.L. Deopura
IIT Delhi, New Delhi, India

8.1 Introduction

Polypropylene (PP) fibers are generally prepared via the melt-spinning route, which essentially consist of two stages: (1) extrusion of fiber and (2) subsequent thermal and mechanical stretching of the fiber. Between the die exit and the pullout rolls (first Godet roller), the extruded fibers are predrawn, water quenched, separated into an orderly arrangement (in the case of multifilament), and dried of adhering surface moisture. The predraw results in a decrease in fiber diameter, which occurs as the molten polymer emerges from the die. The operational variables controlling the uniformity of drawdown are polymer throughput and filament velocity just prior to the quench bath. Upon solidification of the fiber in the quench bath, drawdown is complete (Fig. 8.1).[1]

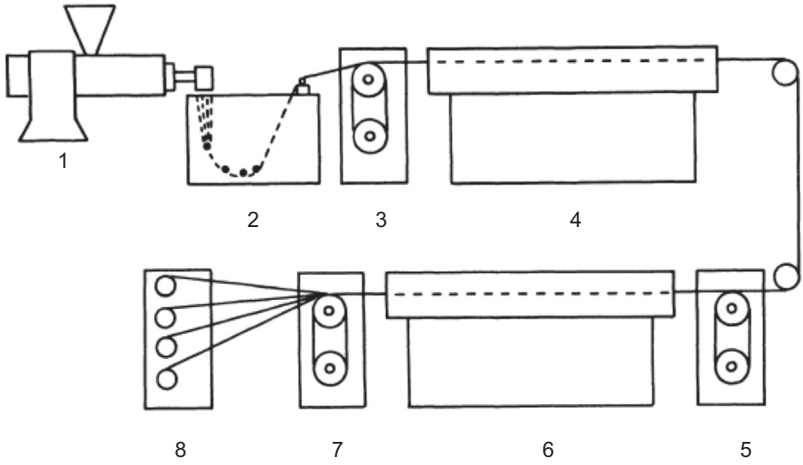

Figure 8.1 A typical line for extrusion of polypropylene monofilaments. (1) Extruder. (2) Quench tank. (3) Pulllout rolls. (4) Draw oven. (5) Draw rolls. (6) Passage for relaxation. (7) Relaxing rolls. (8) Wind-up.
After Galanti A, Mantell C. *Polypropylene fibers and films*. New Jersey: Springer Science; 1965.

Structure and Properties of High-Performance Fibers. http://dx.doi.org/10.1016/B978-0-08-100550-7.00008-5

When isotactic PP is drawn at a low temperature below 100°C, strain hardening occurs and the draw ratio is typically limited to 7−9, which is called the "natural draw ratio." To attain a higher draw ratio, drawing temperatures of 110−170°C are typically used. Since as-spun original fibers have a fairly high crystallinity of 50−60%, a high drawing temperature close to the melting point is useful to soften the lamellae and to transform them to extended-chain crystals. During the drawing, the fiber structure alters from a lamellar to a fibrillar one.[2]

8.2 Synthesis of high-performance polypropylene fibers

Since the introduction of fiber-forming, melt-spinnable, synthetic polymers, fiber manufacturers have looked for ways to increase the strength and stability properties of the fibers made from those polymers. The additional strength and stability properties of the fibers are needed so that applications beyond textile uses could be opened for their products. Such nontextile uses (also known as "industrial uses") include: tire cord; sewing thread; sail cloth; cloth, webs or mats used for road bed construction or other geotextile applications; industrial belts; composite materials; architectural fabrics; reinforcement in hoses; laminated fabrics; ropes; and so on.

High-modulus, high-tenacity fibers have thus offered an interesting arena to the fiber scientist. Fibers in the as-spun state do not have the necessary strength to be put to any use. Thus orientation of the chain molecules in the direction of the fiber axis is necessary to impart the required strength. Production of high-modulus fibers has been tried through various routes. Development of carbon, aramid, gel-spun ultrahigh-molecular-weight polyethylene has opened new vistas in the area of composites. It is interesting that even though the theoretical maximum modulus of polyethylene is approximately 250 GPa, the present ultrahigh modulus fibers have achieved a maximum of 120 GPa[3] and a tensile strength around 4.0 GPa.[4] Similarly for PP, the commercial PP fibers remain in the modulus and tenacity range of 4−8 GPa and 0.35−0.6 GPa, respectively, whereas the theoretical modulus of PP has been found to be 35−42 GPa when measured by X-ray techniques[5,6] and the theoretical strength is 3.9 GPa[7], which is also much higher as compared to commercial fibers. Thus efforts are made to produce high-modulus and high-tenacity fibers.

Controlling either the molecular design or the morphological features can produce ultrahigh-modulus fibers. Altering the molecular design is associated with changing the average length of the molecular chains, the regularity of packing, and the chain stiffness. The morphological way to utilize fibers is to use the intrinsic mechanical anisotropy present in the fibers and to further align them in the direction of the fiber axis.

There are two routes to align molecules parallel to the fiber axis: either they are prealigned in a mechanical field and crystallization takes place in the extended state, that is, the fibers are formed in the spinning process, which is done in gel spinning, or flexible molecules are allowed to be folded and crystallized from the melt or solution and then unfolded by solid-state deformation. This is very commonly accomplished by drawing—a process of stretching the fibers through a passage between a set

of rollers having a positive speed differential. The majority of the literature reports manufacturing of PP through the second route.

Drawing aims at producing long chain molecules whose theoretical modulus is only limited by the extensibility and deformability of the covalent bonds along the fully extended chains. The stretching of polymers, as outlined earlier, has its share of problems. In a system of flexible molecules, it is difficult to achieve the required degree of chain extension for a continuous and smooth stress transfer process and any attempts at chain extension are associated with the entropic forces trying to return the molecules to their original random configuration.

Moreover, drawing may only orient without stretching the chains. But the aim is really to extend the chains. For example, in the case of polyethylene, conventional solid-state drawing with draw ratios of 4−10× orients the sample but fails to extend the polymer chains. For extension, much higher draw ratios in the order of 30−100× are necessary, which is not an easy task because of the retractile entropic forces present.[8]

Drawing of fibers proceeds in a heterogeneous or homogeneous way, depending on the conditions of drawing. In *homogeneous drawing*, which takes place at higher temperature and lower deformation speeds, the diameter decreases continuously. In this kind of drawing, all the points along the specimen length are stretched equally.

In the other class of drawing, known as *heterogeneous*, all points on the test specimen do not undergo uniform extension and the drawing proceeds through a neck. Scientists are of the view that the crystalline lamellae breaks into smaller blocks and this discontinuous behavior of the lamellae is responsible for the sudden change in the diameter of the fiber, exhibited as necking. At higher draw ratios, the fibers become white and opaque. This phenomenon is well known in industrial practice and is related to the formation of microvoids. Since postspinning has been the major route in manufacturing high-modulus PP fibers, it would be interesting to discuss the factors that affect the drawability of such fibers.

8.2.1 Factors affecting drawability

It has been observed that the properties of the spun yarns are influenced by various factors like molecular weight, polydispersity, extrusion temperature, extrusion velocity, air-flow rate, take-up velocity, and temperature.

8.2.1.1 Feed parameters

1. *Molecular weight of the sample*: Drawability increases with molecular weight up to a certain value, after which it decreases. For PP, drawability becomes maximum at $6.7-7.8 \times 10^4$, after which it deteriorates.[9] In a wide range of experiments with PP of different molecular weight (180,000−400,000), Wills et al.[10] reported the maximum modulus at molecular weight of 181,000. Generally, a higher molecular weight implies a higher elongational viscosity, higher degree of crystallinity, and a higher strength and modulus. However, very high molecular weight inhibits spinning. Capaccio et al.[11] have reported an inverse relationship between molecular weight and draw ratio. The nucleation rate also varies inversely with molecular weight, which implies a fiber with lower degree of crystallinity.[12]

2. *Polydispersity*: A higher polydispersity implies deteriorating mechanical properties but enhanced processing ease. Low-molecular-weight species act as a plasticizer and drawability is enhanced with broader molecular weight distribution. Moreover, such polymers yield at lower stress. Many patents specify the polydispersity of the polymer to be processed.
3. *Initial morphology*: Materials with smectic structure (paracrystalline) can be drawn to a higher degree than the monoclinic (α-crystalline) form, as in PP. Nonuniform crystal structure, which is generally obtained in freshly spun yarns or with rapid quenching, facilitates drawing.
4. *Structure of the feed yarn*: The feed yarn should have low crystallinity values. Thus crystallization in the spinline should be inhibited to facilitate further drawing.
5. *Influence of additives*: Some of the additives aid in the drawing of fibers considerably. For PP, stearates of calcium, zinc, and waxes/paraffinic compounds in 2−5% concentration enhance the drawability at high speeds, increase maximum draw ratio, and decrease the void formation.[6]

8.2.1.2 Process parameters

Temperature

Extrusion temperature is important as it controls the viscosity of the polymer. The spinline stress decreases with temperature of extrusion.

The temperature of drawing also limits the drawing performance. Sufficient heat needs to be supplied to enable drawing without break although heat needs to be removed in cases of high work of drawing.

Generally, homogeneous drawing can only occur at higher temperatures, while in cold drawing the sample stretches through a neck. Drawing is generally done in between the T_g and the T_m of the fibers. Raising the temperature until the T_m generally allows for a higher draw. The increase in temperature lowers the temperature necessary for the initiation of the drawing and also the tension in the flow zone. The natural draw ratio decreases while the maximal draw ratio becomes greater. For PP, a two-stage drawing with the first stage at 60°C and the second stage at 120−140°C provides good results.

As seen from Fig. 8.2, which plots load versus the extension for a sample at varying temperatures, at low temperature, generally brittle fracture is seen (a), as the temperature is increased, the sample follows a path of (b) ductile failure, (c) necking, and cold drawing followed by (d) rubber-like behavior.[13]

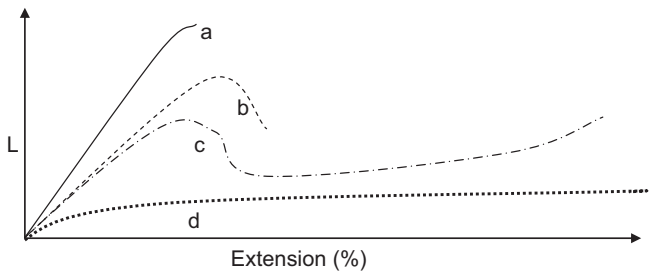

Figure 8.2 Drawing of polypropylene at varying temperatures.

Spinning speed and time

In the spinning zone, time plays a crucial role. For a polymer of given molecular weight, tenacity has been seen to vary with the spinning speed and time. The spinning speed, if too high, leads to melt fracture. The maximum spinning speed, and hence the time, is restricted and is governed by the molecular weight through the following relation where SS implies the spinning speed and MW the molecular weight[14]:

$$SS_{max} = 1858.4 - 2.7966 \times 10^{-2} \times MW + 1.6703 \times 10^{-7} \times (MW)^2 - 3.8969 \times 10^{-13} \times (MW)^3 \quad (8.1)$$

Time is also an important factor affecting drawability, which depends on the drawing speeds. Drawing should take place allowing a time whereby the fiber can take up the heater temperature. The effect of drawing speeds has been studied on polyethylene terephthalate (PET), polybutylene terephthalate, and nylon-6 when the samples were drawn at various speeds above the glass transition temperature. The time of deformation-induced crystallization is dependent on the rate of drawing and higher rates raise the internal temperature of the polymer, thus affecting the rate of crystallization.

Spinline stress and take-up velocity The spinline stress should be as low as possible so as to avoid stress-induced crystallization. The spinline stress is a function of the take-up velocity and the jet stretch defined as amount of attenuation imparted to molten polymers between the spinneret and before solidification. The take-up velocity should be less so as to inhibit crystallization. A higher take-up velocity induces higher stress, which in turn induces higher jet stretch.

Number of drawing stages

It has been confirmed that a multiple-stage drawing has a better effect than a single-stage drawing. Wang et al. reported better tensile properties of PP when drawn in two stages—the first being at a relatively lower temperature of 60°C and subsequently at 140°C when compared to single-stage drawing. Ito et al. has shown that a two-stage drawing process is favorable for preparing high-strength PET fibers.[15] They showed that the initial morphology created in the first-stage draw is extremely important with regard to properties achieved after the second-stage draw.[16]

Environment of drawing

A two-stage draw technique was used for drawing both originally amorphous fibers and fibers that were drawn in situ in CO_2. CO_2-drawn fibers could be drawn to 50% higher draw ratios attaining higher strength, crystallinity, and orientation. The CO_2-induced morphology enhanced the development of the crystalline phase. At a draw temperature of 230°C, fibers with very high crystallinity values (65%) could be obtained. CO_2 can be used effectively for the processing and production of high-performance PET fibers.

Nature of cooling

After leaving the spinneret, the polymer is cooled, for example, by natural cooling during its passage through air, or by quenching or contact with fluid, particularly a liquid. The rate of cooling in air is far in excess of 15°C per minute and by quenching in a liquid, very high rates of cooling may be obtained. The high rate of cooling prevents excessive crystallization of the polymer, which affects the subsequent drawing of the spun filaments.

Previous production of high-modulus polypropylene fibers

There have been various processes employing drawing in one form or another. A summary of the processes, temperature, speed, and final properties of the fibers so produced is given in Table 8.1.

8.3 Structure and properties of high-performance polypropylene fibers

Several processes have been used to produce high-modulus PP fibers. To obtain excellent mechanical properties, high-modulus fiber should have a network structure composed of tie molecules and extended-chain crystals. In such a structure the movement of the amorphous chains is strongly inhibited.[26] A variety of techniques using X-ray, differential scanning calorimetry, nuclear magnetic resonance, infrared, optical, and electric microscopes, etc., as well as dynamic viscoelastic measurements, are utilized for characterizing the superstructure of high-modulus and high-strength fibers. One of the major routes in the characterization of high-modulus PP fibers is to rely on intrinsic birefringence values. Once they are established, the combination of birefringence and X-ray diffraction may then be used to resolve the birefringence of PP into its crystalline and amorphous components (Fig. 8.3).[27] The general observation has been the increase in both the crystalline and amorphous contributions to the overall orientation.[28] In the draw heat-setting process,[29] wherein a fiber is simultaneously drawn and heat-set, because the processing temperature is close to the melting range, all the crystals of sizes related to this and lower temperatures are melted and recrystallized. This leads to a narrow width of melting peak, as evident from Table 8.2.

In another process patented by the authors,[30–32] a gradient heater was used to draw the samples. Initial modulus of drawn fiber was found to be a unique function of the draw ratio quite independent of the initial morphology and molecular weight. Gradient-drawn PP samples were characterized by high draw ratios coupled with high initial modulus. While tensile modulus reflects the average structure, tensile strength relates to the weakest position in the structure. The tensile strength of fibers is determined by intrinsic parameters like the intrinsic elastic modulus of the parent polymer, the intermolecular bonds, and the chain length distribution. Postspinning operations improve the mechanical properties but also introduce defects like inhomogeneities and voids. Thus generally at very high draw ratios though the modulus increases, strength suffers. In the case of gradient drawing, however, high modulus

Table 8.1 Comparison of various drawing processes

SI. No.	Drawing details	Feed material (MFI/MW)	Temperature	Nature of process	Production speed	Resultant fiber properties	References
1.	Two-stage drawing	35 MFI PP	1st stage—60°C 2nd stage—140°C	Continuous	~200 mt/min	Tenacity—1 GPa Modulus—7.1 GPa	17
2.	Constant load oven drawing	0.61 MFI PP MW ~ 4.7×10^5	1st stage—130°C 2nd stage—130°C	Batch	~1.8 cm/min	Tenacity—1.05 GPa Modulus—8.9 GPa	18
3.	Tensile drawing	0.91 MFI PP MW ~ 1.8×10^5	1st stage—110°C 2nd stage—163°C	Batch	~2.8 cm/min	Modulus—12 GPa	19
4.	Hot nip drawing	MW ~ 6×10^5 PP	1st stage—115°C 2nd stage—170°C	Batch	~2 cm/min	Tenacity—0.2 GPa Modulus—13.2 GPa	20
5.	Zone drawing and zone annealing	MW ~ 7.4×10^5 PP	1st stage—150°C 2nd stage—170°C	Batch	~5 cm/min	Tenacity—0.2 GPa Modulus—15 GPa	21
6.	Gel spinning and hot drawing	MW ~ 3.4×10^6 PP	1st stage—150°C	Continuous	~2 cm/min	Tenacity—1.4 GPa Modulus—39 GPa	22
7.	Die drawing	PP	155°C	Batch	~2 m/min	Modulus—20 GPa	23,24
8.	Draw heat setting	17 and 35 MFI PP	60 and 160°C	Batch	~2 m/min	Tenacity—0.711 GPa Modulus—18.06 GPa	25

MFI, Melt flow index; *MW*, molecular weight; *PP*, polypropylene.

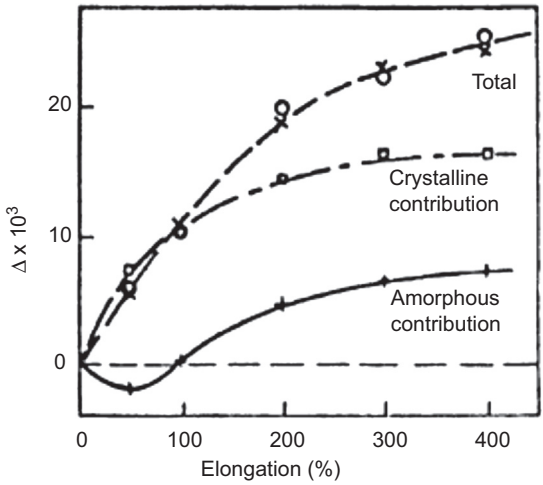

Figure 8.3 Crystalline and amorphous contributions to the birefringence of deformed isotactic polypropylene.

Table 8.2 Differential scanning calorimetry values of draw heat-set samples

Sample	Draw ratio	$\chi_{(DSC)}$ (%)	T_m (peak)	Peak width (°C)
D1	7.6x	52	169	47
DHS11	8.6x	58	169	44
DHS13	12.7x	65	169	39
DHS14	14.7x	67	169	32
DHS22	9.5x	64	169	40
DHS23	14.4x	68	169	33
DHS24	19.3x	72	169	25

coupled with high tenacity values are obtained because of the unique microstructure that has developed. Gradient drawing allows high draw ratios with low void content. It is interesting to note that in spite of the high draw ratio of 17 a very low void fraction results. The incremental drawing over the gradient heater approaching the melting point results in low drawing stress characterized by near absence of voids (9×10^{-4}) and is one of the main reasons behind the high tenacity values of gradient-drawn samples.

The initial morphology of a starting material strongly influences the drawing behavior.[33] By applying the force in the direction parallel to the lamella surface, the

folded molecular chains in lamellae can be easily pulled out from the lamellae because of the weak intramolecular forces. This technique, which was established for ultrahigh-molecular-weight polyethylene, can be applied to isotactic PP with a ultrahigh molecular weight of 10^6 g/mol.

8.4 Applications of high-performance polypropylene fibers

In the monofilament process, filaments are extruded into a water bath and are typically drawn to 250 denier per filament. Different filaments are then combined to form a rope/twine. Rope or twine is produced by twisting numerous bundles intro strands and twisting the different strands into the final rope form. Strands are often braided into lighter-duty ropes. Individual monofilaments may be woven into fabrics. The largest single fiber application of PP is in nonwoven fabrics.

In spunbond and melt blowing, filaments are continuous (no staple fibers) and no carding is necessary as the fibers are extruded; they are collected as webs. Of course the staple fibers of PP are carded or air laid and then bonded.

Composites of both spunbonded and melt blown fabrics, generally referred to as SMS fabrics, are used in various applications. There are, however, some specialized areas where high-modulus PP fibers have been used. In one of the patents,[34] cementitious articles are reinforced with a fabric made at least partially of high-modulus PP monofilament fibers. The PP monofilament yarns have a 3% secant modulus of elasticity of at least 100 g/denier. The high-modulus PP fabric has an intrinsic resistance to the alkaline conditions present in a cementitious composite, as well as a low elongation at break. The high-modulus PP may contain a nucleating agent to facilitate the process of obtaining the desired draw ratio.

Another patent[35] discusses an air-laid composition comprising absorbent, binder, and synthetic fibers, where the synthetic fibers have a modulus greater than about 2 g/denier and a percent crimp of less than about 30%. The binder comprises about 3−15% of the weight of the composition. The synthetic fibers comprise about 10−50% of the weight of the composition. The binder is selected from the class comprising conventional latex systems, hot melt adhesive, or binder fibers, or a mixture of these. The absorbent comprises natural absorbents or super-absorbent polymer, or a combination of these. The natural absorbent materials are selected from the class consisting of wood pulp fluff, cotton, cotton linters, and regenerated cellulose fibers. The super-absorbent polymer is selected from the class of agar, pectin, guar gum, and synthetic hydrogel polymers. The synthetic fibers may possibly be PP having an average length of about 3−18 mm.

In another patent,[36] a protective, impact-resistant material and method, the material comprising a fabric of thermoplastic polymeric fibers has a strength of at least 0.4 GPa, an elastic modulus of at least 5 GPa, and a matrix of polymeric material disposed in the interstices between the fibers, the matrix having an elastic modulus in the range

0.2−3 × 106 psi. The polymeric fibers can be gel-spun polyethylene, PP, etc. The matrix is derived from the fabric. The method of making the material comprises providing a matrix of melted polymeric material transparent to energy of a predetermined type and having a predetermined melting temperature. A fabric of polymeric fibers having a melting temperature higher than the melting temperature of the matrix is placed in the matrix, applying a pressure of 1000−6000 psi to the fabric disposed in the matrix. Then the temperature is raised to the melting temperature of the fabric for the minimum time required to cause consolidation of the fabric and the matrix. The consolidated fabric and matrix is then rapidly cooled to a temperature below the melting temperature of the fabric.

8.5 Conclusion: strengths and weaknesses of current fiber types

PP fibers have several advantages. Because of the compact structure, high crystallinity, and a very low moisture regain, PP fibers show high-resistance to chemicals, mildew, insects, perspiration, rot, stain, and soil. The fibers have good bulk and cover, and are very light weight. They have the lowest static generated in any synthetic fiber.[37] They also have good washability, quick drying properties, and can impart good thermal comfort.[38] The trends in consumption of PP fibers in nonwovens is summarized in Fig. 8.4.

PP as a polymer suffers from some disadvantages. However, these disadvantages are only applicable when the fiber is used for apparel applications. Because of its structure, the fiber is difficult to dye after manufacturing, except after substantial treatment and modification. The high crystallinity and poor thermal conductivity lead to limited texturizability. For industrial applications, low UV and thermal stability of PP when compared to polyesters and polyamides and a tendency to creep are some of the disadvantages.

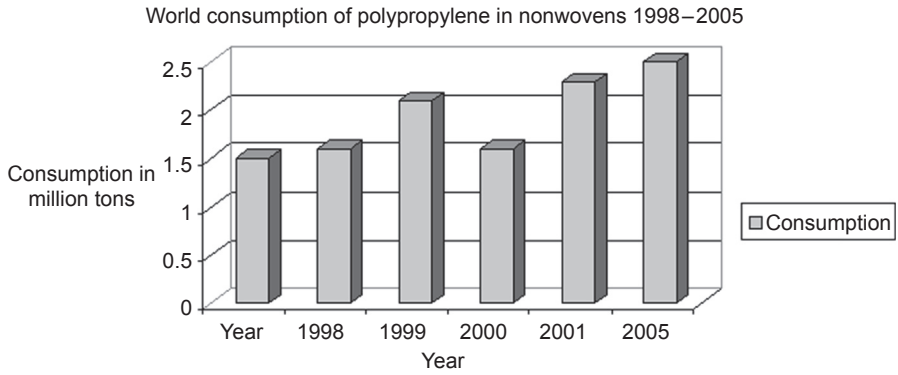

Figure 8.4 Trends in consumption of polypropylene in nonwovens.[39]

8.6 Future trends

The challenge is to produce finer filaments of PP for nonwovens. Interesting application areas are filtration performance of blended microglass and electrospun PP fiber filter media. The use of PP fibers in hybrid composites[40] has also received a lot of attention and needs to be further explored. Use of PP in concrete[41,42] has also received interest. Mechanical and microstructural features of autoclaved aerated concrete reinforced with autoclaved PP,[43] carbon, basalt, and glass fiber are showing interesting results.

References

1. Galanti A, Mantell C. *Polypropylene fibers and films*. New Jersey: Springer Science; 1965.
2. Peterlin A. Mechanical properties of fibrous structure. In: Ciferri A, Ward IM, editors. *Ultra-high modulus polymers*. London: Applied Science; 1977. p. 279–320.
3. Kalb B, Penningsa AJ. *J Mater Sci* 1980;**15**:2584.
4. Smook J, Flinterman M, Pennings AJ. *Polym Bull* 1980;**2**:775.
5. Todokoro H. *Polymer* February 1984;**25**:147.
6. Mirabella Jr FM. *J Polym Sci Part B Polym Phys* 1987;**25**:591.
7. He T. *Polymer* February 1986;**27**:253.
8. Keller A. *Future Trends Polym Sci Technol* 1989:185.
9. Ahmed M. In: *Polypropylene fibres-science and technology*. New York: Elsevier Scientific Publishing Company; 1982. p. 277.
10. Wills AJ, Capaccio G, Ward IM. *J Polym Sci* 1980;**493**.
11. Capaccio G, Crompton TA, Ward IM. *J Polym Sci Polym Phys Ed* 1976;**14**:1641.
12. Ahmed M. In: *Polypropylene fibres-science and technology*. New York: Elsevier Scientific Publishing Company; 1982. p. 187.
13. Ward IM. In: *Structure and properties of oriented polymers*. Chapman and Hall; 1997.
14. USP 4228118 A, Wen-li Wu, William B. Black, Process for producing high tenacity polyethylene fibers, Published 14.10.1980.
15. Ito M, Takahashi K, Kanamoto T. *J Appl Polym Sci* 1990;**40**:1257 [Compendex World Textiles].
16. Ito M, Tanaka K, Kanamoto T. *J Polym Sci Polym Phys Ed* 1987;**25**:2127 [INSPEC Compendex].
17. Wang, et al. *J Text Inst* 1995;**86**:383.
18. Sheehan WC, et al. *J Appl Polm Sci* 1964;**8**:2359.
19. Candia, et al. *J Appl Polm Sci* 1992;**46**:1799.
20. Laughner, et al. *J Appl Polm Sci* 1988;**36**:899.
21. Kunugi. In: *Oriented polymer materials*. Oxford; 1996. p. 394.
22. Cannon. *Polymer* 1982;**23**:1123.
23. Ward IM. In: Lemstra PJ, editor. *Integration of fundamental polymer science & technology*, vol. 2. Chapman and Hall; 1988. p. 559.
24. Taraiya AK, Richardson A, Ward IM. *JAPS* 1987;**33**:2559.
25. Kar P. High modulus polypropylene filaments: preparation, structure and properties, phd thesis; 1998. p. 12–8.

26. Karger-Kocsis J, editor. *Polypropylene − an A−Z reference*. Dordecht: Kluwer Academic Publishers; 1999.
27. Ward M. *Structure and properties of oriented polymers*. Springer-Science+Business Media, B.V.; 1997.
28. Samuels RJ. *J Polym Sci A* 1965;**3**:1741.
29. Kar P. *High modulus polypropylene filaments: preparation, structure and properties* [Ph.D. thesis]. IIT; February 1999.
30. Mukhopadhyay S, Deopura BL, Alagirusamy R. Mechanical properties of polypropylene filaments drawn on varying post spinning temperature gradients. *Fibers Polym* 2006;**7**(4): 432−5.
31. Mukhopadhyay S, Deopura BL, Alagirusamy R. *J Appl Polym Sci* 2006;**101**:838.
32. Mukhopadhyay S, Deopura BL, Alagirusamy R. *J Text Ins* 2005;**96**:349.
33. Kunugi T. In: Karger-Kocsis J, editor. *Polypropylene − an A−Z reference*. Dordecht: Kluwer Academic Publishers; 1999.
34. EP 1718789 A4 20101020 (EN). Fabric reinforced cement.
35. Ouederni M, Campbell K. *Air-laid web with high modulus fibers*. US 20030003830 A1, Published 2 January; 2003.
36. Klocek P, MacKnight WJ, Farris RJ, Lietzau C. *High strength, high modulus continuous polymeric material for durable, impact resistant applications*. US 5573824 A, Published: November 12; 1996.
37. http://www.engr.utk.edu/mse/Textiles/Olefin%20fibers.htm.
38. Slater K. Comfort properties of textiles. *Text Prog* 1977;**9**(4):12−5.
39. Malkan. Advancements in polyolefin resins for polymer-laid nonwovens. In: Hi-Perfab'96 Conference, Singapore, April 24−26, 1996.
40. Yap SP, Bu CH, Johnson Alengaram U, Mo KH, Jumaat MZ. Flexural toughness characteristics of steel−polypropylene hybrid fibre-reinforced oil palm shell concrete. *Mater Des* May 2014;**57**:652−9.
41. Flores Medina N, Barluenga G, Hernández-Olivares F. Combined effect of Polypropylene fibers and Silica Fume to improve the durability of concrete with natural Pozzolans blended cement. *Constr Build Mater* October 15, 2015;**96**:556−66.
42. Liu L-F, Wang P-M, Yang X-J. Effect of polypropylene fiber on dry-shrinkage ratio of cement mortar. *Jianzhu Cailiao Xuebao/J Build Mater* 2005;**8**(4):373−7.
43. Onur Pehlivanlı Z, Uzun İ, Demir İ. Mechanical and microstructural features of autoclaved aerated concrete reinforced with autoclaved polypropylene, carbon, basalt and glass fiber. *Constr Build Mater* October 15, 2015;**96**:428−33.

High-performance nylon fibers

9

M. Najafi [1], *L. Nasri* [2], *R. Kotek* [1]
[1]North Carolina State University, Raleigh, NC, United States; [2]Trützschler Switzerland AG, Winterthur, Switzerland

9.1 Introduction

Nylon or polyamide (PA) is known as the second most important man-made polymer for textiles after polyester [1]. It was first developed by a brilliant chemist, Wallace H. Carothers, in the 1930s at DuPont research facilities [2]. Properties such as stiffness, toughness, lubricity, and resistance to temperature, fatigue, and abrasion make nylon one of the most versatile thermoplastics in use today [3]. The most important application of nylon is as fibers, which cover a wide range of textiles, apparel, and industrial products [4]. Nylon filaments for technical requirements or functions are known as high-performance (technical) fibers. Based on application, technical nylon fibers can be classified into several categories such as high-modulus–high-tenacity (HM-HT) fibers, flame retardant fibers, chemical resistance fibers, and conductive fibers [5]. Among them, the HM-HT fibers are of particular interest as they have high tensile performance as well as good chemical and thermal stability [6]. Thus the main focus of this chapter is on the production and characteristics of HM-HT nylon fibers.

HM-HT nylon fiber is constructed from aliphatic polymers with structural methylene units $(CH_2)_n$ linked together by amide (peptide) groups (NH–CO). PAs are identified as nylon-*n* (PA-*n*) or nylon-*mn* (PA-*mn*), where *m* and *n* represent the number of carbon groups in the related monomeric units (Fig. 9.1) [3]. Nylons are commercially produced in two different ways: polycondensation of difunctional monomers containing amino acids or equal pairs of diamines and dicarboxylic acids, and ring-opening polymerization of lactams. PA-6 and 66 are the two principal nylons used for technical fibers because of the combination of tensile properties, process flexibility, and abrasion resistance. Nylon-6 is synthesized through ring-opening polymerization of caprolactam while nylon-66 is synthesized by polycondensation from adipic acid and hexamethylene diamine [7,8]. High tenacity, high elasticity, good adhesion to rubber, and resistance to abrasion and chemicals make these nylon filaments attractive for various technical applications such as tire cords, surgical sutures, friction bearing, cloths, threads, ropes, and nets [7,9].

$$\text{Nylon-}n\text{: } -[-(\text{NH}-\text{CO})-(-\text{CH}_2)_{n-1}-]- \quad (1)$$

$$\text{Nylon-}mn\text{: } -[-(\text{NH}-\text{CO})-(-\text{CH}_2)_{n-2}-(\text{CO}-\text{NH})-(\text{CH}_2)_m-]- \quad (2)$$

Figure 9.1 Chemical structure of nylon-*n* and nylon-*mn*.
Reprinted from S. Dasgupta, W.B. Hammond, W.A. Goddard, Crystal structures and properties of nylon polymers from theory, J. Am. Chem. Soc. 118 (1996), 12291–12301 with permission of ACS.

Structure and Properties of High-Performance Fibers. http://dx.doi.org/10.1016/B978-0-08-100550-7.00009-7

HM-HT PA fiber has some technical and economic advantages over other similar products. It does not have high process complexity and high production cost of aramid fibers such as M5, Zylon, and Kevlar (Fig. 9.2). These rigid polymers are often difficult to process as they decompose chemically before melting and need strong acid solvents for the filament formation [6,10]. Moreover, nylon has a higher melting point than other flexible polymers such as polypropylene (PP), polyethylene (PE), and polyethylene terephthalate (PET), and thus it has a potential for a wider range of applications. Nevertheless, technical nylon filaments have considerably lower tensile properties than other technical fibers (eg, carbon, aramid) (Fig. 9.2), and this limits their usage in industrial products. It is said that the strength (tenacity) and the stiffness (modulus) are related to molecular orientation and the number of the chain ends inside the fiber. Thus to make stronger nylon yarns the macromolecules need to be thoroughly extended and oriented along the fiber axis and the chain end defects need to be reduced [11]. This can be achieved through modifying fiber formation processes and thermomechanical treatments. In this chapter, we will first elaborate recent advances in spinning methods and treatments for production of HM-HT nylon (PA-6 and PA-66) fibers, and then we will describe the structures, properties, and applications of such high-performance filaments in detail.

9.2 Production of high-performance nylon fibers

9.2.1 Fiber formation

Fiber formation and treatment methods play a critical role in providing structural and tensile properties for textile yarns. It can be said that the shape of the fibers is formed

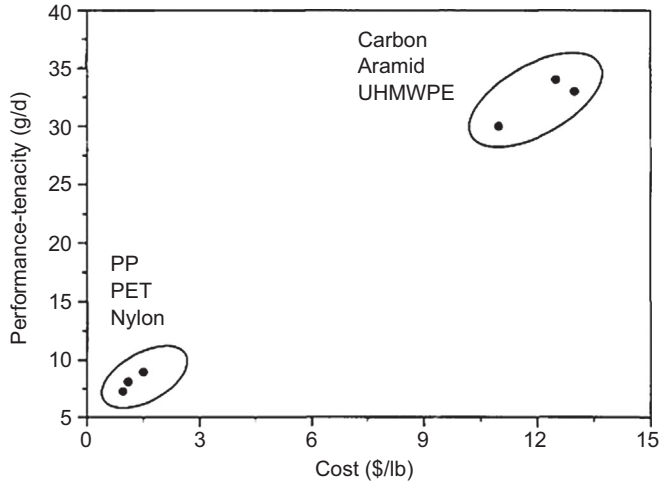

Figure 9.2 Comparison of performance and cost for some technical fibers.
Reprinted from V. Mittal, High performance polymers: an overview, in: V. Mittal (Ed.), High Performance Polymers and Engineering Plastics, first ed., Wiley, 2011, pp. 1−20 with permission of Wiley.

during the spinning process, whereas their structure is shaped mainly during the drawing process [8]. Several techniques such as melt spinning [12,13], dry spinning [14,15], wet spinning [15−17], and gel spinning [18,19] have been used for the production of PA fibers. Among them, melt spinning is of greater interest as it is the simplest eco-friendly method both conceptually and economically, as it also does not have the complexity of chemical reaction, mass transfer, and waste recovery systems that is inherent other techniques [20−22]. Conventional melt spinning produces nylon fibers with low tenacity, low modulus, and high elongation at break, which are not appropriate for technical applications. To improve the tensile performance, additional treatments such as drawing and/or annealing are performed on the filaments/yarns [21,22].

The main challenge in making high-performance fibers from nylons is the strong hydrogen bonding (H-bonding) between the chains. These H-bonds favor rapid crystal formation during the spinning process, hindering further chain mobility and molecular orientation for obtaining higher tensile properties. The highest draw ratio (DR) reported for commercial nylon fibers is about 5−6 [23], which is much lower than the DR of 100 for technical PE fiber [24]. Higher values have been reported in patents and papers, but there is still a problem of commercialization. Also the maximum tenacity and modulus for technical nylon yarns are about 1 N/tex (∼1 GPa) and 9 N/tex (∼9 G) [6], which are far beyond the corresponding theoretical values of 28.3−31.9 GPa and 183−263 GPa [25]. Higher modulus and tenacity nylon fiber can be obtained possibly by suppression of crystallinity or by breaking/weakening the H-bonding [26]. New approaches and innovative methods such as liquid isothermal bath (LIB) [27] and SymTTec [28] have been developed, in this regard. Next we first review the traditional spinning processes and treatments for production of technical nylon fibers, and then we will explain those innovative methods in detail.

9.2.2 Melt spinning

Melt spinning is the simplest spinning method for production of synthetic fibers and yarns. It is based on the extrusion of polymer melt through a spinneret into a cooling environment and the subsequent elongation of the extruded melt into filament bundles (Fig. 9.3). This method is appropriate for polymers such as nylons that are sufficiently stable in the molten state and their viscosity is low enough for extrusion [29]. Melt spinning has several advantages over other fiber formation techniques. It has a higher production rate because of the higher wind-up speed used in the spinning line. Also it is a very simple and eco-friendly method, as it does not have the complexity of chemical reaction and mass transfer that is inherent in other spinning techniques. Moreover, obtaining filaments with uniform structure is easier in melt spinning, as the filaments have no porosity and defect sites inherently found in the fibers of other methods. Also filaments with desired cross-sections (eg, round, trilobal, pentagonal) can be easily made by using the desired spinneret hole configuration [22,30].

The melt-spinning process comprises several steps including: melting, extrusion, extension, solidification, and wind-up (Fig. 9.3). The polymer melt is obtained either

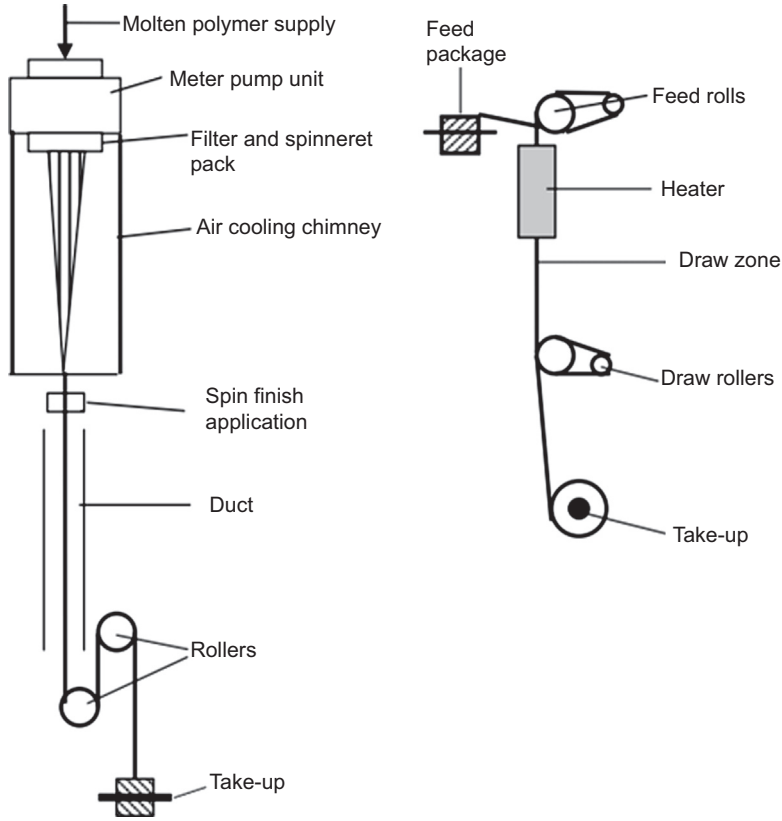

Figure 9.3 Scheme of melt spinning and drawing of nylon yarn.
Reprinted from A.F. Richards, Nylon fibres, in: J.E. McIntyre (Ed.), Synthetic Fibres: Nylon, Polyester, Acrylic, Polyolefin, first ed., Boca Raton: CRC Press; Woodhead Pub., 2005, pp. 20–94 with permission of Woodhead.

from melting the polymer chips or directly from the polymerization vessel. In the case of the chips, the moisture content of the polymer needs to be lowered to a consistent level (about 0.12%) before spinning, as the moisture can result in polymer degradation and poor fiber quality. The polymer passes through several steps in the spinning line to become yarn (Fig. 9.3). First, the chips are melted inside a grid or extruder and moved into a metering pump. The spinning temperature is normally set 30–40°C higher than the polymer melting point (T_m) to reduce the melt viscosity and facilitate the melt extrusion. The metering pump delivers the melt to the spin pack, which contains a top cap, a breaking plate, a filtration medium, and a spinneret. The top cap and breaking plate distribute the polymer evenly inside the spin pack. The filtration medium removes solid impurities (eg, gel and foreign particles) and gas bubbles from the melt. And the spinneret, which is like a shower head, transforms the polymer melt into filaments. Following the spinneret, the filaments are extended and solidified/quenched by air or water. The temperature and humidity in this step need to be controlled precisely, as

they affect considerably the orientation and crystallinity of the final yarn. The filaments become a single yarn by a vacuum gun and are gathered on a bobbin by a winder [7,30].

9.2.2.1 Drawing and annealing

As-spun filaments generally have low tensile properties and cannot be used for technical applications. To improve fiber performance, the molecular orientation and crystal formation need to be increased inside the filaments. This can be achieved by applying specific mechanical and/or thermal treatments (eg, drawing and annealing) on the yarn. During the drawing, the fibers are normally heated at a temperature higher than the polymer glass transition temperature (T_g) to increase chain mobility, and then stretched with a certain DR to align the chains along the fiber axis. Fig. 9.4 displays a scheme of the drawing process for nylon yarns. As the figure shows, the spun yarn is passed through a set of feed rollers and then stretched through another set of rollers known as draw rolls. The yarn between the rolls may be heated up by a heater or an inert gas. The DR is defined as the ratio of surface speed between draw rolls (v_2) and feed rolls (v_1). For apparel application, the nylon yarns are drawn with a low DR of 2−2.5, whereas for industrial usage the yarns are drawn with a high DR of 4−5 [9]. Besides the drawing, annealing is also applied on as-spun or drawn yarns to increase the crystal size and crystallinity. In annealing, the yarn length is essentially kept constant and sometimes a small amount of tension or relaxation may be given to control the dimensional stability and load-elongation behavior. The annealing temperature is normally between T_g and T_m to provide enough molecular mobility for chain folding and crystal formation [8].

Drawing and annealing can be performed on the filaments during or after melt spinning. In this regard, the melt-spinning processes can be classified in two main groups: two-step process (conventional melt spinning) and one-step process (spin−draw process). In the two-step process, the low-oriented yarn (LOY) is produced first at

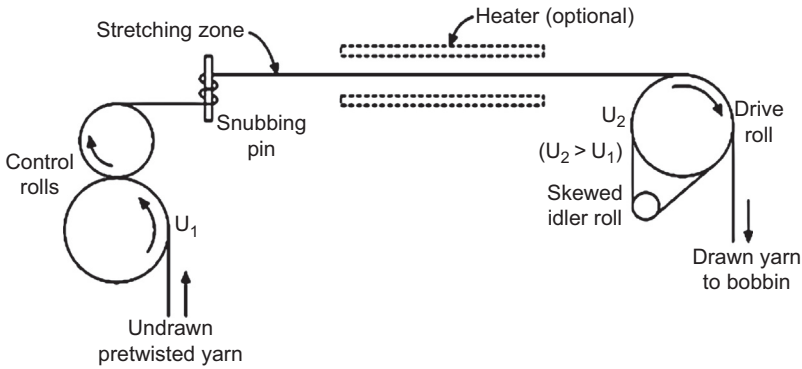

Figure 9.4 Scheme of the drawing process used for polyamide filaments.
Reprinted from S.K. Mukhopadhyay, Manufacture, properties and tensile failure of nylon fibres, in: A.R. Bunsell (Ed.), Handbook of Tensile Properties of Textile and Technical Fibres, first ed., Woodhead Publishing, Oxford, 2009, pp. 197−221 with permission of Woodhead.

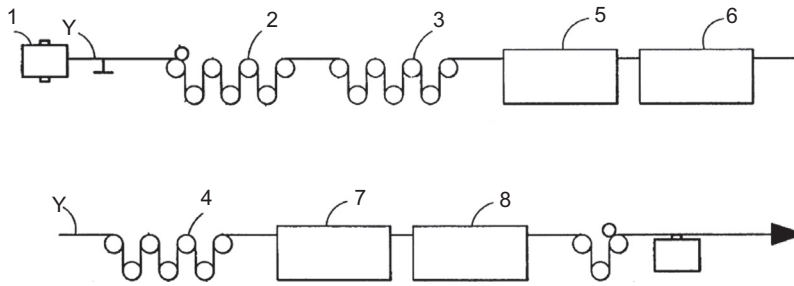

Figure 9.5 Three-stage hot drawing 2, 3, and 4 (DR1: 3.28, DR2: 1.79, and DR3: 5.89), two ovens 5 and 6, and two relaxation ovens 7 and 8 on yarn package 1.
Adapted from R.T. Clark, A. Joseph, High Tenacity, High Modulus Polyamides Yarn and Process for Making Same, US Patent 5106946, 1992.

1000−1500 m/min. The undrawn yarn is normally kept in storage for 4−12 h and then stretched at 400−1000 m/min to become fully drawn yarn (FDY) with higher mechanical properties. Many variations of fiber stretching during/after melt spinning are described in the patent literature [32−40]. Drawing may be performed several times on the yarn to increase the tenacity and modulus, high enough for technical applications. For example, in 1992 Clark and Cofer [33] designed a multistage drawing process for production of technical nylon yarns. The process comprised three drawing steps, each has seven rolls and some heated areas (ovens) (Fig. 9.5). The yarn was stretched with different DRs and temperatures in each step. High tenacity of 12 g/d, high modulus of 75.4 g/d, and low elongation of 11.3% were reported after multistage drawing of nylon yarn.

The two-step process, although it improves the fiber tensile performance, has high production cost, low productivity, and high energy consumption. To address these problems, the drawing and spinning processes are integrated into a one-step continuous process (spin−draw process), where the filaments travel into several drive rolls with different temperatures and velocities before being gathered on the bobbin [7,30,41]. Fig. 9.6 displays a scheme of a spin−draw process for nylon-6 tire cord yarn. As shown in the figure, the draw field is divided into two or more zones by intermediate rolls arranged between feed rolls and draw rolls. In 1984, Koschinek et al. [39] used the spin−draw process for the production of technical yarns from polyesters and polyamides. PA-6 yarn with a high tenacity of 90.4 cN/tex (10.21 g/d) and low elongation of 8% was obtained for DRs of 1.5 and 5.2 (ie, first and second draw zones) and a take-up speed of 2850 m/min.

9.2.2.2 Zone drawing−zone annealing

Zone drawing−zone annealing is an old thermomechanical treatment designed by Kunugi et al. [42,43] for production of high-strength fibers. The apparatus is a modified standard tensile tester in which a 2-mm wide band heater is attached to a movable crosshead (Fig. 9.7). The moving speed and the temperature of the band heater are adjustable and the desirable tension is applied to the end of fiber by using a suitable weight.

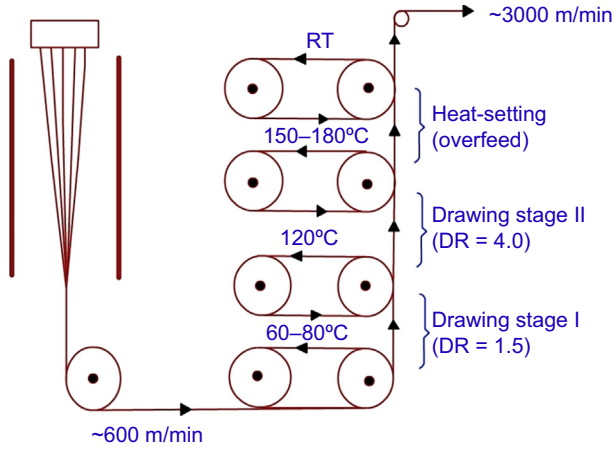

Figure 9.6 Spin–draw process for production of nylon-6 tire cord yarn.
Reprinted from NPTEL:Textile Engineering – Manufactured Fibre Technology- Drawing Machines. [Online]. Available: http://www.nptel.ac.in/courses/116102010/29 with permission of NPTEL.

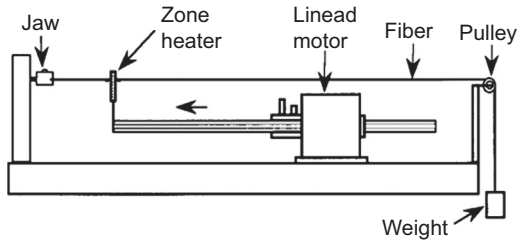

Figure 9.7 Scheme of the apparatus used for zone drawing/annealing.
Reprinted from T. Kunugi, K. Chida, A. Suzuki, Preparation of high-modulus nylon 6 fibers by vibrating hot drawing and zone annealing, J. Appl. Polym. Sci. 67 (1998) 1993–2000 with permission of Wiley.

The method basically comprises two steps: zone drawing (ZD) and zone annealing (ZA). In ZD, the temperature is chosen between glass transition and crystalline temperatures, and the applied tension is low to make highly oriented amorphous fiber. In ZA, higher tension and temperature are applied to form perfectly extended chain crystals in the fiber. The drawing and/or annealing steps need to be repeated several times to provide fibers with high tenacity and modulus. ZD–ZA treatment has already been used on several polymers such as PA, PET, PP, and PE. For nylon-6 fiber, the tenacity and modulus were increased up to high values of 1 and 10 GPa, after ZD (one time) and ZA (six times) [42,44]. Also for nylon-46, three repetitions of high-temperature zone drawing (HT-ZD) on the fibers increased the tenacity and modulus up to 1 and 7.2 GPa, respectively, and reduced the elongation at breakdown to 10.3% [45].

Several designs of ZD–ZA treatments have been applied to nylons fibers. Kunugi and coworkers [44] developed a vibrating hot drawing (VD) method to

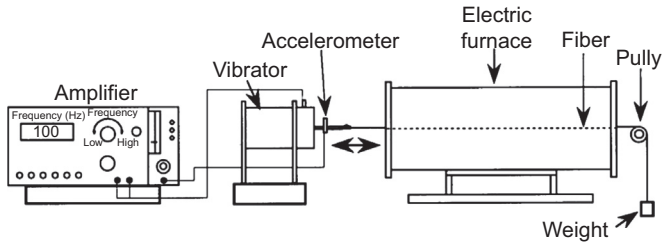

Figure 9.8 Schematic of vibrating hot drawing instrument.
Reprinted from T. Kunugi, K. Chida, A. Suzuki, Preparation of high-modulus nylon 6 fibers by vibrating hot drawing and zone annealing, J. Appl. Polym. Sci. 67 (1998) 1993−2000 with permission of Wiley.

get high-modulus nylon-6 fibers. As displayed in Fig. 9.8, the apparatus consists of an electric furnace, an amplifier, and a vibrator equipped with an accelerometer. Vibrating frequency in the range of 2−20,000 Hz is used and optimum amplitude is selected to have the DR as high as possible. High tenacity of 0.8 GPa, high modulus of 23 GPa, and low elongation of 4.3% were reported after performing VD (two times) and ZA (one time) on nylon-6 fiber. Furthermore, Suzuki et al. [46] investigated the influence of high-tension annealing (HTA) on the tensile properties of nylon-66 fiber. In this method, the fiber is annealed under extremely high tension, close to the strength at break, to extend thoroughly the tie molecules inside the amorphous phase. A tensile strength of 1.42 GPa and Young's modulus of 12.3 GPa were reported after HT-ZD (two times) and HTA (three times) treatments. In another study, Suzuki and Ishihara [47] used carbon dioxide (CO_2) laser heating ZD and annealing to modify the tensile performance of nylon-6 fiber. In this technique, a continuous-wave CO_2 laser beam is placed between supplying and winding spools. The role of the CO_2 laser is to heat the fibers under tension. A DR of 5.2 and dynamic storage modulus of 22 GPa were reported after several laser-heated ZD−ZA treatments on the fiber.

Although ZD−ZA methods are very simple and easy to use, they have several deficiencies preventing them from being used at industrial scale. First, the drawing and/or annealing steps need to be repeated several times to provide fibers with high tenacity and modulus. Also, as the technique is performed in a batch-wise operation, only a limited length of yarn can be treated each time. Moreover, the speed of the band heater for drawing/annealing stages is extremely low (10−40 mm/min). The need for several repetitions and the very low speed indeed affect productivity of the final product. To address these problems, Suzuki et al. [48] developed a continuous version of the technique with higher speed (240 mm/min). The continuous method was performed three times on nylon-66 fibers and the tenacity and modulus were increased up to 1.2 GPa and 8 GPa and strain at break reduced up to 11%. Nevertheless, similar to the batch system, the continuous system needs to be performed several times to provide high-tensile results and the speed is still not high enough for commercial application.

9.2.2.3 High-speed spinning

High-speed spinning is another type of one-step process in which higher wind-up speed (>3000 m/min) is used to improve fiber tensile properties. The idea behind this technology was based on the elimination of the drawing process by using higher wind-up velocity in the spinning line. High-speed spinning has several advantages over the two-step process. It increases productivity, simplifies the production process, and reduces the energy, labor, and overall production costs. It is known that the productivity of high-speed spinning is 6−15 times higher than conventional two-step melt spinning. Moreover, high-speed spinning reduces the lag time between drawing and spinning by reducing the need for a further drawing process [29]. Nevertheless, this spinning method has its own limitations and deficiencies. The tenacity, modulus, and elongation of the high-spun yarns are typically inferior to those of traditional two-step process yarns [49]. Also the filaments may not be quenched and solidified adequately, since they travel the distance between the spinneret and the take-up rollers faster. This issue can considerably impact the structural uniformity and mechanical properties of thicker filaments in particular, as they need more time to be quenched.

The influence of high-speed spinning on tensile properties can be explained by molecular orientation and crystal formation. The higher velocity increases the crystallization rate and reduces the chain mobility and crystallization time. At first the higher take-up stress predominantly increases the birefringence and crystallinity, leading to higher tenacity, higher modulus, and lower elongation (Fig. 9.9). However, above a critical speed, the chain mobility and crystallization time are decreased considerably, resulting in lower orientation, crystallization, and tensile properties (Fig. 9.9) [13]. To get higher tensile performance, higher molecular weight polymer can be used.

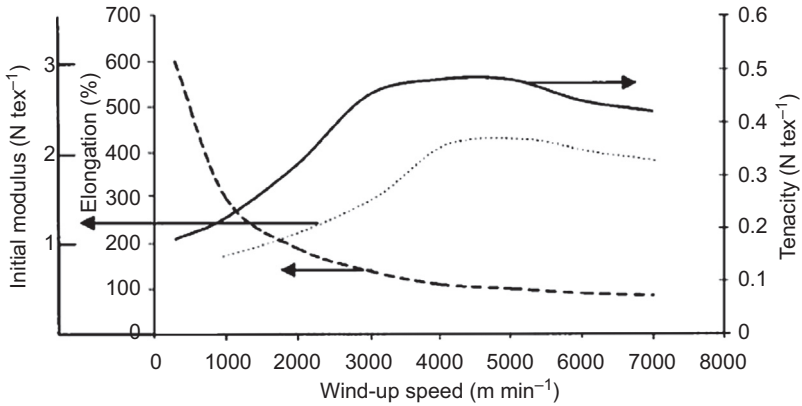

Figure 9.9 Influence of take-up speed on the tenacity (—), initial modulus (——), and elongation (……) of PA-6 fiber.
Reprinted from A.F. Richards, Nylon fibres, in: J.E. McIntyre (Ed.), Synthetic Fibres: Nylon, Polyester, Acrylic, Polyolefin, first ed., CRC Press; Woodhead Pub., Boca Raton, 2005, pp. 20−94 with permission of Woodhead.

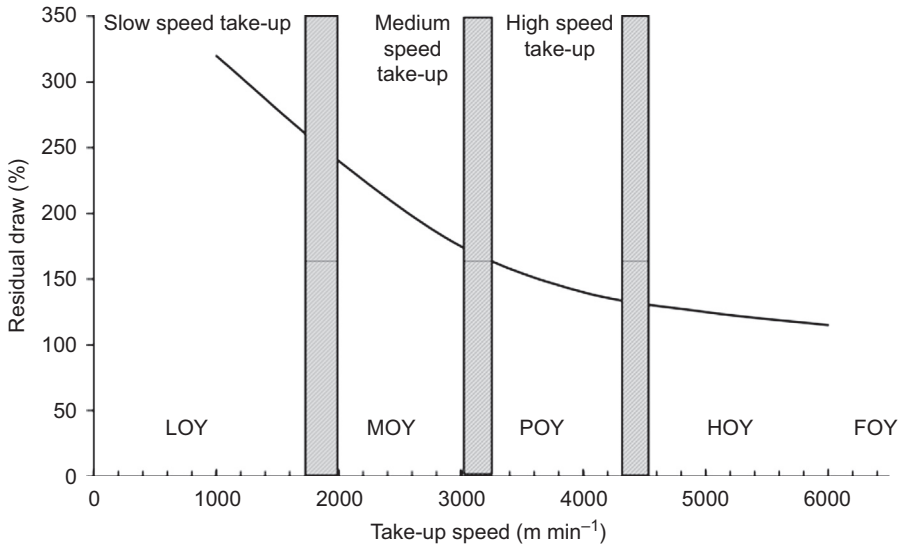

Figure 9.10 Effect of take-up speed on the residual draw ratio of nylon fiber. LOY, MOY, POY, HOY, and FOY stand for low, medium, partially, highly, and fully oriented yarn, respectively. Reprinted from A.F. Richards, Nylon fibres, in: J.E. McIntyre (Ed.), Synthetic Fibres: Nylon, Polyester, Acrylic, Polyolefin, first ed., CRC Press; Woodhead Pub., Boca Raton, 2005, pp. 20–94 with permission of Woodhead.

The more entanglement between the chains at higher molecular weight can lead to higher orientation, crystallization, and mechanical properties [105]. Besides that, drawing the filaments during high-speed spinning (ie, spin–draw process) can modify the tensile characteristics. The problem is that the high take-up and rapid airflow used in such high-speed technology increases considerably the molecular orientation and limits fiber drawability (Fig. 9.10).

In 2005, Samant and Vassilatos [50] developed pneumatic quench to improve fiber drawability at high-speed spinning. In this method, an inert quench gas such as nitrogen is provided to the freshly extruded fibers to control their temperature and attenuation profiles. As Fig. 9.11 shows, the quench gas is directed to travel along the extruded filamentary array to solidify them. Such cooling design reduces the aerodynamic drag on the running filaments and results in lower fiber birefringence and higher DR during the spinning process. Furthermore, the reduced yarn tension can increase productivity via reducing filament breakage at higher take-up speed. The new quench system was applied to the spin–draw process for nylon-66 at different spinning velocities. High tenacity of 10.8 g/d and DR of 5.5 were reported for pneumatic cooling at a spinning speed of 3660 m/min, which were higher than the corresponding values of 9.6 g/d and 4.8 in former cross-flow quenching. Also the tenacity of 10.8 g/d obtained at 3000 m/min by the prior art quench was achieved at 5500 m/min by the pneumatic quench, indicating (5500/3000) = 1.8 times increase in productivity.

Moreover, in 1997 Schippers and Lenk [51] applied additional heat to polymer melt in the region of the spinneret to improve fiber drawing. The heat is generated by an

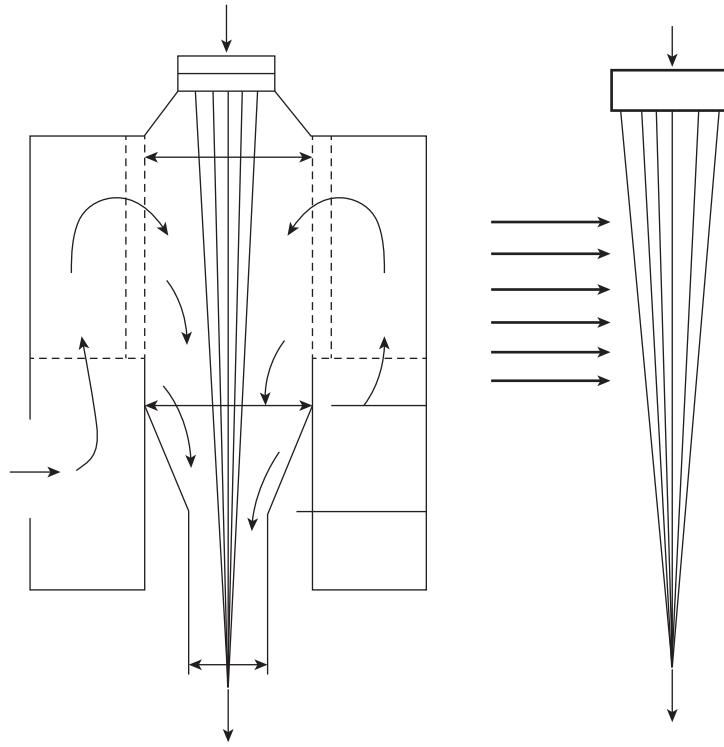

Figure 9.11 Schemes of pneumatic cooling (left) and cross-flow quench (right) systems. Adapted from K.R. Samant, G. Vassilatos, Process of Making Polyamide Filaments, US Patent 6899836 B2, 2005.

annular heating strip or a resistance heating wire and is directed to a conical surface, which faces the spinneret (Fig. 9.12). The temperature of the heater is in the range of 300°C to about 800°C. Such a high temperature can keep the polymer chains in the molten state for a longer time, reducing molecular orientation while increasing fiber elongation and DR in the spin−draw process. The extent of the increased elongation depends on the radiation temperature and the yarn denier. For the thicker filaments, the effect is lesser and higher radiation temperature may be required. The method is suitable for spinning of PA and polyester yarns.

9.2.2.4 Solid-state polymerization

High relative viscosity (RV) nylons are desirable for fiber production as they can improve the tensile properties as well as chemical and abrasion resistance. One way to increase the RV is to increase the amount of catalyst in the polymerization of nylons. The problem is that obtaining the desired high RV with high polymer quality is often difficult because of the high level of crosslinking and/or branching occurring during the process. Another way of increasing the RV or molecular weight is by solid-state

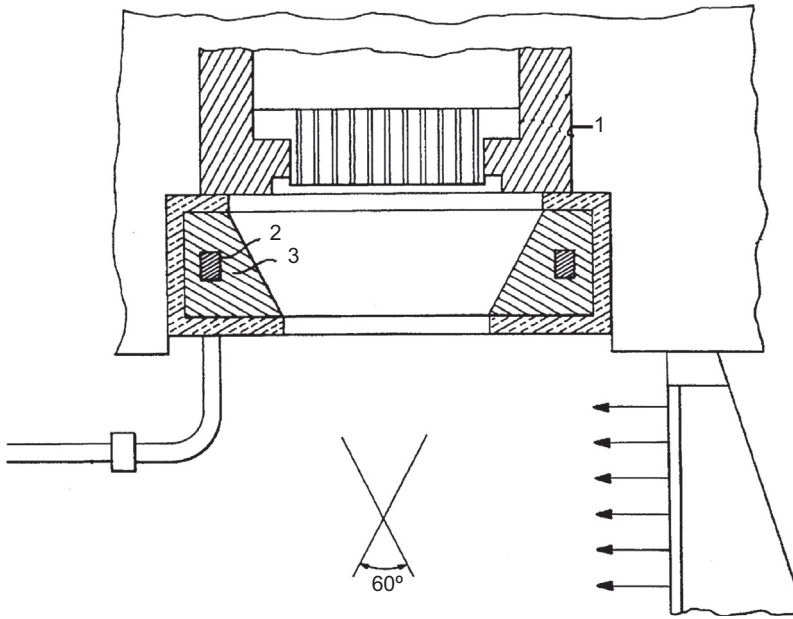

Figure 9.12 Scheme of the heater below the spinneret in melt spinning: 1—spin pack, 2—annular heating strip, 3—radiation heater.
Adapted from E. Schippers, H. Lenk, Method and Apparatus for Producing Multifilament Yarn by a Spin-draw Process, US Patent 5661880, 1997.

polymerization (SSP). In this process, polymer pieces (eg, chips, flake, pellets, etc.) are heated up to high temperatures below the melting point, to facilitate the reaction between the acid and amide ends of the molecules, and to make the polymer chains with longer length [52,53].

The problem with the SSP process on nylon chips is that the obtained polymers have high melting viscosities, which often make their extrusion very complex. In fact, the possible degradation occurring during the melting can reduce the molecular weight and polymer quality. Also the high entanglement between the chains can limit fiber drawing and tensile performance [54]. Such problems limited the integration of the SSP process with the melt-spinning process for manufacturing high molecular weight PA fibers. In the 1970s, researchers found that the SSP process on nylon filaments could improve the tensile properties [52,54]. For example, Silverman et al. [54] applied the SSP process to the drawn spun nylon yarns. The molecular weight increased from 35,000 to 52,000, the tenacity increased from 5.65 to 7.49 g/d, modulus increased from 38 to 51 g/d, and elongation decreased from 15.1 to 17.4% after the SSP process at 160°C for 8 h. Also, in 1991 Knorr [55] applied the SSP process to nylon yarns before being drawn. The SSP process could change the morphology of the as-spun fibers, letting them be drawn to a higher DR. The high DR of 6.98, high tenacity of 11.51 g/d, and low elongation of 12.5% were reported after hot drawing solid-state polymerized nylon-66 yarns by a modified draw tester.

In 2001, Schwinn and Raymon [53] patented a method to use the SSP process with melt spinning for industrial production of nylon filament tow and staple fibers. In that process the flake is heated up to a temperature of about 120−200°C for about 4−24 h by an inert hot gas (eg, nitrogen, argon, or helium) circulating inside the vessel. The flake having a formic acid RV of at least 90 can be removed from the vessel and transferred directly into the melt extruder for filament production. Moreover, Yildririm et al. [56] combined the SSP process with melt spinning and drawing for production of high-performance nylon-66 yarn. A high DR of 5−6.5, high tenacity of 11.34 g/d, low elongation of 13.9%, and low shrinkage of 6.3% were reported.

9.2.3 Dry spinning

Dry spinning comprises the extrusion of polymer solutions through a spinneret into a stream of hot gas (usually air) to evaporate the solvent and solidify the spinning jet (Fig. 9.13). It is a more complicated process than melt spinning because of the complexity of mass transfer in the solidification process, as well as the solvent recovery from the gas outlet [22,57]. The tensile strength and initial modulus of the filaments in this method depend strongly on molecular weight, DR, polymer concentration, and solvent ratio [14]. Dry spinning of nylon-6 has been examined by a couple of studies. Gogolewski and Penning [14] used cosolvent formic acid/chloroform ($HCOOH/CCl_4$) for the spinning. The use of CCl_4 as a nonsolvent improved chain entanglement and increased the DR up to 10, which is twice as high as the achievable DR in conventional melt spinning. The maximum reported tenacity and modulus were 1 GPa and 19 GPa,

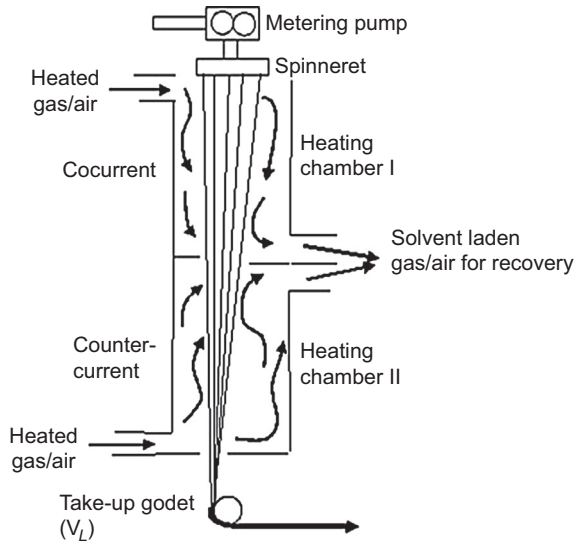

Figure 9.13 A typical dry-spinning process.
Reprinted from NPTEL: Textile Engineering − Manufactured Fibre Technology-Introduction to Solution Spinning. [Online]. Available: http://www.nptel.ac.in/courses/116102010/18 with permission of NPTEL.

respectively, which are superior to those of melt-spun fibers. In another study, Smook et al. [15] used formic acid/dichloromethane ($HCOOH/CH_2Cl_2$) for dry spinning of PA-6. The obtained DR and tenacity were inferior to those of melt-spun fibers.

9.2.4 Wet spinning

Wet spinning is the oldest method for production of synthetic fibers. It involves extrusion of polymer solutions into a coagulation bath where the polymer is precipitated from the solution to form a solid filament (Fig. 9.14). The coagulation bath contains low molecular weight substances miscible with the solvent but immiscible with the polymer. The complexities and problems of wet spinning prevent it being used widely for polymers. The take-up speed depends on hydrodynamic drag in the liquid bath and rarely exceeds over 50−100 m/min. Also obtaining filaments with uniform structure and diameter is very difficult as the fiber morphology is affected considerably by the conditions/compositions of the precipitation/coagulation bath. In fact, the filaments often have inherent problems of high porosity and surface defects, leading them to have more inferior tensile properties than melt-spun filaments [22]. Hancock et al. [16] examined wet spinning of various PAs including nylon-6 and nylon-66. The tensile strength could not exceed 0.15 g/d, probably because of the low molecular weight (3×10^4 g/mol) used for the spinning. In another study, Smook et al. [15] applied wet spinning on higher molecular weight nylon-6 (5×10^5 g/mol) for two different spinning solutions: sulfuric acid (96−100%) and formic acid/lithium chloride, and fibers with higher tenacities of 6 and 57 cN/tex (0.68 g/d and 6.44 g/d) were obtained, respectively.

9.2.5 Gel spinning

Gel spinning, also known as dry−wet spinning, is a fiber formation process for high molecular weight polymers (Fig. 9.15). The partially liquid state of the polymer used in this method can hold the chains somewhat bound together and produce strong

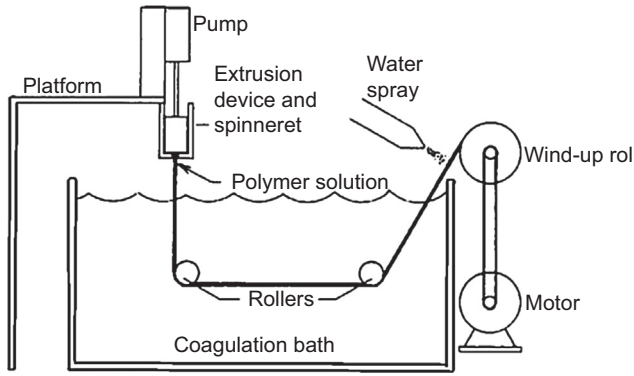

Figure 9.14 Scheme of wet-spinning process.
Reprinted from T.A. Hancock, J.E. Spruiell, J.L. White, Wet spinning of aliphatic and aromatic polyamides, J. Appl. Polym. Sci. 21 (1977) 1227−1247 with permission of Wiley.

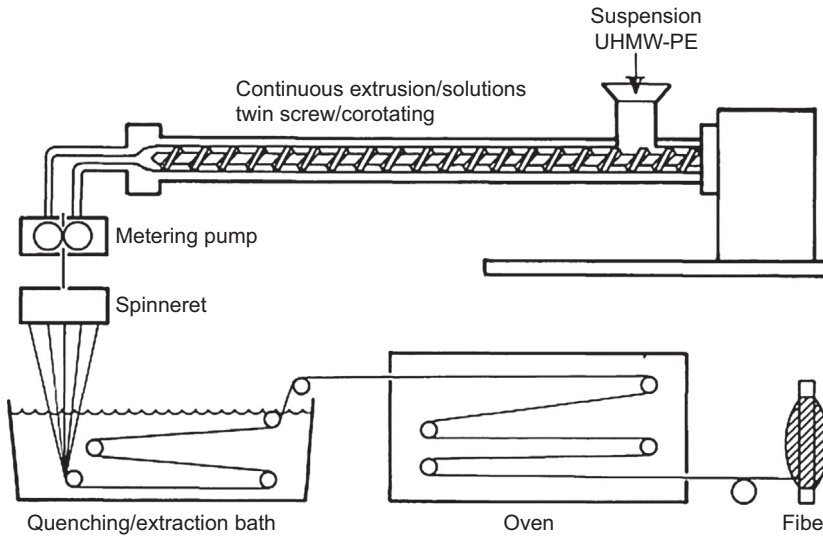

Figure 9.15 Scheme of a gel-spinning process.
Reprinted from P.J. Lemstra, C.W.M. Bastiaansen, H.E.H. Meijer, Chain-extended flexible polymers, Die Angew. Makromol. Chem. 145 (1986) 343−358 with permission of Wiley-VCH Verlag GmbH & Co. KGaA.

interchain forces in the fibers [58,61]. The success of this technology is for the reduced chain entanglements in the gel as well as the efficient drawing of the macromolecules in the flow field [59]. Application of this spinning technique has not been successful for PAs, since the strong hydrogen bonds within the chains make the ultradrawing of the fibers difficult. Gel spinning of nylon-6 has been investigated by several authors. Jia and coworkers [18] used formic acid and anhydrous $CaCl_2$ as the spinning solution, and tetrachloroethane/chloroform solution as the coagulation bath. The role of $CaCl_2$ is to make complex structures with the amide groups, disrupting partially the H-bonds and increasing the fiber drawability. A tenacity of 413 MPa, modulus of 28.8 GPa, and elongation of 50.2% were achieved after a DR of 8. In a similar study, Zhang et al. [60] obtained a tensile strength of 530.5 MPa, initial modulus of 32.3 GPa, and elongation at break of 27.1% after a DR of 10. Moreover, Cho et al. [19] examined gel spinning of nylon-6 in benzyl alcohol solution. A tenacity of 0.6 GPa and modulus of about 6.2 GPa were reported after performing a two-step drawing (DR = 6.2) on the filaments. Also Gupta [26] studied gel spinning/drawing of PA-6 for two different molecular weights (63,000 and 550,000 g/mol). A high tenacity of 1.23 GPa and modulus of 25 GPa were obtained for the higher molecular weight polymer after hot drawing the filament with a DR of 8.97.

9.2.6 Spinning with plasticizers and nanofillers

As mentioned, the strong H-bonding in nylons reduces chain mobility and prohibits high DR in the filaments. To increase the fiber drawability and tensile performance,

such H-bonding needs to be either suppressed or weakened. This can be achieved by utilizing a plasticizer during the fiber formation process, since it can disrupt temporarily the hydrogen bonds between the chains and facilitate their movements. The plasticizer is required to be removed after processing, as it can deteriorate the tensile properties. Iodine, ammonia, inorganic salts, and Lewis acids have been used for plasticization of aliphatic nylons [62–69].

The influence of plasticizers on fiber formation of nylons has been studied by several researchers. Afshari et al. [70], for example, examined the tensile performance of $GaCl_3$–nylon-66 complexed filaments. They used dry-jet wet spinning on high molecular weight nylon-66 ($1.75–2 \times 10^5$ g/mol) for fiber production. Fig. 9.16 displays a scheme of the spinning system. As it can be seen the polymer solution is extruded into the air and drawn before entering the coagulation bath. Based on the X-ray diffraction (XRD) results (Fig. 9.17), the complexation of the PA with the Lewis acid led to complete removal of the crystalline peaks and formation of fully amorphous fiber. The complexed filaments were easily stretched up to a DR of 7 at room temperature (ie, cold drawing). They also performed a hot drawing process on the regenerated (decomplexed) filaments. A low tenacity of 0.343 GPa, high modulus of 12.98 GPa, and low elongation of 12.3% were obtained after a DR of 13.8. The low tenacities observed for both complexed and regenerated filaments were attributed to the existence of nonuniformity or defects inside the fibers.

Moreover, Wei et al. [71] examined the influence of calcium chloride ($CaCl_2$) contents on drawing and tensile properties of melt-spun nylon-6 composite (ie, PA-6/$CaCl_2$) fiber. Tensile properties of the composite fiber were improved consistently with drawing ratio or drawing temperature. A maximum tensile strength of 0.6 GPa and initial modulus of 8.5 GPa were obtained for the 3% $CaCl_2$ content [ie, PA-$6_{0.97}(CaCl2)_{0.03}$] after a DR of 7 at 120°C. In another study, Yang et al. [23] investigated the effect of $CaCl_2$ in dry spinning of high molecular weight ($3–4 \times 10^5$) nylon-6 in formic acid. A molar range (MR) of 0.15–0.3 was found efficient for the complexation

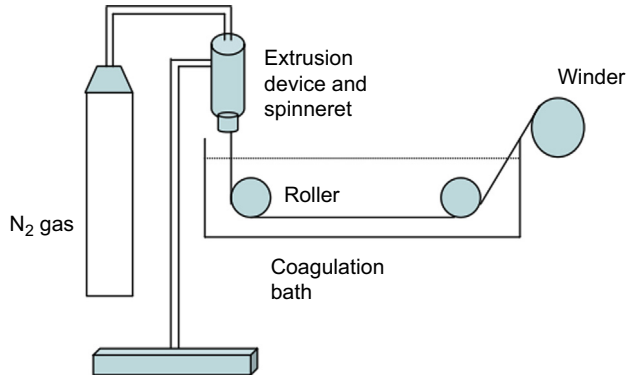

Figure 9.16 Schematic of dry-jet wet-spinning process.
Reprinted from M. Afshari, A. Gupta, D. Jung, R. Kotek, A.E. Tonelli, N. Vasanthan, Properties of films and fibers obtained from Lewis acid–base complexed nylon 6,6, Polym. J. 49 (2008) 1297–1304 with permission of Elsevier.

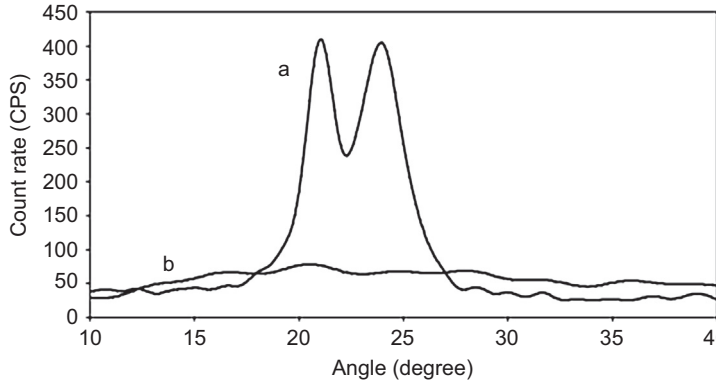

Figure 9.17 Equatorial X-ray scans of (a) decomplexed and drawn nylon-66 filament and (b) nylon-66/$GaCl_3$ complexed filament.
Reprinted from M. Afshari, A. Gupta, D. Jung, R. Kotek, A.E. Tonelli, N. Vasanthan, Properties of films and fibers obtained from Lewis acid−base complexed nylon 6,6, Polym. J. 49 (2008) 1297−1304 with permission of Elsevier.

of $CaCl_2$−PA-6. The fibers were collected at a very low take-up speed of 2−20 m/min. The fibers were stretched at two stages: the first drawing was on the complexed fibers at room temperature with a DR of 3−8, and the second drawing was after the removal of $CaCl_2$ and on the decomplexed fibers at a high temperature of 200°C. For the low MR of 0.15 $CaCl_2$, a low tenacity of 660 MPa, high modulus of 48 GPa, and strain at break of 17.3% were reported after a maximum total DR of 14.4.

Besides the plasticizers, inorganic nanoscale fillers such as nanotubes and clay can improve drawability and tensile strength of nylon-6 fibers. These nanofillers with high specific surface area can act as effective nucleation agents during the crystallization process, and reduce the amount and perfection of the crystals inside the fiber. In this way, polymer chains become more mobile, can be more easily unfolded and pulled out from the crystal, and the DR can be increased [72,73]. The effect of nanoclay on the tensile strength and DR of nylon-6 composite fiber has been studied by some authors. For example, Yeh et al. [73] investigated the influence of nylon-6 clay resin contents and drawing temperature on the drawability and tenacity of melt-spun nylon-6/nylon-6 clay composite fiber. A maximum DR of 7.5 and tenacity of 5.8 g/d were obtained for the 0.5 wt% optimum content (ie, nylon-$6_{0.95}$/nylon-6 $clay_{0.05}$) and 120°C drawing temperature. Similar results were reported by Tsai et al. [72] for the effect of another nanoclay (ie, attaplugite) on the tensile properties of melt-spun composite nylon-6 filaments.

9.2.7 Liquid isothermal bath

LIB is a modified version of the single-step melt-spinning process, in which a liquid bath is used between spinneret and take-up roller [27] (Fig. 9.18). The liquid provides several additional controllable processing variables (eg, temperature, tension, and time) in the spinning line to modify the tensile properties of the fibers. The liquid temperature is about 30−40°C higher than the polymer T_g, to provide enough

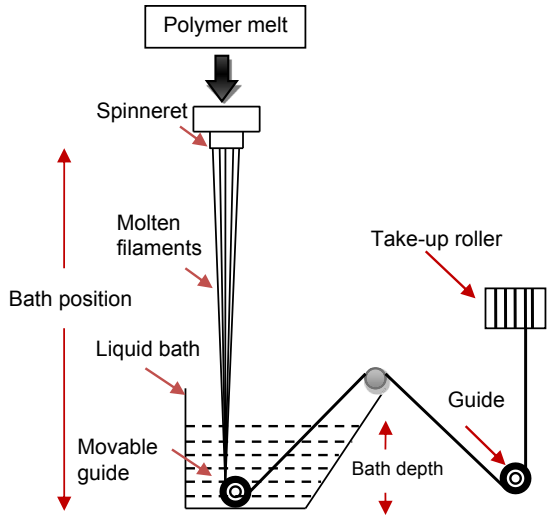

Figure 9.18 Horizontal isothermal bath process
Adapted from M. Najafi, H. Avci, R. Kotek, High-performance filaments by melt spinning low viscosity nylon 6 using horizontal isothermal bath process, Polym. Eng. Sci. 47 (2015) 21–25 with permission of Wiley.

mobility for the chains to be oriented. When the thread line enters the bath at high speeds (>1000 m/min), the polymer chains experience a combined effect of high tension and constant temperature ($>T_g$) for a longer time in the mobile molten state. In this way, crystal formation is delayed and the polymer molecules have an opportunity to be more thoroughly extended, oriented, and ordered in the fiber. Note that there are several forms of the liquid bath method, which basically work in the same way. In the last design the bath is used horizontally (ie, horizontal "liquid" isothermal bath [HIB] method [74]) between the winder and spinneret to make the fiber production industrially feasible (Fig. 9.18) [10].

The superiority of the liquid bath method over other melt-spinning techniques can be explained by molecular orientation and crystal formation. In conventional melt spinning and drawing, the crystals usually have a lower degree of molecular orientation, since crystal formation is affected by the poor mobility of the polymer chains in the solid state [20]. Also in high-speed spinning, rapid crystallization among polymer chains can reduce chain mobility, and prevent further molecular orientation, which affects the mechanical properties of fibers. These challenges can be addressed well in the HIB method as the liquid drag uniformly increases the overall orientation of the fiber at first; and then, under a low DR, the maximum crystallinity can be achieved through transformation of the oriented amorphous region [49].

The liquid bath technique has already been applied to several semicrystalline polymers (eg, PP [21,76], polyethylene naphthalate [77,78], PET [49,79–85], polytrimethylene terephthalate [86], PA-6 [75,87]), and fibers with tensile properties comparable to and even better than melt-spun yarns were produced. Table 9.1

Table 9.1 Tensile and structural properties of HIB and control (no HIB) filaments spun at 3000 m/min

Sample type	Tenacity (g/d)	Modulus (g/d)	Elongation (%)	X_c (%)	F_{OA}	f_c	f_a
Undrawn control	3.79 ± 0.33	10.26 ± 2.54	115.07 ± 13.20	15.55	0.42	0.97	0.37
Drawn control (draw ratio = 1.38)	4.48 ± 0.36	20.83 ± 3.37	38.45 ± 5.84	20.50	0.43	0.9862	0.50
Undrawn HIB	5.46 ± 0.53	17.33 ± 2.11	67.74 ± 17.92	25.90	0.70	0.9837	0.54
Drawn HIB (draw ratio = 1.38)	10.02 ± 0.53	43.88 ± 9.35	26.93 ± 2.48	34.74	0.56	0.9849	0.58

Adapted from M. Najafi, H. Avci, R. Kotek, High-performance filaments by melt spinning low viscosity nylon 6 using horizontal isothermal bath process, Polym. Eng. Sci. 47 (2015) 21−25 with permission of Wiley.

displays the structural and tensile characteristics of HIB nylon-6 fiber before and after the drawing process. Based on the table, the liquid increased the tenacity up to 5.46 g/d by c. 44%, modulus up to 17.33 g/d by ca. 69%, and reduced elongation up to 67.74% by c. 41%. Such modification was obtained only through entering the yarn in a warm ($T = 88°C$) liquid bath for a few milliseconds. After hot drawing at 165°C the tenacity increased from 5.46 to 10.02 g/d by c. 84%, the modulus increased from 17.13 to 43.88 g/d by c. 154%, and the elongation decreased from 67.74 to 26.93 by c. 60%. Such significant tensile results were obtained at a low number average molecular weight (Mn ~23,000 D) of the polymer and very low DR of 1.38, which otherwise would require a much higher M_n polymer and multistage stretching with a higher DR (5−6) in traditional melt spinning and drawing.

The HIB nylon fibers also show interesting orientation and crystallinity results as shown in Table 9.1. The HIB increased considerably the amorphous isotropy (F_{OA}) from 0.42 to 0.7 by 66.6%, and increased the crystallinity (X_c) from 15.55% to 25.9% by 66.55%. Also such treatment raised magnificently the amorphous orientation factor (f_a) from 0.37 to 0.54 by 46%. This is because of the high temperature and frictional drag of the liquid. In fact, as the liquid temperature (88°C) is higher than the polymer T_g, the chains in the amorphous phase are mobile enough to become more oriented and crystallized under the high frictional drag of the liquid. The H-bonding between the amide groups in the chains also promotes crystallization inside the filament. Table 9.1 also shows the influence of the drawing (DR: 1.38) on the structural parameters of the fibers. For HIB fiber, the drawing reduced the F_{OA} to 0.56 while increasing further the X_c and f_a up to 34.74% and 0.58, respectively. Such decrease in the F_{OA} was attributed to the transformation of the oriented amorphous phase to the crystalline region during the drawing [75].

One of the important aspects of the HIB method is the specific precursor developed into the fibers [21]. Fig. 9.19 displays the morphology of the drawn HIB and control (no HIB) filaments. As it can be observed, the control fiber has a nonuniform voided structure, which can be developed further to crazes or cracks, significantly deteriorating the fiber's performance. Also the appearance of a compact fibrillar structure in the drawn HIB fiber can be clearly seen in Fig. 9.19. The compact morphology can provide substantial surface area for the load transfer from the surface to the center of the fiber, contributing considerably to the fiber tensile performance. Such a specific precursor with high crystallinity and high molecular orientations is credible for superior tensile properties of the drawn HIB fiber [75].

9.2.8 SymTTec

As mentioned earlier, the polymer melt in the spinning process goes through a sequence of steps to become filaments/yarns. In each step the macromolecules experience certain tensions and temperatures, the timing and quality of which determine the quality of the subsequent steps and final product. In fact, poor control of such parameters can increase nonuniformity in fiber structure and result in low tensile performance. In this regard, high-tenacity and high-modulus filaments can be obtained by better tension, temperature, and time control in various parts of the spinning line. This is the concept behind SymTTec; the new spin−draw process designed by the

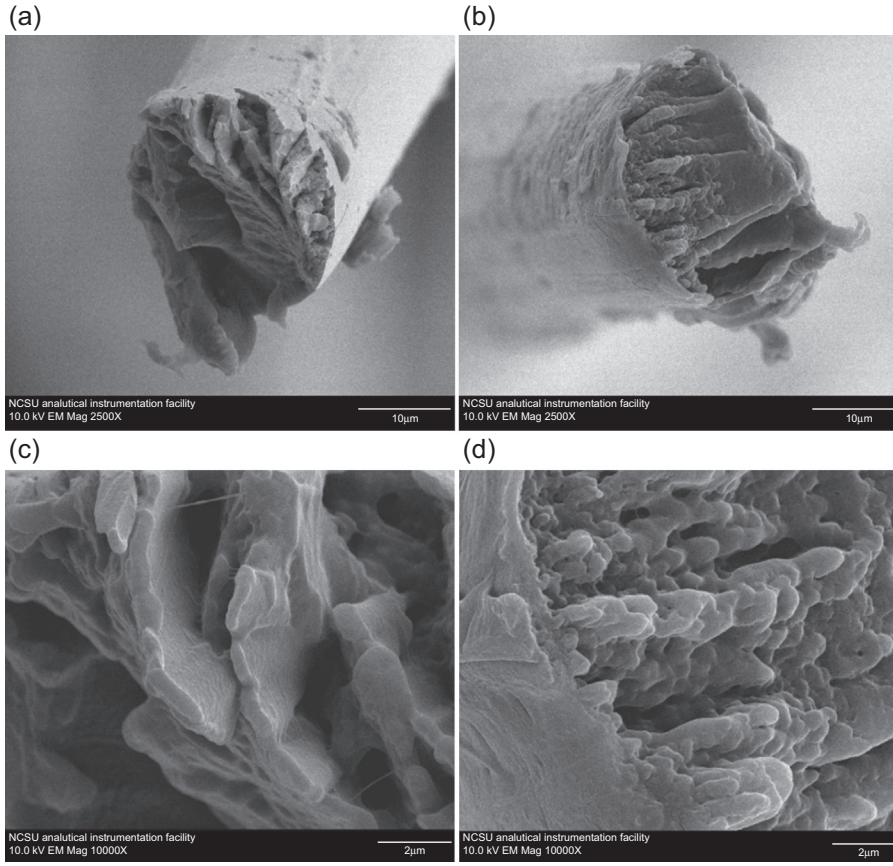

Figure 9.19 Cross-sectional view of the drawn control and HIB nylon-6 filaments (draw ratio = 1.38) at two different magnifications (up: 2500×, 10 μm scale; down: 10,000×, 2 μm scale): drawn control (a, c), and drawn HIB (b, d).
Adapted from M. Najafi, H. Avci, R. Kotek, High-performance filaments by melt spinning low viscosity nylon 6 using horizontal isothermal bath process, Polym. Eng. Sci. 47 (2015) 21−25 with permission of Wiley.

SwissTex Company in 2008. SymTTec or total symmetry is an innovative extrusion method for the production of high-performance polyamide and polyester yarns. In this technology, the design and/or control of all single process-relevant components of the spinning line are modified to create total symmetry in the different parts of the spinning process (Fig. 9.20). Such symmetry improves the homogeneity of melt distribution and the uniformity of individual filaments, and results in yarns with higher tensile performance. Fig. 9.21 compares the tensile results of the SwissTex yarns with some commercial technical nylon-6 yarns [28]. SymTTech increased the tenacity to the high value of 90 cN/tex (10.17 g/d) and reduced the elongation at break below 12%, leading to unique yarn quality, superior to the commercial products.

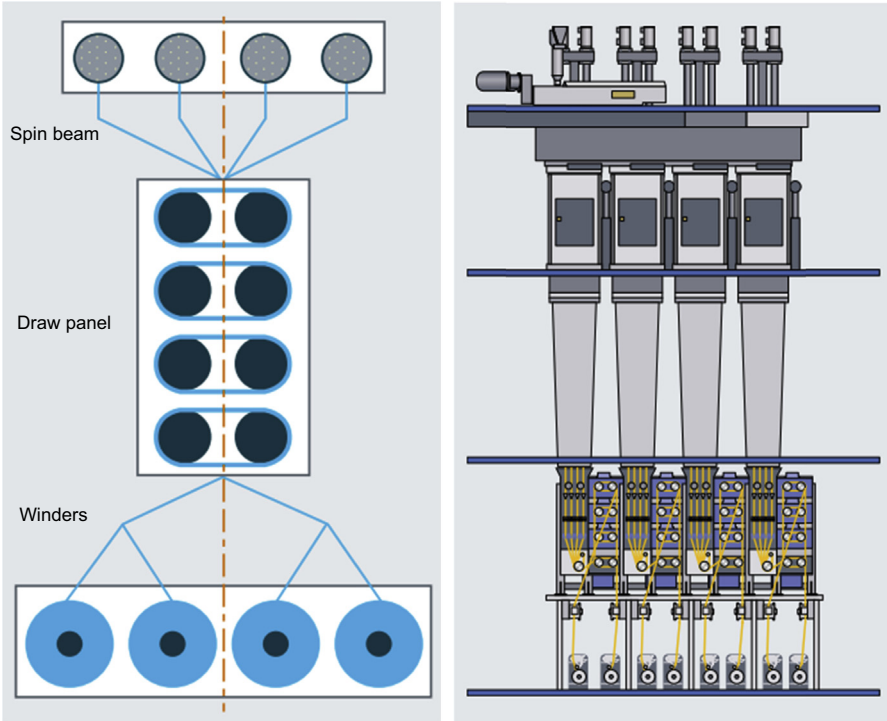

Figure 9.20 Scheme of total symmetry (*left*) and its layout with four positions and 16 ends (*right*).
Reprinted from Swiss Tex, symTTec Technical Yarn Extrusion System, 2008. [Online]. Available: http://www.primetex-technology.com/symttec.pdf and Truetzchler, Man-made Fibers. [Online]. Available: http://www.truetzschler-manmadefibers.com/fileadmin/user_upload/truetzschler-nonwovens/brochures_downloads/man-made-fibers/englisch/MMF_EN.pdf with permission of Truetzschler.

In SymTTec, special focus was given to melt creation and extrusion. It is said that the quality of polymer chips determines the quality of the yarn. Thus SwissTex developed its own conditioning, supply, and dosing systems for the chips. For technical yarns, heat stabilizers or pigments may be added to the chips. The gravimetric dosing system (Fig. 9.22) is used for polymer feeding as it provides exact and constant delivery of the chips into the extruder. The design of the extruder is also modified specifically for high-viscosity polymer to ensure perfect melt quality and increase chain drawability during the spinning process. This is achieved through several modifications in the extrusion system. The geometry/shape of the extruder screw is modified individually for each polymer/project. Moreover, the last four heating zones are cooled by air to modify the regulation time. Also the extruder is equipped with a batch of sensors and control software to provide precise and rapid adjustment of temperature and other control parameters. Besides that, the spin pack is improved to increase the uniformity between the individual filaments. The spin pack components such as

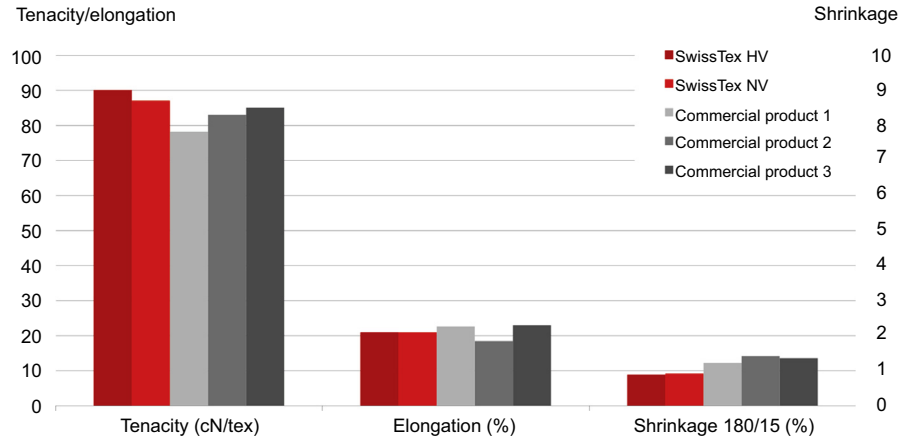

Figure 9.21 Tensile properties of SwissTex and commercial nylon-6 yarns. HV and NV are related to high and normal PA-6 viscosities, respectively.
Reprinted from Swiss Tex, symTTec Technical Yarn Extrusion System, 2008. [Online]. Available: http://www.primetex-technology.com/symttec.pdf with permission of Truetzschler.

Figure 9.22 Extruder with gravimetric dosing system in SymTTec.
Reprinted from Truetzchler, Man-made Fibers. [Online]. Available: http://www.truetzschler-manmadefibers.com/fileadmin/user_upload/truetzschler-nonwovens/brochures_downloads/man-made-fibers/englisch/MMF_EN.pdf with permission of Truetzschler.

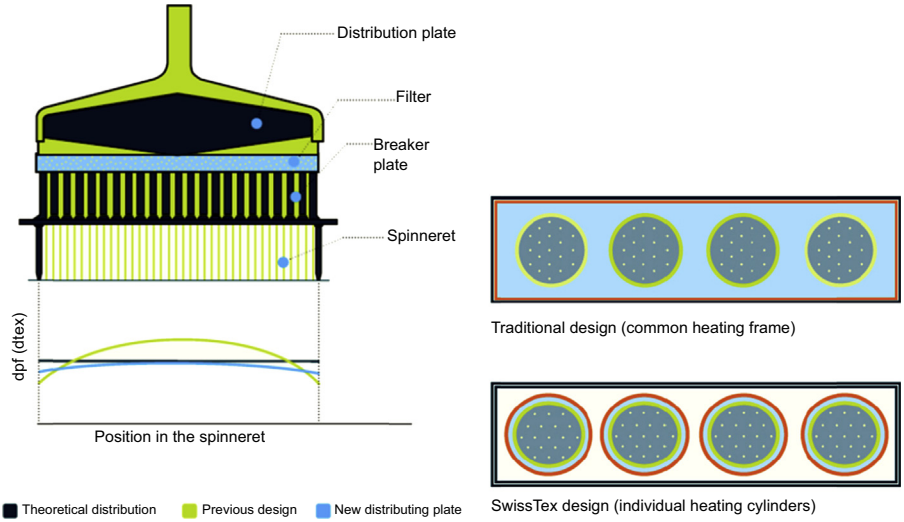

Figure 9.23 *Left*: New designed spin packs for high polymer melt quality in SymTTec. *Right*: Individual annealers for excellent thermal treatment of filaments bundles.
Reprinted from Swiss Tex, symTTec Technical Yarn Extrusion System, 2008. [Online]. Available: http://www.primetex-technology.com/symttec.pdf with permission of Truetzschler.

distribution plate and filters are redesigned to ensure perfect melt distribution, high filtration capability, and high filament regularity (Fig. 9.23). All filaments experience the same mechanical and thermal treatments thanks to the pressure vessel installed in the spinning line. These modifications increase fiber homogeneity and result in higher tensile performance in the final yarn [28,88].

The drawing and quenching steps are also improved in the SymTTec technology. It can be said that the rapid crystal formation and the high fiber friction are two main problems of yarn breakage in polyamides spinning. The crystals act like crosslinking between the chains limiting their movement and fiber stretching. To delay the crystallization the filament temperature and cooling need to be controlled precisely. To obtain this, individual heating cylinders or annealers are installed for each filament bundle to provide excellent thermal treatment and increase the filament uniformity (Fig. 9.23). In this way the filament temperature remains close to the melt temperature in the spin pack, providing more chain mobility and higher fiber drawability. Also quench air parameters such as temperature, relative humidity, and velocity are monitored exactly to control crystal formation in the filaments. To avoid air turbulence and increase filament stability during the filament cooling, holes distribution in the spinnerets, quench unit, and interfloor tubes is modeled and simulated as a complete system. Also the interfloor tubes are redesigned to optimize the air flow and eliminate any turbulence during filament quenching (Fig. 9.24). Besides the crystallization the high friction between the filaments and other surfaces needs to be controlled to reduce the yarn breakage. This is obtained through better designing of spinning line, drawing panels, and winders. Fig. 9.20 displays a scheme of the traveling route

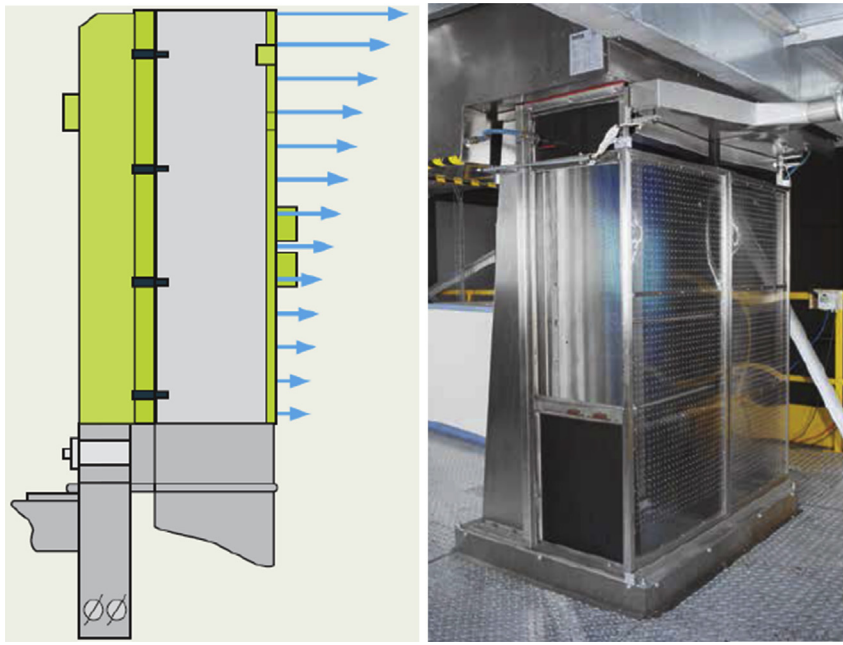

Figure 9.24 Air turbulence-free quench system in SymTTec. The interfloor tube is no longer a passive system, as it can have a considerable effect on yarn cooling.
Reprinted from Swiss Tex, symTTec Technical Yarn Extrusion System, 2008. [Online]. Available: http://www.primetex-technology.com/symttec.pdf with permission of Truetzschler.

of the filaments from the spinneret to the winders in SymTTec. The new design of spinning line lets the yarn to move in a very straight path with limited friction points. The special finish applicator and the large inlet used at the draw panel also reduce the friction and angle of the fibers at the panel inlet, minimizing the probability of yarn breakage during the spinning process [28,88,89].

Winders and draw rolls are among the most technological advancements in SymTTech. The extrusion system is equipped with two winders, each with two ends (Figs. 9.20 and 9.25) to ensure symmetrical geometry for winding. No quality difference between rear, middle, and front yarn packages can be measured. Moreover, drawing panel with one feed roll and four dual shell draw rolls (ie, RIEVAP draw roll; Fig. 9.26) are designed for high-tenacity nylon yarns (Fig. 9.25). The surfaces of the rolls are plasma coated to increase both their lifetime and constant quality over a long production period. Furthermore, the high surface quality of the rolls avoids any surface defects on the yarn and increases the tensile performance. The RIEVAP rollers can also transfer the heat to all filaments in the same way providing consistent yarn quality during drawing. The mechanism of heat transfer in the RIEVAP is based on the heat pipe principle. Fig. 9.27 displays the heat pipe mechanism for a dual shell filled with liquid. Heat pipes are highly efficient for heat conduction between two interfaces, because of high heat transfer coefficient of the liquid for boiling and

Figure 9.25 Draw rolls with five duos.
Reprinted from Swiss Tex, symTTec Technical Yarn Extrusion System, 2008. [Online]. Available: http://www.primetex-technology.com/symttec.pdf with permission of Truetzschler.

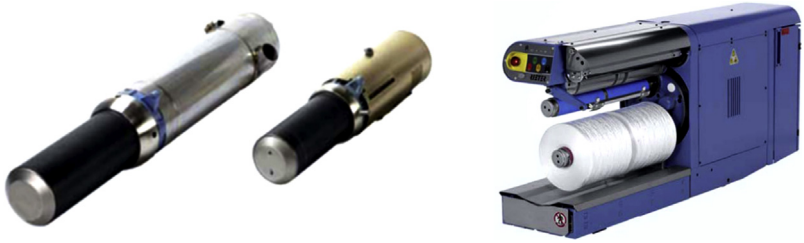

Figure 9.26 RIEVAP dual shell draw rolls (*left*) and high-speed winder (*right*) used in SymTTech.
Reprinted from Swiss Tex, symTTec Technical Yarn Extrusion System, 2008. [Online]. Available: http://www.primetex-technology.com/symttec.pdf with permission of Truetzschler.

condensation. As Fig. 9.27 shows, the liquid is heated and vaporized by induction heating and travels along the heat pipe to the surface of the draw rolls. When the cold filaments reach the roller surface, the vapor condenses back into liquid and returns to hotter areas where it vaporizes again. Such heat transfer system provides an absolutely flat temperature profile over the heated length (Fig. 9.27), and reduces significantly the heat-up time of the rollers and respond time to load changes, ensuring uniform yarn quality [28,88,89].

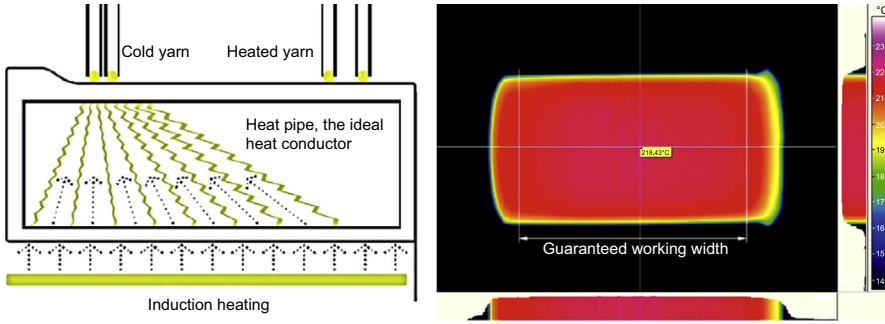

Figure 9.27 Heat pipe mechanism (*left*) and exceptional uniform temperature profile over the heated length (*right*) in the RIEVAP draw roll.
Reprinted from Swiss Tex, RIEVAP-dual Shell Draw Rolls, 2008. [Online]. Available: http://www.primetex-technology.com/drawrolls.pdf with permission of Truetzschler.

9.3 Structure and properties of high-performance nylon fibers

9.3.1 Fiber structure

Fiber morphology plays an important role in tensile properties of high-performance yarns. When fiber deforms under load, various structural units and parameters affect the mechanics of load transfer from the fiber surface to the center. Crystallinity, crystal size and species, molecular orientation, and amorphous structures are among the most important elements affecting fiber tenacity, modulus, and elongation at break [90]. Technical yarns generally have high crystallinity, large crystal size, and high molecular orientation in both crystalline and amorphous phases. To engineer textile yarn for industrial applications, the micro- and nanostructures of fibers need to be identified and modified. In this part, various structural elements of nylon fibers are described in detail, and the way they contribute to the tensile characteristics will be explained.

Industrial nylon yarns are generally produced by melt spinning and drawing. The elongational flow in melt spinning and the plastic deformation during drawing instill microfibrillar morphology inside the fibers [9]. Several models have been made for identifying various structural and morphological features of PA fibers. Perhaps the best illustration for many practical purposes is hierarchical fiber structure proposed by Murthy et al. for nylon-6 (Fig. 9.28) [91]. The model comprises three different phases, namely, crystalline, unoriented (isotropic) amorphous, and oriented (anisotropic) amorphous domains. In the crystalline region there are crystallites, generally in sizes of 5−20 nm in all directions. The crystallites are also called lamellae, as under ideal conditions (eg, crystallization from solution) they can form thin lamella sheets, 5−20 nm thick but only micrometers in width. Inside each lamella the polymer chains are folded back and forth on themselves across the thickness of the platelet [31,92]. The lamellae are connected together by tie molecules inside the interlamellar amorphous region (Figs. 9.28 and 9.29). Tie molecules result from chain unfolding during

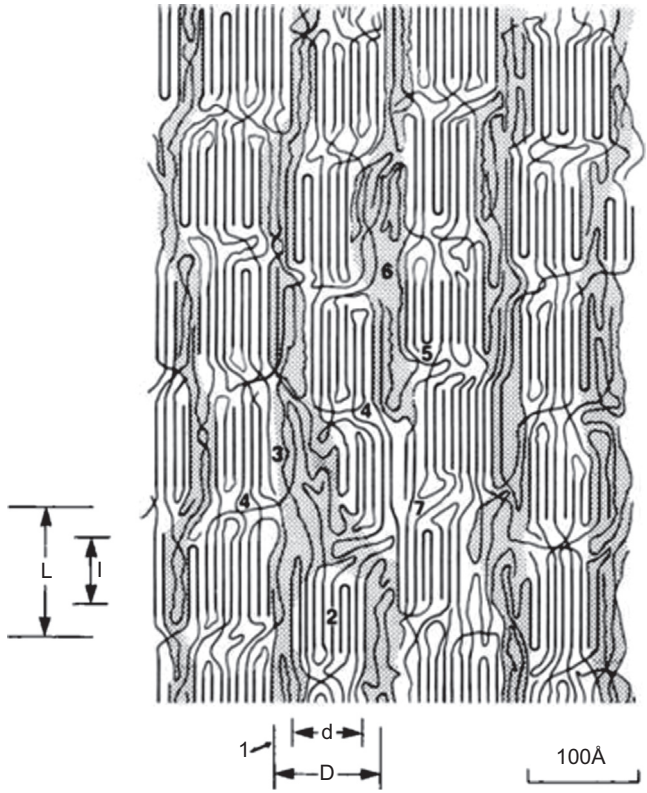

Figure 9.28 Morphological model for nylon-6 fiber: 1—fibril, 2—crystallites, 3—partially extended molecules in the interfibrillar regions, 4—tie molecules in the interlamellar amorphous region, 5—free chain ends, 6—voids and interfibrillar amorphous region.
Reprinted from N.S. Murthy, A.C. Reimschuessel, V. Kramer, Changes in void content and free volume in fibers during heat setting and their influence on dye diffusion and mechanical properties, J. Appl. Polym. Sci. 40 (1990) 249−262 with permission of Wiley.

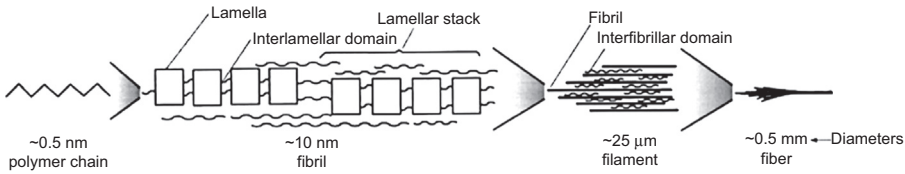

Figure 9.29 Schematic of nylon-6 fiber structure at various scales.
Reprinted from N.S. Murthy, D.T. Grubb, Deformation of lamellar structures: simultaneous small- and wide-angle X-ray scattering studies of polyamide-6, J. Polym. Sci. Part B Polym. Phys. 40 (2002) 691−705 with permission of Wiley.

the drawing process, and their strength and length affect significantly the filament breakage. Under uniaxial stress, the lamellar stacks are lined up along the fiber axis and form a fibril, the strain and modulus of which are the same as those of a fiber (Fig. 9.29). The space between the fibrils is filled by microvoids and interfibrillar amorphous chains. The microvoids are often said to be the initiation of fiber tensile failure. They can be further developed and transformed into cracks, and cause filament breakage [31,92,93].

9.3.1.1 Amorphous structure

The amorphous region in nylon fibers comprises two different phases: oriented amorphous (anisotropic) and unoriented amorphous (isotropic) domains. The oriented components are primarily in the interfibrillar region and the unoriented components are mainly in the interlamellar region (Fig. 9.29) [94]. These amorphous phases are different in packing density and interchain structure. The chain segments inside the oriented amorphous region are more densely packed and their interchain interactions are more like crystals, whereas such interactions for the unoriented amorphous region are similar to the polymer melt [95]. Such structural disparity leads the two amorphous domains to respond differently in processing (ie, drawing and heat setting) and environmental conditions (ie, humidity and temperature). The unoriented components can have a greater influence on dye/moisture diffusion rate than oriented amorphous components, as polymer chains in the unoriented phase can undergo larger changes [96].

9.3.1.2 Crystal structure

The crystal structure of nylons results from the conformation and lateral packing of the macromolecules. Generally, the polyamide chains are packed in such a way that all possible hydrogen bonds in various crystal forms are fully satisfied. To achieve this, the chains adopt either fully extended or slightly twisted configuration, minimizing the occupied volume and the potential energy of the crystal structure, while maintaining appropriate distances between the adjacent chain segments for intermolecular interactions. In polyamides, such interactions include H-bonding and van der Waals' forces that affect the organization of the chains inside the crystal. The H-bonding between the NH and CO moieties in adjacent chains form two-dimensional sheet-like arrangements. These H-bonded sheets that are held together inside a three-dimensional lattice by van der Waals' forces construct the main feature of nylon's crystal structure. Monoclinic, triclinic, and rhombic lattices are the three well-known unit cells for nylon's crystal system. The size and shape of the unit cells are determined by stacking of H-bonded sheets inside the crystal [1,11].

Several crystal structures have been identified for nylons. Among them, α and γ are the two main crystal forms and the others (ie, β, δ, λ, smectic, and metastable phases) can be considered as the various qualifiers of these. The two crystal forms are structurally different in chain direction and conformation. In α form the chains are in antiparallel alignment with fully extended zigzag conformation, whereas in γ

form, the chains are in parallel alignment with twisted helical configuration [92]. The interactions between the chains are not the same in two crystal forms. In γ phase the kink structure enables amide groups to form H-bonding both within and between the molecular sheets, whereas in α phase, H-bonding is exclusively formed inside the molecular sheets [1,4,11]. Formation of α and γ crystals depends on the number of CH_2 groups between the amide moieties in the Polyamide structure. Even in nylons with longer CH_2 groups (PA-8, PA-10, and PA-12) γ is the stable form, and even in nylons with shorter CH_2 groups (PA-4 and PA-6) α is the stable form. Moreover, nylons with odd−odd, odd−even, and even−odd numbers crystallize primarily in the γ form. Fig. 9.30 shows the crystal structures of PA-6 and PA-66. PA-6 can be crystallized in both α and γ phases. However, PA-66 has no γ phase as it has a centrosymmetric structure and no chain directionality [90,92]. The most stable crystalline structure in both nylons is the α form, although their structures are not exactly the same. In nylon-66, the unit cell has a triclinic structure, whereas in nylon-6, α phase has a monoclinic structure.

The α and γ crystal forms have their own physical and mechanical properties and can appear in fiber based on spinning conditions and specific treatments. Table 9.2 compares some physical properties of the two crystal forms for PA-6. α is thermodynamically more stable, whereas γ is kinetically more stable. Also the modulus, density, and melting point of α are higher than those of γ [97]. α can be formed by slow crystallization from the melt or by a solvent, and γ can be produced by rapid crystallization. Both crystal forms can exist inside fiber, although their amount can be affected by spinning conditions. Fibers produced by conventional melt spinning at moderate wind-up speed comprises both α and γ forms. However, filaments obtained at higher take-up speed (>3000 m/min) have mainly γ phase in their crystalline structure because of orientation-induced crystallization. The two crystal forms can be converted together by applying specific treatments on fiber. γ can be transformed to α by heat, strain, or water, and α can be converted to γ by iodine treatment. It was reported that annealing nylon-6 fiber at temperatures >100°C in the presence of moisture can result in γ to α transformation. Also drawing the fiber at high temperature and draw ratio can break H-bonding between the sheets inside γ and lead to α formation [7,90,92,102].

9.3.1.3 Characterization

The fiber structure of nylons can be characterized by the wide angle X-ray diffraction method. Fig. 9.31 shows a typical X-ray intensity versus Bragg angle ($I - 2\theta$) at an equatorial direction for a nylon-6 fiber having both α and γ crystals. The amorphous scattering and crystalline planes can be identified by resolving the plot to various peaks and a halo using peak position parameters such as peak width and peak positions. For example, the two peaks at $2\theta = 20.4$ and 23.60 degrees are for the α(200) and α(002/202) crystalline peaks, that is, α_1 and α_2, and the two peaks at $2\theta = 21.65$ and 23.15 degrees are related to γ(001) and γ(200/201) crystalline peaks, that is, γ_1 and γ_2, and a broad halo centered at 22.15 degrees is associated with the amorphous phase reflection. To determine the crystalline and amorphous parameters, a baseline is created from the first and last points of the plot. The baseline and the deconvoluted

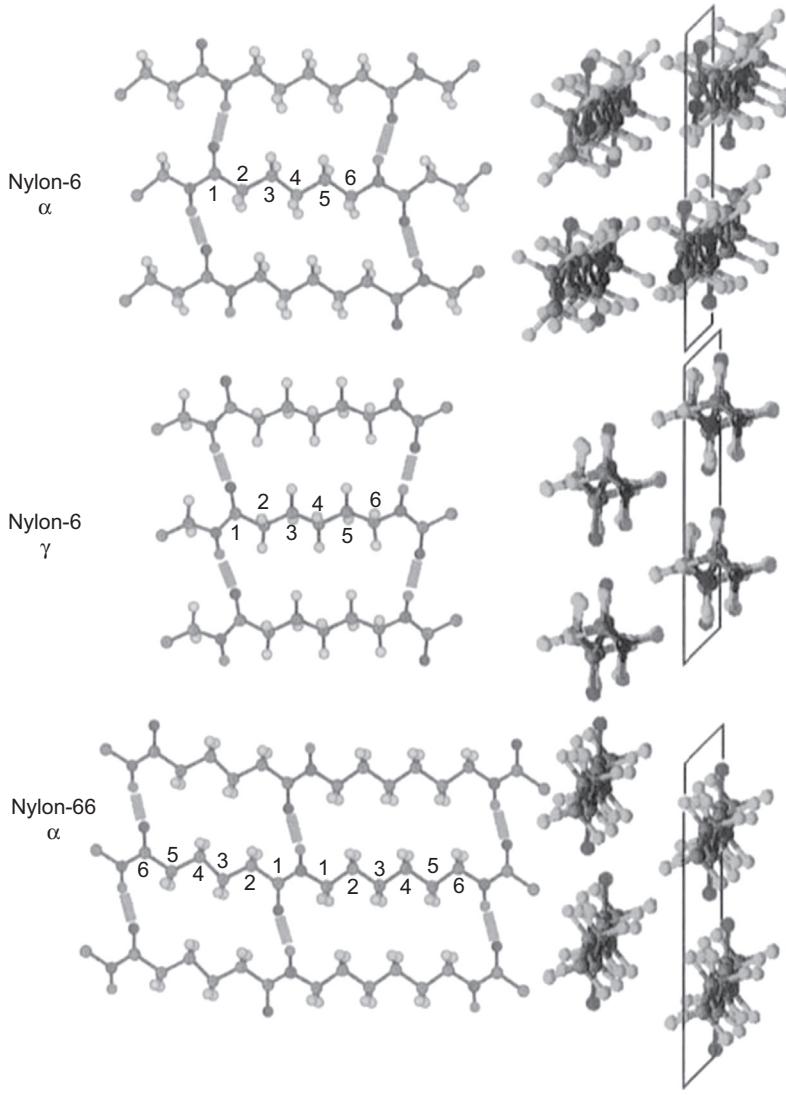

Figure 9.30 Structures of α and γ crystals for nylon-6 and nylon-66.
Reprinted from S. Dasgupta, W.B. Hammond, W.A. Goddard, Crystal structures and properties of nylon polymers from theory, J. Am. Chem. Soc. 118 (1996), 12291−12301 with permission of ACS.

peaks divide the XRD plot into three different regions related to the crystalline, oriented, and unoriented amorphous phases (Fig. 9.31). Fiber crystallinity is determined from the ratio of the areas of the crystalline reflections to the total areas of the scattering curve. Amorphous isotropy is the proportion of the amorphous phases that are preferentially oriented [103]. The crystallinity (X_c) and amorphous isotropy

Table 9.2 Comparison of some physical and structural characteristics of α and γ forms for nylon-6 fiber

Property	α	γ	References
Crystal structure	Monoclinic	Monoclinic	[89]
Lattice constants	$a = 9.56$ Å $b = 17.24$ Å $c = 8.01$ Å $\beta = 67.5$ degrees	$a = 9.56$ Å $b = 15.8-16$ Å $c = 16.88$ Å $\beta = 121$ degrees	[28,94]
Crystallographic reflections	(200), (002/202)	(001), (200/20$\bar{1}$)	[28,95,96]
Density, ρ (g/cm^3)	1.23 (experimental) 1.23 (calculated)	1.16−1.19 (experimental) 1.16 (calculated)	[94]
Heat of fusion, ΔH_f° (g/cm^3)	241	239	[94]
Melting point (°C)	220−221	210−217[a]	[97,98]
Modulus (GPa)	295	135	[99]

[a]The melting points of crystal phases depend on the melt-spinning speed.
Adapted from T.D. Fornes, D.R. Paul, Crystallization behavior of nylon 6 nanocomposites, Polym. J. 44 (2003) 3945−3961 with permission of Elsevier.

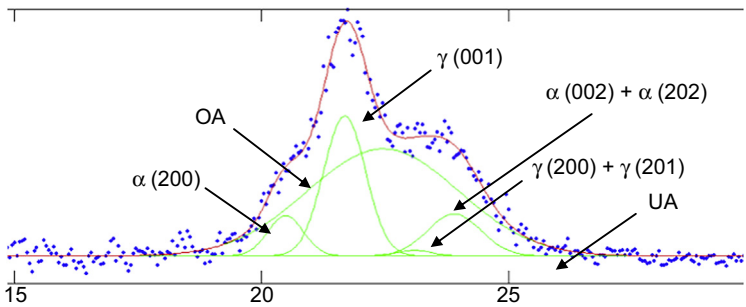

Figure 9.31 Deconvolution of X-ray intensity versus Bragg angle ($I - 2\theta$) plot into crystalline, oriented amorphous (OA) and unoriented amorphous (UA) components for nylon-6 fiber. Adapted from M. Najafi, H. Avci, R. Kotek, High-performance filaments by melt spinning low viscosity nylon 6 using horizontal isothermal bath process, Polym. Eng. Sci. 47 (2015) 21−25 with permission of Wiley.

(F_{OA}) of the samples are calculated from the equatorial X-ray scan by the following equations:

$$X_c = \frac{A(C)}{A(C) + A(OA) + A(IA)} \times 100\% \tag{9.1}$$

$$F_{OA} = \frac{A(OA)}{A(OA) + A(IA)} \tag{9.2}$$

where $A(C)$, $A(OA)$, and $A(IA)$ are the areas of the crystalline, oriented amorphous (ie, halo above the baseline), and isotropic amorphous domain (ie, region under the baseline), respectively.

The apparent crystal sizes are calculated by the Scherrer equation:

$$ACS = \frac{0.9\lambda}{(\Delta 2\theta)\cos\theta} \tag{9.3}$$

where θ is half the value of the peak position, λ is the X-ray wavelength, and $(\Delta 2\theta)$ is the full-width at half-maximum (FWHM) of the crystalline peak in radians.

The crystalline orientation factor (f_c) is related to the orientation distribution of all crystal axes relative to the fiber axis (Fig. 9.32) [7]. It is a function of the angle between fiber axis and specific crystal axis and can be determined using the Herman's function:

$$f_c = \left(3\left(\cos^2\varphi\right) - 1\right)/2 \tag{9.4}$$

where φ is the angle between the crystallographic axis and the fiber axis, $I(\varphi)$ is the azimuthal intensity distribution of the crystalline peaks, and $\Delta\varphi$ is FWHM of the $I - \varphi$ plot.

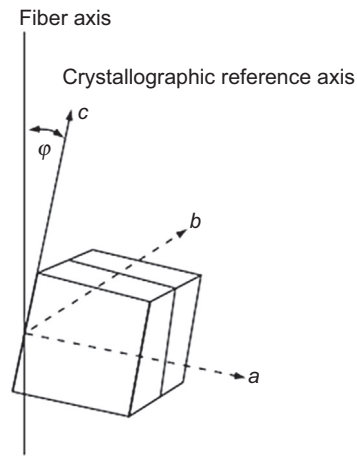

Figure 9.32 Crystal orientation with respect to the fiber axis.
Reprinted from H.H. Yan, Polyamide fibers, in M. Lewin, (Ed.), Handbook of Fiber Chemistry, third ed., CRC/Taylor & Francis, Boca Raton, 2007, pp. 31−138 with permission of CRC Press.

The amorphous orientation function (f_a) is calculated by the well-known Stein and Norris equation (Eq. (9.5)) in which the crystalline orientation is subtracted from birefringence of the fiber [21,98]:

$$f_a = \frac{\Delta n - \chi f_c \Delta n_c^{\circ}}{(1-\chi)\Delta n_a^{\circ}} \tag{9.5}$$

where χ is the fraction of crystallinity obtained by XRD, Δn is the birefringence determined by a polarizing microscope, and Δn_a° and Δn_c° are intrinsic birefringence of the amorphous and crystalline regions [103].

9.3.2 Fiber properties

Fiber properties of technical nylons are determined by the molecular structure and molecular organization. The molecular structure of the nylons comprises the amide (peptide) linkage (NH—CO) and the methylene groups (CH_2). The amide groups can make strong H-bonding between the chains inside the fiber. Such strong H-bonds can give the nylon fiber high strength at high temperatures, toughness at low temperatures, outstanding elasticity, high resiliency, as well as other properties such as stiffness, unique abrasion and wear resistance, low friction coefficient, and good chemical resistance [7—9]. The molecular organization of nylons is related to the arrangement of the polymer chains inside the fiber. Nylon is a flexible and thermoplastic polymer and thus it can be oriented and crystallized inside the fiber at elevated temperatures. The amorphous and crystalline domains are different in molecular orientation, chain mobility, chain packing, number of H-bonding, and interchain spaces. Such structural differences lead the amorphous and crystalline regions to respond differently to heat, chemicals, moisture, and load. Thus the fiber structure as well as the molecular structure can influence the tensile, thermal, and chemical properties of high-performance nylon fibers.

9.3.2.1 Tensile properties

Tensile or mechanical properties are the most important characteristics of nylon fibers. They indicate the behavior of the filaments to forces and deformations, and determine their suitability for a specific application [31]. The principal attributes of tensile properties for technical yarns are tensile strength (tenacity), Young's (initial) modulus, elongation (strain) at break, and shrinkage. Tenacity is the amount of the specific stress (Eq. (9.6)) required to break a fiber. Modulus is related to the initial response of a fiber to loading and equals the slop of the stress—strain curve at the initial point (Fig. 9.33) [104]. Elongation (strain) at break (Eq. (9.7)) is the amount of elongation necessary to break a filament. Shrinkage is the contraction/disorientation of the polymer chains during the heating process and indicates the dimensional stability of the fiber. These tensile characteristics depend on the fiber structure, polymer molecular mass, and thermal history [31]. Strength (tenacity) and stiffness (modulus) are related to molecular orientation and the number of chain

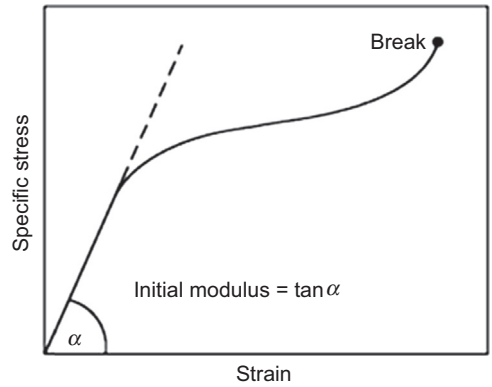

Figure 9.33 Schematic of stress−strain curve.
Adapted from J.W.S. Hearle and W.E. Morton, Tensile properties, In: Physical Properties of Textile Fibres, 4th ed., 2008, with permission of woodhead.

ends inside the fiber [11]. In addition, fiber/polymer shrinkage is associated with relaxation of the amorphous chains, crystalline reorganization, recrystallization, and melting of small crystals [92,103]. Crystal formation and molecular orientation in nylon fiber increase the tenacity and modulus and decrease the elongation (Fig. 9.34) and shrinkage.

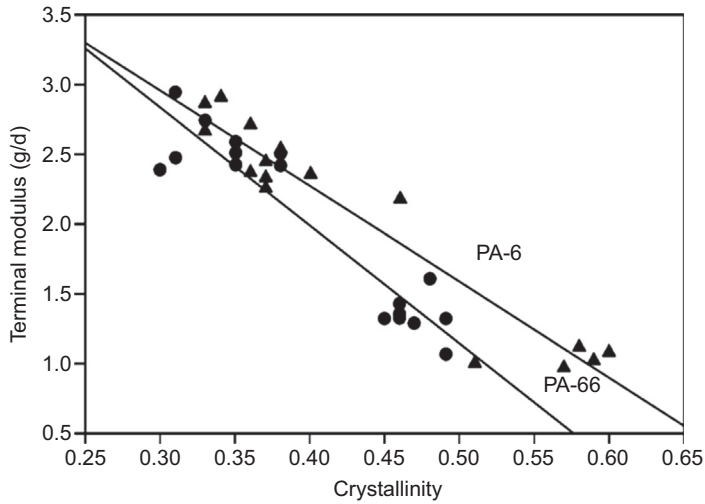

Figure 9.34 Elongation versus crystallinity for PA-6 and PA-66 fibers.
Reprinted from N. Vasanthan, Polyamide fiber formation: structure properties and characterization, in: M.J.S. Eichhorn, J.W.S. Hearle, (Eds.), Handbook of Textile Fibre Structure, first ed., Woodhead Publishing, 2009, pp. 232−252 with permission of Woodhead.

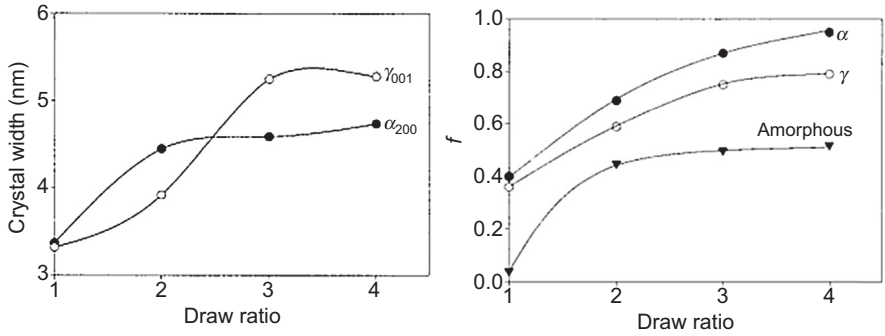

Figure 9.35 Effect of draw ratio on crystal size (*left*) and the orientation factors (*f*) of crystalline and amorphous regions for PA-6 fiber (*right*).
Reprinted from N. Vasanthan, Orientation and structure development in polyamide 6 fibers upon drawing, J. Polym. Sci. Part B Polym. Phys. 41 (2003) 2870−2877 with permission of Wiley.

$$\text{Specific stress(tenacity)} = \frac{\text{load}}{\frac{\text{mass}}{\text{unit length}}} \tag{9.6}$$

$$\text{Tensile strain} = \frac{\text{elongation}}{\text{initial length}} \tag{9.7}$$

High take-up speed and/or thermomechanical treatments used in the production of technical yarn induce crystallization and orientation inside the fibers. The high take-up stress can increase crystallinity, crystal size, and birefringence, whereas it can reduce the amorphous ratio in the nylon fiber [100]. Drawing increases crystal size, fraction, and orientation of the oriented amorphous and crystalline phases while reducing the ratio of the unoriented amorphous phase (Figs. 9.35 and 9.36) [103,107]. Also annealing (heat setting) can raise crystalline factors such as crystallinity, crystal size (Fig. 9.37), and crystalline orientations, although the treatment temperature can affect them [101,106,108]. Such high crystalline and amorphous parameters lead the technical nylon fiber to have high tenacity, high modulus, low elongation, and low shrinkage.

9.3.2.2 Thermal properties

The thermal properties of nylon fibers have a fundamental role in determining the manufacture conditions and product applications. The thermal behavior is affected considerably by the amide linkages in the polymer structure. The melting point (T_m) and glass transition temperature (T_g) of nylons are increased with the number of amide groups per polymer repeat unit (Fig. 9.38), although such increase is not always regular as the even or odd number of CH_2 groups between the NHCO groups can affect it [9,31]. Table 9.3 compares some of the thermal properties of nylon-6 and nylon-66 fibers. As it can be seen, PA-66 has higher T_m and T_g than PA-6 (Table 9.3). The thermal response of nylon fibers is also influenced by their crystalline and amorphous

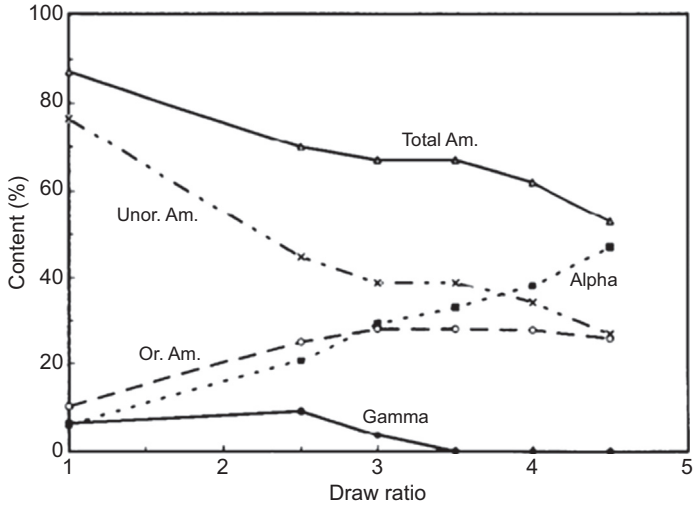

Figure 9.36 Variations of crystalline (alpha, gamma), unoriented amorphous (Unor. Am.), and oriented amorphous (Or. Am.) components upon drawing for nylon-6 fiber.
Reprinted from N.S. Murthy, R.G. Bray, S.T. Correale, R.A.F. Moore, Drawing and annealing of nylon-6 fibres: studies of crystal growth, orientation of amorphous and crystalline domains and their influence on properties, Polym. J. 36 (1995) 3863−3873 with permission of Elsevier.

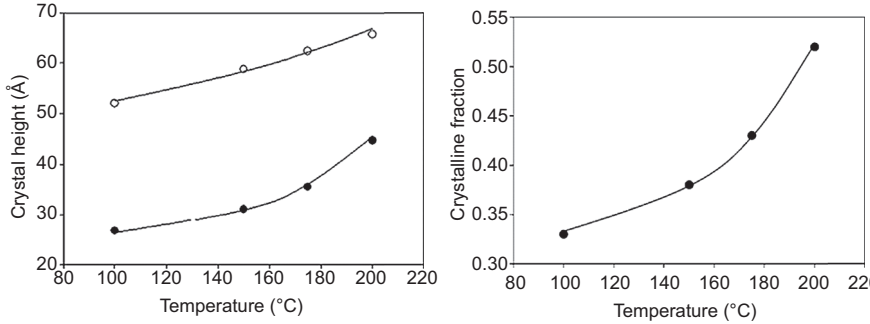

Figure 9.37 Effect of annealing temperature on the crystal size of α (●) and γ (○) (*left*) and crystalline fraction (crystallinity) for PA-6 fiber (*right*).
Reprinted from N. Vasanthan, Effect of the microstructure on the dye diffusion and mechanical properties of polyamide-6 fibers, J. Polym. Sci. Part B Polym. Phys. 45 (2006) 349−357 with permission of Wiley.

parameters. Higher crystallinity (Fig. 9.39), higher orientation (Fig. 9.39), and larger crystals can reduce the chain mobility and increase the T_g. The effect of the molecular orientation on the T_g for PA-6 fibers was examined by Murthy et al. [92,96]. The oriented amorphous phase was found to have a higher T_g (ie, $T_g \sim 80-90°C$) than the unoriented component (ie, $T_g \sim 30-50°C$) because of the high orientation and lower mobility of the chains in that region. HM-HT nylon fibers often have larger crystals,

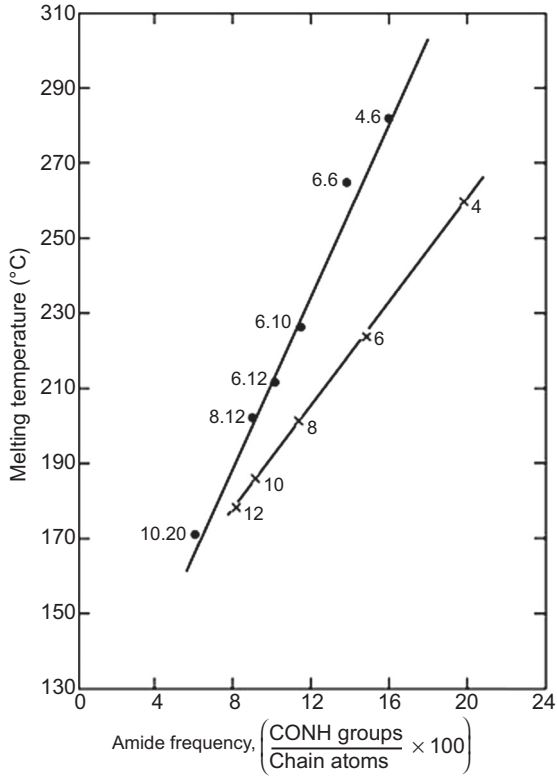

Figure 9.38 Effect of the frequency of amide groups on the melting point of polyamides. The numbers on the curves indicate the specific polyamide.
Reprinted from A. Anton, B.R. Baird, Polyamides, fibers, Encyclopedia Polym. Sci. Technol. 3 (2014) 584–618 with permission of Wiley.

Table 9.3 Thermal and moisture Properties of nylon-6 and nylon-66 fibers

Property	Nylon-6	Nylon-66	References
Melting point (°C)	215–220	255–260	[31]
Glass transition temperature (°C)[a]	45–75	60–80	[7]
Maximum setting temperature (°C)	190	225	[31]
Moisture regain at 21°C, 65% RH (%)	2.8–5.0	4.0–4.5	[2]

[a]The T_g depends on various parameters including moisture regain of the fiber.
Adapted from A.F. Richards, Nylon fibres, in: J.E. McIntyre (Ed.), Synthetic Fibres: Nylon, Polyester, Acrylic, Polyolefin, first ed., CRC Press; Woodhead Pub., Boca Raton, 2005, pp. 20–94 with permission of Woodhead.

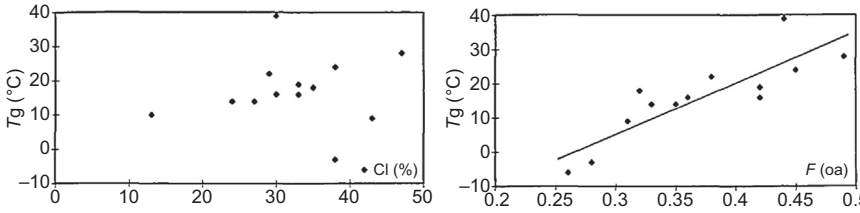

Figure 9.39 Changes of the T_g with crystallinity (*left*) and amorphous isotropy (F_{OA}) (*right*) for nylon-6 fiber.
Reprinted from N.S. Murthy, Fibrillar structure and its relevance to diffusion, shrinkage, and relaxation processes in nylon fibers, Text. Res. J. 67 (1997) 511−520 with permission of Sage.

higher crystalline, and higher amorphous orientations/fractions than the conventional nylon filaments, and thus reveal more resistance to thermal deformation at high temperatures.

9.3.2.3 Chemical properties

The chemical/degradation properties of technical nylon fibers are related to the reaction of the amide groups with acids, alkalis, alcohols, solvents, etc. The CH_2 groups are chemically inert, although the groups near to the NHCO may take part in certain reactions. PA-6 and PA-66 have good chemical resistance to most chemicals such as hydrocarbons, fats, and oils, but they can be degraded by strong alkalis, alcohols, and acids. Aqueous bases and acids hydrolyze nylons, whereas concentrated phenols and acids dissolve them. The amide group is also susceptible to heat, oxygen, light, and moisture [7,9]. The high temperature used in the melt-spinning process may disintegrate PAs to carbon dioxide, ammonia, and water products. Exposure of PA-6 and PA-66 to UV radiation over a long period of time can lead to photooxidative degradation and reduce strength. Nylon fibers are also partially hydrophilic in nature. The moisture content of nylons tends to decrease as the nylon number increases (Table 9.3). Moisture can make H-bonding between the PA chains increase the chain mobility and swell the fiber [7,9,31]. The moisture primarily diffuses in the amorphous regions. HM-HT nylon fibers have low moisture absorption because of their high orientation and crystallinity.

9.4 Applications of high-performance nylon fibers

In 2011, Technon OrbiChem published statistical data for world production of several fibers [109]. As Fig. 9.40 shows, the global production of polyamide fiber has been almost constant over the last 25 years, and it is projected to maintain its position based on technical end uses [109]. Also Fig. 9.41 displays the global production of PA filament by regions. Current production of nylon fiber is about 4 million tons and is expected to increase up to 4.8 million tons by 2025. There has been a reduction in nylon fiber production in North East Asia and East Europe, and the trend is projected to continue in the coming years. China is currently the world's largest

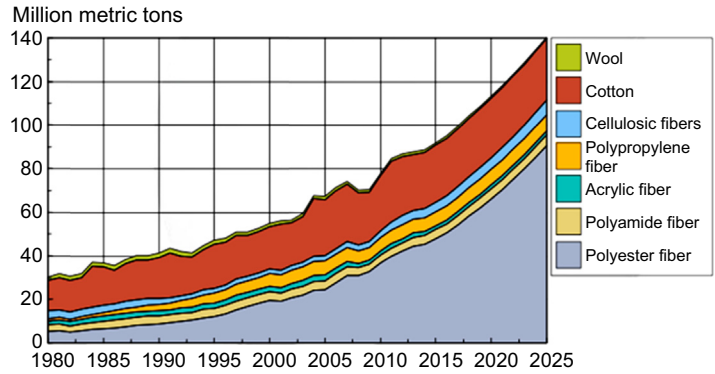

Figure 9.40 Worldwide fiber production 1980−2025.
Reprinted from R. Lee, Tecnon OrbiChem, Impact of crude oil and raw material price changes on world fibres markets, in: 12th International Polyester & Intermediates Forum, Shanghai, China, 2015 with permission of Tecnon OrbiChem.

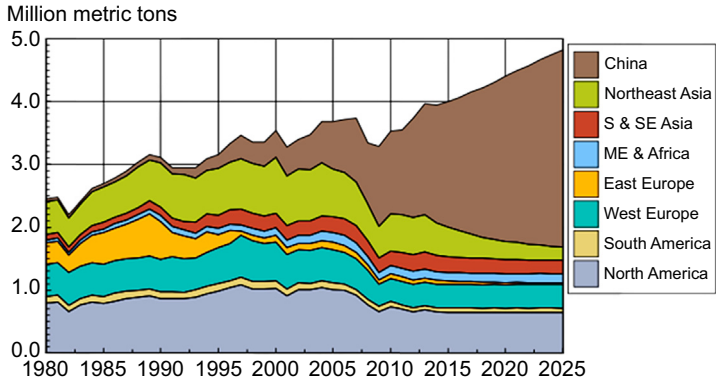

Figure 9.41 World polyamide filament production by regions.
Reprinted from R. Lee, Tecnon OrbiChem, Impact of crude oil and raw material price changes on world fibres markets, in: 12th International Polyester & Intermediates Forum, Shanghai, China, 2015 with permission of Tecnon OrbiChem.

manufacturer of nylons and it is expected to maintain its position as the leading PAs manufacturer in the next decade [109] (Fig. 9.41). Nylon fibers were mainly used in carpets and apparels because of properties such as retention of appearance, excellence wear resistance, and good dyeability [8]. However, over the last few years, nylon has lost some of its market share to polyester in textile and carpet applications because of its excellent easy care and wrinkle resistance [9].

Nylon-6 and nylon-66 are the most common Polyamides used for production of technical fibers. Other nylons such as PA-4, PA-11, PA-12, and PA-46 are also noticeable for industrial uses [7]. However, problems such as large moisture absorption, high production cost, low yield of polymerization, low dimensional stability, and poor tensile properties make them inappropriate for technical filaments [90]. PA-6 and PA-66 fibers/yarns

have been used in a variety of technical products. High tenacity, high elasticity, good adhesion to rubber, and resistance to abrasion and chemicals make such fibers useful for heavy-duty truck, bus, and earthmover tires. Other applications include surgical sutures, tents, fishing lines and nets, industrial threads, climbing and marine ropes, seat belts, upholstery fabrics, dental floss, parachutes, sleeping bags, and tarpaulins [8,9,31].

9.5 Conclusions and future trends

Several spinning methods have been used for the production of high-performance nylons fibers. Among them, melt spinning is still of greater interest, as it is the simplest eco-friendly method both conceptually and economically and it does not have the complexity of chemical reaction, mass transfer, and waste recovery systems that are inherent in other techniques. Traditional melt spinning often produces filaments with low tensile properties, inappropriate for technical applications. To modify the performance, thermal and/or mechanical treatments such as drawing and annealing are required for nylon fibers. Such treatments need to be used in the spinning line to make HT-HM yarns with high production rate and low manufacture cost. Innovative approaches of HIB and SymTTec have been designed in this regard. These techniques can delay rapid crystallization of polyamide chains and increase fiber drawability and tensile performance by better temperature, tension, and time control of the polymer/fiber in the spinning process.

Nevertheless, the tenacity and modulus of nylon fibers are still much lower than the theoretical values. New approaches can be used to obtain higher tensile performance. Higher molecular weight nylons (PA-6 or PA-66) can be used in the HIB process. A tenacity of 10 g/d has already been obtained in the HIB process for low molecular weight PA-6. The higher molecular weight provides more chain entanglements, which can increase chain/fiber stretching and tensile properties. Furthermore, combining SymTTech and HIB methods can lead to higher mechanical characteristics. Because these techniques improve tensile properties in two different ways, their combination can provide both more process parameters (eg, liquid temperature, depth, and temperature) and more polymer/fiber uniformity, and result in stronger fibers. Moreover, utilizing nanofillers and plasticizers in the HIB and/or SymTTec methods can increase the interspace of PA chains, weaken H-bonding, and increase chain mobility and DR. Also copolymerization of nylon-6 or nylon-66 with other aliphatic/aromatic PAs can increase the distance between the chains, modify chain/fiber drawability, and result in higher tensile performance. These suggestions would require more research and understanding of various process and structure properties of nylon fibers.

References

[1] World Nylon Fiber Report − Highlights. [Online]. Available: http://www.yarnsandfibers.com/preferredsupplier/spreports_fullstory.php?id=641.

[2] A. Anton, B.R. Baird, Polyamides, fibers, Encyclopedia Polym. Sci. Technol. 3 (2014) 584−618.

[3] S. Dasgupta, W.B. Hammond, W.a. Goddard, Crystal structures and properties of nylon polymers from theory, J. Am. Chem. Soc. 118 (1996) 12291−12301.
[4] M. Chanda, S.K. Roy, Industrial Polymers, Specialty Polymers, and Their Applications [Electronic Resource], CRC Press, Boca Raton, 2009, pp. 71−80 sec. 1.
[5] R. Chattopadhyay, Introduction: types of technical textile yarn, in: R. Alagirusamy, A. Das (Eds.), Technical Textile Yarns: Industrial and Medical Applications, first ed., Woodhead Publishing, Cambridge, U.K., 2010, pp. 1−56.
[6] J.W.S. Hearle, Introduction, in: J.W.S. Hearle (Ed.), High-performance Fibres, first ed., CRC Press; Woodhead Pub. [In Association With] The Textile Institute, Boca Raton [Fla.], 2001, pp. 1−21.
[7] H.H. Yan, Polyamide fibers, in: M. Lewin (Ed.), Handbook of Fiber Chemistry, third ed., CRC/Taylor & Francis, Boca Raton, 2007, pp. 31−38.
[8] N. Vasanthan, Polyamide fiber formation: structure properties and characterization, in: M.J.S. Eichhorn, J.W.S. Hearle (Eds.), Handbook of Textile Fibre Structure, first ed., Woodhead Publishing, 2009, pp. 232−252.
[9] S.K. Mukhopadhyay, Manufacture, properties and tensile failure of nylon fibres, in: A.R. Bunsell (Ed.), Handbook of Tensile Properties of Textile and Technical Fibres, first ed., Woodhead Publishing, Oxford, 2009, pp. 197−221.
[10] V. Mittal, High performance polymers: an overview, in: V. Mittal (Ed.), High Performance Polymers and Engineering Plastics, first ed., Wiley, 2011, pp. 1−20.
[11] J. Yao, C. Bastiaansen, T. Peijs, High strength and high modulus electrospun nanofibers, J. Fibers 2 (2014) 158−186.
[12] V.G. Bankar, J.E. Spruiell, J.L. White, Melt spinning of nylon 6: structure development and mechanical properties of as-spun filaments, J. Appl. Polym. Sci. 21 (1977) 2341−2358.
[13] S. Murase, M. Kashima, K. Kudo, M. Hirami, Structure and properties of high-speed spun fibers of nylon 6, Macromol. Chem. Phys. 198 (1997) 561−572.
[14] S. Gogolewski, a. J. Pennings, High-modulus fibres of nylon-6 prepared by a dry-spinning method, Polym. J. 26 (9) (1985) 1394−1400.
[15] J. Smook, G.J.H. Vos, H.L. Doppert, A semiempiric model for establishing the drawability of solution-spun linear polyamides and other flexible chain polymers, J. Appl. Polym. Sci. 41 (1990) 105−116.
[16] T.A. Hancock, J.E. Spruiell, J.L. White, Wet spinning of aliphatic and aromatic polyamides, J. Appl. Polym. Sci. 21 (1977) 1227−1247.
[17] R. Kotek, D. Jung, A.E. Tonelli, N. Vasanthan, Novel methods for obtaining high modulus aliphatic polyamide fibers, J. Macromol. Sci. Part C 45 (2005) 201−230.
[18] Q. Jia, Z. Xiong, C. Shi, Preparation and properties of polyamide 6 fibers prepared by the gel spinning method, J. Appl. Polym. Sci. 124 (2012) 5165−5171.
[19] J. Cho, G. Lee, B. Chun, Mechanical properties of nylon 6 fibers gel-spun from benzyl alcohol solution, J. Appl. Polym. Sci. 62 (1996) 771−778.
[20] C.Y. Lin, P.A. Tucker, J.A. Cuculo, Poly(ethylene terephthalate) melt spinning via controlled threadline dynamics, J. Appl. Polym. Sci. 46 (1992) 531−552.
[21] H. Avci, R. Kotek, J. Yoon, Developing an ecologically friendly isothermal bath to obtain a new class high-tenacity and high-modulus polypropylene fibers, J. Mater. Sci. 48 (2013) 7791−7804.
[22] A. Ziabicki, Wet- and dry-spinning, in: Fundamentals of Fibre Formation: The Science of Fibre Spinning and Drawing, Wiley, London, 1976.
[23] Q. J, Z. Yang, H. Yin, X. Li, Z. Liu, Study on dry spinning and structure of low mole ratio complex of calcium chloride-polyamide 6, Polym. Polym. Compos. 21 (2013) 449−456.

[24] J.V. Dingenen, Gel-spun high-performance polyethylene fibres, in: J.W.S. Hearle (Ed.), High-performance Fibres, first ed., CRC Press; Woodhead Pub. [In Association With] The Textile Institute, Boca Raton [Fla.], 2001, pp. 62–92.
[25] J.G. Lim, B.S. Gupta, W. George, The potential for high performance fiber from nylon 6, Prog. Polym. Sci. 14 (6) (1989) 763–809.
[26] A. Gupta, Novel Approaches to Fiber Formation from Hydrogen Bond Forming Polymers, North Carolina State University, 2008. Dissertation. Available, http://repository.lib.ncsu.edu/ir/handle/1840.16/4526.
[27] J.A. Cuculo, P.a. Tucker, G.-Y. Chen, L. Ferdinand, Melt Spinning of Ultra-oriented Crystalline Filaments, US Patent 5268133 A, 1995.
[28] Swiss Tex, symTTec Technical Yarn Extrusion System, 2008 [Online]. Available: http://www.primetex-technology.com/symttec.pdf.
[29] H. Kawai, A. Ziabicki, High-Speed Fiber Spinning: Science and Engineering Aspects, Krieger Pub. Co., Malabar, Fla., 1991.
[30] V.B. Gupta, Melt-spinning process, in: V.B. Gupta, V.K. Kothari (Eds.), Manufactured Fibre Technology, first ed., Chapman & Hall, London, 1997, pp. 67–97.
[31] A.F. Richards, Nylon fibres, in: J.E. McIntyre (Ed.), Synthetic Fibres: Nylon, Polyester, Acrylic, Polyolefin, first ed., CRC Press; Woodhead Pub., Boca Raton, 2005, pp. 20–94.
[32] J.A. Barnes, F. Dempster, High Tenacity Low Shrinkage Polyamide Yarns, US Patent 0124149 A1, 2009.
[33] R.T. Clark, A. Joseph, High Tenacity, High Modulus Polyamides Yarn and Process for Making Same, US Patent 5106946, 1992.
[34] G.C. Stow, W.C. Mallonee, H.D. Barrett, Nylon Tire Cords, US Patent 3343363, 1967.
[35] H. Good, N.,A. Tenn, Process for Drawing a Polyamide Yarn, US Patent 3311691 A, 1968.
[36] H.H. Schenker, Multi-step Stretching of Nylon Cords, US Patent 2807863, 1957.
[37] R. Ono, T. Haga, T. Sakai, Process for the Manufacture of High Tenacity Nylon Filaments, US Patent 3379810, 1968.
[38] R.L.R. Keefe, W.O. Statton, High Tenacity Tire Yarn, US Patent 3564835, 1971.
[39] L. Thone, G. Koschinek, D. Wandel, Process for Spin-stretching of High Strength Technical Yarns, US Patent 4461740, 1984.
[40] H.E. Sundbeck, Stretching Nylon Filaments in a Gas Vortex, US Patent 3551549, 1970.
[41] NPTEL:Textile Engineering – Manufactured Fibre Technology- Drawing Machines. [Online]. Available: http://www.nptel.ac.in/courses/116102010/29.
[42] T. Kunugi, I. Akiyama, M. Hashimoto, Preparation of high-modulus and high-strength nylon-6 fibre by the zone-annealing method, Polym. J. 23 (1982) 1193–1198.
[43] T. Kunugi, I. Akiyama, M. Hashimoto, Mechanical properties and superstructure of high-modulus and high-strength nylon-6 fibre prepared by the zone-annealing method, Polym. J. 23 (1982) 1199–1203.
[44] T. Kunugi, K. Chida, A. Suzuki, Preparation of high-modulus nylon 6 fibers by vibrating hot drawing and zone annealing, J. Appl. Polym. Sci. 67 (1998) 1993–2000.
[45] A. Suzuki, A. Endo, Preparation of high modulus nylon 46 fibres by high-temperature zone-drawing, Polym. J. 38 (1997) 3085–3089.
[46] A. Suzuki, H. Murata, T. Kunugi, Application of a high-tension annealing method to nylon 66 fibres, Polym. J. 39 (1998) 1351–1355.
[47] A. Suzuki, M. Ishihara, Application of CO_2 laser heating zone drawing and zone annealing to nylon 6 fibers, J. Appl. Polym. Sci. 83 (2002) 1711–1716.
[48] A. Suzuki, Y. Chen, T. Kunugi, Application of a continuous zone-drawing method to nylon 66 fibres, Polym. J. 39 (1998) 5335–5341.

[49] G. Wu, Q. Zhou, J. Chen, J.F. Hotter, P.A. Tucker, J.A. Cuculo, The effect of a liquid isothermal bath in the threadline on the structure and properties of poly (ethylene terephthalate) fibers, J. Appl. Polym. Sci. 55 (1995) 1275−1289.
[50] K.R. Samant, G. Vassilatos, Process of Making Polyamide Filaments, US Patent 6899836 B2, 2005.
[51] E. Schippers, H. Lenk, Method and Apparatus for Producing Multifilament Yarn by a Spin-draw Process, US Patent 5661880, 1997.
[52] J.W. Nunning, P.E. Brignac, H.B. Duke, Method for Spinning Polyamide Yarn of Increased Relative Viscosity, US Patent 3551548, 1974.
[53] R.G. West, A.G. Schwinn, High RV Filaments, and Apparatus and Processes for Making High RV Flake and the Filaments, US Patent 6235390 B1, 2003.
[54] P. Silverman, B. Stewart, E.L. Fla, High Molecular Weight Oriented Polyamide Textile Yarn, US Patent 3548484, 1970.
[55] R.S. Knorr, High Tenacity Nylon Yarn, US Patent 5073453, 1991.
[56] I. Yildirim, E. Guven, E. Kop, A Yarn Production Method and a Super Hightenacity Yarn Acquired with This Method, W.O. Patent 2014129991 A1, 2015.
[57] NPTEL: Textile Engineering − Manufactured Fibre Technology-Introduction to Solution Spinning. [Online]. Available: http://www.nptel.ac.in/courses/116102010/18.
[58] H. Yasuda, K. Ban, Y. Ohta, Gel spinning process, in: T. Nakajima (Ed.), Advanced Fiber Spinning Technology, first ed., Woodhead, Cambridge, England, 1994.
[59] H. Chuah, R. Porter, Solid-state co-extrusion of nylon-6 gel, Polym. J. 27 (1986) 1022−1029.
[60] H. Zhang, C. Shi, M. He, Q. Jia, L. Zhang, Structure and property changes of polyamide 6 during the gel-spinning process, J. Appl. Polym. Sci. 130 (2013) 4449−4456.
[61] P.J. Lemstra, C.W.M. Bastiaansen, H.E.H. Meijer, Chain-extended flexible polymers, Die Angew. Makromol. Chem. 145 (1986) 343−358.
[62] T. Kanamoto, A.E. Zachariades, R.S. Porter, The effect of anhydrous ammonia on the crystalline-state deformation of nylons 6 and 6,6, J. Polym. Sci. Polym. Phys. Ed. 20 (1982) 1485−1496.
[63] A.E. Zachariades, R.S. Porter, Reversible plasticization of nylons 6 and 11 with anhydrous ammonia and their deformation by solid-state coextrusion, J. Appl. Polym. Sci. 24 (1979) 1371−1382.
[64] H.H. Chuah, R.S. Porter, A new drawing technique for nylon-6 by reversible plasticization with iodine, Polym. J. 27 (1986) 241−246.
[65] Y. Lee, R. Porter, Structure of nylon 6-iodine complexes and their drawability by solid-state coextrusion, J. Macromol. Sci. Part B 34 (1995) 295−309.
[66] N.S. Murthy, Structure of iodide ions in iodinated nylon 6 and the evolution of hydrogen bonds between parallel chains in nylon 6, J. Macromol. 20 (1987) 309−316.
[67] A. Richardson, I.M. Ward, Production and properties of fibers spun from nylon 6/lithium chloride mixtures, J. Polym. Sci. Polym. Phys. Ed. 19 (1981) 1549−1565.
[68] M. Roberts, S. Jenekhe, Site-specific reversible scission of hydrogen bonds in polymers. an investigation of polyamides and their Lewis acid-base complexes by infrared spectroscopy, Macromolecules 24 (1991) 3142−3146.
[69] N. Vasanthan, R. Kotek, D.-W. Jung, D. Shin, A.E. Tonelli, D.R. Salem, Lewis acid−base complexation of polyamide 66 to control hydrogen bonding, extensibility and crystallinity, Polym. J. 45 (2004) 4077−4085.
[70] M. Afshari, A. Gupta, D. Jung, R. Kotek, A.E. Tonelli, N. Vasanthan, Properties of films and fibers obtained from Lewis acid−base complexed nylon 6,6, Polym. J. 49 (2008) 1297−1304.

[71] W. Wei, L. Qiu, X.L. Wang, H.P. Chen, Y.C. Lai, F.C. Tsai, P. Zhu, J.T. Yeh, Drawing and tensile properties of polyamide 6/calcium chloride composite fibers, J. Polym. Res. 18 (2011) 1841−1850.
[72] F.-C. Tsai, P. Li, J.-T. Yeh, Drawing and ultimate tenacity properties of polyamide 6/Attapulgite composite fibers, J. Appl. Polym. Sci 126 (2012) 1906−1926.
[73] J.-T. Yeh, C.-K. Wang, F.-C. Tsai, Drawing and ultimate tensile properties of nylon 6/nylon 6 clay composite fibers, Polym. Eng. Sci. 52 (2012) 1348−1355.
[74] J.A. Cuculo, R. Kotek, P. Chen, M. Afshari, F. Lundberg, Highly Oriented and Crystalline Thermoplastic Filaments and Method of Making Same, US Patent 20130040521 A1, 2013.
[75] M. Najafi, H. Avci, R. Kotek, High-performance filaments by melt spinning low viscosity nylon 6 using horizontal isothermal bath process, Polym. Eng. Sci. 47 (2015) 21−25.
[76] H. Avci, R. Kotek, B. Toliver, Controlling of threadline dynamics via a novel method to develop ultra-high performance polypropylene filaments, Polym. Eng. Sci. 55 (2014) 1−13.
[77] P. Chen, M. Afshari, J.A. Cuculo, R. Kotek, Direct formation and characterization of a unique precursor morphology in the melt-spinning of polyesters, Macromolecules 42 (2009) 5437−5441.
[78] K. Miyata, H. Ito, T. Kikutani, N. Okui, Effect of liquid isothermal bath in high-speed melt spinning of poly (ethylene 2, 6-naphthalene dicarboxylate), Sen'i Gakkaishi 54 (1998) 661−671.
[79] J.-Y. Chen, P.A. Tucker, J.A. Cuculo, High-performance PET fibers via liquid isothermal bath high-speed spinning: fiber properties and structure resulting from threadline modification and posttreatment, J. Appl. Polym. Sci. 66 (1997) 2441−2455.
[80] T. Kikutani, M. Sato, J. Radhakrishnan, N. Okui, A. Takaku, High melt spinning of PET via LIB mechanism, simulation, 1996, Intern. Polym. Process. 11 (1996) 42−49.
[81] G. Wu, P.A. Tucker, J.A. Cuculo, High performance PET fibre properties achieved at high speed using a combination of threadline modification and traditional post treatment, Polym. J. 38 (1997) 1091−1100.
[82] J. Hotter, J. Cuculo, Effect of liquid isothermal bath position in modified poly (ethylene terephthalate) PET melt spinning process on properties and structure of As-spun and annealed filaments, J. Appl. Polym. Sci. 69 (1998) 2051−2068.
[83] G. Wu, J. Jiang, P. Tucker, J. Cuculo, Oriented noncrystalline structure in PET fibers prepared with threadline modification process, J. Polym. Sci. Polym. Phys. 34 (1996) 2035−2047.
[84] B. Huang, P. Tucker, J. Cuculo, High performance poly (ethylene terephthalate) fibre properties achieved via high speed spinning with a modified liquid isothermal bath process, Polym. J. 38 (1997) 1101−1110.
[85] H. Avci, M. Najafi, A. Kilic, R. Kotek, Highly crystalline and oriented high-strength poly(ethylene terephthalate) fibers by using low molecular weight polymer, J. Appl. Polym. Sci. 42747 (2015) 1−15.
[86] M. Najafi, R. Kotek, High-tenacity PTT fibers by HIB Process, in: Fiber Society Conference, Liberec, Crech Republic, 2014.
[87] M. Najafi, R. Kotek, Unique polyamide fibers by hIB process, in: Fiber Society Conference, Liberec, Crech Republic, 2014.
[88] Truetzchler, Man-made Fibers. [Online]. Available: http://www.truetzschler-manmadefibers.com/fileadmin/user_upload/truetzschler-nonwovens/brochures_downloads/man-made-fibers/englisch/MMF_EN.pdf.

[89] Swiss Tex, RIEVAP-dual Shell Draw Rolls, 2008 [Online]. Available: http://www.primetex-technology.com/drawrolls.pdf.
[90] S.M. Aharoni, n-Nylons, Their Synthesis, Structure, and Properties, J. Wiley, Chichester, 1997.
[91] N.S. Murthy, A.C. Reimschuessel, V. Kramer, Changes in void content and free volume in fibers during heat setting and their influence on dye diffusion and mechanical properties, J. Appl. Polym. Sci. 40 (1990) 249–262.
[92] N.S. Murthy, Hydrogen Bonding, Mobility, and structural transitions in aliphatic polyamides, J. Polym. Sci. Polym. Phys. Ed. 44 (2006) 1763–1782.
[93] J.W.S. Hearle, Tensile failures, in: J.W.S. Hearle, B. Lomas, W.D. Cooke (Eds.), Atlas of Fibre Fracture and Damage to Textiles [Electronic Resource], second ed., Woodhead Publishing Limited: CRC Press, Cambridge, England, 2006, pp. 35–67.
[94] N.S. Murthy, D.T. Grubb, Deformation of lamellar structures: simultaneous small- and wide-angle X-ray scattering studies of polyamide-6, J. Polym. Sci. Part B Polym. Phys. 40 (2002) 691–705.
[95] N.S. Murthy, H. Minor, C. Bednarczyk, S. Krimm, Structure of the amorphous phase in oriented polymers, Macromolecules 26 (1993) 1712–1721.
[96] N.S. Murthy, Fibrillar structure and its relevance to diffusion, shrinkage, and relaxation processes in nylon fibers, Text. Res. J. 67 (1997) 511–520.
[97] T.D. Fornes, D.R. Paul, Crystallization behavior of nylon 6 nanocomposites, Polym. J. 44 (2003) 3945–3961.
[98] D.R. Holmes, C.W. Bunn, D.J. Smith, I. Chemical, The crystal structure of polycaproamide: nylon 6, J. Polym. Sci. 17 (1955) 159–177.
[99] H. Arimoto, M. Ishibashi, M. Hirai, Y. Chatani, Crystal structure of the gamma form of nylon 6, J. Polym. Sci. Part A Polym. Chem. 3 (1965) 317–326.
[100] S.Y. Kwak, J.H. Kim, S.Y. Kim, H.G. Jeong, I.H. Kwon, Microstructural investigation of high-speed melt-spun nylon 6 fibers produced with variable spinning speeds, J. Polym. Sci. Part B Polym. Phys. 38 (2000) 1285–1293.
[101] R. Heuvel, H.M. Huisman, Effects of winding speed, drawing and heating on the crystalline structure of nylon 6 yarns, J. Appl. Polym. Sci. 26 (1981) 713–732.
[102] Y. Li, W.A. Goddard, Nylon 6 crystal structures, folds, and lamellae from theory, Macromolecules 35 (2002) 8440–8455.
[103] N.S. Murthy, R.G. Bray, S.T. Correale, R.A.F. Moore, Drawing and annealing of nylon-6 fibres: studies of crystal growth, orientation of amorphous and crystalline domains and their influence on properties, Polym. J. 36 (1995) 3863–3873.
[104] J.W.S. Hearle, W.E. Morton, Tensile properties, in: Physical Properties of Textile Fibres, 4th ed., Woodhead Pub, 2008.
[105] K. Koyama, J. Suryadevara, E. Joseph, Effect of molecular weight on high-speed melt spinning of nylon 6, J. Appl. Polym. Sci. 31 (1986) 2203–2229.
[106] S.T. Correale, N.S. Murthy, Secondary crystallization and premelting endo- and exotherms in oriented polymers, J. Appl. Polym. Sci. 101 (2006) 447–454.
[107] N. Vasanthan, Orientation and structure development in polyamide 6 fibers upon drawing, J. Polym. Sci. Part B Polym. Phys. 41 (2003) 2870–2877.
[108] N. Vasanthan, Effect of the microstructure on the dye diffusion and mechanical properties of polyamide-6 fibers, J. Polym. Sci. Part B Polym. Phys. 45 (2006) 349–357.
[109] R. Lee, Tecnon OrbiChem, Impact of crude oil and raw material price changes on world fibres markets, in: 12th International Polyester & Intermediates Forum, Shanghai, China, 2015.

High performance fibers from aramid polymers

10

K. Akato [1], *G. Bhat* [2]
[1]The University of Tennessee, Knoxville, TN, United States; [2]The University of Georgia, Athens, Georgia, United States

10.1 Introduction

Aramid fibers (aromatic polyamides) are part of the high-performance engineered fibers family and are one of the most representative commodities, not only in terms of quantity used worldwide, but also in view of high tenacity, high modulus, and good heat and flame resistance [1]. Aramid fibers have in common the same molecular structure, consisting of aromatic ring and amide group. These parts combine to provide fibers with outstanding anisotropy of the superimposed substructure presenting pleated, crystalline, fibrillar, and skin−core characteristics.

Aramid fibers, first developed in the 1960s, have improved throughout the years with multiple investigations into the rheology and processing of liquid crystalline polymer fields [2−4]. DuPont scientist Kwolek was said to be the first person to prepare high molecular weight lyotropic aramids [5]. His work along with the later discovery of fiber-spinning anisotropic solutions by Blades [6] resulted in the commercialization of high-performance polyaramid fiber commonly called Kevlar.

Enormous efforts to industrialize these fibers led to a growing number of different chemical combinations of aromatic and aromatic aliphatic polyamides. In regard to condensing the diversity and still maintaining uniqueness, the US Federal Trade Commission adopted a simple definition for aramid as a fiber of aromatic polyamide type in which at least 85% of the amide linkages are attached directly to two aromatic rings [7]. Only a few aramid fibers were subsequently developed and commercialized (Kevlar, Nomex, Technora, and Twaron are examples) because of the tremendous scientific contributions. Important efforts were also made to establish structure−property relationships of the aramid fibers in view of expanding their usage in different applications [8−10]. Many believe that by solving this complex relationship, these fibers will continue to dominate the market in terms of performance and economic impact.

The potential and varieties of applications of aramid fibers as an engineered material testify to the growing interest in them. They are used in aircraft, marine craft, and automobiles, ropes for offshore oil rigs, and bulletproof vests. They also find application in protective clothing against heat, chemicals, and radiation. This chapter summarizes the establishment of aramid as top high-performance fibers as well as the successful research achievements generated to lift the fibers to their present prominence, especially with respect to polymer preparation, fiber formation, structure−property relationships. In addition, some of the recent developments and understandings with regard to the structure of these fibers and modifications to achieve superior performance are included.

Structure and Properties of High-Performance Fibers. http://dx.doi.org/10.1016/B978-0-08-100550-7.00010-3

10.2 Polymer preparation of aramid fibers

The outstanding mechanical properties of high-performance aramid fibers are achieved by utilizing liquid crystalline solutions during fiber spinning. However, the individual molecules of aramid polymers behave as rigid-rod-like structures with restricted motion or movement as opposed to common fiber-forming polymers that exist as random coils in solution. For this reason, a controlled process is needed to prepare fiber-forming aramid polymers.

10.2.1 Polymerization process

The polymerization of aramid polymers is a controlled process with a goal of producing polymers with a suitable molecular weight that can be used for fiber formation. Since the molecular weight is influenced by factors such as solvent composition, temperature, reactant concentration, mixing, and stoichiometry, numerous efforts have been developed to help understand the process. The knowledge collected to date on the synthesis of aramids distinguishes two different established methods: low-temperature polycondensation (preferably below 50°C to avoid degradation, side reactions, and crosslinking) and direct polycondensation in solution using phosphites (in the presence of metal salts).

Kwolek [5,11,12] was the first to report low-temperature polymerization of aromatic polyamides. In an effort to refine the process, Morgan [13,14] later pointed out the solubility−concentration−temperature relationship along with salt concentration as constant polymer concentration to be key factors affecting polymer characteristic in low-temperature reactions. The goal of the process is to achieve the optimum and narrowest molecular weight distribution suitable for fiber formation. Low-temperature polycondensation can be divided into two other methods. One is referred to as interfacial polycondensation but it is not suitable for fiber formation because of the broad molecular weight distribution generated in this process. Solution polycondensation is preferred because of its efficiency and it only requires a system where the polymerization medium is an inert solvent for at least one of the reactants and solvents or swelling agents for the polymer (if possible a solvent). Most meta- and para-aramid copolymers have been prepared by solution polycondensation [15,16]. Nomex, for example, was prepared using *m*-phenylenediamine and dichloride of *m*-isophthalic acid. Nomex will be described in full in a later section. Fig. 10.1(a) and (b) show the schematic of both the para- and meta-aramid polymers.

Poly(1,4-phenylene terephthalamide) (PPD-T) is a high molecular weight aramid polymer that is prepared by the low-temperature solution technique [17]. A mixture of hexamethyl phosphoric triamide (HMPA) and *N*-methyl-2-pyrrolidone (NMP) is used but it was reported that HMPA alone can produce fiber-forming polymers [18]. Other mixtures of HMPA and dimethyl acetamide (DMAC) were also reported [19,20]. For example, researchers have reported producing high molecular weight PPD-T by mixing HMPA:NMP in a ratio of 1:2 or DMAC:HMPA in a ratio of 1:1.4. In some cases salt is added to the mixture to promote the polymerization

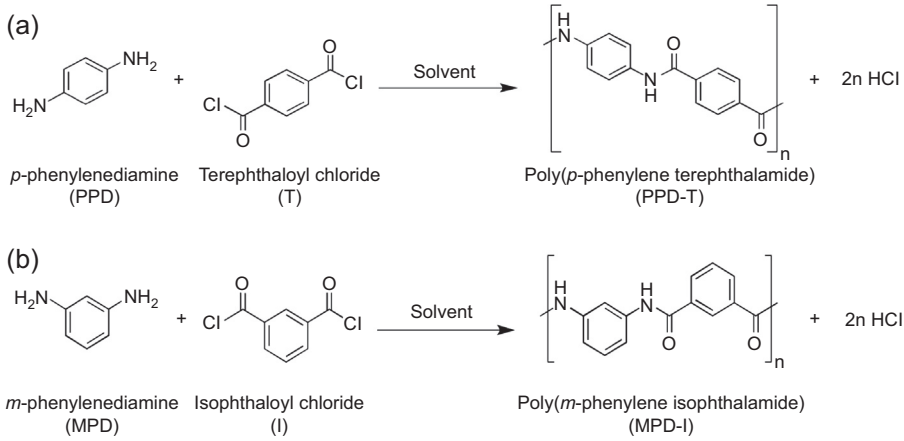

Figure 10.1 Aramid polymer preparation: (A) Kevlar, (B) Nomex [17].

reactions [21]. DuPont developed a system using HMPA as a solvent and NMP containing calcium chloride [17]. The system had a better chemical and thermal stability than 100% HMPA. $CaCl_2$ can be an effective solvent additive as concentration increases. Even though they suggested possible formation of $CaCl_2$/amide complexes, addition of *N*,*N*′ dimethylaniline, an acid acceptor, helped to reach molecular weights necessary to form fibers [22]. The polymerization of PPD-T consisted of rapid molecular weight increase within the first few seconds followed by quick gelation point where polymerization proceeds at a very slow rate. Gelation is controlled by choosing a suitable solvent and allowing the molecular weight to reach its maximum. PPD-T is reported to reach a maximum in 100% HMPA at 0.7 m/L. However, in a mixture of HMPA/NMP at a 2:1 ratio, the maximum is reached at a low concentration of 0.25 m/L. Molecular weight is restricted by unwanted side reactions with solvent at low concentration, which is favorable for fiber-forming polymers, but high concentration often induces gel formation at lower molecular weight. Molecular weight has been one of the important topics of much research [23], especially in terms of improving it since it is affected by many other factors. For industrial PPD-T, the number-average molecular weight is 20,000, the weight-average molecular weight is between 40,000 and 50,000, and the degree of polymerization is around 190. The relationship between the polymer inherent viscosity and reaction time is illustrated in Fig. 10.2. The inherent viscosity is correlated to the polymer molecular weight. Maximum values are reached when initial temperatures are 0−5°C and final temperature is 30°C or less.

10.2.2 Fiber formation

Aramids decompose before or during melting. Even though melt spinning would be ideal from an economic standpoint, it is not possible to produce fiber from the aforementioned. For that reason they are spun in solution form, either by dry- or wet-spinning techniques. High molecular weight aramids are usually dissolved in high

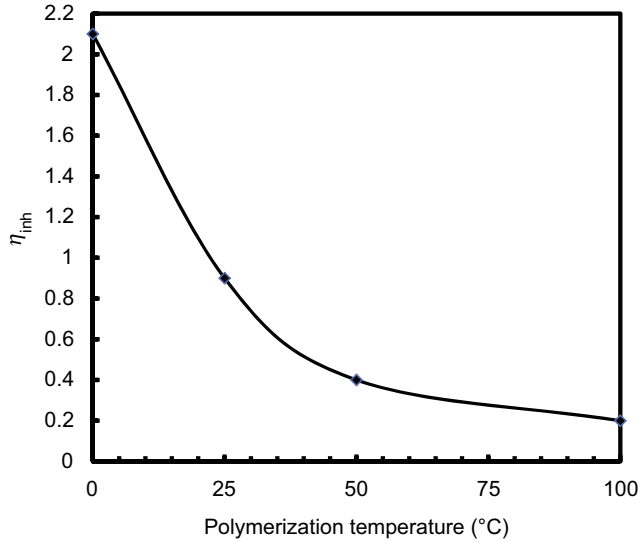

Figure 10.2 Effect of polymerization temperature on inherent viscosity of poly(1,4-benzamide) in tetramethylurea [24].

concentration in different solvents to form a dope with viscosity low enough for fiber drawing with good mechanical properties [25]. Most aramid polymer molecules are lyotropic because they only form a liquid crystalline phase upon addition of solvent. At suitable polymer concentration, the rod-like structures aggregate to form ordered domains (Fig. 10.3). These aggregates exist as a separate phase in an initially continuous isotropic phase. Addition of more polymer leads to a more ordered state until an anisotropic phase is reached. The ordered phase is often referred to as nematic since rod-like chains of varying length are in parallel array. The polymer state of common PPD-T in sulfuric acid solution is illustrated in Fig. 10.4. A concentration of 20% of nematic PPD-T in 100% sulfuric acid is reported to be adequate to form a liquid crystalline state. The viscosity profile also determines the critical concentration at

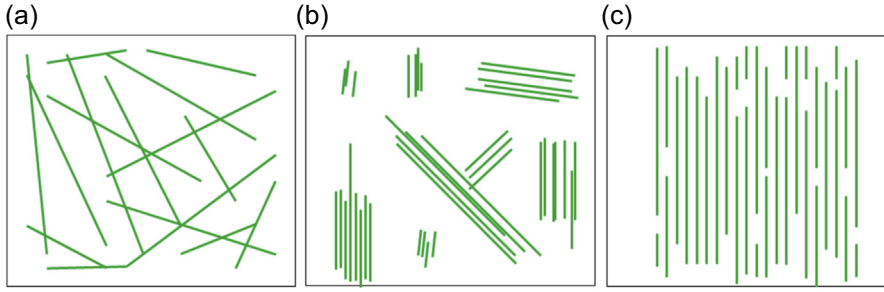

Figure 10.3 Different states of PPD-T rod-like polymers in sulfuric acid: (a) random arrangement, (b) liquid crystalline regions, (c) oriented liquid crystalline.

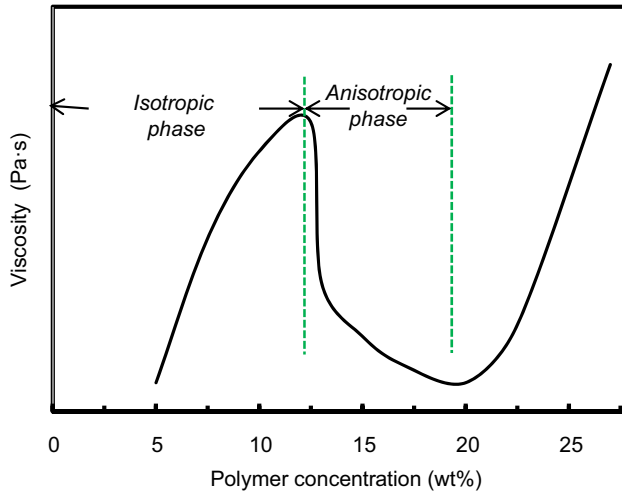

Figure 10.4 Liquid crystalline behavior of PPTA solution, indicating an isotropic phase at concentrations below 12 wt% and an anisotropic phase between concentrations of 12 wt% and 20 wt% [26].

which these high molecular weight aromatic polyamides can transition to a liquid crystalline state. For instance, the viscosity profile of PPD-T in 100% sulfuric acid shows a rapid increase of viscosity with increasing concentration, and a rapid drop once the critical concentration is reached. Blair and Morgan [11] have successfully prepared poly(*p*-phenylene terephthalamide) (PPTA) with the highest inherent viscosity by using a 2:1 ratio by volume of HMPA:NMP. The viscosity profile was consistent in showing the inherent viscosity dropping quite rapidly when reactant concentration is less than 0.25 M but falls gradually when concentration reaches 0.3 M. Examination of solution polymerization of aromatic diamines and aromatic dicarboxylic acid chlorides in DMAC also confirmed a decrease in viscosity at low reactant concentration [20]. The main reason behind the reduction in viscosity was explained by the decrease in reactant mobility caused by onset of gelation before a high value of inherent viscosity could be achieved. The dopes are required to melt before spinning and are adequate for low-temperature coagulation.

In the solution-spinning process, the dope is extruded under heat and pressure through a single or multihole spinneret to a narrow air gap, and then quickly enters the coagulation bath. The crystal domains of the anisotropic solution align along the direction of extensional shear produced by the extrusion through a capillary (Fig. 10.5). Such shear causes an interesting transition of the crystal domains to deorient at the exit of the die but the phenomenon can be overcome by filament attenuation under spinning tension. The attenuated filament, after washing and drying, results in crystalline, high-modulus fibers. In the case of wet spinning, the dope is directly exposed to the coagulation bath as soon as it exits the capillary die, thus preventing a complete attenuation. Such methods give fibers with low tenacity and intermediate modulus. Dry-jet wet spinning is often preferred for aramid fiber production. In this

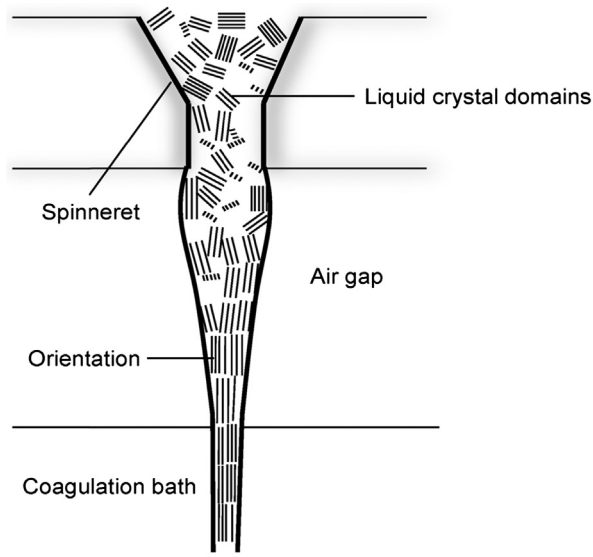

Figure 10.5 Schematic diagram of molecular orientation during the dry-jet wet-spinning process of liquid crystalline solution [26].

process, the thermal condition for optimal flow and spinning and the optimal condition for coagulation can be easily separated [27].

Spinning of aramid fibers is typically followed by heat treatment under tension to increase the modulus (stiffness) and crystallinity. These properties are important for industrial applications and set these aramid fibers apart from other high-performance fibers. The literature has several reports on the effect of heat treatment on aramid fibers [28–32]. Heat treatment has implications that are beneficial after either wet spinning or dry-jet spinning. Wet-spun yarns have been reported to have tenacity and modulus increasing exponentially with increasing temperatures (and draw ratio). Measurements suggest an effective increase in properties starting around the T_g of the polymer ($\sim$360°C) and maximum properties are achieved around the T_m of the polymers ($\sim$550°C). Increase in crystallinity, structure perfection, and orientation are well established during heat treatment. The stretched fibers keep their high orientation that leads to a high degree of crystallinity as well. A jump in modulus was reported for dry-jet-spun yarns at temperatures greater than 200°C but such a jump is essentially temperature independent. The final properties of the nascent fibers are strongly related to the polymer structure and the spinning method. Fig. 10.6 shows the full diagram of the production of PPT-D.

10.3 Structure and properties

Aramid fibers have a high degree of orientation that sets them apart from other synthetic fibers. Their tensile properties are related to the fiber structure at the molecular level. The polymer chain conformation and rigidity, crystal orientation, and crystallinity

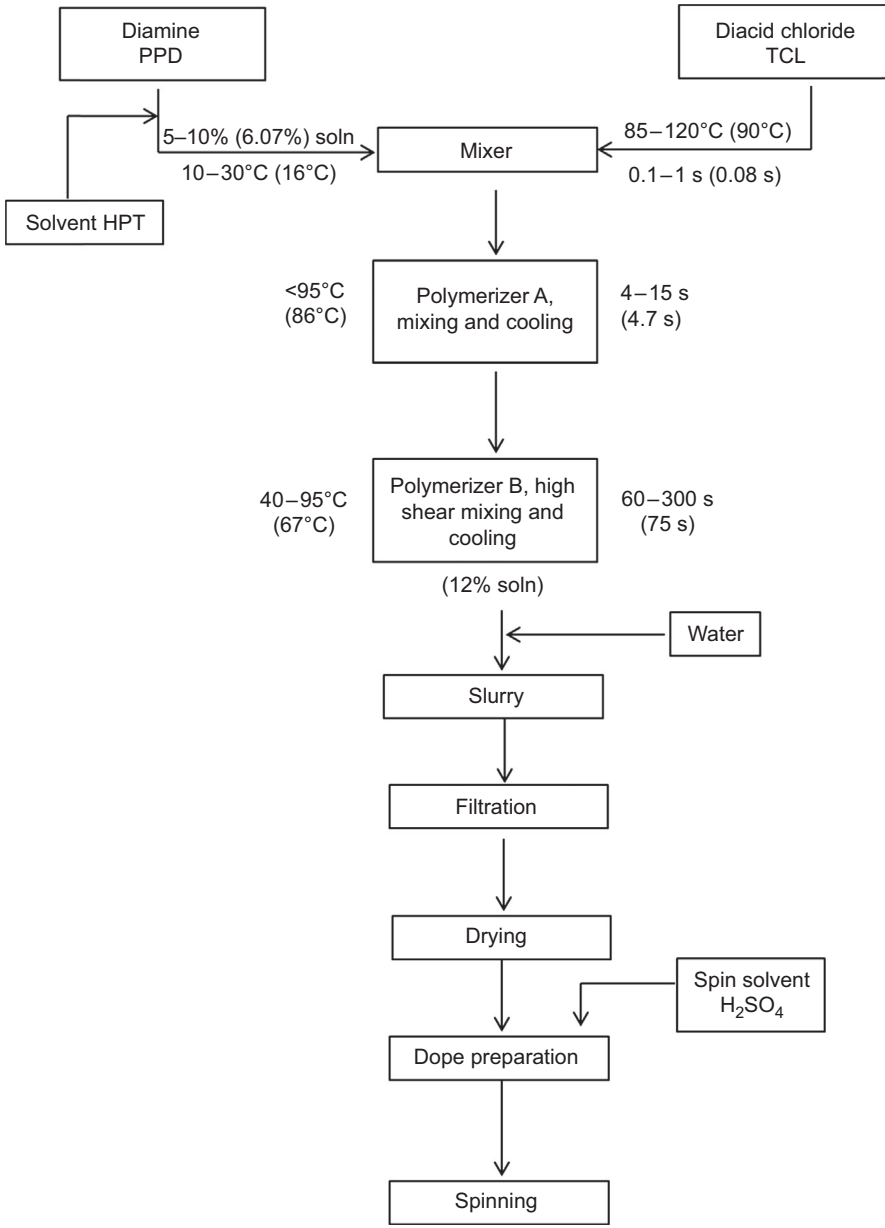

Figure 10.6 Diagram for production PPT-D fibers [17].

contribute to the strength and performance of the fibers. Depending on the processing techniques and the type of polymer structure, different characteristics are reported.

Kevlar is a para-amid fiber with very stiff polymer chains. One advantage is the structure where the backbone consists of carbonyl group and NH centers. The

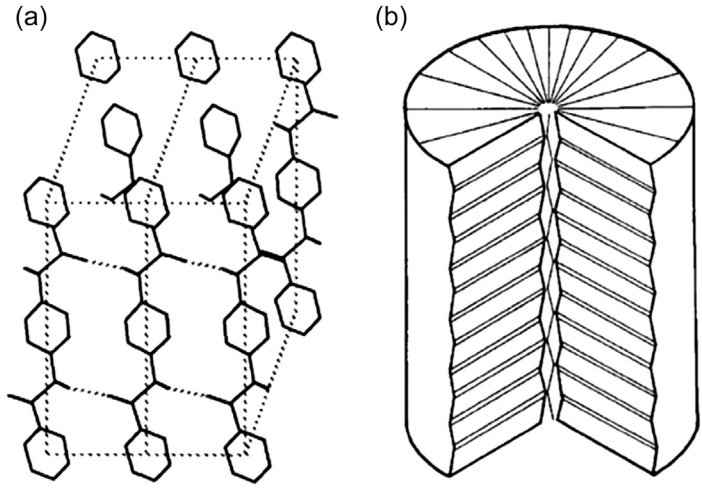

Figure 10.7 (a) Unit cell of Kevlar crystal and (b) radial arrangement pleated sheet structure of Kevlar [33].

quantification of Kevlar structure showed a high degree of alignment of long, straight polymer chains parallel to the fiber axis. Furthermore, it was reported that the fibers possess fibrillar structure [9,33−35]. Electron diffraction and dark field transmission electron microscopy are well suited to determine the degree of orientation in fibers [36]. For Kevlar the results of microstructural studies showed unusual radial orientation of hydrogen-bonded sheets and pleated structure (Fig. 10.8). The latter observation was only reported for a few Kevlars but they are nonexistent in high-end quality Kevlar. The pleated sheet structures are formed within the core region of the fibers as shown in Fig. 10.7(a) and (b). They are the direct result of the relaxation of the local stress field at the onset of coagulation. The pleated conformation of the polymer chains is primarily governed by an association of intra- and intermolecular interactions between the conjugated groups within the Kevlar primary structure. Examples of these interactions are the interchain bonds between the carbonyl group and NH centers and the aromatic stacking interactions between adjacent strands. At the crystalline level, the pleating of fibrils is superimposed on the fibrillary structure of PPTA with a variation from linearity of approximately 5 degrees and periodicity of 500 nm. The outstanding high strength of Kevlar is summarized in four simple ways. It starts with the aromatic and amide groups present in the chain followed by the crystalline arrangement in the way polymer chains are oriented parallel to the fiber axis. The next factor is the closeness of the individual strands through hydrogen bonding between polar amide groups on adjacent chains. Last but not least is the radial orientation of the aromatic components, which gives a high degree of symmetry and regularity to the internal structure of the fibers.

As mentioned earlier, Kevlar possesses tremendous mechanical properties in tension. This is related to the perfect structural characteristics described previously. However, the compressive strength of Kevlar is 1/10 of its ultimate tensile strength. The

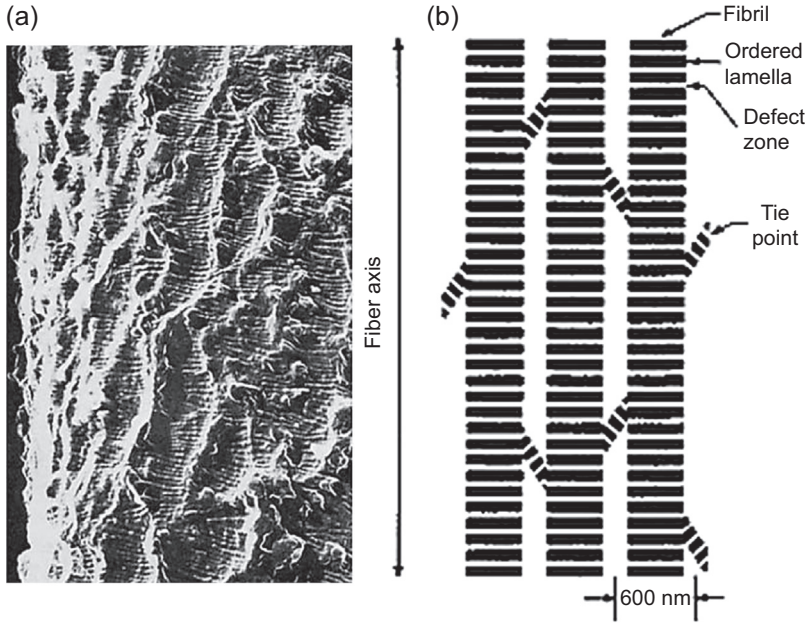

Figure 10.8 Etched surface by transmission electron microscopy and the oriented fibrillar model of the Kevlar fiber [40].

disproportion of high tensile and low compressive properties is often regarded as a limiting factor of the end use of Kevlar in some applications. Numerous efforts were undertaken for the improvement of such inequality. One approach is to incorporate additives or modifiers into the polymer microstructure during polymerization or spinning [37]. Another method was postspinning treatment at elevated temperature or using electron bombardment [38]. These proposed methods have the same goal of facilitating the formation of intermolecular covalent crosslinkages in the fibers.

Aramids are known to absorb moisture because of the hydrophilicity of amide linkages in their structure. For instance, at 20°C and 55% relative humidity, moisture absorption by Kevlar 29 is around 7% and by Kevlar 149 it is 1%. The difference in water uptake is attributed to different factors such as amide groups at the chain ends, intrafibrillar lattice deficits, and inner surfaces of the microvoids that form small water clusters at low vapor pressure [39]. The same amide groups that help with hydrophilicity can be hydrolyzed in the presence of strong acids and bases at high temperatures. Even though aramid fibers do not melt, they can decompose when exposed to high temperature. However, long before decomposition conditions are met, aramid fibers retain most of their physical properties. Kevlar can retain 70% of its modulus and 50% of its strength at 300°C. The excellent thermal stability is attributed to the conjugation between the amide groups and the aromatic rings.

Kevlar is known to have outstanding mechanical properties. However, these properties are observed only in one direction because of the high anisotropy of the material.

A weak hydrogen bond in the transverse direction results in low compressive strengths. Fatigue behavior of aramids is strongly dependent on the failure mode. When in tension, no failure is observed at 60% of breaking strength of 10^7 cycles while the compressive fatigue is even worse. The retention of tensile strength decreases with increase in compressive strain.

In contrast to the Kevlar structure, Nomex, a wholly aromatic polyamide, structure has the rigid phenylene and amide units linked in the meta position. The variability in linear structures is substantial, thus resulting in concomitant reduction in Nomex cohesive energy and crystallization. As a whole, Nomex is a poly(*m*-phenylene isophthalamide) (MPD-I) as described by DuPont in 1961 [17]. It was produced by low-temperature polycondensation of *m*-phenylenediamine and dichloride polyamides in amide solvent. In MPD-I, there are aromatic rings parallel but not coplanar. Both the acid- and amine-derived rings are tilted some 30 degrees from the plane of the amine groups. There are also networks of hydrogen bond link molecules in both the a and b directions and perpendicular to the chain axes. Fig. 10.9 shows the crystal and molecular structure of Nomex polyaramid.

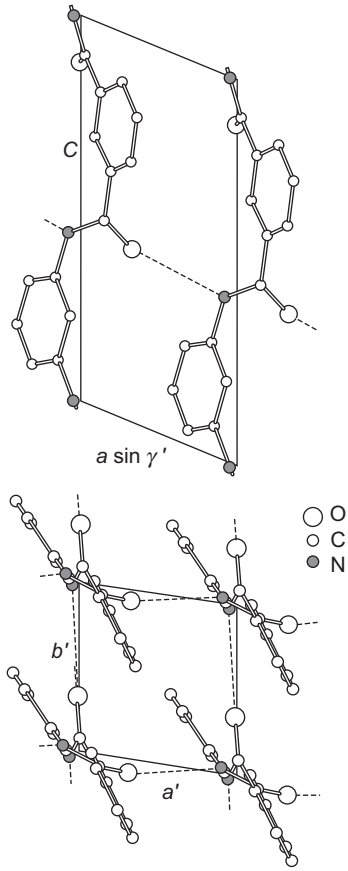

Figure 10.9 Crystal structure of Nomex polyaramid [48].

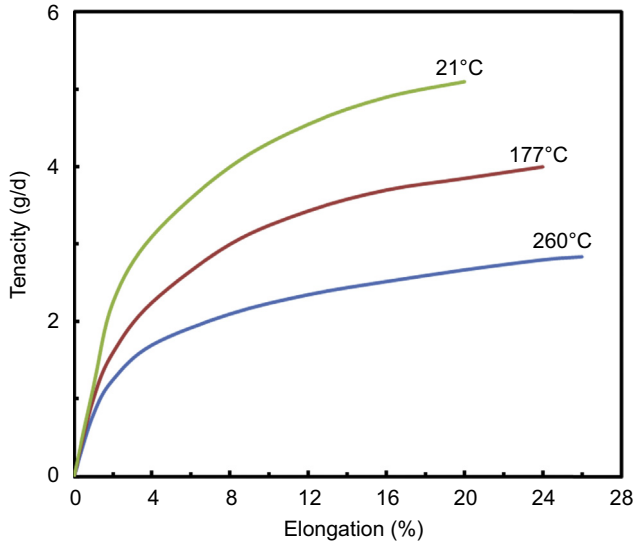

Figure 10.10 Stress–strain curves of Nomex fiber at various temperatures.

The meta-aramid has poor mechanical properties for high-performance fibers. X-ray study of Nomex showed broad peak width indicative of low degree of crystalline orientation [41]. This conformation results in an irregular chain conformation, and thus a lower tensile modulus. Detailed analyses were carried out to identify the effect of thermal exposure on the initial properties of Nomex [42,43]. Fig. 10.10 shows the stress–strain curve of Nomex after exposure to various temperatures for 5 min in air. As observed, the fiber tenacity and modulus decrease with increasing heat treatment temperature, meanwhile the elongation at break increases. However, the fibers still retain more than 60% of their strength. It is important to mention that Nomex was not designed for its strength but rather for its temperature resistance with suitable energy absorption properties.

The other advantage of Nomex is its thermal and dimensional stability. When introduced to a flame or high heat source, Nomex will shrink away because of the high crystallinity. As a result, shrinkage is negligible at high temperature both in air and in hot water for which less than 0.1% was reported. In open flame, Nomex is usually reduced to a thick char that can in return act like as a thermal barrier. The fireproof properties of Nomex are built directly into the molecular structure of the fibers. Nomex has high limiting oxygen index values making it extremely difficult to burn.

Glass transitions of aramid polymers are reported to be in the range of 250°C to >400°C. Because of the high T_g, these fibers are difficult to dye using conventional methods. In response to this, different approaches have been evaluated to improve the dyeability of aramid fibers [44–47]. Polar solvent is one option to ease the dyeability of these fibers. In addition, pretreatment with liquid ammonia or using benzyl alcohol as a carrier was also reported. In pretreatment with liquid ammonia, dyeing conditions call for immersing 2.5 g of meta-aramid in 100 mL of liquid for

10 min at 40°C. The process is usually followed by rinsing with both hot and cold water. However, polar solvents provide chemical energy to the fibers, leading to rearrangement of the polymer chains through breakage and reformation of interchain hydrogen bonding.

Copolymers of meta- and para-aramids were prepared and used to produce fibers. Their possible applications were carefully examined based on the specific performance determined for each one. For instance, copolymerization of terephthaloyl dichloride with p-phenylenediamine and 3-4′ diaminodiphenyl ether (ODA) introduced ODA/PPPT (co-poly-(p-phenylene/3,4-oxydiphenylene terephthalamide)-type aramid commercialized under Technora in 1987 [23]. Other aramid fibers have also been introduced since. Twaron was commercialized in 1988 and recently Russian researchers introduced Armos, a *p*-aromatic hydrocyclic copolyamide.

Most of the recently developed aramid fibers are amorphous to some extent. A comparison study showed that Kevlar is highly crystalline, followed by Nomex (68−95% crystalline). Technora is highly oriented but has relatively lower crystallinity because of the higher flexibility of the copolymer chain and loose crystalline structure. Broad comparison of commercial aramids carried out in the literature encompassed various physical properties and characteristics including crystal lattice parameter, density, equilibrium moisture content, tensile properties at both room and elevated temperatures, thermal properties, and chemical resistance. The strategy here is to have a summary readily available for engineering design issues and choice of material for specific applications.

Publications on the properties, assortment, and applications of aramids, especially the *p*-aramids, suggested classification of these materials into two branches. The first reported dynamic deformation modulus of 130−160 GPa. These materials are in fact designed for high-strength structural and reinforcement of composites with minimal deformability. In addition, average dynamic deformations of 80−120 GPa are obtained for fiber intended for elastomeric composite articles. Some properties of aramid fibers are reported in Table 10.1.

Table 10.1 Comparison of commercial polyaramid high-performance fibers

Properties	Kevlar	Nomex	Technora	Twaron
Density (g/cc)	1.44	1.38	1.39	1.45
Water uptake (%), at 65% relative humidity	3.9	5.2	4.0	5.01
Strength (GPa)	2.9−3.0	0.59−0.86	3.4	2.4−3.6
Modulus (GPa)	70−112	7.9−12.1	72	60−120
Elongation (%)	2.4−3.6	20−45	4.6	2.2−4.4
Flammability (limiting oxygen index)	29	29	25	29−37

10.4 Surface modification of aramid fibers

The possibility of modifying the surface of aramid fibers in a controlled manner has interested researchers for a long time, particularly because of their interest in establishing aramid fibers as reinforcement agents for high-performance composites [49–53]. The goal is obviously restricted because of the poor interfacial adhesion between the aramid fibers and matrix resulting from the relatively smooth and chemically inert surface. Nevertheless, recent efforts to improve the wettability and adhesion have shifted the field to attain the goal.

Various surface modification methods such as plasma technique, ion sputtering, oxidation, and corona discharge have been studied [54–57]. The broad investigation carried out by Li encompassed ammonia plasma treatment of aramid fibers [58]. The strategy here for improving the adhesion performance and surface wettability consisted of introducing nitrogen-containing polar functional groups. A report on the use of dopamine as biomimetic surface modifier agent of meta-aramid fibers describes the improved adhesion of the fiber to rubber matrix [59]. When compared with their untreated counterpart, the adhesion strength has been increased by 62.5%. Wang [60] examined the effect arising from the vapor phase graft polymerization of acrylic acid induced by plasma. The process generated a steady increase in O═C−OH and increased the surface roughness. Fig. 10.11 shows X-ray photoelectron spectroscopy (XPS) spectra of the control and the modified fiber. The differences between the control and the modified aramid fibers are evident based on the surface chemical composition. This is not surprising considering plasma-induced graft polymerization is a reliable process to graft molecular chains onto plasma-treated substrate surfaces.

Kong et al. [61] demonstrated improved adhesion to epoxy of poly(*p*-phenylene terephthalamide) fiber based on treatment in supercritical carbon dioxide with hexamethylene diisocyanate and the atomic force microscopy images are shown in Fig. 10.12. They observed a 22% improvement in the interfacial properties of aramid/epoxy composites. Such improvement is correlated to the superior roughness morphology on the treated fibers, which is caused by a possible new polymer layer obtained from surface crosslinking and grafting reactions of the hexamethylene diisocyanate with the amide group on the surface of the fibers. This is a breakthrough for epoxy reinforcement with aramid fiber applications. An understanding of the adhesion mechanism is important for design and more surface treatment [62–64].

An attempt to evaluate and understand the interfacial adhesion in all aramid/matrix systems is very complicated. Different surface treatments are being developed to promote either the physical or the chemical bonding between the fiber and the matrix [65–71]. Most of them showed little improvement, prompting ongoing research to build a common interpretation of the subject.

Apart from being used as reinforcement agents, aramid fibers have been extensively modified at the surface level for new ventures, and medical, biological, and chemical agent defense protective textiles have attracted a good deal of attention. In this scope, by using atmospheric plasma-induced graft polymerization, it has been shown that free radicals can be attached to the Kevlar surface to improve its antimicrobial activity

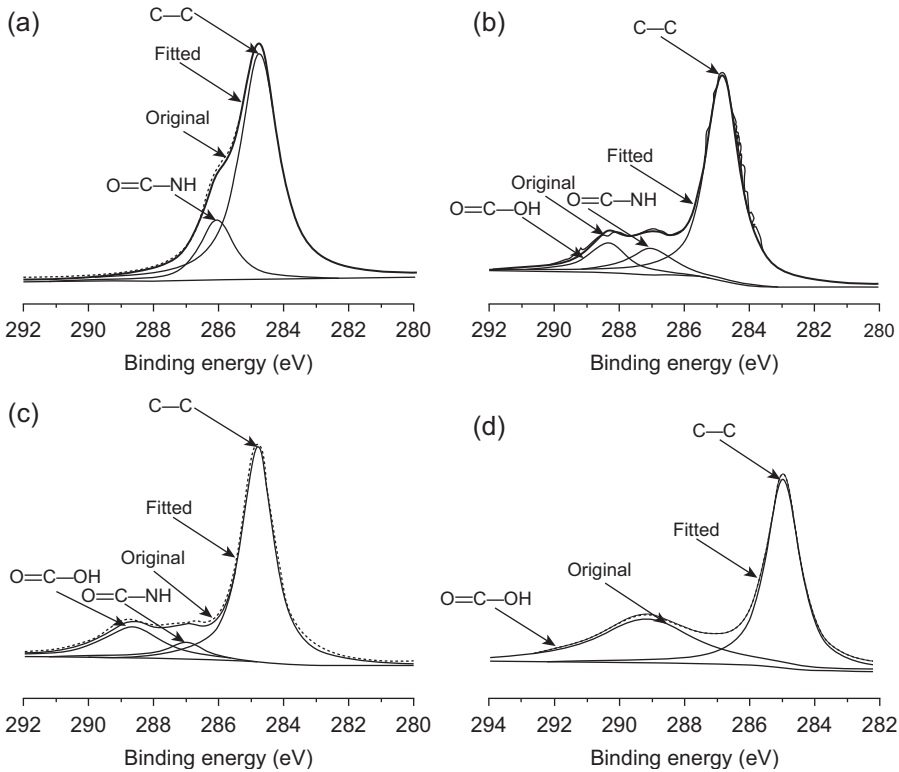

Figure 10.11 Deconvolution of X-ray photoelectron spectroscopy (XPS) core level C1s spectra of the control and the aramid fibers modified by Plasma induced vapor phase graft polymerization (PIVPGP) of acrylic acid (AA) with different plasma treatment times (100 W, N2): (a) control, (b) 5 min, (c) 10 min, and (d) 20 min [60].

through a reduction of bacteria colonies [72]. A systematic investigation by Salter of *N*-chloramide-modified Nomex showed a self-decontaminating regenerable property suitable for military chemical warfare textiles [73]. Many efforts have been devoted to the study of simple chlorine bleaching of aramid fibers to allow regeneration of biocidal function and durable antimicrobial functionality [74].

Wang et al. [75] have successfully prepared a highly electrically conductive meta-aramid fiber for microelectronic or biomedical applications. The method consists first of functionalization of aramid fiber with poly(dopamine) followed by electroless silver plating. The subsequent materials displayed electrical resistivity of 0.61 mΩ cm and the coating was uniform. Others have attempted to coat conductive layers on aramid fiber in the past using techniques such as electrodeposition, electroless plating, self-assembly, and sputtering [76–78]. These methods are cost ineffective, labor intensive, and tedious with limited adhesion between the metal layer and the aramid fibers. The method described by Wang is direct, simple, and eco-friendly as the illustration in Fig. 10.13 shows.

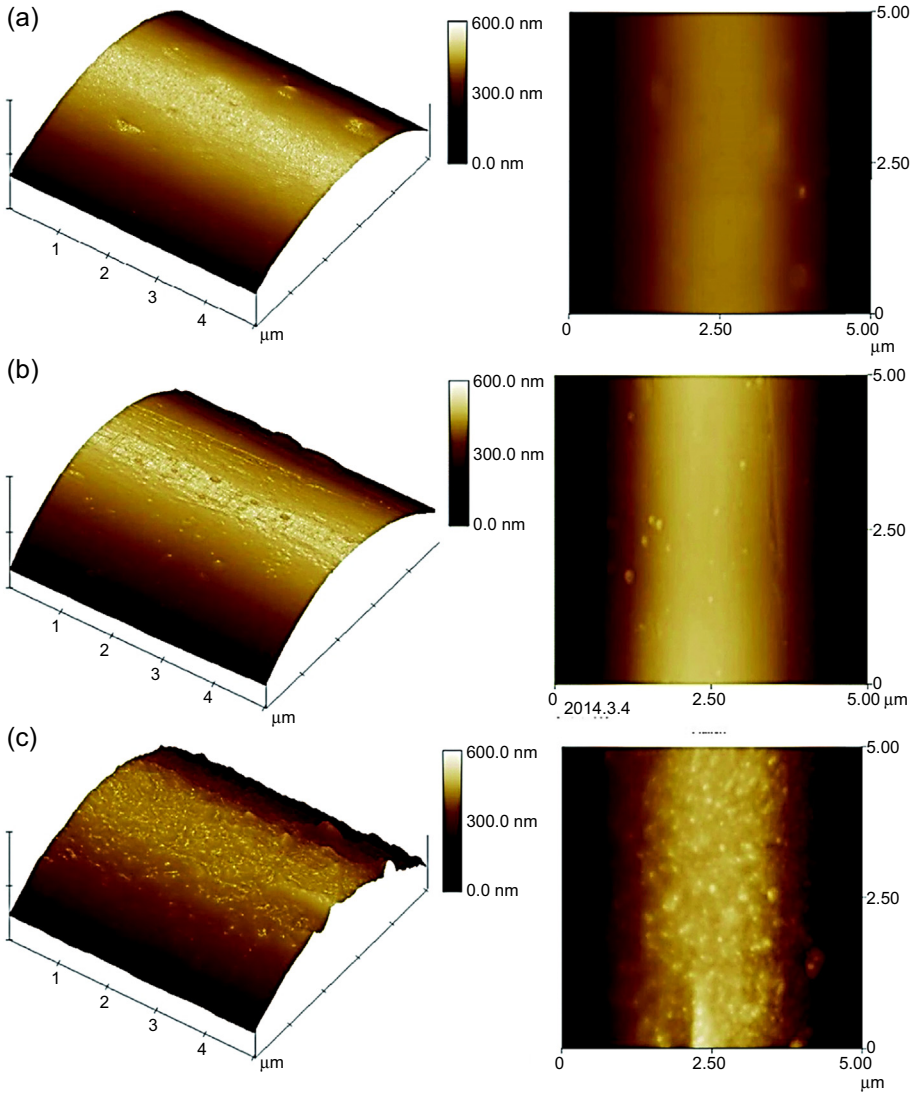

Figure 10.12 Atomic force microscopy images of poly(p-phenylene terephthalamide) fiber (5 µm × 5 µm): (a) untreated PPTA fibers, (b) PPTA fibers treated in supercritical carbon dioxide without hexamethylene diisocyanate, and (c) PPTA fibers treated in ScCO2 with HDI [61].

10.5 Applications

High-performance aramid fibers are well-established material used in various applications. The demand for these engineered materials has increased recently and they are considered as advantageous new materials for novel technical applications. The broad

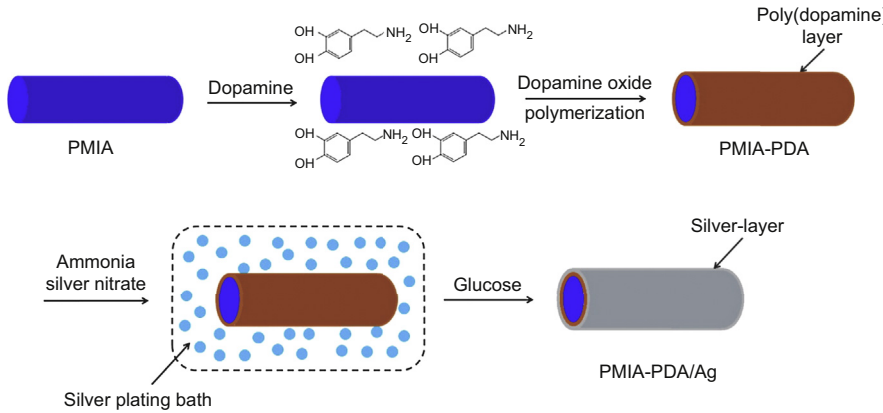

Figure 10.13 Schematic illustration of procedure for fabrication of PMIA−PDA/Ag composite by poly(dopamine)-assisted electroless silver plating [75].

spectrum of aramid fibers can be divided into two vast categories. They are used in apparel-related applications, such as fire protective clothing and bulletproof vests. They are also used in reinforcement applications such as tire cord or automotive components such as gaskets and clutch linings, and in advanced plastic composites used in aircraft and aerospace equipment, military vehicles, sporting goods, and many others including ropes and cables.

Usage of aramid fibers in high-temperature situations is a topic of study. As mentioned earlier, aramid polymers do not melt. They show little decomposition with short exposure to heat but over time degradation becomes significant. Fabric made out of Nomex can be used as protective clothing for firefighters or in electrical insulation [79−84]. Most of these applications do not require excellent tensile properties; hence they are suitable for Nomex fibers. However, some protective apparels such as heat-resistant work wear, cut-resistant protective gloves, and seat cover layers require advanced mechanical properties [85]. To meet the requirements, Kevlar is used in these applications. In addition, it was reported that blends of Kevlar and Nomex were used to take advantage of the unique properties that each bring.

Kevlar finds application as a reinforcement agent for composites [86,87]. The para-aramid is used for ship building, pressure vessels, and sporting goods. The advantages are the light weight, high strength, high modulus, good impact strength, and wear resistance features that are found in para-aramid fibers. For instance, they can be used in aircraft structural components where weight reduction and impact damage tolerance are sought after. Aramid fiber-reinforced composites can absorb two to four times more energy when compared to their carbon fiber-reinforced counterparts. Combining Kevlar and carbon leads to hybrid composites with better properties, for instance, high energy absorption and good structural integrity after crashing. Most of these hybrid composites find applications in commercial aircraft. Aramid fibers are also used in concrete reinforcement to prevent the concrete from cracking between beams.

For ballistic application, only high-performance fabrics that can stop a projectile by absorbing and dissipating its kinetic energy by the work of deformation are considered.

In this instance, aramid fibers are widely used. They are also used for equipment shielding and as a protection for panels. Antiballistic panels can be designed to have laminated structures made of a core layer of foamed material and a shield layer of aramid to stop a projectile passing through.

Dimensional stability is another property that allows aramid fibers to be used in mechanical goods such as conveyor belts, hydraulic hoses, and high-speed tires for trucks and aircraft. However, for these applications, thermal stability is often coupled with low density, high tenacity, low shrinkage, thermal resistance, and chemical resistance.

Properties such as high strength, high modulus, corrosion resistance, good dielectric properties, and heat resistance make aramid fibers suitable for applications in ropes and cables, such as aerial optical cable, electrocable, mechanical construction cable, and mooring lines. Mooring lines are used in oil rigs to probe large depths.

Aramid fibers are finding applications in other, newer fields as their worthiness is still growing. They are used largely in telecommunications. Aramids can be designed intentionally to be hollow for permeation of separation membranes to purify sea water and brackish water. They are also being used in the leisure industry as sailing boat hulls.

New developments in rope technology for high-temperature application have sought out aramid fibers as a potential solution. For such applications, their performance characteristics have been enhanced using specialized additives or by mechanical means. Technora T200 and Twaron 1000, both *p*-aramid types, have been evaluated in this instance because they possess properties that are already suitable. Such properties are the ability to withstand heat for extended periods, good strength, good heat cycling, good abrasion properties, and decent chemical resistance. When a new flame-retardant coating is applied to these fibers, they showed significant improvement. The new flame-retardant-based coating performed better than their polyurethane-based counterpart did.

Although they possess good mechanical properties, the performance of *p*-aramids can be enhanced further by using heat treatment to reach specific desired structures and properties [30]. To the best of our knowledge, a new technique for heating has been carried out and reported in several publications. In these series of experiments, the aramid fibers are treated with hot pins. Small- and wide-angle X-ray scattering techniques showed unambiguously that both structure changes and deformation occurred [88,89], which lead to increase in modulus with simultaneous increase of apparent crystalline size and decrease in tensile strength because pleats start to phase out under tension and formation of microvoids. The recent development in heat treatment is favorable to produce advanced fibers with superior stiffness that are used in composites.

10.6 Conclusion

Given the outstanding properties that high-performance aramid fibers present and the vast array of applications where they are used, it appears that these fibers will continue to be included in advanced and modern technologies. More vigorous interactions

between academia and industry are required for constant adaptation of aramid fibers to new challenges associated with various generations of products. Aramid fibers can still be real actors in tomorrow's solutions scene as some properties can still be optimized.

Extensive investigations have been carried out to shift alternative fibers with comparable mechanical properties and cost effectiveness to challenge the well-established Kevlar and Nomex. Rather than propose a thorough review of these new fibers, we discussed a few examples to show their important properties and performance. For example, M5 fibers obtained from rigid-rod polymer and produced by Magellan Systems International have high compressive strength because of the intermolecular hydrogen bonds formed by its two hydroxyl groups [90]. The lack of compressive strength of Kevlar, its limitation factors, and efforts to improve it are well known [37]. Another example of new high-performance fibers is poly(*p*-phenylene-2,6-benzobisoxazole) (PBO) known commercially as Zylon. Flammability data show PBO time to ignition is three times better than Twaron and four times better than Nomex with minimal heat release rate. These properties go hand in hand with the outstanding tensile modulus and tensile strength of PBO fibers. Polyester-based fibers are cost effective comparable to aramid fibers with acceptable tensile modulus.

References

[1] Rebouillat. High performance fibres. England: Woodhead Publishing; 2000.
[2] Wissbrun KF. Rheology of rod-like polymers in the liquid-crystalline state. Journal of Rheology 1981;25(6):619−62.
[3] Baek SG, Magda JJ, Larson RG. Rheological differences among liquid-crystalline polymers 1. The 1st and 2nd normal stress differences of pbg solutions. Journal of Rheology 1993;37(6):1201−24.
[4] Olmsted PD, Lu CYD. Phase separation of rigid-rod suspensions in shear flow. Physical Review E 1999;60(4):4397−415.
[5] Kwolek SL. In: DuPont, editor. Liquid crystalline polyamides; 1980.
[6] Blades H, U.S. Patent. 1973.
[7] Phillips GTMaHT. New millennium fibers. 2005 [USA].
[8] Young RJ, et al. Relationship between structure and mechanical-properties for aramid fibers. Journal of Materials Science 1992;27(20):5431−40.
[9] Rao Y, Waddon AJ, Farris RJ. Structure-property relation in poly(p-phenylene terephthalamide) (PPTA) fibers. Polymer 2001;42(13):5937−46.
[10] Barton R. Paracrystallinity-modulus relationships in kevlar aramid fibers. Journal of Macromolecular Science-Physics 1985;B24(1−4):119−30.
[11] Morgan PW, Kwolek SL. Interfacial polycondensation 2. Fundamentals of polymer formation at liquid interfaces. Journal of Polymer Science 1959;40(137):299−327.
[12] Morgan PW, Kwolek SL. Interfacial polycondensation 12. Variables affecting stirred polycondensation reactions. Journal of Polymer Science 1962;62(173):33−58.
[13] Morgan PW. Condensation polymers. New York: Interscience Publishers; 1965.
[14] Morgan PW, Kwolek SL. Interfacial polycondensation 13. Viscosity-molecular weight relationship and some molecular characteristics of 6-10 polyamide. Journal of Polymer Science Part A-General Papers 1963;1(4):1147−62.

[15] Yokozawa T, et al. Convenient method of chain-growth polycondensation for well-defined aromatic polyamides. Macromolecular Rapid Communications 2005;26(12):979−81.
[16] Yokozawa T, et al. Chain-growth polycondensation for nonbiological polyamides of defined architecture. Journal of the American Chemical Society 2000;122(34):8313−4.
[17] Jassal M, Ghosh S. Aramid fibres − an overview. Indian Journal of Fibre & Textile Research 2002;27(3):290−306.
[18] Ones RSJ, High M. In: Lewin M, Preston J, editors. High performance aramid fibers. New York: MarcelDekker; 1985.
[19] Oishi Y, Kakimoto MA, Imai Y. Synthesis of aromatic polyamide-imides from N,N′-bis (trimethylsilyl)-substituted aromatic diamines and 4-chloroformylphthalic anhydride. Journal of Polymer Science Part A-Polymer Chemistry 1991;29(13):1925−31.
[20] Oishi Y, Kakimoto MA, Imai Y. Synthesis of aromatic polyamides from N,N′-bis(trimethylsilyl)-substituted aromatic diamines and aromatic diacid chlorides. Macromolecules 1988;21(3):547−50.
[21] Burch RR, Manring LE. N-Alkylation and hofmann elimination from thermal-decomposition of R4N+ salts of aromatic polyamide polyanions − synthesis and stereochemistry of N-alkylated aromatic polyamides. Macromolecules 1991;24(8):1731−5.
[22] Oishi Y, et al. Preparation and properties of new aromatic polyamides from 4,4′-diaminotriphenylamine and aromatic dicarboxylic-acids. Journal of Polymer Science Part A-Polymer Chemistry 1990;28(7):1763−9.
[23] Garcia JM, et al. High-performance aromatic polyamides. Progress in Polymer Science 2010;35(5):623−86.
[24] Kwolek SL, et al. Synthesis, anisotropic solutions, and fibers of poly(1,4-benzamide). Macromolecules 1977;10(6):1390−6.
[25] Radding S. Stephanie Kwolek, Kevlar, US Patents 3,819,587 and RE 30,352. Abstracts of Papers of the American Chemical Society 1998;216:U353.
[26] Yao J, Bastiaansen CW, Peijs T. High strength and high modulus electrospun nanofibers. Fibers 2014;2(2):158−86.
[27] Picken SJ, et al. Liquid crystal main-chain polymers for high-performance fibre applications. Liquid Crystals 2011;38(11−12):1591−605.
[28] Zhong HP, et al. Effect of tension on mechanical properties and structure of aramid fibers during heat treatment. Pts 1-3. In: Kim YH, Yarlagadda P, editors. Advanced technologies in manufacturing, engineering and materials; 2013. p. 856−9.
[29] Hyun BD, et al. Structure and property relations in heat-treated para-aramid fibers. Textile Science and Engineering 2010;47(1):15−21.
[30] Ahmed D, et al. Microstructural developments of poly (p-phenylene terephthalamide) fibers during heat treatment process: a review. Materials Research-Ibero-American Journal of Materials 2014;17(5):1180−200.
[31] Watanabe A, et al. Fatigue behavior of aramid nonwoven fabrics under hot-press conditions − Part IV: effect of fiber fineness on mechanical properties. Textile Research Journal 1998;68(2):77−86.
[32] Watanabe A, Miwa M, Yokoi T. Fatigue behavior of aramid nonwoven fabrics under hot-press conditions − Part VI: effect of stable base fabrics on mechanical properties. Textile Research Journal 1999;69(1):1−10.
[33] Dobb MG, Johnson DJ, Saville BP. Supramolecular structure of a high-modulus polyaromatic fiber (kevlar 49). Journal of Polymer Science Part B-Polymer Physics 1977; 15(12):2201−11.
[34] Pruneda CO, et al. Structure-property relations of kevlar-49 fibers. Abstracts of Papers of the American Chemical Society 1981;182(AUG):138 [POLY].

[35] Warner SB. On the radial structure of kevlar. Macromolecules 1983;16(9):1546−8.
[36] Riekel C, et al. X-ray microdiffraction study of chain orientation in poly(p-phenylene terephthalamide). Macromolecules 1999;32(23):7859−65.
[37] Sweeny W. Improvements in compressive properties of high modulus fibers by cross-linking. Journal of Polymer Science Part A-Polymer Chemistry 1992;30(6):1111−22.
[38] Newell JA, Spence M. Novel applications for high performance polymers. Recent Research Developments in Applied Polymer Science 2002;vol. 1(Pt 1):321−40.
[39] Chatzi EG, Ishida H, Koenig JL. AN FT-IR Study of the water absorbed in kevlar-49 fibers. Applied Spectroscopy 1986;40(6):847−51.
[40] Panar M, et al. Morphology of poly (p-phenylene terephthalamide) fibers. Journal of Polymer Science: Polymer Physics Edition 1983;21(10):1955−69.
[41] Hamilton LE, Sherwood PMA, Reagan BM. X-Ray photoelectron-spectroscopy studies of photochemical changes in high-performance fibers. Applied Spectroscopy 1993;47(2): 139−49.
[42] Jain A, Vijayan K. Thermally induced structural changes in Nomex fibres. Bulletin of Materials Science 2002;25(4):341−6.
[43] Cui Z-y, Ma C, Lv N. Effects of heat treatment on the mechanical and thermal performance of fabric used in firefighter protective clothing. Fibres & Textiles in Eastern Europe 2015; 23(2):74−8.
[44] Cao G, et al. Structural and dyeing properties of aramid treated with 2-phenoxyethanol. Coloration Technology 2015;131(5):384−8.
[45] Islam MT, et al. Use of N-methylformanilide as swelling agent for meta-aramid fibers dyeing: kinetics and equilibrium adsorption of Basic Blue 41. Dyes and Pigments 2015; 113:554−61.
[46] Dyeing of aramid fibres|for use in weaving of fire resistant textile or carpet, pretreating the fibres with tert amine, e.g pyridine soln. Monsanto Co.
[47] Ulery HE. Sorption of basic-dyes by expanded dispersions of nomex (DUP) aromatic polyamide (ARAMID). Journal of the Society of Dyers and Colourists 1974;90(11): 401−10.
[48] Tashiro K, Kobayashi M, Tadokoro H. Elastic-moduli and molecular-structures of several crystalline polymers, including aromatic polyamides. Macromolecules 1977;10(2): 413−20.
[49] Zhang YH, et al. Influence of gamma-ray radiation grafting on interfacial properties of aramid fibers and epoxy resin composites. Composite Interfaces 2008;15(6):611−28.
[50] Zhang SF, Zhang MY. Direct measurement of the adhesion forces between aramid fiber-fibrids surfaces by AFM. In: Jin Y, Zhai H, Li Z, editors. Proceedings of international conference on pulping, papermaking and biotechnology 2008: Icppb '08, vol. 2; 2008. p. 368−76.
[51] Lv M, et al. Friction and wear behaviors of carbon and aramid fibers reinforced polyimide composites in simulated space environment. Tribology International 2015;92:246−54.
[52] Hazarika A, et al. Growth of aligned ZnO nanorods on woven Kevlar (R) fiber and its performance in woven Kevlar (R) fiber/polyester composites. Composites Part A-Applied Science and Manufacturing 2015;78:284−93.
[53] de Lange PJ, et al. Adhesion activation of Twaron (R) aramid fibres studied with low-energy ion scattering and x-ray photoelectron spectroscopy. Surface and Interface Analysis 2001;31(12):1079−84.
[54] Brown JR, Mathys Z. Plasma surface modification of advanced organic fibres .5. Effects on the mechanical properties of aramid/phenolic composites. Journal of Materials Science 1997;32(10):2599−604.

[55] Chen, P., et al., Method modifying the interface of aramid fiber reinforced PPESK resin base composite. Univ Dalian Technology; Shenyang Inst Aeronautical Eng; Shenyang Aviation Ind College.
[56] Plawky U, Londschien M, Michaeli W. Surface modification of an aramid fibre treated in a low-temperature microwave plasma. Journal of Materials Science 1996;31(22):6043−53.
[57] Stepankova M, et al. Using of DSCBD plasma for treatment of kevlar and nomex fibers. Chemicke Listy 2008;102:S1515−8.
[58] Li S, et al. Surface modification of aramid fibers via ammonia - plasma treatment. Journal of Applied Polymer Science 2014;131(10).
[59] Sa R, et al. Surface modification of aramid fibers by bio-inspired poly(dopamine) and epoxy functionalized silane grafting. ACS Applied Materials & Interfaces 2014;6(23): 21730−8.
[60] Wang CX, et al. Surface modification of aramid fiber by plasma induced vapor phase graft polymerization of acrylic acid. I. Influence of plasma conditions. Applied Surface Science 2015;349:333−42.
[61] Kong HJ, et al. Surface modification of poly(p-phenylene terephthalamide) fibers with HDI assisted by supercritical carbon dioxide. RSC Advances 2015;5(72):58916−20.
[62] Mahy J, Jenneskens LW, Grabandt O. The fiber-matrix interphase and the adhesion mechanism of surface-treated Twaron(R) aramid fiber. Composites 1994;25(7):653−60.
[63] Mahy J, et al. Adhesion activation of Twaron (R) aramid fibre. In: Olij WJV, Anderson HR, editors. First international congress on adhesion science and technology − invited papers: festschrift in honor of Dr. K.L. Mittal on the occasion of his 50th birthday; 1998. p. 407−25.
[64] Garton A, Daly JH. The crosslinking of epoxy-resins at interfaces 2. At an aromatic polyamide surface. Journal of Polymer Science Part A-Polymer Chemistry 1985;23(4): 1031−41.
[65] Kalantar J, Drzal LT. The bonding mechanism of aramid fibers to epoxy matrices 1. A review of the literature. Journal of Materials Science 1990;25(10):4186−93.
[66] Kalantar J, Drzal LT. The bonding mechanism of aramid fibers to epoxy matrices 2. An experimental investigation. Journal of Materials Science 1990;25(10):4194−202.
[67] Andrews MC, Bannister DJ, Young RJ. The interfacial properties of aramid/epoxy model composites. Journal of Materials Science 1996;31(15):3893−913.
[68] Padmanabhan K, Kishore. Interlaminar shear of woven fabric kevlar-epoxy composites in 3-point loading. Materials Science and Engineering A-Structural Materials Properties Microstructure and Processing 1995;197(1):113−8.
[69] de Lange PJ, et al. Characterization and micromechanical testing of the interphase of aramid-reinforced epoxy composites. Composites Part A-Applied Science and Manufacturing 2001;32(3−4):331−42.
[70] Park R, Jang J. Impact behavior of aramid fiber/glass fiber hybrid composites: the effect of stacking sequence. Polymer Composites 2001;22(1):80−9.
[71] Zhang XY, et al. Effects of plasma-induced epoxy coatings on surface properties of Twaron fibers and improved adhesion with PPESK resins. Vacuum 2013;97:1−8.
[72] Widodo M, El-Shafei A, Hauser PJ. Surface nanostructuring of kevlar fibers by atmospheric pressure plasma-induced graft polymerization for multifunctional protective clothing. Journal of Polymer Science Part B-Polymer Physics 2012;50(16):1165−72.
[73] Salter B, et al. N-chloramide modified Nomex(A (R)) as a regenerable self-decontaminating material for protection against chemical warfare agents. Journal of Materials Science 2009;44(8):2069−78.

[74] Sun YY, Sun G. Novel refreshable N-halamine polymeric biocides: N-chlorination of aromatic polyamides. Industrial & Engineering Chemistry Research 2004;43(17): 5015−20.
[75] Wang WC, et al. Surface silverized meta-aramid fibers prepared by bio-inspired poly(dopamine) functionalization. ACS Applied Materials & Interfaces 2013;5(6):2062−9.
[76] Love JC, et al. Self-assembled monolayers of thiolates on metals as a form of nanotechnology. Chemical Reviews 2005;105(4):1103−69.
[77] Kobayashi Y, Salgueirino-Maceira V, Liz-Marzan LM. Deposition of sliver nanoparticles on silica spheres by pretreatment steps in electroless plating. Chemistry of Materials 2001; 13(5):1630−3.
[78] Peng C, Jin J, Chen GZ. A comparative study on electrochemical co-deposition and capacitance of composite films of conducting polymers and carbon nanotubes. Electrochimica Acta 2007;53(2):525−37.
[79] Smeulders, B.., Protective clothing for use as fire-brigade uniform, comprises outer fabric with meta aramid and aromatic polyester, where outer fabric comprises Ripstop binding, and aromatic polyester is provided in rib. Ibena Textilwerke Gmbh.
[80] Choi I-R, Jeon G. Study on the protective clothing-thermal characteristics of the protective clothing exposed to the radiation heat. The Research Journal of the Costume Culture 2005; 13(2):314−7.
[81] Lee YS, Jeong JS. A study on the textile for protective clothing of fire fighters. Family and Environment Research 2002;40(5):15−24.
[82] Double woven aramid fabric|for use in protective clothing. [Anonymous].
[83] Dillon IG, Obasuyi E. Permeation of hexane through butyl nomex. American Industrial Hygiene Association Journal 1985;46(5):233−5.
[84] Gu H. Research on thermal properties of Nomex/Viscose FR fibre blended fabric. Materials & Design 2009;30(10):4324−7.
[85] Su FH, et al. Study on the friction and wear properties of the composites made of surface modified-Nomex fabrics. Materials Science and Engineering A-Structural Materials Properties Microstructure and Processing 2006;416(1−2):126−33.
[86] Manero II A, et al. Evaluating the effect of nano-particle additives in Kevlar (R) 29 impact resistant composites. Composites Science and Technology 2015;116:41−9.
[87] Yao J, et al. High performance co-polyimide nanofiber reinforced composites. Polymer 2015;76:46−51.
[88] Ellison MS, Lopes PE, Pennington WT. In-situ x-ray characterization of fiber structure during melt spinning. Journal of Engineered Fibers and Fabrics 2008;3(3):10−21.
[89] Reinhold C, Fischer EW, Peterlin A. Evaluation of small-angle X-Ray scattering of polymers. Journal of Applied Physics 1964;35(1):71−5.
[90] Afshari M, et al. High performance fibers based on rigid and flexible polymers. Polymer Reviews 2008;48(2):230−74.

Electrospun nanofibers

11

E. Zdraveva [1,2], J. Fang [1], B. Mijovic [2], T. Lin [1]
[1]Deakin University, Victoria, Australia; [2]University of Zagreb, Zagreb, Croatia

11.1 Introduction

Nanofibers were initially defined as fibers with diameters below 100 nm. However, the scope of nanofibers has been broadened in recent years with all fibers of diameter less than 1 μm included. Nanofibers have shown high surface-to-volume (or weight) ratio, and their assemblies often have a porous structure with excellent pore interconnectivity. These unique properties together with the functionalities from the materials themselves have resulted in many novel properties and applications.

A number of techniques have been reported to prepare nanofibers, including splitting of bicomponent fibers [1], melt-blowing [2], physical drawing [3], flash-spinning [4], phase separation [5], self-assembling [6], solvent dispersion [7], centrifugal spinning [8], hydrothermal [9], and electrospinning. The fiber-making principle and nanofiber diameter ranges are given in Table 11.1. Among all these techniques, electrospinning is distinct from the others for its versatility to prepare nanofibers from a wide selection of materials, ability to control nanofiber diameter, morphology and fibrous structure, ease of modification through adding various soluble substances or nanomaterials to the solution for electrospinning, the possibility of preparing nanofibers with bicomponent configuration (eg, core—sheath, side-by-side, islands-in-a-sea, and pie-wedges), porous structure, surface porous nanofiber, and even nanotubes.

11.2 Electrospinning

Electrospinning is a process that can directly convert a polymer fluid into dry nanofibers. Although it was invented a century ago, it was only in recent decades that the advantages of electrospinning were discovered. The basic setup for electrospinning comprises a high-voltage power supply, polymer solution container, and a grounded collector, as illustrated in Fig. 11.1.

11.2.1 Brief history

The very early finding concerning electrically drawn drops of water under charged amber was reported in the year of 1600 by W. Gilbert [10]. In 1882, Lord Rayleigh estimated charged liquids, which resulted in fine jets [11]. Some early patents were filed at the beginning of the 20th century by J.F. Cooley [12,13] and W.J. Morton [14] on the methods and apparatus for separation and dispersion of charged fluids.

Structure and Properties of High-Performance Fibers. http://dx.doi.org/10.1016/B978-0-08-100550-7.00011-5

Table 11.1 Nanofiber-making techniques and fiber diameter ranges [1–9]

Techniques	Principle	Diameter range
Splitting of bicomponent fibers	Removal of one polymer out of islands-in-the-sea (or citrus pie)-spun fibers	>800 nm
Melt-blowing	Drawing polymer melt using hot air jet	>800 nm
Physical drawing	Physically drawing polymer solution	>50 nm
Flash-spinning	Simultaneous heating and pressurizing of polymer fluid	>200 nm
Phase separation	Formation of fibers by induced phase separation of solution	50–500 nm
Self-assembling	Self-organization of molecules in solution	<100 nm
Solvent dispersion	Shear-enhanced solvent precipitation in nonsolvent	~100 nm
Centrifugal spinning	Drawing spinning fluid using centrifugal force	>100 nm
Hydrothermal	Formation of fibers in hydrothermal solution	50–120 nm
Electrospinning	Stretching of solution by high electric field	10 nm to a few microns

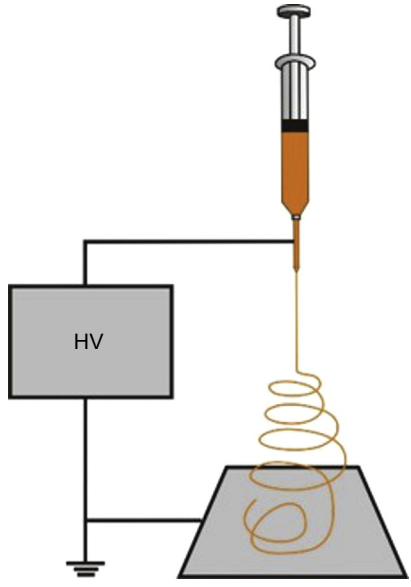

Figure 11.1 Basic electrospinning setup. *HV*, High voltage.

A series of patents were then filed by A. Formhals between 1934 and 1944 to develop devices for electrospinning of cellulose-based solutions [15–20]. The first melt electrospinning patent (on both method and apparatus) was filed by C.L. Norton in 1936 [21].

From 1964 to 1969, G.I. Taylor set the mathematical model of the conical-shaped charged fluid drop. He reported that a cone-like drop existed in equilibrium only with a semivertical angle of 49.3 degrees, and this cone has been named after him as the "Taylor cone." He also reported on the first calculation on the bending instability of jets [22–25]. In the 1990s, D.H. Reneker and his researchers reinvestigated the electrospinning process and reported its potential in making nanofibers [26,27], which set off the boom of electrospinning research.

11.2.2 Physical principle

For electrospinning, the polymer solution is electrically charged and with the increase of the electrical field intensity, the solution receives stronger stretching. This results in the formation of a Taylor cone on the nozzle tip. When the electric field force overcomes the surface tension of the polymer solution, a jet is ejected from the cone. This charged jet then has an intensive interaction with the electric field, leading to thinning of the jet. The solvent evaporation leaves solid fibers [26]. The jet during electrospinning undergoes several phases: Taylor cone, stable straight jet, bending instability (also referred to as "whipping instability"), and dry fiber [28].

11.2.3 Effect parameters

Many parameters influence the final morphology of electrospun nanofibers. These effect factors can be classified into three categories: (1) material properties (eg, concentration, viscosity, conductivity, surface tension), (2) processing parameters (eg, electrical voltage, flow rate, spinning distance), and (3) ambient condition (eg, temperature, humidity).

11.2.3.1 Polymer solutions

To obtain uniform nanofibers, optimal conditions of polymer concentration, viscosity, conductivity, and surface tension are needed. Polymer solution concentration has been reported as the most dominant factor in the formation of uniform nanofibers. There is a direct relationship between the solution concentration and viscosity, and many studies have indicated the increase in the fiber diameter with increasing the solution viscosity [29]. At very low concentrations, no fiber is formed by electrospinning because of low viscosity. This is because a jet from a dilute polymer solution is unable to withstand stretching, and spraying often takes place especially at a high applied voltage [30].

At a low polymer concentration, polymer solution is often electrospun into beaded fibers, whereas at very high concentrations, curly and wavy fibers with straight segments often result (Fig. 11.2). These defects decrease the surface-to-volume ratio [31].

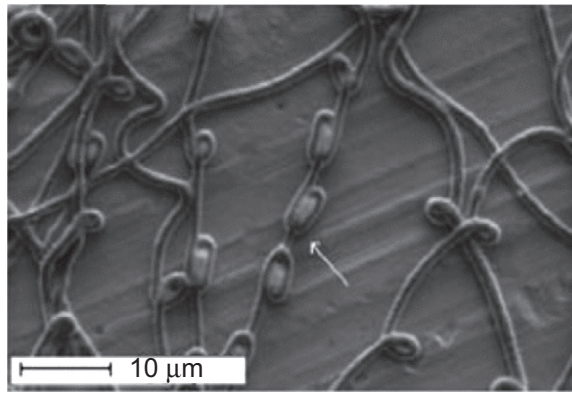

Figure 11.2 Curly and wavy fibers prepared by electrospinning.
Reprinted with permission from Demir MM, et al. Electrospinning of polyurethane fibers. Polymer 2002;43(11):3303−9. Copyright (2002) Elsevier Science Ltd.

The formation of beaded fibers is dependent upon surface tension and viscoelastic characteristics of the polymer solution. Solution viscosity and number of beads formation are inversely proportional. By increasing the viscosity, the distance between the beads increases and the shape changes from sphere to spindle [32].

The solvent is the main factor determining the surface tension of polymer solution. Higher surface tension results in jet instability [33], but low surface tension not always results in fine fibers because the rate of the solvent evaporation also influences fiber diameter. When a multisolvent system is used, for example, a mixture of tetrahydrofuran and *N*,*N*-dimethylformamide for electrospinning of polystyrene (PS) [34], flat and coarse fibers were formed. Fiber diameter also decreased with the increase of polymer molecular weight, independent of the solvent type.

The addition of surfactants also has an influence on the surface tension, other solution properties, and thus fiber morphology. For example, when PS was electrospun with the inclusion of cationic surfactants, such as dodecyltrimethylammonium bromide and tetrabutylammonium chloride, in the electrospinning solution, bead formation was effectively eliminated because of the increased net charge density in the solution [35]. The addition of the nonionic surfactant Triton X-405 slightly changed the surface tension, improved conductivity, and reduced the number of fiber beads [35].

Jet elongation is dependent on the electrical forces that are related to the solution electrical conductivity, applied voltage, and electrospinning distance. Slightly increasing solution conductivity causes stronger stretching of the jet along the axis, and hence results in finer fibers [36]. However, the electric force decreases if the solution conductivity is higher than a critical value. Solvent and polymer, as well as additives such as salts in the solution, contribute to solution conductivity. For example, when different inorganic salts were added to a polyamide 6 (PA 6) solution, both viscosity and electrical conductivity changed while the surface tension was almost unchanged [37].

11.2.3.2 Processing parameters

Applied voltage is the major parameter influencing fiber diameter and morphology. When the applied voltage increases, two opposite effects on the fiber diameter could be observed: (1) stretching force on solution jet normally increases with the increase in applied voltage, which results in finer fibers [38]; (2) higher electrical voltage favored the formation of defects along the fibers [39]. By increasing applied voltage, the bead reduces the size and the interbead distance becomes shorter. Sometimes thicker fibers with more spherical beads were formed by increasing the voltage [40].

However, many studies have reported that the change in fiber diameter with applied voltage was not significant [41,42], and sometimes the fiber diameter even increases with increasing applied voltage [36,43]. These different experimental observations have demonstrated that applied voltage influences many aspects of an electrospinning process.

Generally speaking, the diameter of electrospun nanofibers decreases with increased spinning distance. This is caused by increased jet stretching time [26]. With increased spinning distance, it is more likely to obtain round-shaped fibers. This is because at short spinning distances, wet fibers with irregular cross-section could form because of insufficient solvent evaporation [38].

Flow rate of polymer solution is often controlled by electric field. For needle electrospinning, solution drops come with fibers when the flow rate is larger than a critical value. This is because of the insufficient spinning ability. In the adjustable range, higher flow rates often result in larger fiber diameters and larger beads, because of larger drop formation at the tip of the needle and shorter time for solvent evaporation [40].

11.2.3.3 Ambient condition

The most intensively explored ambient conditions in electrospinning are humidity and temperature. With the change in the humidity during electrospinning, the fiber morphology changes accordingly. Humidity was reported to be closely related to the formation of porous fibers. For example, during electrospinning of PS at different humidities, fibers with different pore shapes, pore sizes, and pore size distributions resulted. At a relative humidity below 25%, the fibers were smooth. Pores were formed on the fiber surface when the humidity was over 38%, with uniform circular shapes and relatively uniform distribution. Uneven pores were observed at up to 59% of humidity, and a very high number of distributed pores as well. The number of pores slightly increased when the humidity increased up to 72%. Fig. 11.3 shows the surface morphology of the porous electrospun PS fibers [44].

It was also reported that increasing polymer solution temperature reduced surface tension, viscosity, and conductivity. The morphology of electrospun PA 6 fibers changed only slightly when the polymer solution temperature was maintained between 30 and 60°C, but the fiber diameter decreased. Further increase in the temperature resulted in increased fiber production rate [37].

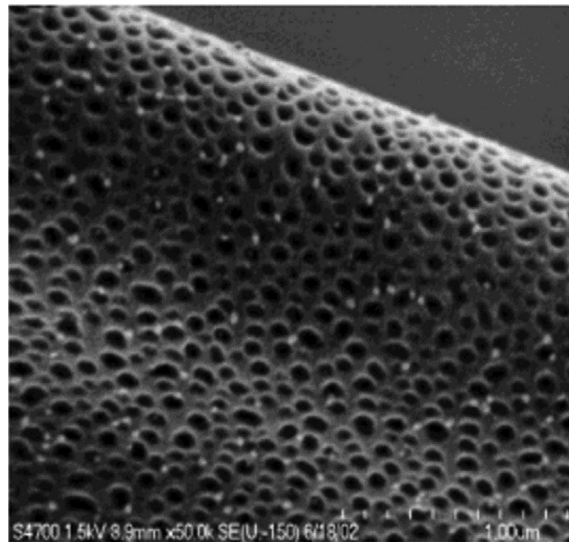

Figure 11.3 PS fiber with surface porous structure electrospun at a humidity of 50%. Reprinted with permission from Casper CL, et al. Controlling surface morphology of electrospun polystyrene fibers: effect of humidity and molecular weight in the electrospinning process. Macromolecules 2004;37(2):573−8. Copyright (2004) American Chemical Society.

11.2.4 Advanced electrospinning

Electrospinning is conventionally performed using a needle-like nozzle. Despite a number of advantages for needle electrospinning, its main drawback is low production rate, which limits the broad applications of electrospun nanofibers. Also it is hard to use a normal needle nozzle to prepare bicomponent nanofibers. Nanofibers produced by conventional electrospinning are mainly in the form of a randomly oriented fiber web. To break those limits, advanced electrospinning techniques have been developed. In this section, three advanced electrospinning techniques, that is, bicomponent electrospinning, needleless electrospinning, and yarn electrospinning, are introduced in detail.

11.2.4.1 Bicomponent electrospinning

Bicomponent electrospinning has been widely used to prepare nanofibers with two component cross-sectional configurations. Some typical bicomponent electrospinning setups and fiber structures are presented in Fig. 11.4. In some early work on bicomponent electrospinning, Sun et al. [45] reported on coaxial electrospinning consisting of a syringe-in-syringe configuration to prepare core−sheath nanofibers. Both polymer solutions in the syringes were pressured to stabilize the process (Fig. 11.4(a)). Further on, Li and Xia [46] demonstrated the fabrication of core−sheath and hollow nanofibers through a coaxial spinneret (Fig. 11.4(b)). Two immiscible liquids, mineral oil and

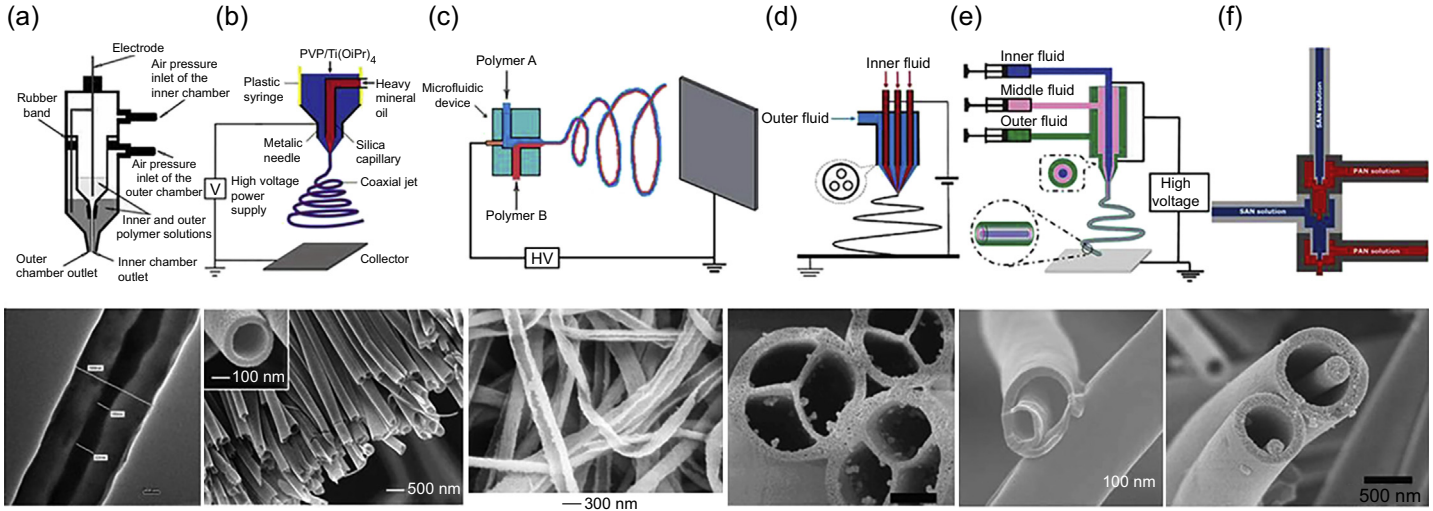

Figure 11.4 Bicomponent electrospinning setups and their corresponding nanofiber structures. (a) Coaxial electrospinning. *(Reprinted with permission from Sun Z, et al. Compound core−shell polymer nanofibers by co-electrospinning. Advanced Materials 2003;15(22):1929−32. Copyright (2003) WILEY-VCH Verlag GmbH & Co. KGaA, Weinheim).* (b) Coaxial electrospinning. *(Reprinted with permission from Li D, Xia Y. Direct fabrication of composite and ceramic hollow nanofibers by electrospinning. Nano Letters 2004;4(5):933−8. Copyright (2004) American Chemical Society.)* (c) Side-by-side electrospinning. *(Reprinted with permission from Lin T, Wang H, Wang X. Self-crimping bicomponent nanofibers electrospun from polyacrylonitrile and elastomeric polyurethane. Advanced Materials 2005;17(22):2699−703. Copyright (2005) WILEY-VCH Verlag GmbH & Co. KGaA, Weinheim.)* (d) Multifluidic electrospinning. *(Reprinted with permission from Zhao Y, Cao X, Jiang L. Bio-mimic multichannel microtubes by a facile method. Journal of the American Chemical Society 2007;129(4):764−5. Copyright (2007) American Chemical Society.)* (e) Triaxial electrospinning. *(Reprinted with permission from Chen H, et al. Nanowire-in-microtube structured core/shell fibers via multifluidic coaxial electrospinning. Langmuir 2010;26(13):11291−6. Copyright (2010) American Chemical Society.)* (f) Quadruple coaxial electrospinning [51].

polyvinylpyrrolidone/titanium tetraisopropoxide [PVP/Ti(OiPr)$_4$], were fed into coaxial capillaries, to form core and sheath, respectively. Nanofibers with continuous or segmented hollow cores were obtained by the removal of the oil through solvent extraction. The work was extended to the fabrication of surface (outer and inner)-functionalized hollow nanofibers containing dye molecules, silane, magnetic nanoparticles, or other species [47].

A different approach in the electrospinning of a side-by-side bicomponent nanofiber was reported by Lin et al. in 2005 (Fig. 11.4(c)) [48]. The group used a microfluidic device as the spinneret to prepare side-by-side polyurethane (PU)/polyacrylonitrile (PAN) nanofibers. The microfluidic device consisted of three channels: two side channels were fed with spinning solutions into the main channel to conduct spinning. Because of the elasticity difference between the elastomeric PU and thermoplastic PAN, self-crimping nanofibers were obtained.

Later on, multifluidic electrospinning was introduced by Zhao et al. [49]. In their setup, three metallic capillaries were inserted in the main solution channel (Fig. 11.4(d)). By filling three capillaries with paraffin oil and using PVP/Ti(OiPr)$_4$ in the main channel, a hollow fiber structure with three channels was obtained by removing the organic compound afterward. With the same spinneret configuration, hollow fibers with up to five channels were also reported by the group. Another multifluidic triaxial electrospinning was conducted by Chen et al. [50] for the fabrication of fibers with a nanowire-in-microtube structure (Fig. 11.4(e)). The setup consisted of three coaxial capillaries. TiO_2 nanofibers were prepared by using Ti(OBu)$_4$ as the outer and the inner precursor, with the middle layer filled with paraffin/water emulsion, later on removed by calcination. Recently, a report on a quadruple coaxial electrospinning setup for the fabrication of double tubular carbon nanofibers was reported (Fig. 11.4(f)). Initially, tetra-layered nanofibers were prepared by coaxial electrospinning of styrene-*co*-acrylonitrile (SAN) and PAN, which were supplied in the nozzle in SAN/PAN/SAN/PAN alternating mode. To produce the hollow double tubular carbon nanofibers (CNFs) the fibers were further heat treated [51].

11.2.4.2 Needleless electrospinning

Needleless electrospinning does not use a needle-like nozzle to generate nanofibers. Instead, numerous solution jets are initiated from an open liquid surface [52]. The first needleless setup was patented by Simm et al. in 1979 [53]. The work described the usage of a rotating ring as a substitute for a needle in conventional electrospinning. The ring was supported by three rollers and partially dipped into the polymer solution container. Fiber fleece was collected by two side conductive conveyor belts. In 2004 Yarin and Zussman [54] described a needleless electrospinning setup combining both magnetic and electric fields. Numerous cones resulting in jets of nanofibers were driven from the surface of a polymer solution as the top layer in a container. The lower layer of the fluid was filled with magnetic fluid, which caused the upper layer to initiate multiple jets under an external magnetic field. The first commercial needleless electrospinning was constructed by Jirsak et al. in 2005 [55,56]. It was an upward needleless electrospinning setup, in which a rotating cylinder was immersed in the solution

container to generate the nanofibers. In 2006 a porous cylinder tube spinneret was reported by Dosunmu et al. [57]. Polymer solution was forced through the tube pores and collected by a surrounding coaxial wire mesh collector. To help draw the jet away from the tube, air was fed from the top of the tube. In 2007 Liu and He [58] reported on a needleless electrospinning where nanofiber jets were generated from a bubbled fluid surface. The bubbles were formed by blowing compressed air into the fluid. Downward needleless electrospinning was also reported. A flat cap single hole [59], splashing metal roller [60], and rotating metallic cone [61] were used for the generation of nanofibers. These setups are schematically illustrated in Fig. 11.5(a)–(c).

Depending on the shape of the needleless spinnerets, versatile types of electrospinning setups were reported in the period from 2009 to 2012. Fig. 11.6 shows a list of spinnerets with different shapes, such as conical coil, cylinders, cones, and wires in different configurations.

Wang et al. [62] reported on a novel conical wire-coil spinneret in 2009. The spinneret was made of 1-mm copper wire in the shape of a cone with a gap of 1 mm (Fig. 11.6(a)). The fiber productivity of polyvinyl alcohol (PVA) was reported as 0.86 g/h and 2.75 g/h at 45 kV and 70 kV, respectively. The authors also reported that possibly because of the low level of humidity during fiber generation, there was no corona discharge during the spinning. This work was further extended and patented with a modified fiber generator in the shape of a spiral coil dipped partially into polymer solution container and slowly rotating [63]. Nanofiber productivity was then significantly increased to 2.94 g/h and 9.42 g/h at 45 kV and 60 kV, respectively (Fig. 11.6(b)) [64]. In this setup (Fig. 11.6(c)) nanofiber productivity can be increased by increasing the number of copper rings used as spinnerets. It has been reported that the productivity increased from 3.5 g/h to 6.6 g/h at 60 kV from single to double rings [65]. When this spiral coil spinneret was compared with cylinder (Fig. 11.6(d))

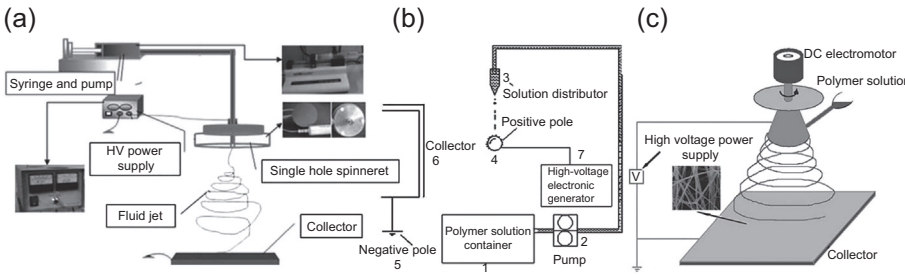

Figure 11.5 Downward needleless electrospinning setups. (a) Flat cap. *(Reprinted with permission from Zhou FL, Gong RH, Porat I. Polymeric nanofibers via flat spinneret electrospinning. Polymer Engineering and Science 2009;49(12):2475–81. Copyright (2009) Society of Plastics Engineers.)* (b) Splashing roller. *(Reprinted with permission from Tang S, Zeng YC, Wang XH. Splashing needleless electrospinning of nanofibers. Polymer Engineering and Science 2010;50(11):2252–7. Copyright (2010) Society of Plastics Engineers.)* (c) Rotating metallic cone. *(Reprinted with permission from Lu BA, et al. Superhigh-throughput needleless electrospinning using a rotary cone as spinneret. Small 2010;6(15):1612–6. Copyright (2010) Wiley-VCH Verlag GmbH & Co. KGaA, Weinheim.)*

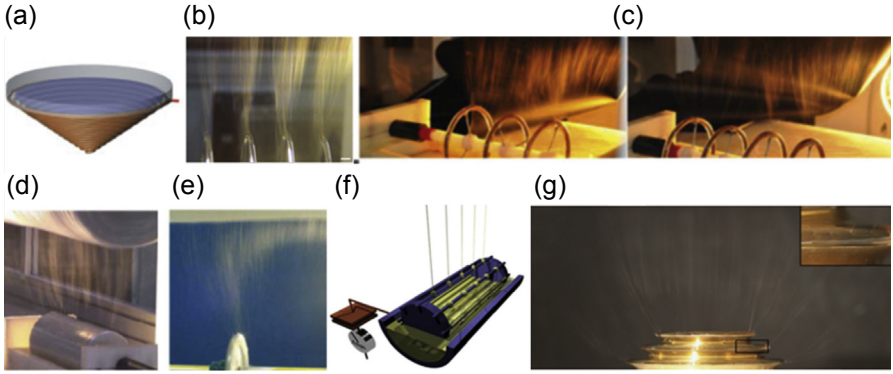

Figure 11.6 Different needleless electrospinning spinnerets. (a) Conical wire-coil. *(Reprinted with permission from Wang X, et al. Needleless electrospinning of nanofibers with a conical wire coil. Polymer Engineering and Science 2009;49(8):1582−6. Copyright (2009) Society of Plastics Engineers.)* (b) Spiral coil [64]. (c) Spiral coils with different number of coils. *(With kind permission from Springer Science + Business Media Wang, X, Lin T, Wang XG. Scaling up the production rate of nanofibers by needleless electrospinning from multiple ring. Fibers and Polymers 2014;15(5):961−5 [Fig. 1(d) and (e)].)* (d) Cylinder. *(Reprinted with permission from Niu HT, Lin T, Wang XG. Needleless electrospinning. I. A comparison of cylinder and disk nozzles. Journal of Applied Polymer Science 2009;114(6):3524−30. Copyright (2009) Wiley Periodicals Inc.)* (e) Disk. *(Reprinted with permission from Niu HT, Lin T, Wang XG. Needleless electrospinning. I. A comparison of cylinder and disk nozzles. Journal of Applied Polymer Science 2009;114(6):3524−30. Copyright (2009) Wiley Periodicals Inc.)* (f) Stationary/rotary wires. *(Reprinted with permission from Forward KM, Flores A, Rutledge GC. Production of core/shell fibers by electrospinning from a free surface. Chemical Engineering Science 2013;104(0):250−9. Copyright (2013) Elsevier.)* (g) Stepped copper pyramid. *(Reprinted with permission from Jiang G, Zhang S, Qin X. High throughput of quality nanofibers via one stepped pyramid-shaped spinneret. Materials Letters 2013;106(0):56−8. Copyright (2013) Elsevier.)*

and disk (Fig. 11.6(e)) spinnerets, it was concluded that it had much better electric field distribution along the spinneret structure, which contributed to its high fiber productivity [66−68].

Spinnerets with stationary/rotary wires (Fig. 11.6(f)) [69] and stepped copper pyramid (Fig. 11.6(g)) [70] were reported. Both stationary and rotary wire spinnerets were introduced by Elmarco Company in their commercial electrospinning production line. The stationary wire spinnerets use a traveling brush to repeatedly coat a thin layer of spinning solution onto the wire to maintain the solution stability. In the pyramid-shaped spinneret, polymer solution was pumped from the bottom and a number of jets were formed from all pyramid edges with a PVA nanofiber productivity of 4 g/h.

11.2.4.3 Yarn electrospinning

Most electrospinning setups produce nonwoven-like fiber webs; the process is less likely to use electrospun nanofiber webs in traditional textiles because textile fabrics

are made of yarn through weaving or knitting. Therefore it is of practical importance to electrospin nanofibers in the form of yarns. The first trial in the formation of nanofiber yarns was described in some early patents. In his first patent, Formhals described the production of a bundle of aligned parallel nanofibers, following postprocess twisting to obtain the yarn [15]. Improvements in the nanofiber yarn collection, twisting, reduced entanglement, and strength were further gained with his later patents.

Other studies described production of twisted bundles with twisting units or movable collectors (Fig. 11.7(a)−(d)). Water coagulation baths were also reported to enhance fiber entanglement during the formation of nanofiber bundles (Fig. 11.7(e) and (f)).

Ko et al. [71] reported on a setup for the alignment of nanofiber bundles through an air tube and a rotating drum, following twisting (Fig. 11.7(a)). Kim et al. [72] described a setup for the production of nanofiber yarn, collected by a rotating conductive plate (Fig. 11.7(b)). The yarns were further drawn, heat treated, and twisted. Higher alignment of nanofiber bundles was achieved using dynamic collectors, where the fibers' orientation was related to the collector rotation rate. Bazbous and Stylios [73] described a setup consisting of two grounded disks in Y−Z and X−Z planes, with a gap of 40 mm. The first disk was used to twist the bundle of the vertically deposited nanofibers, while the second one was for winding (Fig. 11.7(c)).

In 2011, Ali et al. [74] described direct twisting of nanofiber bundles to form a yarn, with a production rate of 5 m/min. The setup consisted of two oppositely charged nozzles and an intermediate funnel collector providing direct drawing and twisting of a fiber bundle from a hollow nanofiber cone (Fig. 11.7(d)). This setup is capable of continuously producing nanofiber yarns with controlled twist level, which makes it of greater importance than other setups for large-scale nanofiber yarn production.

Water-based collector setups were reported by Khil et al. [75] and Teo et al. [76]. The first setup described the formation of a strand of nanofibers deposited in a coagulation bath. The fibers were random and were guided with a filament guide bar to the take-up winder (Fig. 11.7(e)). The second setup describes the formation and stretching of nanofiber yarn by a vortex on the bottom of a bath with a diameter of 5 mm (Fig. 11.7(f)). The main drawback of the setup was the possibility of fiber entanglement or noncoherent structure formation because of the faster harvest of the fibers than the water flow or opposite, respectively.

11.3 Morphology of electrospun nanofibers

11.3.1 Diverse single nanofibers

The most common electrospun nanofibers are continuous and straight fibers. Nonstraight fibers can be obtained because of the buckling effect, which is different from bending instability during electrospinning. The final appearance of the fibers is dependent on jet length and collector type (stationary, movable, or with a liquid bath). For example, by collecting electrospun PS on a water surface, different buckling patterns were collected, as shown in Fig. 11.8 [77].

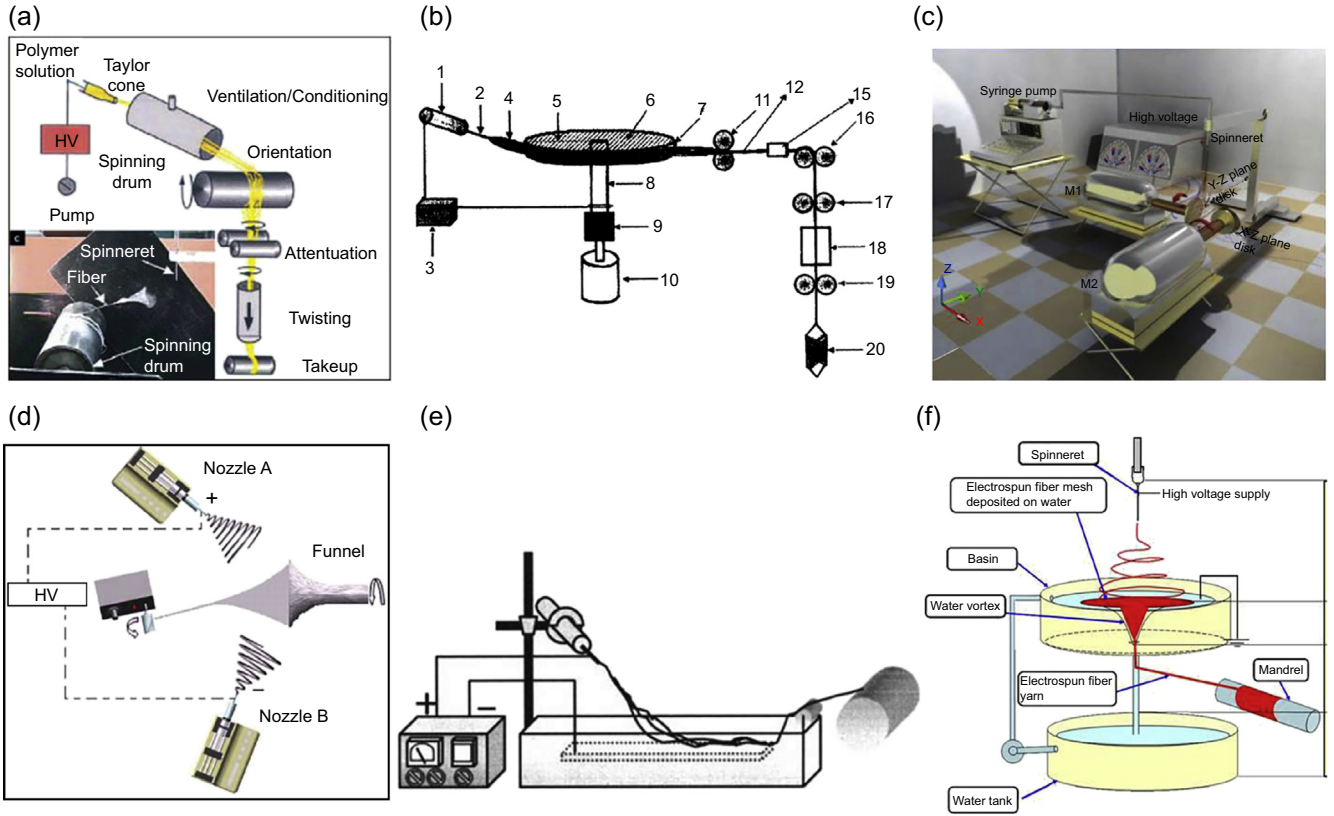

Figure 11.7 Examples of continuous nanofiber bundle and nanofiber yarn fabrication through a range of devices. (a) Air tube. *(Reprinted with permission from Ko F, et al. Electrospinning of continuous carbon nanotube-filled nanofiber yarns. Advanced Materials 2003;15(14):1161−5. Copyright (2003) Wiley-VCH Verlag GmbH & Co. KGaA, Weinheim.)* (b) Rotating plate [72]. (c) Dual disks. *(Reprinted from Bazbouz MB, Stylios GK. Novel mechanism for spinning continuous twisted composite nanofiber yarns. European Polymer Journal 2008;44(1):1−12. Copyright (2008) Elsevier.)* (d) Funnel. *(Ali U, et al. Direct electrospinning of highly twisted, continuous nanofiber yarns. Journal of the Textile Institute 2012;103(1):80−8. Copyright the Textile Institute. Reprinted by permission of Taylor & Francis Ltd., www.tandfonline.com on behalf of the Textile Institute.)* (e) Coagulation bath. *(Reprinted from Teo WE, et al. A dynamic liquid support system for continuous electrospun yarn fabrication. Polymer 2007;48(12):3400−5. Copyright (2004) Wiley Periodicals Inc.)* (f) Vortex-forming bath. *(Reprinted from Teo WE, et al. A dynamic liquid support system for continuous electrospun yarn fabrication. Polymer 2007;48(12):3400−5. Copyright (2007) Elsevier.)*

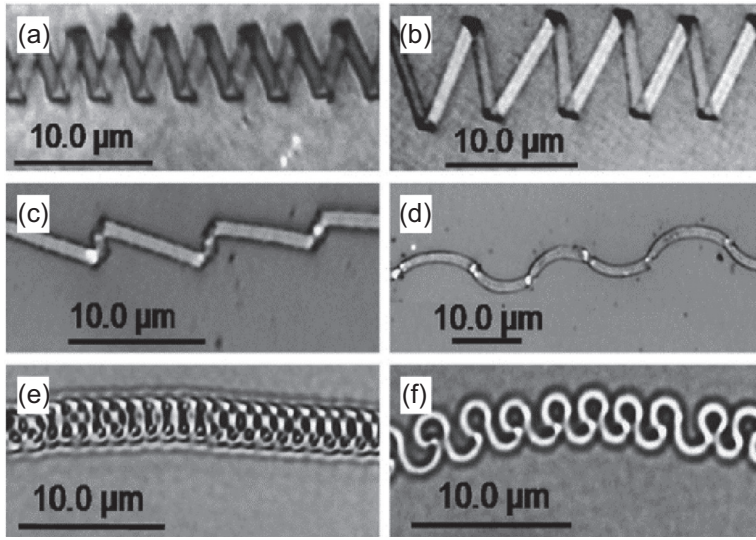

Figure 11.8 Buckling patterns of electrospun PA 6 collected on a water surface.
Reprinted with permission from Han T, Reneker DH, Yarin AL. Buckling of jets in electrospinning. Polymer 2007;48(20):6064−76. Copyright (2007) Elsevier Ltd.

Necklace-like structured fibers could also be prepared by encapsulating SiO_2 nanoparticles into electrospun fibers. As shown in Fig. 11.9, the fibers have different morphologies depending on particle size. The smallest size particles tended to aggregate while the larger particles tended to disperse one by one in the fibers. The medium-sized particles (265 nm) led to a necklace-like structure while blackberry-like fibers were collected with large particles (910 nm) [78].

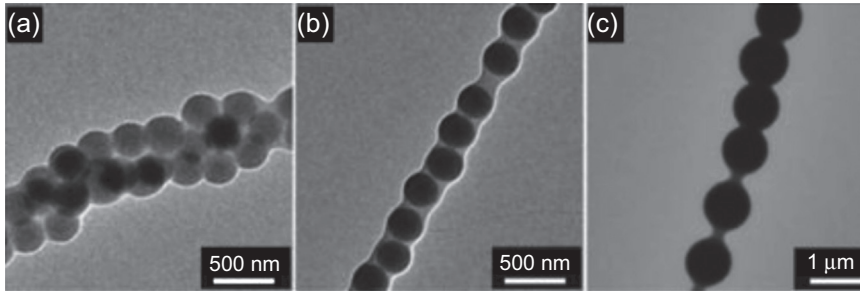

Figure 11.9 Morphology of electrospun PVA fibers with SiO_2 diameters of (a) 143 nm, (b) 265 nm, and (c) 910 nm.
Reprinted with permission from Jin Y, et al. Fabrication of necklace-like structures via electrospinning. Langmuir 2009;26(2):1186−90. Copyright (2009) American Chemical Society.

11.3.2 Aligned nanofibers

Different from randomly oriented fibrous structures in normal electrospun nanofiber webs, aligned fibers are electrospun using many different fiber-collecting techniques. The most straightforward method to prepare aligned fibers is to use a rotating mandrel collector, which has a high linear speed matching the deposition speed of the electrospun fibers. As shown in Fig. 11.10(a), two layers of oriented fibers are formed with the position of the parallel fibers in an angle of 90 degrees [79].

Another method to electrospin aligned nanofibers is the addition of an auxiliary electrode pair or using a pair of parallel strip collectors. Once one end of the nanofiber deposits on one electrode, another end of the fiber is attached by another electrode because of electrostatic attraction, thus forming aligned fibers between the pair. Aligned

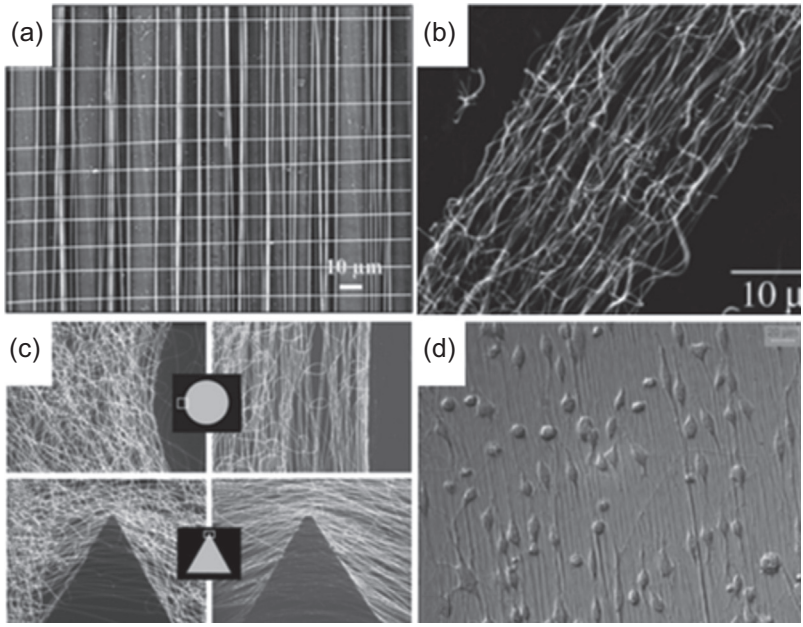

Figure 11.10 (a) Two-nanofiber layer alignment at 90 degrees. *(Reproduced from Yuan H, et al. Stable jet electrospinning for easy fabrication of aligned ultrafine fibers. Journal of Materials Chemistry 2012;22(37):19634−8 with permission of the Royal Society of Chemistry.)* (b) Alignment of electrospun fibers after 40 min of electrospinning. *(Reprinted with permission from Katta P, et al. Continuous electrospinning of aligned polymer nanofibers onto a wire drum collector. Nano Letters 2004;4(11):2215−8. Copyright (2004) American Chemical Society.)* (c) Deposition of the electrospun fibers on patterned electrodes with different insulating areas. *(Reprinted with permission from Li D, et al. Collecting electrospun nanofibers with patterned electrodes. Nano Letters 2005;5(5):913−6. Copyright (2005) American Chemical Society.)* (d) Neural stem cell attachment on aligned nanofiber scaffolds. *(Reprinted from Yang F, et al. Electrospinning of nano/micro scale poly (L-lactic acid) aligned fibers and their potential in neural tissue engineering. Biomaterials 2005;26(15):2603−10. Copyright (2005) with permission from Elsevier.)*

fibers were deposited on a copper wire-framed rotating drum with a rotation speed of 1 rpm. The fiber deposition was caused by the attraction of the fibers by the wires, which results in perpendicular stretching to the parallel wires (Fig. 11.10(b)) [80].

More complex fibrous architectures can be prepared by using specially designed collector electrodes. For example, a quartz wafer with gold patterns can be used to collect random-orientated, circulated triangulated, squared, or rectangular-shaped fibrous architecture, depending on the way the gold patterns are connected (Fig. 11.10(c)) [81].

Nanofiber alignment have an influence on cell response. Neural stem cells showed elongation and neurite growth parallel to the aligned fibers (Fig. 11.10(d)). In regard to degree of orientation, up to 94% of the neurites showed parallel orientation for nanofibers. Compared to random fibrous scaffolds, the aligned ones showed cell−matrix interactions, presented as filament-like structures extending from the cell to the fibers [82].

11.3.3 Nanofiber yarns

There are two types of nanofiber yarns: parallel nanofiber bundles and twisted nanofiber yarns reported in the literature. A liquid reservoir was used to collect nanofibers into a continuous filament bundle with the productivity of 180 m/h and 3720 fibers in the yarn cross-section (Fig. 11.11(a)) [83]. The nanofibers in the bundles are highly aligned; however, there are no twists, therefore the bundles have a hairy appearance. Similarly, an aligned but wavy fiber bundle was formed by the vortex bath setup (Fig. 11.11(b)). The bundle tightness was caused by the water present between the fibers acting as a lubricant [76].

By simply rotating one of two parallel rings, multifilament twisted yarn was produced (Fig. 11.11(c)). The yarn reported was up to 5 μm in diameter and 50 mm in length [84]. Highly twisted nanofiber yarn can be collected by guiding nanofibers from an intermediate fibrous cone (Fig. 11.11(d)) [74]. Both fiber and yarn diameters decreased with increasing funnel rotating speed. By increasing the funnel rotating speed from 500 to 2000 rpm, the twist angle increased from 20 to 51 degrees. The tensile property of the twisted nanofiber yarn is dependent on yarn twist level. For a poly(vinylidenefluoride-hexafluoropropylene) (PVDF-HFP) nanofiber yarn with a twist level of 420 (turns per meter, tpm), the tensile strength and elongation at break were 2 MPa and 250%, respectively. By increasing the twist level from 420 to 6000 tpm, the tensile strength was recorded as 60.4 MPa for the yarn with a twist level of 350 tpm.

Fig. 11.11(e) shows a directly twisted yarn with a length of 30−40 cm. Posttreatment with organic solvent resulted in a reduction of the fiber−fiber interaction, and therefore better mechanical performance [85]. The coil structure in Fig. 11.11(f) was obtained by an overtwist of fiber yarns. The diameter of the yarn was 175 μm while for the coil it was 306 μm. The coils made up of aligned fiber yarns showed a significant strain of 740%, compared to the aligned fiber yarns' strain of 160%. The yarns showed greater toughness (98 J/g) than the coils (56 J/g) because of the higher fiber−fiber interaction and greater interaction length, which results in easier load transfer [86].

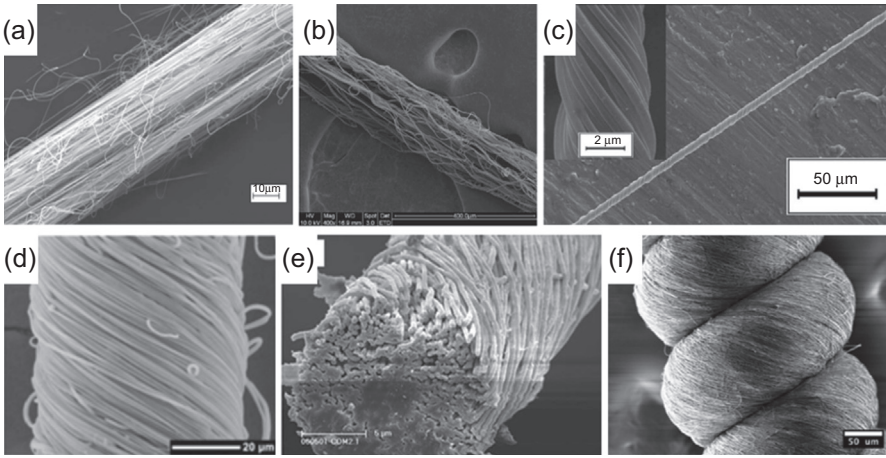

Figure 11.11 Morphology of fibers bundles. (a) Aligned fibers from coagulation bath. *(Reprinted with permission from Smit E, Bűttner U, Sanderson RD. Continuous yarns from electrospun fibers. Polymer 2005;46(8):2419−23. Copyright (2007) Elsevier Ltd.)* (b) Aligned and wavy bundles from vortex coagulation bath. *(Reprinted with permission from Teo WE, et al. A dynamic liquid support system for continuous electrospun yarn fabrication. Polymer 2007;48(12):3400−5. Copyright (2007) Elsevier.)* Twisted fiber yarns: (c) By ring rotation. *(Reprinted with permission from Dalton PD, Klee D, Möller M. Electrospinning with dual collection rings. Polymer 2005;46(3):611−4. Copyright (2004) Elsevier Ltd.)* (d) Funnel rotation. *(Ali U, et al. Direct electrospinning of highly twisted, continuous nanofiber yarns. Journal of the Textile Institute 2012;103(1):80−8. Copyright the Textile Institute, reprinted by permission of Taylor & Francis Ltd., www.tandfonline.com on behalf of the Textile Institute.)* (e) Cylinder rotation. *(Reprinted with permission from Liu LQ, et al. One-step electrospun nanofiber-based composite ropes. Applied Physics Letters 2007;90(8):083108-1. Copyright (2007) AIP Publishing LLC.)* (f) Overtwisted yarns—coils. *(Reprinted with permission from Baniasadi M, et al. High-performance coils and yarns of polymeric piezoelectric nanofibers. ACS Applied Materials & Interfaces 2015;7(9):5358−66. Copyright (2015) American Chemical Society.)*

11.3.4 3D fibrous architectures

By combining electrospinning with a rapid prototyping technique (projection-microstereolithography), that is, depositing electrospun fibers onto a 3D resin pattern, a 3D micropatterned fibrous structure was prepared. The 3D patterns can be of any shape such as sinusoidal, sawtooth, hexagonal, and reentrant honeycomb. The fibrous structures comprised dense and loosely deposited structures (Fig. 11.12(a)) [87]. Similarly, honeycomb micropatterned constructs (Fig. 11.12(b)) were prepared by both electrospinning/electrospraying and photolithography on silicon wafers [88]. Some nanofibers were reported to self-organize into honeycomb patterns. As shown in Fig. 11.12(c), the pattern contains both micropores and mesopores and the fibrous pattern can be prepared to a thickness of several centimeters. These 3D structures were

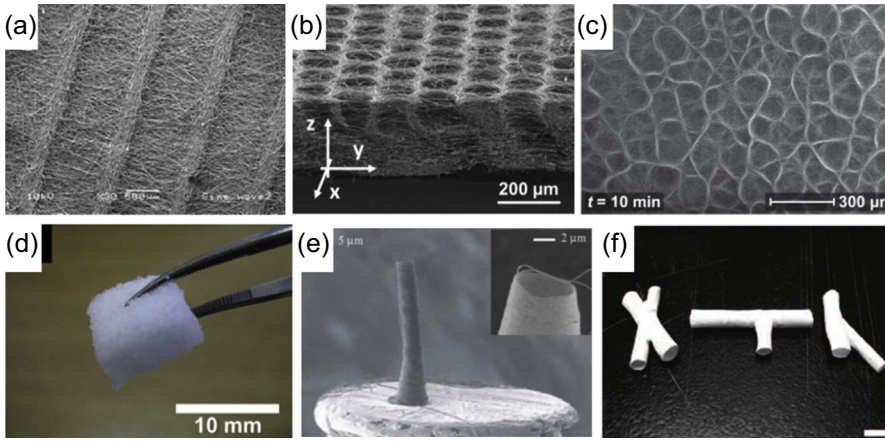

Figure 11.12 (a) Sinusoidal patterned electrospun structures [87]. (b) 3D columnar structure [88]. (c) Self-assembled electrospun structures. *(Reproduced from Ahirwal D, et al. From self-assembly of electrospun nanofibers to 3D cm thick hierarchical foams. Soft Matter 2013; 9(11):3164−72 with permission of the Royal Society of Chemistry.)* (d) HA/collagen and deposited NaCl nanofibrous structure. *(Reprinted with permission from Kim TG, Chung HJ, Park TG. Macroporous and nanofibrous hyaluronic acid/collagen hybrid scaffold fabricated by concurrent electrospinning and deposition/leaching of salt particles. Acta Biomaterialia 2008;4(6):1611−9. Copyright (2008) Acta Materialia Inc. Published by Elsevier Ltd.)* (e) Hollow coiled electrospun structure. *(Reprinted with permission from Kim HY, et al. Nanopottery: coiling of electrospun polymer nanofibers. Nano Letters 2010;10(6):2138−40. Copyright (2010) American Chemical Society.)* (f) Tubes with interconnected tubular structures. *(Reprinted with permission from Zhang D, Chang J. Electrospinning of three-dimensional nanofibrous tubes with controllable architectures. Nano Letters 2008;8(10): 3283−7. Copyright (2008) American Chemical Society.)*

formed attributable to heterogeneous distribution of electric charges and irregular aggregation of fibers [89].

A 3D porous fibrous structure was also fabricated by combining electrospinning with a porogen leaching method. For example, a hyaluronic acid (HA)/collagen blend was electrospun by simultaneous deposition of sodium chloride salt patriciates to fiber web through a sieving method (Fig. 11.12(d)). After crosslinking of the polymer and leaching the salt porogen, macropores can be inserted to the fibrous structure. Increasing the collagen portion in the fibers stabilizes the fiber structure [90].

A pin collector was reported to fabricate a hollow coiled structure (Fig. 11.12(e)). With an increase in polymer concentration, the modulus of the coiled fibers decreased. The coil radius increases with increase in the fiber diameter [91]. In addition, branched fibrous tubes can be prepared using 3D columnar collectors (Fig. 11.12(f)). Both single and multiple tubes with two or more patterned architectures in the tube were reported. The surface of the tubular structures was also varied including two and more patterns per tube [92].

11.4 Applications of electrospun nanofibers

11.4.1 Biomedicine

Electrospun nanofibers have shown enormous applications in the biomedical field. Until now research has been mostly focused on the development of tissue engineering scaffolds. The primary advantage of these fibrous scaffolds is that nanofibrous structure mimics the native extracellular matrix [93]. In addition, functional compounds, such as drugs or growth factors, can be encapsulated into nanofibers.

Biodegradable synthetic polymers such as polycaprolactone (PCL), polylactic acid (PLA), copolymers [eg, like poly(lactic-*co*-glycolic acid) (PLGA), poly (L-lactide-co-caprolactone) (PLLC)], or naturally derived materials (eg, collagen, gelatin, silk fibroin, chitosan, cellulose) have been used to prepare scaffolds. Different types of cells have been seeded on electrospun scaffolds. Most of the electrospun nanofibers show support to cell attachment, spreading, and growth.

Some of the earlier papers reported bone tissue engineering using nanofiber scaffolds made of PCL [94] and silk fibroin/poly(ethylene oxide) (PEO) [95], PLGA [96]. Bone marrow stromal cells showed proliferation on silk fibroin nanofibers. PLGA accommodated human mesenchymal stem cell differentiation into chondrocytes and osteoblasts. Chondrocytes were also reported to penetrate into lacunae-like structures. Silk fibroin/PEO nanofiber scaffolds were also functionalized with bone morphogenetic protein 2 and hydroxyapatite nanoparticles [97]. Both protein and nanohydroxyapatite enhanced mineralization and the presence of the protein resulted in higher calcination level.

Cell behavior on electrospun scaffolds is affected by scaffold topography and its chemical feature. For example, cell density increased with the increase of nanofiber diameters. Fibrous scaffold with diameters greater than 2 μm were observed to guide lamellapodia along fibers (Fig. 11.13) [98].

Cells showed better infiltration in fibrous scaffold with fibers of diameter in the range of 10−30 μm. In the case of free-standing fibers suspended in cell culture medium, cells also infiltrated into the structure. It was indicated that the finest fibers allowing cells to attach and migrate were 10 μm in diameter. The fiber gap to be bridged by the cells was a maximum of 200 μm, but was not dependent on the possible angle between fibers [99].

Apart from enhancing cell adhesion, migration, and growth, electrospun mats provide good absorption to fluids (eg, wound exudates), exchange of gases, and evaporation of water, which are useful for developing wound-dressing materials for skin. For example, emulsion electrospun fibers were prepared from polylactide-co-poly (ethylene glycol) containing a fibroblast growth factor (bFGF) to be potentially used in patients with diabetic mellitus skin wounds. In vivo studies on diabetic rats in the skin dorsal area showed enhanced epithelization and continuous growth of skin appendages because of sustained release of the bFGF [100].

Aligned fibers were reported to facilitate cell infiltration in vitro and in vivo. A scaffold made of aligned PLLA fibers functionalized with heparin provided greater spacing for bovine aortic endothelial cells to enter between fibers compared to random fibrous

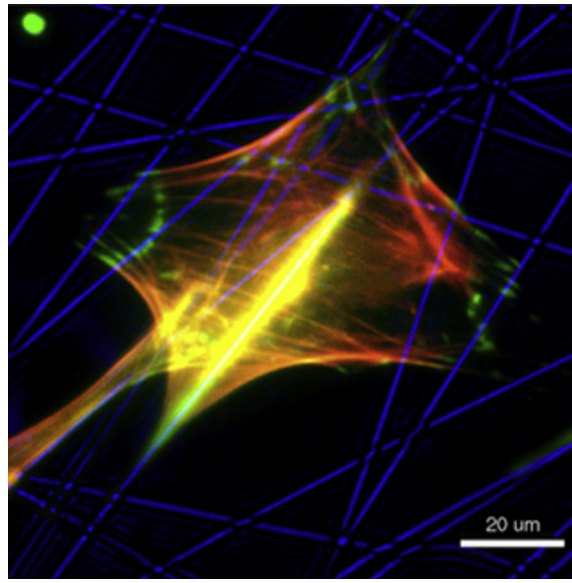

Figure 11.13 Superimposed image of immunofluorescent-stained cells adhesion onto image of poly(D,L-lactide)fibers.
Reprinted with permission from Badami AS, et al. Effect of fiber diameter on spreading, proliferation, and differentiation of osteoblastic cells on electrospun poly(lactic acid) substrates. Biomaterials 2006;27(4):596−606. Copyright (2005) Elsevier Ltd.

scaffolds. Heparin further improved cell penetration because of its anticlotting ability, especially in the in vivo dermal wound rat model [101].

To mimic natural blood vessels, fibrous tubular scaffolds were prepared by electrospinning a blend of collagen type I, elastin, and poly(D,L-lactide-*co*-glycolide). Endothelial and smooth muscle cells showed growth, proliferation, and maturation on the scaffold. Biocompatibility was further confirmed by in vivo subcutaneous implantation of the grafts in mice [102]. Dual porous scaffolds with good structural integrity were prepared by combining electrospinning with compression molding and salt/leaching gas-forming techniques. The scaffolds provided both micro- and nanopores for cell growth and nutrient and waste transport, respectively [103]. To prevent arterial stenosis after graft surgery, PCL fibrous scaffolds were functionalized by the addition of heparin. The release of heparin inhibited the proliferation of vascular smooth muscle cells and movement into the vein intima [104].

Human skeletal muscle cells were adhered, proliferated, and fused into myotubes on hybrid-based PCL/collagen type I scaffolds. The scaffolds were prepared in both random and aligned configurations. Aligned fibrous scaffolds showed enhancement in cell organization and the myotubes growing on the aligned nanofiber appeared longer compared to random scaffolds [105]. Similarly, the topographical features of PU scaffolds influenced the maturation of skeletal myotubes from myoblasts. Aligned PU fibrous scaffolds not only provided cell alignment along fiber length, but also

improved cell elongation, fusion, and upregulation of stretch-activated ion channels over random fiber scaffolds. Further electromechanical stimulation resulted in an increase of the striated myotubes from 70% to 85% [106].

The alignment of electrospun PLLA scaffolds was also examined for the behavior of dorsal root ganglia explant cultures from rat embryos. Highly aligned fibers enhanced radial neurite outgrowth and provoked ganglia elongated shapes. Schwann cells adhered to aligned fibrous scaffolds resulting in an extremely narrow morphology. Because of Schwann cells and growth cones sensation of the contact guidance cue below, above, and on both sides, neurites were observed to migrate down the fiber bundles [107].

Topographical guidance and electrical stimulation were reported to benefit the growth and differentiation of rat pheochromocytoma 12 (PC12) cells and hippocampal neurons. An electroconductive polypyrrole coating was formed on PLGA nanofiber scaffolds. Regardless of the conductive coating, longer neurites and more elliptical cells were observed on aligned fibers. Neurite outgrowth of PC12 cells was promoted by both aligned fibers and electrical stimulation. Longer neurites were observed when electrical stimulation was performed at a low potential. The number of neurites per cell on the other hand was not significantly affected by fiber alignment or electrical stimulation [108].

Electrospun nanofibers were also used as drug delivery vehicles because of the ability to carry and deliver the medicine in a controlled manner. For this purpose, nanofibers were produced from either single polymer or polymer blends through conventional, coaxial, or emulsion electrospinning. To further assist in the sustained release, nanoparticles and liposomes were incorporated in the nanofibers or applied on the fiber surface.

Poorly water soluble drugs, such as itraconazole and ketanserin, were loaded into electrospun PU. Both model drugs had an amorphous dispersion in the PU matrix. At low loadings, fast release resulted, while sustained release occurred at higher loadings. For itraconazole, no burst initial release happened. However, ketanserin released at a faster pace at the initial stage because of higher solubility and diffusivity, as well as fiber imperfections [109]. To tailor the release profile of antibiotics, nanofibers were electrospun from polymer blends, for example, PCL and PLA. A specific range of release rates can be obtained based on the system compositions [110].

To reduce release rate, a polymer coating was applied to electrospun fibers that contain drug. Poly(*p*-xylylene) was deposited on electrospun PVA by chemical vapor deposition. The release of the protein from the PVA fibers was retarded and controlled by the coating thickness [111]. Target drug delivery was proposed for the treatment of leukemia cells. A complex system comprising PLA nanofibers functionalized with TiO_2 nanoparticles and loaded with daunorubicin was studied. Because of the synergistic effect of the compounds, drug diffusion outside of cancer cells was prevented, and its permeation and accumulation onto the target cells was efficiently enhanced [112].

11.4.2 Energy and electronics

Electrospun nanofibers were extensively studied for their potential to fabricate supercapacitors, batteries, solar cells, piezoelectric systems, and sensors.

11.4.2.1 Supercapacitors

Supercapacitors can store electricity through either electrostatic charge absorption/desorption (electric double-layer capacitors) or redox reaction (pseudocapacitors). Compared with lithium-ion batteries, supercapacitors have higher power density, higher recharging rate, and more charge/discharge cycles. When PAN-based CNFs were activated at a temperature of 700 or 800°C, they showed high specific surface area and low mesopore volume fraction. At high current density, high capacitance was obtained for nanofibers with low surface area, while at lower current density the opposite case was observed [113]. Dependence on the activation temperature was also observed on CNFs made of electrospun polybenzimidazol. The CNFs activated at 800°C were reported to have a surface area of 1220 m^2/g, and the electrode showed a specific capacitance of 178 F/g [114]. To improve the electrochemical performance, activated CNFs were embedded with carbon nanotubes and further coated with polypyrrole. The surface modification led to a 236% increase in the specific capacitance (333 F/g), which was explained by the high surface mesoporous area, good charge transfer, and electrical conductivity [115].

Pseudosupercapacitors based on transitional metal oxide nanofibers were reported from MnO_2 nanofibers, and they showed the highest specific capacitance among all metal oxide nanofibers. A coaxial AAI-CNF@MnO_2 electrode was prepared from CNFs made of PAN−iron acetylacetonate (AAI) nanofiber precursor and MnO_2 coating. The AAI itself increased the capacitance five times compared to pristine CNFs. Further, with the addition of MnO_2, the electrode showed a capacitance of 311 F/g at 2 mV/s and a retention of 51% at 200 mV/s, when the loading was up to 39%. When the MnO_2 loading increased to 59%, the capacitance and rate capability were reduced to 216 F/g and 26%, respectively [116]. To improve electron and proton conductivity, fibers were prepared from an electrically conductive core with a hydrous shell. For example, the core was prepared from an electrospun RuO_2/poly(vinyl acetate) (PVAc) precursor and the shell was from electrochemical deposition of a thin layer of $RuO_2 \cdot nH_2O$. The capacitance of the electrode materials was reported to be 104.3 F/g (based on total mass) and 886.9 F/g (based on the mass of the deposited layer) [117]. Composite nanofibers from RuO_2 and Mn_3O_4 were fabricated to improve pseudocapacitive properties. The fibers consisted of amorphous RuO_2 with a partially crystalline Mn_3O_4 phase and its specific capacitance was 293 F/g at a scan rate of 10 mV/s. The capacity loss at a scan rate of 2000 mV/s was 55% [118].

11.4.2.2 Li-ion batteries

Electrospun nanofibers show great potential in the battery area. They can be used as battery separator, anode, or cathode, depending on material and structure. Ultralong hierarchical vanadium oxide nanowires were prepared by electrospinning ammonium metavanadate/PVA solution and subsequent calcination. The nanowires consisted of small nanorods along their length. They were used as a cathode material in Li-ion batteries and showed discharge capacity of 390 mAh/g and 201 mAh/g after the 50th cycle at 1.75 V and 4 V, respectively. The high performance and stability of

the battery come from the ability to prevent self-aggregation of the nanorods, which maintained a large surface area and effective contact area [119].

The Li-ion battery separators are often required to have a highly porous structure to absorb the liquid electrolyte and good mechanical stability to retain the structure. Electrospun PVDF was used as a separator in Li-ion batteries. After heat treatment to improve its physical integrity and ethylene plasma treatment to introduce some interfiber bonding, the PVDF nanofiber membranes filled with a lithium salt electrolyte solution showed ion conductivities of $1.6-2.0 \times 10^{-3}$ S/cm [120].

Porous CNFs loaded with MnO_2 particles were prepared from PAN/$Mn(OAc)_2$ precursor solution. The nanofibers were directly used as Li-ion battery anodes. The battery showed high initial charge/discharge capacity of 1155 mAh/g and 785 mAh/g, respectively, with a coulombic efficiency of 68.0%. After 50 cycles of charge/discharge, the reversible capacity was 597 mAh/g (retention capacity, 76.1%) [121]. Activated CNFs were prepared from PAN/$ZnCl_2$ composite precursor. At a $ZnCl_2$ loading the charge/discharge initial capacities were 970 mAh/g and 515 mAh/g, respectively [122]. In addition, carbon-based anode electrochemical performance was improved by inserting SnO_2 nanoparticles in the fibers. Compared to a commercial Sn nanoparticle electrode, which degrades after 20 cycles, the anode discharge capacity was still 648 mAh/g after 140 cycles [123].

11.4.2.3 Dye-sensitized solar cells

Dye-sensitized solar cells (DSSC) are also called Grätzel cells, after Professor Michael Grätzel for his pioneering contribution in this field. A typical DSSC device comprises a semiconductor photoanode (also referred to as "working electrode," mostly TiO_2), covered with a thin layer of dye sensitizer, a counter electrode and electrolyte. The dye sensitizer under light illumination generates photoelectrons that inject into the conduction band of the TiO_2. The electrons flow out through the back contact and external load to reach the counter electrode, where they are involved in the reduction of the redox mediator, which is oxidized by the sensitizer. For some time the generated electrons are held by the electrode; more likely they are depleted by either recombination with the oxidized dye molecules or participating in a redox reaction. Compared with a commonly used working electrode containing a thin layer of TiO_2 nanoparticles, one-dimensional electrospun nanofiber-based electrodes have the advantages of significantly reduced grain boundaries, better electron transport pathway, and longer electron lifetime.

Hierarchically structured TiO_2 nanofibers prepared from PVAc and titanium (IV) propoxide precursor solution were used as working electrodes in DSSCs. After heat treatment, nanorod-in-nanofiber structures were formed and amorphous TiO_2 was converted into anatase phase. The nanofibers contained both macro- and mesopores. The highest power conversion efficiency obtained was 7.93% at a light intensity of 30 mW/cm^2, with an open circuit voltage of 630 mV, current of 5.6 mA/cm^2, and fill factor of 67.5% [124]. In addition, photoanodes were made by mixing TiO_2 nanofibers with conventional TiO_2 nanoparticles. The solar cell device showed a current density of 16.8 mA/cm^2 and energy conversion efficiency of 8.8% [125]. It was 44% higher in efficiency compared to one made of TiO_2 nanoparticle photoanode.

11.4.2.4 Piezoelectric devices

Piezoelectric materials can convert a mechanical deformation into electricity. They have been used for making electrical transducers, mechanical sensors, and energy harvesters. Conventionally, piezoelectric materials are prepared either from inorganic compounds containing toxic elements or polymers, which require a series of treatments including drawing at a high ratio and poling in a high electric field at an elevated temperature.

Electrospinning has shown advantages in processing piezoelectric polymers for energy harvesting applications. Using polyvinyl fluoride (PVDF) or poly(vinylidene fluoride-*co*-trifluoroethylene) as the models, several groups have reported the interesting piezoelectric property of electrospun nanofibers. The piezoelectricity of PVDF originates from its β crystal phase. Energy harvesting devices have been developed from this polymer. Aligned electrospun PVDF nanofibers were prepared using a conventional electrospinning technique. When dipole alignment was improved by in-plane polling treatment, the nanofiber device generated a voltage output of 15−20 mV. Biomechanical and biochemical energy were also converted into low electric voltage, for example, 50 mV and 95 mV, respectively, using nanofibers [126]. Single PVDF nanofibers prepared by a near-field electrospinning technique showed piezoelectricity without postelectrospinning polling treatment. However, the nanofiber device still showed a low-voltage output, in the range of 5−30 mV [127].

Larger voltage output was reported on randomly oriented electrospun PVDF nanofiber webs. Without polling treatment, the electrospun nanofibers can generate a voltage as high as 0.43 V under 5 Hz compression [128]. The group also reported the piezoelectricity of PVDF nanofibers prepared by a needleless electrospinning technique. When a rotary disk was used as fiber generator during electrospinning, the resulting PVDF nanofiber webs showed voltage output in the range of 1−2.6 V, depending on the applied voltage used for electrospinning [129].

11.4.2.5 Sensors

Sensors function to detect a physicochemical state or its change (eg, gas, pH value, chemicals, or biochemical species), and transduce it mostly into electric or optical output. Most sensors are required to have a large surface area and a highly porous structure to support fast access of the analyte and large signal-to-noise ratio. Nanofibrous materials match well with these features. In particular, electrospinning offers opportunities to process various sensing materials (eg, functional polymers and inorganic oxide) into nanofibers, and the fiber properties are easily modified through adding a dopant, functional chemical, or polymer into solution for electrospinning.

Electrospun poly(acrylic acid) (PAA) [130] and PVA/PAA [131]-coated quartz crystal microbalance were used as gas sensors to detect ammonia. The sensors were able to detect trace ammonia on ppm/ppb levels. For the sensor made of pure PAA nanofibers, it was able to detect 130 ppb ammonia in air. The sensor showed higher sensitivity for finer nanofibers or at a higher humidity environment level. When the PVA/PAA blend was used, the sensor sensitivity increased with the increase of the

PAA composition. Compared to the film counterpart, the nanofiber device had higher sensitivity attributable to the higher surface area.

A biosensor was prepared from electrospun PVA/glucose oxidase for the detection of glucose. Compared to the cast films, the electrospun sensor showed much faster response to 0.5 mM glucose. The sensor showed a linear response in the range of 1−10 mM. The sensor had a high stability. After refrigeration for 20 days, the activity was only reduced by 60% [132]. Ni particle-loaded carbon was also reported to detect glucose. The sensor showed a detection limit of 1 μm [133].

11.4.3 Environmental protection

Air and water pollution have become the main concern in the world. Filtration is of high importance to remove particle pollutants from the environment. One of the main applications for electrospun nanofibers is in the filtration area. Their large surface area and high porosity provide them with high particle collection efficiency and low flow resistance.

In one report on the filtration behavior of electrospun polyvinyl chloride (PVC)/PU nanofiber membranes, NaCl particles of 300−500 nm were used for test [134]. With an increase of the nanofiber areal density to 20.72 g/m^2, the filtration efficiency increased to 99.5%, while the pressure drop was only 144 Pa (face velocity, 5.3 cm/s).

Electrospun membranes were also used for oil/water separation. Water-stabilized electrospun PVA was attached to poly(ether sulfone) microfibrous nonwoven substrate and further coated with hydrophilic polyether−polyamide or crosslinked PVA hydrogel with multiwalled carbon nanotubes (MWCNTs). The PVA/MWCNT coating layer provided a nonfouling effect for 24 h, with the incorporation of MWCNTs providing nanochannels to speed up water permeation. The membrane showed a filtration rejection efficiency of 99.8% at a water flux of 330 L/m^{2}h. The PVA-coated substrate was reported to have two times higher flux rate than the polyether−polyamide one [135]. Electrospun waste-expanded PS fibers were mixed with microglass fibers for water/oil separation. The nanofiber-containing filter had higher separation efficiency up to 88.1% than neat glass filter (efficiency, 67.5%) [136]. To improve filter efficiency, boehmite nanoparticles were introduced into electrospun PA 6 nanofibers. The electret effect of boehmite increased particle capture without increasing the air flow resistance. This boehmite-containing filter membrane showed a filtration index of 0.943 mm/H_2O at a resistance value of 25 Pa [137].

11.4.4 Chemistry area

In the chemistry area, nanofibers are ideal catalyst carriers for chemical reactions. Pd nanoparticles were loaded on electrospun CNFs as a catalyst for the Sonogashira coupling reaction. The Pd CNF catalyst showed a high catalytic activity, with a reaction yield of 85% and a recovery rate of 100% after 10 reaction cycles [138]. Commercial Pt/C on electrospun CNFs showed catalytic activity for methanol oxidation. It had an exchange current density 4.49 times higher than Pt/C supported by commercial carbon paper. The porous structure of nanofiber mats and good

dispersion of the Pt/C particles in the fibrous matrix allowed the system to have lower charge transfer resistance for methanol oxidation [139].

Electrocatalytic electrodes were prepared by electroless plating of Pd on electrospun PA 6 nanofibers. The Pd-coated PA 6 nanofiber was used for ethanol oxidation. The current density of the system at the first scan was 34.76 mA/cm^2 and the current had 5.4% reduction after 20 cycles of the reaction [140]. In addition, Pt nanoparticles were also loaded on graphene-modified CNFs for electrocatalytic reaction. The system showed fast charge transfer rate during methanol oxidation and long-term stability [141].

TiO_2 nanofibers were reported as a photocatalyst for hydrogen evolution. At 450°C, the nanofibers showed an evolution hydrogen rate of 270 μmol/g, which was 2.8 times higher than TiO_2 nanofibers prepared by the hydrothermal method [142]. TiO_2/SnS_2 nanofibers prepared by electrospinning and subsequent hydrothermal method showed photocatalytic activity in the degradation of organic dyes and phenols. Under UV irradiation for 50 and 60 min, the nanofibers showed a degradation ratio for methyl orange and 4-nitrophenol of 92.7% and 88.8%, respectively [143]. A similar effect was reported on TiO_2 nanofibers decorated with ZnO nanoparticles for the degradation of methyl red and rhodamine B dyes [144,145].

Enzymes were also immobilized on electrospun nanofibers to improve their catalyzing ability. Electrospun PVA and PEO/casein nanofibers containing lipase were prepared for hydrolysis of olive oil. Compared to cast counterparts the PVA/lipase had six times higher catalytic activity [146]. Cellulose immobilized on PVA nanofibers (glutaraldehyde crosslinked) showed two times greater activity than free cellulose in cast films [147]. In addition, phospholipid-modified PAN nanofibers were used to immobilize lipase from *Candida rugosa*. The nanofibers showed increased enzyme activity retention of up to 76.8% compared to 56.4% for the pure PAN nanofibers [148]. Electrospun poly(acrylonitrile-*co*-acrylic acid) (PANCAA) nanofibers with MWCNTs were used for the immobilization of catalase. The MWCNT-containing system showed larger retention of enzyme activity (up to 47.9%) than pure PANCAA nanofibers. The increased activity retention was attributed to MWCNTs' improved charge transfer [149].

11.4.5 Functional textiles

Electrospun nanofibers show the potential to be used for making protective clothing. They form a barrier layer against hazardous liquids or vapors. For textile application, wear comfort must be considered. The nanofiber barrier layer should not alter the heat and moisture transport properties of fabric, as well as the air permeability.

It was reported that when electrospun PU nanofibers were deposited onto spunbonded polypropylene nonwoven fabric, the pesticide penetration of the fabric was reduced by 25%. In comparison to polytetrafluoroethylene membranes, the nanofiber layer was light weight, an order of magnitude smaller. Although the air permeability of the functional fabric was reduced with the increase in the areal density of the PU nanofibers, it was still at a satisfactory level of 100 cm^3/s/cm^2. The nanofiber layer did not change the water vapor transport of the fabric [150].

To provide thermophysiological comfort, textiles need to have both water vapor and heat transfer properties. A dual-layered electrospun fabric was prepared from hydrophilic PAN (outer) and hydrophobic PS (inner) mats and its moisture transport performance was evaluated. The fabric showed a push−pull effect toward moisture by changing the PS layer into hydrophilic. In practice this means that the fabric will allow sweat transfer from the inner to the outer hydrophilic layer [151].

Dual layer nanofibers were reported to have one-way transport ability to water or oils [152]. For example, PVDF-HFP and a blend of PVDP-HFP, FD-POSS (fluorinated decyl polyhedral oligomeric silsesquioxanes), and FAS (fluorinated alkylsilane) were electrospun in sequence to form a dual layer nanofiber membrane. The membrane showed superhydrophobicity on both sides but had a one-way oil transport from the PVDF-HFP/FD-POSS/FAS layer. This smart membrane showed enhanced oil/water separation.

11.4.6 Others

Electrospun nanofibers also show potential to be used in the field of material reinforcement. When electrospun nylon 6/fibrillary silicate nanofibers were embedded in 2,2′-bis-[4-(methacryloxypropoxy)-phenyl]-propane/ tri (ethylene glycol) dimethacrylate (Bis-GMA/TEGDMA) dental composites at low mass fractions, the flexural strength and elastic modulus were improved by 23% and 25%, respectively [153]. High-performance nanofiber-reinforced films were prepared from polyimide (PI)/carbon nanotube electrospun nanofibers embedded within a PI matrix, using poly(amic acid) as the precursor for the imidization process. These transparent composite films showed improved mechanical properties by 138% for tensile strength and 104% for elongation at break [154].

Electrospun nanofibers were also used for sound absorption. Electrospun PAN nanofibers with different fiber morphologies and thicknesses showed improved sound reduction [155]. The sound absorption of electrospun nanofibers from PVP, PS, and PVC was reported to increase by reducing fiber diameters. The absorption coefficients reached almost 1 at 2000 and 6000 Hz. The high sound absorption was explained by the large surface area, which provided strong interaction with sound waves [156].

11.5 Outlook

This chapter summarized electrospinning and structures, properties and applications of electrospun nanofibers. Electrospinning shows diversity in producing single fibers, random and aligned fibrous structures, 3D complex architectures, and yarns. Electrospun nanofibers offer broad applications in diverse areas. It is expected that with further development of large-scale electrospinning and nanofiber yarn production techniques, more success in practical applications of nanofibers and development of novel 3D fibrous architectures will be attained.

References

[1] Makoto K, et al. Method for manufacturing fibrous configuration composed of a plurality of mutually entangled bundles of extremely fine fibers. 1971 [Google Patents].
[2] Wente AV. Manufacture of superfine organic fibers. Washington, DC: Naval Research Laboratory; 1997.
[3] Joachim C. Drawing a single nanofibre over hundreds of microns. EPL (Europhysics Letters) 1998;42(2):215.
[4] Ingersoll HG. Fibrillated strand. 1963 [Google Patents].
[5] Ma PX, Zhang R. Synthetic nano-scale fibrous extracellular matrix. Journal of Biomedical Materials Research Part A 1999;46(1):60−72.
[6] Liu G, Qiao L, Guo A. Diblock copolymer nanofibers. Macromolecules 1996;29(16): 5508−10.
[7] Sutti A, Lin T, Wang X. Shear-enhanced solution precipitation: a simple process to produce short polymeric nanofibers. Journal of Nanoscience and Nanotechnology 2011; 11(10):8947−52.
[8] Lozano K, Sarkar K. Superfine fiber creating spinneret and uses thereof. 2014. US 8828294 B2.
[9] Cao M, et al. Preparation of ultrahigh-aspect-ratio hydroxyapatite nanofibers in reverse micelles under hydrothermal conditions. Langmuir 2004;20(11):4784−6.
[10] Gilbert W. On the magnet. Basics Books; 1958.
[11] Rayleigh L. On the equilibrium of liquid conducting masses charged with electricity. Philosophical Magazine 1882;14:184−6.
[12] Cooley JF. Apparatus for electrically dispersing fluids. 1902 [Google Patents].
[13] Cooley JF. Improved methods of and apparatus for electrically separating the relatively volatile liquid component from the component of relatively fixed substances of composite fluids. 1900.
[14] Morton WJ. Method of dispersing fluids. 1902 [Google Patents].
[15] Anton F. Process and apparatus for preparing artificial threads. 1934 [Google Patents].
[16] Anton F. Artificial fiber construction. 1938 [Google Patents].
[17] Anton F. Method and apparatus for the production of fibers. 1938 [Google Patents].
[18] Anton F. Artificial thread and method of producing same. 1940 [Google Patents].
[19] Anton F. Production of artificial fibers from fiber forming liquids. 1943 [Google Patents].
[20] Anton F. Method and apparatus for spinning. 1944 [Google Patents].
[21] Norton CL. Method of and apparatus for producing fibrous or filamentary material. 1936 [Google Patents].
[22] Taylor G. Electrically driven jets. Proceedings of the Royal Society of London A. Mathematical, Physical and Engineering Sciences 1969;313(1515):453−75.
[23] Taylor G. Disintegration of water drops in an electric field. Proceedings of the Royal Society A 1964;280(1382):383−97.
[24] Taylor G, McEwan A. The stability of a horizontal fluid interface in a vertical electric field. Journal of Fluid Mechanics 1965;22(01):1−15.
[25] Taylor GI. Conical free surfaces and fluid interfaces. In: Görtler H, editor. Applied mechanics. Springer Berlin Heidelberg; 1966. p. 790−6.
[26] Doshi J, Reneker DH. Electrospinning process and applications of electrospun fibers. Journal of Electrostatics 1995;35(2−3):151−60.
[27] Reneker DH, Chun I. Nanometre diameter fibres of polymer, produced by electrospinning. Nanotechnology 1996;7(3):216.

[28] Angammana CJ, Jayaram SH. A theoretical understanding of the physical mechanisms of electrospinning. In: Proceedings of ESA annual meeting on electrostatics; 2011.
[29] Sukigara S, et al. Regeneration of *Bombyx mori* silk by electrospinning—part 1: processing parameters and geometric properties. Polymer 2003;44(19):5721−7.
[30] Bailey VAG. Electrostatic spraying of liquids. Research studies Press LTD Taunton, Somerset/John Wiley & Sons Inc., New York 1988, 197 Seiten. Physik in unserer Zeit 1989;20(5):160.
[31] Demir MM, et al. Electrospinning of polyurethane fibers. Polymer 2002;43(11): 3303−9.
[32] Naveen Kumar HMP, et al. Compatibility studies of chitosan/PVA blend in 2% aqueous acetic acid solution at 30°C. Carbohydrate Polymers 2010;82(2):251−5.
[33] Hohman MM, et al. Electrospinning and electrically forced jets. II. Applications. Physics of Fluids 2001;13(8).
[34] Eda G, Shivkumar S. Bead-to-fiber transition in electrospun polystyrene. Journal of Applied Polymer Science 2007;106(1):475−87.
[35] Lin T, et al. The charge effect of cationic surfactants on the elimination of fibre beads in the electrospinning of polystyrene. Nanotechnology 2004;15(9):1375.
[36] Tan SH, et al. Systematic parameter study for ultra-fine fiber fabrication via electrospinning process. Polymer 2005;46(16):6128−34.
[37] Mit-uppatham C, Nithitanakul M, Supaphol P. Ultrafine electrospun polyamide-6 fibers: effect of solution conditions on morphology and average fiber diameter. Macromolecular Chemistry and Physics 2004;205(17):2327−38.
[38] Buchko CJ, et al. Processing and microstructural characterization of porous biocompatible protein polymer thin films. Polymer 1999;40(26):7397−407.
[39] Deitzel JM, et al. The effect of processing variables on the morphology of electrospun nanofibers and textiles. Polymer 2001;42(1):261−72.
[40] Zong X, et al. Structure and process relationship of electrospun bioabsorbable nanofiber membranes. Polymer 2002;43(16):4403−12.
[41] Yuan X, et al. Morphology of ultrafine polysulfone fibers prepared by electrospinning. Polymer International 2004;53(11):1704−10.
[42] Mo XM, et al. Electrospun P(LLA-CL) nanofiber: a biomimetic extracellular matrix for smooth muscle cell and endothelial cell proliferation. Biomaterials 2004;25(10): 1883−90.
[43] Zhang C, et al. Study on morphology of electrospun poly(vinyl alcohol) mats. European Polymer Journal 2005;41(3):423−32.
[44] Casper CL, et al. Controlling surface morphology of electrospun polystyrene fibers: effect of humidity and molecular weight in the electrospinning process. Macromolecules 2004; 37(2):573−8.
[45] Sun Z, et al. Compound core−shell polymer nanofibers by co-electrospinning. Advanced Materials 2003;15(22):1929−32.
[46] Li D, Xia Y. Direct fabrication of composite and ceramic hollow nanofibers by electrospinning. Nano Letters 2004;4(5):933−8.
[47] Li D, McCann JT, Xia Y. Use of electrospinning to directly fabricate hollow nanofibers with functionalized inner and outer surfaces. Small 2005;1(1):83−6.
[48] Lin T, Wang H, Wang X. Self-crimping bicomponent nanofibers electrospun from polyacrylonitrile and elastomeric polyurethane. Advanced Materials 2005;17(22): 2699−703.
[49] Zhao Y, Cao X, Jiang L. Bio-mimic multichannel microtubes by a facile method. Journal of the American Chemical Society 2007;129(4):764−5.

[50] Chen H, et al. Nanowire-in-microtube structured core/shell fibers via multifluidic coaxial electrospinning. Langmuir 2010;26(13):11291−6.
[51] Lee BS, Yang HS, Yu WR. Fabrication of double-tubular carbon nanofibers using quadruple coaxial electrospinning. Nanotechnology 2014;25(46):465602.
[52] Niu H, Lin T. Fiber generators in needleless electrospinning. Journal of Nanomaterials 2012;2012:1−13.
[53] Simm W, et al. Fibre fleece of electrostatically spun fibres and methods of making same. 1979 [Google Patents].
[54] Yarin AL, Zussman E. Upward needleless electrospinning of multiple nanofibers. Polymer 2004;45(9):2977−80.
[55] Jirsak O, et al. A method of nanofibres production from a polymer solution using electrostatic spinning and a device for carrying out the method. 2005 [Google Patents].
[56] Jirsak O, et al. Method of nanofibres production from a polymer solution using electrostatic spinning and a device for carrying out the method. 2009 [Google Patents].
[57] Dosunmu O, et al. Electrospinning of polymer nanofibres from multiple jets on a porous tubular surface. Nanotechnology 2006;17(4):1123.
[58] Liu Y, He JH. Bubble electrospinning for mass production of nanofibers. International Journal of Nonlinear Sciences and Numerical Simulation 2007;8(3):393−6.
[59] Zhou FL, Gong RH, Porat I. Polymeric nanofibers via flat spinneret electrospinning. Polymer Engineering and Science 2009;49(12):2475−81.
[60] Tang S, Zeng YC, Wang XH. Splashing needleless electrospinning of nanofibers. Polymer Engineering and Science 2010;50(11):2252−7.
[61] Lu BA, et al. Superhigh-throughput needleless electrospinning using a rotary cone as spinneret. Small 2010;6(15):1612−6.
[62] Wang X, et al. Needleless electrospinning of nanofibers with a conical wire coil. Polymer Engineering and Science 2009;49(8):1582−6.
[63] Lin T, et al. Electrostatic spinning assembly. 2010. WO 2010043002 A1.
[64] Wang X, et al. Needleless electrospinning of uniform nanofibers using spiral coil spinnerets. Journal of Nanomaterials 2012:9.
[65] Wang X, Lin T, Wang XG. Scaling up the production rate of nanofibers by needleless electrospinning from multiple ring. Fibers and Polymers 2014;15(5):961−5.
[66] Niu HT, Lin T, Wang XG. Needleless electrospinning. I. A comparison of cylinder and disk nozzles. Journal of Applied Polymer Science 2009;114(6):3524−30.
[67] Niu HT, Wang XG, Lin T. Upward needleless electrospinning of nanofibers. Journal of Engineered Fibers and Fabrics 2012;7:17−22.
[68] Niu HT, Wang XG, Lin T. Needleless electrospinning: influences of fibre generator geometry. Journal of the Textile Institute 2012;103(7):787−94.
[69] Forward KM, Flores A, Rutledge GC. Production of core/shell fibers by electrospinning from a free surface. Chemical Engineering Science 2013;104(0):250−9.
[70] Jiang G, Zhang S, Qin X. High throughput of quality nanofibers via one stepped pyramid-shaped spinneret. Materials Letters 2013;106(0):56−8.
[71] Ko F, et al. Electrospinning of continuous carbon nanotube-filled nanofiber yarns. Advanced Materials 2003;15(14):1161−5.
[72] Kim H. Method of manufacturing a continuous filament by electrospinning and continuous filament manufactured thereby. 2009 [Google Patents].
[73] Bazbouz MB, Stylios GK. Novel mechanism for spinning continuous twisted composite nanofiber yarns. European Polymer Journal 2008;44(1):1−12.
[74] Ali U, et al. Direct electrospinning of highly twisted, continuous nanofiber yarns. Journal of the Textile Institute 2012;103(1):80−8.

[75] Khil MS, et al. Novel fabricated matrix via electrospinning for tissue engineering. Journal of Biomedical Materials Research Part B Applied Biomaterials 2005;72(1): 117−24.
[76] Teo WE, et al. A dynamic liquid support system for continuous electrospun yarn fabrication. Polymer 2007;48(12):3400−5.
[77] Han T, Reneker DH, Yarin AL. Buckling of jets in electrospinning. Polymer 2007;48(20): 6064−76.
[78] Jin Y, et al. Fabrication of necklace-like structures via electrospinning. Langmuir 2009; 26(2):1186−90.
[79] Yuan H, et al. Stable jet electrospinning for easy fabrication of aligned ultrafine fibers. Journal of Materials Chemistry 2012;22(37):19634−8.
[80] Katta P, et al. Continuous electrospinning of aligned polymer nanofibers onto a wire drum collector. Nano Letters 2004;4(11):2215−8.
[81] Li D, et al. Collecting electrospun nanofibers with patterned electrodes. Nano Letters 2005;5(5):913−6.
[82] Yang F, et al. Electrospinning of nano/micro scale poly (L-lactic acid) aligned fibers and their potential in neural tissue engineering. Biomaterials 2005;26(15):2603−10.
[83] Smit E, Bűttner U, Sanderson RD. Continuous yarns from electrospun fibers. Polymer 2005;46(8):2419−23.
[84] Dalton PD, Klee D, Möller M. Electrospinning with dual collection rings. Polymer 2005; 46(3):611−4.
[85] Liu LQ, et al. One-step electrospun nanofiber-based composite ropes. Applied Physics Letters 2007;90(8):083108−1.
[86] Baniasadi M, et al. High-performance coils and yarns of polymeric piezoelectric nanofibers. ACS Applied Materials & Interfaces 2015;7(9):5358−66.
[87] Rogers CM, et al. A novel technique for the production of electrospun scaffolds with tailored three-dimensional micro-patterns employing additive manufacturing. Biofabrication 2014;6(3):035003.
[88] Wittmer CR, et al. Well-organized 3D nanofibrous composite constructs using cooperative effects between electrospinning and electrospraying. Polymer 2014;55(22): 5781−7.
[89] Ahirwal D, et al. From self-assembly of electrospun nanofibers to 3D cm thick hierarchical foams. Soft Matter 2013;9(11):3164−72.
[90] Kim TG, Chung HJ, Park TG. Macroporous and nanofibrous hyaluronic acid/collagen hybrid scaffold fabricated by concurrent electrospinning and deposition/leaching of salt particles. Acta Biomaterialia 2008;4(6):1611−9.
[91] Kim HY, et al. Nanopottery: coiling of electrospun polymer nanofibers. Nano Letters 2010;10(6):2138−40.
[92] Zhang D, Chang J. Electrospinning of three-dimensional nanofibrous tubes with controllable architectures. Nano Letters 2008;8(10):3283−7.
[93] Agarwal S, Wendorff JH, Greiner A. Use of electrospinning technique for biomedical applications. Polymer 2008;49(26):5603−21.
[94] Yoshimoto H, et al. A biodegradable nanofiber scaffold by electrospinning and its potential for bone tissue engineering. Biomaterials 2003;24(12):2077−82.
[95] Jin HJ, et al. Human bone marrow stromal cell responses on electrospun silk fibroin mats. Biomaterials 2004;25(6):1039−47.
[96] Xin XJ, Hussain M, Mao JJ. Continuing differentiation of human mesenchymal stem cells and induced chondrogenic and osteogenic lineages in electrospun PLGA nanofiber scaffold. Biomaterials 2007;28(2):316−25.

[97] Li CM, et al. Electrospun silk-BMP-2 scaffolds for bone tissue engineering. Biomaterials 2006;27(16):3115−24.
[98] Badami AS, et al. Effect of fiber diameter on spreading, proliferation, and differentiation of osteoblastic cells on electrospun poly(lactic acid) substrates. Biomaterials 2006;27(4): 596−606.
[99] Sun T, et al. Development of a 3D cell culture system for investigating cell interactions with electrospun fibers. Biotechnology and Bioengineering 2007;97(5):1318−28.
[100] Yang Y, et al. Promotion of skin regeneration in diabetic rats by electrospun core-sheath fibers loaded with basic fibroblast growth factor. Biomaterials 2011;32(18): 4243−54.
[101] Kurpinski KT, et al. The effect of fiber alignment and heparin coating on cell infiltration into nanofibrous PLLA scaffolds. Biomaterials 2010;31(13):3536−42.
[102] Stitzel J, et al. Controlled fabrication of a biological vascular substitute. Biomaterials 2006;27(7):1088−94.
[103] Lee YH, et al. Electrospun dual-porosity structure and biodegradation morphology of Montmorillonite reinforced PLLA nanocomposite scaffolds. Biomaterials 2005;26(16): 3165−72.
[104] Luong Van E, et al. Controlled release of heparin from poly(epsilon-caprolactone) electrospun fibers. Biomaterials 2006;27(9):2042−50.
[105] Choi JS, et al. The influence of electrospun aligned poly(epsilon-caprolactone)/collagen nanofiber meshes on the formation of self-aligned skeletal muscle myotubes. Biomaterials 2008;29(19):2899−906.
[106] Liao IC, et al. Effect of electromechanical stimulation on the maturation of myotubes on aligned electrospun fibers. Cellular and Molecular Bioengineering 2008;1(2−3):133−45.
[107] Corey JM, et al. Aligned electrospun nanofibers specify the direction of dorsal root ganglia neurite growth. Journal of Biomedical Materials Research Part A 2007;83A(3): 636−45.
[108] Lee JY, et al. Polypyrrole-coated electrospun PLGA nanofibers for neural tissue applications. Biomaterials 2009;30(26):4325−35.
[109] Verreck G, et al. Incorporation of drugs in an amorphous state into electrospun nanofibers composed of a water-insoluble, nonbiodegradable polymer. Journal of Controlled Release 2003;92(3):349−60.
[110] Buschle-Diller G, et al. Release of antibiotics from electrospun bicomponent fibers. Cellulose 2007;14(6):553−62.
[111] Zeng J, et al. Poly(vinyl alcohol) nanofibers by electrospinning as a protein delivery system and the retardation of enzyme release by additional polymer coatings. Biomacromolecules 2005;6(3):1484−8.
[112] Chen C, et al. Poly (lactic acid)(PLA) based nanocomposites—a novel way of drug-releasing. Biomedical Materials 2007;2(4):L1.
[113] Kim C, Yang K. Electrochemical properties of carbon nanofiber web as an electrode for supercapacitor prepared by electrospinning. Applied Physics Letters 2003;83(6): 1216−8.
[114] Kim C, et al. Characteristics of supercapacitor electrodes of PBI-based carbon nanofiber web prepared by electrospinning. Electrochimica Acta 2004;50(2−3):877−81.
[115] Ju YW, et al. Electrochemical properties of electrospun PAN/MWCNT carbon nanofibers electrodes coated with polypyrrole. Electrochimica Acta 2008;53(19):5796−803.
[116] Zhi MJ, et al. Highly conductive electrospun carbon nanofiber/MnO_2 coaxial nano-cables for high energy and power density supercapacitors. Journal of Power Sources 2012;208: 345−53.

[117] Hyun TS, et al. Facile synthesis and electrochemical properties of RuO_2 nanofibers with ionically conducting hydrous layer. Journal of Materials Chemistry 2010;20(41): 9172−9.
[118] Youn DY, et al. Facile synthesis of highly conductive RuO_2-Mn_3O_4 composite nanofibers via electrospinning and their electrochemical properties. Journal of the Electrochemical Society 2011;158(8):A970−5.
[119] Mai LQ, et al. Electrospun ultralong hierarchical vanadium oxide nanowires with high performance for lithium ion batteries. Nano Letters 2010;10(11):4750−5.
[120] Choi S-S, et al. Electrospun PVDF nanofiber web as polymer electrolyte or separator. Electrochimica Acta 2004;50(2−3):339−43.
[121] Ji L, Zhang X. Manganese oxide nanoparticle-loaded porous carbon nanofibers as anode materials for high-performance lithium-ion batteries. Electrochemistry Communications 2009;11(4):795−8.
[122] Ji LW, Zhang XW. Generation of activated carbon nanofibers from electrospun polyacrylonitrile-zinc chloride composites for use as anodes in lithium-ion batteries. Electrochemistry Communications 2009;11(3):684−7.
[123] Yu Y, et al. Tin nanoparticles encapsulated in porous multichannel carbon microtubes: preparation by single-nozzle electrospinning and application as anode material for high-performance Li-based batteries. Journal of the American Chemical Society 2009;131(44): 15984.
[124] Hwang D, et al. High-efficiency, solid-state, dye-sensitized solar cells using hierarchically structured TiO_2 nanofibers. ACS Applied Materials & Interfaces 2011;3(5): 1521−7.
[125] Joshi P, et al. Composite of TiO_2 nanofibers and nanoparticles for dye-sensitized solar cells with significantly improved efficiency. Energy & Environmental Science 2010; 3(10):1507−10.
[126] Hansen BJ, et al. Hybrid nanogenerator for concurrently harvesting biomechanical and biochemical energy. ACS Nano 2010;4(7):3647−52.
[127] Chang C, et al. Direct-write piezoelectric polymeric nanogenerator with high energy conversion efficiency. Nano Letters 2010;10(2):726−31.
[128] Fang J, Wang X, Lin T. Electrical power generator from randomly oriented electrospun poly (vinylidene fluoride) nanofibre membranes. Journal of Materials Chemistry 2011; 21(30):11088−91.
[129] Fang J, et al. Enhanced mechanical energy harvesting using needleless electrospun poly (vinylidene fluoride) nanofibre webs. Energy & Environmental Science 2013;6(7): 2196−202.
[130] Ding B, Yamazaki M, Shiratori S. Electrospun fibrous polyacrylic acid membrane-based gas sensors. Sensors and Actuators B-Chemical 2005;106(1):477−83.
[131] Ding B, et al. Electrospun nanofibrous membranes coated quartz crystal microbalance as gas sensor for NH_3 detection. Sensors and Actuators B-Chemical 2004;101(3): 373−80.
[132] Ren GL, et al. Electrospun poly(vinyl alcohol)/glucose oxidase biocomposite membranes for biosensor applications. Reactive & Functional Polymers 2006;66(12):1559−64.
[133] Liu Y, et al. Nonenzymatic glucose sensor based on renewable electrospun Ni nanoparticle-loaded carbon nanofiber paste electrode. Biosensors & Bioelectronics 2009; 24(11):3329−34.
[134] Wang N, et al. Tortuously structured polyvinyl chloride/polyurethane fibrous membranes for high-efficiency fine particulate filtration. Journal of Colloid and Interface Science 2013;398:240−6.

[135] Wang XF, et al. High flux filtration medium based on nanofibrous substrate with hydrophilic nanocomposite coating. Environmental Science & Technology 2005;39(19): 7684−91.
[136] Shin C, Chase GG, Reneker DH. Recycled expanded polystyrene nanofibers applied in filter media. Colloids and Surfaces A Physicochemical and Engineering Aspects 2005; 262(1−3):211−5.
[137] Yeom BY, Shim E, Pourdeyhimi B. Boehmite nanoparticles incorporated electrospun nylon-6 nanofiber web for new electret filter media. Macromolecular Research 2010; 18(9):884−90.
[138] Chen LP, et al. Novel Pd-carrying composite carbon nanofibers based on polyacrylonitrile as a catalyst for Sonogashira coupling reaction. Catalysis Communications 2008;9(13): 2221−5.
[139] Li MY, et al. Electrospinning-derived carbon fibrous mats improving the performance of commercial Pt/C for methanol oxidation. Journal of Power Sources 2009;191(2):351−6.
[140] Su L, et al. Free-standing palladium/polyamide 6 nanofibers for electrooxidation of alcohols in alkaline medium. Journal of Physical Chemistry C 2009;113(36):16174−80.
[141] Chang YZ, et al. Graphene-modified carbon fiber mats used to improve the activity and stability of Pt catalyst for methanol electrochemical oxidation. Carbon 2011;49(15): 5158−65.
[142] Chuangchote S, et al. Photocatalytic activity for hydrogen evolution of electrospun TiO_2 nanofibers. ACS Applied Materials & Interfaces 2009;1(5):1140−3.
[143] Zhang ZY, et al. Hierarchical assembly of ultrathin hexagonal SnS_2 nanosheets onto electrospun TiO_2 nanofibers: enhanced photocatalytic activity based on photoinduced interfacial charge transfer. Nanoscale 2013;5(2):606−18.
[144] Liu RL, et al. Fabrication of TiO_2/ZnO composite nanofibers by electrospinning and their photocatalytic property. Materials Chemistry and Physics 2010;121(3):432−9.
[145] Kanjwal MA, et al. Photocatalytic activity of ZnO-TiO_2 hierarchical nanostructure prepared by combined electrospinning and hydrothermal techniques. Macromolecular Research 2010;18(3):233−40.
[146] Xie JB, Hsieh YL. Ultra-high surface fibrous membranes from electrospinning of natural proteins: casein and lipase enzyme. Journal of Materials Science 2003;38(10):2125−33.
[147] Wu LL, Yuan XY, Sheng J. Immobilization of cellulase in nanofibrous PVA membranes by electrospinning. Journal of Membrane Science 2005;250(1−2):167−73.
[148] Huang XJ, et al. Electrospun nanofibers modified with phospholipid moieties for enzyme immobilization. Macromolecular Rapid Communications 2006;27(16):1341−5.
[149] Wang ZG, et al. Nanofibrous membranes containing carbon nanotubes: electrospun for redox enzyme immobilization. Macromolecular Rapid Communications 2006;27(7): 516−21.
[150] Lee S, Obendorf SK. Use of electrospun nanofiber web for protective textile materials as barriers to liquid penetration. Textile Research Journal 2007;77(9):696−702.
[151] Dong Y, et al. Tailoring surface hydrophilicity of porous electrospun nanofibers to enhance capillary and push−pull effects for moisture wicking. ACS Applied Materials & Interfaces 2014;6(16):14087−95.
[152] Wang H, et al. Dual-layer superamphiphobic/superhydrophobic-oleophilic nanofibrous membranes with unidirectional oil-transport ability and strengthened oil−water separation performance. Advanced Materials Interfaces 2015;2(4).
[153] Tian M, et al. Bis-GMA/TEGDMA dental composites reinforced with electrospun nylon 6 nanocomposite nanofibers containing highly aligned fibrillar silicate single crystals. Polymer 2007;48(9):2720−8.

[154] Chen D, et al. High performance polyimide composite films prepared by homogeneity reinforcement of electrospun nanofibers. Composites Science and Technology 2011; 71(13):1556−62.
[155] Xiang HF, et al. Sound absorption behaviour of electrospun polyacrylonitrile nanofibrous membranes. Chinese Journal of Polymer Science 2011;29(6):650−7.
[156] Khan WS, Asmatulu R, Yildirim MB. Acoustical properties of electrospun fibers for aircraft interior noise reduction. Journal of Aerospace Engineering 2012;25(3):376−82.

High performance polyimide fibers

12

J. Chang, H. Niu, D. Wu
Beijing University of Chemical Technology, Beijing, China

12.1 Introduction

High-performance polyimide (PI) fibers with excellent mechanical properties, superior chemical and radiation resistance, outstanding thermal-oxidative stabilities, and unique electric properties (Ohya et al., 1997; Hasegawa and Horie, 2001; Liaw et al., 2012; Mengxian, 2006) have been of great interest to researchers in recent years with respect to the cyclic imide and aromatic groups in the polymer backbone. As one of the most promising high-performance polymeric fibers for present and future, PI fibers have been utilized in diverse fields such as electrical, microelectronics, engineering, and aerospace applications (Bessonov, 1987; Ghosh, 1996; Sroog, 1991). Also high-performance PI fibers have undergone significant development in the past decades. PI fibers were initially proposed by American and Soviet researchers (Sasaki et al., 1981; Makino et al., 1984; Ohmura et al., 1983); however, the mechanical properties of PI fibers were very poor because of the limitation of spinning equipment and the synthesis method. After several years' research and development, high-performance PI fibers with outstanding properties have deserved much attention. In this regard, to obtain high-performance PI fibers, much effort has been given to fundamental studies of the relationship between structures and properties, which was of critical importance to establish a general rule in designing and preparing high-performance PI fibers.

Currently, two main techniques are well developed in preparing PI fibers (Cheng et al., 1991; Eashoo et al., 1993; Zhang et al., 2004a; Niu et al., 2013). The first refers to the one-step method in which PI fibers are produced directly from organ-soluble PIs synthesized via a polycondensation reaction of dianhydrides and diamines in toxic phenol solvents (Kaneda et al., 1986a,b). In this method, microporous structures and other defects can be avoided, resulting in the ultrahigh tensile strength and initial modulus of PI fibers. Unfortunately, the selection of organ-soluble monomers and environment-friendly solvents has restricted the development of industrial production of PI fibers in the one-step method (Niu et al., 2013; Dong et al., 2013). The other and more widely practiced technique is the two-step method, in which poly(amic acid) (PAA) fibers are obtained by extruding PAA solution into a coagulation bath and subsequently converting into corresponding PI fibers through thermal or chemical imidization (Chen et al., 2009; Park and Farris, 2001; Dorogy and St. Clair, 1991a,b; 1993). The industrial production of PI fibers is more likely to be realized in this method since there are extensive amounts of monomer candidates for

Structure and Properties of High-Performance Fibers. http://dx.doi.org/10.1016/B978-0-08-100550-7.00012-7

polymerization. However, the mechanical properties of PI fibers are in need of further improvement in the two-step method because of the defects generated during the dual-diffusion and imidization route (Kaneda et al., 1986a,b). Despite its weakness, the two-step technology has provided diverse opportunities for large-scale applications.

Generally, the mechanical properties of PI fibers are closely related to the rigidity of the polymer backbone, chemical structures of the main chains, degree of crystallinity, molecular packing and orientation, and structural defects in the fibers (Hsiao and Chen, 2002; Hasegawa et al., 1999a,b; Liu et al., 2012). Also there is no doubt that these factors are strongly affected by different preparation methods because of the variation of aggregation state and morphologies in the fibers. Herein we attempt to cover the important topics concerning the correlation between structures and properties of the PI fibers on the basis of preparation methods.

12.2 One-step method for polyimide synthesis

As is well known, the earliest commercialized P84 fibers were derived from 3,3′,4,4′-benzophenonetetracarboxylic dianhydride (BTDA), 4,4′-diphenylmethane diisocyanate (MDI), and 2,4-toluene diisocyanate (TDI) by the one-step method (Qiao et al., 2005; Xiang et al., 2011). However, because of the limitation of spinning equipment and technology, the fibers possess poor mechanical properties with a tensile strength of 0.5 GPa, initial modulus of 2.12 GPa, and elongation of 20%. In this regard, P84 fibers are commonly used in thermal and irraditional resistance applications (Mengxian, 2006). The typical preparation of PI in the one-step method is shown in Fig. 12.1. Herein, some representatives of PI fibers adopted in the one-step technology are listed based on different dianhydrides such as 3,3′,4,4′-biphenyltetracarboxylic dianhydride (BPDA), 4,4′-oxydiphthalic anhydride (ODPA), and BTDA.

12.2.1 BPDA-based polyimide fibers

Cheng et al. (1991) have synthesized a type of PI fiber derived from BPDA and 2,2′-bis(trifluoromethyl)-4,4′-diaminobiphenyl (PFMB/TFMB) using a one-step dry-jet wet-spinning method (Eashoo et al., 1993). The fibers were drawn 10 times over 400°C to get the resultant PI fibers with tensile strength and initial modulus of

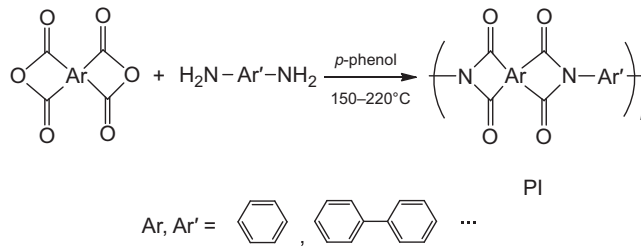

Figure 12.1 The preparation of PI fibers in the one-step method.

3.2 and 130 GPa, respectively. By means of convenience in the one-step method without removal of the micromolecules, the fibers could yield larger drawing to quickly build up well-defined crystalline structures. When the draw ratio increased to 8, the fibers exhibited a crystallinity of 50% and crystal orientation of 0.87, while the values were 10% and 0.75 for as-spun fibers, respectively. For aromatic PI fibers, crystallinity and crystal orientation are two crucial factors that determine the final performance of fibers. Subsequently, the extensively improved mechanical properties of BPDA/PFMB fibers in the one-step method are mainly attributed to the elevated drawing ratio, giving critical evidence of a draw ratio-dependent feature. Similarly, Li et al. (1996) prepared novel soluble high-performance PI fibers in *p*-chlorophenol with BPDA and 2,2′-dimethyl-4,4′-diaminobiphenyl (DMB) by the one-step dry-jet wet-spinning method (Eashoo et al., 1994). The tensile strength and initial modulus were up to 3.3 and 130 GPa with a maximum drawing ratio of 10, respectively, ascribing to the readily aligned rigid chain molecules and ordered crystalline regions regarding the presence of external forces. Above all, in the one-step method, the supermolecular structures could be retained without the imidization process, which exerts considerable effects on the mechanical properties of PI fibers. However, the residual toxic phenol solvents in the fibers are difficult to remove and will inevitably influence the performance of the resulting PI fibers. Accordingly, the development of the one-step method was limited and needed to be further improved. The chemical structures of BPDA/PFMB and BPDA/DMB fibers are illustrated in Fig. 12.2.

Furthermore, Zhang et al. (2004a,b,c) have prepared kind of BPDA/ODA homo-PI fibers via a one-step dry-jet wet-spinning method. The chemical structure of the fibers is given in Fig. 12.3. The fibers exhibited a tensile strength and initial modulus of 2.4 and 114 GPa with a drawing ratio of 5.5, while the value for as-spun fibers was 0.42 and 33 GPa, respectively. Thus it was possible to obtain PI fibers with high strength and modulus by drawing in the one-step method. Hence the fibrils and microvoids could be identified from the fractured cross-sectional morphologies, which had affected the mechanical properties of the PI fibers. The fibers also exhibited excellent

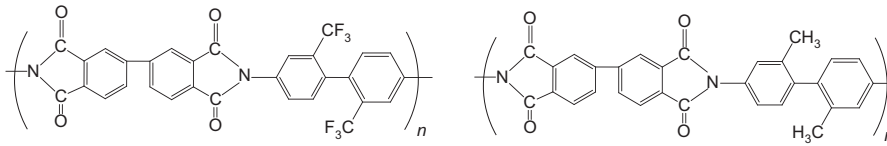

BPDA/PFMB BPDA/DMB

Figure 12.2 The chemical structures of BPDA/PFMB and BPDA/DMB fibers.

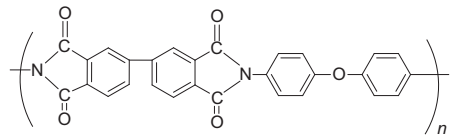

Figure 12.3 The chemical structure of BPDA/ODA-type PI fibers.

thermal stabilities with *5% weight loss temperature* (T_{d5}) around 400°C in air atmosphere, negative value of linear coefficient of thermal expansion (CTE) below 400°C, and *glass transition temperature* (T_g) ranging from 276 to 297°C with the frequency increased from 0.1 to 100 Hz.

12.2.2 ODPA-based polyimide fibers

Kim et al. (1996) have synthesized PI fibers derived from ODPA and DMB via a one-step dry-jet wet-spinning method, whose chemical structure is illustrated in Fig. 12.4. The fibers obtained an optimum tensile strength of 0.77 GPa and initial modulus of 41 GPa when drawn 4.4 times. The improved mechanical properties were critically dependent on the increased crystallinity and orientation of the fibers. As the overall and crystal orientation developed differently with high drawing ratio, further improvement of tensile strength with high drawing ratios was related to the increase of orientation in the noncrystalline region of the fibers.

12.2.3 BTDA-based polyimide fibers

Dong et al. (2013) prepared a series of PI fibers based on BTDA, 2-(4-aminophenyl)-5-aminobenzimidazole (BIA) and TFMB via a one-step wet-spinning method as illustrated in Fig. 12.5. The heterocyclic diamine BIA provided strong intermolecular hydrogen-bonding (H-bonding) interaction that strengthened the mechanical properties of the PI fibers, while the diamine TFMB possessed a rigid nonplanar structure with two bulky trifluoromethyl groups, resulting in great benefits for improving solubility of the PIs. Consequently, the final PI fibers exhibited a tensile strength of 2.25 GPa and initial modulus of 102 GPa with a drawing ratio of 3.0 when the molar ratio of TFMA/BIA was 50/50. Because of the presence of $-CF_3$ groups, the PI fibers showed excellent solubility in aprotic polar solvents. Meanwhile, the fibers exhibited excellent thermal stabilities of up to 591°C in nitrogen and 563°C in air for a 5% weight loss and (T_g) values above 340°C.

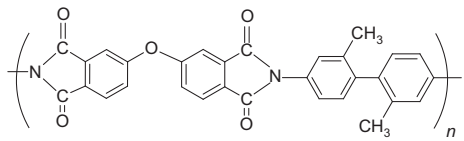

Figure 12.4 The chemical structure of ODPA/DMB fibers.

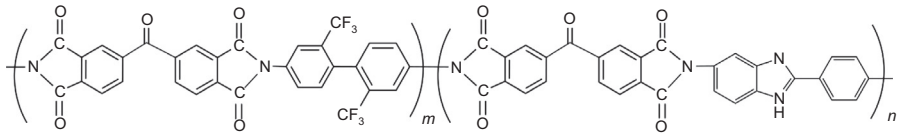

Figure 12.5 The chemical structure of BTDA/TFMB/BIA fibers.

In summary, the typical synthesis route in the one-step method involves the polycondensation of dianhydrides and diamines in phenol solvent, which is then spun into final PI fibers directly. The prepared PI fibers exhibited high strength/high modulus with high molecular weight; however, the selection of soluble reaction components and environment-friendly solvents has severely limited the development and large-scale production of PI fibers. In this regard, the other technique, the two-step method, has attracted much attention and has been commonly adopted in obtaining aromatic PI fibers recently.

12.3 Two-step method for polyimide synthesis

The typical approach in preparing PI in the two-step method is illustrated in Fig. 12.6. As for two-step method, the first patent for PI fibers was published in the 1960s, when the PI fibers were prepared with pyromellitic dianhydride (PMDA), 4,4′-oxydianiline (ODA), and 4,4′-thiodianiline (TDA) in dimethylacetamide (DMAc) solvent (Samuel and Edgar, 1968). The mechanical properties of the prepared PI fibers were not high because of the poor processing conditions. In this aspect, attributing to the convenience of designing macromolecular structures and synthesis, a novel integrated continuous two-step method was developed to yield PI fibers from as-spun PAA fibers (Wu et al., 2014).

Fig. 12.7 depicts a typical schematic diagram of the preparation of PI fibers via the integrated continuous two-step wet-spinning method, and each part in the diagram is described. The spinning solution was primarily extruded into the coagulation bath through a spinneret to get as-spun PAA fibers. After removing the residual solvents in the washing bath, the fibers were dried and delivered into the furnace with temperatures ranging from 200 to 500°C, with continual drawing on the rollers to be converted into PI fibers. In particular, it should be noted that the as-spun PAA fibers were spun from isotropic solutions in which the molecules were not well oriented. During thermal treatment, the molecules had much opportunities to rearrange themselves , resulting in the drastically improved mechanical performances of the resulting PI fibers as compared with those of as-spun PAA fibers. Also the aggregation state of the molecules is strongly dependent on the spinning conditions and chemical structures

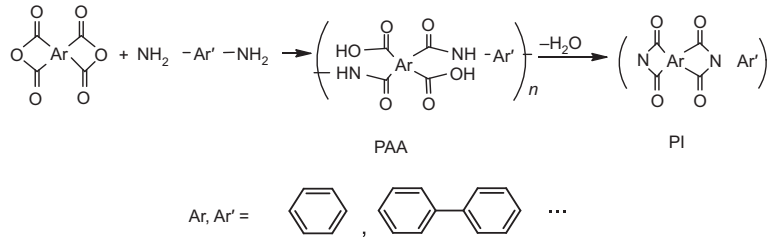

Figure 12.6 The preparation of PI fibers in the two-step method.

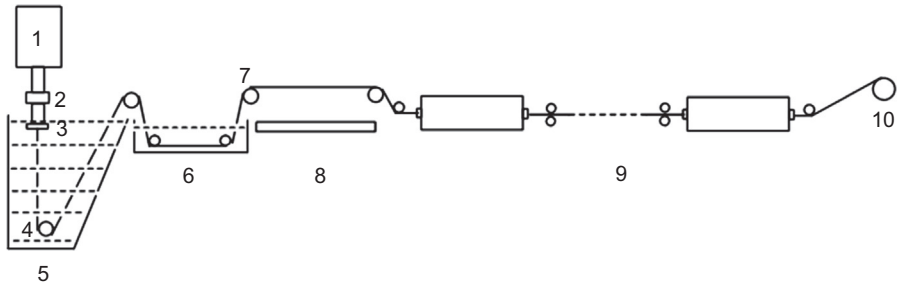

Figure 12.7 Schematic diagram of the preparation of PI fibers in the two-step wet-spinning method: 1—storage tank; 2—metering pump; 3—spinneret plate; 4—godet roller; 5—coagulating bath; 6—washing bath; 7—hot roller; 8—hot plate; 9—tubular heating furnace; 10—winding device.
Niu, H., 2012. Preparation and properties research of polyimide fibers with high strength and high modulus (Doctoral thesis). Beijing University of Chemical Technology.

of the polymer backbone in the two-step technique. Herein, two aspects including spinning conditions and chemical structures are covered to understand the structure–property relationship of PI fibers.

12.3.1 The structure–property relationship of polyimide fibers with different spinning conditions

During the fiber formation process, there are three factors that mainly govern the final performances of the PI fibers: (1) the coagulation bath (Wang et al., 2009; Chen et al., 2007), (2) the drawing ratio (Cheng et al., 1991; Eashoo et al., 1993; Wu et al., 1995) and (3) the imidization temperature (Niu et al., 2012).

12.3.1.1 Coagulation bath

The PAA precursor fibers were obtained in the coagulation bath, and therefore the quality of the as-spun fibers will directly affect the properties of the corresponding PI fibers. Usually, the coagulation bath consists of a mixture of deionized water and (or) other solvents such as DMAc, dimethylformamide (DMF), dimethyl sulfoxide (DMSO), *N*-methyl-2-ketopyrrolidone (NMP), and ethanol (Mengxian, 2006). Different constitution, temperature, and concentration of the coagulation bath will give rise to different fractured cross-sectional morphologies and performances of the fibers, which are similar to the case of carbon fibers (Dong et al., 2007; Um et al., 2004; Bahrami et al., 2003). During wet spinning, the dual-diffusion process will happen as the solvents diffuse into the coagulation bath and the coagulants diffuse into the fibers. If the inner force and external force cannot reach equilibrium for the solvents and coagulants, the defects will inevitably generate in the fibers. For example, if solidification proceeds too fast, the "skin–core" structures are likely to be generated because of the rapid solidification of the surface layer of the fibers. On the contrary, the

fibers may contain too many solvents in the fibers. Both phenomena will post a negative impact on the performance of the fibers. However, the literature is scant regarding the coagulation conditions on the properties of PI fibers.

12.3.1.2 Drawing ratios

In the one-step method, the fibers could endure large drawing ratios even up to 10, leading to significant improvement in the performances of the PI fibers, yet the exploration of the drawing ratio was not comprehensive enough. In the two-step method, after the PAA precursor fibers were obtained, the fibers were then transferred to PI fibers by the thermal imidization process. During the process, the macromolecule chains will rearrange themselves into the defect-free positions under external drawing because of the removal of micromolecules. Hence it provides opportunities for the polymer chains to form ordered molecular arrangement under deformation, leading to remarkable changes on the properties of the fibers.

Dong et al. (2014) prepared a series of PI fibers derived from BTDA, TFMB, and BIA (the molar ratio of TFMB/BIA = 1/9) with different drawing ratios such as 0, 1.5, 1.6, 1.9, 2.0, and 2.3 by a typical two-step method. For as-spun fibers with a drawing ratio $\lambda = 0$, the fibers exhibited a tensile strength and initial modulus of 0.57 and 4.3 GPa, respectively. Correspondingly, the value increased to 2.13 and 109.2 GPa, nearly 3.7 and 25.4 times the strength and modulus of the as-spun fibers. Also the drawing process resulted in the formation of high crystal orientation and ordered crystal structures, orientation of the microvoids along the fibers, and reduction in the size of the microvoids in the fibers, giving evidence of the remarkably enhanced mechanical properties of the PI fibers. In light of the results, it was believable that the microvoids in the fibers were stretched to be longer upon the drawing process, leading to decreased radius and increased length of the microvoids. However, when the drawing ratio increased to 2.3, a rapid decrease in length could be observed because of the breakage of the microvoids under high strain. Moreover, it was found that increased drawing ratios led to increased T_g value with decreased intensities of α relaxations, which was suggested to be caused by the highly ordered crystalline regions and regular macromolecular packing during the drawing process. Ultimately, the performances of the PI fibers were dramatically improved with the increased drawing ratios, giving evidence of the existence of drawing-dependent structures.

With respect to the wet-spinning process, during the thermal or chemical imidization route, the rearrangement of the macromolecule chains will occur depending on the removal of H_2O micromolecules, leading to imperfection in the fibers. In this regard, the microvoids along the fiber axial direction can be characterized by small-angle X-ray scattering (SAXS) (Grubb and Prasad, 1992; Wu et al., 2000). The radius of microvoids can be described by Guinier functions in Eq. (12.3) (Jiang et al., 2012a,b; Wang et al., 2008) as follows:

$$I(q) = I_0 \exp\left(\frac{-q^2R^2}{5}\right) \tag{12.1}$$

where R is the radius of the microvoids with circular cross-section, q is the scattering vector ($q = 4\pi \sin\theta/\lambda$, where 2θ is the scattering angle), and $I(q)$ is the scattering intensity in reciprocal. Through the Fankuchen successive tangent method, the average radius of microvoids can be calculated according to Eq. (12.2):

$$R = \sum R_i W_i (i = 1, 2, 3\ldots) \tag{12.2}$$

where R_i is the radius of different sizes of microvoids and W_i is the corresponding volume percentage of the microvoids. Then the average fibril length L and misorientation B_ϕ are determined by Eq. (12.3) (Ran et al., 2001; Ruland, 1969; Feng et al., 2008) proposed by Ruland:

$$s^2 B_{\text{obs}}^2 = \frac{1}{L^2} + s^2 B_\phi^2 \tag{12.3}$$

where B_{obs} is the angular spread of the data fitting by Gaussian−Gaussian function and s is the scattering vector ($s = 2\sin\theta/\lambda$).

In addition, Zhang et al. (2015b) have also obtained a series of PI fibers prepared with BPDA, *p*-PDA, BIA, and ODA by the two-step wet-spinning method. The PI fibers reached an optimum tensile strength and initial modulus of 2.8 and 136 GPa at a drawing ratio of 3.0, respectively. The 2D wide-angle X-ray diffraction (WAXD) patterns of the PI fibers prepared with different drawing ratios are adapted as presented in Fig. 12.8. It can be observed that with the increased drawing ratio, the diffraction streaks become much stronger and clearer in both directions, indicating the formation of highly ordered crystal structures. On the other hand, the drawing process gave rise to increased molecular orientation along the fiber axis, which was calculated based on the Hermans equation in Eq. (12.4) (Cheng et al., 1991; Eashoo et al., 1993, 1994; Li et al., 1996). The increased orientation will naturally promote the improvement of the performances of the fibers.

$$f = \left(3 < \cos^2\phi > -1\right)/2 \tag{12.4}$$

where f is the degree of molecular orientation along the fiber axis direction and ϕ is the angle between the fiber axis and c-axis crystal unit cell. The numerical values of the mean-square cosines in the equation are determined by corrected intensity distribution $I(\phi)$ diffracted from the crystalline plane by Gaussian fitting following Eq. (12.5):

$$< \cos^2\phi > = \frac{\int_0^{\pi/2} I(\phi)\sin\phi\cos^2\phi d\phi}{\int_0^{\pi/2} I(\phi)\sin\phi d\phi} \tag{12.5}$$

Moreover, atomic force microscopy (AFM) was employed to observe the surface roughness of the fibers with different drawing ratios, which is revealed in Fig. 12.9. The root mean-square roughness (R_q) and the arithmetic mean roughness

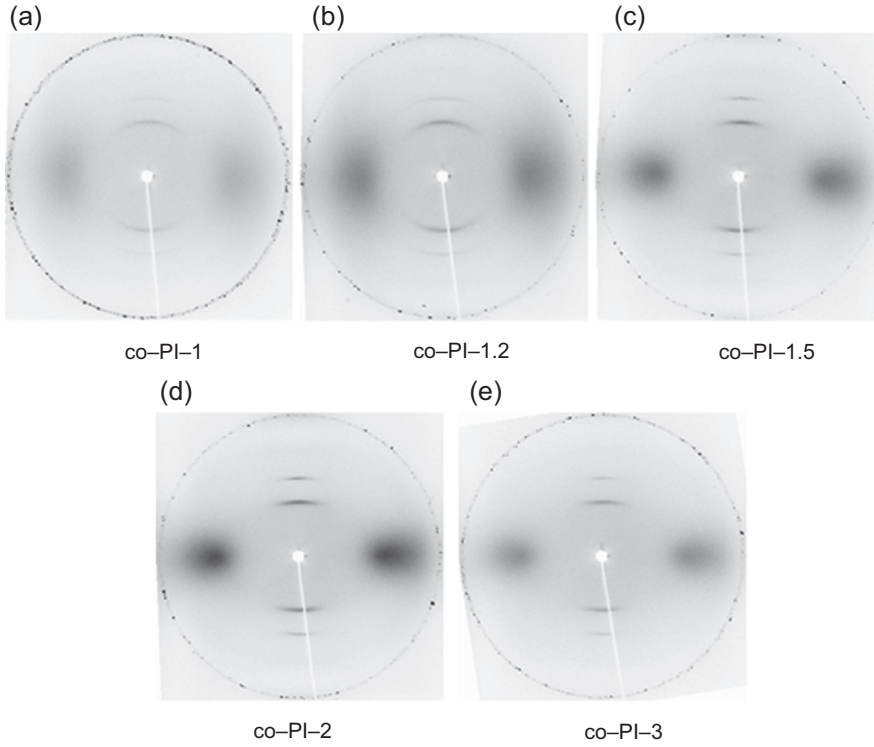

Figure 12.8 WAXD patterns of PI fibers with various drawing ratios.
Zhang, M., Niu, H., Lin, Z., et al., 2015b. Preparation of high performance copolyimide fibers via increasing draw ratios. Macromolecular Materials and Engineering 300 (11), 1096−1107.

(R_a) can be calculated from Eq. (12.6) (Gadelmawla et al., 2002; Fang and Chang, 2003):

$$R_q = \sqrt{\frac{1}{N^2}\sum_{i=1}^{N}\sum_{j=1}^{N}(Z_{ij} - Z_{av})^2}$$
$$R_a = \frac{1}{N}\sum_{i=1}^{N}\sum_{j=1}^{N}(Z_{ij} - Z_{cp})^2 \tag{12.6}$$

where N is the number of data points in the images, i and j are the pixel locations on the AFM images, Z_{ij} is the height value at i and j locations, Z_{av} is the average height value within the given area, and Z_{cp} is the height value from the center plane. The results showed that the roughness of the PI surfaces was increased along with the increased drawing ratio, ascribing to the different abilities of deformation between the core and

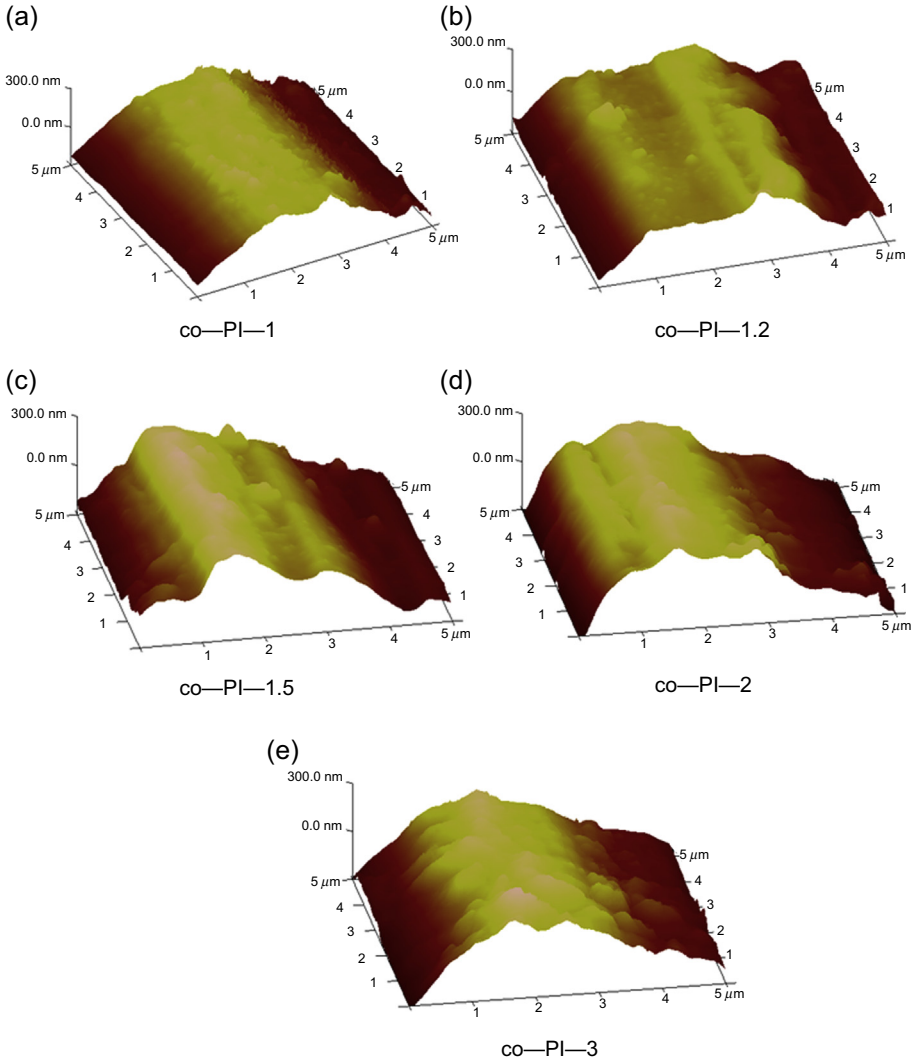

Figure 12.9 AFM observations of PI fibers with various drawing ratios.
Zhang, M., Niu, H., Lin, Z., et al., 2015b. Preparation of high performance copolyimide fibers via increasing draw ratios. Macromolecular Materials and Engineering 300, 1096-1107.

skin structures of the fibers. The soft core was readily stretched, whereas the tough skin was difficult to draw during the imidization process, resulting in the appearance of small notches and protuberances on the fiber surfaces. Furthermore, sketches of the structures and structural evolutions with the increased drawing ratios of the fibers are illustrated in Figs. 12.10 and 12.11, respectively. The fibers were composed of fibrils and exhibit skin−core structures in which the fibrils near the surface were packed more

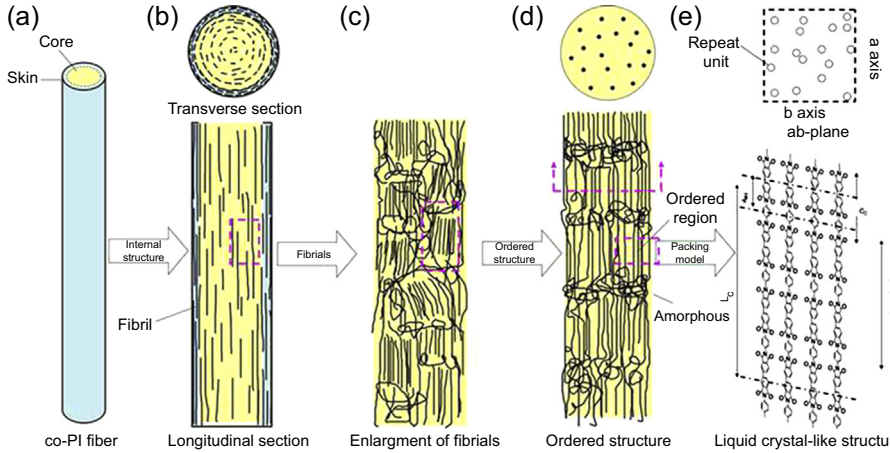

Figure 12.10 Sketch of the structures of PI fibers.
Zhang, M., Niu, H., Lin, Z., et al., 2015b. Preparation of high performance copolyimide fibers via increasing draw ratios. Macromolecular Materials and Engineering 300 (11), 1096−1107.

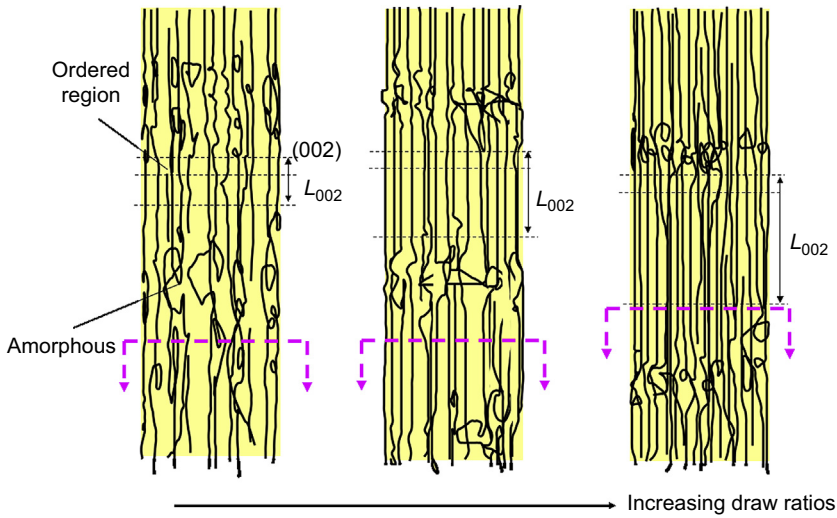

Figure 12.11 Sketch of the structural evolution of PI fibers with increased drawing ratios.
Zhang, M., Niu, H., Lin, Z., et al., 2015b. Preparation of high performance copolyimide fibers via increasing draw ratios. Macromolecular Materials and Engineering 300 (11), 1096−1107.

compactly with ordered molecular arrangement. Although the well-defined 3D crystalline structures were not observed depending upon the poor lateral packing in the transverse directions, the fibers still exhibited "semectic-like" ordered structures along the fiber axial direction, including the ordered and amorphous regions. Accompanied by the increased drawing ratio, the packing in both regions became denser and ordered, leading to the relatively perfect "smectic-like" structures with regular molecular arrangement.

12.3.1.3 Imidization temperature

The mechanical properties of the PI fibers were significantly promoted during the thermal imidization process, namely, the performances of the fibers were mainly determined by the imidization conditions. Basically, the imidization conditions encompass imidization temperature and imidization time. Yet, it was discovered that the final properties of the PI fibers were critically dependent on the imidization temperature, and thus the influence of imidization time could be ignored (Xu et al., 2013).

Niu et al. have investigated the effect of thermal treatment temperatures on the structures and properties of BPDA/*p*-PDA/AAQ PI fibers. The cited mechanical and thermal properties data are displayed in Table 12.1 (Niu et al., 2012). After being treated with elevated temperatures, the tensile strength and modulus increased significantly, and reached optimum values of 2.6 and 112.3 GPa at 390°C, respectively, suggesting gradually increased imidization degree (ID) with increased treatment temperatures. Unfortunately, in contrast, further increase in temperature resulted in decreased tensile strength, modulus, and T_{d5} value because of the slight degradation of the polymer chains at elevated temperatures (Dine-Hart and Wright, 1967). Moreover, the 2D WAXD patterns and corresponding cross-sectional morphologies of the fibers with different thermal imidization temperatures are demonstrated in Fig. 12.12. It was noted that followed by the increased temperatures, an increasing numbers of microfibril structures along the longitudinal axis were observed, indicating elevated orientation in the fiber axis direction. Similarly, the clear diffraction streaks in the WAXD patterns have also verified the increased high orientation in the meridian direction. In conclusion, the microstructure, mechanical, and thermal properties of the PI fibers strongly depended on the ID with the increase of the thermal treatment temperatures. Therefore, the thermal imidization temperature plays an important role in controlling the final performances of the resultant PI fibers.

Table 12.1 The mechanical and thermal properties of the fibers with different thermal treatment temperatures

Fibers Thermal treatment temperature (°C)	Tensile strength (GPa)	Initial Modulus (GPa)	Elongation (%)	T_{d5} (°C)		T_g (°C)
				N_2	Air	
Co-PAA	0.15	10.6	3.8	–	–	–
240	0.53	83.1	0.6	–	–	–
240–300	1.7	88.9	2.0	–	–	–
240–360	2.5	109.4	2.6	601	561	396
240–390	2.6	112.3	2.7	611	565	404
240–420	2.5	100.1	2.7	585	558	415

Co-PAA, Copoly(amic) acid.

Niu, H, Qi, S, Han, E., et al., 2012. Fabrication of high-performance copolyimide fibers from 3,3′,4,4′-biphenyltetracarboxylic dianhydride, *p*-phenylenediamine and 2-(4-aminophenyl)-6-amino-4(3H)-quinazolinone. Materials Letters 89, 63–65.

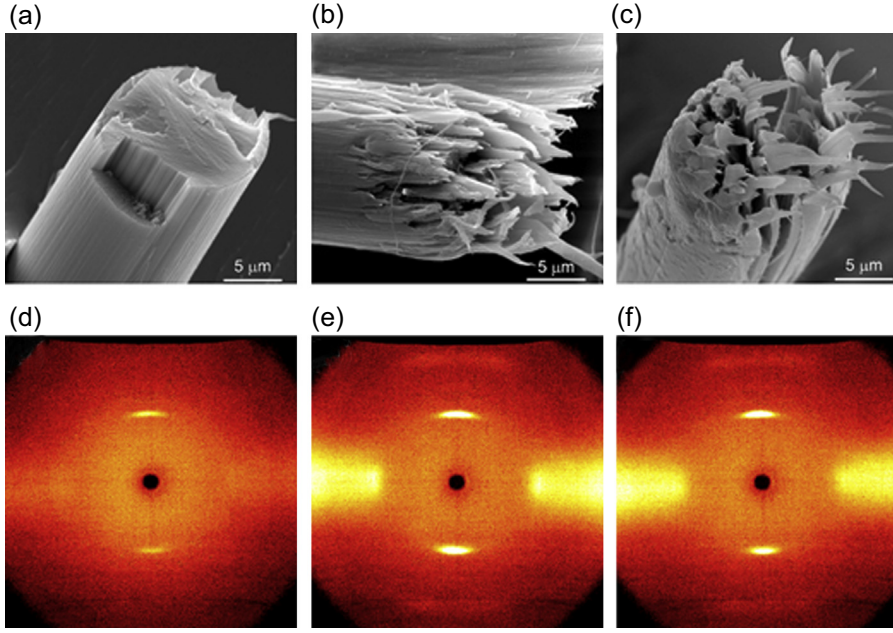

Figure 12.12 Fractured cross-sectional morphologies (a–c) and 2D WAXD patterns (d–f) of the PI fibers: (a, d) 240°C; (b, e) 240–300°C; (c, f) 240–390°C.
Niu, H., Qi, S., Han, E., et al., 2012. Fabrication of high-performance copolyimide fibers from 3,3′,4,4′-biphenyltetracarboxylic dianhydride, p-phenylenediamine and 2-(4-aminophenyl)-6-amino-4(3H)-quinazolinone. Materials Letters 89, 63–65.

12.3.2 The structure–property relationship of polyimide fibers with different chemical structures

As is known, subtle variations in the structures of the dianhydride and diamine components have a tremendous effect on the properties of the final PI fibers. For example, the fibers derived from the PMDA/ODA system exhibited tensile strength, initial modulus, and elongation up to 0.4 GPa, 5.2 GPa, and 11.1%, respectively, with T_g around 400°C (Park and Farris, 2001). The fibers prepared in the BPDA/*p*-PDA system possessed tensile strength, initial modulus, and elongation of 1.07 GPa, 50.39 GPa, and 1.12%, respectively, with T_g around 340°C (Chang et al., 2015b). Thus, such features directly lead to various performances of the PI fibers. Herein, different preparation systems based on various dianhydrides are summarized.

12.3.2.1 PMDA-based polyimide fibers

Among all the preparation systems, the PMDA/ODA system is considered as the simplest because of the high reactivity of the two monomers when reacted with other dianhydrides/diamines, whose chemical structure is shown in Fig. 12.13. The PMDA/ODA polymer backbone consists of rigid PMDA units and flexible ODA units, thus

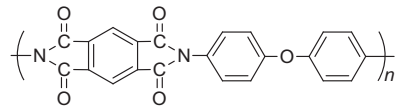

Figure 12.13 The chemical structure of PMDA/ODA-type PI fibers.

leading to a contradiction in the performance of the resultant PI fibers. As stated by the previous review, the rigid polymer chains gave rise to excellent thermal-oxidative stability with 10% weight loss temperature (T_{d10}) over 540°C in air atmosphere and glass transition temperature of 410°C. On the other hand, the flexible ODA units contorted the chain symmetry and thus made it harder for the chain to pack into the crystal lattice, resulting in poor degree of lateral molecular arrangement (Ratta, 1999). Therefore, the fibers could not achieve high mechanical properties through thermal drawing.

Xu et al. (2013) have investigated the effect of ID on the final performance of PMDA/ODA PI fibers via the two-step dry-spinning process. The ID was measured using Fourier transform infrared spectroscopy (FTIR) and thermogravimetric analysis (TGA) according to the Eqs. (12.7) and (12.8), respectively.

$$\alpha = \frac{(D_{1380}/D_{1498})_p}{(D_{1380}/D_{1498})_c} \times 100\% \tag{12.7}$$

where α is the ID calculated by FTIR, D is the area of the peak, and subscripts p and c represent precursor fibers and the fully cured PI fibers, respectively. The peak at 1380 cm^{-1} (C−N−C stretching) was selected for quantifying the ID of the fibers, and the aromatic band at 1498 cm^{-1} (C−C stretching of the *p*-substituted benzene backbone) was selected as the internal standard (Marek et al., 1990; Wang et al., 2012; Zhai et al., 2008).

$$\beta = \left(1 - \frac{1 - m_p}{1 - m_t}\right) \times 100\% \tag{12.8}$$

where β is the ID measured by TGA analysis, m_p is the mass retention of the PAA precursor fibers, and m_t denotes the theoretic mass retention of PAA−DMAc complexation after full imidization. Both measurements proved that the ID was readily affected by imidization temperature rather than spinning speed. In addition, with the increased rolling speed, the fibers became much thinner, and were more sensitive to heat treatment and accelerated the imidization process. The fibers drawn for 2.8 times possessed the tensile strength of 0.84 GPa, initial modulus of 6.96 GPa, and elongation of 12.6%.

Gao et al. (2008) prepared a series of copolyimide (co-PI) fibers by incorporating BIA moieties into the PMDA/ODA backbone in a typical two-step wet-spinning method. The mechanical properties of the resulting PI fibers were improved as compared with those of pure PI fibers, and the optimum tensile strength and initial modulus reached 1.53 and 220.5 GPa at a BIA/ODA molar ratio of 7/3, respectively. The introduction of BIA led to the intense increase of rigidity of polymer chains, which

was the main reason for the drastically improved mechanical and thermal properties of the PI fibers. Meanwhile, the presence of BIA did not affect the aggregation structures of the fibers as the fibers still exhibited amorphous and broad peaks around 20 degrees.

Su et al. (2011) also proposed an approach in preparing PMDA/ODA/*p*-PDA co-PI fibers through a dry-jet wet-spinning method. Because of the increased rigidity of polymer chains induced by the incorporation of *p*-PDA, the co-PI fibers possessed a tensile strength of 0.7 GPa and initial modulus of 25.3 GPa at a *p*-PDA/ODA molar ratio of 2/8, while the value was 0.4 and 4.7 GPa for pure PMDA/ODA fibers, respectively.

12.3.2.2 BPDA-based polyimide fibers

Recently, PI fibers derived from BPDA and *p*-PDA, known as Upilex-S type, are preferred because of the stiff and linear chain structure, strong intermolecular association, and high molecular orientation, and are presented in Fig. 12.14 (Hasegawa and Horie, 2001; Hasegawa et al., 1999a; Zhuang et al., 2012; Huang et al., 2013). However, the stiffness of the polymer chains resulted in poor processability of the fibers simultaneously. Therefore, with the aim of obtaining PI fibers with better mechanical properties, incorporating other monomers into the rigid BPDA/*p*-PDA backbone was considered as the most efficient approach in modifying the chemical structures of PI fibers.

It was addressed that the fibers derived from BPDA, *p*-PDA, and 2-(4-aminophenyl)-6-amino-4(3H)-quinazolinone (AAQ) in the two-step wet-spinning method exhibited a tensile strength and initial modulus up to 2.8 and 115.2 GPa at a *p*-PDA/AAQ molar ratio of 5/5, respectively (Niu et al., 2013). The superior mechanical properties originated from the high rigidity of polymer chains and additional intermolecular associations induced by the presence of AAQ.

Zhang et al. (2015a) have prepared a series of co-PI fibers by the random copolymerization of BPDA, *p*-PDA, BIA, and ODA in the two-step wet-spinning method. The effect of the BIA and ODA moieties on the mechanical properties, molecular packing, and morphologies of the fibers was systematically investigated. The results showed that the introduction of both BIA and ODA could improve the mechanical properties of PI fibers, but the improvement induced by BIA moieties was larger than that of ODA moieties. For instance, the fibers with the *p*-PDA/BIA/ODA molar ratio of 6/1/3 possessed a tensile strength and initial modulus of 2.19 and 60.85 GPa, while the value increased to 2.72 and 94.33 GPa when the molar ratio of *p*-PDA/BIA/ODA was 6/3/1, respectively. The introduction of ODA led to the increase of mobility of the polymer chains, while the BIA has introduced additional intermolecular

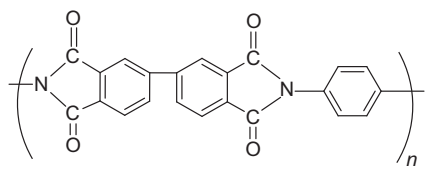

Figure 12.14 The chemical structure of BPDA/*p*-PDA-type PI fibers.

associations such as H-bonding, giving rise to the reduction in size of the microvoids and mechanical properties of PI fibers. Because of the different mechanisms involved in improving the mechanical properties of PI fibers, the fibers with more ODA moieties exhibited increased disruption of lateral molecular packing and reduced thermal-oxidative stabilities. However, the case was opposite for BIA moieties.

Chang et al. (2015a,b) have introduced ODPA and ODA containing ether groups into the BPDA/*p*-PDA polymer backbone via a two-step wet-spinning method, respectively. It was found that the introduction of flexible monomer ODPA or ODA into the rigid BPDA/*p*-PDA system led to a reduction in the size of microvoids in the fibers, which was supposed to be mainly dominated by the tremendously improved mechanical properties of fibers. The fibers containing ODPA moieties exhibited a tensile strength and initial modulus in the range of 1.07−1.58 GPa and 50.39−67.75 GPa, respectively. The morphology evolution performed by SAXS is reproduced in Fig. 12.15. The intense and elongated streaks near the beamstop along the meridian direction reflect the oriented needle-like structures of microvoids, which aligned parallel to the fiber axis. Meanwhile, the optimum mechanical properties of PI fibers containing ODA contents were obtained with a tensile strength of 2.53 GPa at a *p*-PDA/ODA molar ratio of 5/5, which was approximately 3.7 times the tensile strength of BPDA/*p*-PDA PI fibers.

Yin et al. (2015a) have investigated the effect of different molar ratios of BIA/BOA on the performances of PI fibers via a two-step wet-spinning method. The optimum tensile strength and modulus obtained was 1.74 and 74.4 GPa when the molar ratio of BPDA/BIA/BOA was 10/7/3, respectively. The fibers exhibited different crystalline behavior with different molar ratios of BIA/BOA as characterized by 2D WAXD. The PI fibers had better molecular alignment with increased proportion of BIA, and the degree of crystallinity and crystal orientation was found to be 32.4% and 0.81 at a BIA/BOA molar ratio of 7/3. Also the size of the microvoids of the PI fibers in this molar ratio was relatively small. The high crystallinity, orientation, and homogeneous structures at a BIA/BOA molar ratio of 7/3 have explained the corresponding

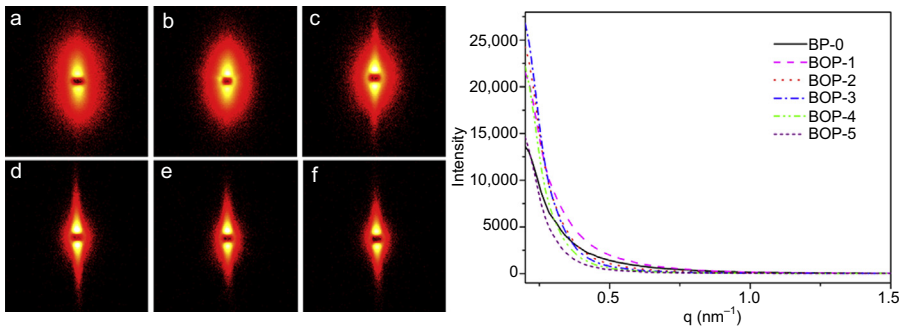

Figure 12.15 The 2D SAXS patterns (left) and corresponding 1D SAXS profiles (right) of the PI fibers.

Chang, J., Niu, H., Zhang, M., et al., 2015b. Structures and properties of polyimide fibers containing ether units. Journal of Materials Science 50, 4104−4114.

high tensile strength and initial modulus. Similarly, PI fibers prepared with BPDA, 4-amino-*N*-(4-aminophenyl) benzamide (DABA) and BIA in the two-step wet-spinning method possessed a tensile strength and initial modulus up to 1.96 and 108.3 GPa, respectively (Yin et al., 2015b).

Huang et al. (2012) have introduced the monomer 3,3′-dimethylbenzidine (OTOL), TFMB, and 2-(4-aminophenyl)-5-aminobenzoxazole (BOA) into the BPDA/*p*-PDA polymer backbone with the dry-jet wet-spinning method, respectively (Senbiaoa et al., 2012; Sen-biao et al., 2012). In a similar manner, the mobility of the polymer chains was improved with the incorporated third monomer, which favored large drawing during the thermal treatment process and reduced the influence of the voids. Therefore, the mechanical properties were subtly improved, whereas, and in contrast, further addition of the third monomer reduced the stacking density of the polymer chains, which was not conducive to the improvement in the mechanical properties of PI fibers.

Luo et al. (2014) have prepared homo-BPDA/BIA PI fibers via the two-step wet-spinning method. The crystallinity of the fibers enhanced from 1.8 to 24.5% when the annealing temperatures increased from 390 to 400°C, which was manifested as a sudden crystallization process. The increased crystallinity of the fibers led to the simultaneous improvement in mechanical properties, and the tensile strength increased from 1.31 to 1.68 GPa in the same temperature range. In this experiment, the H-bonding interactions played a crucial role in determining the macromolecular packing in the fibers. The H-bonding acted as the physical crosslinking points in the fibers, restricting the regular arrangement of the molecules, and thus led to the poor degree of order of the corresponding PAA fibers. The degree of order X of macromolecules can be confirmed by Eq. (12.9):

$$X = \frac{U_0}{I_0} \times \frac{I_X}{U_X} \times 100\% \tag{12.9}$$

where U_0 and U_X denote the backgrounds of the reference sample and experimental sample, while I_0 and I_X are integral intensities of diffraction lines of the reference sample and experimental sample, respectively (Liu et al., 2005). Moreover, curve-fitting deconvolution of the WAXD profiles could be performed to separate crystallization and amorphous contributions. The crystallinity (X_c) was calculated based on Eq. (12.10):

$$X_c = \frac{A_c}{A_c + A_a} \times 100\% \tag{12.10}$$

where A_c and A_a represent the area of all the crystal peaks and the area of the amorphous peak, respectively (Sengupta et al., 2005; Manful et al., 2008). When the temperature increased to 400°C, the H-bonding became weakened, and the physical crosslinking points were destroyed. Consequently, this feature led to the structural evolution of the macromolecular packing and sudden crystallization behavior in the fibers.

In conclusion, increasing attention has been paid to the designation of new structures of PI fibers in need of improving the mechanical properties without sacrificing the inherent unique properties in the two-step method, which promotes PI fibers to be more promising in the class of high-performance polymeric fibers.

12.4 Applications of polyimide fibers

Because of the accumulated progress, a number of advances have been made in the field of PI fibers, which offers tremendous opportunities for their use in a diverse range of applications. Generally, PI fibers exhibit excellent chemical and thermal stabilities, and hence can be used for thermal and irradiation resistance such as high-temperature filtration and fire retardant applications. In addition, the high-strength/high-modulus feature promises that PI fibers can be utilized in aerospace areas when compounded with resin materials. On the other hand, it is established that PI fibers containing fluorine groups in the polymer backbone have better light transmittance, hydrophobic properties, as well as low dielectric permittivity, which are suitable for optical communication applications and microelectronics industry. Also, PI fibers were found to be a good candidate in fabricating high-performance carbon fibers, contributing to the high molecular orientation of the macromolecular chains. Therefore, large-scale production of PI fibers is in need of further improvement to optimize the preparation process to meet the requirements for engineering applications.

12.5 Conclusion

Since PI fibers were initially presented, the one-step method was generally adopted in preparing PI fibers. The fibers prepared using this technique could achieve large drawing ratios (up to 10), and the tensile strength and modulus were up to 3.3 and 130 GPa, respectively. Because of the limitation in choosing environment-friendly solvents and organ-soluble monomers, the situation raised a critical demand for the researchers to turn their focus to a two-step method. With the two-step method, various kinds of PI fibers were produced with different functional groups by means of the extensive amounts of monomers to be selected. However, the mechanical properties were not high as compared with those in the one-step method. The decrease in mechanical properties was attributed to defects such as microvoids generated during dual-diffusion and thermal imidization processes. Recently, novel PI fibers derived from the BPDA/*p*-PDA/BIA system were prepared via a two-step wet-spinning method, with tensile strength and initial modulus up to 2.8 and 115.2 GPa, respectively. Thus, it is essential to mention that high-performance PI fibers could be obtained through the designation of polymer backbone and advanced spinning technology.

As for the two-step technique, spinning conditions such as drawing ratio and imidization temperature were also two crucial factors in determining the final performances of the resulting PI fibers. Further increasing the drawing ratio could lead to the ordered

molecular alignment in the fibers and reduced size of microvoids, which were distributed approximately parallel to the fiber axis, and finally result in the dramatically enhanced mechanical properties of the PI fibers. On the other hand, appropriate imidization temperature will accelerate the imidization process, which was conducive to improving the mechanical and thermal properties of the PI fibers. Meanwhile, excessive thermal treatment temperature could inevitably lead to the slight degradation of the polymer chains and finally give rise to the reduction in the performances of the fibers.

Above all, some useful information was provided as a general rule in designing and preparing PI fibers with high tensile strength and initial modulus. However, the properties of the fibers were still in need of further optimization. Therefore, novel PI fibers with various functions, by utilizing new kinds of monomers or approaches, should be explored to meet the requirement of industrial development. Meanwhile, with the specific features, PI fibers will be expanded in more applications in the future.

Acknowledgments

The authors greatly thank the financial support from the National Key Basic Research Program of China (973 Program, No. 2014CB643606), National Natural Science Foundation of China (NSFC, Project No. 51373008), and Higher School Specialized Research Fund for Doctoral Priority Areas of Development Project (No. 20130010130001).

References

Bahrami, S., Bajaj, P., Sen, K., 2003. Effect of coagulation conditions on properties of poly (acrylonitrile−carboxylic acid) fibers. Journal of Applied Polymer Science 89 (7), 1825−1837.

Bessonov, M., 1987. Polyimides−thermally stable polymers: Consultants Bureau.

Chang, J., Niu, H., He, M., et al., 2015a. Structure−property relationship of polyimide fibers containing ether groups. Journal of Applied Polymer Science 132 (34), 42474.

Chang, J., Niu, H., Zhang, M., et al., 2015b. Structures and properties of polyimide fibers containing ether units. Journal of Materials Science 50 (11), 4104−4114.

Chen, D., Liu, T., Zhou, X., et al., 2009. Electrospinning fabrication of high strength and toughness polyimide nanofiber membranes containing multiwalled carbon nanotubes. Journal of Physical Chemistry B 113 (29), 9741−9748.

Chen, J., Wang, C.G., Ge, H.Y., et al., 2007. Effect of coagulation temperature on the properties of poly(acrylonitrile-itaconic acid) fibers in wet spinning. Journal of Polymer Research 14 (3), 223−228.

Cheng, S.Z., Wu, Z., Mark, E., 1991. A high-performance aromatic polyimide fibre: 1. Structure, properties and mechanical-history dependence. Polymer 32 (10), 1803−1810.

Dine-Hart, R., Wright, W., 1967. Preparation and fabrication of aromatic polyimides. Journal of Applied Polymer Science 11 (5), 609−627.

Dong, J., Yin, C., Luo, W., et al., 2013. Synthesis of organ-soluble copolyimides by one-step polymerization and fabrication of high performance fibers. Journal of Materials Science 48 (21), 7594−7602.

Dong, J., Yin, C.Q., Lin, J.Y., et al., 2014. Evolution of the microstructure and morphology of polyimide fibers during heat-drawing process. RSC Advances 4 (84), 44666−44673.

Dong, X.G., Wang, C.G., Bai, Y.J., et al., 2007. Effect of DMSO/H_2O coagulation bath on the structure and property of polyacrylonitrile fibers during wet-spinning. Journal of Applied Polymer Science 105 (3), 1221−1227.

Dorogy Jr., W.E., St. Clair, A.K., 1991a. Wet Spinning of Solid Polyamic Acid Fibers. US Patent, 5023034.

Dorogy, W.E., St. Clair, A.K., 1991b. Wet spinning of solid polyamic acid fibers. Journal of Applied Polymer Science 43 (3), 501−519.

Dorogy, W.E., St. Clair, A.K., 1993. Fibers from a soluble, fluorinated polyimide. Journal of Applied Polymer Science 49 (3), 501−510.

Eashoo, M., Shen, D., Wu, Z., et al., 1993. High-performance aromatic polyimide fibres: 2. Thermal mechanical and dynamic properties. Polymer 34 (15), 3209−3215.

Eashoo, M., Wu, Z., Zhang, A., et al., 1994. High performance aromatic polyimide fibers, 3. A polyimide synthesized from 3,3′,4,4′-biphenyltetracarboxylic dianhydride and 2,2′-dimethyl-4,4′-diaminobiphenyl. Macromolecular Chemistry and Physics 195 (6), 2207−2225.

Fang, T.H., Chang, W.J., 2003. Effects of AFM-based nanomachining process on aluminum surface. Journal of Physics and Chemistry of Solids 64 (6), 913−918.

Feng, S., Xiong, X., Zhang, G., et al., 2008. Hierarchical structure in oriented fibers of a dendronized polymer. Macromolecules 42 (1), 281−287.

Gadelmawla, E.S., Koura, M.M., Maksoud, T.M.A., et al., 2002. Roughness parameters. Journal of Materials Processing Technology 123 (1), 133−145.

Gao, G., Dong, L., Liu, X., et al., 2008. Structure and properties of novel PMDA/ODA/PABZ polyimide fibers. Polymer Engineering and Science 48 (5), 912−917.

Ghosh, M., 1996. Polyimides: Fundamentals and Applications. CRC Press.

Grubb, D.T., Prasad, K., 1992. High-modulus polyethylene fiber structure as shown by X-ray diffraction. Macromolecules 25 (18), 4575−4582.

Hasegawa, M., Sensui, N., Shindo, Y., et al., 1999a. Improvement of thermoplasticity for s-BPDA/PDA by copolymerization and blend with novel asymmetric BPDA-based polyimides. Journal of Polymer Science Part B: Polymer Physics 37 (17), 2499−2511.

Hasegawa, M., Sensui, N., Shindo, Y., et al., 1999b. Structure and properties of novel asymmetric biphenyl type polyimides. Homo-and copolymers and blends. Macromolecules 32 (2), 387−396.

Hasegawa, T., Horie, K., 2001. Photophysics, photochemistry, and optical properties of polyimides. Progress in Polymer Science 26 (2), 259−335.

Hsiao, S., Chen, Y., 2002. Structure-property study of polyimides derived from PMDA and BPDA dianhydrides with structurally different diamines. European Polymer Journal 38 (4), 815−828.

Huang, S.B., Gao, Z.M., Ma, X.Y., et al., 2012. The properties, morphology and structure of BPDA/PPD/BOA polyimide fibers. e-Polymers 12 (1), 990−1002.

Huang, S.B., Jiang, Z.Y., Ma, X.Y., et al., 2013. Properties, morphology and structure of BPDA/PPD/ODA polyimide fibres. Plastics Rubber and Composites 42 (10), 407−415.

Jiang, G.S., Huang, W.F., Li, L., et al., 2012a. Structure and properties of regenerated cellulose fibers from different technology processes. Carbohydrate Polymers 87 (3), 2012−2018.

Jiang, G.S., Yuan, Y., Wang, B.C., et al., 2012b. Analysis of regenerated cellulose fibers with ionic liquids as a solvent as spinning speed is increased. Cellulose 19 (4), 1075−1083.

Kaneda, T., Katsura, T., Nakagawa, K., et al., 1986a. High-strength-high-modulus polyimide fibers I. One-step synthesis of spinnable polyimides. Journal of Applied Polymer Science 32 (1), 3133−3149.

Kaneda, T., Katsura, T., Nakagawa, K., et al., 1986b. High-strength−high-modulus polyimide fibers II. Spinning and properties of fibers. Journal of Applied Polymer Science 32 (1), 3151−3176.

Kim, Y.H., Harris, F.W., Cheng, S.Z.D., 1996. Crystal structure and mechanical properties of ODPA-DMB polyimide fibers. Thermochimica Acta 282−283 (0), 411−423.

Li, W., Wu, Z., Jiang, H., et al., 1996. High-performance aromatic polyimide fibres. Journal of Materials Science 31 (16), 4423−4431.

Liaw, D.J., Wang, K.L., Huang, Y.C., et al., 2012. Advanced polyimide materials: syntheses, physical properties and applications. Progress in Polymer Science 37 (7), 907−974.

Liu, J.P., Zhang, Q.H., Xia, Q.M., et al., 2012. Synthesis, characterization and properties of polyimides derived from a symmetrical diamine containing bis-benzimidazole rings. Polymer Degradation and Stability 97 (6), 987−994.

Liu, X., Guo, L., Gu, Y., 2005. A novel aromatic polyimide with rigid biphenyl side-groups: formation and evolution of structures in thermoreversible gel. Polymer 46 (25), 11949−11957.

Luo, L., Yao, J., Wang, X., et al., 2014. The evolution of macromolecular packing and sudden crystallization in rigid-rod polyimide via effect of multiple H-bonding on charge transfer (CT) interactions. Polymer 55 (16), 4258−4269.

Makino, H., Kusuki, Y., Harada, T., et al., 1984. Process for Producing Aromatic Polyimide Hollow Filaments. US Patent, 4460526.

Manful, J.T., Grimm, C.C., Gayin, J., et al., 2008. Effect of variable parboiling on crystallinity of rice samples. Cereal Chemistry 85 (1), 92−95.

Marek, M., Schmidt, P., Schneider, B., et al., 1990. Imidization of polypromellitamic acid based on 4, 4′-methylenedianiline. Die Makromolekulare Chemie 191 (11), 2631−2637.

Mengxian, D., 2006. Polyimides: Chemistry, Relationship between Structure and Properties and Materials. Science Press, Beijing.

Niu, H., Huang, M., Qi, S., et al., 2013. High-performance copolyimide fibers containing quinazolinone moiety: preparation, structure and properties. Polymer 54 (6), 1700−1708.

Niu, H., Qi, S., Han, E., et al., 2012. Fabrication of high-performance copolyimide fibers from 3,3′,4,4′-biphenyltetracarboxylic dianhydride, p-phenylenediamine and 2-(4-aminophenyl)-6-amino-4(3H)-quinazolinone. Materials Letters 89, 63−65.

Ohmura, K., Shibasaki, I., Kimura, T., 1983. Polyamide-imide Compositions and Articles for Electrical Use Prepared Therefrom. US Patent, 4377652.

Ohya, H., Kudryavsev, V., Semenova, S.I., 1997. Polyimide Membranes: Applications, Fabrications and Properties. CRC Press.

Park, S.K., Farris, R.J., 2001. Dry-jet wet spinning of aromatic polyamic acid fiber using chemical imidization. Polymer 42 (26), 10087−10093.

Qiao, X.Y., Chung, T.S., Pramoda, K.P., 2005. Fabrication and characterization of BTDA-TDI/MDI (P84) co-polyimide membranes for the pervaporation dehydration of isopropanol. Journal of Membrane Science 264 (1), 176−189.

Ran, S., Fang, D., Zong, X., et al., 2001. Structural changes during deformation of Kevlar fibers via on-line synchrotron SAXS/WAXD techniques. Polymer 42 (4), 1601−1612.

Ratta, V., 1999. Crystallization, Morphology, Thermal Stability and Adhesive Properties of Novel High Performance Semicrystalline Polyimides. Virginia Polytechnic Institute and State University.

Ruland, W., 1969. Small-angle scattering studies on carbonized cellulose fibers. Journal of Polymer Science Part C: Polymer Symposia 28 (1), 143−151.

Samuel, I.R., Edgar, S.C., 1968. Formation of Polypyromellitimide Filaments. US Patent, 3415782.

Sasaki, I., Itatani, H., Kashima, M., et al., 1981. Aromatic Polyimide Resin Composition. US Patent, 4290936.

Sen-biao, H., Zhong-min, G., Xiao-ye, M., et al., 2012. Properties, morphology and structure of BPDA/PPD/TFMB polyimide fibers. Chemical Research in Chinese Universities 28 (4), 752−756.

Senbiaoa, H., Xiaoyea, M., Haiquana, G., et al., 2012. Mechanical property, morphology and structure of BPDA/PPD/OTOL polyimide fibers. Chinese Journal of Applied Chemistry 29 (8), 863−867.

Sengupta, R., Tikku, V., Somani, A.K., et al., 2005. Electron beam irradiated polyamide-6,6 films—I: characterization by wide angle X-ray scattering and infrared spectroscopy. Radiation Physics and Chemistry 72 (5), 625−633.

Sroog, C., 1991. Polyimides. Progress in Polymer Science 16 (4), 561−694.

Su, J., Chen, L., Tang, T., et al., 2011. Preparation and characterization of ternary copolyimide fibers via partly imidized method. High Performance Polymers 23 (4), 273−280.

Um, I.C., Kweon, H., Lee, K.G., et al., 2004. Wet spinning of silk polymer. I. Effect of coagulation conditions on the morphological feature of filament. International Journal of Biological Macromolecules 34 (1−2), 89−105.

Wang, C.G., Dong, X.G., Wang, Q.F., 2009. Effect of coagulation on the structure and property of PAN nascent fibers during dry jet wet-spinning. Journal of Polymer Research 16 (6), 719−724.

Wang, W., Chen, X., Cai, Q., et al., 2008. In situ SAXS study on size changes of platinum nanoparticles with temperature. European Physical Journal B 65 (1), 57−64.

Wang, Y., Yang, Y., Jia, Z.X., et al., 2012. Effect of pre-imidization on the aggregation structure and properties of polyimide films. Polymer 53 (19), 4157−4163.

Wu, D., Han, E., Li, L., et al., 2014. Methods of Preparing Polyimide Fibers with Kidney-shaped Cross-sections. US Patent, 8911649.

Wu, J., Schultz, J.M., Yeh, F., et al., 2000. In-situ simultaneous synchrotron small-and wide-angle X-ray scattering measurement of poly (vinylidene fluoride) fibers under deformation. Macromolecules 33 (5), 1765−1777.

Wu, T., Chvalun, S., Blackwell, J., et al., 1995. Effect of draw ratio on the structure of aromatic copolyimide fibers of random monomer sequence. Acta Polymerica 46 (3), 261−266.

Xiang, H.B., Huang, Z., Liu, L.Q., et al., 2011. Structure and properties of polyimide (BTDA-TDI/MDI co-polyimide) fibers obtained by wet-spinning. Macromolecular Research 19 (7), 645−653.

Xu, Y., Wang, S.H., Li, Z.T., et al., 2013. Polyimide fibers prepared by dry-spinning process: imidization degree and mechanical properties. Journal of Materials Science 48 (22), 7863−7868.

Yin, C., Dong, J., Zhang, D., et al., 2015a. Enhanced mechanical and hydrophobic properties of polyimide fibers containing benzimidazole and benzoxazole units. European Polymer Journal 67, 88−98.

Yin, C., Dong, J., Zhang, Z., et al., 2015b. Structure and properties of polyimide fibers containing benzimidazole and Amide Units. Journal of Polymer Science, Part B: Polymer Physics 53 (3), 183−191.

Zhai, Y., Yang, Q., Zhu, R.Q., et al., 2008. The study on imidization degree of polyamic acid in solution and ordering degree of its polyimide film. Journal of Materials Science 43 (1), 338−344.

Zhang, M., Niu, H., Chang, J., et al., 2015a. High-performance fibers based on copolyimides containing benzimidazole and ether moieties: molecular packing, morphology, hydrogen-bonding interactions and properties. Polymer Engineering & Science 55 (11), 2615−2625.

Zhang, M., Niu, H., Lin, Z., et al., 2015b. Preparation of high performance copolyimide fibers via increasing draw ratios. Macromolecular Materials and Engineering 300 (11), 1096−1107.

Zhang, Q.H., Dai, M., Ding, M.X., et al., 2004a. Mechanical properties of BPDA−ODA polyimide fibers. European Polymer Journal 40 (11), 2487−2493.

Zhang, Q.H., Dai, M., Ding, M.X., et al., 2004b. Morphology of polyimide fibers derived from 3,3′,4,4′-biphenyltetracarboxylic dianhydride and 4,4′-oxydianiline. Journal of Applied Polymer Science 93 (2), 669−675.

Zhang, Q.H., Luo, W.Q., Gao, L.X., et al., 2004c. Thermal mechanical and dynamic mechanical property of biphenyl polyimide fibers. Journal of Applied Polymer Science 92 (3), 1653−1657.

Zhuang, Y., Liu, X., Gu, Y., 2012. Molecular packing and properties of poly(benzoxazole-benzimidazole-imide) copolymers. Polymer Chemistry 3 (6), 1517−1525.

Silk from silkworms and spiders as high-performance fibers

13

K. Murugesh Babu
Bapuji Institute of Engineering and Technology, Davangere, Karnataka, India

13.1 Introduction to silks from silkworms

Silk is one of the oldest fibers known to man. Silk is an animal fiber produced by certain insects to build their cocoons and webs. Although many insects produce silk, only the filament produced by the mulberry silk moth, *Bombyx mori*, and a few others in the same genus is used by the commercial silk industry (Jolly et al., 1979). The silk produced by other insects, mainly spiders, is used in a small number of other commercial capacities, for example, weapon and telescope crosshairs and other optical instruments (Spring and Hudson, 2002).

Silk fibers from silkworms have been used in textiles for nearly 5000 years. The primary reasons for this long-time use have been the unique luster, tactile properties, durability, and dyeability of silks. Silk fibers are remarkable materials displaying unusual mechanical properties: strong, extensible, and mechanically compressible (Matsumoto et al., 2006). Silk is rightly called the queen of textiles for its luster, sensuousness, and glamor (Manohar Reddy, 2009). Silk's natural beauty and properties of comfort in warm weather and warmth during colder months have made it useful in high-fashion clothing. Silk fibers have outstanding natural properties that rival the most advanced synthetic polymers, yet the production of silk does not require harsh processing conditions and hence widespread investigations are ongoing, even for the artificial synthesis of silk fibers (Chen et al., 2003).

13.2 Introduction to sericulture

Sericulture is the rearing of silkworms for the production of raw silk. The major activities of sericulture comprise food-plant cultivation to feed the silkworms, which spin silk cocoons, and reeling the cocoons for unwinding the silk filament for value-added benefits such as processing and weaving. Although there are several commercial species of silkworms, *B. mori* is the most widely used. Sericulture is ideally suited for improving the rural economy of a country, as it is practiced as a subsidiary industry to agriculture. Recent research has also shown that sericulture can be developed as a highly rewarding agroindustry.

Structure and Properties of High-Performance Fibers. http://dx.doi.org/10.1016/B978-0-08-100550-7.00013-9

13.3 Types of silk and their importance

13.3.1 Types of silk

There are five major types of silk of commercial importance, obtained from different species of silkworms, which in turn feed on a number of food plants (except mulberry); other varieties of silks are generally termed nonmulberry silks. India has the unique distinction of producing all these commercial varieties of silk.

13.3.1.1 Mulberry

The bulk of the commercial silk produced in the world comes from this variety and often silk is generally referred to as mulberry silk. Mulberry silk (Fig. 13.1) comes from the silkworm *B. mori* L., which feeds solely on the leaves of mulberry plants. These silkworms are completely domesticated and reared indoors. In India, the major mulberry silk-producing states are Karnataka, Andhra Pradesh, West Bengal, Tamil Nadu, and Jammu and Kashmir, which together account for 92% of the country's total mulberry raw silk production.

13.3.1.2 Types of mulberry silk

Bombyx mori, the domesticated silkworm, has been reared for over 2000 years. During this long history, many mutations have occurred. The mutants have been further classified with each other resulting in a combination of various genes producing a large number of silkworm races. The silkworm races are classified on the basis of:

1. Place of origin
2. Voltinism
3. Molting

13.3.2 Place of origin

13.3.2.1 Indian races

These races are aboriginal in India and South East Asia. The larval stage is longer and they are robust against high temperature and humidity. The size of the cocoon and

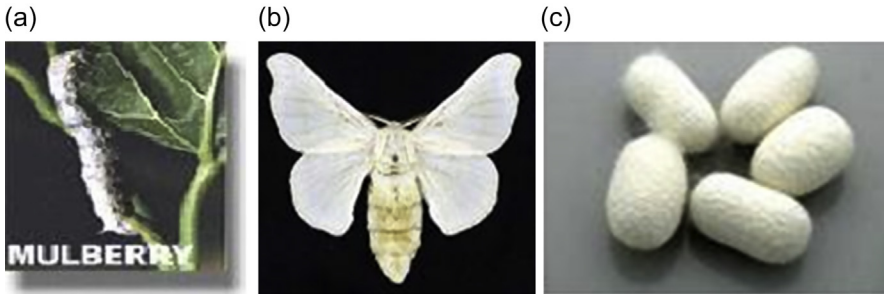

Figure 13.1 Mulberry silk: (a) worm, (b) moth, (c) cocoons.

larvae is small. In many cases the cocoon is spindle shaped and its color is green, yellow, or white. The cocoon shell is thin with less shell percentage. They are mainly multivoltines.

13.3.2.2 Japanese races

These races are aboriginal in Japan. The larvae are robust. The cocoon is peanut shaped. The sizes of the larvae do not correspond with the long larval duration. The cocoon color is usually white but few are also green or yellow. The ratio of double cocoons is more. The quality of the silk filament is inferior and it is thick and short. They are univoltine or bivoltine.

13.3.2.3 Chinese races

These races are aboriginal in China. The larvae are robust against high temperature but weak against high humidity. The larvae are plain and active. They voraciously eat mulberry leaves and grow quickly. The cocoon shape is, in many cases, elliptical, spherical, and spindle shaped in a few cases. The cocoon color is white, golden yellow, green, red, or beige. The cocoon filament is fine and reelability is good. They are univoltine, bivoltine, and multivoltine.

13.3.2.4 European races

These races are aboriginal in Europe and Central Asia. Larval duration is long and they actively eat mulberry leaves. Larvae are weak against high temperature and high humidity. The cocoon size is big with a little constriction. The cocoon reelability is good.

Tasar

Tasar (Tussah) is copperish color, coarse silk mainly used for furnishings and interiors. It is less lustrous than mulberry silk, but has its own feel and appeal. Tasar silk (Fig. 13.2) is generated by the silkworm *Antheraea mylitta*, which mainly thrives on the food plants Asan and Arjun. The rearings are conducted in nature on the trees in the open. In India, tasar silk is mainly produced in the states of Jharkhand, Chattisgarh,

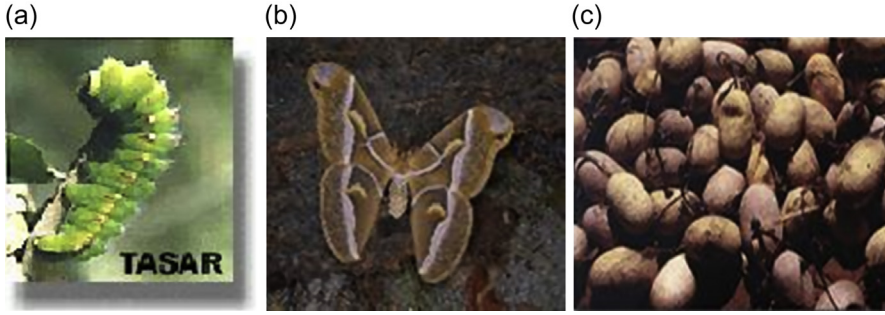

Figure 13.2 Tasar silk: (a) worm, (b) moth, (c) cocoons.

Figure 13.3 Oak tasar silk: (a) worm, (b) moth, (c) cocoons.

and Orissa, as well as Maharashtra, West Bengal, and Andhra Pradesh. Tasar culture is the mainstay for many a tribal community in India.

Oak tasar

This is a finer variety of tasar generated by the silkworm *Antheraea proyeli* J. (Fig. 13.3) in India, which feeds on natural food plants of oak, found in abundance in the sub-Himalayan belt of India covering the states of Manipur, Himachal Pradesh, Uttar Pradesh, Assam, Meghalaya, and Jammu and Kashmir. China is the major producer of oak tasar in the world and this comes from another silkworm known as *Antheraea pernyi*.

Eri

Also known as endi or errandi, eri is a multivoltine silk spun from open-ended cocoons, unlike other varieties of silk. Eri silk (Fig. 13.4) is the product of the domesticated silkworm *Philosamia ricini* that feeds mainly on castor leaves. Eri culture is a household activity practiced mainly for protein-rich pupae, a tribal delicacy. As a result, the eri cocoons are open mouthed and are spun. The silk is used indigenously for preparation of chaddars (wraps) used by tribes. In India, this culture is practiced mainly in the northeastern states and Assam. It is also found in Bihar, West Bengal, and Orissa.

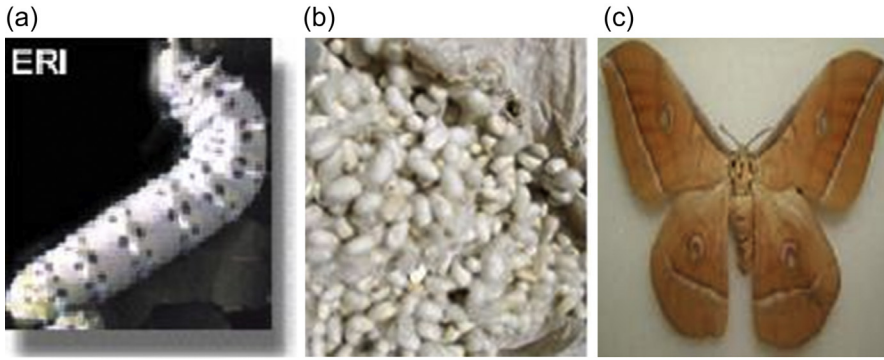

Figure 13.4 Eri silk: (a) worm, (b) Caterpillar, (c) cocoons.

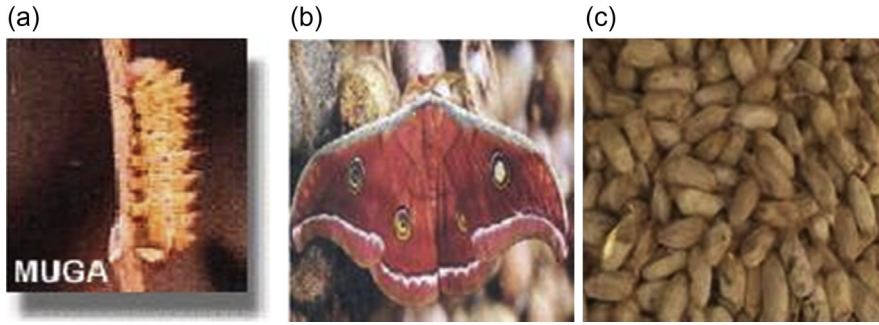

Figure 13.5 Muga silk: (a) worm, (b) caterpillar, (c) cocoons.

Muga

This golden yellow-colored silk is an integral part of India and the pride of Assam state. It is obtained from the semidomesticated multivoltine silkworm *Antheraea assamensis*. These silkworms (Fig. 13.5) feed on the aromatic leaves of Som and Soalu plants and are reared on trees similar to that of tasar. Muga culture is specific to the state of Assam and is an important part of the tradition and culture of that state. The muga silk, a high value product, is used in products like sarees, mekhalas, chaddars, etc.

13.3.2.5 Anaphe silk

This silk of southern and central Africa is produced by silkworms of the genus *Anaphe*: *Anaphe moloneyi* Druce, *Anaphe panda* Boisduval, *Anaphe reticulate* Walker, *Anaphe carteri* Walsingham, *Anaphe venta* Butler, and *Anaphe infracta* Walsingham. They spin cocoons in communes, all enclosed by a thin layer of silk. The tribal people collect them from the forest and spin the fluff into a raw silk that is soft and fairly lustrous. The silk obtained from *A. infracta* is known locally as "book," and that from *A. moloneyi* as "tissnian-tsamia" and "koko." The fabric is elastic and stronger than that of mulberry silk. Anaphe silk is used in velvet and plush.

13.3.2.6 Fagara silk

Fagara is obtained from the giant silkmoth *Attacus atlas* L. and a few other related species or races inhabiting the Indo-Australian biographic region, China, and the Sudan. They spin light-brown cocoons nearly 6 cm long with penduncles of varying lengths (2−10 cm).

13.3.2.7 Coan silk

The larvae of *Pachypasa otus* D., from the Mediterranean biographic region (southern Italy, Greece, Romania, Turkey, etc.), feed primarily on trees such as pine, ash, cypress, juniper, and oak. They spin white cocoons measuring about 8.9 × 7.6 cm. In ancient times this silk was used to make the crimson-dyed apparel worn by the

dignitaries of Rome; however, commercial production came to an end long ago because of the limited output and the emergence of superior varieties of silk.

13.3.2.8 Mussel silk

Where the nonmulberry silks previously described are of insect origin, mussel silk is obtained from a bivalve, *Pinna squamosa*, found in the shallow waters along the Italian and Dalmatian shores of the Adriatic. The strong brown filament or byssus is combed and then spun into a silk popularly known as "fish wool." Its production is largely confined to Taranto, Italy.

13.4 High-performance requirements for silk

13.4.1 Requirements for composites

The silk fiber produced by spiders, silkworms, scorpions, mites, and flies may have different composition, structure, and material properties depending upon the specific source. These flaws can be avoided by spinning under controlled conditions to produce a uniform cross-sectional area of silk fiber. Many of the properties of native silks (as opposed to regenerated silks) also make them potential sustainable alternative reinforcement materials, alongside plant fibers, for engineering (ie, nonbiomedical) composites. Two key issues that require specific attention in the development of silk fiber-reinforced plastics with useful properties are: (1) selection of a complementary matrix, and (2) understanding the role of the interface.

To produce silk fiber composites, the essential requirements are: (1) using a high-failure strain and low-processing temperature hermoset matrix, (2) maximizing the reinforcing effect of low-stiffness ductile silk, (3) facilitating impregnation and avoiding fiber degradation, and (4) employing high fiber volume fractions to ensure that the fibers carry a larger fraction of the load. The fundamental philosophy in fiber-reinforced polymers is the development of a brittle fiber−ductile matrix system (Harris, 1999) where the fibers, compared to the matrix, have a much lower failure strain coupled with a much higher stiffness. Commonly used polymer matrices (including thermosets like epoxy, and thermoplastics like polypropylene) have a relatively low stiffness (<4 GPa) and high failure strain ($>5\%$, even up to 1000%). The strong and stiff fibers are required to carry most of the load, while the ductile matrix provides crack blunting and bridging mechanisms (Harris, 1999). Silk fibers are different from traditional reinforcing fibers (including E-glass and flax) in that mulberry silk fibers have a relatively low stiffness (5−15 GPa) and high failure strain (15−25%), while traditional reinforcing fibers have a high stiffness (>50 GPa) and low failure strain (1−5%).

13.4.2 Requirements for medical products

Silk fiber has a long history of use in medicine because of its nonsepticity and degradability. Further, silkworms efficiently convert the plant nutrients consumed by

its larvae into silk protein, a major advantage of producing such high-value protein at a cheaper cost in a shorter span of time. Hence silk can be used as a biomaterial in various forms, such as films, membranes, gels, sponges, powders, artificial ligaments, and scaffolds. Silk applications also include burn-wound dressings for faster healing, enzyme immobilization matrices, nets, vascular prostheses, and structural implants (Cao and Wang, 2009). Silk fibroin, a natural protein of the domestic silkworm *B. mori* provides an important set of options for biomaterials and scaffolds because of its high tensile strength, controllable biodegradability, hemostatic properties, noncytotoxicity, low antigenicity, and noninflammatory characteristics (Li et al., 2003; Jin et al., 2004; Mauney et al., 2007). Importantly, the biocompatible and bioresorbable properties of silks, their amenability to aqueous or organic solvent processing into various "regenerated" forms (including aqueous solutions, films, hydrogels, porous sponges, regenerated fibers and cords, and nonwoven mats), alongside their unique combination of high strength and toughness, make them ideal for a wide range of clinical applications: from braided suture threads for surgical options, to porous, reinforced-composite scaffolds for cartilage and bone repair (Vepari and Kaplan, 2007; Hardy and Scheibel, 2010; Altman et al., 2003; Hakimi et al, 2007). Naturally, considerable research has focused on biocomposites based on regenerated silks for such biomedical applications (Vepari and Kaplan, 2007; Hardy and Scheibel, 2010; Altman et al., 2003; Hakimi et al, 2007).

The prime requirement of biomaterials is biocompatibility; like silk fibers, biomaterials can perform phenomenal mechanical properties as biopolymers suitable for medical uses. The properties of high oxygen and vapor permeability make silk fiber ideal for soft tissue applications and in spite of its higher adhering ability to tissue cells, it is still biodegradable. Silk fiber shows no toxicity to living bodies during degradation because it is composed of amino acids similar to those found in humans (Sehnal, 2008), for instance, silk sutures have lesser incidence of swelling and infection than any other material. Additional applications of silk biomaterials include new generation soft contact lenses, artificial corneas, skin grafts, and epilepsy drug permeable devices (Dalpra et al, 2005).

13.5 Synthesis of silk fibers from silkworms

13.5.1 Introduction to synthesis of silk from silkworms

Sericulture is the cultivation of cocoons for their filaments. The best raw silk is obtained from the species of moth called *B. mori*. Breeding of silkworms occurs once a year but under controlled conditions they may be hatched three times a year. The female moth lays around 350−400 eggs and the moths die soon after. As they are subject to hereditary infection, the eggs from infected moths are destroyed, which results in production of fine silk. Larvae of about 3 mm are hatched from the eggs. For about 20−30 days, they are carefully nurtured and are fed five times a day on chopped mulberry leaves. In the meantime, the larvae change their skin four times and are formed

into caterpillars about 9 cm long. Now they are ready to spin cocoons for which racks, clusters of twigs, or straw are provided.

The caterpillars have small openings under their jaws called spinnerets through which they secrete a protein-like substance. This substance solidifies when it comes in contact with air and the filament thus formed is spun around the silkworm in a figure of 8. In 3 days the cocoon is complete, and is about the size of a peanut shell. The filament is held together by sericin or silk gum. The life of the worm comes to an end by the process of "stoving" or "stifling" in which the cocoons are heated. Some of the cocoons are preserved so that the pupa or chrysalis inside them develops into moths for further breeding.

13.6 Silk reeling and silk fiber manufacture

Silk reeling is the process of unwinding the silk filaments from the cocoons and a process by which a number of cocoon baves are reeled together to produce a single thread. This is achieved by unwinding filaments collectively from a group of cooked cocoons at one end in a warm water bath and winding the resultant thread onto a fast-moving reel. Raw silk reeling may be classified by the direct reeling method on a standard-sized reel, indirect reeling method on small reels, and the transfer of reeled silk from small reels onto standard-sized reels on a rereeling machine. The last technique is primarily applied in modern silk-reeling processes (Mahadevappa et al., 2001).

The reeled silk is formed into silk yarn or silk thread through a process called "throwing." The spinning process of other natural fibers corresponds to it. The raw silk skeins are sorted according to their color, size, and quantity and washed in warm water with soap or oil to soften the sericin. After drying the skeins, they are placed on reels from where the silk is wound on bobbins. During winding, the silk strands are given the desired amount of twist. The strands may be doubled and then given a twist in similar or opposite directions. To obtain equal diameter throughout the length, the yarn is run through rollers. Many kinds of silk yarns are manufactured by giving different amounts of twists. The remaining sericin is removed from silk yarn by the process of "degumming" in which the yarn is washed with soap and water to bring out its natural shine and soft feel.

13.7 Silk reeling (cocoon sorting, cocoon stifling, cocoon riddling, cocoon cooking, etc.)

13.7.1 Stages in silk filament production

13.7.1.1 Cocoon sorting

Cocoon sorting is a process of sorting out defective cocoons from a number of good cocoons. The process also includes segregating cocoons according to their size. The defective cocoons can be classified as: (1) double cocoons, (2) pierced cocoons,

(3) urinated cocoons, (4) flimsy cocoons, (5) pointed or constricted cocoons, (6) mold attacked cocoons, or (7) immature cocoons.

The process of sorting according to size is carried out with special equipment known as a riddling machine. The segregation of uniform-sized cocoons is extremely important since size has an influence on cooking and reeling properties.

13.7.1.2 Cocoon stifling

The main purpose of stifling is to kill the pupa inside the cocoon so as to avoid its emergence as a moth and thereby preserve the continuity of the filament. In addition, this operation enables the cocoons to be dried so that the cocoon can be stored for a long period of time. Cocoon stifling is generally done by the following methods: sun drying, steam stifling, and hot air drying. Other methods of killing the pupa include the use of infrared rays, cold air killing, use of poisonous gases, etc.

13.7.1.3 Cocoon cooking

The object of cocoon cooking is to soften the sericin so that the cocoon shell is loosened enabling the filament to unwind smoothly during reeling. Different methods of cooking are adapted such as open-pan cooking, three-pan cooking, pressurized cooking, conveyor cooking, etc.

13.8 Types of silk-reeling machines

13.8.1 Country charka

This is a traditional type of reeling machine with a crude way of unwinding the filaments from the cocoons. The silk produced from this machine is mainly utilized in the handloom sectors wherein the cost factor of the raw material has to be kept low to make the finished product saleable. In addition, the establishment of a charka unit does not need big investment or special skill. This enables charka silk to be sold at a minimum price, which is very much wanted by the handloom industry. Also inferior quality multivoltine and defective cocoons available at lower prices can be reeled more economically on charka than on cottage basin or multiend basins.

Charka silk is generally coarse and suffers from many defects since no improved devices such as a button/slub catcher or a standard croissure system in reeling are used. Charka silk is not rereeled. Production of silk per charka per day is about a kilogram with coarse denier.

13.8.2 Cottage basin

This reeling device is an improved version over charka and it is designed on the principle of a Japanese multiend reeling machine. Here cocoon cooking is done separately in a boiling water basin and reeling is done in a hot water basin. Each basin has six

ends and each thread is first passed through a button to clean the slubs, waste, etc. Later on it is independently passed through a travellette-type croissure, which is more efficient than that in charka. After the croissure, the thread passes through a traverse guide and finally onto a small reel.

Since rereeling is done to prepare standard-sized hanks from small reels, the quality of silk produced on this machine is superior to charka silk. Production of silk per day per basin is about 800 g. Superior quality cocoons like bivoltine can be reeled on this device.

13.8.3 Multiend reeling machine

This reeling device is a further improved version of the cottage basin and it is power driven. In multiend basins, there are some additional attachments such as a jetteboute, which picks up the filaments to increase the efficiency of feeding. The distribution system is further improved and individual brake motion for each reel is also provided so that the overall working efficiency of the basin is enhanced. Normally, each basin consists of 10 ends.

In principle, the multiend reeling machine is supposed to be a modern reeling device and it is possible to use superior quality cocoons like bivoltines on these machines with better performance. Raw silk production per day per basin varies from 600 to 800 g in these machines and the quality of silk is superior compared to that of cottage basin/domestic basin.

13.8.4 Automatic reeling machine

The automatic reeling technique has as its components a pressurized cocoon boiling machine, automatic cocoon feeder, and a mechanical brushing unit. In addition, it is equipped with an automatic denier control device, wherein human error in maintaining the uniformity of denier is avoided to a large extent, thereby ensuring minimum size deviation. Automatic reeling is the improved version of the multiend reeling method, designed and extensively used in Japan for reeling univoltine and bivoltine cocoons. It is a Japanese version of the sunken system, which is suitable for better quality cocoons in producing quality raw silk.

13.9 Structure and properties of silk from silkworms for high-performance requirements

13.9.1 Introduction

Silks belong to a group of high molecular weight organic polymers characterized by repetitive hydrophobic and hydrophilic peptide sequences (Altman et al., 2003). Silks are fibrous protein polymers that are spun into fibers by some arthropods such as silkworms, spiders, scorpions, mites, and fleas (Altman et al., 2003, Craig, 1997). There are thousands of silk-spinning insects and spiders, yet only a few have been

investigated in detail. Silks differ in composition, structure, and properties depending on their specific source and function (Altman et al., 2003; Craig et al., 1999, Sheu et al., 2004). They are naturally produced by spiders or insects, such as *Nephila clavipes* and *B. mori*, respectively (Becker et al., 2003, Bell et al., 2002). Silkworm fibers are classified as domestic silk and wild silk. Wild silks are produced by caterpillars other than the mulberry silkworm and they differ from the domesticated varieties in color, size, and texture. The cocoons gathered in the wild usually have been damaged by the emerging moth before the cocoons are gathered, so the silk thread that makes up the cocoon has been torn into shorter lengths. Domestic silkworms like *B. mori* are commercially reared and the pupae are killed by dipping them in boiling water before the adult moths emerge allowing the whole cocoon to be unraveled as one continuous thread. There are other commercially exploited silkworms other than *B. mori*, which can be used to rear the silk, which are known as nonmulberry silkworms like *A. mylitta* (tasar), *P. ricini* (eri), and *A. assama* (muga). Silks are also produced by spiders and insects that secrete glycine-rich silks characterized by their unique synthesis and processing features, as well as strength and extensibility.

13.9.2 Composition of silk

Silk in contrast to all the other natural fibers does not have a cellular structure. In this respect and in the way it is formed, it closely resembles synthetic fiber. The double thread or bave separated from the mulberry silkworm cocoon consists of two filaments or brins of fibroin enveloped and bound together by silk glue, sericin. Morphologically, silk is a very simple fiber. It consists of two single, compact, endless threads that are extruded by the silkworm as it spins its cocoon, which are surrounded and covered by the silk gum or sericin as shown in Fig. 13.6. The denier of the filament varies within the cocoon.

Apart from fibroin and sericin (which are proteins) raw silk contains small quantities of either or alcohol soluble organic matter. Silk, which is naturally colored yellow, green, etc., contains a small amount of coloring matter. Some ash remains after burning silk. The content of all these substances is not constant and varies within wide limits depending on the species of the silkworm and on the place and conditions of rearing.

The silk filament contains 72−81% fibroin, 19−28% sericin, 0.8−1.0% fat and wax, and 1.0−1.4% coloring matter and ash of the total weight. The silkworm extrudes the liquid fiber from the two excretory canals of sericteries, which unite in the spinneret in its head, each of them termed a brin. The two brins cemented together in the spinneret by sericin become a single continuous fiber called the bave or filament. The seric bave is thus made by the union of two brins held together by sericin (Paolo Carboni, 1952). Fibroin is a valuable protein along with sericin; sericin acts as a glue to fix fibroin fiber together in a cocoon. Sericin and fibroin protein is useful because of its properties and has been found to possess various biological functions.

13.9.3 Microstructure and appearance

Silk fibers (*B. mori*) spun out from silkworm cocoons consist of fibroin in the inner layer and sericin in the outer layer. Each raw silk thread has a lengthwise striation,

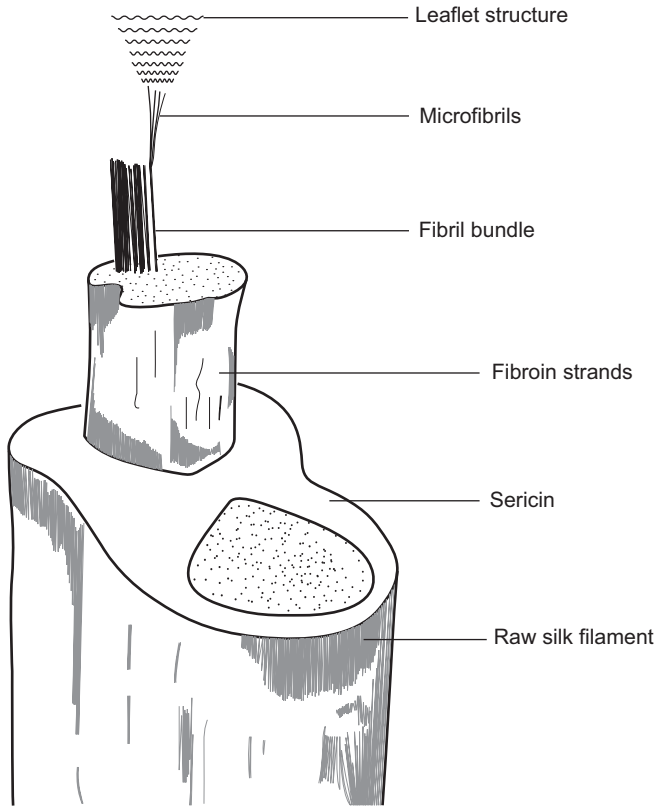

Figure 13.6 Structure of silk.

consisting of two fibroin filaments of 10−14 m each embedded in sericin. The chemical compositions are, in general, silk fibroin 75−83%, sericin 17−25%, waxes about 1.5%, and others about 1.0% by weight. Silk fibers are biodegradable and highly crystalline with well-aligned structure. It has been known that they also have higher tensile strength than glass fiber or synthetic organic fiber, good elasticity, and excellent resilience. Silk fiber is normally stable up to 140°C and the thermal decomposition temperature is greater than 1500°C. The densities of silk fibers are in the range of 1320−1400 kg/m^3 with sericin and 1300−1380 kg/m^3 without sericin. Silk fibers are also commercially available in a continuous fiber type.

13.9.4 Longitudinal view

Scanning electron micrographs of longitudinal views of undegummed and degummed silk fibers are presented in Fig. 13.7(a) and (b), respectively.

It may be observed that mulberry shows a more or less smooth surface (Fig.13.7(b)) whereas the nonmulberry silks such as tasar, muga, and eri (Fig. 13.7(c−e)) all have striations on their surface compared to mulberry.

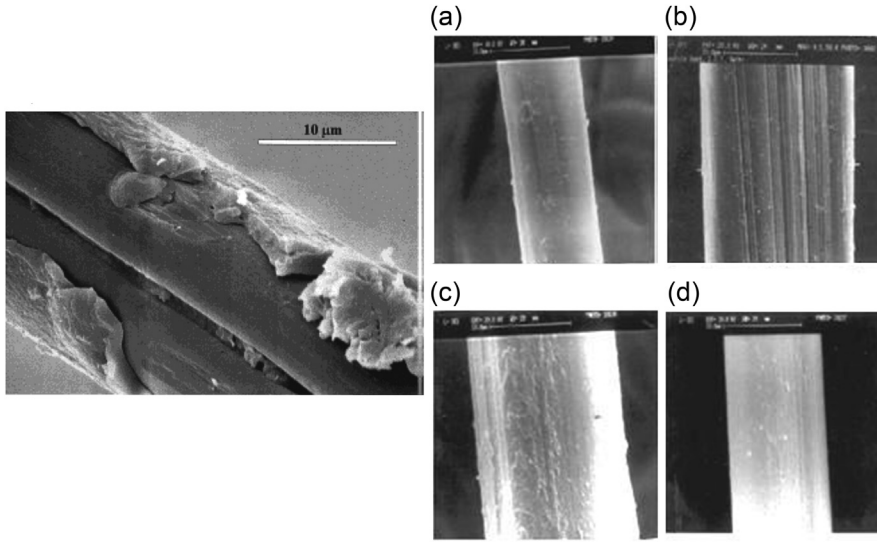

Figure 13.7 (a) The longitudinal view of silk fibers (undegummed). (b–e) The longitudinal view of silk fibers (degummed). (b) Mulberry, (c) tasar, (d) muga, (e) eri.

13.10 Cross-sectional view

Scanning electron micrographs of the cross section of silk fibers are presented in Fig. 13.8. The cross-section of silk fiber, which is made of two types of protein, namely, sericin and fibroin, is shown in the figure. It is found that two strands of fibroin filaments are enveloped by nonfibrous sericin. When a strand of fibroin filament is enlarged for its inner structure, it appears like a bundle of fibrils in which a large number of fibrils are accumulated (Minagawa, 2000).

There are variations depending upon the variety of silkworms and also among the individual cocoons. It may be observed that, in this respect, the mulberry and nonmulberry silks exhibit an altogether different cross-sectional morphology. The mulberry silks show a more or less triangular cross-section and a smooth surface (Fig. 13.8(a)). Among the nonmulberry varieties, tasar and muga exhibit an elongated rectangular or a wedge-shaped cross-section and a large cross-sectional area (Fig. 13.8(b) and (c)). The eri silk has a more or less triangular shape (Fig. 13.8(d)).

Usually in the case of the cocoon fibers of domestic silkworms like mulberry and eri, the cross-section is irregular ranging from triangular shape to circular shape. Moreover, even in the same fibroin filament, there are variations in the cross-section area depending upon the level of the cocoon layer.

13.10.1 Density of silk

Sen and Murugesh Babu (2004) have reported density values of different varieties of silks (Table 13.1). Both mulberry varieties show higher density values compared to

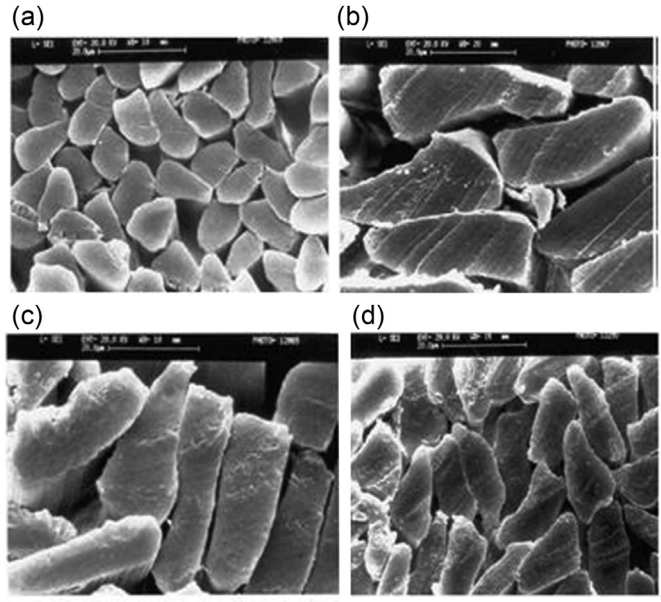

Figure 13.8 The cross-sectional view of silk fibers (degummed). (a) Mulberry, (b) tasar, (c) muga, (d) eri.

those of nonmulberry silks. The higher density values of mulberry silks also indicate a higher degree of order and compact molecular packing compared to those of nonmulberry silks. The mulberry (bivoltine) variety shows higher density than that of the mulberry (crossbreed) variety. It is interesting to note an increasing trend in density values from the outer to the inner layers for all the varieties, which definitely suggests a possible increase in the degree of crystallinity and crystallite orientation as one moves from the outer to the innermost layers. Among the three nonmulberry silks, muga exhibits the highest density, followed by tasar and eri.

Table 13.1 Density ρ values for different varieties of silk

	ρ (g/cm^3)		
Type of silk	**Outer layer**	**Middle layer**	**Inner layer**
Mulberry (bivoltine)	1.350	1.361	1.365
Mulberry (crossbreed)	1.342	1.35	1.356
Tasar	1.300	1.33	1.340
Muga	1.332	1.34	1.348
Eri	1.28	1.29	1.295

Table 13.2 Moisture regain (%) of silk fibers

Type of silk	Moisture regain (%)		
	Outer layer	Inner layer	% Change
Mulberry (bivoltine)	8.52	8.14	4.46
Mulberry (crossbreed)	8.63	8.28	4.05
Tasar	10.76	10.27	4.55
Muga	9.82	9.47	3.56
Eri	10.21	9.79	4.11

13.10.2 Moisture regain

Moisture regain of different varieties of silk has also been reported (Sen and Murugesh Babu, 2004). The results of the moisture regain of different varieties of silk fibers determined under standard conditions are presented in Table 13.2. All three nonmulberry silk fibers show higher moisture regain values compared to those of the mulberry varieties. Among these, tasar shows the highest value (10.76%), followed by eri (10.21%) and muga (9.82%) for the outer layers. On the other hand, mulberry bivoltine and crossbreed varieties show lower values of 8.52% and 8.63%, respectively. The higher moisture regain of nonmulberry silks suggests that all three nonmulberry silk varieties may consist of a higher ratio of hydrophilic to hydrophobic amino acid residues in their chemical architecture compared to that of the mulberry varieties. Interestingly, moisture regain of the inner layers is about 4.0−4.5% less compared to that of the outer layers, suggesting compactness of the inner layers.

13.11 Amino acid composition

The amino acid composition varies in different varieties of silk. Three major amino acids such as serine, glycine, and alanine may be found in mulberry and nonmulberry varieties. Among the other major amino acids present are tyrosine and valine. In general in mulberry silks, glycine, alanine, and serine together constitute about 82%, of which about 10% is serine. Tyrosine and valine may be considered next to these at about 5.5% and 2.5%, respectively. The overall composition of acidic amino groups (ie, aspartic and glutamic acids) in the mulberry variety is greater than that of the basic amino acids. The other important aspect is the composition of amino acids with bulkier side groups. The presence of bulky side groups can hamper close packing of molecules and hinder the crystallization process. In general, a large portion of the mulberry fibroin is made up of simple amino acids such as glycine and alanine, suggesting a favorable condition for crystallization (Sen and Murugesh Babu, 2004) (Fig. 13.9).

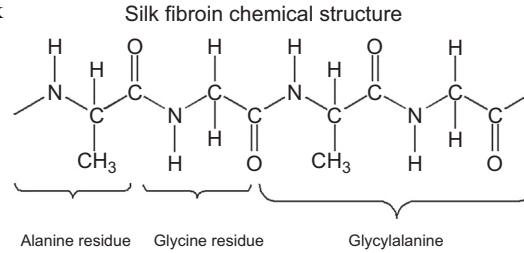

Figure 13.9 Chemical structure of silk fibroin.

Compared to the mulberry silks, the total amount of glycine, alanine, and serine constitute about 73% in the nonmulberry variety, less by about 10%. All the nonmulberry silks exhibit a high proportion of alanine compared to that in the mulberry variety. The proportion of alanine is about 34% in tasar, 36% in eri, and 35% in muga. This value is consistent but is lower than that particularly for muga (~44%). On the other hand, the glycine content in these varieties is about 27–29%, which is lower than that found in the mulberry varieties (~43%).

In addition, the nonmulberry varieties have a substantial proportion of amino acids with bulky side groups, especially aspartic acid (4–6%) and arginine (4–5%), which means that not only the acidic but also basic amino acid levels are greater. It is interesting to note the presence of sulfur-containing amino acids (ie, cysteine and methionine) in all the varieties of silk. Methionine content in nonmulberry silks is slightly higher (0.28–0.34%) compared to that found in mulberry varieties (0.11–0.19%), whereas the cysteine content is comparable (Sen and Murugesh Babu, 2004). Amino acid composition of different varieties of silk is presented in Table 13.3.

13.11.1 X-ray diffraction studies

Silk fibroin, the fibrous protein of the silk cocoon, has been studied extensively by a number of investigators from various points of view. Many researchers have reported extensive studies on X-ray diffraction of different varieties of silk.

13.11.2 Crystalline structure

The silkworm cocoon and spider dragline silks are characterized as an anti-parallel β-pleated sheet wherein the polymer chain axis is parallel to the fiber axis. Other silks are known to form α-helical (bees, wasps, ants) or cross-β-sheet (many insects) structures. The cross-β-sheets are characterized by a polymer chain axis perpendicular to the fiber axis and a higher serine content. Most silks assume a range of different secondary structures during processing from soluble protein in the glands to insoluble spun fibers (Kaplan, 2004). The crystalline structure of silk was first described in the 1950s as an anti-parallel, hydrogen-bonded β-sheet based on the characterization of *B. mori* fibroin (Marsh, 1955), and further modifications to this early model have

Table 13.3 Amino acid composition of silk fibers

Amino acid composition (mol%)				
Amino acid	***Bombyx mori* (mulberry)**	***Antheraea mylitta* (tasar)**	***Antheraea assama* (muga)**	***Philosamia ricini* (eri)**
Aspartic acid	1.64	6.12	4.97	3.89
Glutamic acid	1.77	1.27	1.36	1.31
Serine	10.38	9.87	6.11	8.89
Glycine	43.45	27.65	28.41	29.35
Hystidine	0.13	0.78	0.72	0.75
Arginine	1.13	4.99	4.72	4.12
Threonine	0.92	0.26	0.21	0.18
Alanine	27.56	34.12	34.72	36.33
Proline	0.79	2.21	2.18	2.07
Tyrosine	5.58	6.82	5.12	5.84
Valine	2.37	1.72	1.5	1.32
Metheonine	0.19	0.28	0.32	0.34
Cysteine	0.13	0.15	0.12	0.11
Isoleucine	0.75	0.61	0.51	0.45
Leucine	0.73	0.78	0.71	0.69
Phenylalanine	0.14	0.34	0.28	0.23
Tryptophan	0.73	1.26	2.18	1.68
Lysine	0.23	0.17	0.24	0.23

been made over the years (Fraser and MacRae, 1973; Colonna-Cesari et al., 1975). The antiparallel β-pleated sheet configuration of *B. mori* is shown in Fig. 13.10.

Most silkworm cocoon and spider dragline silk fibers contain assembled antiparallel β-pleated sheet crystalline structures (Fig. 13.10) (Marsh et al., 1955, Lucas et al., 1960; Fraser and MacRae, 1973). Silks are considered semicrystalline materials with 30−50% crystallinity in spider silks, 62−65% in cocoon silk fibroin from the silkworm *B. mori*, and 50−63% in wild-type silkworm cocoons. In the β-sheet crystals the polymer chain axis is parallel to the fiber axis. Furthermore, the polyalanine repeats or the glycine−alanine repeats are the major primary structure sequences responsible for β-sheet formation. The β-sheets consisting of the glycine−alanine crystalline repeats in the silkworm fiber are asymmetric, with one surface primarily projecting alanyl methyl groups and the other surface of the same sheet containing hydrogen atoms from the glycine residues (Matsumoto et al., 2006).

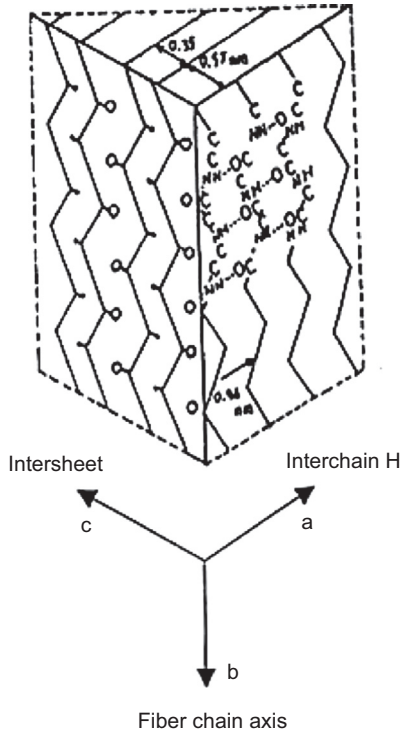

Figure 13.10 The antiparallel β-pleated sheet configuration of *B. mori*. The chain axis is parallel to the fiber axis.

Molecules of silk fibroin are the polypeptide chain with formula $(-CHR-\ominus CO-NH-)_n$ with $n = 1100$ and R being one of the various amino acid residues. The polypeptide chain has not only a backbone but also side chains consisting of radicals R (substituent) of amino acids. Naturally, the degree of branching of the polypeptide chain depends on the amino acids contained in the protein. Thus side chains form 19% of the weight in silk fibroin.

The side chains may be nonpolar, as, for instance, hydrocarbon residues,

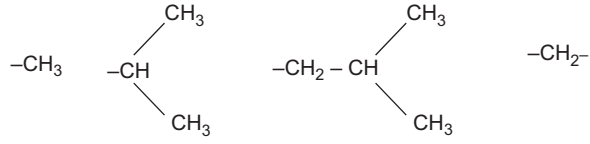

and may contain polar groups such as:

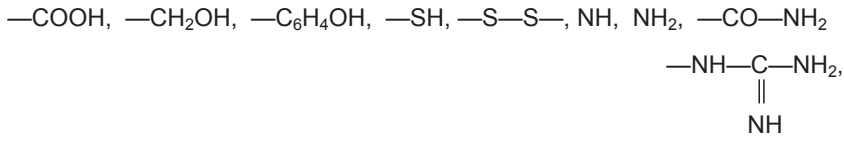

13.11.2.1 Crystallinity

Silk as mentioned earlier is a semi-crystalline material. Earlier studies by X-ray diffraction analysis indicated 62−65% crystallinity in cocoon silk fibroin from the silkworm, 50−63% in wild-type silkworm cocoons, and lesser amounts in spider silk (Warwicker, 1956).

Physical parameters such as crystallinity, crystallite size, and crystallite orientation have been determined from X-ray diffraction. In a study on mulberry, tasar, muga, and eri (Bhat and Nadiger, 1980), it was observed that the mulberry and nonmulberry silks exhibit different wide-angle X-ray diffraction (WAXD) patterns (Fig. 13.11). Mulberry shows a broad 28 peak at 20 degrees corresponding to (201) reflection. On the other hand, all the nonmulberry silks exhibit similar X-ray diffraction patterns showing two major peaks at 28 equal to 17.1 and 20.2 degrees corresponding to (002) and (201) planes. Using X-ray diffraction, Warwicker (1960) observed that the different silk fibroins could be classified into five groups. Mulberry (*B. mori*) has been placed in group I and tasar, muga, and eri (*Antheraea* silks) in group 3a. Group 3a includes most *Antheraea* species, together with other silks belonging to the family Saturniidae. The antiparallel β-sheet structure is the molecular conformation assumed by the fibroin chains in the crystalline regions, with unit-cell dimensions similar to that of $(Ala)_n$ in β-form.

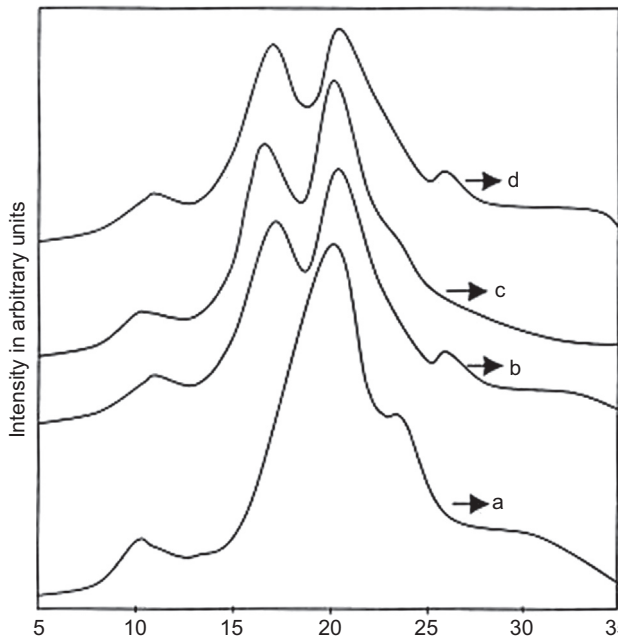

Figure 13.11 WAXD patterns of (a) mulberry, (b) tasar, (c) muga, (d) eri (Bhat and Nadiger, 1980).

Table 13.4 Density and crystallinity values for various silk fibers

Variety	Sex	Density (g/cm^3)	Percentage crystallinity (X-ray)
Antheraea myllita	M	1.329	39.5
(tropical tasar)	F	1.334	39.6
Antheraea proylei	M	1.345	44.6
(temp. tasar)	F	1.344	41.8
Antheraea assama	M	1.314	42.7
(muga)	F	1.327	43.7
Ariake	M	1.354	37.2
(mulberry extra coarse)	F	1.356	35.2
Shunreix shongetsu	M	1.333	43.1
(mulberry extra fine)	F	1.320	41.9

The density and the degree of crystallinity values for male and female varieties as obtained by X-ray diffraction analysis for mulberry, tasar, and muga are reported in Table 13.4. The data have been compiled from the work of Iizuka et al. (1996, 1994, 1993a,b,c) and Iizuka and Itoh (1997). No definite trend may be observed between the male and female varieties. It may be observed from the data that no significant differences exist between the mulberry and nonmulberry varieties. However, the data obtained for the temperate tasar, muga, and mulberry (extra fine) may be compared with those for unhydrolyzed samples obtained by Bhat and Nadiger (1980). No literature is available that gives any idea about any differences in crystallinity or lateral order along the length of the silk filament. All the values seem to be the average values. Considering the fact that some workers have reported gradual reduction of denier, elongation-at-break, degumming loss, etc. in the inner layers of cocoons, it is reasonable to expect the change in the these parameters along the length of the filament.

13.11.2.2 Crystallite size

NY Bhat et a1. (1980) investigated the crystallite size of hydrolysates (silk treated with HCl for different duration) of Indian silk varieties by WAXD (Table 13.5). A quick glance at the results reveals that the nonmulberry silk varieties seem to have larger crystals as compared to mulberry silk. The higher alanine content, as also the predominance of Ala−Ala links in the crystalline region, may be responsible for the higher size. From their results, they concluded that after the HCI treatment, the crystallite size calculated from the 002 plane increased from 27 to 60 Å for tasar, 30 to 56 Å for eri, and 32 to 59 Å for muga. Interestingly, the crystallite size for mulberry control fibers was 10 Å from the 002 plane and the size increased to 20 Å after 96 h of

Table 13.5 Average crystallite size for silk and their hydrolysates

Variety of silk	Planes	Control sample (Å)	48-h hydrofibroin (Å)	(48 + 48)-h hydrofibroin (Å)
Mulberry	002	10	15	20
	201	19	20	25
Tasar	002	27	68	60
	201	47	56	52
Eri	002	30	56	56
	201	47	47	60
Muga	002	32	47	59
	201	39	43	47

treatment. Further, there was no significant increase in the crystallite size of mulberry silk calculated from the 002 plane, whereas all the three nonmulberry silks showed a considerable increase in their crystallite size for the 002 plane after the acid treatment. Similar trends were seen from the data obtained for the 201 plane too.

The authors opined that, in the case of wild silks, the process of acid hydrolysis leads to the Ala−Ala segments aligning parallel to the existing microcrystal and thus causing the crystal to grow. However, the higher crystallite size that may also be related to the crystal geometry of nonmulberry silks compared to mulberry silks needed to be investigated further.

13.11.2.3 Orientation (birefringence and sonic modulus)

Birefringence of different varieties of silk fibers has been reported by Kushal Sen and Murugesh Babu (2004). The Beckeline method was used for determination of the birefringence. A series of mixtures using two liquids [ie, liquid paraffin (refractive index, $\eta = 1.465$) and 1-chloronaphthaline ($\eta = 1.633$)] were prepared for determination of the refractive index of single filaments in both the parallel and the perpendicular directions. The refractive index of the mixture, in which the Beckeline vanished under a polarizing microscope, was taken as the refractive index of fiber. The birefringence (Δ_n) was calculated using the relation:

$$\Delta_n = \eta \parallel - \eta \perp$$

where $\eta||$ is the refractive index of the fiber in the parallel direction and $\eta \perp$ is the refractive index of the fiber in the perpendicular direction to the plane of the polarizer light. An average of five readings was reported.

The birefringence (Δ_n) value gives an idea about the overall molecular orientation, whereas the sonic modulus (S_ε) gives a combined effect of order and orientation.

Table 13.6 Birefringence (Δ_n) and sonic modulus (S_ε) values for different varieties of silks

Type of silk	Δ_n			S_ε (g/den)		
	Outer layer	Middle layer	Inner layer	Outer layer	Middle layer	Inner layer
Mulberry (bivoltine)	0.054	0.055	0.056	165	170	206
Mulberry (crossbreed)	0.051	0.052	0.052	153	167	192
Tasar	0.041	0.042	0.042	106	107	115
Muga	0.040	0.041	0.042	103	108	114
Eri	0.034	0.035	0.035	101	106	109

The values of Δ_n and S_ε are listed in Table 13.6. Both birefringence and sonic modulus were found to increase from the outer to the inner layers within the same variety. This trend was observed in all varieties.

13.11.3 IR spectroscopy

The IR studies on silk fibroin (Bhat and Ahirrao, 1983, Bhat and Ahirrao, 1985, Nadiger and Bhat, 1985, Baruah et al., 1991, Magoshi et al., 1979) suggest that the appearance of absorption bands at 1660, 1540, 1235, and 650 cm^{-1} corresponds to amide 1, amide 2, amide 3, and amide 4, respectively, characteristic of the random coil conformation (amorphous), and those appearing at 1630, 1535, 1265, and 700 cm^{-1} indicate the β-conformation (crystalline).

The calculation of crystallinity index from IR spectroscopy has been done by previous workers using the ratios of intensity bands ofthe crystalline region corresponding to that of amorphous region. Drukker et al. (1953) have reported a crystallinity value of 63% for *B. mori* silk using bands at 1528 cm^{-1} and 1560 cm^{-1}. However, the authors emphasized that the value obtained was not exact, as the resolution of these bands was not exceptionally good. This value certainly appears high compared to those obtained from WAXD. Similar studies on mulberry and wild varieties of Indian silk were done (Bhat and Nadiger, 1980) using the ratio of absorbance of bands at 1265 cm^{-1}(β-form) and 1235 cm^{-1}[α-(random coil conformation) form]. It may be observed from their data (Table 13.7) that mulberry and muga silks showed higher crystallinity indices (0.66 and 0.60, respectively) compared to tasar (0.50) and eri (0.50).

In a study on crystallinity of silk hydrolysates, NV Bhat et al. (1980) reported the IR spectra of different varieties of silk in the range of 1400−800 cm^{-1} (Fig. 13.12). They assigned the band at 1015 cm^{-1} to Gly−Gly linkage, the band at 970 cm^{-1} to Ala−Ala linkage, and those at 998 and 975 cm^{-1} to Ala−Gly linkages. In mulberry, the bands at 1015 cm^{-1} and 970 cm^{-1} were totally absent while the bands at 975 and

Table 13.7 Crystallinity indices for various silk fibers

Variety	X-ray index		IR crystallinity index		Electron diffraction index	
	Control	Hydrolyzed (96 h)	Control	Hydrolyzed (96 h)	Control	Hydrolyzed (96 h)
Mulberry	0.42	0.48	0.66	0.74	0.62	–
Tasar	0.43	0.77	0.50	0.66	0.60	–
Muga	0.44	0.72	0.60	0.64	0.62	–
Eri	0.43	0.65	0.50	0.82	0.63	–

998 cm^{-1} were present. The nonmulberry silks showed a strong band at 970 cm^{-1}. The intensity of these bands at respective wave numbers was further enhanced in hydrolyzed silk samples of both the mulberry and nonmulberry varieties. The band at 1015 cm^{-1}, which was corresponding to Gly−Gly linkage, totally disappeared in the hydrolyzed samples of wild varieties. On the basis of these results, they concluded that the crystalline structure of mulberry must have been formed mostly by the

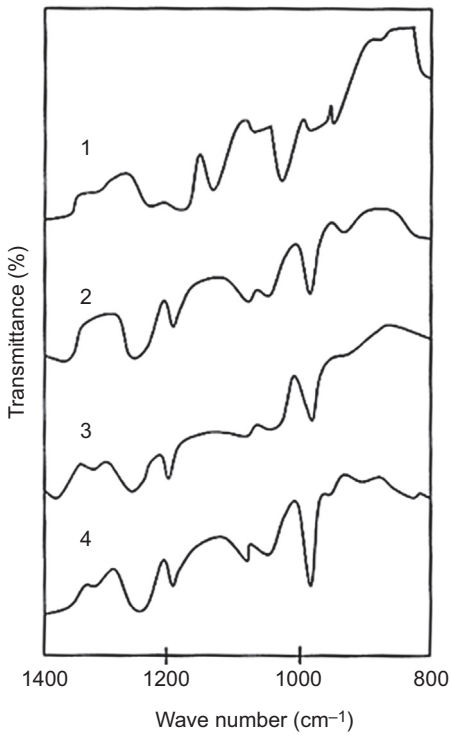

Figure 13.12 Infrared spectra of different varieties of silk: (1) mulberry, (2) tasar, (3) muga, (4) eri.

sequence of glycine and alanine linkages and that of wild silks by nonlabile Ala−Ala linkages.

13.12 Spider silk: synthesis, structure, and properties

13.12.1 Introduction to spider silks

Spider silk is a natural filamentous protein fiber produced by spiders. Scientists and engineers have long envied spiders' ability to manufacture a material that is simultaneously strong, fine, and tough. This combination of properties makes spider silk an extremely attractive fiber for numerous applications in medicine, defense, and the leisure industry. The fibrous threads produced by the eight-legged spiders possess extraordinary properties. Many spider silks have better mechanical properties than silkworm's silk (Gosline et al., 1999). Spiders can spin up to seven different types of silk, each one tailor-made to fit a specific function. To date, most researchers have focused their attention on "dragline" silk, used by spiders as a safety line and also as the frame for their webs (Fig. 13.13) (Gould, 2002).

Spider silks are characterized by remarkable diversity in their chemistry, structure, and functions, ranging from orb web construction to adhesives and cocoons. These unique materials have prompted efforts to explore potential applications of spider silk equivalent to those of silkworm silks, which have undergone 5000 years of domestication and have a variety of uses, from textiles to biomedical materials. These silks are much less talked about than ordinary silk despite their many superior properties. Their unique combination of strength and elasticity is judged to be superior to that of synthetic high-tech fibers made of polyamide or polyester (Mukhopadhyay and Sakthivel, 2005). Weight-by-weight spider silk is five times stronger than steel, finer than human hair, more resilient than any synthetic fiber, and completely biodegradable. Compared to silkworm silk, it is more waterproof and can absorb three times

Figure 13.13 Dragline silk produced by spiders.

the impact force of Kevlar without breaking. All these properties are achieved in a fiber manufactured under conditions of ambient temperatures, low pressures, and with water as a solvent.

13.12.2 Spider web and types of spider silk

Spider dragline silk is a semicrystalline biopolymer with a unique combination of high tensile strength, high elasticity, and high modulus. The 0.2−10 mm diameter silk fibers have a higher breaking energy than other natural or synthetic fibrous polymers, far exceeding that of high-tensile steel and Kevlar on a weight-for-weight basis (Gosline et al., 1984).

Spider webs can take a variety of forms but the most common type is the orb web. Different families of spiders (*Araneus*, *Nephila*) build orb webs and other families of spiders construct tangle and sheet webs. The golden orb web spider (Fig. 13.14) has the most spectacular and most investigated silk of all spiders. These spiders are known to make a large, golden-colored web. These webs can be 2 m in diameter and some tribes (Native tribes in the Western Pacific Islands, American Native Indians on the Columbia River) use these webs as fishing nets (Champion deCrespigny et al., 2001). Their draglines have extraordinary properties. They are hard to breed in laboratory conditions. They measure around 5 cm in length without legs and up to 25 cm with stretched legs.

Orb-weaving spiders are able to synthesize as many as seven different types of silks by specialized glands (Table 13.8). The information contained within the silk proteins for each of these different types of silks provides important insights into protein structure−function relationships. Spider silks are used for nearly all aspects of a spider's life including capturing and swathing prey or protecting the cocoon, to name just a few. As different as their utilization by the spider, individual properties of the silks are distinct.

Figure 13.14 *Nephila clavipes*, golden orb spider.

Table 13.8 Different types of spider silks

SI. no.	Silk gland	Use	Spinneret
1	Major ampullate	Dragline, frame threads	Anterior
2	Minor ampullate	Dragline reinforcement	Median
3	Pyriform	Attachment disk	Anterior
4	Aciniform	Swathing prey	Median, posterior
5	Cylindrical (tubuliform)	Cocoon construction	Median, posterior
6	Aggregate	Sticky silk glue for capture spiral	Posterior
7	Flagelliform	Capture spiral	Posterior

13.12.3 Chemical composition

The molecular structure of silk consists of regions of protein crystals separated by less organized protein chains. The primary structural modules give rise to diverse secondary structures that, in their turn, direct functions of different silks. As the most heavily studied secondary structure of silks, crystalline β-sheets contribute to the high tensile strength of silk fibers. Beta-sheets form through natural physical crosslinking of amino acid sequences, which in spider and silkworm silk consist of multiple repeats of mainly alanine, glycine−alanine, or glycine−alanine−serine. The noncrystalline regions of silk are commonly made up of: (1) β-spirals similar to a β-turn composed of GPGXX repeats (where X is mostly glutamine) and (2) helical structures composed of GGX (Kaplan et al., 1994, 1997). These semiamorphous regions provide silk with elasticity. For example, the flagelliform silk from *Nephila clavipes* is rich in the GPGXX motif, and this sequence results in a highly elastic fiber that functions in prey capture. In addition to the crystalline and semiamorphous regions, nonrepetitive regions are present at the amino and carboxyl termini of the proteins. Although the impact of these termini on mechanical response is not fully understood, it has been speculated that they might play a role in the controlled assembly of silk proteins (Scheibel, 2004; Van Beek et al., 2002).

Each silk-producing creature synthesizes silk proteins that offer a rich diversity of primary sequences and secondary structures. For example, the common amino acid modules in the silk fibers synthesized by the Araneomorphae (true spiders) can be grouped into four categories: poly-Ala, poly-Ala−Gly, GPGXX, GGX and a spacer sequence (Hayashi et al., 1999). Most recently, Garb and colleagues characterized six novel silk proteins from the Mygalomorphae (tarantulas) that do not contain these four categories found in true spider spidroins. These newly characterized tarantula silks, as a result, do not possess high-tensile strength and elasticity. This finding supports the hypothesized role of poly-Ala and GPGXX modules in forming dragline and flagelliform silks (Garb et al., 2007). In most of the these cases, the fundamental

process of silk protein self-assembly into functional materials remains consistent, with the more hydrophobic domains, mainly the alanine, glycine–alanine, and glycine–alanine–serine repeats, driving the process. In most spider silks, β-sheet formation is achieved in a spinning duct caused by the progressive loss of water in the gland and alignment of the hydrophobic regions during flow (Huemmerich, 2004; Vollrath and Knight, 2001, Jin and Kaplan, 2003, Bini et al., 2004, Exler et al., 2007). Exceptions are the more hydrophilic silks, such as those involved in adhesion, wherein charge interactions can play a more dominant role than the hydrophobic interactions. Self-assembly without chemical crosslinking provides stability while still allowing enzymatic digestion (Scheibel, 2004) or slow degradation under appropriate environmental conditions (Horan et al., 2005).

13.12.4 Amino acid composition and molecular components of dragline silk

The major and minor ampullate fibroins contain the highest levels of glycine and alanine relative to other spider silk family members; these levels approach >50% of the total amino acid content (Casem et al, 1999; Lombardi and Kaplan, 1990). Biochemical experiments show dragline silk is a composite material largely composed of two structural proteins or spidroins (contraction of the words spider and fibroin) called MaSp1 and MaSp2 (Xu and Lewis, 1990; Hinman and Lewis, 1992). Structural studies demonstrate the major ampullate spidroins form the core of the fiber that is wrapped inside a glycoprotein coat. Although the identities of the constituents of the glycoprotein layer remain unknown, experimental evidence supports that this layer is added in the ampulla prior to extrusion (Casem et al., 2002; Sponner et al., 2005). The molecular sequences coding for the dragline silk fibroins were the first to be identified from *N. clavipes* (Xu and Lewis, 1990). Recently, the complete genetic blueprints for MaSp1 and MaSp2 were determined from *Latrodectus hesperus* (Ayoub et al., 2007). The predicted sequences for these fibroins encode large molecular weight proteins that are approximately 3500 amino acids in length. These spidroins are highly modular, each containing internal repetitive block repeats that are flanked by N- and C-terminal nonrepetitive ends comprised of approximately 100 amino acids. The internal block repeats are rich in glycine and alanine; these regions form polyalanine or polyalanine–glycine stretches that are interrupted by glycine-rich regions. The polyalanine segments form β-sheet crystal domains and are responsible for high tensile strength while the glycine-rich regions adopt 31-helix-type structures and β-turns that link the crystalline domains (Simmons et al., 1996). These interconnecting glycine-rich regions constitute the semiamorphous regions and have been implicated in the extensibility of the fibers. Extensibility of dragline silk fibers also has been attributed to glycine–proline–glycine–X–X (GPGXX) repeats within the MaSp2 protein sequence and the formation of β-spirals. MaSp2 proteins have been shown to be tightly packed in certain core regions of fibers from *N. clavipes*, whereas MaSp1 appears to be uniformly distributed along the radial axis (Sponner et al., 2005). These data demonstrate that MaSp1 and MaSp2 are not evenly distributed

down the long axis of natural fibers. The biochemical mechanisms that modulate their differential localization are not well understood, but could be explained by differences in expression levels and/or their protein sequences that control partitioning during extrusion.

Table 13.9 shows the amino acid composition of dragline silk in comparison with other protein fibers such as silkworm silk and wool keratin (Kapaln et al., 1997). It may be observed that, in addition to fibroin, other components like glycoprotein, inorganic salts, sulfur-containing amino acids, and ionic forms of amines may be found in spider silk (Schulz and Toft, 1993; http/www/zoology.ubc.ca, 2005). The presence of these components plays crucial roles like identification of species, regulation of water content of web, and protection against microorganisms. The presence of 12-methyltetradecanic acid and 14-methylhexadecanoic acid to the minor amounts impart antimicrobial properties to the spider silk. Wax-like esters are also present on the surface of spider silk. The structural hierarchy in the assembly of spider silk is shown in Fig. 13.15 and the secondary structure of dragline silk is presented in Fig. 13.16.

Table 13.9 Amino acid composition (mol%) of spider dragline silk and other protein fibers

Amino acid	Silkworm silk	Wool fiber	Spider silk
Glycine	43.7	8.4	37.1
Alanine	28.8	5.5	21.1
Valine	2.2	5.6	1.8
Leucine	0.5	7.8	3.8
Isoleucine	0.7	3.3	0.9
Serine	11.9	11.6	4.5
Threonine	0.9	6.9	1.7
Aspartic acid	1.3	5.9	2.5
Glutamic acid	1.0	11.3	9.2
Phenylalanine	0.6	2.8	0.7
Tyrosine	5.1	3.5	–
Lysine	0.3	2.6	0.5
Histidine	0.2	0.9	0.5
Arginine	0.5	6.4	7.6
Proline	0.5	6.8	4.3
Tryptophan	0.3	0.5	2.9
Cysteine	0.2	9.8	0.3
Metheonine	0.1	0.4	0.4

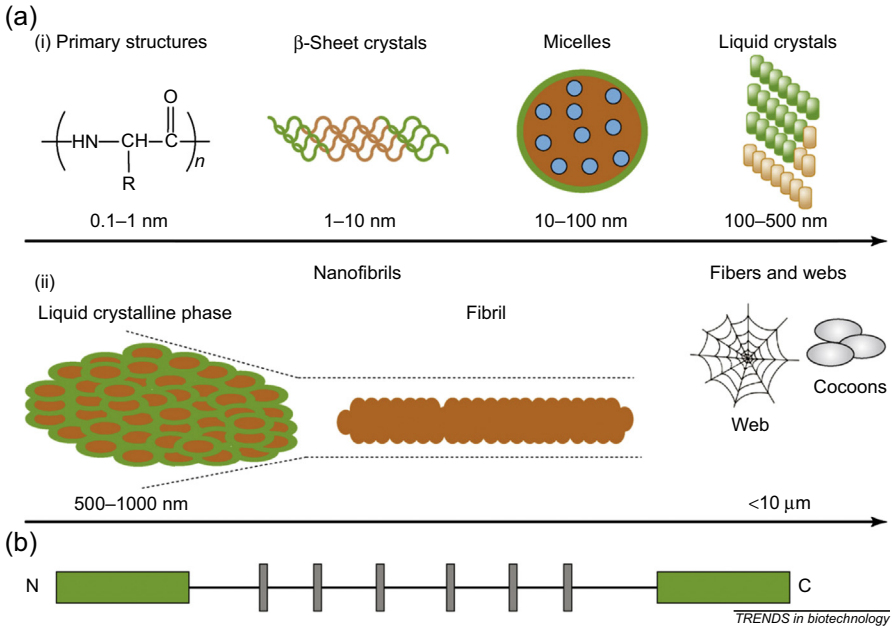

Figure 13.15 Structural hierarchy in silk assembly related to assembly into fibers. (a) (i) Spider silk proteins consist of repeats of amino acid sequences that self-assemble into β-sheets. This self-assembly is driven by hydrogen bonding and also by hydrophobic regions. These interactions result in the formation of inter- or intramolecular protein chain interactions. The β-sheet structures further assemble into soft micelles in a manner that excludes the hydrophilic ends to the perimeter. The interiors of the micelles contain water (*blue regions in the figure*) caused by the presence of small "spacers" that are more hydrophilic than the dominant hydrophobic domains. This does not represent a multishell structure; rather, it is caused by the partitioning of the hydrophilic chain ends to the surface of the micelles and the location to the interior of the large and dominant hydrophobic domains and small hydrophilic spacers. With increasing protein concentration, micelles transform into gel-like states leading to metastable liquid crystalline structures. (ii) Triggers, such as physical shearing, or environmental factors, such as low pH, methanol, ultrasonication, and electric fields, convert the gel states and liquid crystals into a more stable β-sheet structure. The resulting fibrils emerging from spinning ducts are combined into higher-ordered structures as naturally constructed webs or cocoons. (b) Molecular structure of a spider silk protein. In silks that are used for web architecture and other strong fibers, the underlying molecular structure consists mainly of hydrophobic regions (*illustrated by thin black lines*). These large hydrophobic regions are interspersed with small hydrophilic spacers (*illustrated by gray vertical rectangles*) and are flanked by nonrepetitive domains at the N- and C-termini (*green horizontal rectangles*).

13.12.5 Properties of spider silk

In the world of natural fibers, spider silk has long been recognized as an important fiber for its unique combination of high strength and rupture elongation. Spider silk is shown to possess strength as high as 1.75 GPa at a breaking elongation of over

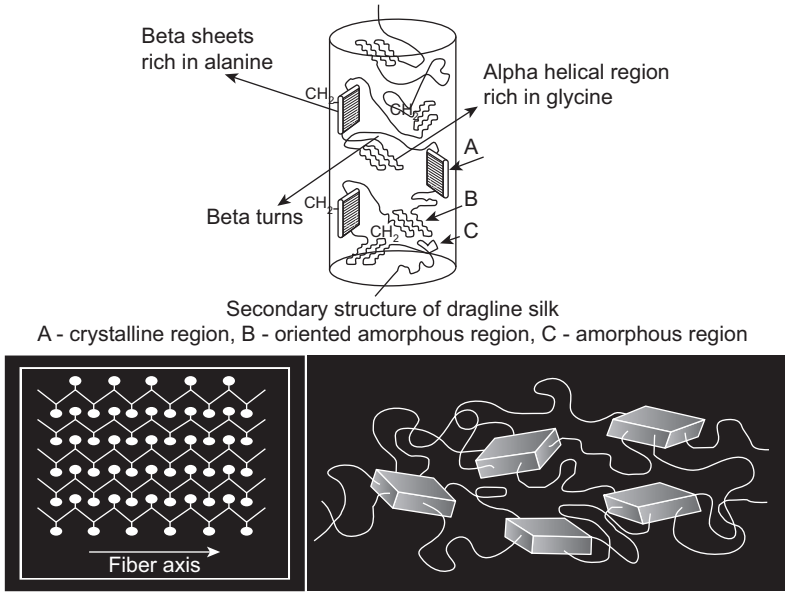

Figure 13.16 Secondary structure of dragline silk.

26%. With toughness three times more than that of aramid and other industrial fibers, spider silk continues to attract the attention of fiber scientists and technologists.

Properties of spider silk vary by species and by functions. Depending upon the species, an individual spider has more than five different silk glands where silks of different properties are produced before extrusion through three pairs of spinnerets. The dragline originates in the ampullate gland and is extruded through the anterior spinnerets. Spider dragline is the strongest and toughest of the silks a spider makes, and is the structural framework of a spider web and the lifetime of a spider.

The major reason for studying spider silk, beyond inherent curiosity, is its unique mechanical properties. To survive, the spider must use a minimum amount of silk in its web to capture prey, and yet the web must be able to stop and capture an insect flying at high velocity. To do this the web must absorb the energy of the insect without creating rebound, which would trampoline the prey off the web. A recent study has concluded that the web and the spider silk used to construct it are nearly optimally designed for each other. The crucial factors in this optimization are tensile strength and elasticity. Even though it is not as strong as some fibers, it is much more elastic. This allows it to absorb more energy prior to breaking than any commonly used material (Lewis, 1992).

Another fascinating evolutionary adaptation of dragline silk is its ability to supercontract. The fiber will contract to less than 60% of its original length when it is wetted. This results in nearly a 1000-fold decrease in the elastic modulus and an increased extensibility (Gosline et al., 1984). The practical application for the spider is that the web will tighten each day when it is wetted with dew, thus maintaining its shape

and tension. There are several polymers that exhibit supercontraction in organic solvents but virtually none that will supercontract in water alone (Work, 1977). This supercontraction is reversible and repeatable and can do mechanical work such as lifting a weight. An important feature in conjunction with supercontraction is the insolubility of the silks. Extreme chaotropic agents are required to solubilize any of the silks.

13.12.6 Mechanical properties of spider silk

13.12.6.1 Tensile behavior

The material properties of spider silk vary from specimen to specimen, as demonstrated in the past studies of the *N. clavipes* spider by Frank K.Ko et al. (2005). The spider silk was tested by simple elongation at a strain rate of 100% per minute using a gauge length of 1.25 cm. The stress−strain curve of the spider silk showed a sigmoidal shape (Fig. 13.17) indicating a balanced strength and elongation of 1.75 GPa (15.8 g/den) and 36%, respectively. A comparison of tensile properties of spider silk with other fibers is presented in Table 13.10.

The stress−strain curve is characterized by three distinct regions: the 0−5% strain region characterized by a high initial modulus of 34 GPa, the 5−21% strain region having a pseudo yield point at 5% before strain hardening to a maximum modulus of 22 GPa at 22% elongation, and the 21−36% region exhibiting a gradual reduction of modulus until reaching a failure strength of 1.75 GPa. The area under the stress−strain curves showed a toughness level of 2.8 g/den. This is much higher than the toughness of the aramid fiber (0.26 g/den) and nylon-6 fiber (0.9 g/den).

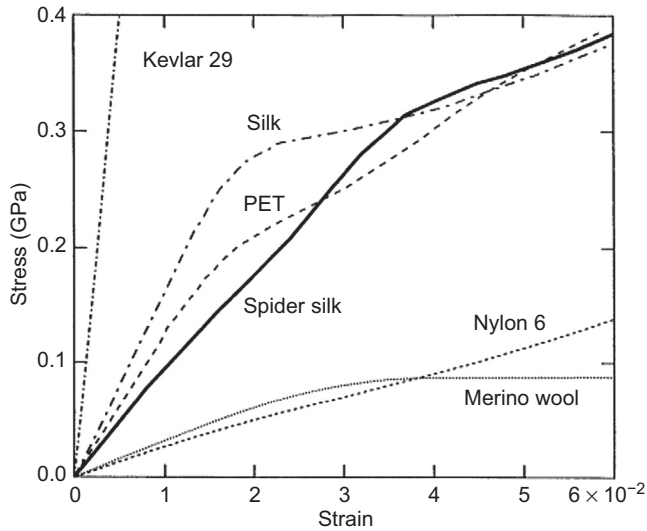

Figure 13.17 Tensile properties of spider silk compared to other fibers.

Table 13.10 Comparison of tensile properties of silk with other high-performance fibers

	Density (g/cm^3)	Tenacity (GPa)	Extensibility (%)	Toughness (MJ/m^3)
Nylon-6,6	1.1	0.95	18	80
Kevlar 49	1.4	3.6	3	50
Dragline of *Araneus diadematus*	1.3	1.1	27	160
Egg sac of *Araneus diadematus*	1.3	0.3	25−50	70
Bombyx mori silk (mulberry silk)	1.3	0.6	18	70
Wool	1.3	0.2	50	60
Polylactic acid	1.24	0.7	22	90
Carbon fiber	1.8	4	1.3	25
High-tensile steel	7.8	1.5	1	6

Spider silk has an intriguing combination of high strength, extensibility, and resistance to compression (Cunniff et al., 1994a,b). Some silks exhibit over 200% elongation and others maintain tensile strengths approaching those of high-performance fibers. These unique values are what make the fiber so interesting. A combination of such high modulus and tenacity values coupled with such high elongation makes the fiber highly versatile for various uses.

The stress−strain characteristics of dragline silks show large inter- and intraspecific differences between spiders in different families (Madsen et al., 1999). Moreover, there can be a large daily variability in silk from individuals of the same species; and the spider's condition can (and frequently does) affect silk properties, starvation, for example, can lead to decreased breaking elongation. Speed of silk production also affects silk properties such that with increasing speed: (1) breaking elongation decreases; (2) breaking stress increases; and (3) Young's modulus increases. Finally, the spider's body temperature during silk production also plays an important role. Since spiders are ectotherms, this means that an individual can to some extent modify silk parameters by adjusting the time of building and the speed of running. However, the spider also seems to be able to modify silk parameters by direct nervous control (Madsen and Vollrath, 2000) as well as indirectly by its diet.

13.12.6.2 Elasticity

The extreme elasticity of this natural fiber comes from long spirals in the protein's configuration (http://www.sciencenews.org/sn_arc98/2_21_98/fob2.htm), as proposed researchers from the University of Wyoming in Laramie. The helices present

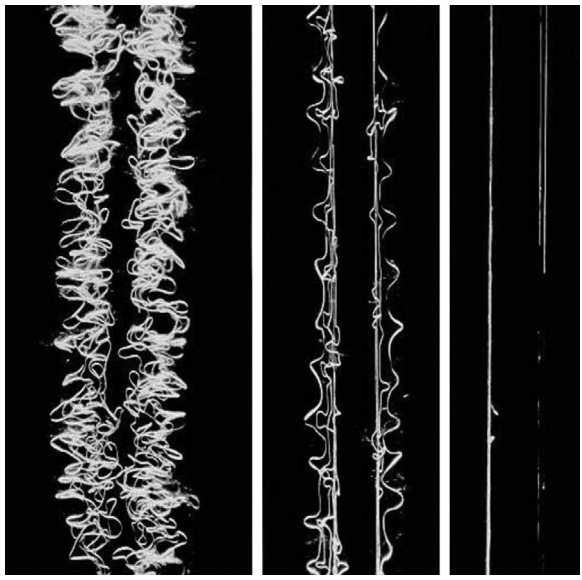

Figure 13.18 A strand of a social spider, *Stegodyphus sarasinorum*, is shown in normal size, and stretched five times and 20 times its original length.

in the protein molecules act as molecular springs and make it elastic. A strand of spider silk of normal size, stretched five times and 20 times its original length, showing its extensibility, is shown in Fig. 13.18.

It has been found that capture silk protein from *N. clavipes* has a chain of thousands of amino acids having regions in which a sequence of five amino acids is repeated over and over, as many as 63 times. The researchers suggest that the segments of the protein with the repeating blocks form long, spring-like shapes. At the end of each five-amino-acid block, the protein kinks back on itself in a 180 degree turn. The series of turns eventually forms a spiral that "looks exactly like a molecular spring."

Dragline silk proteins and capture silk proteins have similar turn-forming blocks of amino acids. However, these blocks repeat an average of 43 times in the capture silk, compared to only nine times in the dragline silk. That fivefold difference in length corresponds to the difference in elasticity between the two proteins.

13.12.7 Applications

13.12.7.1 Spider silk composites

The combination of high strength, toughness, and light weight makes spider silks attractive for high-performance fiber and composite applications (Arcidiacono et al., 2002) and for biomedical applications. Whether the silk material is to be used as an individual fiber or woven into a textile structure, it is critical that production techniques are developed to generate long lengths of material in sufficient quantity and with mechanical performance that is at least equal to the native spider silks. Traditionally, silkworm silks have been the focus of research to generate silk fiber materials. Techniques

to form fibers from silkworm proteins, such as solvent extrusion, electrospinning and microfluidic approaches, might be appropriate for spider silk proteins as well. The advantages and limitations of each system might determine their use in specific applications or their commercial exploitation.

13.12.7.2 Spider silk as a biomaterial

One attractive application of spider silks is to emulate the diverse material functions of this family of proteins as a source of novel biomaterial designs. Insight into the assembly and processing of spider silk proteins into various material forms has been a longstanding focus and has allowed the broadening of the field of applications for silks in general. Specifically, medical devices and tissue engineering applications are perhaps the most promising areas for the utilization of spider silks. Recent progress with reprocessed or native silkworm silk fibers has been realized, and similar approaches could be used with spider silks when they become available in sufficient quantities. For example, in ligament tissue engineering, a combination of fiber twisting and braiding of silkworm silk fibers was able to direct stem cell- and ligament cell-based reconstruction through the alignment and mechanical strength of the twisted silk structure (Altman et al., 2003, 2002). Spider silk fibers were manually collected from the major ampullate dragline and seeded with human Schwann cells to demonstrate biocompatibility, suggesting a promising strategy for future treatment of peripheral nerve injuries (Allmeling et al., 2006).

13.12.7.3 Biotechnological applications of spider silk

Current research in spider silk involves its potential use as an incredibly strong and versatile material. The interest in spider silk is mainly because of a combination of its mechanical properties and the nonpolluting way in which it is made. The production of modern synthetic super-fibers such as Kevlar involves petrochemical processing, which contributes to pollution. Kevlar is also drawn from concentrated sulfuric acid. In contrast, the production of spider silk is completely environmentally friendly. It is made by spiders at ambient temperature and pressure and is drawn from water. In addition, silk is completely biodegradable. If the production of spider silk ever becomes industrially viable, it could be a good alternative to Kevlar and be used to make a diverse range of items such as:

- Bulletproof clothing
- Wear-resistant lightweight clothing
- Ropes, nets, seat belts, parachutes
- Rust-free panels on motor vehicles or boats
- Biodegradable bottles
- Bandages, surgical thread
- Artificial tendons or ligaments, supports for weak blood vessels

Scientists hope soon be able to spin spider silk without the aid of spiders—achieving an age-old human quest to harness one of nature's most remarkable materials. Randy Lewis is a professor of molecular biology at the University of Wyoming in Laramie.

His team of researchers has successfully sequenced genes related to spider silk production, uncovering the formula that spiders use to make silk from proteins. The most common method is introducing silk spider genes into other organisms so that they can produce silk proteins that might later be used to create artificial silk threads. Host organisms range from simple bacteria to goats. There have been attempts to generate transgenic tobacco and potato plants that express remarkable amounts of recombinant *N. clavipes* dragline proteins. In the process the team acquired a better understanding of how the silk's structure is related to its amazing strength and elastic properties. By cracking the genetic code of spider silk, scientists hope not only to be able to duplicate the material but perhaps even to improve on it. Over hundreds of millions of years the 37,000 known species of spiders (and others unknown) have evolved and diversified many silks for their unique purposes. Best known and studied is silk secreted by a spider's major ampullate glands. The silk is also used to create spiders' familiar "wagon wheel" webs. Spider silk has incredible tensile strength and is often touted as being several times stronger than steel of the same thickness. What's even more unique, however, is spider silk's elasticity. "When we say spider silk is tougher than things like Kevlar [a plastic used to make body armor], Kevlar has higher tensile strength but it's not very stretchy," said Todd Blackledge, an entomologist at the University of Akron (Gole and Kumar, 2013). These properties suggest a potential for many applications for spider silk: extremely thin sutures for eye or nerve surgery, plasters and other wound covers, artificial ligaments and tendons, textiles for parachutes, protective clothing and body armor, ropes, fishing nets, and so on. "One that's initially surprising is air bags," Lewis added. "Right now an air bag just sort of blasts you back into a seat. But if it were made out of this material it would actually be made to absorb energy and really reduce impact." Current research focuses around these problems and a possible solution would be to adapt the composition of silk proteins to alter its properties. Research is still in its early stages but unraveling the secrets of spider silk is under way.

13.13 Applications of high-performance silk fibers

Special silk-fiber composites might be used in microelectronics and fiber optics or as "smart" structural fabrics with antistatic properties. Electrostatic properties may also lead to a first market for the more complex minimachine silks of the capture thread type, be they of the droplet or woolly kind, and they might find employment in active filters, which, after all, is an area where orb webs already excel.

For medical applications, surgical threads, biomaterial membranes, and scaffolds, cell-growth supporting substrates and controlled release matrices are envisioned because of the low inflammatory potential of the silk proteins, the antithrombic nature of the material, and the opportunity to generate a wide range of mechanical properties by bioengineering the primary sequences contained in the silk. Most current applications for silks involve silkworm fibroin because of the limited availability of spider silks.

It is known that the orb-weaving spider produces one of the world's toughest fibers. Using recombinant DNA technology, DuPont scientists in the United States have created

synthetic spider silk as a model for a new generation of advanced materials. It has been suggested that a single strand of spider silk, thick as a pencil, could stop a 747 Jumbo Jet in flight (Syed, 2006). Whatever comparison one uses, the dragline silk of the orb-weaving spider is an impressive material. On an equal weight basis, it is stronger than steel. In addition, spider silk is very elastic. It is this combination of strength and stretch that makes the energy-to-break of spider silk so high. Simply put, it is the toughest material known. Spider silk is merely the most dramatic example of a sizable family of biopolymers possessing a combination of properties that synthetic materials cannot yet approach. Researchers at DuPont are looking to these natural materials as paradigms for the design and synthesis of a new generation of advanced structural materials.

13.14 Summary

Silk fibers are remarkable materials displaying unusual mechanical properties: strong, extensible, and mechanically compressible. Silks also display interesting thermal and electromagnetic responses, particularly in the UV range for insect entrapment and form crystalline phases related to processing. Silk fibers combine reasonable modulus (about 16 GPa for cocoon silk) with a very high strain to failure (order 20%), which means they can absorb a considerable amount of energy upon failure. Research has shown that silk fabrics perform best in penetration impact resistance when embedded in a matrix of high strain to failure and when the fiber−matrix adhesion is relatively modest. Silk fibers were used in optical instruments as late as the mid-1900s because of their fine and uniform diameter and high strength and stability over a range of temperatures and humidity. Some spider silks exhibit over 200% elongation and others maintain tensile strengths approaching those of high-performance fibers. In terms of energy absorption prior to break, spider silks are unmatched in the world of synthetic or natural fibers. Naturalist reports suggest that some spider silks were used in the South Pacific for gill nets, dip nets, and fishing—a testimony to the remarkable mechanical properties and durability of this family of protein polymers. Silks have historically been used in medicine as sutures over the past 100 years and are currently used in this mode along with a variety of consumer product applications. The novel mechanical and visual features of silk fibers from silkworms and spiders have driven interest in this family of structural protein fibers for centuries. The ability to manipulate silkworms for domesticated production of silk fiber, the opportunity to exploit spider silks via genetic engineering, and future options to mimic the novel features of this family of protein fibers using synthetic approaches continue to drive strong interest in these protein fibers. With growing applicability of these fibers in biomedical and consumer product applications, this interest is likely to continue to expand.

13.15 Future trends

Because of the advent of improved analytical techniques, together with the tools of biotechnology, a new generation of products is envisioned with silk. The ability to tailor polymer structure to a precise degree leads to interesting possibilities in the control of macroscopic functional properties of fibers, membranes, and coatings, as well as

improved control of processing windows. Biotechnology offers the tools with which to solve limitations in spider silk production that have not been overcome with traditional domestication and breeding approaches, such as those used successfully with the silkworm. This is of interest because of the variety of silk structures available and the higher modulus and strength as compared to silkworm silk. Though the traditional practices make silk to construct only textiles, the new approach extends its application toward nutritional, cosmetic, pharmaceutical, biomaterial, biomedical and bioengineering, automobile, house building, and art craft applications. The inclination rightly suits silk because of faster production rate and increasing global demand for its variable eco-friendly composites and viable contributing impact on value, employment, and environmental safety.

The threads that the spider weaves for the construction of the fabric and the security thread that generates to move, usually known by its acronym in English as threads more, they are more resistant fibers known today. This thread combines two properties that do not usually appear simultaneously in artificial materials: a great mechanical resistance (force required to break the thread) comparable to that of the best steel, and an exceptional capacity for deformation (increase in the length of the thread with respect to its initial length), between 10 and 100 times more than any other fiber. Although there is still no equivalent commercial thread, its possible applications are very diverse: from armored military vehicles or bulletproof vests to fine sutures for use in ocular operations or micro- and neurosurgery.

Special silk fiber composites might be used in microelectronics and fiber optics or as "smart" structural fabrics with antistatic properties. Electrostatic properties may also lead to a first market for the more complex minimachine silks of the capture thread type, be they of the droplet or woolly kind, and they might find employment in active filters, which, after all, is an area where orb webs already excel. For medical applications, surgical threads, biomaterial membranes, and scaffolds, cell growth-supporting substrates and controlled release matrices are envisioned because of the low inflammatory potential of the silk proteins, the antithrombic nature of the material, and the opportunity to generate a wide range of mechanical properties by bioengineering the primary sequences contained in the silk. Most current applications for silks involve silkworm fibroin because of the limited availability of spider silks. The combination of high strength and superb toughness is likely to push dragline silks into impact and tearproof textiles or other structural fabrics where strong, flexible materials are desirable. Technosilks might benefit from the fact that environmental concerns are growing and that the market is already primed and waiting for artificial spider silks.

References

Allmeling, C., et al., 2006. Use of spider silk fibres as an innovative material in a biocompatible artificial nerve conduit. Journal of Cellular and Molecular Medicine 10, 770−777.

Altman, G.H., et al., 2002. Silk matrix for tissue engineered anterior cruciate ligaments. Biomaterials 23, 4131−4141.

Altman, G., Diaz, F., Jakuba, C., Calabro, T., Horan, R.L., Chen, J., Lu, H., Richmond, J., Kaplan, D.L., 2003. Silk-based biomaterials. Biomaterials 24, 401−416.

Arcidiacono, S., et al., 2002. Aqueous processing and fibre spinning of recombinant spider silks. Macromolecules 35, 1262−1266, 49.

Ayoub, N.A., Garb, J.E., Tinghitella, R.M., Collin, M.A., Hayashi, C.Y., 2007. Blueprint for a high-performance biomaterial: full-length spider dragline silk genes. PLoS One 2, e514.
Baruah, G.C., Talukdar, C., Bora, M.N., 1991. Indian Journal of Physics 65B (6), 651−654.
Becker, N., Oroudjev, E., Mutz, S., Cleveland, J.P., Hansma, P.K., Hayashi, C.Y., et al., 2003. Molecular nanosprings in spider capture-silk threads. Natural Materials 2, 278−283.
Bell, F.I., McEwen, I.J., Viney, C., 2002. Fibre science: supercontraction stress in wet spider Dragline. Nature 416, 37.
Bhat, N.V., Ahirrao, S.M., 1983. Journal of Applied Polymer Science 28, 1273−1280.
Bhat, N.V., Ahirrao, S.M., 1985. Textile Research Journal 55 (1), 65−71.
Bhat, N.V., Nadiger, G.S., 1980. Journal of Applied Polymer Science 25, 921−932.
Bini, E., et al., 2004. Mapping domain structures in silks from insects and spiders related to protein assembly. Journal of Molecular Biology 335, 27−40.
Cao, Y., Wang, B., 2009. Biodegradation of silk biomaterials. International Journal of Molecular Sciences 10, 1514−1524.
Carboni, P., 1952. Silk, Biology, Chemistry and Technology. Chapman & Hall Ltd., London.
Casem, M.L., Turner, D., Houchin, K., 1999. Protein and amino acid composition of silks from the cob weaver, *Latrodectushesperus* (black widow). International Journal of Biological Macromolecules 24 (2−3), 103−108.
Casem, M.L., Tran, L.P., Moore, A.M., 2002. Ultrastructure of the major ampullate gland of the black widow spider, Latrodectus Hesperus. Tissue Cell 34 (6), 427−436.
Champion de Crespigny, F.E., Herberstein, M.E., Elgar, M.A., January 2001. Food caching in orb-web spiders (Araneae: Araneoidea). Naturwissenschaften 88 (1), 42−45.
Chen, Z., Kimura, M., Suzuki, M., Kondo, Y., Hanabusa, K., Shirai, H., 2003. synthesis and characterization of new acrylic polymer containing silk protein. Fibre 59 (5), 168−172.
Colonna−Cesari, F., Premilat, S., Lotz, B., 1975. Journal of Molecular Biology 95, 71.
Craig, C.L., Hsu, M., Kaplan, D., Pierce, N.E., 1999. A comparison of the composition of silk proteins produced by spiders and insects. International Journal of Biological Macromolecules 24, 109−181.
Craig, C.L., 1997. Evolution of arthropod silks. Annual Review of Entomology 42, 231−267.
Cunniff, P.M., Fossey, S.A., Auerbach, M.A., 1994a. Polymers for Advanced Technologies 5, 401.
Cunniff, P.M., Fossey, S.A., Auerbach, M.A., Song, J.W., 1994b. Silk polymers: materials science and biotechnology. In: American Chemical Society Symposium Series, vol. 544, p. 34. http://pubs.acs.org/books/publish.shtml.
Dalpra, I., Freddi, G., Minic, J., Chiarini, A., Armato, U., 2005. De novo engineering of reticular connective tissue *in vivo* by silk fibroin nonwoven materials. Biomaterials 26, 1987−1999.
Drukker, B., Hainsworth, R., Smith, S.G., 1953. Journal of the Textile Institute 44, T420.
Exler, J.H., et al., 2007. The amphiphilic properties of spider silks are important for spinning. Angewandte Chemie, International Edition in English 46, 3559−3562.
Fraser, R.D.B., MacRae, T.P., 1973. Silks. In: Conformation in Fibrous Proteins. Academic Press, New York.
Garb, J.E., et al., 2007. Expansion and intragenic homogenization of spider silk genes since the Triassic: evidence from Mygalomorphae (tarantulas and their kin) spidroins. Molecular Biology and Evolution 24, 2454−2464.
Gole, R.S., Kumar, P., 2013. Spider's Silk: Investigation of Spinning Process, Web Material and Its Properties. Department of Biological Sciences and Bioengineering, Indian Institute of Technology Kanpur, Kanpur-208016.
Gosline, J.M., Denny, M.W., DeMont, M.E., 1984. Nature 309.
Gosline, J.M., Guerette, P.A., Ortlepp, C.S., Savage, K.N., 1999. The mechanical design of spider silks: from fibroin sequence to mechanical function. Journal of Experimental Biology 202, 3295−3303.

Gould, P., December 2002. Exploiting spider's silk. Materials Today 42–47.
Hakimi, O., Knight, D.P., Vollrath, F., Vadgama, P., 2007. Spider and mulberry silkworm silks as compatible biomaterials. Composites: Part B 38, 324–337.
Hardy, J., Scheibel, T.R., 2010. Composite materials based on silk proteins. Progress in Polymer Science 1093–1115.
Harris, B., 1999. Engineering Composite Materials. The Institute of Materials, London.
Hayashi, C.Y., et al., 1999. Hypotheses that correlate the sequence, structure, and mechanical properties of spider silk proteins. International Journal of Biological Macromolecules 24, 271–275.
Hinman, M.B., Lewis, R.V., 1992. Isolation of a clone encoding a second dragline silk fibroin. Nephila clavipes dragline silk is a two-protein fibre. J Biol Chem 267 (27), 19320–19324. Sep 25.
Horan, R.L., et al., 2005. In vitro degradation of silk fibroin. Biomaterials 26, 3385–3393.
Huemmerich, D., et al., 2004. Novel assembly properties of recombinant spider dragline silk proteins. Current Biology 14, 2070–2074.
Huemmerich, D., et al., 2006. Processing and modification of films made from recombinant spider silk proteins. Applied Physics A 82, 219–222.
Iijuka, E., Itoh, H., 1997. International Journal of Wild Silkmoth & Silk 3, 37.
Iizuka, E., Kawano, R., Kitani, Y., Okachi, Y., Shimizu, M., Fukuda, A., 1993a. Indian Journal of Sericulture 32, 27.
Iizuka, E., Okachi, Y., Shimizer, M., Fukuda, A., Hashizume, M., 1993b. Journal of Sericulture 1, 1.
Iizuka, E., Okachi, Y., Shimizer, M., Fukuda, A., Hashizume, M., 1993c. Indian Journal of Sericulture 32, 175.
Iizuka, E., Vegaki, K., Takamatsu, H., Okachi, Y., Kawai, E., 1994. Journal of Sericultural Science of Japan 63, 64.
Iizuka, E., Teramoto, A., Lu, Q., Min, Si-sia, Shimizu, O., 1996. Journal of Sericulture Science of Japan 65 (2), 134–136.
Jin, H.J., Kaplan, D.L., 2003. Mechanism of silk processing in insects and spiders. Nature 424, 1057–1061.
Jin, H.J., Park, J., Valluzzi, R., Cebe, P., Kaplan, D.L., 2004. Bio-material films of *Bombyxmori* silk fibroin with poly ethylene oxide. Biomacromolecules 5, 711–717.
Jolly, M.S., Sen, S.K., Sonwalker, T.N., Prasad, G.K., 1979. Non-mulberry silks. In: Rangaswami, G., Narasimhanna, M.N., Kashivishwanathan, K., Sastri, C.R., Jolly, M.S. (Eds.), Manual on Sericulture. Food and Agriculture Organization of the United Nations, Rome, pp. 1–178.
Kaplan, D., et al. (Eds.), 1994. Silk Polymers: Materials Science and Biotechnology. American Chemical Society.
Kaplan, D.L., Mellow, C.M., Arcidiacono, S., Fossey, S., Senecal, K., Muller, W., 1997. In: Protein Based Materials. Birkhauser, Boston, pp. 104–107.
Kaplan, D.L., 2004. Silk. In: EPST, vol. 11, pp. 841–850.
Ko, F.K., Kawabata, S., Inoue, M., Niwa, M., Fossey, S., Song, J.W., 2005. www.web.mit.edu/course/3/3.064/www/slides/Ko_spider_silk.pdf.
Lewis, R.V., 1992. Spider silk: the unraveling of a mystery. Accounts of Chemical Research 25 (9).
Li, M., Ogiso, M., Minoura, N., 2003. Enzymatic degradation behavior of porous silk fibroin sheets. Biomaterials 24, 357–365.
Lombardi, S., Kaplan, D.L., 1990. The amino acid composition of major ampullate gland silk (Dragline) of *Nephilaclavipes*(Araneae, Tetragnathidae). Journal of Arachnology 18, 297–306.
Lucas, F., Shaw, J.T.B., Smith, S.G., 1960. Comparative studies of fibroins. I. The amino acid composition of various fibroins and its significance in relation to their crystal structure and taxonomy. Journal of Molecular Biology 2, 339–349.
Madsen, B., Vollrath, F., 2000. Naturwissenschaften 87, 148.

Madsen, B., Shao, Z., Vollrath, F., 1999. International Journal of Biological Macromolecules 24, 301.
Magoshi, J., mizuide, M., Magoshi, Y., 1979. Journal of Polymer Science 17, 515–520.
Mahadevappa, D., Halliyal, V.G., Shankar, D.G., Bhandiwad, R., 2001. Mulberry Silk Reeling Technology. Oxford and IBH publication Co., India.
Manohar Reddy, R., 2009. Innovative and Multidirectional Applications of Natural Fibre, Silk A Review. Academic Journal of Entomology 2 (2), 71–75.
Marsh, R.E., Corey, R.B., Pauling, L., 1955. An investigation of the structure of silk fibroin. Biochimica et Biophysica Acta 16, 1–34.
Matsumoto, A., Kim, H.J., Tsai, I.Y., Wang, X., Cebe, P., Kaplan, D.L., 2006. Silk. In: Hand Book of Fibre Chemistry. Taylor & Francis Group, LLC.
Mauney, J.R., Nguyen, T., Gillen, K., Kirker, C., Gimble, J.M., Kaplan, D.L., 2007. Engineering adipose-like tissue *in vitro* &*in vivo* utilizing human bone marrow and adipose-derived mesenchymal stem cells with silk fibroin 3D scaffolds. Biomaterials 28, 5280–5290.
Minagawa, M., 2000. In: Hojo, N. (Ed.), Structure of silk yarn, vol-I. Oxford & IBH Publishing Co. Pvt. Ltd., New Delhi, pp. 185–208.
Mukhopadhyay, S., Sakthivel, J.C., 2005. Journal of Industrial Textiles 35, 91.
Nadiger, G.S., Bhat, N.V., 1985. Journal of Applied Polymer Science 30, 4127–4136.
Scheibel, T., 2004. Spider silks: recombinant synthesis, assembly, spinning, and engineering of synthetic proteins. Microbial Cell Factories 3, 14.
Schulz, S., Toft, S., 1993. Branched long chain alkyl methyl ethers: a new class of lipids from spider silk. Tetrahedron 49 (31), 6805–6820.
Sehnal, F., 2008. Prospects of the practical use of silk sericins. Entomological Research 38, 1–8.
Sen, K., Murugesh Babu, K., 2004. Studies on Indian silk. I. Macrocharacterization and analysis of amino acid composition. Journal of Applied Polymer Science 92, 1080–1097.
Sheu, H.S., Phyu, K.W., Jean, Y.C., Chiang, Y.P., Tso, I.M., Wu, H.C., et al., 2004. Lattice deformation and thermal stability of crystals in spider silk. International Journal of Biological Macromolecules 34, 325–331.
Simmons, A.H., Michal, C.A., Jelinski, L.W., 1996. Molecular orientation and two-component nature of the crystalline fraction of spider silk. Science 271 (5245), 84–87.
Sponner, A., Unger, E., Grosse, F., Weisshart, K., 2005. Differential polymerization of the two main protein components of dragline silk during fibre spinning. Nature Materials 4 (10), 772–775.
Spring, C., Hudson, J., 2002. Silk in Africa. University of Washington Press, Seattle.
Syed, I.B., 2006. Spider Silks. Islamic Research Foundation International, Inc., 7102 W. Shefford Lane, Louisville, KY 40242–6462, USA. http://WWW.IRFI.ORG.
Van Beek, J.D., et al., 2002. The molecular structure of spider dragline silk: folding and orientation of the protein backbone. Proceedings of the National Academy of Sciences of the United States of America 99, 10266–10271.
Vepari, C., Kaplan, D.L., 2007. Silk as a biomaterial. Progress in Polymer Science 32, 991–1007.
Vollrath, F., Knight, D.P., 2001. Liquid crystalline spinning of spider silk. Nature 410, 541–548.
Warwicker, J.O., 1956. Transactions of the Faraday Society 52, 554–557.
Warwicker, J.O., 1960. Comparative studies of fibroins, The crystal structure of various fibroins. Journal of Molecular Biology 2, 350–362.
Work, R.W., 1977. Transactions of the American Microscopical Society 100, 1–20.
Xu, M., Lewis, R.V., 1990. Structure of a protein super fibre: spider dragline silk. Proceedings of the National Academy of Sciences of the United States of America 87, 7120–7124.

Wool as a high-performance fiber

14

K.R. Millington, J.A. Rippon
CSIRO Manufacturing, Geelong Technology Precinct, Waurn Ponds, Victoria, Australia

14.1 Introduction

The term "high-performance fibers" (HPF) usually refers to fiber applications outside their traditional role of providing fashionable clothing and basic furnishing textiles, such as rugs, carpets, and curtains. Some publications have used a somewhat narrower definition for HPF based on their physical and chemical properties, including high modulus high tenacity, high elasticity, high chemical, or thermal resistance (Hearle, 2001), which excludes natural fibers such as wool and cotton. However, wool is a unique fiber, having many desirable properties that synthetic fiber manufacturers are still unable to emulate. In particular, the handling and comfort properties of fine Merino wools, wool's moisture transport properties, and its ability to liberate heat when wetted out make wool a highly desirable premium fiber. In addition, it has a number of technical applications, in particular for flame-resistant safety apparel and interior textiles, for felts, antimicrobial medical textiles, use for thermal and sound insulation, filtration, and even in composite materials. Such applications are possible because of the many unique properties of protein fibers, and wool in particular, that are described in the following sections.

14.2 Structure and properties of the wool fiber

14.2.1 Fiber structure

The textile industry uses fibers obtained from a wide variety of animals, of which the wool from sheep is the most important (Rippon, 2013a; Christoe et al., 2003). The earliest sheep were covered in a brownish coat consisting of coarse fibers. Selective breeding has produced animals with finer wool and the cream color we know today. Wool is classified according to fiber length and diameter. Coarse wools, which generally range in diameter from 28 to 45 μm, are mostly used in interior textiles, such as carpets and upholstery. Fine wools (<25 μm) are used in apparel. The most important breed for producing fine wool is the Merino. This originated in Spain, from where it was introduced to Australia around 200 years ago, where the sheep were developed to produce wool with desirable attributes of fineness, length, luster, crimp, and color. Basic Merino types include strong (broad) wool 23–24.5 μm, medium wool 19.6–22.9 μm, fine wool 18.6–19.5 μm, superfine wool 15–18.5 μm, and ultrafine wool 11.5–15 μm.

Structure and Properties of High-Performance Fibers. http://dx.doi.org/10.1016/B978-0-08-100550-7.00014-0

Raw wool contains around 25−70% of impurities; these consist of wool grease, suint (residuals from perspiration), dirt, and vegetable matter, such as seeds and burrs. Wool grease consists of a mixture of fatty acids and esters; and suint is composed of potassium salts of fatty acids, plus phosphate, sulfate, and nitrogenous compounds. Wool grease, suint, and dirt are removed by scouring. In worsted processing, vegetable matter is removed by carding and combing, whereas on the woolen system it is removed by carbonizing with sulfuric acid.

Wool is a member of a group of materials known as α-keratins, because they contain proteins with an α-helical conformation (Mercer and Maltosy, 1968). Other keratins containing proteins with an α-helical conformation include horns and beaks. A characteristic of these hard keratins is a higher concentration of sulfur than is found in soft keratins, such as those in skin. The sulfur is mainly present in the form of cystine. Wool fibers grow from the bulbous base of follicles within the skin of sheep and growth is complete immediately above the bulb (Jones et al., 1998). At this point the process of keratinization commences and this is finished by the time the fiber emerges from the skin. Keratinization involves the formation of cystine residues containing disulfide crosslinks ($-CH_2-S-S-CH_2-$), formed from pairs of cystine residues ($-CH_2SH$).

Wool fibers consist of a complex mixture of approximately 170 different proteins (Zahn et al., 1980). These range in relative molecular mass from below 10,000 Da to greater than 50,000 Da (Gillespie, 1990; Lindley, 1977). The basic structural units of proteins are amino acids (Rippon, 2013a). Intact wool contains 20 amino acids, which have the general formula $NH_2CH(R)COOH$, where (R) is the amino acid side chain. Proteins are formed by the condensation of amino acids via their terminal amino and carboxyl groups, to produce secondary amide bonds (ie, peptide bonds; $-NHCH(R)CO-$). Linear polypeptides of high relative molecular mass are produced by multiple condensations. The side chains present in the amino acid residues of polypeptides can be aliphatic, aromatic, or other cyclic groups. They vary in size and chemical behavior and play an important role in both the physical and chemical properties of wool. The nonpolar (hydrocarbon) side chains of glycine, alanine, phenylalanine, valine, leucine, and isoleucine are of low chemical reactivity: whereas the hydroxyl groups of the polar side chains of serine, threonine, and tyrosine are chemically more reactive. The side chains that have the most influence on the chemical reactivity of wool are those containing acidic or basic groups. Acidic carboxyl groups are present in the residues of aspartic and glutamic acids; and basic groups are contained in the residues of histidine, arginine, and lysine (ie, imidazole, guanidine, and amino groups, respectively). The side chains in wool fibers contain approximately equal numbers of basic amino and acidic carboxyl groups. These groups are responsible for the ability of wool to combine with large amounts of acids and alkalis (Alexander and Hudson, 1963). They are also important in dyeing because of their interactions with anionic wool dyes (Rippon, 2013a). In an aqueous medium, the ionization of these groups gives rise to the amphoteric properties of wool. Thus wool carries a net positive charge below pH4 and a net negative charge above pH8. In the range pH4−8, both types of group are fully ionized and the net charge carried by the fiber is zero (the fiber is in the isoelectric state).

Wool reacts with a much larger range of chemicals than other textiles fibers. The three main types of reactive groups are peptide bonds, the side chains of some of

the amino acids, as discussed earlier, and disulfide crosslinks. The chemical reactivity of wool has been discussed in detail in various textbooks and reviews (Alexander and Hudson, 1963; Hinton, 1974; Maclaren and Milligan, 1981; Rippon and Evans, 2012). The reactivity of wool has led to the development of many industrial processes, for example, in the areas of shrinkproofing (Christoe et al., 2003; Rippon, 2008; Rippon and Evans, 2012), dyeing (Lewis, 1990; Christoe et al., 2003; Rippon and Evans, 2012), flame resistance (Benisek, 1976; Horrocks, 1986), and finishing (Taylor, 1985; Brady, 1997; Whewell, 1971), which are discussed later in this chapter.

The individual polypeptide chains in wool are held together by a variety of covalent crosslinks and noncovalent interactions. The most important covalent crosslink is the disulfide bond of cystine, which accounts for most of the sulfur in wool. Disulfide linkages can occur between either separate polypeptide chains or different parts of the same chain. These bonds are largely responsible for stabilizing wool fibers, particularly in the wet state (Zahn and Blankenburg, 1964). Cleavage and rearrangement of disulfide bonds is involved in important processes such as setting and shrinkproofing (Rippon, 2008, 2013a; Christoe et al., 2003; Rippon, 2008). Another type of covalent crosslink is the isodipeptide bond; these bonds are formed between the ε-amino groups of lysine and the β- or γ-carboxyl groups of aspartic or glutamic acid. Other bonds that contribute to the stabilization of wool are: hydrogen bonds between amide groups and other hydrogen donating and accepting groups: ionic interactions (salt linkages) between ionized carboxyl and amino groups: and hydrophobic interactions (sometimes called "hydrophobic bonds") between the nonpolar groups of alanine, phenylalanine, valine, leucine, and isoleucine. Both hydrogen bonds and ionic interactions contribute significantly to the physical properties of dry wool, but are progressively disrupted as wool absorbs water. Thus the contribution of salt linkages and hydrogen bonds to the physical properties of wet wool is less than it is for dry wool. Furthermore, because of the amphoteric nature of wool, discussed previously, the contribution of salt linkages is also dependent on pH. Even when the wool fiber is completely saturated, some of the interactions within the fiber are undisturbed. Unlike hydrogen bonds and salt linkages, hydrophobic interactions are not easily disrupted by water and make a significant contribution to the mechanical strength of wool even at high water content (Zahn and Blankenburg, 1964). They are important in the setting of wool and in the smooth-drying properties of fabrics (Christoe et al., 2003).

Although classified as a keratin, clean wool contains only (approximately) 82% of proteins that contain sufficient sulfur for them to be characterized as keratinous (usually regarded as more than 3% sulfur by mass). Approximately 17% of wool consists of proteins that are termed "nonkeratinous" because of their relatively low concentration of cystine (and hence lower crosslink density) compared with the true keratinous proteins (Baumann, 1979; Leeder, 1986; Feldtman et al., 1983; Feldtman and Leeder, 1984; Rippon and Leeder, 1986). The nonkeratinous proteins of wool are more labile and have a lower resistance to chemical attack than wool keratinous proteins. In addition to proteins, wool also contains approximately 1% by mass of nonproteinaceous matter, which consists of lipids plus a small amount of polysaccharide material. Both the nonkeratinous proteins and the lipids are not uniformly distributed throughout the fiber, but are concentrated in specific regions (Rippon, 2013a).

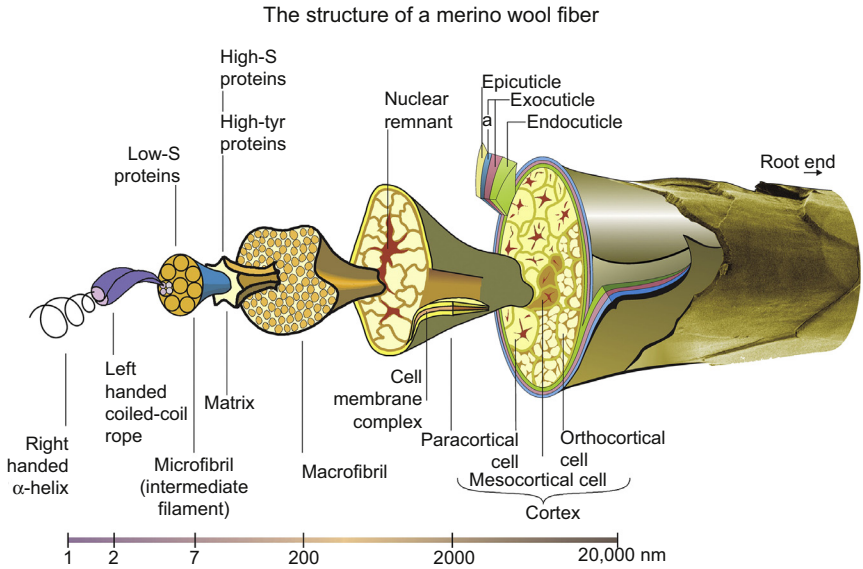

Figure 14.1 Schematic diagram of the structure and morphology of a Merino wool fiber. Courtesy of CSIRO.

In common with other mammalian fibers, wool is a biological composite consisting of regions that vary from each other in physical and chemical composition. The complex morphological structure of a fine wool fiber is shown schematically in Fig. 14.1.

Fine wool fibers contain two types of cells: external cuticle cells and those of the internal cortex (Rippon, 2013a; Jones et al., 1998). Coarse wool fibers (diameters >35 μm) often contain a third type of cell (medulla). These form a central core of cells along the fiber axis. Air-filled spaces between medullar cells improve the thermal insulation of the fiber for minimal weight. Cuticle cells are separated from the underlying cortex and cortical cells are separated from each other by the cell membrane complex. This component is a continuous region that extends throughout the whole cortex (Leeder, 1986).

Cuticle cells, or scales, which account for approximately 10% of the fiber mass, form a sheath around the cortex. Cuticle cells, which overlap both along and around the circumference of each fiber like tiles on a roof, can be seen clearly in the light or scanning electron microscope (Fig. 14.2). This structure makes wool unique among textile fibers. Cuticle cells are responsible for wool's ability to felt when agitated under moist conditions (Rippon, 2008) and for wettability and tactile properties (Leeder and Rippon, 1985).

Except where two cells overlap, the cuticle of fine wool is usually one cell thick and the overlap is approximately 15% (Rippon, 2008). Cuticle cells range in thickness from 0.3 to 0.5 μm and are approximately 30 μm long and 20 μm wide. Sections of cuticle cells show that they consist of an upper sulfur-rich region (the exocuticle) and an underlying region of lower sulfur content (the endocuticle) (Fig. 14.3).

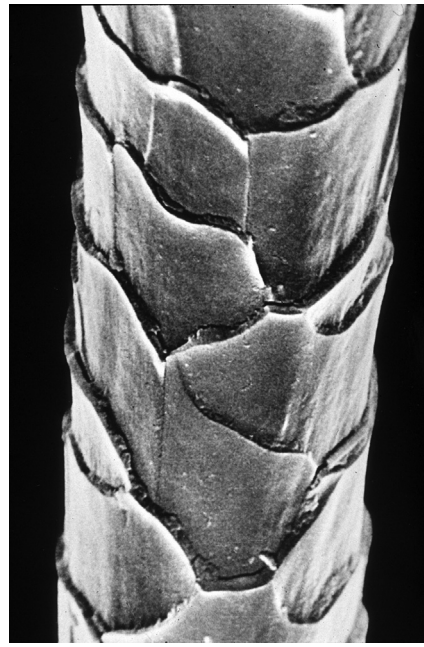

Figure 14.2 Scanning electron micrograph of a clean Merino wool fiber. Courtesy of CSIRO.

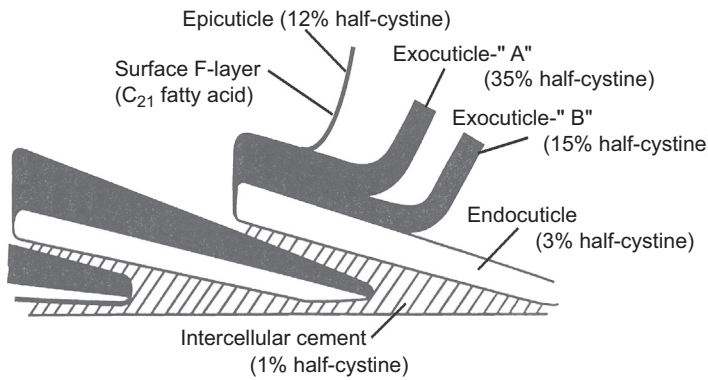

Figure 14.3 Schematic diagram of the cuticle structure of fine wool. Courtesy of CSIRO.

From chemical and physical analysis of the components of cuticle cells it has been concluded that the cuticle has a more amorphous structure than the rest of the fiber (Bradbury et al., 1965). It is also less extensible than the cortex because it has a higher concentration of cystine (and therefore a higher crosslink density). The lower extensibility results in a tendency for cuticle cells to crack when wool fibers are stretched

(Lehmann, 1941). Cracking does not, however, lead to detachment of cuticle cells from the cortex, which is very important for wool mechanical processing such as spinning and weaving (Ruetsch and Weigmann, 1995).

Each cuticle cell is surrounded by a chemically resistant membrane, which is approximately 2−7 nm thick and accounts for around 0.1% of the fiber mass (Bradbury, 1973). The underside of this component forms part of the cell membrane complex, which separates cuticle cells from the cells of the fiber cortex. On the exposed surface of cuticle cells, this resistant membrane is called the epicuticle. Although the epicuticle is proteinaceous, wool fibers from which grease has been removed are hydrophobic. This behavior is caused by a lipid subcomponent that is covalently bound to the surface of the epicuticle; this has been called the F-layer (Rippon, 2013a; Leeder and Rippon, 1985; Leeder et al., 1985a; Evans et al., 1985; Ward et al., 1993). This lipid component of the wool epicuticle consists mainly of an unusual fatty acid (18-methyl eicosanoic acid), which is believed to be bound to the surface by a thioester bond (Evans et al., 1985; Evans and Lanczki, 1997).

The cells of the internal cortex make up almost 90% of the wool fiber and are largely responsible for its mechanical properties. The complex structure of the cortex of a fine wool fiber is shown in Figs. 14.1 and 14.4.

Cortical cells, which are spindle shaped, are approximately 100 μm long and 3−6 μm wide (Bradbury, 1973). They are aligned along the fiber axis in a closely packed, overlapping configuration. Cortical cells consist of rod-like elements

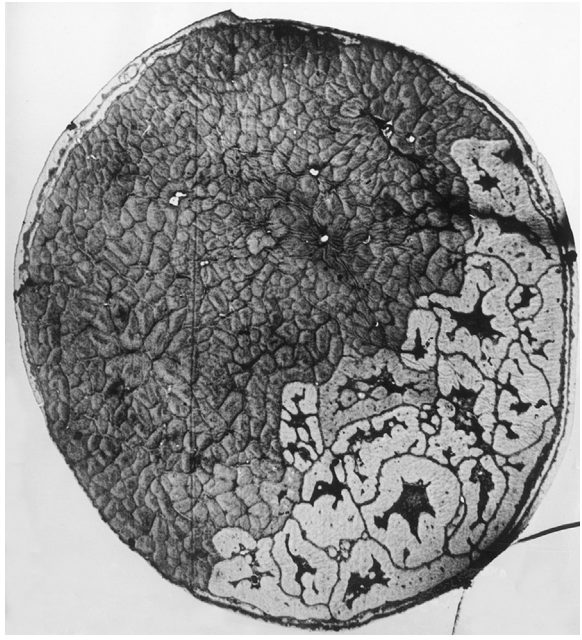

Figure 14.4 Transmission electron micrograph of a cross-section of 21 μm Merino wool fiber. Courtesy of CSIRO.

composed of highly ordered, crystalline proteins, called intermediate filaments (or microfibrils in the older literature). Some of the proteins in the intermediate filaments are helical and crystalline, and these give wool its elasticity, resilience, and good wrinkle recovery. These are embedded in a region (the matrix) containing relatively amorphous proteins that are richer in sulfur than the proteins of the intermediate filaments (Rippon, 2013a). The matrix proteins are responsible for the ability of wool to absorb a relatively large amount of water, compared with other fibers, without feeling wet (around 30% by mass of the dry fiber) (Leeder, 1984). The matrix proteins are also important in dyeing because they are where dyes are located when wool is dyed to equilibrium (Rippon, 2013b; Leeder et al., 1985b).

The intermediate filaments and matrix are organized into aggregates, called macrofibrils (Fig. 14.1) (Rogers, 1959). These are cylindrical units around 0.3 μm in diameter and ranging in length from 10 μm to the entire length of a cortical cell. It has been estimated that each macrofibril contains an average of 19 intermediate filaments (Fraser et al., 2003). Macrofibrils of greater diameter are believed to form from fusion of smaller macrofibrils. Macrofibrils are grouped together to form two main types of cortical cells (ortho and para). In fine Merino wools, these two types are present in approximately equal amounts and are arranged bilaterally. Coarser wools (diameter >25 μm) have a less distinct segmentation of the two types of cells and a small amount of a third type of cell (the mesocortex) with a structure between that of the ortho and para cells may also be present. One coarse wool type (Lincoln) has an annular arrangement, with an orthocortical core surrounded by paracortical cells.

The ortho- and paracortex differ in a number of ways (Kaplin and Whiteley, 1985). As discussed previously, wool contains around 17% of proteins with a sulfur content of less than 3%, the so-called "nonkeratinous" proteins. The ortho- and paracortical cells are characterized by the manner in which these nonkeratinous proteins are distributed within them. Paracortical cells are generally better outlined than those of the orthocortex with the nonkeratinous material being concentrated in prominent regions called nuclear remnants (Figs. 14.1 and 14.4). Where a mesocortex is present, this also contains nuclear remnants. In the cells of the orthocortex, nuclear remnants are less apparent because the nonkeratinous material is distributed more evenly between the macrofibrils, rather than being concentrated in specific regions. Thus the network of intermacrofibrillar material clearly defines the macrofibrils of the orthocortex compared with paracortical cells.

Ortho- and paracortical cells also differ both in the proportion of intermediate filaments and matrix material and in the packing arrangement of these within the macrofibrils. Although the proteins of the intermediate filaments are similar in both types of cell, there are some differences in the matrix proteins, with the paracortex containing proteins with the highest sulfur content. The ortho/para segmentation of wool is responsible for the highly desirable crimp of fine wools. In these wools, the orthocortex is always oriented toward the outside of the crimp curl. This results in the two segments twisting around the fiber in phase with the crimp (Rippon, 2013a). Fiber crimp gives wool fabrics bulkiness because it prevents fibers from packing closely together. Bulkiness in a fabric increases the amount of entrapped air, which enhances insulating properties.

The differences in the physical and chemical structure of the ortho- and paracortex influence the rate and extent of uptake of dyes and chemicals and are therefore important in wool processing. In general, the orthocortex is more accessible to reagents and more chemically reactive than the paracortex (Bradbury, 1973).

14.2.2 Fiber properties

Although other textile fibers may have individual properties that are better than those of wool, its complex physical and chemical structure, described earlier, gives wool a large range of useful properties that is not found in any other textile fiber (Leeder, 1984). Furthermore, advances in the knowledge of the fine structure and chemical composition of wool has led to methods of further improving its chemical and physical properties. Some of these will be discussed in the following sections.

14.2.2.1 Water sorption

Wool has a water-repellent surface, which arises from the waxy lipids that are covalently bound to the outer layer of the cuticle cells (F-layer). When this layer is removed the underlying proteinaceous surface is hydrophilic and easily wetted (Leeder and Rippon, 1985). Despite its hydrophobic surface, wool is a hygroscopic material that absorbs or desorbs large amounts of water with changes in the surrounding relative humidity. In common with dyes and chemicals, water probably enters and leaves wool fibers via the cell membrane complex, which extends to the surface between overlapping cuticle cells and extends throughout the whole fiber between the internal cortical cells. Sorbed water is associated with the amorphous regions of the fiber matrix, in particular with polar side chains and peptide groups (Watt, 1980). The amount of water sorbed by wool is called "regain," which is the mass of water expressed as a percentage of the dry mass of the fiber. The water sorption/desorption isotherm of wool shows a pronounced hysteresis; this is around 2% higher on the desorption curve than on the absorption curve (Watt and Darcy, 1979). The moisture regain of wool at saturation is around 33%, which is considerably higher than that of other textile fibers (Morton and Hearle, 1993). When wool absorbs water, heat is liberated (heat of wetting) (Haly and Snaith, 1973). It has been calculated that when a 1 kg wool garment at 20°C and 25% relative humidity is moved into an environment at 10°C and 95% relative humidity, 40 kJ of heat is released (Leeder, 1984). The heat is generated progressively as the wool absorbs moisture. This reduces discomfort when a person wearing wool moves from a dry indoor environment to a cold damp atmosphere outdoors. This property gives wool an important advantage over other textile fibers.

Sweat accumulating on the skin underneath a garment causes discomfort for the wearer. This is reduced if the garment is made from hygroscopic material, which can sorb moisture and transport it away from the skin (Barnes and Holcombe, 1996).

At a given relative humidity, wool has similar moisture sorption to human skin. It also has the ability to absorb up to 33% of its mass without feeling wet. These properties enable wool garments to act as an excellent moisture buffer during physical activity, by transporting perspiration away from the skin and keeping the moisture content around a level consistent with wearer comfort. This property has been exploited in a

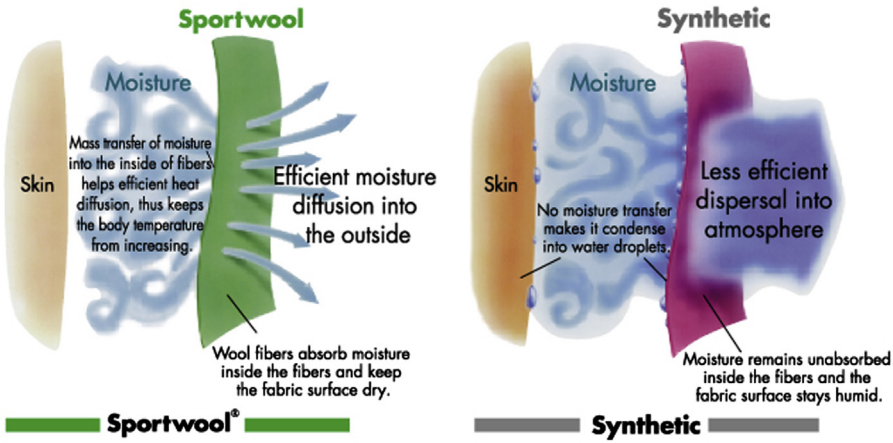

Figure 14.5 Schematic drawing showing the principle of moisture transport away from the skin by Sportwool fabric.
Courtesy of Australian Wool Innovation.

wool-containing fabric designed by CSIRO (Australia) for use in active sportswear (Sportwool) (CSIRO, 2010; Collis, 2002), as shown schematically in Fig. 14.5. The original Sportwool fabric had a double jersey knitted structure with hydrophilic shrink-resist treated wool on the inside and hydrophobic synthetic fiber (polyester) on the outside.

14.2.2.2 Tensile properties

The tensile properties of wool have been explained in terms of a two-phase composite model, involving the water-resistant crystalline regions of the intermediate filaments embedded in a relatively hydrophilic matrix (Wortmann and Zahn, 1994; Hearle, 2002). The arrangement of the intermediate filaments parallel to the longitudinal fiber axis results in wool fibers being anisotropic. As the state of the fiber is changed from dry to wet the longitudinal modulus decreases threefold (Huson, 1998), whereas the torsional modulus, which depends on the stiffness of the amorphous matrix, decreases by a factor greater than 10 (Mitchell and Feughelman, 1960).

The longitudinal load–extension curves of wool show three distinct regions, as shown in Fig. 14.6 (Hearle, 2002). After the initial removal of fiber crimp, the first region AB is near-linear, up to about 2% strain, called the preyield or Hookean region. For wet fibers, this is generally associated with stretching of the α-helices within the intermediate filaments. With decreasing regain the matrix phase becomes increasingly more important in determining load–extension behavior. In the yield region BC, which occurs between 2% and 30% extension, the α-helices progressively unfold to form a β-pleated sheet configuration, similar to that of silk and feathers. Very little increase in load is observed during this stage and complete recovery is still possible, provided the fiber is allowed to relax in water. Beyond 30% extension, the

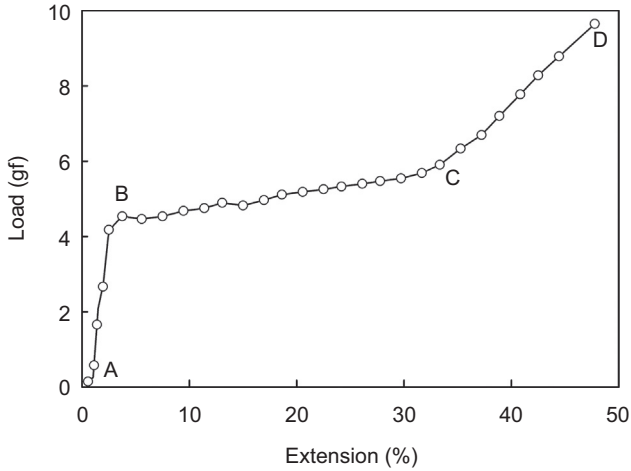

Figure 14.6 Load−extension curve of a Corriedale wool fiber in water at 20°C. AB is the Hookean region, BC the yield region, and CD the postyield region.
Redrawn from Hearle, J.W.S., 2002. Physical properties of wool. In: Simpson, W.S., Crawshaw, G.H. (Eds.), Wool: Science and Technology. Woodhead, Cambridge, UK, pp. 80−129.

fiber is in the postyield region; it becomes increasingly stiffer and eventually breaks. This is believed to be caused by resistance to the unfolding of the intermediate filaments (Wortmann and Zahn, 1994) together with the rubber-like properties of the matrix (Hearle, 2000). The modulus of the fiber in the preyield region is both time and water dependent, whereas the equilibrium modulus (1.4 GPa) is independent of water content and corresponds to the modulus of the crystalline phase (Feughelman and Robinson, 1971). The time, temperature, and water dependence can be attributed to the viscoelastic properties of the matrix phase.

The elastic recovery of wool after deformation has a practical importance because it helps wool fabrics to maintain their shape and bulk over long periods of use. In this respect, wool is superior to other natural fibers used in clothing, such as cotton and linen. Resilience is also important in nonapparel products, such as carpets, because it helps to prevent flattening during use.

14.2.2.3 Setting

The setting operation is used to remove stresses introduced into yarns and fabrics during manufacture. These stresses would otherwise cause twisting and snarling of yarns during winding and warping, or knitting, and distortion of fabrics during hot, wet treatments, for example, in dyeing. Yarns are set by steaming and fabrics either by steaming or immersion in hot water. Fabrics are also usually set in a flat state at the end of a finishing sequence to give dimensional stability and to improve the handle (Brady, 1997; Rippon and Evans, 2012). Garments are set to their required shape by steam pressing; this is also used to insert pleats and creases.

Wool setting is unique in that it can involve two types that differ on the basis of stability. These are temporary (sometimes called cohesive) set and permanent set.

Set that is retained after 15 min in water at 70°C is called permanent set and set that is removed under these conditions is temporary set. Wool that has been permanently set will be stable to most of the conditions encountered by a garment during wear and cleaning, whereas temporary set will be lost under these conditions. In fact, immersion in water at room temperature is usually sufficient to remove temporary set from wool.

The stress relaxation that is involved in setting occurs at the molecular level; in this the protein structure is rearranged and stabilized in the new configuration by various types of chemical bonds and interactions. At ambient temperature and water content, wool is below its glass transition temperature and the matrix is glass-like. When fiber deformation occurs under these conditions, stress relaxation is slow. When heated, however, the matrix becomes more rubbery, which allows stress relaxation to occur at a faster rate. When the fibers are cooled and dried in the deformed state, they will maintain their new shape. When no rearrangement of chemical bonds occurs, the new shape is stabilized via hydrogen bonds and ionic interactions, such as those discussed in Section 14.2.1. This set is temporary because it is released when the matrix is again made rubbery by wetting and/or heating.

Permanent set is more stable than temporary set because it also involves the rearrangement of covalent bonds, in particular the disulfide crosslinks that are present between the peptide chains. This occurs by a mechanism of thiol/disulfide interchange (Fig. 14.7) (Burley, 1955). The rate of permanent setting is increased by factors that

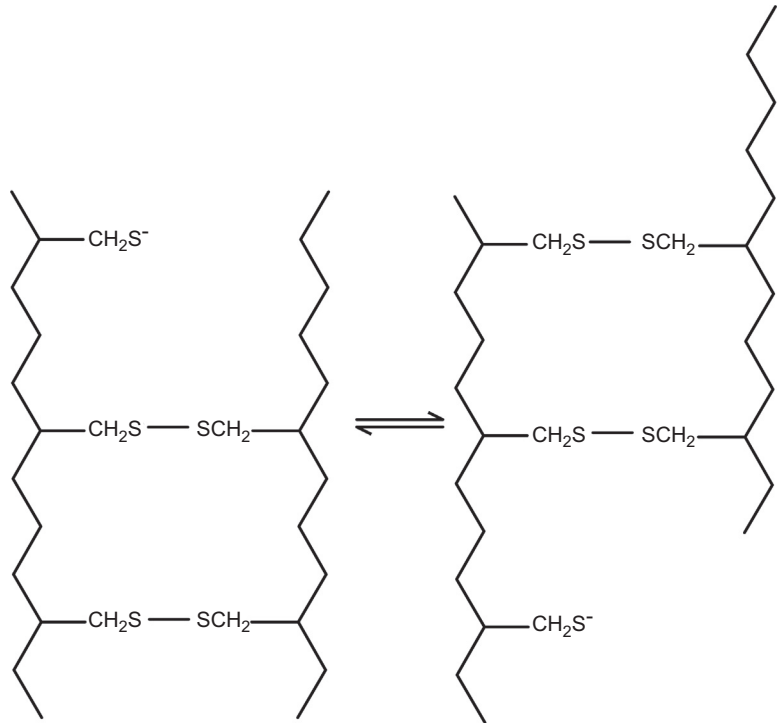

Figure 14.7 Thiol−disulfide interchange reaction involved in the setting of wool.

facilitate the fission of disulfide bonds, for example, by raising the pH and with a reducing agent. Increasing the temperature and moisture content (eg, in steaming) also increases the rate of setting by promoting the mobility of the protein chains making it easier for them to adopt lower energy configurations. At higher temperatures, a contribution to stabilization of the new structure is also made by rearrangement of hydrophobic interactions between the hydrocarbon side chains of valine, phenylalanine, and leucine. These hydrophobic interactions are not readily disrupted by water (Zahn and Blankenburg, 1964; Asquith and Puri, 1968).

During the setting of wool under alkaline conditions with a reducing agent, in addition to rearranging, some of the disulfide bonds undergo reactions that result in the formation of new types of crosslinks, namely, lanthionine and lysinoalanine bonds (Ziegler, 1965; Rippon and Evans, 2012). These bonds are more stable than the disulfide crosslinks and make an important contribution to the stability of permanently set wool.

Important industrial processes for setting wool include crabbing, which involves treating a roll of fabric in boiling water for several minutes and then cooling it rapidly in cold water. This method gives a level of set of 40−85%. Higher productivity is obtained with continuous methods of crabbing, but these give lower levels of set. As part of the finishing operation, fabrics are set by "decatizing." In this the fabric is interleaved with a cotton or cotton/synthetic wrapper and wound onto a perforated drum. Steam is blown through the roll for up to 10 min, after which the fabric is cooled with a stream of cold air. This method gives a level of permanent set of up to 40%. Where required, higher levels can be obtained by steaming the batch in an autoclave for 3−5 min at 120−130°C.

An important process that uses reducing agents to insert permanent creases and pleats in wool garments is the Siroset Process developed by CSIRO (Farnworth and Delmenico, 1971). In this, garments are sprayed with a reducing agent, such as monoethanolamine bisulfite and then pressed using a steam/bake cycle of around 60 s.

14.2.2.4 Thermal properties

The crystalline α-helical polypeptide chains within the intermediate filaments occupy around 70% of the dry volume of wool (Feughelman, 1989). This phase melts irreversibly at a temperature that is both time and regain dependent (Haly and Snaith, 1967). Normal dyeing and finishing procedures do not melt wool, but care has to be taken when processing blends of wool with synthetic fibers that may require higher temperatures than those used for pure wool. The amorphous matrix phase is relatively highly crosslinked because it contains a higher concentration of cystine than the intermediate filaments. In common with other materials containing an amorphous phase, wool fibers exhibit a glass transition temperature (T_g) (Wortmann et al., 1984). Water acts as a plasticizer and lowers the T_g from a value of 170°C for the dry fiber to below zero when fully saturated. Creases can be temporarily set into wool by deforming fibers at temperatures above the T_g and then fixing the creases by changing the conditions to below the T_g; for example, by heating and cooling, wetting and drying, or a combination of both, such as occurs in steam pressing.

14.2.2.5 Wrinkling and wrinkle recovery

Until the development of polyester, wool had better wrinkle recovery properties than other textile fibers, including cotton, silk, linen, nylon, and viscose rayon. The wrinkle recovery properties of wool are controlled by the tensile and thermal behavior discussed earlier. Of particular importance are the highly elastic properties of the crystalline α-helical peptides of the intermediate filaments and the viscoelastic properties of the fiber matrix. Whereas the elastic components deform and recover very quickly, the viscous regions of the matrix lag behind in both deformation and also in recovery following removal of the deforming force. Wrinkle recovery is poorer when wrinkles are inserted under conditions above the T_g and when recovery occurs below the T_g. This is likely to occur under hot and humid conditions where local wetting (in the form of perspiration) and wrinkle insertion occur simultaneously. When the fabric moves away from the skin, there is insufficient time for the wrinkles to recover before the fabric dries. Loss of moisture causes the T_g of the fabric to rise to a temperature above that of the environment and the wrinkles remain in place. The advantage of wool over other fibers is that wrinkles inserted during wear are easily removed. This can be achieved by hanging a garment overnight in a humid atmosphere (eg, a bathroom). These conditions enhance relaxation of the matrix, thus allowing recovery of the elastic helical proteins.

It is worth noting that when required for some textile products, the excellent wrinkle recovery of wool can be further improved by blending wool with polyester.

14.2.2.6 Friction and felting properties

Wool fibers feel smoother than most other textile fibers and are unique in displaying a directional frictional effect (DFE). This property is caused by the presence of the cuticle cells, because descaled wool does not show a DFE (King, 1927). In the fleece of a sheep, cuticle cells point from the root of a fiber to the tip, which results in the surface friction being greater when rubbed against the scales (tip to root) than when rubbed with the scales (root to tip). The DFE helps to keep the fleece clean by assisting in repelling dirt (Fraser et al., 1980).

The DFE is also responsible for wool's unique property among textile fibers of felting. This occurs when under the action of an applied force, the DFE causes fibers in a yarn, fabric, or garment to migrate preferentially in one direction (Rippon, 2008). Although felting can occur in the dry state, it occurs more readily in the presence of water (eg, in laundering).

It was originally believed that felting occurs by interlocking of the scales involving a ratchet mechanism (Alexander and Hudson, 1963). This mechanism would require the scales to be regularly spaced and for the fibers to be parallel over most of their length, neither of which is the case (Makinson, 1979). Furthermore, felted wool samples have never been found to contain fibers with interlocked scales. A ratchet mechanism, however, can produce the DFE as a result of interaction between the tips of scales and asperities on other scales. When fibers are drawn against the scales, the fiber tips deform and then recover as they slide past the asperities. When fibers are drawn in the with-scale direction, scales on adjacent fibers are flattened on the surface and the fibers slide past each other.

In addition to the DFE, some other properties also influence the rate and extent of felting of wool. These are fiber diameter, length, crimp, and elasticity (Rippon, 2008; Pierlot, 1997). In general, finer fibers felt more readily than coarse wools (Speakman and Stott, 1931). Elasticity is also particularly important because it affects the extension and contraction of the fibers under an applied force, with felting increasing with the ease of extensibility (Mitchell and Feughelman, 1967; Speakman et al., 1933). Factors that affect extensibility, such as liquor temperature and pH, have a marked influence on felting ability. Although the felting of wool during washing is regarded as a disadvantage, compared with other textile fibers, this property has been utilized in the manufacture of products that cannot be made from other fibers (Marsh, 1966; Moncrieff, 1953; Nason, 1965). Thus controlled felting (called milling or fulling) has been used since ancient times to increase the density of fabrics by closing up the structure. It is used in the manufacture of wool products such as blankets, woven and knitted garments, hats, billiard cloths, papermaking felts, and piano hammers (Stulov, 1995, 2004). When a wool product has been milled to the required level, further felting can be prevented, for example, during laundering, by application of a shrinkproofing treatment, as described in Section 14.3.1.

14.3 Fiber modification to improve performance

14.3.1 Shrink-resist treatments

Felting shrinkage can be deceased or prevented by overcoming the effect of the DFE for wet fibers. This can be done by completely removing the scales with an abrasive (Speakman and Whewell, 1945), by treatment with an oxidizing agent (Hojo, 1985), or an enzyme (Levene and Shakkour, 1995). Descaling reveals the underlying cortex, which is smoother and more lustrous than the surface of untreated wool. The treatments, however, can produce up to a 10% weight loss and weakening of the fiber. Consequently, commercial shrinkproofing methods do not involve complete removal of cuticle cells.

The most widely used commercial shrinkproofing treatments fall into three categories: namely, chemical treatments, polymer-only treatments, and chemical treatment followed by application of a polymer. The highest level of shrinkproofing that is required for machine washable products is difficult to achieve with a chemical treatment on its own (Kettlewell et al., 2015). It can, however, be obtained on garments and fabrics by a treatment involving application of a polymer, or on wool tops and garments by a chemical treatment followed by application of a polymer. The various methods operate by different mechanisms.

14.3.1.1 Chemical treatments

Chemical treatments are also called “degradative” treatments, because they involve some chemical attack on the fiber. Although the conditions used for chemical treatments have been optimized in an attempt to restrict reaction to the fiber surface,

some modification of the whole fiber usually occurs. In the past, oxidizing agents, reducing agents, alkalis, and corona or plasma discharge have been used commercially (Rippon, 2008; Rippon and Evans, 2012). More recently, the most common types of chemical treatments use oxidation, either with chlorine or permonosulfuric acid (PMS), also called Caro's acid ($HOOSO_3H$). Chlorination decreases felting shrinkage by oxidizing disulfide bonds in the highly crosslinked exocuticle to cysteic acid $\left(-SO_3^-\right)$ residues, and also by breaking some peptide bonds at tyrosine residues. These reactions generate peptide fragments that are retained within the epicuticular membrane. The fragments are osmotically active and cause the scales to swell and become softer in water (Makinson, 1979; Rippon, 2008). This produces a large increase in the friction in the with-scale direction and a smaller increase in the friction against the scales. The net effect is to decrease the DFE, which reduces the tendency for preferential migration of fibers, and therefore felting. In addition to its effect of swelling the cuticle cells, chlorination also removes a large proportion of the covalently bound surface lipids (F-layer) (Negri et al., 1992). Removal of surface lipids contributes to shrink resistance by increasing interfiber friction in both the with- and against-scale directions. Lipid removal is, however, responsible for the harsh handle of chlorinated wool (Leeder and Rippon, 1985). Both sodium hypochlorite and chlorine gas dissolved in water can be used for chlorinating wool (Kettlewell et al., 2015). Although used in the continuous treatment of wool tops, garments and fabrics, an uneven treatment can occur because of very rapid reaction between wool and chlorine. This is avoided by the use of dichloroisocyanuric acid (DCCA) as the chlorinating agent. The release of chlorine from this chemical can be controlled by careful adjustment of pH and temperature.

Treatment with PMS has been used to decrease the felting shrinkage of wool. It reacts with the fiber more slowly than chlorine, making it more suitable for garment treatment (Rippon, 2008; Rippon and Evans, 2012). When used alone it produces little change in either surface friction or shrink resistance. A post-treatment with either sodium sulfite or bisulfite, however, lowers the DFE because of an increase in with-scale friction, with little change in the friction against the scales. In contrast to chlorination, which produces cysteic acid residues, PMS followed by a sulfite or bisulfite after-treatment produces Bunte salt residues $\left(-SSO_3^-\right)$ in the exocuticle. Furthermore, unlike chlorination, PMS treatment does not break peptide bonds to produce the osmotically active peptides responsible for the greater swelling of the cuticle of chlorinated wool. Moreover, PMS treatment does not remove a significant amount of the lipids of the F-layer. It has, therefore, a softer handle than chlorinated wool, but PMS is far less robust than chlorination as a commercial shrinkproofing treatment, particularly for superfine and ultrafine wools.

14.3.1.2 Polymer-only treatments (fabrics)

Polymers are used extensively to decrease the felting shrinkage of woven and knitted fabrics. They are usually applied by a pad-dry method. The most important group of polymers are based on a poly(propylene oxide) backbone with reactive groups that can undergo self-crosslinking reactions during the drying step following application to the

wool. The most commonly used polymer in this group contains carbamoyl sulfonate groups $\left(-NHCOSO_3^-\right)$, for example, Synthappret BAP (Tanatex). Another important group of polymers used on fabrics are silicone elastomers, for example, DC-109 (Dow Corning). The poly(propylene oxide)-based polymers overcome the DFE by forming interfiber bonds (called spot welds) (Rippon and Rushforth, 1976), which prevent the fibers from migrating during washing. Silicone polymers, however, have a lower surface energy than the former group and spread on untreated wool to form a continuous layer on the fiber surface, joining two or more fibers together. Silicone elastomers are not as effective as polycarbamoyl sulfonates.

14.3.1.3 Chemical treatment plus polymer (garments)

Although treatment by oxidation with either chlorine or PMS gives a level of shrink resistance that is usually adequate for woven goods, it is insufficient to meet the higher demands of machine washability now required for knitted garments. This can, however, be achieved by treating the garments with a low-level oxidative treatment, followed by the application of a polymer. The most effective treatment is carried out with DCCA. This increases the surface energy of the wool and makes it more wettable by removing the F-layer surface lipids and by oxidizing cystine in the exocuticle to cysteic acid residues. The polymers used are cationic and are attracted to the fiber surface by the anionic cysteic acid residues. Several polymers are used, with the most common one being a polyamide/epichlorohydrin condensate (Hercosett 125; Hercules Chemical Co.) (Kettlewell et al., 2015; Rippon, 2008). The chemical changes to the fiber surface produced by chlorination raise the surface energy and enable the polymer to spread evenly. During curing, the polymer self-crosslinks and also reacts with thiol and amine groups near the fiber surface. The cured polymer acts by a mechanism that involves fiber−fiber bonding and scale masking via fiber encapsulation. The latter occurs because Hercosett polymer swells in water to around five times its dry volume. Thus an application level of 2% on mass of wool produces a swollen layer that is thicker than the height of cuticle cells on 20 μm wool fibers (0.5 μm) (Makinson and Lead, 1973).

PMS can also be used as an alternative to DCCA for the pretreatment step. PMS is, however, not as versatile as DCCA because fewer polymers are suitable for use following this treatment.

14.3.1.4 Chemical treatment plus polymer (top treatment)

Most machine washable products are made from wool that has been continuously treated in top form by a process developed by CSIRO and the International Wool Secretariat (Connell, 2003; Kettlewell et al., 2015). It is carried out on specialized equipment in many countries around the world. Parallel slivers of wool are treated at 5−10 m/min by the following steps:

acid chlorination → antichlor → neutralize → rinse →
polymer → softener → dry

A detailed description of the treatment conditions and machinery used for this method has been recently published (Kettlewell et al., 2015).

Polymers that rely on fiber−fiber bonding are unsuitable for application on wool tops because the bonds would be broken during subsequent processing. The most commonly used polymer for the continuous treatment of tops is the polyamide/epichlorohydrin resin (Hercosett 125), discussed previously. In this method, most of the shrink-resist effect is caused by the effect of the chlorination step. The function of the resin is to raise the level of shrink resistance to meet the requirement for full machine washability. The polymer spreads readily on chlorinated wool and encapsulates the fibers. It decreases felting mainly by masking the scales, with some contribution from increased adhesion between fibers from the swollen polymer (Makinson and Lead, 1973). Any fiber−fiber bonds that are formed in the treatment are broken during processing, but this does not affect the level of shrink resistance obtained.

14.3.2 Dyeing

In common with other textile fibers, most wool products are dyed. The majority of dyes used to color wool are sodium salts of aromatic anions. They range in molecular weight from around 300 Da to around 900 Da, depending on the type of dye. Water solubility is provided by sulfonic acid groups, or, in a few cases, by carboxyl or nonionic groups (Christoe et al., 2003; Rippon, 2013b). Wool dyes are divided into a number of groups: these include acid dyes, chrome dyes, premetallized dyes, and reactive dyes. These classifications are based on the dye structure, molecular weight, and method of application. An important advantage of wool is that the range of dye types available enables dyes to be selected for particular applications: for example, levelness of uptake on different substrates, brightness of shade and fastness to light and washing. Wool is usually dyed by batch methods from acidic aqueous liquors as loose fiber, top, yarn, fabric, or garments. In a typical dyeing cycle, the dyebath temperature is increased slowly from around 40°C to 98−100°C, where it is held for a time ranging from 30 min to over 2 h, depending on the type of dye and depth of shade (Rippon and Evans, 2012). Equilibrium exhaustion of dye from the dyebath is much higher for wool than for cellulosic fibers (typically >98% for wool, compared with 60−70% for cotton). Furthermore, because dyes exhaust readily onto wool, large amounts of electrolytes and other chemicals are not required to promote exhaustion. This contrasts with cellulosic fibers, which require very high concentrations of an electrolyte, such as sodium sulfate to promote exhaustion (Rippon and Evans, 2012). This makes the coloration of wool a relatively environmentally-friendly procedure.

As was discussed earlier, wool is an amphoteric material and in an acidic dyebath it carries a net positive charge. This provides an electrostatic attraction for the negatively charged dye anions and is responsible for the transfer of dye molecules onto the fiber (Rippon, 2013b). This mechanism enables wool dyers to obtain an even dye uptake by controlling the rate of dye sorption by changing the dyebath pH. The rate of dye uptake can also be varied by the addition of specific reagents that compete with the anionic dye molecules for the cationic groups in the fiber. Although ionic interactions are important in attracting dye molecules to the fiber in the early stages of dyeing, other

types of interaction, such as van de Waals' forces and hydrophobic interactions, are responsible for the affinity and wetfastness properties of dyed wool (Rippon, 2013b). Unlike other fibers, wool does not behave as a homogeneous cylinder that takes up dye uniformly along the surface. The mechanism of wool dyeing is determined by the complex morphological structure of the fiber. It is now established that for wool with an intact cuticle, the dye molecules enter the fiber via the cell membrane complex at the junctions where the cuticle cells overlap (Fig. 14.3) (Leeder et al., 1985b; Rippon, 2013b). They then diffuse along the cell membrane complex and other nonkeratinous regions, from where they progressively transfer into the cortical cells, where they are finally located in the regions containing the sulfur-rich hydrophobic matrix proteins surrounding the intermediate filaments. At equilibrium, dye is also located in the A-layer of the cuticle. Equilibrium within the fiber is not usually established until sometime after the dyebath appears to be exhausted; this is the reason why a prolonged time at a high temperature is required to produce dyed wool with good fastness properties (Rippon, 2013b). If dye largely remains in the nonkeratinous regions, it can rapidly diffuse out of the fiber, thus giving poor wetfastness properties. Reactive dyes contain groups that form covalent bonds with wool proteins. They may, therefore, show a somewhat different distribution inside the fiber and may be present in the nonkeratinous regions to a greater extent than their nonreactive analogs. However, because they are bound to the wool, this does not affect their overall fastness properties (Rippon, 2013b).

When wool is dyed at the boil, some damage to the fiber can occur. This can cause yellowing and weaken the fibers (Rippon et al., 1995). By using a special auxiliary (Valsol LTA-N, now called Neargal LT-WD: Nearchemica), wool can be dyed at temperatures below the boil (typically 85−90°C). Satisfactory dyeings are produced with considerably less yellowing and fiber damage compared with wool dyed at the boil.

14.3.3 Stretching to reduce mean fiber diameter (OPTIM)

Changing the configuration of wool by permanent setting has been used to produce a new textile fiber, OPTIM Fine (Phillips and Warner, 1994; CSIRO, 2011; Bhoyro et al., 2001). OPTIM Fine is manufactured by simultaneously stretching and setting, on specialized equipment, wool fibers that have been pretreated with an aqueous solution of a reducing agent (eg, sodium bisulfite). The fibers are prevented from slipping during the whole operation by using false twist to maintain cohesion within the assembly. The fibers are then permanently set in the extended configuration by steaming. Stretching by 40−50% decreases the diameter of 19 μm wool fibers to around 15−16 μm. Stretching and setting wool by this amount changes the intermediate filaments in the cortex from an α-crystalline helical structure to a β-pleated sheet, similar to the structure of silk (Bendit, 1960). The false twist applied to prevent fiber slippage imparts a large transverse force to the assembly. This changes the almost circular cross-section of wool to an irregular shape with a high proportion of flat surfaces (Fig. 14.8). This change in the shape of the fiber surface is responsible for the high luster of OPTIM Fine compared with the parent wool. OPTIM Fine fibers are also stronger than those of the parent wool and are suitable for making fine yarns (either

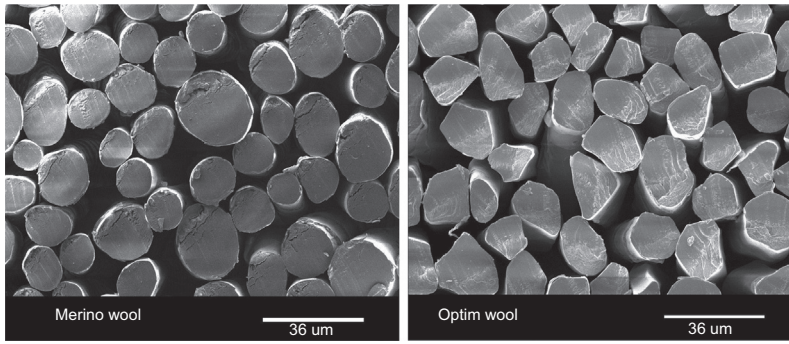

Figure 14.8 Cross-sections of wool and OPTIM Fine fibers.
Courtesy of CSIRO.

alone or in blends with silk, cashmere or alpaca) that are used for the manufacture of high-value fabrics where softness, luster, and lightness are important.

Another textile product made from wool can also be produced on the equipment used to manufacture OPTIM Fine, namely, OPTIM Max (Bhoyro et al., 2001). Whereas OPTIM Fine fibers are permanently set, those of OPTIM Max are held in a stretched configuration by cohesive set. This is done by omitting the sodium bisulfite reducing agent and also decreasing the steaming time. When yarns made from a blend of OPTIM Max and unstretched wool are relaxed in hot water, the OPTIM Max fibers contract by around 25%. The retracted fibers cause the untreated wool fibers in the blend to buckle. This increases the volume of the yarn and results in an increased cover factor in knitted products.

14.3.4 Bleaching to improve whiteness

Cotton and most synthetic textile fibers contain very few chromophores that absorb visible light, and therefore they appear very white and exhibit high reflectance across the entire visible range (750−400 nm). However, wool and other protein fibers (including silk) contain traces of natural yellow chromophores of unknown origin, and yellow protein oxidation products, which also contribute to the familiar off-white, cream color of wool. The presence of yellow chromophores has been demonstrated by comparing the UV−visible absorption spectrum of wool with its constituent UV-absorbing amino acids (Nicholls and Pailthorpe, 1976). Diffuse reflectance spectroscopy studies also suggest that the amino acid residues that absorb in the near-UV, tryptophan, tyrosine, and in particular cystine in the solid state may tail into the visible region and contribute to absorption of visible light (Millington, 2012).

When wool products in bright whites and pastel shades are required, the wool needs to be bleached to remove these yellow chromophores. There are several reviews on the bleaching of wool (Duffield, 1996; Duffield and Lewis, 1985; Millington, 2013). It is bleached with hydrogen peroxide, usually using a 0.5−1% w/v solution at 60°C for at least an hour at pH 8.5−9 in the presence of a suitable stabilizer and metal chelator. The active bleaching species is the perhydroxy anion −OOH, which oxidizes many

of the chromophores, rendering them colorless. However, some chromophores persist in wool and the efficiency of wool bleaching compared with cotton and other fibers is low. To maximize the achievable whiteness on wool it is necessary to carry out a double bleaching operation, where hydrogen peroxide bleaching is followed by reductive bleaching, most commonly with sodium hydrosulfite ($Na_2S_2O_4$). However, even after double bleaching, some residual yellowness persists.

It is possible to significantly improve the whiteness of bleached wool by applying a fluorescent whitening agent (FWA). This is usually done by adding the FWA to the reducing bleach bath during double bleaching. The FWA absorbs UVA wavelengths and emits blue fluorescence, which compensates for the residual yellowness of the bleached wool. Commercial FWAs for wool are based on sulfonated stilbenes, distyrylbiphenyls (DSBPs), or pyrazoles.

14.3.5 Photostabilization

The photostability of wool and silk is poor compared to cotton and synthetic apparel fibers. Much research has been done on this problem since the 1960s and there are several reviews on the photoyellowing of wool and its mechanism (Millington, 2006b,c, 2009, 2013). The UV wavelengths present in sunlight cause rapid photoyellowing of bleached and FWA-treated wool, particularly if the wool is wet after laundering, as shown in Fig. 14.9. In common with most other polymers and biomaterials,

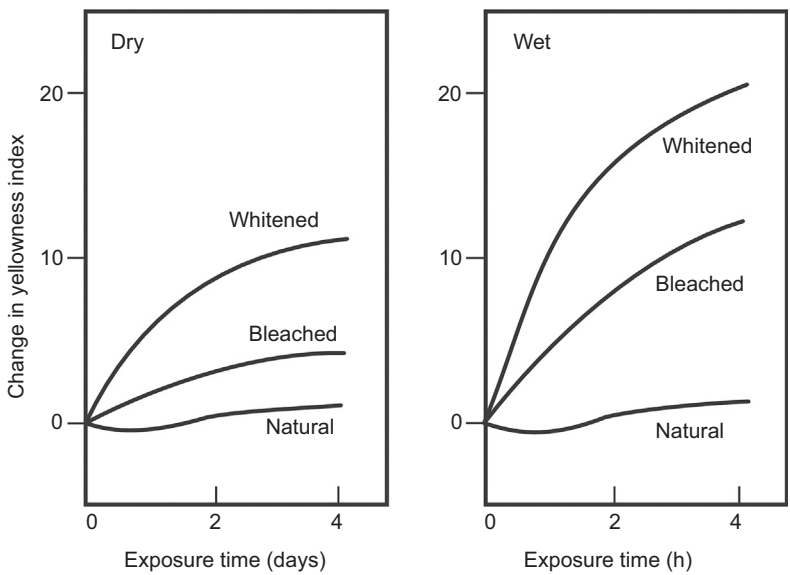

Figure 14.9 Photoyellowing rates of dry and wet wool fabrics exposed to simulated sunlight. Redrawn from Leaver, I.H., Ramsay, G.C., 1969. Studies in wool yellowing. 27. The role of water in the photoyellowing of fluorescent whitened wool. Textile Research Journal 39, 730–733.

the mechanism of wool photoyellowing by UV occurs via a free radical mechanism established by Bolland and Gee in the late 1940s known as autoxidation (Bolland, 1949; Bolland and Gee, 1946). Evidence for this is provided by the presence of free radicals in wool after exposure to UV light, which can be detected using a variety of different techniques. These include electron spin resonance spectroscopy (Shatkay and Michaeli, 1970; Windle, 1964), use of a radical-specific fluorescent probe (Millington and Kirschenbaum, 2002), and photoinduced chemiluminescence (Zhang et al., 2008; Millington et al., 2008).

Further evidence for a free radical mechanism is provided by analysis of the yellow products formed when wool is exposed to UV radiation. Analysis of trypsin digests of heavily irradiated wool fabrics using liquid chromatography-tandem mass spectrometry (HPLC/MS/MS) techniques has confirmed the presence of 13 different yellow chromophores in 25 photomodified peptide sequences (Fig. 14.10) (Dyer et al., 2006a,b, 2005). All of these chromophores are oxidation products derived from tryptophan and tyrosine residues in the keratin intermediate filaments and high glycine tyrosine proteins present in the wool fiber cortex. The products are highly consistent with a free radical oxidation mechanism.

The very rapid photoyellowing of FWA-treated wool under wet conditions is probably caused by photoinduced electron transfer (PET) reactions from the wool to the FWA, leading to high concentrations of O_2^- and H_2O_2 at the fabric surface (Millington and Maurdev, 2005). UV or simulated sunlight irradiation of wool in the presence of H_2O_2 leads to much more rapid yellowing than observed in water. In addition, stilbene and DSBP FWAs themselves can also produce yellow photoproducts when exposed to UV light in the presence of H_2O_2. A strongly yellow stilbene quinone has been identified using HPLC/MS/MS after irradiating a DSBP FWA in the presence of H_2O_2 (Dyer et al., 2008).

Treatments that reduce the number of free radicals formed when wool is exposed to UV light will reduce the rate of photoyellowing. For example, the combination of an antioxidant (*N*-acetylcysteine) and a metal chelator (oxalic acid) was highly effective when applied as a rinse treatment for reducing the rate of photoyellowing of FWA-treated wool (Millington, 2006a). However, the treatment was not substantive and the benefits were lost after laundering. The only current commercial treatment for wool is a sulfonated 2-hydroxyphenylbenzotriazole UV absorber that can be exhausted onto wool. This was developed and commercialized by CSIRO in Australia in 1990 (Leaver and Wilshire, 1990; Mosimann et al., 1990) and is now available as UVFast W (Huntsman). One of the problems with this additive is that when applied to very white or bleached wool it causes yellowing, which negates any benefits of peroxide bleaching. An improved application method from a reductive bleach bath, developed by the Sheep CRC in Australia as the *Everwhite* process, alleviates this problem (Millington et al., 2014).

When wool is exposed to visible light in the absence of UV wavelengths, such as sunlight after passing through a window made from borosilicate glass, photobleaching occurs. Wavelengths in the range 400−600 nm lead to photobleaching, but blue light (400−450 nm) is the most effective range. Blue light is absorbed strongly by preexisting yellow chromophores in the wool, and in the excited state these can react more

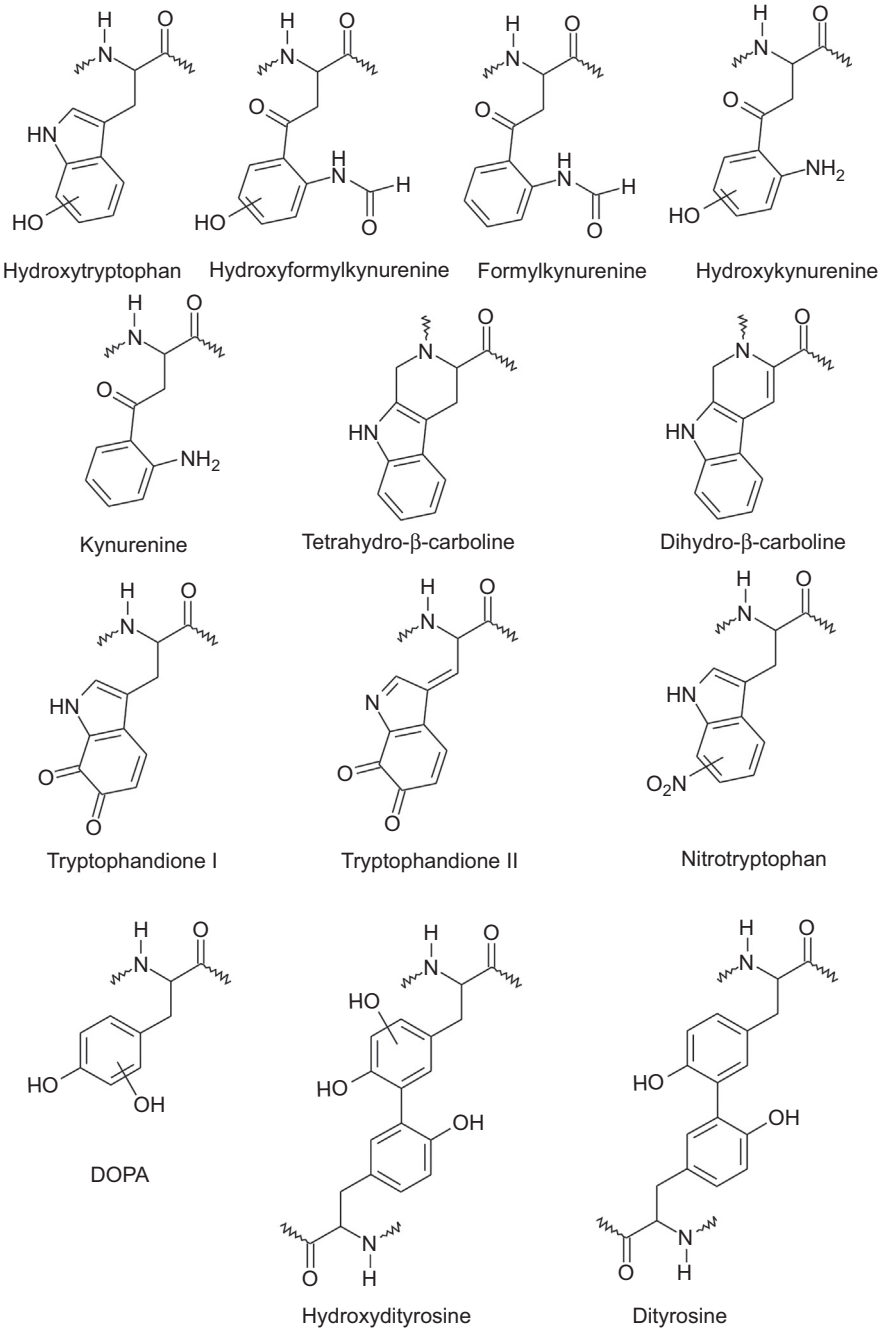

Figure 14.10 Thirteen yellow chromophores derived from Trp and Tyr residues identified in trypsin digests of photoirradiated wool fabric by HPLC/MS/MS (Dyer et al., 2005). Redrawn from Millington, K.R., 2009. Improving the whiteness and photostability of wool. In: Johnson, N.A.G., Russell, I.M. (Eds.), Advances in Wool Technology. Woodhead, Cambridge, UK, pp. 217–247.

rapidly with oxygen to form colorless products. Photobleaching can lead to unacceptable changes in shade, particularly for carpets and upholstery fabrics that have areas that are continually exposed to sunlight filtered through window glass. New Zealand workers developed an additive (Lanalbin APB, Archroma) for application to wool that yellows on exposure to visible light at the same rate as photobleaching occurs, negating its effects (AgResearch, 2012).

14.3.6 Flame resistance

Wool has the highest flame resistance of all the common textile fibers. The high natural flame resistance of wool is caused by its unique chemical and physical structure. Unlike other textiles fibers, which are composed mainly of carbon and oxygen, wool fibers contain a high proportion of nitrogen (ca. 14%). This is a major factor in its high ignition temperature of 570−600°C and in its limiting oxygen concentration of 25−26%, required to support combustion, which is higher than the normal ambient atmospheric oxygen concentration of 21%. Moreover, after ignition the low heat of combustion (4.9 kcal/g) and high moisture content (ca. 15%) of wool are responsible for the flame spreading slowly and being easy to extinguish (Shaw and White, 1984). Furthermore, in contrast to thermoplastic fibers, such as polyester, wool does not melt or drip when it does burn. In wool fibers, the outer layer of cuticle cells are separated from the cortex by the lightly crosslinked cell membrane complex. When the fibers are heated, the cuticle cells tend to separate from the cortex and, because of their high concentration of sulfur, produce a foam (char) that insulates the bulk of the fiber from oxygen.

For many end uses, no additional fire-retardant treatment is needed; in particular with heavier, denser fabrics with a flat surface that tends to exclude air. For some applications, however, the high natural flame resistance of wool is not high enough to meet mandatory regulations. Chemical treatments have therefore been developed to meet the required standards. Early treatments used borates and the phosphate treatments already in use for cotton. These were replaced in the 1970s by the Zirpro Process, developed by The International Wool Secretariat. These treatments evolved from the observation that the chrome mordant used in the application of chrome dyes improved the flame resistance of wool. To avoid the discoloration of undyed wool caused by chromium, other transition metals that bind to wool were investigated. It was found that compounds of zirconium or titanium gave similar improvements in flame retardancy without the discoloration caused by chromium (Benisek, 1974a).

Zirpro treatment involves exhaustion of negatively charged salts of zirconium or titanium onto wool under acidic conditions. A treatment level of 3% on weight of wool is sufficient to give the required improvement in flame retardancy with minimal effect on other properties, such as color, handle, and moisture absorption. A range of Zirpro treatments has been developed that combine flame resistance with shrink resistance, insect resistance, oil and water repellency, and dyeing (Benisek, 1974b). The Zirpro technology has been used extensively for wool in aircraft interiors, theater curtains and for carpets in public buildings, where high flame resistance is required by legislation.

The use of flameproofing treatments is also very important for protective clothing and safety apparel, for example, uniforms worn by firefighters (Cardamone and Kanchager, 2007) and in industries where workers are exposed to molten metals (Benisek and Edmondson, 1981). The performance of a fabric against molten metal splashes is a complex phenomenon that depends on the weight, thickness, density, and surface properties, including surface tension of the fabric as well as the chemical and physical properties of the fiber and any flame-retardant treatment present. Most molten metals have poor adhesion on flameproofed wool fabrics and tend to run off. The unique protective properties of wool can be explained by surface charring on exposure to heat, with the inner layers of the fiber being temporarily protected by this insulating char (Benisek and Edmondson, 1981).

14.3.7 Insect-resist treatments

Wool is a tough material that under most conditions is resistant to degradation by water, acids, sunlight, mildew, and rot. However, at the end of its useful life, wool will degrade in soil to release valuable nutrients. This occurs under the action of organisms produced by proteolytic enzymes. This property makes wool a totally renewable, sustainable material, unlike the synthetic fibers that are derived from a finite resource (oil).

In addition to degradation by soil organisms, keratinous materials such as wool, fur, skin, claws, and feathers are also susceptible to attack by the larvae of some species of moths and beetles. Wool cannot be digested by most insects because the extensive network of disulfide crosslinks prevents access of the digesting proteolytic enzymes to the peptide bonds. A small number of moths and beetles have, however, developed the ability to digest wool. This is believed to be because alkaline-reducing conditions in the larval gut break disulfide bonds, thus allowing the wool to be digested by the proteolytic enzymes (McPhee, 1971). Wool products stored for a long time, carpets, wool insulation, and heritage materials are particularly susceptible, making this a potentially serious problem.

Wool goods can be protected from insect damage by insect-resist (IR) agents, usually applied as part of the manufacturing process. A variety of IR agents have been used (Barton, 2000; Ingham et al., 2012; Simpson, 2002). Synthetic pyrethroids, which were originally developed for agricultural use, have been widely used. Except when used on wool insulation, these agents are applied either in scouring or dyeing. This approach eliminates the need for a separate processing step and, particularly when applied from a hot dyebath, maximizes penetration into the fiber, thus ensuring good fastness to washing and drycleaning. Another important benefit of good penetration of the IR agent into the fibers is that contact with nontarget insects is minimized, because the active agent is released only after the fiber has been digested.

Over the past 30 years the most commonly used synthetic pyrethroid has been Permethrin. This has the advantages of low cost, low water solubility, and, when applied correctly, good fastness. Although it has low mammalian toxicity, unfortunately it has relatively high toxicity to aquatic species. This has resulted in very stringent effluent requirements, particularly in the United Kingdom. In an attempt to avoid this problem, alternative application techniques have been investigated. These include increasing

exhaustion onto the fiber by using low liquor application methods, dry methods of application, and application using a polymeric binder. Exhaustion from a dyebath can be increased by the use of a special auxiliary (Valsol LTA-N) (Barton, 2000; Rippon and Harrigan, 1994; Rippon et al., 1995). A dry application method has been developed (Lanaguard Process: Ag Research, NZ), in which a mixture of Permethrin and a polymeric carrier is sprinkled onto wool carpets, followed by baking in an oven. When the polymer melts, the IR agent diffuses into the fiber surface (Barton, 2000). Permethrin has also been applied to fabrics using a polyurethane binder in a pad/dry/cure application (Cleyman, 2010).

In addition to its toxicity to aquatic life, another problem for Permethrin is the development of resistance to its effect by moths and, in particular, beetles. As a result of this, another synthetic pyrethroid (Bifenthrin) was introduced as a replacement for Permethrin (Barton, 2000). Compared with Permethrin, this is less toxic to aquatic life, has better washfastness, is more effective at low concentrations, and, very importantly, has no current resistance problems with carpet beetles. An alternative to pyrethroids (Chlorfenapyr) was also introduced in 2007 (Mills, 2007). At the present time, immunity to IR agents is confined to pyrethroid-type compounds, particularly Permethrin. Resistance is not expected to develop in the near future with Chlorfenapyr because it is not a pyrethroid. Chlorfenapyr has a further advantage in that it is less toxic to aquatic life than both Permethrin and Bifenthrin (Ingham et al., 2012). The search is still on for alternative IR agents and a surfactant-based dye-leveling agent (Ecolan CEA: Chemcolour, NZ) has been introduced as an IR agent. This is claimed to provide good protection against insects together with excellent fastness properties (Ingham et al., 2012).

14.3.8 Applications for wool as an insulation material

14.3.8.1 Thermal insulation

Wool is an efficient insulating material that has been used for generations in outerwear such as winter jackets and coats. Mongolian nomads also used sheep wool pads for insulation of the walls and floors of their dwellings (yurts). The use of wool as an insulating material for homes is rising in popularity in Western countries, particularly in Europe and Australasia. Many of its physical properties make it attractive for applications in insulation, including its moisture buffering and absorption properties, thermal performance, acoustic qualities, ability to regulate temperature, and natural flame resistance (Corscadden et al., 2014). Wool insulation is usually made from fibers that are either mechanically held together or bonded using between 5–15% recycled polyester adhesive to form insulating batts or rolls. Unlike fiberglass, wool insulation can be installed without protective clothing as it does not cause irritation to the skin, eyes, or respiratory tract. Wool is also a renewable resource, as the average sheep produces about 5 kg of raw wool per year. The technical feasibility and economics of manufacturing wool insulation for the North American market has recently been published (Corscadden et al., 2014). Wool insulation is often treated with borax to enhance its fire retardant and pest repellent qualities. The level of borax is around 4% of dry

weight, although the scouring baths have a higher load of 8−9%. Borax is a suspected reproductive toxin having been considered relatively safe for many years; animal ingestion studies in several species at high doses indicate that borates cause reproductive and developmental effects (Chapin and Ku, 1994; Moore et al., 1997).

There is increased interest in utilizing the absorptive capacity of porous materials to create passive control of humidity variations in indoor air (Peuhkuri et al., 2004). Use of passive control techniques will lead to increased energy efficiency for climate control in buildings. Thus interest in the moisture buffer capacity of materials suitable for application in building construction, in particular as insulating materials, is increasing. Wool insulation is already available and it outperforms more traditional materials such as fiberglass and perlite in buffering indoor relative humidity (Peuhkuri et al., 2004).

14.3.8.2 Sound insulation

The acoustic product market is dominated by foam panels and fiberboards, because of their effectiveness as sound absorbers and relatively low cost (Miao, 2005). Wool is usually considered too expensive to use as a core absorber. However, its growing use as a thermal insulation material has prompted some studies on its acoustic performance. Wool is a low flow resistivity material with practical forms, such as batts and knops, having densities of 10−100 kg/m^{-3} with flow resistivities from 500−15,000 MKS rayls/m (Ballagh, 1996). To achieve useful acoustic performance the thickness of wool materials needs to be quite high, >50 mm. Such materials can increase the sound transmission loss in stud walls by up to 6 dB or more (Ballagh, 1996). Wool materials can also be used as duct linings, where their low flow resistivity is an advantage.

When wool fabrics are used as covers for conventional acoustic panels, they significantly increased the acoustic absorption, particularly in the midfrequency range (500−2000 Hz) (Miao, 2005). Wool carpets are also effective at reducing surface noise, echoing, and airborne noise (McNeil, 2014).

14.3.9 Sorption and filtration

14.3.9.1 Odor sorption by wool clothing

The complex chemical and physical structure of wool allows body odors to be adsorbed and trapped within the fiber until laundering (Leeder, 1984). Furthermore, the various acidic, basic, and hydrophobic groups in the peptide side chains enables wool to bind many toxic gases, including those involved in toxic building syndrome.

Perspiration generated during strenuous exercise swells the fibers in a wool garment, thus allowing odor molecules of various sizes to diffuse into the structure. When exercise is stopped, the sorbed moisture evaporates and the swollen fibers contract and trap the odor molecules within the structure. When the garment is laundered the temperature of the wash water is usually sufficient to swell the fibers and release the odor molecules into the water.

In addition to trapping odors, other factors also make wool a better fiber than synthetics for applications where the wearer generates large amounts of perspiration.

Sweat has no inherent odor, but it provides an excellent environment for the multiplication of bacteria present on the surface of the skin. These bacteria are responsible for odor generation. The moisture absorbing properties of wool, by removing moisture from the skin surface, provide a less favorable environment for bacterial growth than synthetics, which absorb very little moisture. Some compounds associated with body odor, such as ammonia and volatile fatty acids, are readily absorbed by wool, which also contributes to wool's advantages in reducing the build-up of odor in next-to-skin applications (Johnson et al., 2003).

Furthermore, even without washing, it has been shown that wool socks were less odorous after wearing than socks made from synthetic fibers. Odors are prevented from developing, and when they do form, they are trapped inside the fiber.

14.3.9.2 Atmospheric airborne pollutant removal

The quality of indoor air is affected by many factors, including the external atmosphere and the type of heating and efficiency of ventilation. Also important are the materials used in construction of the building itself and its internal furnishings, floor coverings, and finishes, all of which can emit volatile organic compounds. Wool's structure, in particular the side chains of the various amino acids, gives it the ability to absorb and bind many of the noxious compounds in polluted indoor air (Leeder, 1984; Johnson et al., 2003; Causer et al., 1995; Crawshaw, 1978; Wortmann et al., 2005).

Three pollutants that are produced by domestic appliances, open fires, and the combustion of petroleum products, coal, and wood are nitrogen dioxide, sulfur dioxide, and formaldehyde. Wool carpets absorb more nitrogen dioxide than carpets made from nylon. Furthermore, wool has an additional advantage over nylon because it releases less of the bound gas when the carpet becomes warm.

The high acid binding capacity of wool enables it to absorb and retain sulfur dioxide to a greater extent than do other textile fibers. Furthermore, because sulfur dioxide is a reducing agent, it can react with disulfide bonds in wool via sulfitolysis reactions. This reaction is irreversible, with less than 1% of the trapped gas being released over a two hour period.

Formaldehyde-based chemicals are used in the manufacture of some household products, such as furniture made from chipboard and some textiles. The level of formaldehyde in indoor air can exceed recommended levels as it is slowly released; this is exacerbated at higher temperatures and humidity. Formaldehyde reacts readily with proteins, including wool, where it binds irreversibly with the protein side chains, thus permanently removing it from the air. Furthermore, as the rate of emission of the gas increases with temperature and humidity, the rate of absorption by wool also increases rapidly. It has been shown that by using wool carpets and wall coverings in buildings with high formaldehyde emissions, the concentration of the gas can be decreased to levels below the World Health Organization recommendation of 0.05 ppm.

Wool and keratin-derived materials have also been considered to protect from exposure to chemical warfare agents such as mustard gas (Ghosh and Collie, 2014). Agents that are designed to interact with human skin will also react with keratin, since keratin is

a major component of skin. Organophosphates form covalent adducts with tyrosine and serine residues in skin, and wool protective clothing could be valuable, as it was during the two World Wars (Ghosh and Collie, 2014).

14.3.9.3 Electrostatic air filters

Wool has had a long history as a filter material for trapping airborne particles. It was first recognized in the 1930s that the performance of wool filters could be improved significantly when naturally occurring resin powders were added (Hansen, 1932). The resin−wool combination generated electrostatic charge within the filter structure to assist the mechanical capture of particles and hence achieve higher particle collection efficiencies, while maintaining a low resistance to air flow. Electrostatic filters are far more effective than simple mechanical filters, particularly for particles in the size range 0.15−0.5 μm, which are difficult to capture by other mechanisms (Wang, 2001). Nowadays resin−wool filters have largely been superseded by split-fiber electret filters and mixed fiber electrostatic filters. A combination of carded and needle-punched carbonized wool with polypropylene works very well as an electrostatic filter, in particular when blended at a ratio to maintain equal surface areas for the two components (Schutz and Humphries, 2010). For fibers of equal diameter, this corresponds to a 60:40 wool/polypropylene blend. For applications that require high heat resistance, such as respiratory filters for firefighters, the polypropylene component can be replaced by aramid fibers (Schutz and Church, 2011).

14.3.9.4 Metal adsorption properties

Wool keratin has a high affinity for metal ions and can adsorb relatively large amounts from aqueous solutions. In particular, adsorption of soft acids, that is, the cations of less electropositive, more polarizable metals such as mercury, gold, platinum, silver, and lead ions from dilute aqueous (10−20 mM) solution, led to increases in the weight of the wool by 11−34% (Masri et al., 1974). The higher adsorption of soft acids by wool is caused by interaction with thiol groups in the fiber. Thus chemically reducing the disulfide groups to thiols further increases wool's affinity for soft metal ions (Masri and Friedman, 1974). In the 1970s, use of waste wool recovered from carpets was proposed as a means of removing traces of mercury from effluent produced by the chlor-alkali industry (Laurie and Barraclough, 1979). Mercury metal is used as the cathode in the electrolysis of brine to produce chlorine and caustic soda.

The use of wool as a filter media to adsorb toxic metal ions from drinking water or effluent streams has been examined by a number of workers (McNeil, 2001). Wool powders have an increased surface area compared to fibers, and have also been examined as potential metal ion adsorbents. The rate of uptake of copper (II) ions by wool powder was significantly faster than that for wool fiber by a factor of ∼40 (Naik et al., 2010). Also in comparison with commercial cationic exchange resins, wool powders showed significantly higher (two- to ninefold) metal ion loading capacity. Other keratinous materials, such as keratin proteins extracted from chicken feathers and human hair, have been considered for similar applications (Ghosh and Collie, 2014).

14.3.9.5 Absorption of oil from environmental spills

Pollution of offshore and shoreline waters with crude oil continues to be a serious environmental issue. Fibrous sorbents are highly effective for cleaning up and limiting the spread of oil slicks on water because they can be made into knops, batts, or fabrics with good buoyancy properties, which, when contained within a course-mesh outer fabric, can be formed into long booms. The natural fibers cotton and wool have higher sorption capabilities for oil than synthetic fibers (Johnson et al., 1973). Synthetic fibers are also important components of surface booms because of their hydrophobic properties, which maintain buoyancy. The long-chain aliphatic lipids covalently bound to the surface of the wool cuticle confer oleophilic properties, which enable wool to sorb up to 40 times its own weight in oil, depending on the viscosity and nature of the oil (Johnson et al., 2003). Waste or recycled wool materials are ideal for this application to minimize costs. One study has shown that a needle-punched nonwoven material produced from waste 80:20 wool−PET knitwear sorbs 11−14 times its own weight of three different grades of oil from seawater, and that the oil can be removed by compression of the loaded fabric through a pad mangle. This sorption/compression process was repeated for five cycles with oil sorption maintained at over 11 times its own weight for all three oil grades (Radetic et al., 2003). A comparison of natural wool, a wool-based nonwoven fabric, and three inorganic sorbents for extracting motor oil from water showed that natural wool was clearly the most efficient material (Rajakovic-Ognjanovic et al., 2008). The use of wool knops to produce "pillows," booms, and filters to sorb oil from spills has been commercialized as Woolspill in the United Kingdom (EnviroPro, 2015).

14.3.10 Blending with other fibers to improve specific performance attributes

Wool can be blended with other fibers to improve its performance, comfort, protection, durability and easy-care characteristics, and also to impart special functionality (Miao, 2009). Woven wool fabrics containing 20−30% of polyester have improved wrinkle recovery performance compared to similar 100% wool fabric (De Boos et al., 1975). The felting shrinkage of wool can be limited by blending with nonfelting fibers such as cotton and polyester. Wool-poor polyester blends (wool ratio $<50\%$) require no special finishing to prevent felting shrinkage for machine washing. However, wool-rich garments (wool ratio $>60\%$) usually require special finishing and garment setting procedures. For wool cotton blends, 20% wool has little influence on machine washing performance, but with higher levels of untreated wool, shrinkage can occur (Byrne, 1998). The prickle sensation, which is caused by small numbers of broad wool fibers with diameters $>30\ \mu m$, can also be reduced by blending wool with fine fibers. Another strategy is to prevent broad wool fibers from direct contact with skin by using bilayer fabrics, with fine cotton or synthetic fibers only facing the skin. Blending wool with small amounts of elastomeric fibers such as Lycra (commonly up to 5%) can improve garment shape retention and

comfort. Blending can also be used to improve the comfort and performance of flame-resistant clothing and the moisture transport properties of fabrics.

14.3.11 Applications in medical textiles

14.3.11.1 Medical sheepskins

In the 1960s and 1970s, sheepskins were reported to help prevent pressure ulcers (bed sores). However, a major problem for hospitals using sheepskins was the hardening of the leather, which occurred during laundering. In 1998, CSIRO introduced a new high-performance medical sheepskin, the Australian Medical Sheepskin. This has a denser and higher wool pile and can withstand multiple washes at 80°C, representing a significant advance in leather technology (Montgomery, 1996). A randomized controlled trial at an Australian hospital in Melbourne showed that the Australian Medical Sheepskin reduces the incidence of pressure ulcers by 58% (Jolley et al., 2004). Similar findings were obtained in a subsequent trial on somatic nursing home patients (Mistiaen et al., 2010).

14.3.11.2 Wound dressings

Keratin proteins have been shown to play a key role in wound healing. Keratin is a fundamental component of human skin, and the role of proteins from the skin keratin family in wound healing has been extensively researched (Kim et al., 2006). Keratin proteins can be extracted from wool using processes that do not hydrolyze peptide bonds, which allows the keratin proteins to retain a form and function similar to native keratins (Kelly, 2009). The keratin proteins can then be purified and incorporated into dressings and topical creams (Keraplast). These treatments are often used for the treatment of persistent wounds and have been found to be therapeutic (Batzer et al., 2014; Than et al., 2012).

14.3.11.3 Bioscaffolds

Keratin-based materials have shown significant promise to enable the regeneration of human and animal tissues because of their intrinsic biocompatibility, biodegradability, mechanical durability, and natural abundance (Rouse and Van Dyke, 2010). The ability of extracted keratin proteins to self-assemble and polymerize into complex three-dimensional structures has led to their development as scaffolds for tissue engineering. Fabrication of wool keratin scaffolds for long-term cell cultivation was first reported by Tachibana et al. in 2002 (Tachibana et al., 2002). The matrices were created by lyophilization of aqueous wool keratin solutions after controlled freezing, which resulted in a rigid and heat-stable structure with a homogeneously porous microarchitecture. More recently electrospinning has been used to create suitable matrices to encourage cell growth (Rouse and Van Dyke, 2010). Often silk fibroin is used in combination with keratin to improve processability by electrospinning (Zoccola et al., 2008). The use of keratin-based biomaterials for biomedical applications has recently been reviewed (Rouse and Van Dyke, 2010).

14.3.12 Ballistic applications

Ballistic fabrics are used to make protective clothing that helps absorb the impact and reduce or prohibit penetration to the body from firearm-fired projectiles and shrapnel from explosions. Kevlar is one of the most common fibers used in making modern ballistic protective clothing. Kevlar typically has high strength combined with low weight. The high bulk of a ballistic panel makes it difficult for body heat and moisture to pass through and as a consequence the wearer often feels uncomfortable, particularly in warm environments. Blending Kevlar with wool enabled the number of layers used in a ballistic panel to be decreased, thereby reducing its bulk as compared to the 100% Kevlar panel, for comparable ballistic performance (Sinnppoo et al., 2010). The wool was claimed to improve the energy absorption mechanism of yarn "pull-in" because of the increased friction along the wool yarns and Kevlar filaments. Sinnppoo et al. also reported that blending Kevlar with wool improved fabric performance while it was wet. Incorporating wool in a ballistic fabric also has the additional benefit of transferring moisture through the fabric, and potentially improving wearer thermal comfort (Mahbub et al., 2013).

14.3.13 UV protection

Depletion of the ozone layer has made protection from the sun's harmful UV radiation more important, and most people are now aware of the need to wear clothing to help prevent the development of disfiguring or life-threatening skin cancers. The extent to which a woven or a knitted fabric transmits, absorbs, or reflects the UV radiation present in sunlight determines its UV-protection properties. Transmission, absorption, and reflection are in turn dependent on the fiber, fabric construction (thickness and porosity), and finish (Gambichler et al., 2002). The UV-blocking properties of natural fibers have recently been reviewed (Zimniewska and Batog, 2012). Undyed lightweight wool fabrics offer excellent protection from solar UV radiation compared with undyed cotton and synthetics of similar construction, because of the UV-absorbing amino acid residues present in the keratin structure, which also cause photoyellowing (see Section 14.3.5) (Crews et al., 1999). The excellent UV protection properties of wool were confirmed by a study in 2001 (Gambichler et al., 2001), which investigated 236 apparel textiles to determine their UV protection factor (UPF). The fabrics were provided by a leading European garment manufacturer and the mean weight of the samples was 158 g/m^2. They were investigated unstretched and in dry condition, and, in accordance with the European standard, the UPFs were determined spectrophotometrically. The results showed that 33% of fabrics had a UPF $<$15% and 19% had a UPF $\geq$15 and $<$30, showing that more than half of the fabrics failed to satisfy the European standard for UV protective clothing of UPF 30+. Many fabrics commonly worn in summer performed poorly in the test. Of the cotton samples, for example, 79% had a UPF $\leq$20 while 100% of the linen samples fell below the standard of UPF 30+. Some synthetic fabrics also performed poorly, with 89% of the viscose samples failing the test. Only one apparel textile in the study had all its samples pass the test, which was Merino wool. Wool's poorest sample produced a result of UPF 40+, while more than 70% of wool samples had a UPF $\geq$50+.

14.3.14 Wool composites

Composite materials are comprised of a tough matrix material containing strong elastic reinforcements that are well bonded to the matrix. Fibers commonly used for polymer composites are glass and carbon fibers and aramids, which have high tensile strength and bond well to tough matrix resins such as epoxies. Composite materials that use wool are not common, because the price of premium wools is generally high and its surface lipid content makes it a difficult fiber to bond with. However, recently some applications for using waste wool in novel composites have been reported. An Italian group disrupted wool into its histological components using ultrasound and enzymes, and used the cortical cells to produce composite films in a cellulose acetate matrix for potential applications as bioscaffolds (see Section 14.3.11) (Aluigi et al., 2008). However, the adhesion between the cortical cells and the matrix was poor. The same group later used sulfitolysis to extract keratin proteins from wool, which were used as fillers in a poly(L-lactide) matrix (Aluigi et al., 2014).

Spanish and Scottish researchers added wool to clay soils for producing bricks in wet climatic conditions as a potential source of sustainable, nontoxic, and locally produced building materials (Galan-Marin et al., 2010b). The bricks were comprised of local Scottish clay, alginate, a natural polymer extracted from seaweed, and raw unprocessed wool (Galan-Marin et al., 2010a). The bricks could be used without firing, which saves energy, and mechanical tests showed them to be up to 74% stronger in compression than similar bricks made without adding wool. Wool also increased the flexural strength of the bricks.

14.4 Conclusion: strengths and weaknesses

This chapter has shown that wool has many highly positive attributes as a high-performance fiber. It is natural and renewable, not derived from fossil fuels. Every year sheep grow a new fleece. Wool products use less energy than synthetic fibers during manufacture. It is sun safe—wool has naturally high UV protection compared to cotton and synthetic fibers of similar weight and construction. It has natural flame retardant properties—wool fiber has a higher ignition threshold than many other fibers and is flame retardant up to 600°C. It does not melt and drip and produces fewer toxic fumes in a fire. Dyes exhaust almost completely onto wool, producing no colored dyehouse effluent, in stark contrast to cotton and other cellulosic fibers. Wool is biodegradable—when disposed of, natural wool fiber takes only a few years to decompose, and with a high nitrogen content, wool can act as a fertilizer. It is breathable—wool's natural structure allows it to absorb and release water vapor into the atmosphere, keeping you warm in winter and cool in summer. Wool is nonallergenic—wool is not known to cause allergy and does not promote the growth of bacteria. With microscopic cuticle scales, wool fibers can trap dust in the top layers until vacuumed away. It is durable and elastic—a wool fiber can be bent 20,000 times without breaking and still have the power to recover and return to its natural shape. Modern wool garments have easy-care properties—they can be machine washed; retaining a small amount of

natural oil, wool fiber resists dirt and grease. It is multiclimatic—wool acclimatizes to its surroundings and can act as a buffer to prevent rapid changes in indoor relative humidity. It is naturally insulating—wool can insulate the home providing and retaining warmth, and reducing energy costs and noise.

There are a few negative attributes, including the natural cream color of wool and its poor bleachability, which are an impediment to achieving the ultimate bright shades achievable on cotton and synthetics. Also the poor photostability of bleached and fluorescent-brightened wool compared to other fibers is an issue for applications in summer and trans-seasonal apparel, where bright whites and pastel shades are essential. The need to protect wool from attack by certain moths and beetles using pesticides, which are toxic to marine life, is also problematic. The prickle sensation, caused by the presence of a small number of coarse fibers in mid-micron wools with mean fiber diameters >21 μm, has historically caused some reluctance in consumers with sensitive skin to consider wool garments. Fibers coarser than 32 μm are considered responsible for prickle (Naylor et al., 1997). With the move nowadays toward superfine and ultrafine Merino wools for apparel, the association of wool with prickliness has become far less common.

The positive attributes of wool, developed both by evolution and selective breeding over many generations, are unique and have established wool as a high-quality fiber. Provided that other fibers remain unable to match wool's key properties through further research and technological developments, wool's future as a quality high-performance fiber will remain secure.

14.5 Future trends

Wool currently comprises about 1.3% of the global fiber market (Lenzing Group, 2015), with the major fibers being synthetics (62.6%) and cotton (29.5%). Synthetic fibers such as polyester, which recently overtook cotton as the fiber with the largest market share, are produced from petrochemicals and at the current rate of consumption, world oil resources are only expected to last for up to 60 more years. Hence the long-term production of low-cost synthetic fibers from oil is unsustainable. But whether this results in more demand for natural fibers in the future, or the development of new sustainable fiber industries, is an open question.

Australia is the largest wool producing nation, contributing 25% of global wool production, with other major producers being China and New Zealand. For apparel use, Australian Merino flocks produce 77% of wool <24 μm diameter and 88% of fine wool with <20 μm diameter (New Merino, 2015). In Australia, sheep numbers have declined significantly over the last 25 years, from 163 million in 1991 to around 72 million in 2015. One of the factors responsible for this decline is the volatility of wool prices, with large fluctuations resulting in some farmers leaving the wool industry to take up other activities, in particular cropping. Climate change is likely to have further implications on the future sustainability of sheep farming and wool growing in some areas of Australia, particularly with regards to its effects on forage, water resources, land carrying capacity, and animal health (Harle et al., 2007). However, an

analysis has shown that on the whole the Australian wool industry is considered to be relatively robust to the effects of climate change up to 2030 (Harle et al., 2007). Wool remains an A$2.5 billion industry, equivalent to 5% of the gross value of agricultural production in Australia (Australian Bureau of Statistics, 2015).

Sources of further information and advice

Many of the books, chapters, and reviews listed in the bibliography provide more detailed information on various aspects of wool science and technology, and its high-performance applications.

CSIRO carried out wool R&D for many decades and established dedicated wool research laboratories in Australia from 1948. The history of CSIRO wool research and the stories behind many of the commercial breakthroughs made in the 50 years to 1998 are described in:

Williams, V.A. 1998. *From Fleece to Fabric*, Geelong, CSIRO Wool Technology. ISBN 0643 06,446X

Many of the important individual CSIRO achievements in wool R&D are also described online at: http://www.csiropedia.csiro.au/display/CSIROpedia/Achievements+A-Z

Some of the high-performance attributes of wool are further described in factsheets that can be downloaded from a website based on the work of the Wool Research Organisation of New Zealand (WRONZ) at: http://www.campaignforwool.co.nz/technical-and-information/.

References

Agresearch, 2012. Lanalbin® APB. Available from: http://www.climatecloud.org.nz/our-science/textiles-biomaterials/textile-chemistry/Pages/lanalbin-apb.aspx.

Alexander, P., Hudson, R.F., 1963. Wool: Its Chemistry and Physics. Chapman & Hall, London.

Aluigi, A., Vineis, C., Ceria, A., Tonin, C., 2008. Composite biomaterials from fibre wastes: characterization of wool-cellulose acetate blends. Composites Part A: Applied Science and Manufacturing 39, 126−132.

Aluigi, A., Tonetti, C., Rombaldoni, F., Puglia, D., Fortunati, E., Armentano, I., Santulli, C., Torre, L., Kenny, J.M., 2014. Keratins extracted from Merino wool and Brown Alpaca fibres as potential fillers for PLLA-based biocomposites. Journal of Materials Science 49, 6257−6269.

Asquith, R.S., Puri, A.K., 1968. Stability to aftertreatments of wool set in thioglycollic acid. Journal of the Society of Dyers and Colourists 84, 461−462.

Australian Bureau of Statistics, 2015. Value of Agricultural Commodities Produced, Australia, 2013−14. Available from: http://www.abs.gov.au/ausstats/abs@.nsf/mf/7503.0.

Ballagh, K.O., 1996. Acoustical properties of wool. Applied Acoustics 48, 101−120.

Barnes, J.C., Holcombe, B.V., 1996. Moisture sorption and transport in clothing during wear. Textile Research Journal 66, 777−786.

Barton, J., 2000. It's a bug's life − or is it? International Dyer 195, 14−16.

Batzer, A.T., Marsh, C., Kirsner, R.S., 2014. The use of keratin-based wound products on refractory wounds. International Wound Journal 1−6.

Baumann, H., 1979. Applied aspects of keratin chemistry. In: Parry, D.A.D., Creamer, L.K. (Eds.), Fibrous Proteins: Scientific, Industrial and Medical Aspects, vol. 1. London Academic Press, pp. 299–370.

Bendit, E.G., 1960. A quantitative X-ray diffraction study of the alpha-beta transformation in wool keratin. Textile Research Journal 20, 547–555.

Benisek, L., Edmondson, G.K., 1981. Protective clothing fabrics. Part 1. Against molten metal hazards. Textile Research Journal 51, 182–190.

Benisek, L., 1974a. Improvement of the natural flame-resistance of wool: Part I. Metal-complex applications. Journal of the Textile Institute 65, 102–108.

Benisek, L., 1974b. Improvement of the natural flame-resistance of wool: Part II. Multipurpose finishes. Journal of the Textile Institute 65, 140–145.

Benisek, L., 1976. Development of flame resist treatments for wool. Wool Science Review 52, 30–63.

Bhoyro, A.Y., Church, J.S., King, D.G., O'loughlin, G.J., Phillips, D.G., Rippon, J.A., 2001. Wool's space age response – Optim Fine and Optim Max. In: Proc. Textile Institute World Conference, 1st – 4th April, 2001 (Melbourne).

Bolland, J.L., Gee, G., 1946. Kinetic studies in the chemistry of rubber and related materials 2. The kinetics of oxidation of unconjugated olefins. Transactions of the Faraday Society 42, 236–243.

Bolland, J.L., 1949. Kinetics of olefin oxidation. Quarterly Reviews 3, 1–21.

Bradbury, J.H., Chapman, G.V., King, N.L.R., 1965. The chemical composition of wool. 2. Analysis of major histological components produced by ultrasonic disintegration. Australian Journal of Biological Sciences 18, 353.

Bradbury, J.H., 1973. The structure and chemistry of keratin fibers. Advances in Protein Chemistry 27, 111–211.

Brady, P.R., 1997. Finishing and Wool Fabric Properties: A Guide to the Theory and Practice of Finishing Woven Wool Fabrics. CSIRO Wool Technology, Geelong.

Burley, R.W., 1955. Some observations of the extension, contraction and supercontraction of wool fibres. Procedings of the 1st International Wool Textile Conference, Melbourne, Vol D, pp. 88–117.

Byrne, K.M., 1998. Easy care wool/cotton blends. In: Proceedings of the Beltwide Cotton Production Conference, San Diego, pp. 771–775.

Cardamone, J.M., Kanchager, A.P., 2007. Method of Inhibiting the Burning of Natural Fibers, Synthetic Fibers, or Mixtures Thereof, or Fabric or Yarn Composed of Natural Fibers, Synthetic Fibers, or Mixtures Thereof, and Products Produced by Such Methods (USA patent application).

Causer, S.M., Mcmillan, R.C., Bryson, W.G., 1995. The role of wool carpets in controlling indoor air pollution. In: Proc. 9th Intern. Wool Textile Res.Conf. Biella, Italy, vol. I, pp. 155–161.

Chapin, R.E., Ku, W.W., 1994. The reproductive toxicity of boric-acid. Environmental Health Perspectives 102, 87–91.

Christoe, J.R., Denning, R.J., Evans, D.J., Huson, M.G., Jones, L.N., Lamb, P.R., Millington, K.R., Phillips, D.G., Pierlot, A.P., Rippon, J.A., Russell, I.M., 2003. Wool. In: Rippon, J.A. (Ed.), Encyclopedia of Polymer Science and Technology, fourth ed., vol. 12. John Wiley & Sons, Chichester, UK, pp. 546–586.

Cleyman, J., 2010. Anti-insect treatments for outerwear, tents and battledress uniforms. International Dyer 195, 23–25.

Collis, B., 2002. Fields of Discovery: Australia's CSIRO. Allen & Unwin, Sydney, pp. 152–192.

Connell, D.L., 2003. Wool finishes: the control of shrinkage. In: Heywood, D. (Ed.), Textile Finishing. Society of Dyers and Colourists, Bradford, UK, pp. 372–397.

Corscadden, K., Biggs, J.N., Stiles, D.K., 2014. Sheep's wool insulation: a sustainable alternative use for a renewable resource? Resources Conservation and Recycling 86, 9–15.

Crawshaw, G.H., January, 1978. The role of wool carpets in controlling indoor air pollution. Textile Institute and Industry. pp. 12–15.

Crews, P.C., Kachman, S., Beyer, A.G., 1999. Influences on UVR transmission of undyed woven fabrics. Textile Chemist and Colorist 31, 17–26.

CSIRO, 2010. Sportwool™. Available from: http://www.csiropedia.csiro.au/pages/viewpage.action?pageId=426177.

CSIRO, 2011. OPTIM™ Fibre Processing. Available from: http://www.csiropedia.csiro.au/pages/viewpage.action?pageId=426494.

De Boos, A., Jones, F.W., Leeder, J.D., Taylor, D.S., 1975. The wrinkling of wool and wool/polyester blends. In: Proceedings of 5th International Wool Research Conference, Aachen, vol. 3, pp. 472–481.

Duffield, P.A., Lewis, D.M., 1985. The yellowing and bleaching of wool. Review of Progress in Coloration 38–51.

Duffield, P.A., 1996. Review of Wool Bleaching Processes. The Woolmark Company.

Dyer, J.M., Bringans, S.D., Plowman, J.E., Bryson, W.G., 2005. Chromophores in photo-yellowed wool fabric characterised by mass spectrometry. In: Proc 11th Int Wool Text Res Conf, Leeds. CDROM, UK. Paper 98FWSA.

Dyer, J.M., Bringans, S.D., Bryson, W.G., 2006a. Characterisation of photo-oxidation products within photoyellowed wool proteins: tryptophan and tyrosine derived chromophores. Photochemical & Photobiological Sciences 5, 698–706.

Dyer, J.M., Bringans, S.D., Bryson, W.G., 2006b. Determination of photo-oxidation products within photoyellowed bleached wool proteins. Photochemistry and Photobiology 82, 551–557.

Dyer, J.M., Cornellison, C.D., Bringans, S.D., Maurdev, G., Millington, K.R., 2008. The photoyellowing of stilbene-derived fluorescent whitening agents – mass spectrometric characterization of yellow photoproducts. Photochemistry and Photobiology 84, 145–153.

Enviropro, 2015. WoolSpill Slicklickers. Available from: http://cms.esi.info/Media/documents/Hydro_WoolspillSlick_ML.pdf.

Evans, D.J., Lanczki, M., 1997. Cleavage of integral surface lipids of wool by aminolysis. Textile Research Journal 67, 435–444.

Evans, D.J., Leeder, J.D., Rippon, J.A., Rivett, D.E., 1985. Separation and analysis of the surface lipids of the wool fibre. In: Proc. 7th Int. Wool Text. Res. Conf., Tokyo, vol. I, pp. 135–142.

Farnworth, A.J., Delmenico, J., 1971. Permanent Setting of Wool. Merrow Publishing, Watford, UK.

Feldtman, H.D., Leeder, J.D., 1984. Effect of polar organic solvents on the abrasion resistance of wool. Textile Research Journal 54, 26–31.

Feldtman, H.D., Leeder, J.D., Rippon, J.A., 1983. The composite structure of wool. In: Postle, R., Kawabata, S., Niwa, M. (Eds.), Objective Evaluation of Apparel Fabrics. Text. Mach. Soc. Japan, Osaka, pp. 125–135.

Feughelman, M., Robinson, M.S., 1971. Some mechanical properties of wool fibers in the "Hookean" region from zero to 100% relative humidity. Textile Research Journal 41, 469–474.

Feughelman, M., 1989. A note on the water-impenetrable component of alpha-keratin fibers. Textile Research Journal 59, 739–742.
Fraser, R.D.B., Jones, L.N., Macrae, T.P., Suzuki, E., Tulloch, P.A., 1980. The fine structure of wool. In: Proc. 6th Int. Wool Text. Res. Conf., Pretoria, South Africa, vol. 1, pp. 1–33.
Fraser, R.D.B., Rogers, G.E., Parry, D.A.D., 2003. Nucleation and growth of macrofibrils in trichocyte (hard-alpha) keratins. Journal of Structural Biology 143, 85–93.
Galan-Marin, C., Rivera-Gomez, C., Petric-Gray, J., 2010a. Effect of animal fibres reinforcement on stabilized earth mechanical properties. Journal of Biobased Materials and Bioenergy 4, 121–128.
Galan-Marin, C., Rivera-Gomez, C., Petric, J., 2010b. Clay-based composite stabilized with natural polymer and fibre. Construction and Building Materials 24, 1462–1468.
Gambichler, T., Rotterdam, S., Altmeyer, P., Hoffmann, K., 2001. Protection against ultraviolet radiation by commercial summer clothing: need for standardised testing and labelling. BMC Dermatology 1, 6.
Gambichler, T., Altmeyer, P., Hoffmann, K., 2002. Role of clothes in sun protection. Recent Results in Cancer Research 160, 15–25.
Ghosh, A., Collie, S.R., 2014. Keratinous materials as novel absorbent systems for toxic pollutants. Defence Science Journal 64, 209–221.
Gillespie, J.M., 1990. The proteins of hair and other hard alpha-keratins. In: Goldman, R.D., Steinert, P.M. (Eds.), Cellular and Molecular Biology of Intermediate Filaments. Plenum Press, New York, pp. 95–128.
Haly, A.R., Snaith, J.W., 1967. Differential thermal analysis of wool – phase-transition endotherm under various conditions. Textile Research Journal 37, 898–907.
Haly, A.R., Snaith, J.W., 1973. Heat of wetting of annealed wool. Textile Research Journal 43 (1), 54–57.
Hansen, N.L., 1932. Method for the Manufacture of Smoke Filters or Collective Filters (UK patent application 384,052).
Harle, K.J., Howden, S.M., Hunt, L.P., Dunlop, M., 2007. The potential impact of climate change on the Australian wool industry by 2030. Agricultural Systems 93, 61–89.
Hearle, J.W.S., 2000. A critical review of the structural mechanics of wool and hair fibres. International Journal of Biological Macromolecules 27, 123–138.
Hearle, J.W.S., 2001. High Performance Fibres. Woodhead, Cambridge.
Hearle, J.W.S., 2002. Physical properties of wool. In: Simpson, W.S., Crawshaw, G.H. (Eds.), Wool: Science and Technology. Woodhead, Cambridge, UK, pp. 80–129.
Hinton, E.H., 1974. Survey and critique of literature on crosslinking agents and mechanisms as related to wool keratin. Textile Research Journal 44, 233–292.
Hojo, H., 1985. Improvement of wool fibres by removing exocuticle in the presence of metallic ions. In: Proc. 7th Int. Wool Text. Res. Conf.,Tokyo, vol. 4, pp. 322–331.
Horrocks, A.R., 1986. Flame resistant finishing of textiles. Review of Progress in Coloration and Related Topics 16, 62–101.
Huson, M.G., 1998. Physical properties of wool fibers in electrolyte solutions. Textile Research Journal 68, 595–605.
Ingham, P.E., Mcneil, S.J., Sunderland, M.R., 2012. Functional finishes for Wool-Eco considerations. Eco-dyeing, Finishing and Green Chemistry 441, 33–43.
Johnson, R.F., Manjreka, T.G., Halligan, J.E., 1973. Removal of oil from water surfaces by sorption on unstructured fibers. Environmental Science & Technology 7, 439–443.
Johnson, N.A.G., Wood, E.J., Ingham, P.E., Mcneil, S.J., Mcfarlane, I.D., 2003. Wool as a technical fibre. Journal of the Textile Institute 94, 26–41.

Jolley, D.J., Wright, R., Mcgowan, S., Hickey, M.B., Campbell, D.A., Sinclair, R.D., Montgomery, K.C., 2004. Preventing pressure ulcers with the Australian Medical Sheepskin: an open-label randomised controlled trial. Medical Journal of Australia 180, 324–327.

Jones, L.N., Rivett, D.E., Tucker, D.J., 1998. Wool and related mammalian fibres. In: Lewin, M., Pearce, E.M. (Eds.), Handbook of Fibre Chemistry. Marcel Dekker, New York, pp. 355–413.

Kaplin, I.J., Whiteley, K.J., 1985. The structure of keratin macrofibrils. Part 1: keratins of high sulfur content. In: Proc. 7th Int. Wool Text. Res. Conf., Tokyo, Japan, vol. I, pp. 95–104.

Kelly, R., 2009. Application of wool keratins ranging from industrial materials to medical devices. In: Johnson, N.A.G., Russell, I.M. (Eds.), Advances in Wool Technology. Woodhead, Cambridge, UK, pp. 323–331.

Keraplast. Wound Care: a new paradigm in wound healing, Available from: http://www.keraplast.com/wound-care.

Kettlewell, R., De Boos, A., Jackson, J., 2015. Commercial shrink-resist finishes for wool. In: Paul, R. (Ed.), Functional Finishes for Textiles. Improving Comfort, Performance and Protection. Woodhead, Cambridge, pp. 193–226.

Kim, S., Wong, P., Coulombe, P.A., 2006. A keratin cytoskeletal protein regulates protein synthesis and epithelial cell growth. Nature 441, 362–365.

King, A.T., 1927. Unscaled fibers. A new aspect of fiber research. Biochemical Journal 21, 434–436.

Laurie, S.H., Barraclough, A., 1979. Use of waste wool for the removal of mercury from industrial effluents, particularly those from the chlor-alkali industry. International Journal of Environmental Studies 14, 139–149.

Leaver, I.H., Ramsay, G.C., 1969. Studies in wool yellowing. 27. The role of water in the photoyellowing of fluorescent whitened wool. Textile Research Journal 39, 730–733.

Leaver, I.H., Wilshire, J.F.K., 1990. A new and better photoprotective treatment for wool. Chemistry in Australia 174.

Leeder, J.D., Rippon, J.A., 1985. Changes induced in the properties of wool by specific epicuticle modification. Journal of the Society of Dyers and Colourists 101, 11–16.

Leeder, J.D., Rippon, J.A., Rivett, D.E., 1985a. Modification of the surface properties of wool by treatment with anhydrous alkali. In: Proc. 7th Int. Wool Text. Res. Conf., Tokyo, vol. IV, pp. 312–321.

Leeder, J.D., Rippon, J.A., Rothery, F.E., Stapleton, I.W., 1985b. Use of the transmission electron microscope to study dyeing and diffusion processes. In: Proc. 7th Int. Wool Text. Res. Conf., Tokyo, vol. V, pp. 99–108.

Leeder, J.D., 1984. Wool: Nature's Wonder Fibre. Australasian Textiles Publishing, Ocean Grove, VIC.

Leeder, J.D., 1986. The cell membrane complex and its influence on the properties of the wool fibre. Wool Science Review 3–35.

Lehmann, E., 1941. Chemical and histological studies on wool. Melliand Textilberichte 22, 145.

Lenzing Group, 2015. The Global Fiber Market in 2014. Available from: http://www.lenzing.com/en/investors/equity-story/global-fiber-market.html.

Levene, R., Shakkour, G., 1995. Wool fibers of enhanced luster obtained by Enzymatic Descaling. Journal of the Society of Dyers and Colourists 111, 352–359.

Lewis, D.M., 1990. Dyeing and wet processing of wool. In: Proc 8th Int Wool Text Res Conf, Christchurch, NZ, vol. IV, pp. 1–49.

Lindley, H., 1977. The chemical composition and structure of wool. In: Asquith, R.S. (Ed.), Chemistry of Natural Protein Fibres. Plenum Press, New York, pp. 147–191.

Maclaren, J.A., Milligan, B., 1981. Wool Science: The Chemical Reactivity of the Fibre. Science Press, Marrickville NSW.
Mahbub, R.F., Ratnapandian, S., Wang, L.J., Arnold, L.N., 2013. Evaluation of comfort properties of coated Kevlar/wool ballistic fabric. Advances in Textile Engineering and Materials Iii 821−822 (Pts 1 and 2), 342−347.
Makinson, K.R., Lead, J.A., 1973. The nature and function of the resin in the chlorine/resin shrink-proofing treatment of wool tops. Textile Research Journal 43, 669−681.
Makinson, K.R., 1979. Shrinkproofing of Wool. Marcel Dekker, New York.
Marsh, T.T., 1966. Introduction to Textile Finishing. Chapman and Hall, London.
Masri, M.S., Friedman, M., 1974. Effect of chemical modification of wool on metal-ion binding. Journal of Applied Polymer Science 18, 2367−2377.
Masri, M.S., Reuter, F.W., Friedman, M., 1974. Interaction of wool with metal cations. Textile Research Journal 44, 298−300.
Mcneil, S.J., 2001. Heavy metal removal using wool filters. Asian Textile Journal 88−90.
Mcneil, S.J., 2014. Acoustic Advantages of Wool Carpeting. AgResearch technical Bulletin. (Christchurch, NZ).
Mcphee, J.R., 1971. The Mothproofing of Wool. Merrow, Watford, UK.
Mercer, E.H., Maltosy, A.G., 1968. Keratin. In: Montagna, W., Dobson, R.L. (Eds.), Advances in Biology of Skin and Hair Growth. Pergamon Press, Oxford, pp. 555−569.
Miao, M.H., 2005. Wool for acoustic absorption. In: Proc. 11th Int Wool Text Res Conf, Leeds, UK.
Miao, M.H., 2009. High-performance wool blends. In: Johnson, N.A.G., Russell, I.M. (Eds.), Advances in Wool Technology. Woodhead, Cambridge, pp. 284−307.
Millington, K.R., Kirschenbaum, L.J., 2002. Detection of hydroxyl radicals in photoirradiated wool, cotton, nylon and polyester fabrics using a fluorescent probe. Coloration Technology 118, 6−14.
Millington, K.R., Maurdev, G., 2005. The mechanism of photoyellowing of fluorescent whitened wool. In: Proc 11th Int Wool Text Res Conf, Leeds, UK.
Millington, K.R., Deledicque, C., Jones, M.J., Maurdev, G., 2008. Photo-induced chemiluminescence from fibrous polymers and proteins. Polymer Degradation and Stability 93, 640−647.
Millington, K.R., Del Giudice, M., Sun, L., 2014. Improving the photostability of bleached wool without increasing its yellowness. Coloration Technology 130, 413−417.
Millington, K.R., 2006a. Improving the photostability of whitened wool by applying an antioxidant and metal chelator rinse. Coloration Technology 122, 49−56.
Millington, K.R., 2006b. Photoyellowing of wool. Part 1: factors affecting photoyellowing and experimental techniques. Coloration Technology 122, 169−186.
Millington, K.R., 2006c. Photoyellowing of wool. Part 2: photoyellowing mechanisms and methods of prevention. Coloration Technology 122, 301−316.
Millington, K.R., 2009. Improving the whiteness and photostability of wool. In: Johnson, N.A.G., Russell, I.M. (Eds.), Advances in Wool Technology. Woodhead, Cambridge, UK, pp. 217−247.
Millington, K.R., 2012. Diffuse reflectance spectroscopy of fibrous proteins. Amino Acids 43, 1277−1285.
Millington, K.R., 2013. Bleaching and whitening of wool: photostability of whites. In: Lewis, D.M., Rippon, J.A. (Eds.), The Coloration of Wool and Other Keratin Fibres. Wiley, Chichester, UK, pp. 131−155.
Mills, W., 2007. Beating moths the clean way. Wool Record 166−230.

Mistiaen, P., Achterberg, W., Ament, A., Halfens, R., Huizinga, J., Montgomery, K., Post, H., Spreeuwenberg, P., Francke, A.L., 2010. The effectiveness of the Australian Medical Sheepskin for the prevention of pressure ulcers in somatic nursing home patients: a prospective multicenter randomized-controlled trial (ISRCTN17553857). Wound Repair and Regeneration 18, 572–579.

Mitchell, T.W., Feughelman, M., 1960. The torsional properties of single wool fibers: Part I: torque-twist relationships and torsional relaxation in wet and dry fibers. Textile Research Journal 30, 662–667.

Mitchell, T.W., Feughelman, M., 1967. Mechanical properties of wool fibers in water at temperatures above 100°C. Textile Research Journal 37, 660–666.

Moncrieff, R.W., 1953. Wool Shrinkage and its Prevention. National Trades Press, London.

Montgomery, K.C., 1996. Medical Sheepskins: A Literature Review. CSIRO Division of Wool Technology, Clayton, Melbourne.

Moore, J.A., Callahan, M., Chapin, R., Daston, G.P., Erickson, D., Faustman, E., Foster, P., Friedman, J.M., Goldman, L., Golub, M., Hughes, C., Kavlock, R.J., Kimmel, C.A., Lamb, J.C., Lewis, S.C., Lunchick, C., Morseth, S., Mortensen, B.K., Oflaherty, E.J., Palmer, A.K., Ramlow, J., Rodier, P.M., Rudo, K., Ryan, L., Schwetz, B.A., Scialli, A., Selevan, S., Tyl, R., Campbell, M., Carney, E., Faber, W., Hellwig, J., Murphy, S.R., Smith, M.A., Strong, P.L., Weiner, M., 1997. An assessment of boric acid and borax using the IEHR Evaluative process for assessing human developmental and reproductive toxicity of agents. Reproductive Toxicology 11, 123–160.

Morton, W.E., Hearle, J.W.S., 1993. Physical Properties of Textile Fibres, third ed. The Textile Institute, Manchester.

Mosimann, W., Benisek, L., Burdeska, K., Leaver, I.H., Myers, P.C., Reinert, G., Wilshire, J.F.K., 1990. A new commercial UV absorber for the protection of wool and wool dyeings. In: Proc 8th Int Wool Text Res Conf, Christchurch, NZ, vol. IV, pp. 239–249.

Naik, R., Wen, G.Q., Dharmaprakash, M.S., Hureau, S., Uedono, A., Wang, X.G., Liu, X., Cookson, P.G., Smith, S.V., 2010. Metal ion binding properties of novel wool powders. Journal of Applied Polymer Science 115, 1642–1650.

Nason, R., 1965. Fulling – past and present. American Dyestuff Reporter 54, 1008–1012.

Naylor, G.R.S., Phillips, D.G., Veitch, C.J., Dolling, M., Marland, D.J., 1997. Fabric-evoked prickle in worsted spun single jersey fabrics. Part 1. The role of fiber end diameter characteristics. Textile Research Journal 67, 288–295.

Negri, A.P., Cornell, H.J., Rivett, D.E., 1992. Effects of processing on the bound and free fatty-acid levels in wool. Textile Research Journal 62, 381–387.

New Merino, 2015. Global Merino Production by Country. Available from: http://newmerino.com.au/global-wool-facts/.

Nicholls, C.H., Pailthorpe, M.T., 1976. Primary reactions in the photoyellowing of wool keratin. Journal of the Textile Institute 67, 397–403.

Peuhkuri, R., Rode, C., Hansen, K.K., 2004. Moisture buffer capacity of different insulation materials. In: Proceedings of Buildings IX. American Society of Heating, Refrigerating and Air-Conditioning Engineers (ASHRAE), Clearwater, Florida.

Phillips, D.G., Warner, J.J., 1994. Apparatus for Stretching Staple Fibers. USP 5365729.

Pierlot, A.P., 1997. Influence of glass transition on the felting shrinkage of wool fabric. Textile Research Journal 67, 616–618.

Radetic, M.M., Jocic, D.M., Jovancic, P.M., Petrovic, Z.L., Thomas, H.F., 2003. Recycled wool-based nonwoven material as an oil sorbent. Environmental Science & Technology 37, 1008–1012.

Rajakovic-Ognjanovic, V., Aleksic, G., Rajakovic, L., 2008. Governing factors for motor oil removal from water with different sorption materials. Journal of Hazardous Materials 154, 558−563.

Rippon, J.A., Evans, D.J., 2012. Improving the properties of natural fibres by chemical treatments. In: Kozlowski, R. (Ed.), Handbook of Natural Fibres, Processing and Applications, vol. 2. Woodhead, Cambridge, pp. 63−140.

Rippon, J.A., Harrigan, F.J., 1994. Dyeing Process for Keratin Materials, with Improved Exhaustion of Bath Constituents. USP 5496379.

Rippon, J.A., Leeder, J.D., 1986. The effect of treatment with perchloroethylene on the abrasion resistance of wool fabric. Journal of the Society of Dyers and Colourists 102, 171−176.

Rippon, J.A., Rushforth, M.A., 1976. The use of the water-soluble bisulphate addition product of a polyisocyanate. Textilveredlung 11, 224−229.

Rippon, J.A., Harrigan, F.J., Tilson, A.R., 1995. The Sirolan-LTD wool dyeing process: improved product quality with economic benefits and cleaner effluent. In: Proc. 9th Internat. Wool Text. Res. Conf., Biella, Italy, vol. III, pp. 122−131.

Rippon, J.A., 2008. Friction, felting and shrink-proofing of wool. In: Gupta, B.S. (Ed.), Friction in Textile Materials. Woodhead, Cambridge, pp. 253−291.

Rippon, J.A., 2013a. The structure of wool. In: Lewis, D.M., Rippon, J.A. (Eds.), The Coloration of Wool and Other Keratin Fibres. Wiley, Chichester, UK, pp. 1−42.

Rippon, J.A., 2013b. The chemical and physical basis for wool dyeing. In: Lewis, D.M., Rippon, J.A. (Eds.), The Coloration of Wool and Other Keratin Fibres. John Wiley, Chichester, UK, pp. 43−74.

Rogers, G.E., 1959. Electron microscope studies of hair and wool. Annals of the New York Academy of Sciences 83, 378−399.

Rouse, J.G., Van Dyke, M.E., 2010. A review of keratin-based biomaterials for biomedical applications. Materials 3, 999−1014.

Ruetsch, S.B., Weigmann, H.D., 1995. Mechanism of tensile stress release in the keratin fibre cuticle. In: Proc. 9th Internat. Wool Text. Res. Conf.,Biella, vol. II, pp. 44−55.

Schutz, J.A., Church, J.S., 2011. Respiratory protection for physiologically straining environments. Textile Research Journal 81, 1367−1380.

Schutz, J.A., Humphries, W., 2010. A study of wool/polypropylene non-wovens as an alternative to the Hansen filter. Textile Research Journal 80, 1265−1277.

Shatkay, A., Michaeli, I., 1970. Electron paramagnetic resonance study of wool irradiated by ultraviolet and visible light. Radiation Research 43, 485−498.

Shaw, T., White, M.A., 1984. The chemical technology of wool finishing. In: Lewin, M., Sello, S.B. (Eds.), Handbook of Fiber Science and Technology, Chemical Processing of Fibers and Fabrics, vol. II. Marcel Dekker, New York, pp. 317−442.

Simpson, W.S., 2002. Chemical processes for enhanced appearance and performance. In: Simpson, W.S., Crawshaw, G.H. (Eds.), Wool: Science and Technology. Woodhead, Cambridge, pp. 215−236.

Sinnppoo, K., Arnold, L.N., Padhye, R., 2010. Application of wool in high-velocity ballistic protective fabrics. Textile Research Journal 80, 1083−1092.

Speakman, J.B., Stott, E., 1931. A contribution to the theory of milling: a method of measuring the scaliness of wool. Journal of the Textile Institute 22, T339−T348.

Speakman, J.B., Whewell, E., 1945. The use of abrasives to make wool unshrinkable. Journal of the Textile Institute 36, T48−T56.

Speakman, J.B., Stott, E., Chang, H., 1933. A contribution to the theory of milling. Journal of the Textile Institute 24, T273−T292.

Stulov, A., 1995. Hysteretic model of the grand piano hammer felt. Journal of the Acoustical Society of America 97, 2577−2585.

Stulov, A., 2004. Dynamic behavior and mechanical features of wool felt. Acta Mechanica 169, 13−21.

Tachibana, A., Furuta, Y., Takeshima, H., Tanabe, T., Yamauchi, K., 2002. Fabrication of wool keratin sponge scaffolds for long-term cell cultivation. Journal of Biotechnology 93, 165−170.

Taylor, D.S., 1985. Wool technologies - present and future. In: Proc. 7th Int. Wool Text. Res. Conf., Tokyo, vol. I, pp. 27−69.

Than, M.P., Smith, R.A., Hammond, C., Kelly, R., Marsh, C., Maderal, A.D., Kirsner, R.S., 2012. Keratin-based wound care products for treatment of resistant vascular wounds. Journal of Clinical and Aesthetic Dermatology 5, 31−35.

Wang, C.S., 2001. Electrostatic forces in fibrous filters − a review. Powder Technology 118, 166−170.

Ward, R.J., Willis, H.A., George, G.A., Guise, G.B., Denning, R.J., Evans, D.J., Short, R.D., 1993. Surface-analysis of wool by X-ray photoelectron-spectroscopy and static secondary-ion mass-spectrometry. Textile Research Journal 63, 362−368.

Watt, I.C., Darcy, R.L., 1979. Water-vapor adsorption-isotherms of wool. Journal of the Textile Institute 70, 298−307.

Watt, I.C., 1980. Sorption of water-vapor by keratin. Journal of Macromolecular Science-reviews in Macromolecular Chemistry and Physics C18, 169−245.

Whewell, C.S., 1971. The chemistry of wool finishing. In: Asquith, R.S. (Ed.), Chemistry of Natural Protein Fibers. Plenum Press, New York, pp. 333−370.

Windle, J.J., 1964. Origin of free radicals in wool. In: Proc Tech Wool Conference, San Francisco and Albany, ARS-74−29. US Dept Agriculture, pp. 74−81.

Wortmann, F.J., Zahn, H., 1994. The stress/strain curve of alpha-keratin fibers and the structure of the intermediate filament. Textile Research Journal 64, 737−743.

Wortmann, F.J., Rigby, B.J., Phillips, D.G., 1984. Glass-transition temperature of wool as a function of regain. Textile Research Journal 54, 6−8.

Wortmann, G., Thomé, S., Föhles, J., Wortmann, F.-J., 2005. Sorption of aldehydes from indoor air by wool: formaldehyde as an example. In: Proc 11th Int Wool Text Res Conf, Leeds, UK.

Zahn, H., Blankenburg, G., 1964. Action of alcohol water mixtures on wool. Textile Research Journal 34, 176−177.

Zahn, H., Fohles, J., Nienhaus, M., Schwan, A., Spel, M., 1980. Wool as a biological composite structure. Industrial & Engineering Chemistry Product Research and Development 19, 496−501.

Zhang, H., Millington, K.R., Wang, X.G., 2008. A morphology-related study on photo-degradation of protein fibres. Journal of Photochemistry and Photobiology B-biology 92, 135−143.

Ziegler, K., 1965. The influence of alkali treatment on wool. In: Proc. 3rd Internat. Wool Text. Res. Conf., Paris, vol. 2, pp. 403−417.

Zimniewska, M., Batog, J., 2012. Ultraviolet-blocking properties of natural fibres. In: Kozlowski, R.M. (Ed.), Handbook of Natural Fibres, Processing and Applications, vol. 2. Woodhead, Cambridge, pp. 185−215.

Zoccola, M., Aluigi, A., Vineis, C., Tonin, C., Ferrero, F., Piacentino, M.G., 2008. Study on cast membranes and electrospun nanofibers made from keratin/fibroin blends. Biomacromolecules 9, 2819−2825.

Index

'*Note*: Page numbers followed by "f" indicate figures and "t" indicate tables.'